

REPUBLIC OF CAMEROON

Peace-Work-Fatherland

UNIVERSITY OF YAOUNDE I

FACULTY OF SCIENCE

POSTGRADUATE SCHOOL OF SCIENCE,
TECHNOLOGY AND GEOSCIENCES

RESEARCH AND POSTGRADUATE TRAINING
UNIT FOR CHEMISTRY AND APPLICATIONS



REPUBLIQUE DU CAMEROUN

Paix-Travail-Patrie

UNIVERSITE DE YAOUNDE I

FACULTE DES SCIENCES

CENTRE DE RECHERCHE ET DE FORMATION
DOCTORALE EN SCIENCES, TECHNOLOGIES
ET GEOSCIENCES

UNITE DE RECHERCHE ET DE FORMATION
DOCTORALE CHIMIE ET APPLICATIONS

DEPARTMENT OF ORGANIC CHEMISTRY

DEPARTEMENT DE CHIMIE ORGANIQUE

**CHEMICAL INVESTIGATION AND
ANTILEISHMANIAL ACTIVITY OF THREE
CAMEROONIAN MEDICINAL PLANTS:
ROTHMANNIA HISPIDA (K. SCHUM) FAGERL.,
NAUCLEA LATIFOLIA (J.E. SMITH) (RUBIACEAE)
AND *BAPHIA LEPTBOTRYS* HARMS (FABACEAE)**

THESIS

Presented and publicly defended in view of the requirement of Doctorate/Ph.D in Organic
Chemistry

By:

Argan Kelly WONKAM NKWENTI

Registration number: 16X5885

Master of Science in Organic Chemistry


Under the supervision of:

Bruno LENTA NDJAKOU

Professor



2021

THE UNIVERSITY OF YAOUNDE I Faculty of Science Division of Programming and Follow-up of Academic Affairs		UNIVERSITÉ DE YAOUNDÉ 1 Faculté des Sciences Division de la Programmation et du Suivi des Activités Académiques
LIST OF PERMANENT TEACHING STAFF		LISTE DES ENSEIGNANTS PERMANENTS

LIST OF PERMANENT TEACHING STAFF

ACADEMIC YEAR 2021/2022

(By Department and by Grade)

UPDATE DATE: 22 September 2021

ADMINISTRATION

DEAN: TCHOUANKEU Jean-Claude, Associate Professor

VICE DEAN/DPSAA: ATCHADE Alex de Théodore, Associate Professor

VICE DEAN/DSSE: NYEGUE Maximilienne Ascension, Professor

VICE DEAN/DRC: ABOSSOLO Monique, Associate Professor

Head of Administrative and Financial Division: NDOYE FOE Florentine Marie Chantal, Associate Professor

Head of Academic Affairs, Education and Research Division DAASR: AJEAGAH Gideon AGHAINDUM, Professor

1- DEPARTMENT OF BIOCHEMISTRY (BC) (38)

N°	NAMES AND SURNAMES	Grade	Observations
1	BIGOGA DAIGA Jude	Professor	On duty
2	FEKAM BOYOM Fabrice	Professor	On duty
3	FOKOU Elie	Professor	On duty
4	KANSCI Germain	Professor	On duty
5	MBACHAM FON Wilfried	Professor	On duty
6	MOUNDIPA FEWOU Paul	Professor	<i>Head of Department</i>
7	NINTCHOM PENLAP V. spouse BENG	Professor	On duty
8	OBEN Julius ENYONG	Professor	On duty

9	ACHU Merci BIH	Associate Professor	On duty
10	ATOGHO Barbara Mma	Associate Professor	On duty
11	AZANTSA KINGUE GABIN BORIS	Associate Professor	On duty
12	BELINGA born NDOYE FOE F. M. C.	Associate Professor	<i>Head AFD/FS</i>
13	BOUDJEKO Thaddée	Associate Professor	On duty
14	DJUIDJE NGOUNOUE Marcelline	Associate Professor	On duty
15	EFFA ONOMO Pierre	Associate Professor	On duty
16	EWANE Cécile Anne	Associate Professor	On duty

17	MOFOR born TEUGWA Clotilde	Associate Professor	<i>Service Inspector MINESUP</i>
18	NANA Louise spouse WAKAM	Associate Professor	On duty
19	NGONDI Judith Laure	Associate Professor	On duty
20	NGUEFACK Julienne	Associate Professor	On duty
21	NJAYOU Frédéric Nico	Associate Professor	On duty
22	TCHANA KOUATCHOUA Angèle	Associate Professor	On duty

23	AKINDEH MBUH NJI	Lecturer	On duty
24	BEBEE Fadimatou	Lecturer	On duty
25	BEBOY EDJENGUELE Sara Nathalie	Lecturer	On duty
26	DAKOLE DABOY Charles	Lecturer	On duty
27	DJUUKWO NKONGA Ruth Viviane	Lecturer	On duty
28	DONGMO LEKAGNE Joseph Blaise	Lecturer	On duty
29	FONKOUA Martin	Lecturer	On duty
30	KOTUE KAPTUE Charles	Lecturer	On duty
31	LUNGA Paul KEILAH	Lecturer	On duty
32	MANANGA Marlyse Joséphine	Lecturer	On duty
33	MBONG ANGIE M. Mary Anne	Lecturer	On duty
34	Palmer MASUMBE NETONGO	Lecturer	On duty
35	PECHANGOU NSANGOU Sylvain	Lecturer	On duty

36	MBOUCHE FANMOE Marceline Joëlle	Assistant lecturer	On duty
37	OWONA AYISSI Vincent Brice	Assistant lecturer	On duty
38	WILFRIED ANGIE Abia	Assistant lecturer	On duty

2- DEPARTMENT OF BIOLOGY AND ANIMAL PHYSIOLOGY (BAP) (46)

1	AJEAGAH Gideon AGHAINDUM	Professor	<i>VICE-DEAN DSSE</i>
2	BILONG BILONG Charles-Félix	Professor	<i>Head of Department</i>
3	DIMO Théophile	Professor	On duty
4	DJIETO LORDON Champlain	Professor	On duty
5	DZEUFUET DJOMENI Paul Désiré	Professor	Vice Dean/FMBS/UYI
6	ESSOMBA born NTSAMA MBALA	Professor	On duty
7	FOMENA Abraham	Professor	On duty
8	KAMTCHOUING Pierre	Professor	On duty
9	KEKEUNOU Sévilor	Professor	On duty
10	NJAMEN Dieudonné	Professor	On duty
11	NJIOKOU Flobert	Professor	On duty
12	NOLA Moïse	Professor	<i>Service Inspector of Coord.Progr./MINSANTE</i>
13	TAN Paul VERNYUY	Professor	On duty

14	TCHUEM TCHUENTE Louis Albert	Professor	On duty
15	ZEBAZE TOGOUET Serge Hubert	Professor	On duty

16	BILANDA Danielle Claude	Associate Professor	On duty
17	DJIOGUE Séfirin	Associate Professor	On duty
18	JATSA BOUKENG Hermine spouse MEGAPTCHÉ	Associate Professor	On duty
19	LEKEUFACK FOLEFACK Guy B.	Associate Professor	On duty
20	MEGNEKOU Rosette	Associate Professor	On duty
21	MONY Ruth spouse NTONE	Associate Professor	On duty
22	NGUEGUIM TSOFAK Florence	Associate Professor	On duty
23	TOMBI Jeannette	Associate Professor	On duty

24	ALENE Désirée Chantal	Lecturer	On duty
25	ATSAMO Albert Donatien	Lecturer	On duty
26	BELLET EDIMO Oscar Roger	Lecturer	On duty
27	DONFACK Mireille	Lecturer	On duty
28	ETEME ENAMA Serge	Lecturer	On duty
29	GOUNOUE KAMKUMO Raceline	Lecturer	On duty
30	KANDEDA KAVAYE Antoine	Lecturer	On duty
31	MAHOB Raymond Joseph	Lecturer	On duty
32	MBENOUN MASSE Paul Serge	Lecturer	On duty
33	MOUNGANG Luciane Marlyse	Lecturer	On duty
34	MVEYO NDANKEU Yves Patrick	Lecturer	On duty
35	NGOUATEU KENFACK Omer Bébé	Lecturer	On duty
36	NGUEMBOK	Lecturer	On duty
37	NJUA Clarisse Yafi	Lecturer	<i>Head Div. UBA</i>
38	NOAH EWOTI Olive Vivien	Lecturer	On duty
39	TADU Zephyrin	Lecturer	On duty
40	TAMSA ARFAO Antoine	Lecturer	On duty
41	YEDE	Lecturer	On duty

42	BASSOCK BAYIHA Etienne Didier	Assistant lecturer	On duty
43	ESSAMA MBIDA Désirée Sandrine	Assistant lecturer	On duty
44	KOGA MANG DOBARA	Assistant lecturer	On duty
45	LEME BANOCK Lucie	Assistant lecturer	On duty
46	YOUNOUSSA LAME	Assistant lecturer	On duty

3- DEPARTMENT OF BIOLOGY AND VEGETAL PHYSIOLOGY (BVP) (31)			
---	--	--	--

1	AMBANG Zachée	Professor	<i>Head of Division/UYII</i>
2	BELL Joseph Martin	Professor	On duty
3	DJOCGOUE Pierre François	Professor	On duty
4	MBOLO Marie	Professor	On duty

5	MOSSEBO Dominique Claude	Professor	On duty
6	YOUMBI Emmanuel	Professor	Head of Department
7	ZAPFACK Louis	Professor	On duty

8	ANGONI Hyacinthe	Associate Professor	On duty
9	BIYE Elvire Hortense	Associate Professor	On duty
10	MALA Armand William	Associate Professor	On duty
11	MBARGA BINDZI Marie Alain	Associate Professor	<i>TA/MINESUP</i>
12	NDONGO BEKOLO	Associate Professor	<i>CE/MINRESI</i>
13	NGODO MELINGUI Jean Baptiste	Associate Professor	On duty
14	NGONKEU MAGAPTCHE Eddy L.	Associate Professor	On duty
15	TONFACK Libert Brice	Associate Professor	On duty
16	TSOATA Esaïe	Associate Professor	On duty

17	DJEUANI Astride Carole	Lecturer	On duty
18	GOMANDJE Christelle	Lecturer	On duty
19	MAFFO MAFFO Nicole Liliane	Lecturer	On duty
20	MAHBOU SOMO TOUKAM. Gabriel	Lecturer	On duty
21	NGALLE Hermine BILLE	Lecturer	On duty
22	NNANGA MEBENGA Ruth Laure	Lecturer	On duty
23	NOUKEU KOUAKAM Armelle	Lecturer	On duty
24	ONANA JEAN MICHEL	Lecturer	On duty

25	GODSWILL NTSOMBOH NTSEFONG	Assistant lecturer	On duty
26	KABELONG BANAHU Louis-Paul-Roger	Assistant lecturer	On duty
27	KONO Léon Dieudonné	Assistant lecturer	On duty
28	LIBALAH Moses BAKONCK	Assistant lecturer	On duty
29	LIKENG-LI-NGUE Benoit C	Assistant lecturer	On duty
30	TAEDOUNG Evariste Hermann	Assistant lecturer	On duty
31	TEMEGNE NONO Carine	Assistant lecturer	On duty

4- DEPARTMENT OF INORGANIC CHEMISTRY (IC) (33)

1	AGWARA ONDOH Moïse	Professor	<i>Head of Department</i>
2	DJOUFAC WOUMFO Emmanuel	Professor	On duty
3	Florence UFI CHINJE spouse MELO	Professor	<i>Rector Univ.Ngaoundere</i>
4	GHOOGOMU Paul MINGO	Professor	<i>Minister in Charge of Miss.PR</i>
5	NANSEU Njiki Charles Péguy	Professor	On duty
6	NDIFON Peter TEKE	Professor	<i>TA MINRESI</i>
7	NDIKONTAR Maurice KOR	Professor	<i>Vice-Dean Univ. Bamenda</i>
8	NENWA Justin	Professor	On duty
9	NGAMENI Emmanuel	Professor	<i>Dean FS Uds</i>
10	NGOMO Horace MANGA	Professor	<i>Vice Chancellor/UB</i>

11	ACAYANKA Elie	Associate Professor	On duty
12	BABALE born DJAM DOUDOU	Associate Professor	<i>Mission Officer P.R.</i>
13	EMADACK Alphonse	Associate Professor	On duty
14	KAMGANG YOUBI Georges	Associate Professor	On duty
15	KEMMEGNE MBOUGUEM Jean C.	Associate Professor	On duty
16	KONG SAKEO	Associate Professor	On duty
17	NDI NSAMI Julius	Associate Professor	On duty
18	NJIOMOU C. spouse DJANGANG	Associate Professor	On duty
19	NJOYA Dayirou	Associate Professor	On duty
20	TCHAKOUTE KOUAMO Hervé	Associate Professor	On duty

21	BELIBI BELIBI Placide Désiré	Lecturer	<i>CS/ENS Bertoua</i>
22	CHEUMANI YONA Arnaud M.	Lecturer	On duty
23	KENNE DEDZO GUSTAVE	Lecturer	On duty
24	KOUOTOU DAOUDA	Lecturer	On duty
25	MAKON Thomas Beauregard	Lecturer	On duty
26	MBEY Jean Aime	Lecturer	On duty
27	NCHIMI NONO KATIA	Lecturer	On duty
28	NEBAH born NDO SIRI Bridget NDOYE	Lecturer	<i>TA/MINFEM</i>
29	NYAMEN Linda Dyorisse	Lecturer	On duty
30	PABOUDAM GBAMBIE A.	Lecturer	On duty
31	NJANKWA NJABONG N. Eric	Assistant lecturer	On duty
32	PATOUOSSA ISSOFA	Assistant lecturer	On duty
33	SIEWE Jean Mermoz	Assistant lecturer	On duty

5- DEPARTMENT OF ORGANIC CHEMISTRY (OC) (40)

1	DONGO Etienne	Professor	<i>Vice-Dean/DSEE FSE</i>
2	GHO GOMU TIH Robert Ralph	Professor	<i>Dir. IBAF/UDA</i>
3	NGOUELA Silvère Augustin	Professor	<i>Head of Department UDS</i>
4	NYASSE Barthélemy	Professor	On duty
5	PEGNYEMB Dieudonné Emmanuel	Professor	<i>Director MINESUP/Head of Department</i>
6	WANDJI Jean	Professor	<i>On duty</i>

7	Alex de Théodore ATCHADE	Associate Professor	Vice-Dean/DPSAA
8	AMBASSA Pantaléon	Associate Professor	On duty
9	EYONG Kenneth OBEN	Associate Professor	On duty
10	FOLEFOC Gabriel NGOSONG	Associate Professor	On duty
11	FOTSO WABO Ghislain	Associate Professor	On duty
12	KEUMEDJIO Félix	Associate Professor	On duty

13	KENMOGNE Marguerite	Associate Professor	On duty
14	KOUAM Jacques	Associate Professor	On duty
15	MBAZOA born DJAMA Céline	Associate Professor	On duty
16	MKOUNGA Pierre	Associate Professor	On duty
17	MVOT AKAK CARINE	Associate Professor	On duty
18	NGO MBING Joséphine	Associate Professor	<i>Assistant Director MINRESI</i>
19	NGONO BIKOBO Dominique Serge	Associate Professor	<i>C.E/MINESUP</i>
20	NOTE LOUGBOT Olivier Placide	Associate Professor	<i>C.S/MINESUP</i>
21	NOUNGOUE TCHAMO Diderot	Associate Professor	On duty
22	TABOPDA KUATE Turibio	Associate Professor	On duty
23	TAGATSING FOTSING Maurice	Associate Professor	On duty
24	TCHOUANKEU Jean-Claude	Associate Professor	<i>Dean/FS/Uyi</i>
25	TIH née NGO BILONG E. Anastasie	Associate Professor	On duty
26	YANKEP Emmanuel	Associate Professor	On duty
27	ZONDEGOUMBA Ernestine	Associate Professor	On duty

28	KAMTO Eutrophe Le Doux	Lecturer	On duty
29	NGNINTEDO Dominique	Lecturer	On duty
30	NGOMO Orléans	Lecturer	On duty
31	OUAHOUE WACHE Blandine M.	Lecturer	On duty
32	SIELINOUE TEDJON Valérie	Lecturer	On duty

33	MESSI Angélique Nicolas	Assistant lecturer	On duty
34	MUNVERA MFIFEN Aristide	Assistant lecturer	On duty
35	NONO NONO Éric Carly	Assistant lecturer	On duty
36	OUETE NANTCHOUANG Judith	Assistant lecturer	On duty
37	TCHAMGOUE Joseph	Assistant lecturer	On duty
38	TSAFFACK Maurice	Assistant lecturer	On duty
39	TSAMO TONTSA Armelle	Assistant lecturer	On duty
40	TSEMEUGNE Joseph	Assistant lecturer	On duty

6- DEPARTMENT OF INFORMATIC (IN) (25)

1	ATSA ETOUNDI Roger	Professor	<i>Head Div.MINESUP</i>
2	FOUDA NDJODO Marcel Laurent	Professor	<i>Head Dpt ENS/Head IGA.MINESUP</i>

3	NDOUNDAM René	Associate Professor	On duty
---	---------------	---------------------	---------

4	ABESSOLO ALO'O Gislain	Lecturer	<i>Head of Department</i>
5	AMINOUE Halidou	Lecturer	On duty
6	DJAM Xaviera YOUH – KIMBI	Lecturer	On duty
7	DOMGA KOMGUEM Rodrigue	Lecturer	On duty

8	EBELE Serge Alain	Lecturer	On duty
9	KOUOKAM KOUOKAM E. A.	Lecturer	On duty
10	MELATAGIA YONTA Paulin	Lecturer	On duty
11	MONTHE DJIADEU Valery M.	Lecturer	On duty
12	MOTO MPONG Serge Alain	Lecturer	On duty
13	OLLE OLLE Daniel Claude Delort	Lecturer	<i>Deputy Director Enset Ebolowa</i>
14	TAPAMO Hyppolite	Lecturer	On duty
15	TINDO Gilbert	Lecturer	On duty
16	TSOPZE Norbert	Lecturer	On duty
17	WAKU KOUAMOU Jules	Lecturer	On duty

18	BAYEM Jacques Narcisse	Assistant lecturer	On duty
19	EKODECK Stéphane Gaël Raymond	Assistant lecturer	On duty
20	HAMZA Adamou	Assistant lecturer	On duty
21	JIOMEKONG AZANZI Fidel	Assistant lecturer	On duty
22	MAKEMBE S. Oswald	Assistant lecturer	On duty
23	MESSI NGUELE Thomas	Assistant lecturer	On duty
24	MEYEMDOU Nadège Sylvianne	Assistant lecturer	On duty
25	NKONDOCK MI. BAHANACK N.	Assistant lecturer	On duty

7- DEPARTMENT OF MATHEMATICS (MA) (30)

1	AYISSI Raoult Domingo	Professor	<i>Head of Department</i>
2	EMVUDU WONO Yves S.	Professor	<i>Inspector MINESUP</i>

3	KIANPI Maurice	Associate Professor	On duty
4	MBANG Joseph	Associate Professor	On duty
5	MBEHOU Mohamed	Associate Professor	On duty
6	MBELE BIDIMA Martin Ledoux	Associate Professor	On duty
7	NKUIMI JUGNIA Célestin	Associate Professor	On duty
8	NOUNDJEU Pierre	Associate Professor	<i>Head of Programs & Diplomas</i>
9	TCHAPNDA NJABO Sophonie B.	Associate Professor	<i>Director/AIMS Rwanda</i>
10	TCHOUNDJA Edgar Landry	Associate Professor	On duty

11	AGHOUKENG JIOFACK Jean Gérard	Lecturer	<i>Head Cell MINPLAMAT</i>
12	CHENDJOU Gilbert	Lecturer	On duty
13	DJIADEU NGAHA Michel	Lecturer	On duty
14	DOUANLA YONTA Herman	Lecturer	On duty
15	FOMEKONG Christophe	Lecturer	On duty
16	KIKI Maxime Armand	Lecturer	On duty

17	MBAKOP Guy Merlin	Lecturer	On duty
18	MENGUE MENGUE David Joe	Lecturer	On duty
19	NGUEFACK Bernard	Lecturer	On duty
20	NIMPA PEFOUKEU Romain	Lecturer	On duty
21	POLA DOUNDOU Emmanuel	Lecturer	On duty
22	TAKAM SOH Patrice	Lecturer	On duty
23	TCHANGANG Roger Duclos	Lecturer	On duty
24	TETSADJIO TCHILEPECK M. E.	Lecturer	On duty
25	TIAYA TSAGUE N. Anne-Marie	Lecturer	On duty
26	BITYE MVONDO Esther Claudine	Assistant lecturer	On duty
27	MBATAKOU Salomon Joseph	Assistant lecturer	On duty
28	MBIAKOP Hilaire George	Assistant lecturer	On duty
29	MEFENZA NOUNTU Thiery	Assistant lecturer	On duty
30	TCHEUTIA Daniel Duviol	Assistant lecturer	On duty

8- DEPARTMENT OF MICROBIOLOGY (MIB) (18)

1	ESSIA NGANG Jean Justin	Professor	<i>Head of Department</i>
2	NYEGUE Maximilienne Ascension	Professor	<i>VICE-Dean/DSSE</i>
3	NWAGA Dieudonné M.	Professor	On duty

4	ASSAM ASSAM Jean Paul	Associate Professor	On duty
5	BOYOMO ONANA	Associate Professor	On duty
6	RIWOM Sara Honorine	Associate Professor	On duty
7	SADO KAMDEM Sylvain Leroy	Associate Professor	On duty

8	BODA Maurice	Lecturer	On duty
9	BOUGNOM Blaise Pascal	Lecturer	On duty
10	ESSONO OBOUGOU Germain G.	Lecturer	On duty
11	NJIKI BIKOÏ Jacky	Lecturer	On duty
12	TCHIKOUA Roger	Lecturer	On duty
13	ESSONO Damien Marie	Assistant lecturer	On duty
14	LAMYE Glory MOH	Assistant lecturer	On duty
15	MEYIN A EBONG Solange	Assistant lecturer	On duty
16	NKOUDOU ZE Nardis	Assistant lecturer	On duty
17	SAKE NGANE Carole Stéphanie	Assistant lecturer	On duty
18	TOBOLBAÏ Richard	Assistant lecturer	On duty

9. DEPARTMENT OF PHYSIC (PHY) (44)

1	BEN- BOLIE Germain Hubert	Professor	On duty
2	DJUIDJE KENMOE spouse ALOYEM	Professor	On duty
3	EKOBENA FOU DA Henri Paul	Professor	<i>Vice Rector</i>

4	ESSIMBI ZOBO Bernard	Professor	On duty
5	KOFANE Timoléon Crépin	Professor	On duty
6	NANA ENGO Serge Guy	Professor	On duty
7	NANA NBENDJO Blaise	Professor	On duty
8	NDJAKA Jean Marie Bienvenu	Professor	Head of Department
9	NJANDJOCK NOUCK Philippe	Professor	On duty
10	NOUAYOU Robert	Professor	On duty
11	PEMHA Elkana	Professor	On duty
12	TABOD Charles TABOD	Professor	<i>Dean Univ/Bda</i>
13	TCHAWOUA Clément	Professor	On duty
14	WOAFO Paul	Professor	On duty
15	ZEKENG Serge Sylvain	Professor	On duty

16	BIYA MOTTO Frédéric	Associate Professor	DG/HYDRO Mekin
17	BODO Bertrand	Associate Professor	On duty
18	ENYEGUE A NYAM spouse BELINGA	Associate Professor	On duty
19	EYEBE FOUDA Jean sire	Associate Professor	On duty
20	FEWO Serge Ibraïd	Associate Professor	On duty
21	HONA Jacques	Associate Professor	On duty
22	MBANE BIOUELE César	Associate Professor	On duty
23	MBINACK Clément	Associate Professor	On duty
24	NDOP Joseph	Associate Professor	On duty
25	SAIDOU	Associate Professor	MINRESI
26	SIEWE SIEWE Martin	Associate Professor	On duty
27	SIMO Elie	Associate Professor	On duty
28	VONDOU Derbetini Appolinaire	Associate Professor	On duty
29	WAKATA born BEYA Annie	Associate Professor	<i>Director ENS/Uy1</i>

30	ABDOURAHIMI	Lecturer	On duty
31	CHAMANI Roméo	Lecturer	On duty
32	EDONGUE HERVAIS	Lecturer	On duty
33	FOUEDJIO David	Lecturer	<i>Head Cell. MINADER</i>
34	MBONO SAMBA Yves Christian U.	Lecturer	On duty
35	MEL'I Joelle Larissa	Lecturer	On duty
36	MVOGO ALAIN	Lecturer	On duty
37	OBOUNOU Marcel	Lecturer	<i>DA/Univ Inter State/Sangmalima</i>
38	WOULACHE Rosalie Laure	Lecturer	On duty

39	AYISSI EYEBE Guy François Valérie	Assistant lecturer	On duty
40	DJIOTANG TCHOTCHOU Lucie Angennes	Assistant lecturer	On duty
41	LAMARA Maurice	Assistant lecturer	On duty

42	OTTOU ABE Martin Thierry	Assistant lecturer	On duty
43	TEYOU NGOUPOU Ariel	Assistant lecturer	On duty
44	WANDJI NYAMSI William	Assistant lecturer	On duty

10- DEPARTMENT OF EARTH SCIENCES (ES) (43)

1	BITOM Dieudonné	Professor	<i>Dean/FASA/UDs</i>
2	FOUATEU Rose spouse YONGUE	Professor	On duty
3	NDAM NGOUPAYOU Jules-Remy	Professor	On duty
4	NDJIGUI Paul Désiré	Professor	<i>Head of Department</i>
5	NGOS III Simon	Professor	On duty
6	NKOUMBOU Charles	Professor	On duty
7	NZENTI Jean-Paul	Professor	On duty

8	ABOSSOLO born ANGUE Monique	Associate Professor	<i>Vice-Dean/DRC</i>
9	BISSO Dieudonné	Associate Professor	<i>Director/Barrage Project Memve'ele</i>
10	EKOMANE Emile	Associate Professor	On duty
11	GANNO Sylvestre	Associate Professor	On duty
12	GHOGOMU Richard TANWI	Associate Professor	<i>CD/Uma</i>
13	MOUNDI Amidou	Associate Professor	<i>TA/ MINIMDT</i>
14	NGUEUTCHOUA Gabriel	Associate Professor	<i>CEA/MINRESI</i>
15	NJILAH Isaac KONFOR	Associate Professor	On duty
16	NYECK Bruno	Associate Professor	On duty
17	ONANA Vincent Laurent	Associate Professor	<i>Head of Maintenance & Equipment</i>
18	TCHAKOUNTE J. spouse NUMBEM	Associate Professor	<i>Head cell MINRESI</i>
19	TCHOUANKOUE Jean-Pierre	Associate Professor	On duty
20	TEMDJIM Robert	Associate Professor	On duty
21	YENE ATANGANA Joseph Q.	Associate Professor	<i>Head Div./MINTP</i>
22	ZO'O ZAME Philémon		<i>DG/ART</i>

23	ANABA ONANA Achille Basile	Lecturer	On duty
24	BEKOA Etienne	Lecturer	On duty
25	ELISE SABABA	Lecturer	On duty
26	ESSONO Jean	Lecturer	On duty
27	EYONG JOHN TAKEM	Lecturer	On duty
28	FUH Calistus Gentry	Lecturer	<i>State Sec. /MINMIDT</i>
29	LAMILEN BILLA Daniel	Lecturer	On duty
30	MBESSE CECILE OLIVE	Lecturer	On duty
31	MBIDA YEM	Lecturer	On duty
32	METANG Victor	Lecturer	On duty
33	MINYEM Dieudonné-Lucien	Lecturer	<i>CD/Uma</i>
34	NGO BELNOUN Rose Noël	Lecturer	On duty
35	NGO BIDJECK Louise Marie	Lecturer	On duty

36	NOMO NEGUE Emmanuel	Lecturer	On duty
37	NTSAMA ATANGANA Jacqueline	Lecturer	On duty
38	TCHAPTCHET TCHATO De P.	Lecturer	On duty
39	TEHNA Nathanaël	Lecturer	On duty
40	TEMGA Jean Pierre	Lecturer	On duty
42	FEUMBA Roger	Assistant lecturer	On duty
43	MBANGA NYOBE Jules	Assistant lecturer	On duty

Quantified distribution of teachers from the Faculty of Sciences of the University of Yaoundé 1

NUMBER OF TEACHERS					
DEPARTMENT	Professors	Associate Professors	Lecturers	Assistant lecturers	Total
BCH	8 (01)	14 (10)	13 (05)	3 (02)	38 (18)
BAP	15 (01)	8 (06)	18 (05)	05 (02)	46 (14)
BVP	07 (01)	9 (01)	8 (06)	07 (01)	31 (9)
IC	10 (01)	10 (02)	10 (02)	03 (0)	33 (5)
OC	6 (0)	21 (05)	05 (02)	08 (02)	40 (9)
IN	2 (0)	1 (0)	14 (01)	08 (01)	25 (2)
MAT	2 (0)	8 (0)	15 (01)	05 (02)	30 (3)
MIB	3 (0)	4 (02)	05 (01)	06 (02)	18 (5)
PHY	15 (0)	14 (02)	09 (03)	06 (01)	44 (6)
ES	7 (1)	15 (01)	18 (05)	02 (0)	42 (7)
Total	75 (5)	104 (29)	115 (31)	53 (13)	347 (82)

A total of **347 (82)** with:
 -Professors **75 (5)**
 -Associate Professors **104 (29)**
 -Lecturers **115 (31)**
 -Assistant lecturers **53 (13)**
 () = Number of Women **82**

DECLARATION

I, the undersigned, **Bruno LENTA NDJAKOU** (Professor), certify that the work presented in this thesis and entitled «Chemical investigation and antileishmanial activity of three Cameroonian medicinal plants: *Rothmannia hispida* (K. Schum) Fagerl., *Nauclea latifolia* (J.E. Smith) (Rubiaceae) and *Baphia leptobotrys* Harms (Fabaceae)» was carried out by Mrs **Argan Kelly WONKAM NKWENTI** (Master in Organic Chemistry, Registration number 16X5885), in the Natural Substances of Therapeutic Interest and Organic Synthesis (LASUNITSO) research group at the Higher Teacher Training College (HTTC), University of Yaoundé 1.

This work has not yet been the subject of any submission for the acquisition of any academic degree.

Supervisor

Bruno NDJAKOU LENTA

Professor

DEDICATION

In loving memory of my mother and grandparents

ACKNOWLEDGEMENTS

I address my deep gratitude to:

Professor Bruno LENTA NDJAKOU who guided this work from the beginning to the end. He warmly welcoming me into his research team. He gave me the opportunity to learn from his long and great experience and knowledge in the field of research while leading me on the path of fine-tuned work and rigor.

Professor Silvère Augustin NGOUELA, Head of Department of Chemistry at the Faculty of Science, University of Dschang, for the advice, the great availability and the encouragement.

Professor Dieudonné Emmanuel PEGNYEMB, Head of the Department of Organic Chemistry at the Faculty of Science of the University of Yaoundé 1, for his dynamism and dedication in the smooth running of the Department.

Professor Ephrem Augustin NKENGFACK, for his advice and encouragement during the production of this thesis.

All the teachers of the Department of Organic Chemistry of the Faculty of Science, University of Yaoundé 1, for their dedication in teaching and transferring knowledge.

The **YaBiNaPA** (Yaounde-Bielefeld Graduate School of Natural Products with Antiparasite and Antibacterial activities) members, **Professor Norbert SEWALD** and **Dr Marcel FRESE** from the University of Bielefeld (Germany), **Professors Bonaventure NGADJUI**, **Théophile DIMO**, **Fabrice FEKAM BOYOM**, **Décaux FOTSO WABO KAPCHE** and **Siméon FOGUE KOUAM** from the University of Yaoundé 1, for their support, advice and collaboration in the construction of this work.

Professors Jean Rodolphe CHOUNA, **Jean Jules BANKEU KEZETAS** and **Engelbert AWANTU FUSI**, for their encouragement, invaluable advice and assistance during the production of this thesis.

Drs Eugenie MADIESTE, **Gervais HAPPI MOUTHE**, **Jean-Bosco JOUDA**, **Aimé TCHUENMOGNE TCHUENTE**, **Joseph TCHAMGOUE**, **Billy TCHENITEGNI TOUSSIE** and **Gabin BITCHAGNO**, for their availability and multiple advice throughout this work.

All the laboratory seniors: **Drs Yannick Stéphane FONGANG FOTSING**, **Brice MITTERANT MBA'NING**, **Erik DONFACK VOUFFO**, **Rosine NGAMGWE**, **Jules NGATCHOU**, **Joël ATEBA**, **Flaure ESSOUNG**, **Stephanie DIETAGOUM**, **Donald KAGHO** and **Mrs Claire WALEGUELE**, for their welcome, advice and constant assistance.

My laboratory mates: **Johanne Kevine DONGMO JUMETA, Suzy Ardo CHOUNA DONFACK, Armelle TSAKOU TAFUO, Clemence GOUNI, Jean Koffi GARBA, Larissa BOUZÉKO, Ruland NGUENGANG TCHUINKEU, Joël MENATCHE NJOPNU, Tatiana YOUMBI, Ingrid MATEFO, Jenny TABET, Elfried NGASSAM, Alix FEUMBOU NOUSSI, Andrel KADJI and Gaelle DIFFO**, for their support and collaboration in the construction of this work.

The **Deutscher Akademischer Austauschdienst (DAAD)** through **YaBiNaPA project N° 57316173**, for the grant that enable us to have various material and financial resources.

Professors Jean Duplex WANSI and Alain François WAFFO KAMDEM, for their encouragement and advice during the production of this thesis.

My father **Mr Haddison NKWENTI**, for our forever and ever love and support.

My daughter **Carla NKWENTI**, my sisters and brother **Mrs Solange WONGUE NKWENTI, Cyane Thérine MEUKILEDJE NKWENTI** and **Mr Loic Steve PIDI BARA**, for their unconditional love, support and encouragement.

Me Fabrice Renad TCHOUMEN, Lawyer at the Cameroon Bar, for his advice and support.

Mr Léopold YIMGA DJAMEN, the Regional Delegate of Basic Education for Littoral Region, for his encouragement and support.

My brother in law **Yannick DJOUBOUOSSIE**, for his invaluable advice and encouragement.

Mr Joseph Claude ASSENGUE FOU DA, the General Treasurer at the Treasury of Bafoussam, for his encouragement, advice and support.

My aunts and uncles **Mrs Pelagie TCHOUANYIM, Madeleine NGUENANG, Nathalie MEUKILEDJE, Mr Chirak NGOUONMEDJE and Charlie TAMEU**, for their precious advice and encouragement.

TABLE OF CONTENTS

LIST OF PERMANENT TEACHING STAFF	i
DECLARATION.....	xii
DEDICATION.....	xiii
ACKNOWLEDGEMENTS.....	xiv
TABLE OF CONTENTS.....	xvi
LIST OF ABBREVIATIONS, ACRONYMS AND SYMBOLS	xix
LIST OF TABLES	xx
LIST OF FIGURES	xxiii
LIST OF SCHEMES.....	xxviii
ABSTRACT	xxix
RESUME.....	xxxi
GENERAL INTRODUCTION	1
PART I: LITERATURE REVIEW	3
I.1. OVERVIEW ON LEISHMANIASIS	3
I.1.1. Definition	3
I.1.2. Epidemiology	3
I.1.3. The vector of leishmaniasis	3
I.1.4. The parasite	4
I.1.5. Life cycle of the sandfly	4
I.1.6. Symptoms, diagnosis and treatment of leishmaniasis.....	5
I.2. OVERVIEW ON THE INVESTIGATED PLANTS.....	14
I.2.1. Overview on the Rubiaceae family	14
I.2.1.1. Overview on the genus <i>Rothmannia</i> Thunb.....	15
I.2.1.2. Overview on the genus <i>Nauclea</i> L.....	16
I.2.2. Overview on the Fabaceae family.....	18
I.2.2.1. Overview on the genus <i>Baphia</i> (Lodd.).....	19
I.3. USES OF THE INVESTIGATED PLANTS	21
I.3.1. Uses of plants of the genus <i>Rothmannia</i>	21

I.3.2. Uses of plants of the genus <i>Nauclea</i>	21
I.3.3. Uses of plants of the genus <i>Baphia</i>	22
I.4. PREVIOUS CHEMICAL AND BIOLOGICAL INVESTIGATIONS ON THE SELECTED PLANTS	23
I.4.1. Previous chemical investigations on the studied plants	23
I.4.1.1. Previous chemical investigations on plants of the Gardenieae tribe.....	23
I.4.1.2. Previous chemical investigations on plants of the genus <i>Nauclea</i>	30
I.4.1.3. Previous chemical investigations on plants of the genus <i>Baphia</i>	37
I.4.2. Previous biological investigations on the studied plants	42
I.4.2.1. Previous biological investigations on plants of the Gardenieae tribe	42
I.4.2.2. Previous biological investigations on plants of the genus <i>Nauclea</i>	43
I.4.2.3. Previous biological investigations on plants of the genus <i>Baphia</i>	44
I.5. OVERVIEW ON CERAMIDES	45
I.5.1. Definition and general classification of lipids	45
I.5.2. Definition and occurrence of ceramides	45
I.5.3. Biosynthesis and preparation of ceramides.....	46
I.5.4. Biological function of ceramides	49
I.5.5. General method for the structure elucidation of ceramides	50
PART II: RESULTS AND DISCUSSION	54
II.1. Chemical study of <i>Rothmannia hispida</i> , <i>Nauclea latifolia</i> and <i>Baphia leptobotrys</i>	54
II.1.1. Extraction of plant material	54
II.1.2. Antileishmanial screening and cytotoxicity assay	55
II.1.3. Acute toxicity study.....	55
II.1.4. Isolation of compounds	57
II.1.5. Structural elucidation of the isolated compounds.....	63
II.2. CHEMOPHENETIC SIGNIFICANCE OF THE ISOLATED COMPOUNDS	203
II.3. BIOLOGICAL ACTIVITIES OF THE ISOLATED COMPOUNDS	205
II.3.1. Antileishmanial activity of extracts, fractions and isolated compounds	205
II.3.2. Attempt of preformulation of phytomedicine from <i>N. latifolia</i> fruits	211
CONCLUSION AND PERSPECTIVES	214

PART III: MATERIAL AND METHODS	216
III.1. APPARATUS AND PLANT MATERIALS	216
III.1.1. Apparatus	216
III.1.2. Plant materials	217
III.2. SOME CHARACTERISTIC TESTS USED IN THE IDENTIFICATION OF SECONDARY METABOLITES.....	217
III.3. EXTRACTION, FRACTIONATION, ISOLATION AND PURIFICATION OF COMPOUNDS.....	219
III.3.1. Extraction	219
III.3.2. Fractionation of crude extracts and isolation of compounds.....	220
III.4. METHANOLYSIS.....	227
III.5. EVALUATION OF BIOLOGICAL ACTIVITIES	227
III.5.1. Antileishmanial assay.....	227
III.5.2. Cytotoxicity assay	228
III.5.3. Acute toxicity assay.....	228
III.5.4. Trial of preformulation.....	229
III.6. PHYSICAL AND CHEMICAL CHARACTERISTICS OF THE ISOLATED COMPOUNDS.....	230
REFERENCES	241
ANNEXE	264

LIST OF ABBREVIATIONS, ACRONYMS AND SYMBOLS

<i>B. leptobotrys</i>	<i>Baphia leptobotrys</i>
CC	Column Chromatography
CDC	Centers for Disease Control and Prevention
CL	Cutaneous Leishmaniasis
COSY	Correlation Spectroscopy
d	Doublet
DEPT	Distortionless Enhancement by Polarization Transfer
DMSO	Dimethyl Sulfoxide
EI	Electron Impact
ESI	Electro Spray Ionization
ESIMS	Electro Spray Ionization Mass Spectrum
HMBC	Heteronuclear Multiple Bond Correlation
HMQC	Heteronuclear Single Quantum Coherence
HRESI	High Resolution Electrospray Ionization
IC ₅₀	Inhibitory Concentration 50
IR	Infrared
<i>J</i>	Coupling Constant in Hertz
VL	Visceral Leishmaniasis
m	Multiplet
<i>N. latifolia</i>	<i>Nauclea latifolia</i>
MIC	Minimal Inhibitory Concentration
NMR ¹³ C	Carbon 13 Nuclear Magnetic Resonance
NMR ¹ H	Proton Nuclear Magnetic Resonance
OECD	Organisation for Economic Cooperation and Development
q	Quartet
<i>R. hispida</i>	<i>Rothmannia hispida</i>
s	Singlet
SI	Selectivity Index
TLC	Thin Layer Chromatography
t	Triplet
WHO	World Health Organization
δ	Chemical shift in ppm

LIST OF TABLES

Table 1: Current drugs used for the treatment of VL and CL	9
Table 2: Mechanism of actions of some antileishmanial drugs	10
Table 3: Current antileishmanial drugs, their associated toxicities and evidence of resistance development.....	11
Table 4: Some antileishmanial compounds obtained from medicinal plants.....	13
Table 5: Place of harvest of <i>N. latifolia</i> in Cameroon.....	18
Table 6: Place of harvest of <i>B. leptobotrys</i> in Cameroon.....	21
Table 7: Some plants of the genus <i>Rothmannia</i> and their uses in traditional medicine.....	21
Table 8: Some plants of the genus <i>Nauclea</i> and their uses in traditional medicine	22
Table 9: Traditional uses of some species of the genus <i>Baphia</i>	23
Table 10: Some iridoids isolated from plants of the Gardenieae tribe.....	24
Table 11: Some flavonoids isolated from plants of the Gardenieae tribe	25
Table 12: Some phenolic compounds isolated from plants of the Gardenieae tribe.....	27
Table 13: Some coumarins isolated from plants of the Gardenieae tribe	28
Table 14: Some alkaloids isolated from plants of the Gardenieae tribe.....	28
Table 15: Structure of some triterpenoids isolated from plants of the Gardenieae tribe.....	30
Table 16: Some triterpenoids isolated from plants of the genus <i>Nauclea</i>	32
Table 17: Some alkaloids isolated from the genus <i>Nauclea</i>	34
Table 18: Some phenolic compounds isolated from plants of the genus <i>Nauclea</i>	37
Table 19: Some flavonoids isolated from <i>Baphia</i> species	38
Table 20: Some prenylated xanthenes from plants of the genus <i>Baphia</i>	40
Table 21: Some imminosugars isolated from plants of the genus <i>Baphia</i>	41
Table 22: Some triterpenoids isolated from plants of the genus <i>Baphia</i>	42
Table 23: Effects of the methanol extract on some clinical parameters.....	56
Table 24: ¹ H (500 MHz) and ¹³ C (125 MHz) NMR data of rothmanniamide in pyridine- <i>d</i> ₅ ..	67
Table 25: ¹ H (500 MHz) and ¹³ C (125 MHz) NMR data of <i>n</i> -heptadecyl-4-hydroxy- <i>trans</i> -cinnamate in pyridine- <i>d</i> ₅	73
Table 26: ¹ H (500 MHz) and ¹³ C (125 MHz) NMR data of WN14 in CDCl ₃ compared to 2,6-dimethoxybenzoquinone [CDCl ₃ , NMR ¹³ C (100 MHz), NMR ¹ H (400 MHz)]	77
Table 27: ¹ H (600 MHz) and ¹³ C (150 MHz) NMR data of RH20 in pyridine- <i>d</i> ₅ compared to astragalin [DMSO- <i>d</i> ₆ , NMR ¹³ C (150 MHz) and DMSO- <i>d</i> ₆ +D ₂ O, NMR ¹ H (600 MHz)]	81
Table 28: ¹ H (500 MHz) and ¹³ C (125 MHz) NMR data of RHE1 in CDCl ₃ compared to lichexanthone [CDCl ₃ , NMR ¹³ C (125 MHz), NMR ¹ H (500 MHz)]	85
Table 29: ¹ H (500 MHz) and ¹³ C (125 MHz) NMR data of BLE4 in CDCl ₃ compared to germanicol caffeoyl ester [CDCl ₃ , NMR ¹³ C (150 MHz) and NMR ¹ H (600 MHz)]	90
Table 30: ¹ H (500 MHz) and ¹³ C (125 MHz) NMR data of BLE10 in pyridine- <i>d</i> ₅ compared to 3- <i>β</i> - <i>O</i> - <i>E</i> -3,5-dihydroxycinnamoyl-11-oxo-olean-12-ene [Pyridine- <i>d</i> ₅ , NMR ¹³ C (100 MHz) and NMR ¹ H (400 MHz)].....	96

Table 31: ^{13}C (125 MHz) NMR data of WN1 ($\text{CDCl}_3/\text{methanol-}d_4$) and RH11 (pyridine- d_5) compared to oleanolic acid and hederagenin	104
Table 32: ^{13}C (125 MHz) NMR data of RH5 in CDCl_3 compared to uvaol and erythrodiol. 108	
Table 33: ^{13}C (125 MHz) NMR data of WN5, RH6 (pyridine- d_5) and RH9 (acetone- $d_6/\text{methanol-}d_4$) compared to myrianthic acid, ursolic acid [$\text{DMSO-}d_6$, NMR ^{13}C (100 MHz)] and carisursane A [methanol- d_4 , NMR ^{13}C (100 MHz)].....	117
Table 34: ^1H (500 MHz) and ^{13}C (125 MHz) NMR data of RH15 in CDCl_3 compared to lupeol palmitate [CDCl_3 , NMR ^{13}C (100 MHz)]	122
Table 35: ^{13}C (125 MHz) NMR data of SNC11 (pyridine- d_5), BLE30 and RH16 in CDCl_3 compared to betulinic acid [CDCl_3 , NMR ^{13}C (100 MHz)], lupenone [CDCl_3 , NMR ^{13}C (75 MHz)] and lupeol.....	128
Table 36: ^1H (500 MHz) and ^{13}C (125 MHz) NMR data of SNC1 in CDCl_3 compared to friedelin [CDCl_3 , NMR ^{13}C (100 MHz), NMR ^1H (400 MHz)]	131
Table 37: ^1H (500 MHz) and ^{13}C (125 MHz) NMR data of SNCL2 (CDCl_3) and SNC4 (pyridine- d_5) compared to β -friedelinol [CDCl_3 , NMR ^{13}C (150 MHz)] and 3-oxofriedelan-25-oic acid [CDCl_3 , NMR ^{13}C (125 MHz), ^1H (500 MHz)]	141
Table 38: ^1H (500 MHz) and ^{13}C (125 MHz) NMR data of WN15 in CDCl_3 compared to trimethyl citrate.....	143
Table 39: ^1H (500 MHz) and ^{13}C (125 MHz) NMR data of WN34 in methanol- d_4 compared to dimethyl citrate	147
Table 40: ^1H (500 MHz) and ^{13}C (125 MHz) NMR data of WN36 in methanol- d_4 compared to methyl citrate [$\text{DMSO-}d_6$, NMR ^{13}C (125 MHz), NMR ^1H (500 MHz)].....	149
Table 41: ^1H (500 MHz) and ^{13}C (125 MHz) NMR data of SNC6 in CDCl_3 compared to asperphenamate [CDCl_3 , NMR ^{13}C (175 MHz), NMR ^1H (700 MHz)].....	154
Table 42: ^1H (500 MHz) and ^{13}C (125 MHz) NMR data of SNC6 in D_2O compared to 4-hydroxy- <i>N</i> -methylproline [D_2O , NMR ^{13}C (20.1 MHz), NMR ^1H (270 MHz)]	159
Table 43: ^1H (500 MHz) and ^{13}C (125 MHz) NMR data of WN17 in methanol- d_4 compared to monomethyl ester of 1H-pyrrole-2,5-dicarboxylic acid [$\text{DMSO-}d_6$, NMR ^{13}C (125 MHz), NMR ^1H (500 MHz)]	163
Table 44: ^1H (500 MHz) and ^{13}C (125 MHz) NMR data of NLB3 in methanol- d_4 compared to loganin [$\text{DMSO-}d_6$, NMR ^{13}C (200 MHz) and $\text{DMSO-}d_6 + \text{D}_2\text{O}$, NMR ^1H (600 MHz)]168	
Table 45: ^1H (500 MHz) and ^{13}C (125 MHz) NMR data of BLE8 in $\text{CDCl}_3/\text{methanol-}d_4$ compared to ergosterol peroxide [CDCl_3 , NMR ^{13}C (125 MHz) and NMR ^1H (500 MHz)]	173
Table 46: ^{13}C (125 MHz) NMR data of BLEF32 in acetone- d_6 compared to 7-ketostigmasterol and 7-keto- β -sitosterol [CDCl_3 , NMR ^{13}C (150 MHz)].....	178
Table 47: ^1H (500 MHz) and ^{13}C (125 MHz) NMR data of BLE22 in $\text{DMSO-}d_6$ compared to D-mannitol ($\text{DMSO-}d_6$)	185
Table 48: ^{13}C (125 MHz) NMR data of BLE21 and NLB4 in methanol- d_4 compared to methyl β -D-glucopyranoside, β -D-glucopyranoside and α -D-glucopyranoside.....	191
Table 49: ^1H (500 MHz) and ^{13}C (125 MHz) NMR data of WN3 in CDCl_3 compared to glycerol palmitate.....	194

Table 50: ^1H (500 MHz) and ^{13}C (125 MHz) NMR data of BLE34 in CDCl_3	197
Table 51: ^1H (500 MHz) and ^{13}C (125 MHz) NMR data of WN32 in CDCl_3 compared to 1,4-dimethylbenzene-1,4-dicarboxylate	201
Table 52: Criteria of evaluation of the antileishmanial activity of extracts, fractions and pure compounds	206
Table 53: Criteria of evaluation of the cytotoxicity activity	206
Table 54: Antileishmanial activity and selectivity indices of crude extract and compounds from <i>R. hispida</i> against promastigotes	206
Table 55: Antileishmanial activity and selectivity indices of crude extracts and compounds from <i>B. leptobotrys</i>	210
Table 56: Chromatogram of fraction F1	220
Table 57: Chromatogram of fraction F2	221
Table 58: Chromatogram of fraction F3	222
Table 59: Chromatogram of the <i>n</i> -hexane fraction	222
Table 60: Chromatogram of the dichloromethane fraction	223
Table 61: Chromatogram of the ethyl acetate fraction	224
Table 62: Chromatogram of the <i>n</i> -butanol fraction	224
Table 63: Chromatogram of the trunk bark crude extract of <i>B. leptobotrys</i>	225
Table 64: Chromatogram of the leaves crude extract of <i>B. leptobotrys</i>	226

LIST OF FIGURES

Figure 1: Life cycle of <i>Leishmania</i> parasites	5
Figure 2: Geographical distribution of plants of the Rubiaceae family	15
Figure 3: Picture of <i>Rothmannia hispida</i> (K. Schum) Fagerl branches bearing leaves and fruits	16
Figure 4: Pictures of <i>N. latifolia</i>	17
Figure 5: Distribution of <i>N. latifolia</i> in Africa	18
Figure 6: Branches of <i>Baphia leptobotrys</i> bearing leaves.....	20
Figure 7: Map showing the distribution of <i>B. leptobotrys</i> in the coastal tropical Africa.....	20
Figure 8: Effects of the methanol extract on the weight development of rats in acute toxicity	56
Figure 9: Effects of methanol extract of NLFr on the relative weight of organs in acute toxicity	57
Figure 10a: HRESI mass spectrum of RHE7	67
Figure 10b: ESI mass fragments of RHE7.....	68
Figure 11: IR spectrum of RHE7	68
Figure 12: ¹³ C NMR spectrum of RHE7 (pyridine- <i>d</i> ₅ , 125 MHz).....	68
Figure 13: DEPT spectrum of RHE7	69
Figure 14: HMQC spectrum of RHE7	69
Figure 15: ¹ H NMR of RHE7 (pyridine- <i>d</i> ₅ , 500 MHz).....	69
Figure 16: COSY spectrum of RHE7.....	70
Figure 17: HMBC spectrum of RHE7.....	70
Figure 18: ESI mass spectrum of long-chain base of RHE7	71
Figure 19: HRESI mass spectrum of RHE3	73
Figure 20: ¹ H NMR spectrum (pyridine- <i>d</i> ₅ , 500 MHz) of RHE3	74
Figure 21: ¹³ C NMR spectrum (Pyridine- <i>d</i> ₅ , 125 MHz) of RHE3.....	74
Figure 22: HMQC spectrum of RHE3	74
Figure 23: COSY spectrum of compound RHE3.....	75
Figure 24: HMBC spectrum of RHE3.....	75
Figure 25: HRESI mass spectrum of WN14	77
Figure 26: ¹ H NMR spectrum (CDCl ₃ , 500 MHz) of WN14	77
Figure 27: ¹³ C NMR spectrum (CDCl ₃ , 125 MHz) of WN14	78
Figure 28: DEPT spectrum of WN14.....	78
Figure 29: HMQC spectrum of WN14.....	78
Figure 30: HMBC spectrum of WN14	79
Figure 31: HRESI mass spectrum of RH20	81
Figure 32: ¹ H NMR spectrum (pyridine- <i>d</i> ₅ , 600 MHz) of RH20.....	82
Figure 33: ¹³ C NMR spectrum (pyridine- <i>d</i> ₅ , 150 MHz) of RH20	82
Figure 34: HMQC spectrum of RH20.....	82
Figure 35: HMBC spectrum of RH20	83
Figure 36: HRESI mass spectrum of RHE1	85
Figure 37: ¹ H NMR spectrum (CDCl ₃ , 500 MHz) of RHE1	86

Figure 38: ^{13}C NMR spectrum (CDCl_3 , 125 MHz) of RHE1	86
Figure 39: HMQC spectrum of RHE1	86
Figure 40: HMBC spectrum of RHE1	87
Figure 41: HRESI mass spectrum of BLE4	91
Figure 42: ^1H NMR spectrum (CDCl_3 , 500 MHz) of BLE4	91
Figure 43: ^{13}C NMR spectrum (CDCl_3 , 125 MHz) of BLE4	91
Figure 44: HMQC spectrum of BLE4	92
Figure 45: HMBC spectrum of BLE4	92
Figure 46: COSY spectrum of BLE4	93
Figure 47: HRESI mass spectrum of BLE10	97
Figure 48: ^1H NMR spectrum (Pyridine- d_5 , 500 MHz) of BLE10	97
Figure 49: ^{13}C NMR spectrum (Pyridine- d_5 , 125 MHz) of BLE10	97
Figure 50: HMQC spectrum of BLE10	98
Figure 51: COSY spectrum of BLE10	98
Figure 52: HMBC spectrum of BLE10	99
Figure 53: HRESI mass spectrum of RH11	101
Figure 54: ^1H NMR spectrum (pyridine- d_5 , 500 MHz) of RH11	101
Figure 55: ^{13}C NMR spectrum (pyridine- d_5 , 125 MHz) of RH11	101
Figure 56: HMQC spectrum of RH11	102
Figure 57: HMBC spectrum of RH11	102
Figure 58: ^1H NMR spectrum ($\text{CDCl}_3/\text{methanol-}d_4$, 500 MHz) of WN1	105
Figure 59: ^{13}C NMR spectrum ($\text{CDCl}_3/\text{methanol-}d_4$, 125 MHz) of WN1	105
Figure 60: HRESI mass spectrum of RH5	109
Figure 61: ^1H NMR spectrum (CDCl_3 , 500 MHz) of RH5	109
Figure 62: ^{13}C NMR spectrum (CDCl_3 , 125 MHz) of RH5	109
Figure 63: HMQC spectrum of RH5	110
Figure 64: HMBC spectrum of RH5	110
Figure 65: HRESI mass spectrum of RH6	112
Figure 66: ^1H NMR spectrum (500 MHz, pyridine- d_5) of RH6.....	112
Figure 67: ^{13}C NMR spectrum (pyridine- d_5 , 125 MHz) of RH6	112
Figure 68: ^1H NMR spectrum (acetone- $d_6/\text{methanol-}d_4$, 500 MHz) of WN5.....	114
Figure 69: ^{13}C NMR spectrum (acetone- $d_6/\text{methanol-}d_4$, 125 MHz) of WN5	114
Figure 70: HMQC spectrum of WN5	114
Figure 71: COSY spectrum of WN5	115
Figure 72: HMBC spectrum of WN5	115
Figure 73: HRESI mass spectrum of RH9	118
Figure 74: ^1H spectrum (acetone- $d_6/\text{methanol-}d_4$, 500 MHz) of RH9	118
Figure 75: ^{13}C spectrum (acetone- $d_6/\text{methanol-}d_4$, 125 MHz) of RH9	118
Figure 76: HMQC spectrum of RH9	119
Figure 77: HMBC spectrum of RH9	119
Figure 78: HRESI spectrum of RH15	123
Figure 79: ^1H NMR spectrum (CDCl_3 , 500 MHz) of RH15	123

Figure 80: ^{13}C NMR spectrum (CDCl_3 , 125 MHz) of RH15	123
Figure 81: HMBC spectrum of RH15	124
Figure 82: HRAPCI spectrum of RH15	124
Figure 83: ^1H NMR spectrum (CDCl_3 , 500 MHz) of RH16.....	125
Figure 84: ^{13}C NMR spectrum (CDCl_3 , 125 MHz) of RH16.....	125
Figure 85: HRESI mass spectrum of BLE30	126
Figure 86: ^1H NMR spectrum (500 MHz, CDCl_3) of BLE30.....	127
Figure 87: ^{13}C NMR spectrum (125 MHz, CDCl_3) of BLE30.....	127
Figure 88: ^1H NMR spectrum (pyridine- d_5 , 500 MHz) of SNC11	129
Figure 89: ^{13}C NMR spectrum (pyridine- d_5 , 125 MHz) of SNC11	129
Figure 90: HRESI mass spectrum of SNC1	132
Figure 91: ^1H NMR spectrum (CDCl_3 , 500 MHz) of SNC1.....	132
Figure 92: COSY spectrum of SNC1	132
Figure 93: ^{13}C NMR spectrum (CDCl_3 , 125 MHz) of SNC1.....	133
Figure 94: HMQC spectrum of SNC1.....	133
Figure 95: HMBC spectrum of SNC1	133
Figure 96: HRESI mass spectrum of SNC2	135
Figure 97: ^1H NMR spectrum (CDCl_3 , 500 MHz) of SNC2.....	135
Figure 98: ^{13}C NMR spectrum (CDCl_3 , 125 MHz) of SNC2.....	135
Figure 99: HMBC spectrum of SNC2.....	136
Figure 100: ^1H NMR spectrum (CDCl_3 , 500 MHz) of SNCL2	137
Figure 101: ^{13}C NMR spectrum (CDCl_3 , 125 MHz) of SNCL2	137
Figure 102: HMBC spectrum of SNCL2	138
Figure 103: HRESI mass spectrum of SNC4	139
Figure 104: ^1H NMR spectrum (pyridine- d_5 , 500 MHz) of SNC4	139
Figure 105: ^{13}C NMR spectrum (pyridine- d_5 , 125 MHz) of SNC4	140
Figure 106: HMBC spectrum of SNC4	140
Figure 107: HRESI mass spectrum of WN15	143
Figure 108: ^1H NMR spectrum (CDCl_3 , 500 MHz) of WN15.....	144
Figure 109: ^{13}C NMR spectrum (CDCl_3 , 125 MHz) of WN15.....	144
Figure 110: DEPT spectrum of WN15.....	144
Figure 111: HMQC spectrum of WN15.....	145
Figure 112: COSY spectrum of WN15	145
Figure 113: HMBC spectrum of WN15	146
Figure 114: HRESI mass spectrum of WN34	147
Figure 115: ^1H NMR spectrum (methanol- d_4 , 500 MHz) of WN34.....	148
Figure 116: ^{13}C NMR spectrum (methanol- d_4 , 125 MHz) of WN34.....	148
Figure 117: HRESI mass spectrum of WN36	149
Figure 118: ^1H NMR spectrum (methanol- d_4 , 500 MHz) of WN36.....	150
Figure 119: ^{13}C NMR spectrum (methanol- d_4 , 125 MHz) of WN36.....	150
Figure 120: HRESI mass spectrum of SNC6.....	155
Figure 121: ^1H NMR spectrum (CDCl_3 , 500 MHz) of SNC6.....	155

Figure 122: ^{13}C NMR spectrum (CDCl_3 , 125 MHz) of SNC6.....	155
Figure 123: DEPT spectrum of SNC6.....	156
Figure 124: HMQC spectrum of SNC6.....	156
Figure 125: COSY spectrum of SNC6.....	157
Figure 126: HMBC spectrum of SNC6.....	157
Figure 127: HRESI mass spectrum of SNC10	160
Figure 128: ^1H NMR spectrum (D_2O , 500 MHz) of SNC10	160
Figure 129: ^{13}C NMR spectrum (D_2O , 125 MHz) of SNC10	160
Figure 130: HMQC spectrum of SNC10.....	161
Figure 131: COSY spectrum of SNC10	161
Figure 132: HMBC spectrum of SNC10.....	162
Figure 133: HRESI mass spectrum of WN17	164
Figure 134: ^1H NMR spectrum (methanol- d_4 , 500 MHz) of WN17	164
Figure 135: ^{13}C NMR spectrum (methanol- d_4 , 125 MHz) of WN17.....	164
Figure 136: DEPT spectrum of WN17.....	165
Figure 137: HMQC spectrum of WN17.....	165
Figure 138: HMBC spectrum of WN17	165
Figure 139: HRESI mass spectrum of NLB3	169
Figure 140: ^1H NMR spectrum (methanol- d_4 , 500 MHz) of NLB3.....	169
Figure 141: ^{13}C NMR spectrum (methanol- d_4 , 125 MHz) of NLB3	169
Figure 142: DEPT spectrum of NLB1	170
Figure 143: HMQC spectrum of NLB3	170
Figure 144: HMBC spectrum of NLB3.....	170
Figure 145: COSY spectrum of NLB3.....	171
Figure 146: ESIMS spectrum of BLE8	174
Figure 147: ^1H NMR spectrum (CDCl_3 /methanol- d_4 , 500 MHz) of BLE8	174
Figure 148: ^{13}C NMR spectrum (CDCl_3 /methanol- d_4 , 125 MHz) of BLE8	174
Figure 149: DEPT spectrum of BLE8.....	175
Figure 150: HMQC spectrum of BLE8.....	175
Figure 151: HMBC spectrum of BLE8	175
Figure 152: HRESI mass spectrum of BLEF32	179
Figure 153: ^1H NMR spectrum (acetone- d_6 , 500 MHz) of BLEF32	179
Figure 154: ^{13}C NMR spectrum (acetone- d_6 , 125 MHz) of BLEF32	179
Figure 155: HMBC spectrum of BLEF32.....	180
Figure 156: HRESI mass spectrum of RHE2.....	181
Figure 157: ^1H NMR spectrum (CDCl_3 , 500 MHz) of RHE2	181
Figure 158: ^1H NMR spectrum (CDCl_3 , 500 MHz) of RH4.....	182
Figure 159: HRESI mass spectrum of BLE19	183
Figure 160: ^1H NMR spectrum (Pyridine- d_5 , 500 MHz) of BLE19	183
Figure 161: ^{13}C NMR spectrum (Pyridine- d_5 , 125 MHz) of BLE19	184
Figure 162: HRESI mass spectrum of BLE22	186
Figure 163: ^1H NMR spectrum ($\text{DMSO-}d_6$, 500 MHz) of BLE22	186

Figure 164: ¹³ C NMR spectrum (DMSO- <i>d</i> ₆ , 125 MHz) of BLE22	186
Figure 165: HMQC spectrum of BLE22	187
Figure 166: COSY spectrum of BLE22	187
Figure 167: HMBC spectrum of BLE22	188
Figure 168: ¹ H NMR spectrum (methanol- <i>d</i> ₄ , 500 MHz) of BLE21	189
Figure 169: ¹³ C NMR spectrum (methanol- <i>d</i> ₄ , 125 MHz) of BLE21	189
Figure 170: HMBC spectrum of BLE21	190
Figure 171: HRESI mass spectrum of NLB4.....	191
Figure 172: ¹ H NMR spectrum (methanol- <i>d</i> ₄ , 500 MHz) of NLB4.....	192
Figure 173: ¹³ C NMR spectrum (Methanol- <i>d</i> ₄ , 125 MHz) of NLB4	192
Figure 174: HRESI mass spectrum of WN3	194
Figure 175: ¹ H NMR spectrum (CDCl ₃ , 500 MHz) of WN3.....	194
Figure 176: ¹³ C NMR spectrum (CDCl ₃ , 125 MHz) of WN3.....	195
Figure 177: HMQC spectrum of WN3.....	195
Figure 178: HMBC spectrum of WN3	195
Figure 179: COSY spectrum of WN3	196
Figure 180: ¹ H NMR spectrum (CDCl ₃ , 500 MHz) of BLE34.....	197
Figure 181: ¹³ C NMR spectrum (CDCl ₃ , 125 MHz) of BLE34.....	197
Figure 182: HMBC spectrum of BLE34	198
Figure 183: HRESI mass spectrum of RHE5	199
Figure 184: ¹ H NMR spectrum (pyridine- <i>d</i> ₅ , 500 MHz) of RHE5	199
Figure 185: HRESI mass spectrum of RH3	200
Figure 186: ¹ H NMR spectrum (CDCl ₃ , 500 MHz) of RH3	200
Figure 187: ¹ H NMR spectrum (CDCl ₃ , 500 MHz) of WN32.....	202
Figure 188: ¹³ C NMR spectrum (CDCl ₃ , 125 MHz) of WN32.....	202
Figure 189: HMQC spectrum of WN32.....	202
Figure 190: HMBC spectrum of WN32	203
Figure 191: Preformulation from the fruits of <i>N. latifolia</i>	213
Figure 192: Steps involved in oral acute toxicity assay	229

LIST OF SCHEMES

Scheme 1: Classification of lipids containing fatty acid moiety (Vance and Vance, 2008)	46
Scheme 2: Biosynthesis of ceramides from palmitoyl-coenzyme.....	48
Scheme 3: Biosynthesis of ceramides from sphingomyelin.....	49
Scheme 4: Conversion of cerebrosides to ceramides (Carter <i>et al.</i> , 1961).....	49
Scheme 5: Mass fragmentation pattern of tithioniamide (Meffo <i>et al.</i> , 2006).....	51
Scheme 6: Protocol of extraction and isolation of compounds from the leaves of <i>R. hispida</i>	59
Scheme 7: Protocol of extraction and isolation of compounds from the fruits of <i>N. latifolia</i>	60
Scheme 8: Protocol of extraction and isolation of compounds from the trunk bark of <i>B. leptobotrys</i>	61
Scheme 9: Protocol of extraction and isolation of compounds from the leaves of <i>B. leptobotrys</i> . 62	
Scheme 10: Important HMBC and COSY correlations of RHE7	65
Scheme 11: Mass fragmentation pattern of RHE7	65
Scheme 12: Methanolysis of RHE7	66
Scheme 13: Key HMBC correlation of RHE3	72
Scheme 14: HMBC correlations of WN14.....	76
Scheme 15: Key HMBC correlation of RH20.....	80
Scheme 16: Key HMBC correlations of RHE1	84
Scheme 17: Some Key HMBC and COSY correlations of BLE4.....	89
Scheme 18: Some Key HMBC and COSY correlations of BLE10.....	95
Scheme 19: Key HMBC correlations of RH11	100
Scheme 20: Key HMBC correlations of RH5	107
Scheme 21: Some key COSY and HMBC correlations of WN5	113
Scheme 22: Some key COSY and HMBC correlation of RH9	116
Scheme 23: Key HMBC correlation of RH15.....	121
Scheme 24: Some key COSY and HMBC correlations of SNC1	130
Scheme 25: Key HMBC correlations of SNC2.....	134
Scheme 26: Key HMBC correlations of SNCL2	136
Scheme 27: Some key HMBC correlations of SNC4.....	138
Scheme 28: Some key COSY and HMBC correlations of WN15	142
Scheme 29: Key HMBC correlations of SNC6.....	153
Scheme 30: Some key COSY and HMBC of SNC10	159
Scheme 31: Key HMBC correlations of WN17	163
Scheme 32: Some key COSY and HMBC correlations of NLB3	167
Scheme 33: key HMBC correlations of BLE8.....	172
Scheme 34: Some key HMBC correlations of BLEF32.....	177
Scheme 35: Some key COSY and HMBC correlations of BLE22	185
Scheme 36: Key HMBC correlation of BLE21.....	189
Scheme 37: Some key COSY and HMBC correlations of WN3	193
Scheme 38: Key HMBC correlations of BLE34	196
Scheme 39: Key HMBC correlations of WN32.....	201
Scheme 40: Antileishmanial activity and selectivity indices of crude extracts, fractions and compounds from <i>N. latifolia</i>	208

ABSTRACT

Leishmaniasis is a neglected tropical disease caused by an intracellular flagellate protozoan parasite belonging to the *Leishmania* genus. About 20 different species of *Leishmania* have been discovered to be pathogenic to humans, including *Leishmania donovani* that causes the most deadly visceral leishmaniasis. Worldwide, between 12 to 15 million of people are infected and 350 million are at risk of acquiring the disease. An estimated 1.5 to 2 million of new cases occur each year, and it causes 70,000 deaths per year. This thesis reports the antileishmanial activity and the chemical investigation of three cameroonian medicinal plants: *Baphia leptobotrys*, *Rothmannia hispida* and *Nauclea latifolia* which displayed good antileishmanial activity *in vitro* on the strain of *Leishmania donovani* 1S (MHOM/SD/62/1S) promastigotes during preliminary screening with IC₅₀ values of 63.40, 15.50 and 2.20 µg/mL, respectively and with good selectivities towards Raw 264.7 macrophage cells. The assessment of the toxic effects of the methanol extract of *N. latifolia* for acute toxicity in female rats showed a Lethal Dose 50 (LD₅₀) greater than 5000 mg/kg. Using the different separation methods (flash chromatography, liquid-liquid partition and column chromatography), the crude extracts were fractionated into fourteen fractions which were assessed for their activity against the same strain. The *n*-hexane and CH₂Cl₂ fractions of the MeOH extract of *N. latifolia* fruits were the most active with IC₅₀ values of 7.06 and 30.57 µg/mL, respectively and showed good selectivities on the same mammalian cells.

The fractions studied led to the isolation of forty-five compounds which were characterized by usual spectroscopic and spectrophotometric techniques (IR, MS, 1D and 2D NMR). One of the compounds, the rothmanniamide is a new derivative and the other *n*-heptadecyl-*trans*-cinnamate is isolated for the first time from natural source. The forty-three remaining compounds were grouped into ten classes of secondary metabolites including three phenolic derivatives (2,6-dimethoxybenzoquinone, lichexanthone, kaempferol-3-*O*- β -D-glucopyranoside), seventeen pentacyclic triterpenoids (germanicol caffeoyl ester, 3- β -*O*-(*E*)-3,5-dihydroxycinnamoyl-11-oxo-olean-12-ene, oleanolic acid, hederagenin, erythrodiol, uvaol, ursolic acid, 30-*nor*-2 α ,3 β -dihydroxyurs-12-ene, myrianthic acid, lupeol, lupenone, lupeol palmitate, betulinic acid, fridelin, friedelinol, 3-oxofriedelan-29-al, 3-oxofriedelan-25-oic acid), seven steroids (stigmasterol, β -sitosterol, stigmasta-22-en-3-ol, 7-ketostigmasterol, 7-keto- β -sitosterol, ergosterol peroxide, daucosterol), three citric acid derivatives (trimethyl citrate, dimethyl citrate, methyl citrate), one pyrrole derivative (monomethyl ester of 1H-pyrrole-2,5-dicarboxylic acid), two amino acid derivatives (*N*-benzoylphenylalaninyl-*N*-

benzoylphenylalaninate, 4-hydroxy-*N*-methylproline), four sugar derivatives (D-mannitol, methyl β -D-glucopyranoside, β -glucoside, α -glucoside), one iridoid (loganin 6-*O*- β -glucopyranoside), four fatty derivatives (glycerol palmitate, glycerol tripalmitate, docosanoic acid, triacontanol) and one benzoic acid derivative (1,4-dimethylbenzene-1,4-dicarboxylate). Germanicol caffeoyl ester, 3- β -*O*-(*E*)-3,5-dihydroxycinnamoyl-11-oxo-olean-12-ene, 3-oxofriedelan-29-al and 3-oxofriedelan-25-oic acid were isolated for the first time from Fabaceae family, 30-*nor*-2 α ,3 β -dihydroxyurs-12-ene, monomethyl ester of 1H-pyrrole-2,5-dicarboxylic acid and dimethyl citrate were isolated for the first time from the Rubiaceae family.

The isolated compounds were assessed for their antileishmanial activity against the same strain of *Leishmania donovani* strain and for their cytotoxicity towards Raw 264.7 macrophage cells. Ursolic acid (IC₅₀ = 0.88 μ g/mL), 30-*nor*-2 α ,3 β -dihydroxyurs-12-ene (IC₅₀ = 1.75 μ g/mL), ergosterol peroxide (IC₅₀ = 4.04 μ g/mL), 2,6-dimethoxybenzoquinone (IC₅₀ = 1.67 μ g/mL), germanicol caffeoyl ester (IC₅₀ = 6.03 μ g/mL), monomethyl ester of 1H-pyrrole-2,5-dicarboxylic acid (IC₅₀ = 8.11 μ g/mL) and hederagenin (IC₅₀ = 9.12 μ g/mL) were the most potent compounds compared to the reference drug amphotericin B (IC₅₀ = 0.33 μ g/mL). Except for 2,6-dimethoxybenzoquinone (SI = 0.29), all the potent compounds were selective (SI > 3.40). A trial of preformulation was performed using the methanol extract of *N. latifolia* fruits to fight against visceral leishmaniasis.

Keywords: Rubiaceae, Fabaceae, *Rothmannia hispida*, *Nauclea latifolia*, *Baphia leptobotrys*, chemophenetic significance, antileishmanial activity, cytotoxicity.

RESUME

La leishmaniose est une maladie tropicale négligée causée par un parasite protozoaire flagellé intracellulaire appartenant au genre *Leishmania*. Environ 20 espèces différentes de *Leishmania* ont été découvertes comme étant pathogènes à l'homme, y compris *Leishmania donovani* qui cause la leishmaniose viscérale, la plus mortelle. Dans le monde, entre 12 à 15 millions de personnes sont infectées et 350 millions risquent de contracter la maladie. On estime que entre 1,5 à 2 millions de nouveaux cas surviennent chaque année et causent 70 000 décès. Cette thèse rapporte l'investigation chimique et l'évaluation de l'activité antileishmaniale de trois plantes médicinales camerounaises: *Baphia leptobotrys*, *Rothmannia hispida* et *Nauclea latifolia* qui ont montré de bonnes activités antileishmaniales *in vitro* sur la souche de *Leishmania donovani* 1S (MHOM/SD/62/1S) promastigotes lors du criblage préliminaire avec des valeurs de CI_{50} de 63,40; 15,50 et 2,20 $\mu\text{g/mL}$, respectivement et avec de bonnes sélectivités sur les cellules macrophages Raw 264.7. L'évaluation des effets toxiques de l'extrait au méthanol des fruits de *N. latifolia*, largement consommés par les populations des zones tropicales pour la toxicité aiguë chez les rats femelles a montré une dose létale 50 (DL_{50}) supérieure à 5000 mg/kg.

Au moyen des différentes méthodes de séparation (chromatographie flash, partition liquide-liquide et la chromatographie sur colonne), les extraits bruts ont été fractionnés en quatorze fractions qui ont été évaluées pour leur activité contre la même souche. Les fractions à l'hexane et au CH_2Cl_2 de l'extrait au MeOH de fruits de *N. latifolia* ont été les plus actives avec des valeurs de CI_{50} de 7,06 et 30,57 $\mu\text{g/mL}$, respectivement et avec de bonnes sélectivités sur les mêmes cellules de mammifères. Les fractions étudiées ont conduit à l'isolement de quarante-cinq composés qui ont été tous caractérisés par les techniques spectroscopiques et spectrophotométriques usuelles (IR, SM, RMN 1D et 2D). L'un de ces composés, la rothmanniamide est un dérivé nouveau et l'autre *n*-heptadécyl *trans*-cinnamate est isolé pour la première fois de source naturelle. Les quarante-trois autres composés appartiennent à dix classes de métabolites secondaires incluant trois dérivés phénoliques (2,6-diméthoxyquinone, lichexanthone, kaempférol 3-*O*- β -D-glucopyranoside), dix-sept triterpénoïdes pentacycliques (cafféate de germanicol, 3- β -*O*-(*E*)-3,5-dihydroxycinnamoyl-11-oxo-olean-12-ène, acide oléanolique, hédéragénine, érythrodiol, uvaol, acide ursolique, 30-*nor*-2 α ,3 β -dihydroxyurs-12-ène, acide myrianthique, lupéol, lupénone, palmitate de lupéol, acide bétulinique, fridéline, β -friedélinol, 3-oxofriedélan-29-al, acide 3-oxofriedélan-25-oïque), sept phytostéroïdes (stigmastérol, β -sitostérol, stigmasta-22-én-3-ol, 7-

oxostigmastérol, 7-oxo- β -sitostérol, peroxyde d'ergostérol, daucostérol); trois dérivés d'acide citrique (citrate de triméthyle, citrate de diméthyle, citrate de méthyle), un dérivé de pyrrole (ester monométhyle de l'acide 1H-pyrrole-2,5-dicarboxylique), deux dérivés d'acides aminés (*N*-benzoylphenylalaninyl-*N*-benzoylphenylalaninate, 4-hydroxy-*N*-méthylproline), quatre dérivés de sucres (D-mannitol, méthyl β -D-glucopyranoside, β -glucoside, α -glucoside), un iridoïde (loganine 6-*O*- β -glucopyranoside), quatre dérivés gras (palmitate de glycérol, tripalmitate de glycérol, acide docosanoïque, triacontanol), un dérivé d'acide benzoïque (1,4-diméthylbenzène-1,4-dicarboxylate). Le cafféate de germanicol, le 3- β -*O*-(*E*)-3,5-dihydroxycinnamoyl-11-oxo-oléan-12-ène, la 3-oxofriedelan-29-al et l'acide 3-oxofriedelan-25-oïque ont été isolés pour la première fois de la famille des Fabaceae; 30-*nor*-2 α ,3 β -dihydroxyurs-12-ène, l'ester monométhyle de l'acide 1H-pyrrole-2,5-dicarboxylique et le citrate de diméthyle ont été isolés pour la première fois de la famille des Rubiaceae.

Les composés isolés ont été évalués pour leur activité antileishmaniale contre la même souche de *Leishmania donovani* et pour leur cytotoxicité envers les cellules macrophages Raw 264.7. L'acide ursolique (CI₅₀ = 0,88 μ g/mL), 30-*nor*-2 α ,3 β -dihydroxyurs-12-ène (CI₅₀ = 1,75 μ g/mL), peroxyde d'ergostérol (CI₅₀ = 4,04 μ g/mL), 2,6-diméthoxybenzoquinone (CI₅₀ = 1,67 μ g/mL), le cafféate de germanicol (CI₅₀ = 6,03 μ g/mL) ester monométhyle de l'acide 1H-pyrrole-2,5-dicarboxylique (IC₅₀ = 8.11 μ g/mL) et l'hédéragénine (CI₅₀ = 9,12 μ g/mL) ont été les plus actives comparés à l'amphotéricine B (CI₅₀ = 0,33 μ g/mL), la molécule de référence. À l'exception de la 2,6-diméthoxybenzoquinone (SI = 0,29), tous les composés très actifs ont été sélectifs (SI > 3,40). Un essai de préformulation a été réalisé avec l'extrait au méthanol des fruits de *N. latifolia* pour lutter contre la leishmaniose viscérale.

Mots clés: Rubiaceae, Fabaceae, *Rothmannia hispida*, *Nauclea latifolia*, *Baphia leptobotrys*, signification chimiothérapeutique, activité antileishmaniale, cytotoxicité.

GENERAL INTRODUCTION

Leishmaniasis is a neglected tropical disease caused by an intracellular flagellate protozoan parasite belonging to the *Leishmania* genus. About 20 different species of *Leishmania* have been discovered to be pathogenic to humans (Akhoundi *et al.*, 2016), including *Leishmania donovani* that causes the most deadly visceral leishmaniasis. Worldwide, between 12 to 15 million people are infected and 350 million are at risk of acquiring the disease. An estimated 1.5 to 2 million new cases occur each year, and it causes 70,000 deaths per year (Torres-Guerrero *et al.*, 2017). The four major clinical leishmaniasis forms occurring in humans are visceral (VL), post-kala-azar dermal leishmaniasis, cutaneous (CL) and mucocutaneous leishmaniasis which differ in immunopathology as well as in morbidity and mortality (Singh *et al.*, 2014). Leishmaniasis is endemic in developing countries of Asia, Africa, America and Mediterranean region. In Cameroon, both CL and VL are endemic in the northern part of the country, including the Mokolo (Dondji *et al.*, 1998; Ngouateu *et al.*, 2012) and Kousseri towns (Kaptue *et al.*, 1992; Dondji *et al.*, 2001; Tateng *et al.*, 2019). The current chemotherapeutic approaches used to control the disease include the first line drugs sodium stibogluconate, meglumine antimoniate and the alternative drugs amphotericin B, pentamidine and paromomycin (Singh *et al.*, 2014). However, these drugs face short comings such as emerging drug resistance, toxicity and side effects which limit their efficiency in some cases (Croft and Coombs, 2003; Ullah *et al.*, 2016). Due to the high costs involved in the development and registration of new drugs, the pharmaceutical industry has little interest in research and development of new compounds for the treatment of tropical diseases (Alvar *et al.*, 2006; Ullah *et al.*, 2016). Therefore, in the absence of a vaccine, there is an urgent need to support new research on natural products and search for new drugs showing antileishmanial activity (WHO, 2000). Indeed, plants commonly used in traditional medicine constitute a source of bioactive compounds available, which can be used either directly in therapy or as a bridgehead for the synthesis of new biologically active molecules. Extracts or bioactive substances derived from medicinal plants are possibly the valuable and satisfying source of new therapeutic entities against *leishmania* parasites (Ullah *et al.*, 2016). Plants extracts from the Rubiaceae and Fabaceae families are known to possess antileishmanial activity (Ahua *et al.*, 2007; Sattar *et al.*, 2012; Santana *et al.*, 2015; Ullah *et al.*, 2016; Bapela *et al.*, 2017). In addition, most of these plants are sources of compounds with antileishmanial potency (Singh *et al.*, 2014; Lima *et al.*, 2015).

Therefore, we undertook in the frame of this thesis, the investigation of the chemical profile and the evaluation of the antileishmanial activity of extracts, fractions and compounds from *Rothmannia hispida*, *Nauclea latifolia* (Rubiaceae) and *Baphia leptobotrys* (Fabaceae). Our interest in these three species is justified firstly by their uses in traditional medicine. *R. hispida* is reported to be used in traditional medicine for the treatment of skin infections, ulcers and fever (Udia *et al.*, 2013); *N. latifolia* is used in folk medicine in Central and West Africa for body pain, fever, jaundice, malaria, anemia, skin infections and diarrhea (Igoli *et al.*, 2011; Haudecoeur *et al.*, 2018), while the decoction of the stem bark of *B. leptobotrys* is taken orally in the Dja biosphere in Cameroon to treat jaundice (Betti and Lejoly, 2009). Secondly, these plants exhibited antileishmanial activity during preliminary screening. Thirdly, no chemical and biological study has been done on *B. leptobotrys* and few chemical and biological studies have been done on *R. hispida* and the fruits of *N. latifolia* and despite their uses in traditional medicine, very little biological works have focused on the evaluation of their antileishmanial potential.

The objective of this work was to search for potential extracts, fractions or compounds with antileishmanial activity from *R. hispida*, *N. latifolia* and *B. leptobotrys*.

Specifically, this work consisted to:

- ✚ harvest different plant parts, extract the different plant parts, fractionate the different extracts and screen extracts and fractions for antileishmanial activity;
- ✚ isolate, purify and characterize secondary metabolites;
- ✚ perform *in vitro* antileishmanial assay on the isolated compounds, cytotoxicity assay on extracts, fractions and isolated compounds and toxicity assay on the most active extract in view to formulate a phytodrug.

This thesis, which summarizes the essential of our work, has three main parts: a first part which covers the bibliographic study with a brief overview on leishmaniasis and a brief botanical description as well as the previous chemical and biological works on the studied plants, a second part devoted to results and discussion, and a third part which describes the equipment and the various techniques used as well as the work methodology.

PART I: LITERATURE REVIEW

I.1. OVERVIEW ON LEISHMANIASIS

I.1.1. Definition

Leishmaniasis is a parasitic infection of the monocyte-macrophage system, which pathogen is *Leishmania* flagellated protozoan belonging to the Trypanosomatidae family and the genus *Leishmania* (Akhoundi *et al.*, 2016). There are four main forms of the disease including visceral leishmaniasis (VL, also known as kala-azar), post-kala-azar dermal leishmaniasis, cutaneous leishmaniasis (CL) and mucocutaneous leishmaniasis. Although CL is the most common form of the disease, VL is the most serious and is almost fatal if untreated (WHO, 2020; Desjeux, 2004).

I.1.2. Epidemiology

According to the World Health Organization (WHO), leishmaniasis is one of the seven most important tropical diseases and it represents a serious world health problem that presents a broad spectrum of clinical manifestations (Torres-Guerrero *et al.*, 2017). Worldwide, between 12 and 15 million people are infected and 350 million are at risk of acquiring the disease. An estimated 1.5 to 2 million new cases occur each year, and it causes 70,000 deaths per year (Torres-Guerrero *et al.*, 2017). Leishmaniasis is endemic in Asia, Africa, America and the Mediterranean region. In 2018, out of the 200 countries that were reported to the WHO, 97 were considered endemic or have previously reported cases of leishmaniasis. 88 and 78 countries were considered endemic for CL and VL, respectively (WHO, 2020).

According to the WHO, in the Eastern Mediterranean Region (EMR), 18 out of the 22 countries were endemic to CL; in the American Regions (AMR), 21 out of the 36 countries were also endemic, while in the European Region (EUR), 25 out of the 53 countries were endemic: In the African Region (AFR) and in the South-East Asia Region (SEAR), 19 out of the 47 countries and 4 out of the 11 countries, respectively were equally endemic (WHO, 2020).

For VL, the ratios were 18 out of the 22 countries in EMR, 6 out of the 11 countries in SEAR, 27 out of the 53 countries in EUR, 12 out of the 36 countries in AMR and 14 out of 47 countries in AFR. In the Western Pacific Region (WPR) the proportions of endemic countries were lower than in the other regions, with only China out of 31 countries, being the endemic for both VL and CL (WHO, 2020).

I.1.3. The vector of leishmaniasis

The transmission of leishmaniasis occurs through the bite of female sandflies (Akhoundi *et al.*, 2016). African, European and Asian countries (Old World) are affected by

sandflies of the genus *Phlebotomus*, while American countries of (New world) are affected by *Lutzomyia* species (Reithinger *et al.*, 2007; Kevric *et al.*, 2015; Borghi *et al.*, 2017). Additionally, leishmaniasis can be classified as anthroponotic or zoonotic, depending on whether the natural reservoir is human or animal, respectively (WHO, 2017).

I.1.4. The parasite

Most forms of the disease are transmissible only to animals, but some can be transmitted to humans (zoonosis). Human infection is caused by about 20 out of the 30 species that infect mammals. Among these are grouped the complex of *Leishmania donovani* with three varieties (*L. donovani*, *L. infantum* and *L. chagasi*), the *L. mexicana* complex with three main varieties (*L. mexicana*, *L. amazonensis* and *L. venezuelensis*), *L. Tropica*, *L. major*, *L. aethiopica*. In addition to these species of the genus *Leishmania*, there is the subgenus *Viannia* with four main species (*L. (V.) braziliensis*, *L. (V.) guyanensis*, *L. (V.) panamensis* and *L. (V.) peruvian*) (Ullah *et al.*, 2016). The different species are morphologically indistinguishable, but they can be differentiated by isoenzyme analysis, DNA sequence analysis or monoclonal antibodies (Alvar *et al.*, 2012). Although these species are different, they nevertheless have the same life cycle.

I.1.5. Life cycle of the sandfly

The parasites have two life basic stages: an extracellular mobile stage (promastigote) exclusive to an invertebrate host and an intracellular non-mobile stage (amastigote) inside a host mammalian vertebrate (Borghi *et al.*, 2017). In the vertebrate host organism, *Leishmania* parasites infect phagocytic cells, including macrophages, which are believed to be the major cellular compartments for *Leishmania* in the mammalian host vertebrate (Kobets *et al.*, 2012).

Sandflies inject the larvae at the infectious stage, metacyclic promastigotes, during the blood meal (1). Metacyclic promastigotes that reach the puncture wound are phagocytosed by macrophages (2) and developed into amastigotes (3). Amastigotes multiply in infected cells and reach different tissues, depending (at least in part) on which *Leishmania* species is involved (4). These different specificities of tissue damage are the cause of the clinical manifestations which differ in the various forms of leishmaniasis. Sandflies become infected during blood meals on an infected host when they ingest macrophages carrying amastigotes (5, 6). In the sandfly intestine, the parasites differentiate into promastigotes (7), which multiply and differentiate into metacyclic promastigotes and migrate into the sandfly proboscis (8) (Reithinger *et al.*, 2007; Borghi *et al.*, 2017). Figure 1 below shows the life cycle of *leishmania* parasites (Borghi *et al.*, 2017).

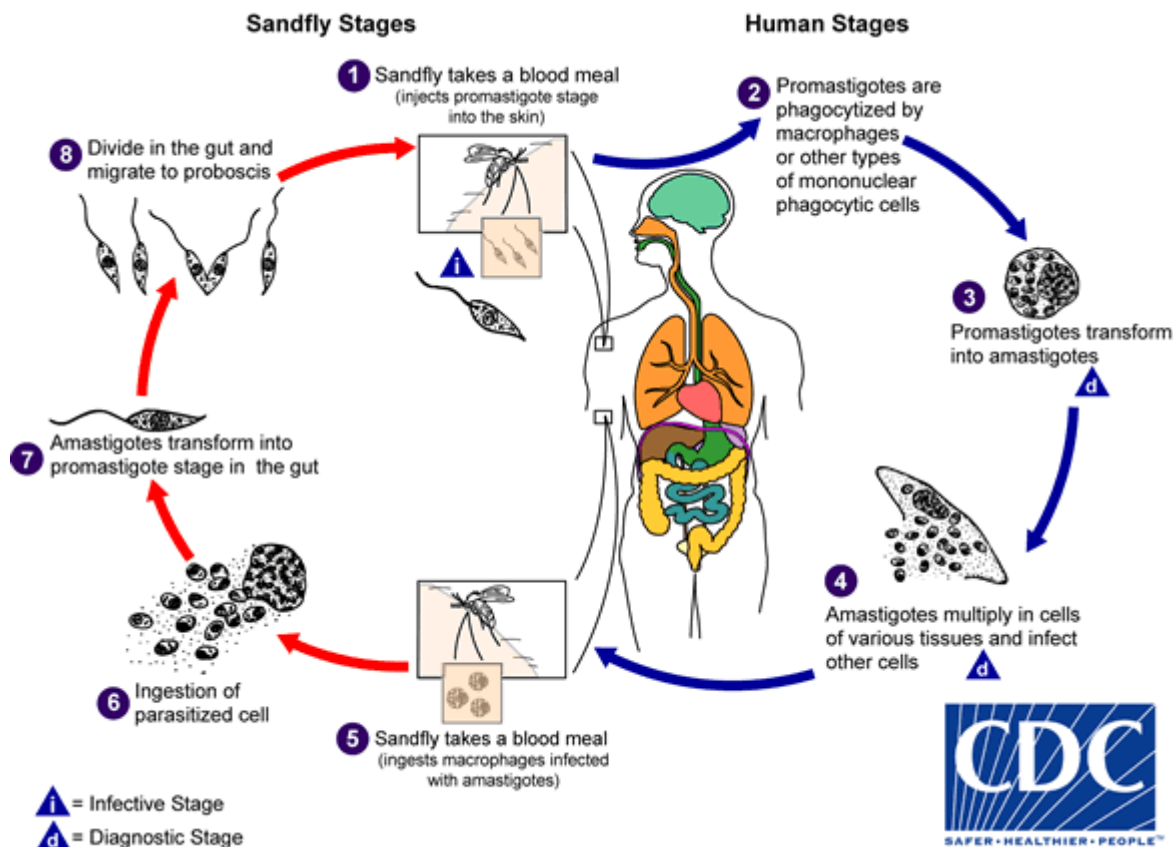


Figure 1: Life cycle of *Leishmania* parasites

I.1.6. Symptoms, diagnosis and treatment of leishmaniasis

I.1.6.1. Symptoms of leishmaniasis

Symptoms of leishmaniasis are skin sores that appear a few weeks or months after the bite of the sandfly. We can also cite other manifestations such as fever, anemia, damage of the liver and spleen (splenomegaly, which is the enlargement of the spleen) (OMS, 2017).

a- Cutaneous leishmaniasis

It is frequently self-healing in the Old World but, when the lesions are multiple and disabling with disfiguring scars, it creates a lifelong aesthetic stigma. It is a recidivist leishmaniasis, very difficult to treat, long-lasting, destructive and disfiguring (Desjeux, 2004).

b- Mucocutaneous leishmaniasis

Also known as "espundia", it causes extensive destruction of oral-nasal and pharyngeal cavities with hideous disfiguring lesions, mutilation of the face and great suffering for life. Although mostly related to *Leishmania* species of the New World such as *L. braziliensis* and *L. guyanensis*, it has been also reported in the Old World due to *L. donovani*, *L. major* and in immuno-suppressed patients due to *L. infantum* (Desjeux, 2004).

c- Visceral leishmaniasis

Also known as "kala azar" or black fever, VL is the most severe form (nearly always fatal if left untreated), characterized by: prolonged and irregular fever often associated with rigor and chills, loss of weight, splenomegaly, hepatomegaly and/or lymphadenopathies and progressive anaemia. It causes large-scale epidemics with high fatality rate. Advanced untreated visceral leishmaniasis can be fatal, particularly if other pre-existing conditions such as tuberculosis, pneumonia, and dysentery are present. After recovery, some patients develop post kala-azar dermal leishmaniasis (Desjeux, 2004; Singh *et al.*, 2006).

d-Post-kala-azar dermal leishmaniasis

It is a complication of visceral leishmaniasis, it is characterised by a macular, maculopapular and nodular rash in a patient who has recovered from VL and who is otherwise well. The rash usually starts around the mouth from where it spreads to other parts of the body depending on severity (Desjeux, 2004; Murray, 2005).

I.1.6.2. Diagnosis of leishmaniasis

Laboratory diagnosis of the disease is achieved by the demonstration of the parasites in amastigote form, in materials obtained from the patient including skin lesions in the CL case and in the spleen (as the most reliable sample), bone marrow and lymph node aspirate in the case with VL (Khan *et al.*, 2014). The diagnosis of VL is complex because other commonly occurring diseases such as malaria, typhoid, and tuberculosis share its clinical features; many of these diseases can be present along with VL (as co-infection) (Singh *et al.*, 2006).

The smears are stained with giemsa/leishman stains for the presence of amastigotes inside the macrophages. The aspirates can be inoculated into BALB/c mice which are genetically susceptible to *Leishmania*, and as a result, they will become infected over time (Khan *et al.*, 2014). For this purpose, the use of methods such as splenic puncture, aspiration of bone marrow, fine-needle biopsy of lymph nodes and culture is helpful in the case of VL (Khan *et al.*, 2014; Oryan, 2015). However, these procedures are risky and invasive.

There are several serological tests including direct agglutination test, complement fixation test, enzyme-linked immunosorbent assay (ELISA) and indirect immunofluorescent antibody test (Daneshbod *et al.*, 2011). However, they are unable to distinguish past and current infections.

Other methodologies include cytology and culture of the aspirates, histopathologic examination and immunohistochemistry (Khan *et al.*, 2014; Oryan, 2015). Molecular assays

such as polymerase chain reaction (PCR) assay could be applied for the diagnosis of the parasite in the tissues and organs of patients and also in the blood of asymptomatic healthy persons living in the endemic regions who may serve as parasite reservoirs, sometimes with 100% sensitivity (Abbasi *et al.*, 2013).

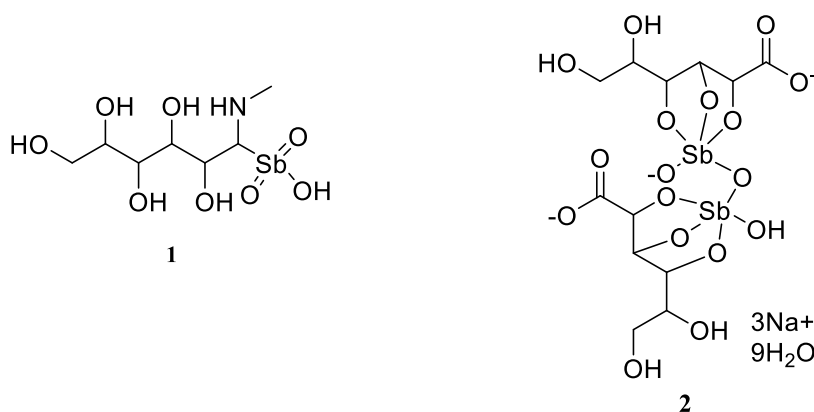
I.1.6.3. Treatment of leishmaniasis

The spectrum and efficacy of available antileishmanial drugs is limited. Drugs that were developed to treat leishmaniasis can be divided into several groups: the first-line drugs and alternative drugs (Kobets *et al.*, 2012; Singh *et al.*, 2014).

➤ First Line Drugs

Over more than five decades, pentavalent antimonials are being used in the treatment for all forms of leishmaniasis worldwide.

Pentavalent antimonials (Sb_v) have been the first-line drug for more than 70 years. The drug is provided in two formulations: meglumine antimoniate (**1**) and sodium stibogluconate (**2**) known in pharmacies as Glucantime and Pentostam, respectively (Kobets *et al.*, 2012; Singh *et al.*, 2014).



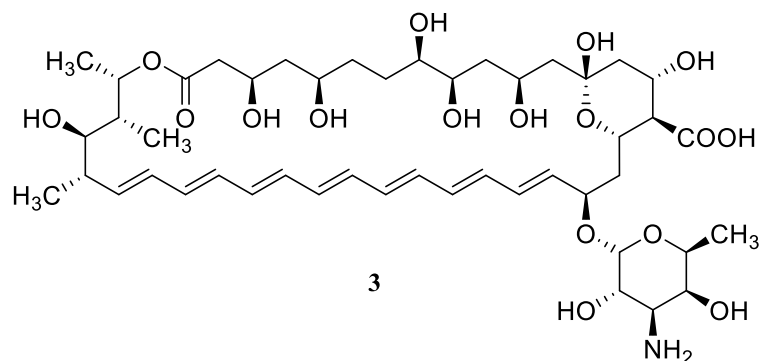
Further, various genes identified in antimonial unresponsive clinical isolates suggest the multifactorial mechanism of resistance and hence this disease seriously requires therapeutic alternatives (Singh *et al.*, 2006).

➤ Alternative Drugs

A range of alternative drugs including amphotericin B (**3**), pentamidine (**4**), miltefosine (**5**), paromomycin (**6**), azithromycin (**7**), sitamaquine (**8**), dapsone (**9**), allopurinol (**10**), rifampicin (**11**) and azoles (itraconazole **12**, ketokonazole **13** and fluconazole **14**) have been introduced (Kobets *et al.*, 2012; Singh *et al.*, 2014).

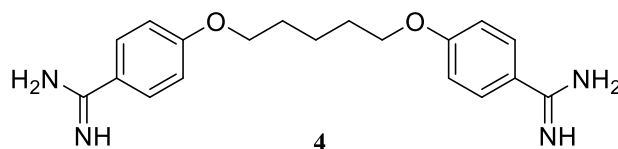
-Amphotericin B

It is the first drug of choice which is widely used in endemic regions where antimonials resistance is common. Three lipid-associated formulations of amphotericin B (**3**) are commercially available: liposomal amphotericin B (L-AMB), amphotericin B lipid complex (ABLC) and amphotericin B colloidal dispersion (ABCD) known in pharmacies as Ambisome™, Abelcet® and Amphocil™/Amphotec™, respectively (Hiemenz and Walsh., 1996; Kobets *et al.*, 2012; Singh *et al.*, 2014).



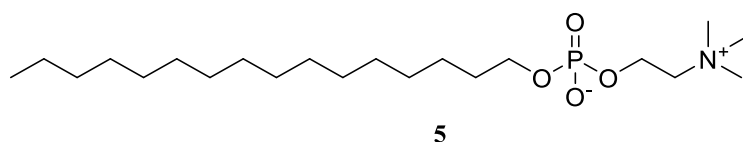
-Pentamidine

Pentamidine (**4**), as the isethionate salt (Pentacarinat®) and previously as the methylsulfonate salt (Lomidine®), has been used as alternative treatments for both VL and CL (Croft and Yardley, 2002).



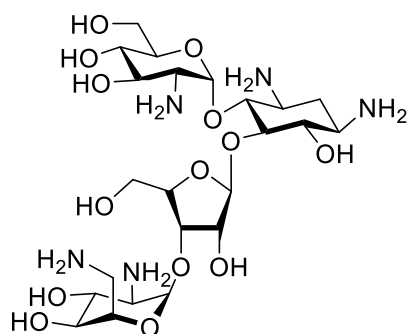
-Miltefosine

The alkylphospholipid derivative miltefosine (hexadecylphosphocholine) is the first orally effective antileishmanial agent (Kobets *et al.*, 2012).



-Paromomycin

It is an expensive but effective treatment for fighting leishmaniasis (Singh *et al.*, 2014).

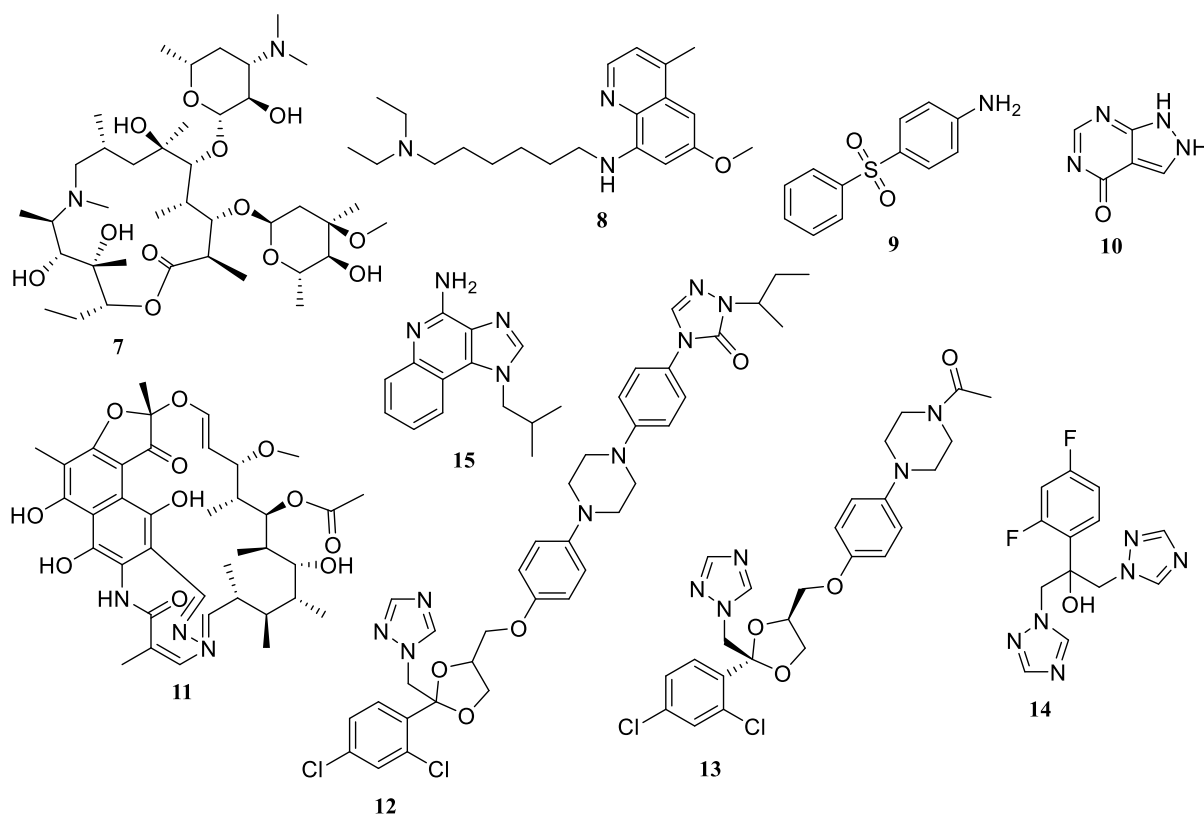


6

The table 1 below summarizes the current drugs used for the treatment of some forms of leishmaniasis (Croft *et al.*, 2006).

Table 1: Current drugs used for the treatment of VL and CL

Visceral leishmaniasis	
First line drugs	Sodium stibogluconate (Pentostam, SSG); meglumine antimoniate (Glucantime)
Alternative drugs	Amphotericin B (Fungizone) Liposomal amphotericin B (AmBisome) Pentamidine
Clinical trials	Sitamaquine (oral, Phase II) Other amphotericin B formulations
Cutaneous leishmaniasis	
First line drugs	Sodium stibogluconate (Pentostam); meglumine antimoniate (Glucantime)
Alternative drugs	Amphotericin B (Fungizone) Pentamidine Paromomycin (topical formulations with methylbenzethonium chloride or urea)
Clinical trials	Miltefosine (oral, Phase III) Paromomycin (topical formulation with gentamicin and surfactants, Phase II) Imiquimod (topical immunomodulator, Phase II) Also anti-fungal azoles–ketoconazole, fluconazole, itraconazole



The mechanism of action of some of these antileishmanial drugs are depicted in table 2 below (Singh *et al.*, 2014; Kobets *et al.*, 2012; Croft and Coombs, 2003).

Table 2: Mechanism of actions of some antileishmanial drugs

Generic name of drug (chemical type)	Mechanism of action
Pentavalent antimonials: Meglumine antimoniate (Glucantime), Sodium stibogluconate (Pentostam)	-Activated within the amastigote, but not in the promastigote, by conversion to a lethal trivalent form; -Activation mechanism not known; -Active trivalent SbIII form inhibits trypanothione reductase and exposes parasite to oxidative stress of the host.
Amphotericin B (polyene antibiotic)	Complexes with 24-substituted sterols, such as ergosterol in cell membrane, thus causing pores which alter ion balance and results in cell death.
Pentamidine (diamidine)	-Accumulated by the parasite; effects include binding to kinetoplast DNA; -Primary mode of action uncertain.
Paromomycin (aminoglycoside antibiotic) (also known as aminosidine or monomycin)	-Inhibits protein synthesis by binding to 30S subunit ribosomes, causing misreading; -Induces a drop of mitochondrial dehydrogenases activities, seemingly due to a shortage of respiratory substrates and the decrease of mitochondrial potential.
Miltefosine (hexadecylphosphocholine)	Primary effect uncertain, inhibition of ether remodelling, phosphatidylcholine biosynthesis, signal transduction and calcium homeostasis.

Table 2: Mechanism of actions of some antileishmanial drugs (continued)

Sitamaquine (8-aminoquinoline, originally WR6026)	Causes dose-dependent inhibition of respiratory chain complex II (succinate dehydrogenase) of the respiratory chain, promotes oxidative stress and apoptosis-like death of <i>Leishmania</i> parasites.
Imiquimod (imidazoquinoline)	Stimulates nitric oxide production from macrophages.
Dapsone	Inhibits choline incorporation into lecithin of the cell membrane, which leads to decreasing phospholipid synthesis.
Rifampicin	Blocks RNA synthesis by specially binding to and inhibiting the DNA-dependent RNA polymerase.
Itraconazole, ketokonazole and fluconazole	Inhibit 14- α -demethylation of lanosterol to ergosterol during cell wall synthesis and promote membrane permeability of <i>Leishmania</i> parasites.

However, the development of new antileishmanial drugs has been constantly required in the clinical therapy to minimize side effects as well as to overcome the evidences of increasing resistance to the existing drugs and also their availability problem (Sangshetti *et al.*, 2015). The toxicity and evidence of resistance of some antileishmanial drugs are presented in the table 3 below (Sangshetti *et al.*, 2015; Kobets *et al.*, 2012).

Table 3: Current antileishmanial drugs, their associated toxicities and evidence of resistance development

Current drugs	Toxicity	Resistance
Pentavalent antimonials	<ul style="list-style-type: none"> -Pancreatitis -Pancytopenia -Reversible peripheral neuropathy -Elevations in serum aminotransferases -Pain at the site of injection -Stiff joints -Gastrointestinal problems -Hepatic renal insufficiency (nephrotoxicity) -Cardiotoxicity -Accumulate inside liver and spleen 	Resistance was developed in Bihar state, India
Amphotericin B	<ul style="list-style-type: none"> -Nephrotoxicity -Fever with rigor and chills -Bone pain -Hypotension -Anorexia -Dyspnoea -Thrombophlebitis -Myocarditis -Hypokalemia 	Resistance in laboratory strains

Table 3: Current antileishmanial drugs, their associated toxicities and evidence of resistance development (continued)

Miltefosine	-Gastrointestinal disturbances -Hepatotoxicity -Renal toxicity	-Resistance in laboratory strains - <i>L. braziliensis</i> , <i>L. guyanensis</i> and <i>L. mexicana</i> are insensitive towards miltefosine
Paromomycin	-Elevated hepatic transaminases -Ototoxicity -Pain at injection-site -Nausea -Abdominal cramps -Diarrhoea	Laboratory strain of <i>L. donovani</i> promastigote developed resistance
Pentamidine	-Myalgia -Pain at the injection site -Nausea -Headache -Metallic taste -Burning sensation, numbness, hypotension -Irreversible insulin dependent diabetes mellitus and death	Unresponsiveness in India, emergence of drug resistance especially in HIV coinfections

The lack of an efficient vaccine and resistance to drugs administered for the treatment of leishmaniasis, coupled with their high cost, parenteral route of administration and toxicity, have been regarded as a great concern especially in endemic areas of developing countries. Hence, there could be no doubt that the search for novel agents having antileishmanial or leishmanicidal potency is one of the critical challenges in the field of the current drug discovery program and is of worldwide concern (Oryan, 2015). Natural products are often overlooked in antiprotozoal chemotherapy.

I.1.6.4. Plants as a source of antileishmanial agents

Plant extracts have been used traditionally in the treatment of leishmaniasis and they have given rise to interesting lead compounds against leishmaniasis (Kobets *et al.*, 2012; Croft and Yardley, 2002). However, due to lack of serious interest (leishmaniasis is a neglected disease) none of them has undergone clinical evaluation (Croft and Yardley, 2002). The table 4 below shows some antileishmanial compounds isolated from some medicinal plants.

Table 4: Some antileishmanial compounds obtained from medicinal plants

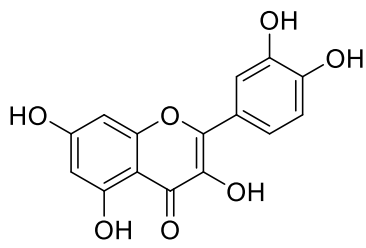
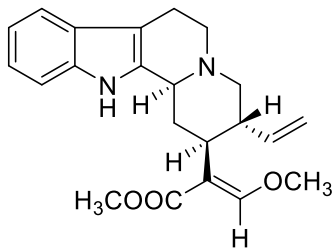
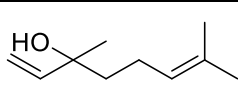
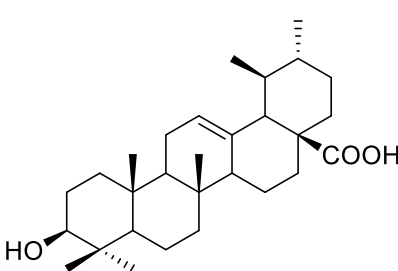
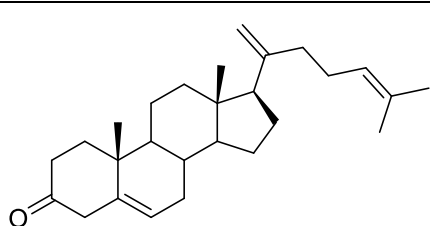
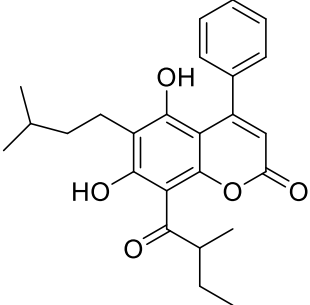
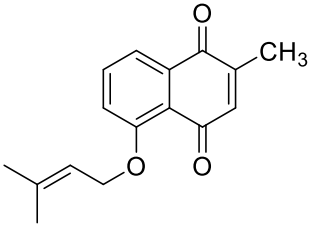
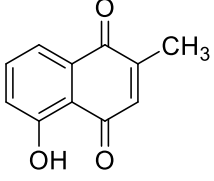
Classes	Antileishmanial compounds	Plants origins and references
Flavonoid	 <p>Quercetin (16) IC₅₀ of 4.3 μg/mL against amastigotes of <i>L. amazonensis</i></p>	<i>Cecropia pachystachya</i> (Urticaceae) da Silva <i>et al.</i> , 2012
Alkaloid	 <p>Corynantheine (17) IC₅₀ of 3 μg/mL against <i>L. major</i></p>	Bark of <i>Corynanthe pachyceras</i> (Rubiaceae) Staerk <i>et al.</i> , 2000
Monoterpenoid	 <p>Linalool (18) IC₅₀ of 28 ng/mL and 143 ng/mL against promastigotes and amastigotes of <i>L. amazonensis</i>, respectively</p>	Oil of <i>Croton cajucara</i> (Euphorbiaceae) Do Socorro <i>et al.</i> , 2003
Terpenoid	 <p>Ursolic acid (19) IC₅₀ of 1.3 μg/mL against amastigotes <i>L. major</i></p>	Aerial parts <i>Mitracarpus frigidus</i> (Rubiaceae) Fabri <i>et al.</i> , 2014
Steroid	 <p>Pentalinosterol (20) IC₅₀ of 3.3 μg/mL against amastigotes of <i>L. Mexicana</i></p>	Roots of <i>Pentalinon andrieuxii</i> (Apocynaceae) Pan <i>et al.</i> , 2012

Tableau 4: Some antileishmanial compounds obtained from some plants (continued)

<p>Coumarin</p>	 <p>5,7-Dihydroxy-8-(2-methylbutanoyl)-6-(3-methylbutyl)-4-phenyl-chroman-2-one (21) IC₅₀ of 0.9 µg/mL against promastigotes of <i>L. amazonensis</i></p>	<p>Leaves of <i>Calophyllum brasiliense</i> (Calophyllaceae) Brenzan <i>et al.</i>, 2012</p>
<p>Naphtoquinones</p>	 <p>2-Methyl-5-(3-methyl-but-2-enyloxy)-[1,4]naphthoquinone (22) EC₅₀ of 1.9 and 3.46 µg/mL against promastigotes and amastigotes of <i>L. donovani</i></p>	<p>Roots of <i>Plumbago zeylanica</i> (Plumbaginaceae) Mishra <i>et al.</i>, 2013</p>
	 <p>Plumbagin (23) IC₅₀ of 2.24 and 5.87 µg/mL against amastigotes of <i>L. donovani</i> and <i>L. amazonensis</i>, respectively.</p>	<p>Stem barks of <i>Pera benensis</i> (Peraceae) Fournet <i>et al.</i>, 1992</p>

I.2. OVERVIEW ON THE INVESTIGATED PLANTS

The tree investigated plants belong to two families including Rubiaceae and Fabaceae.

I.2.1. Overview on the Rubiaceae family

The Rubiaceae family is divided into three subfamilies (Cinchonoideae, Ixoroideae and Rubioideae) and more than 44 tribes. It is a family of flowering plants comprising approximately 13,143 species divided into 620 genera. They are found in all continents, and are mostly widespread in tropical or subtropical areas (Bremer and Eriksson, 2009). The figure 2 below shows the distribution of plants of the Rubiaceae family in the world. It is an easily recognizable family characterized by opposite leaves that are simple and entire, with

interpetiolar stipules, tubular sympetalous corollas and an inferior ovary. The flowers, which are usually bisexual, have a 4-5 lobed calyx and generally a 4-5 lobed corolla, 4 or 5 stamens and two carpels (Takhtajan, 2009). A wide variety of growth forms among which shrubs are the most common, are found in the Rubiaceae. Members of the family can also be trees, lianas or herbs (Takhtajan, 2009). The subfamily Ixoroideae contains 15 tribes such as Coffeae, Ixoreae, Condamieae, Alberteae, Gardenieae etc. The subfamily Cinchonoidae comprises 9 tribes such as Chiococceae, Cinchoneae, Guettardeae, Hamelieae, Naucleaeae etc. (Bremer, 2009).

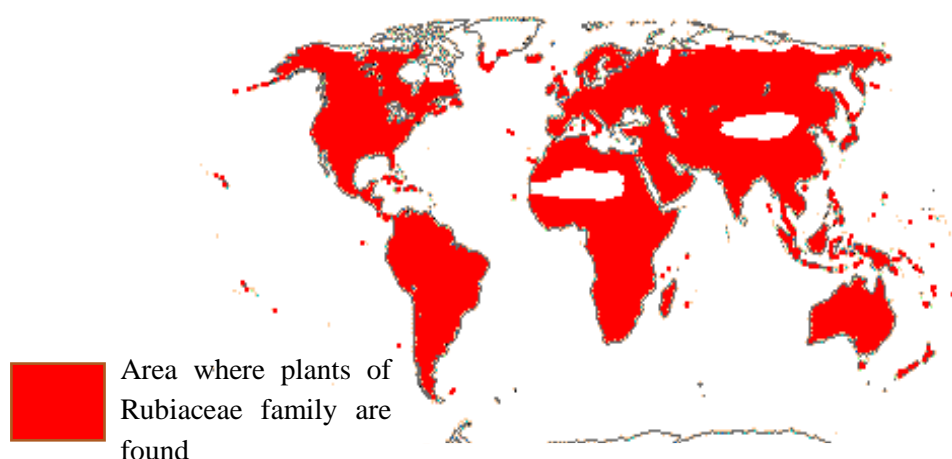


Figure 2: Geographical distribution of plants of the Rubiaceae family (Beniddir, 2012)

I.2.1.1. Overview on the genus *Rothmannia* Thunb.

The genus *Rothmannia* (Ixoroideae) belongs to Gardenieae tribe and comprises about 40 species widely distributed in tropical Africa and Asia (Ling *et al.*, 2001). They are usually small trees or shrubs. Leaves are arranged in three, the flowers are funnel-shaped and scented, while the fruits are either cylindrical or club-like in shape (Vivien and Faure, 2011). Some of the species found in Cameroon include *R. lateriflora*, *R. longiflora*, *R. octomera*, *R. talbotii*, *R. whitfieldi* and *R. hispida* (Sonke and Simo, 1996).

I.2.1.1.1. Overview on *Rothmannia hispida* (K. Schum) Fagerl

Rothmannia hispida (K. Schum) Fagerl (Syn. *Randia hispida* K.Schum) is a small tree or shrub of about 10 m tall with hairy twigs. Leaves are silky and hairy in appearance with petiole of 0.4-1 cm long; they have a blade elliptical, with acuminate apex, 3-9 × 10-19.5 cm, and obtuse base. Leaves have 5-8 pairs of secondary nerves with absent domaties and deltoid stipules. They have 0.3-1 cm long and 0.4-0.7 cm basal width.

Flowers are solitary, sessile with calyx pubescent outside, and a long tube 2.5-6 cm, with 5 linear lobes 2.5-5 cm long. They have hairy corolla, whitish, corolline tube 13.5-20 cm long, bearing 5 lobes 1-4 cm long, overlapping to the right in the flower bud. They are also characterized by medifixed anthers, ovary lobe, grooved style, and stigmas formed of two joined blades.

Fruits are 6-11 cm long, ellipsoid, 2-3×5.5-6.5 cm and have persistent calycinal tube with thick pericarp and numerous seeds (Lewis and Elvis-Lewis, 1977; Sonke and Simo; 1996, Antai *et al.*, 2010).

Rothmannia hispida is widely distributed in Cameroon, Nigeria, Congo, Ivory Coast and Gabon (Sonke and Simo, 1996). Figure 3 below shows the leaves and fruits of *R. hispida*.



Figure 3: Picture of *Rothmannia hispida* (K. Schum) Fagerl branches bearing leaves and fruits

I.2.1.2. Overview on the genus *Nauclea* L.

The genus *Nauclea* (Cinchonoidae) comprises 35 species which are characterized by trees or shrubs, rarely subsarmentous with terminal buds (Plassart, 2015). The stipules are of two possible forms useful for the determination of the species: short and deltoids, broad and oval, and more or less quickly deciduous. The leaves are shiny, green, opposite and pinnate, petiolate, medium or large, generally very developed on young feet or on shoots. The corolla of the flowers is long, the inflorescences are solitary and terminal, the ovaries are completely welded together; the stamens have a very short net and a bilocular anther. The style is long and narrow, going far beyond the corolla. The fruit is massively spheroid syncarpic, sometimes spongy, honeycombed or reticulate, more or less fleshy. The seeds are wingless and sometimes marginal (Plassart, 2015).

Plants of this genus are distributed in tropical areas of Africa and Asia. In Africa, there are seven species of the genus *Nauclea* which are *N. pobeguinii*, *N. diderrichii*, *N. gilleti*, *N.*

vanderguchtii, *N. xanthoxylon*, *N. nyasica* and *N. latifolia* (Löfstrand *et al.*, 2014) which will be the subject of our work.

I.2.1.2.1. Overview on *Nauclea latifolia* (J.E. Smith)

Also called *Sarcocephalus latifolius* (J.E. Smith), from the greek "sarks" which means flesh and "kephalé" which means head, with allusion to the fruit in the shape of a fleshy spherical mass (Plassart, 2015). Other synonyms attributed to it are *N. esculenta*, *S. sassandrae*, *S. russianggeri* and *S. esculentus*

Nauclea latifolia is a straggling shrub or tree up to 10 m high, sometimes reaching 33 m high (El-Amin, 1990; Gidado *et al.*, 2005). The fruits are globosely or ovoid, 5-7.5 cm across, red-brown pitted with pentagonal scars of the flowers, weighing 40-80 g (James and Ugbede, 2011). The edible part is fibrous, high in water, crimson in colour, acidic in taste. The seeds are numerous embedded in sweet edible pulps (Fadipe, 2014a). Seeds colour is bright yellow and the weight is light. The peels are thin and its colour is crimson, easy to separate like blanched potato (Abdel-Rahman *et al.*, 2014). The flowers are white and the flower's head about 5 cm across or more, fragrant, on stout peduncles in about 2 cm long (Nworgu *et al.*, 2008). Flowering occurs from March to August and fruiting from May to March. The bole is crooked, the bark is grey or brown, deeply fissured. It has branchlest stout, glabrous or minutely puberulous. Leaves are broadly oblong-elleptic to obviate or nearly oblong-orbicular (Nworgu *et al.*, 2008), 10-20 × 7-12 cm, glabrous with red petioles, 1.5-2 cm long; stipules are broad, ovate and persistent (Badiaga, 2016). Figure 4 below shows the whole plant and fruits of *N. latifolia*.



Figure 4: Pictures of *N. latifolia*

N. latifolia is spread in tropical regions of Africa and Asia (Gidado *et al.*, 2005), mainly in savanna forest regions of Cameroon, Nigeria, Niger, Congo, Tanzania, Malawi,

Tchad, Sudan and Ethiopia (Michel, 2004). Figure 5 and Table 5 below present the geographical distribution of *N. latifolia* in Africa and the localities of Cameroon where *N. latifolia* has already been harvested, respectively (National Herbarium of Cameroon).



Figure 5: Distribution of *N. latifolia* in Africa (Plassart, 2015)

Table 5: Place of harvest of *N. latifolia* in Cameroon

Regions	Localities
Far North	Mokolo, Mogode and Mayo Djakmé (Béré)
North	Garoua
Adamaoua	Banyo, Yoko and Tibati-Makouba
Centre	Bafia, Eséka, Makénéne
North West	Kumbo
South West	Botanical Garden of Limbé
East	Bertoua (Batouri), Bétaré Oya

I.2.2. Overview on the Fabaceae family

Also called Leguminosae, Fabaceae is the third largest family of flowering plants after Orchidaceae (orchids) and Asteraceae (sun flower) with approximately 730 genus and over 19400 species worldwide (Zahra and Soroush, 2010). This family consists of a large number of domesticated species (trees, shrubs, vines and herbs) harvested as crops for human consumption, used as a source of oil, fuel, fibre and fertilizers. Fabaceae is commonly found in the tropical rain forests and dry forest of America and Africa. The family is divided into six different subfamilies, namely Caesalpinioideae, Cercidoideae, Detarioideae, Dialioideae, Duparquetioideae, and Faboideae/Papilionoideae (LPWG, 2017). Species of the Papilionoideae (Fabiodeae) subfamily are characterized by the presence of nodules on their roots which contain nitrogen fixing bacteria (Gilbert and Boutique, 1952). They are

characterized by simple to compound leaves (pinnate), regular or irregular flowers that are bisexual.

Amongst the 730 genera that exist in the plant family Fabaceae, the genus *Baphia* belonging to the subfamily Papilionioideae and tribe Baphieae (Soladoye, 1985; LPWG, 2017) is of interest in this study.

I.2.2.1. Overview on the genus *Baphia* (Lodd.)

The name *Baphia* originates from a greek word "báptō" which means to dip or to dye. Plants in this genus are legumes that bear simple leaves. According to Kapingu and Magadula (2008), the genus *Baphia* is usually erect or scrambling shrubs, lianas and small to large trees of up to 45 m with about 78 species, found in the tropical and subtropical regions of the world (Soladoye, 1985; Cheek *et al.*, 2014).

About 45 species of *Baphia* are distributed in tropical regions of Africa (Soladoye, 1985). The *Baphia* species are easily recognized by their simple (unifoliate) leaves and free stamens (Soladoye, 1985; Cheek *et al.*, 2014). Some common species of the genus *Baphia* are *B. nitida*, *B. pubescens*, *B. massaiensis*, *B. kirkii*, *B. dubia*, *B. barachybotrys*, *B. abyssinica*, and *B. leptobotrys*, the species of focus in this study.

I.2.2.1.1. Overview on *Baphia leptobotrys* (Harms)

Also called "Sawe" by the Baka populations of Cameroon, *Baphia leptobotrys* (Harms) is a shrub sometimes scrambled, lianescent or arborescent with glabrous branches (Betti and Lejoly, 2009).

Leaves are largely oval or oblong- elliptical, rounded or rounded at the base, broadly acuminate at the top (Figure 6). They have a densely yellowish ovary and bears brown seeds (Soladoye, 1985).



Figure 6: Branches of *Baphia leptobotrys* bearing leaves

It is mostly found in riverine areas in secondary forest, abandoned farmland and near sea level. The species is distributed in South East Nigeria and coastal areas of Cameroon (Soladoye, 1985). It is one of the many species found in the Takamanda forest reserve in the South-West region of Cameroon (Sunderland *et al.*, 2003). Its geographical distribution is shown on the map in Figure 7 below (Soladoye, 1985).



Figure 7: Map showing the distribution of *B. leptobotrys* in the coastal tropical Africa

Baphia leptobotrys is a fairly widespread species in Cameroon. According to information recorded at the National Herbarium of Cameroon, it was collected in various regions of the country as shown in Table 6 below.

Table 6: Place of harvest of *B. leptobotrys* in Cameroon

Regions	Localities
Centre	Eséka, Oveng, Kribi-Nyabessan
Littoral	Masseng, Edea, Masok
Sud	Kribi, Meuban, Djoum

I.3. USES OF THE INVESTIGATED PLANTS

I.3.1. Uses of plants of the genus *Rothmannia*

Several species of the genus *Rothmannia* have been reported to possess medicinal properties for the treatment of many human ailments in different areas. Table 7 gives a summary of plants of the genus *Rothmannia* and their uses in traditional medicines.

Table 7: Some plants of the genus *Rothmannia* and their uses in traditional medicine

Species	Uses	References
<i>R. engleriana</i> (roots)	Infusion from the roots is used against stomach ache and also against snake bites.	Jansen, 2005
<i>R. hispida</i> (leaves, roots, fruits and seeds)	-When the juice from the fruits and seeds is mixed with palm oil and applied on the skin, it treats skin disease; -In Nigeria the roots are used to treat intestinal pain. -In Democratic Republic of Congo, infusion of the roots is given to treat throat abscesses, toothache and leprosy. The seeds are used to treat ulcers; -In Sierra Leone the leaves are used to treat skin diseases.	
<i>R. lujae</i> (barks)	The decoction is used to fight against abdominal disorder.	
<i>R. macrophylla</i> (roots)	Used as contraceptives.	Sui-Kiong, 2001

I.3.2. Uses of plants of the genus *Nauclea*

Plants of the genus *Nauclea* have been reported to be used for various medicinal purposes. The Table 8 below shows some of the uses of the plants of the genus *Nauclea* in traditional medicine.

Table 8: Some plants of the genus *Nauclea* and their uses in traditional medicine

Species	Uses
<i>N. latifolia</i> (bark, leaves, roots, fruits and stem)	-In Nigeria, it is used in skin diseases treatment (Haudecoeur <i>et al.</i> , 2018). It is used as a chewing stick and as a remedy against stomach ache and tuberculosis. The infusion of the roots or leaves is used to treat viral diseases such as jaundice, yellow fever or measles (Gbile and Adesina, 1987); -In West and South Africa, infusions and decoctions of the stem, bark and leaves are used for the treatment of malaria, stomach aches, fever, diarrhea, nematode infections, yellow fever, rheumatism, hepatitis, and diabetes (Maitera <i>et al.</i> , 2011; Haudecoeur <i>et al.</i> , 2018); -In Uganda, root maceration is used to treat hernia (Tchacondo <i>et al.</i> , 2011). -In Cameroon, a root decoction is used in the treatment of fever, convulsions, headaches, inflammatory pain and neuropathic pain (Taiwe <i>et al.</i> , 2014);
<i>N. officinalis</i> (root, stem and branch)	-In China, root, stem and branch are cut into pieces, dried and used for treatment of pink eye, fever, acute jaundice and stomachache in (Sun <i>et al.</i> , 2008).
<i>N. subdita</i> (leaves)	-Leaves are used for the treatment of stomach ache, diabetes, skin problems and blood pressure (Fatin <i>et al.</i> , 2012).
<i>N. orientalis</i> (leaves, bark and stem)	-Leaves and bark are used against abdominal pains, animal bites, wounds, tumors and toothaches. A decoction of the stem and bark is used in Vietnam for the treatment of fever and ascites (He <i>et al.</i> , 2005).
<i>N. diderrichii</i> (bark, fruits and roots)	-In Cameroon, the bark decoction is used for the treatment of sexual asthenia (Townsend, 2014). The bark, root and fruits are used in skin diseases management (Haudecoeur <i>et al.</i> , 2018).
<i>N. pobeguini</i> (stem bark, root and leaves)	-In Nigeria and the Democratic Republic of Congo, the decoction of the stem bark of the roots or leaves is used against abdominal pain, back pain (Mesia <i>et al.</i> , 2010).
<i>N. vanderguchtii</i> (leaves and bark)	-In Cameroon, maceration of the leaves and bark is used treat dermatosis and wounds (Jiofack <i>et al.</i> , 2010; Haudecoeur <i>et al.</i> , 2018).

I.3.3. Uses of plants of the genus *Baphia*

Several species of the genus *Baphia* have been reported to possess medicinal properties for the treatment of many human ailments in different areas. These uses are summarized in table 9 below.

Table 9: Traditional uses of some species of the genus *Baphia*

Species	Uses
<i>B. leptobotrys</i> (stem bark)	-Used in the Dja biosphere in Cameroon to treat jaundice. Taken by oral means as a decoction of the stem bark. It is also used to treat wounds (Betti and Lejoly, 2009).
<i>B. massaiensis</i> (bark, leaves, root)	-Used to treat impotence, infertility, wounds, sores, body measles, dizziness, and haemorrhages during pregnancy and birth as well as in baby tonics (Keroletswe <i>et al.</i> , 2018).
<i>B. nitida</i> (twigs, leaves)	-Leaves are used to treat sterility in women. Its twigs are used locally in Western Nigeria as chewing sticks for treatment of tooth ache (Omobuwajo <i>et al.</i> , 1992); -Leaves are used for the treatment of inflamed and infected umbilical cords (Onwukaeme, 1995); -Leaves are used in traditional medicine for gastrointestinal complains (Chaabi <i>et al.</i> , 2010; Onyekwere <i>et al.</i> , 2014); -It is applied against ringworm, stiff joints, sprains and rheumatic pains (Onyekwere <i>et al.</i> , 2014).
<i>B. bancoensis</i> (roots)	In Ivory coast the juice of the plant is used as remedy to suppurating eyes (Yao-Kouassi <i>et al.</i> , 2008).
<i>B. pubescens</i> (bark, leaves, root)	-According to Ogunwa <i>et al.</i> (2017), the bark and leaves are used to heal sores and wounds in Nigeria, Ghana and Ivory Coast for instance, due to their haemostatic and anti-inflammatory efficacy; -The dried root is used, mixed with oil and water, to treat ringworm by Ghanaians and Nigerians; -In the Benin Republic, the decoction of the leaves is often used to manage diabetes and jaundice, while both leaves and bark extracts are used to treat cardiac pain, asthma, headache, constipation, diarrhea and venereal diseases.

I.4. PREVIOUS CHEMICAL AND BIOLOGICAL INVESTIGATIONS ON THE SELECTED PLANTS

I.4.1. Previous chemical investigations on the studied plants

I.4.1.1. Previous chemical investigations on plants of the Gardenieae tribe

Although very little studies have been carried out on plants of the genus *Rothmannia*, it belongs to the subfamily Ixoroideae and the Gardenieae tribe. The previous chemical work carried out on the species of the Ixoroideae subfamily and particularly of the tribe has led to the isolation and characterization of several classes of secondary metabolites, the most important of which are iridoids, flavonoids, terpenoids, coumarins, alkaloids and other phenolic compounds.

I.4.1.1.1. Iridoids

Iridoids are monoterpenoids consisting of a cyclopentane fused to a 6-atom ring, one of which is oxygen. They are present in many plants of the genus *Rothmannia*. Table 10 below presents some iridoids isolated from plants of the Gardenieae tribe.

Table 10: Some iridoids isolated from plants of the Gardenieae tribe

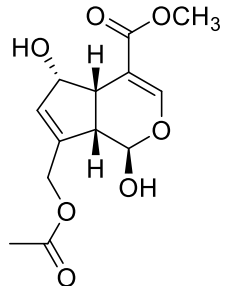
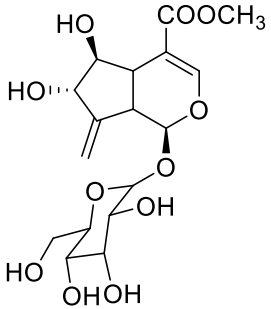
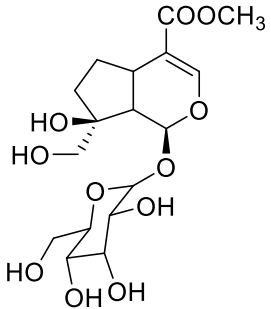
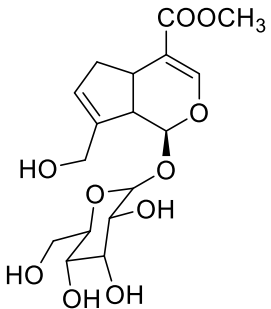
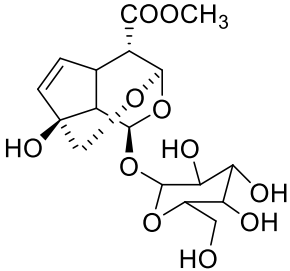
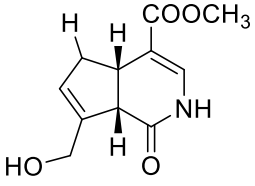
Structures	Species and sources	References
 <p>6β-Hydroxy-10-O-acetylgenipine (24)</p>	<p><i>R. wittii</i> (bark and fruit)</p>	<p>Chaipukdee <i>et al.</i>, 2016</p>
 <p>6β-Hydroxy-7-epigardoside methyl ester (25)</p>	<p><i>Alibertia edulis</i> (stem)</p>	<p>da silva <i>et al.</i>, 2008</p>
 <p>Gardenoside (26)</p>	<p><i>Randia spinosa</i> (stem)</p>	<p>Hamerski <i>et al.</i>, 2005</p>
 <p>Geniposidic acid (27)</p>	<p><i>Genipa americana</i> (fruit)</p>	<p>Ono <i>et al.</i>, 2005</p>

Table 10: Some iridoids isolated from plants of the Gardenieae tribe (continued)

 <p>Macrophylloside (28)</p>	<p><i>R. macrophylla</i> (leaves)</p>	<p>Ling <i>et al.</i>, 2001</p>
 <p>Gardenamide A (29)</p>	<p><i>R. urcelliformis</i> (fruit)</p>	<p>Bringmann <i>et al.</i>, 2001</p>

I.4.1.1.2. Flavonoids

Flavonoids are secondary metabolites responsible for the varied color of the flowers and fruits of many plants. From a structural point of view, they have a basic skeleton with fifteen carbon atoms (C₁₅) and made of two aromatic rings linked by a chain with three carbon atoms corresponding to diphenylpropane (**30**) (Dacosta, 2003). Table 11 below shows some examples of flavonoids isolated from plants of the Gardenieae tribe.

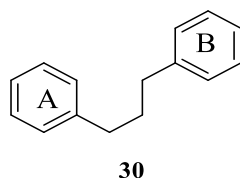


Table 11: Some flavonoids isolated from plants of the Gardenieae tribe

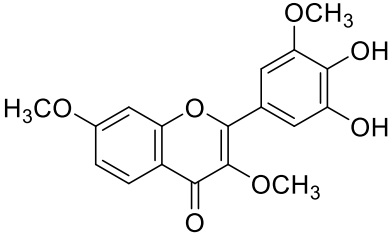
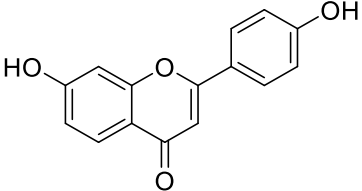
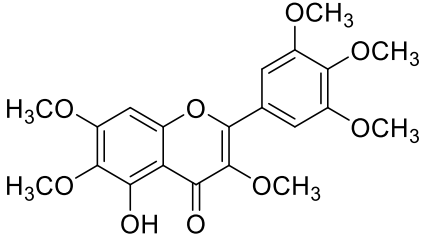
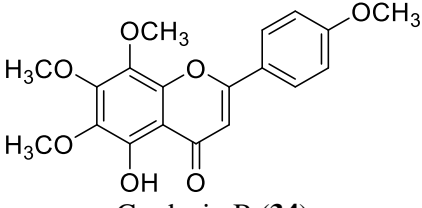
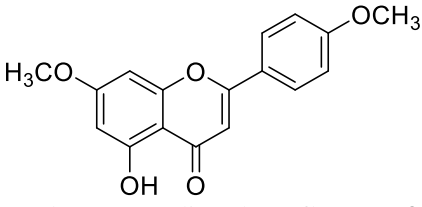
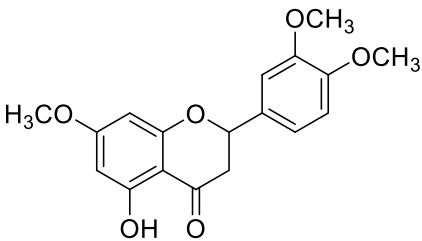
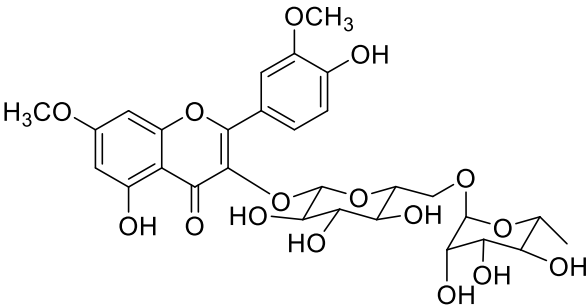
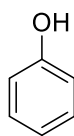
Structures	Species and sources	References
 <p>4',5'-Dihydroxy-3,3',7-trimethoxyflavone (31)</p>	<p><i>Duroia hirsuta</i> (root)</p>	<p>Aquino <i>et al.</i>, 1999</p>
 <p>4',7-Dihydroxyflavone (32)</p>	<p><i>Gardenia sootepensis</i> (flower)</p>	<p>Liang <i>et al.</i>, 1991</p>

Table 11: Some flavonoids isolated from plants of the Gardenieae tribe (continued)

 <p>5-Hydroxy-3,6,7,3',4',5'-hexamethoxyflavone (33)</p>	<p><i>Gardenia fosbergii</i> (buds)</p>	<p>Gunatilaka <i>et al.</i>, 1979</p>
 <p>Gardenin B (34)</p>	<p><i>Gardenia gummifera</i> (gum)</p>	<p>Krishnamurti <i>et al.</i>, 1972</p>
 <p>5-Hydroxy-7,4'-dimethoxyflavone (35)</p>	<p><i>Gardenia erubescens</i> (stem)</p>	<p>Adelakun and Okogun, 1996</p>
 <p>5-Hydroxy-7,3',4'-trimethoxyflavanone (36)</p>		
 <p>Ramnazin-3-O-rutinoside (37)</p>	<p><i>Tocoyena brasiliensis</i> (leaves)</p>	<p>Hamerski <i>et al.</i>, 2005</p>

I.4.1.1.3. Other phenolic compounds

Phenolic compounds are aromatic chemical compounds carrying a hydroxy group (-OH), corresponding to the basic skeleton (38). Approximately, 8000 natural compounds belong to this family; they have in common a benzene nucleus carrying at least one hydroxy group. Depending on the number of phenolic units present, they are classified into simple phenolic compounds and polyphenols (Muanda, 2010) (Table 12).



38

Table 12: Some phenolic compounds isolated from plants of the Gardenieae tribe

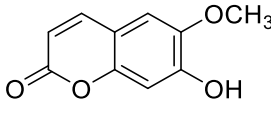
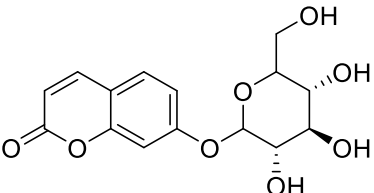
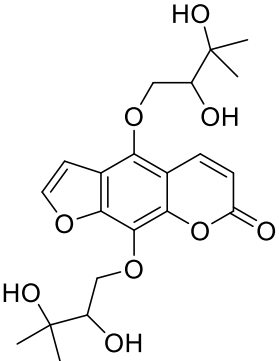
Structures	Species and sources	References
<p>1-(3-Hydroxy-4-methoxy-5-methylphenyl)-ethanone (39)</p>	<i>Lamprothamnus zanguebaricus</i> (stem bark)	Khan <i>et al.</i> , 2003
<p>1-(3-Hydroxy-4-methoxyphenyl)-ethanone (40)</p>		
<p>2-(Hydroxy)-phenyl-<i>O</i>-β-D-glucopyranoside (41)</p>	<i>Oxyanthus speciosus</i> (leaves)	Nahrstedt <i>et al.</i> , 1995
<p>Protocatechuic acid (42)</p>	<i>Alibertia macrophylla</i> (stem)	da silva <i>et al.</i> , 2007
<p><i>p</i>-Hydroxybenzaldehyde (43)</p>	<i>Rothmannia merrilli</i> (leaves)	Tan <i>et al.</i> , 2014

I.4.1.1.4. Coumarins

The word coumarin derives from "Coumarou", a South American vernacular name taken from *Dypteryx odorata* Willd., also called "Tonka" bean from which the first coumarin was isolated in 1820. Coumarins are 2H-1-benzopyran-2-one which are lactones of *O*-hydroxy-2-cinnamic acids (Borges *et al.*, 2005).

Table 13 below depicts the structures of some coumarins isolated from plants of the Gardenieae tribe.

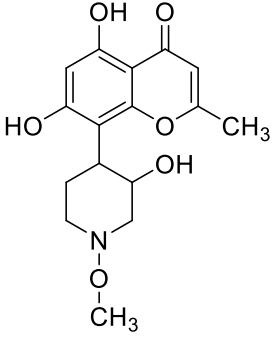
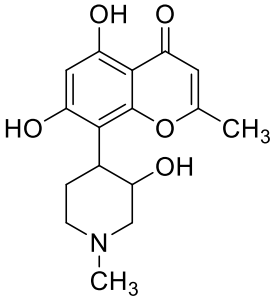
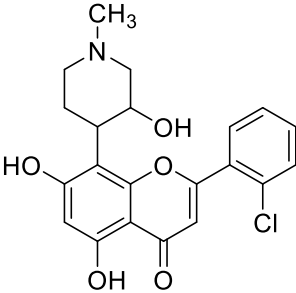
Table 13: Some coumarins isolated from plants of the Gardenieae tribe

Structures	Species and sources	References
 Scopoletin (44)	<i>Alibertia myrciifolia</i> (stem)	Luciano <i>et al.</i> , 2004
 Skimmine (45)	<i>Gardenia jasminoides</i> (fruit)	Moon <i>et al.</i> , 2002
 5,8-Di-(2,3-dihydroxy-3-methylbutyloxy)psoralen (46)		

I.4.1.1.5. Alkaloids

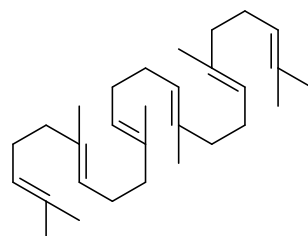
Alkaloids are organic molecules originating mainly from plants and containing at least one nitrogen atom in their chemical structure with a variable degree of basicity and marked pharmacological properties (Bruneton, 1999). They are mainly extracted from flowering plants, but they are also found in some animals such as ants, frogs and ladybugs (Mauro, 2006). The following Table 14 shows the structures of some alkaloids isolated from plants of the Gardenieae tribe.

Table 14: Some alkaloids isolated from plants of the Gardenieae tribe

Structures	Species and source	Reference
 <p>Rohitukine <i>N</i>-oxide (47)</p>	<i>Schumanniophyton problematicum</i> (bark and stem)	Kumara <i>et al.</i> , 2014
 <p>Rohitukine (48)</p>		
 <p>Flavopiridol (49)</p>		

I.4.1.1.6. Triterpenoids

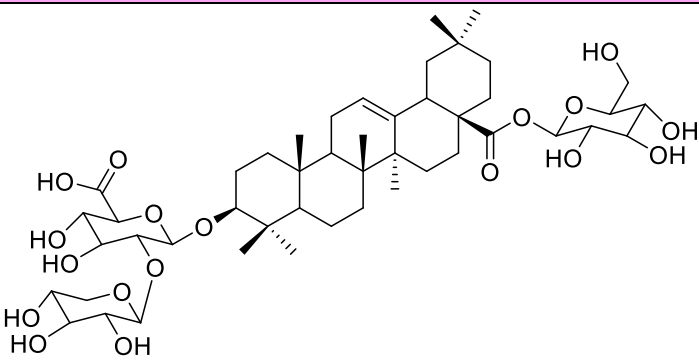
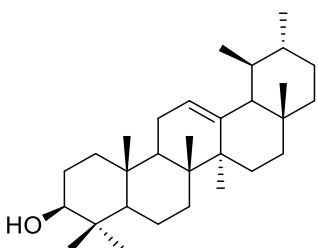
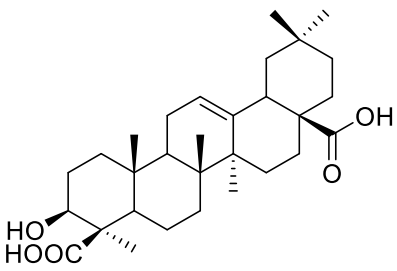
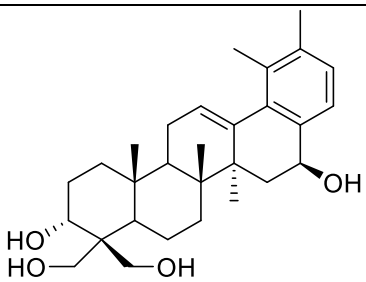
Triterpenoids form a group of natural products containing in their skeleton thirty carbon atoms and derived from squalene (**50**) by a series of cyclization and modifications. They are mostly pentacyclic compounds (Bruneton, 1999).



Squalene (**50**)

Table 15 presents the structures of some triterpenoids isolated from plants of the Gardenieae tribe.

Table 15: Structure of some triterpenoids isolated from plants of the Gardenieae tribe

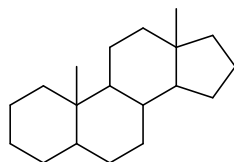
Structures	Species and sources	References
 <p>Pseudoginsenoside-RT1 (51)</p>	<i>Randia siamensis</i> (fruit)	Jansakul <i>et al.</i> , 1999
 <p>α-Amyrin (52)</p>	<i>G. turgida</i> (root)	Joshi <i>et al.</i> , 1979
 <p>Gypsogenic acid (53)</p>		Reddy <i>et al.</i> , 1973
 <p>3α,16β,23,24-tetrahydroxy-28-nor-ursane-12,17,19,21-tetraene (54)</p>	<i>G. jasminoides</i> (fruit)	Fang-min <i>et al.</i> , 2015

I.4.1.2. Previous chemical investigations on plants of the genus *Nauclea*

Previous phytochemical work on plants of the genus *Nauclea* revealed the presence of several classes of secondary metabolites belonging to several classes of compounds such as steroids, triterpenoids, phenolic compounds and alkaloids (Haudecoeur *et al.*, 2018; Bankeu *et al.*, 2018).

1.4.1.2.1. Steroids

Steroids are very common secondary metabolites in plants derived from triterpenoids through the loss of two or three methyl groups. They are characterized by a perhydrocyclopentanophenanthrenic or sterane nucleus (**55**) comprising methyls in positions 10 and 13 (Moss, 1989; Bruneton, 1999).



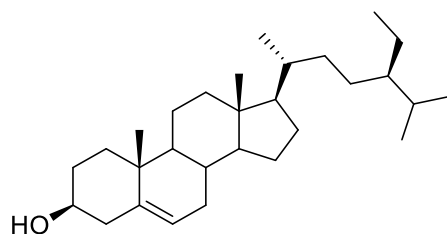
55

The chemical composition of African *Nauclea* species began to be unraveled in 1953 with the discovery of the steroid β -sitosterol (**56**) and its palmitate ester (**57**) as the first identified metabolite of *N. diderrichii* (King and Jurd, 1953).



56

57



R = glc: β -sitosterol glucoside (**58**)

R = stearylglc: β -sitosterol 6'-stearylglucoside (**59**)

1.4.1.2.2. Triterpenoids

Some triterpenoids isolated from plants of the genus *Nauclea* are grouped in Table 16.

Table 16: Some triterpenoids isolated from plants of the genus *Nauclea*

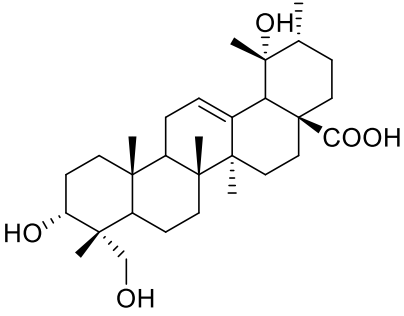
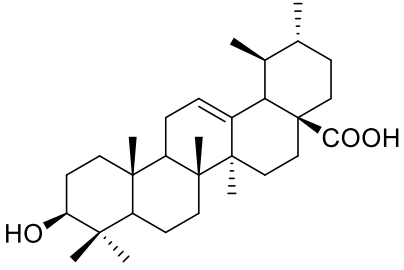
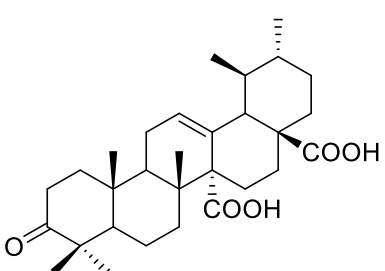
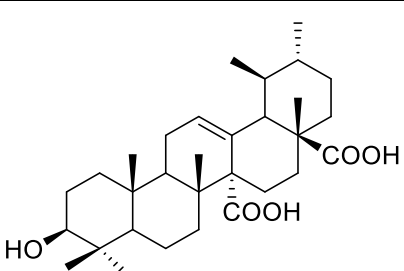
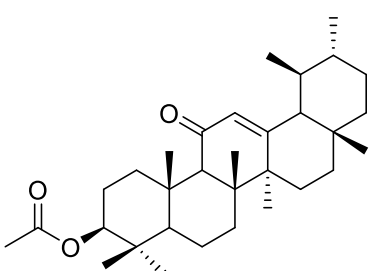
Structures	Species and sources	References
 <p>Rotundic acid (60)</p>	<p><i>N. latifolia</i> (roots)</p>	<p>Ngnokam <i>et al.</i>, 2003</p>
 <p>Ursolic acid (19)</p>	<p><i>N. latifolia</i> (heartwood)</p>	<p>Bankeu <i>et al.</i>, 2019</p>
 <p>Quafrinoic acid (61)</p>		
 <p>Quinovic acid (62)</p>		
 <p>3-Acetoxy-11-keto-urs-12-ene (63)</p>	<p><i>N. pobeguinii</i> (bark)</p>	<p>Kuete <i>et al.</i>, 2015</p>

Table 16: Some triterpenoids isolated from plants of the genus *Nauclea* (continued)

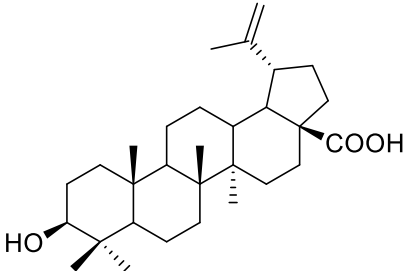
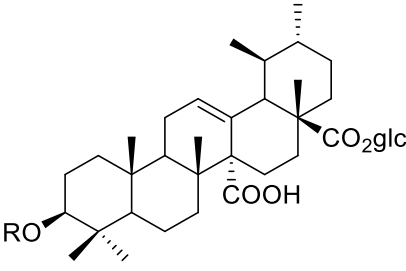
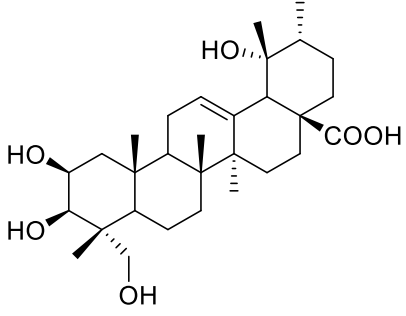
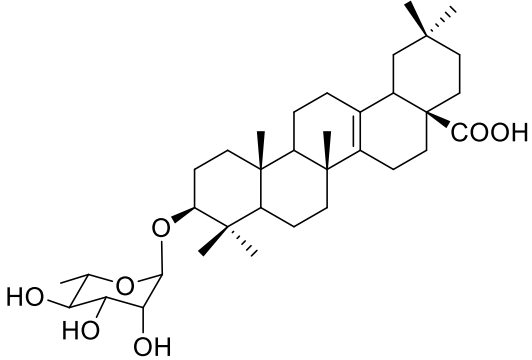
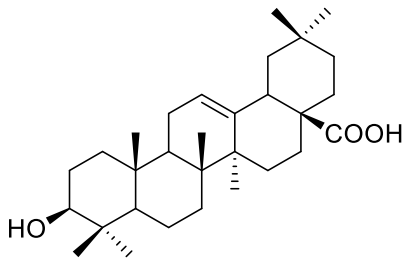
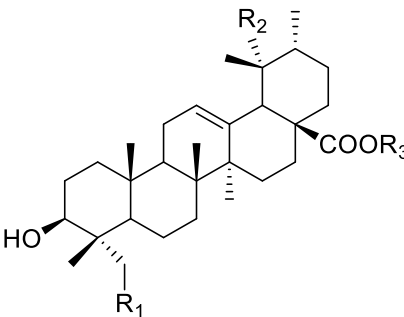
 <p style="text-align: center;">Betulinic acid (64)</p>	<p><i>N. pobeguinii</i> (bark)</p>	<p>Bankeu <i>et al.</i>, 2018</p>
 <p style="text-align: center;">R = β-D-glc Quinovic acid 28-glucosyl ester 3-O-β-D-glucopyranosyl (65) R = β-D-fuc Quinovic acid 28-glucosyl ester 3-O-β-D-fucopyranosyl (66) R = α-L-rha- Quinovic acid 28-glucosyl ester 3-O-β-D-rhamnopyranosyl (67)</p>	<p><i>N. diderrichii</i> (bark)</p>	<p>Di Giorgio <i>et al.</i>, 2006.</p>
 <p style="text-align: center;">$2\beta,3\beta,19\alpha,23$-Tetrahydroxy-urs-12-en-28-oic acid (68)</p>	<p><i>N. officinalis</i> (stem)</p>	<p>Wang <i>et al.</i>, 2014</p>
 <p style="text-align: center;">Pyrocincholic acid 3β-O-α-L-rhamnopyranoside (69)</p>		

Table 16: Some triterpenoids isolated from plants of the genus *Nauclea* (continued)

 <p>Oleanolic acid (70)</p>		Wang <i>et al.</i> , 2014
 <p> $R_1 = R_2 = H, R_3 = CH_3$ 3α-Hydroxyurs-12-en-28-oic acid methyl ester (71) $R_1 = OH, R_2 = R_3 = H$ $3\alpha, 23$-Dihydroxyurs-12-en-28-oic acid (72) $R_1 = R_2 = OH, R_3 = CH_3$ $3\alpha, 19\alpha, 23$-Trihydroxyurs-12-en-28-oic acid methyl ester (73) </p>	<i>N. orientalis</i> (stems)	He <i>et al.</i> , 2005

1.4.1.2.3 Alkaloids

The various alkaloids identified in *N. latifolia* are of monoterpene types with indole or indoloquinolizide structures. Some alkaloids extracted from the various organs of *Nauclea* genus are grouped in Table 17 below.

Table 17: Some alkaloids isolated from the genus *Nauclea*

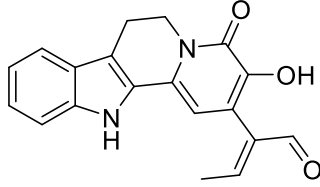
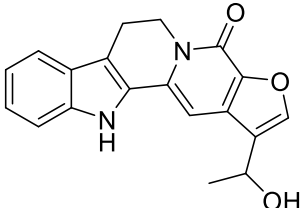
Structures	Species and sources	References
 <p>Latifoliaindole A (74)</p>	<i>N. latifolia</i> (heartwood)	Bankeu <i>et al.</i> , 2019
 <p>Latifoliaindole B (75)</p>		

Table 17: Some alkaloids isolated from the genus *Nauclea* (continued)

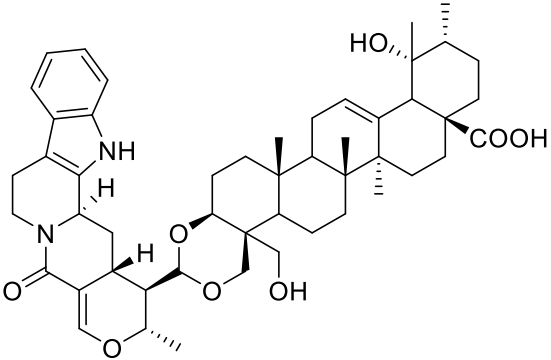
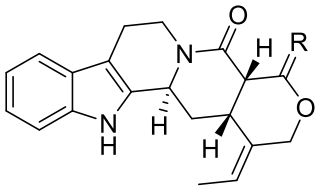
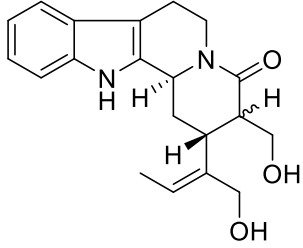
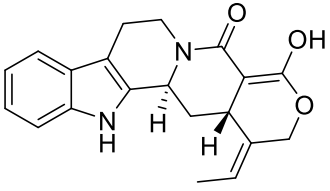
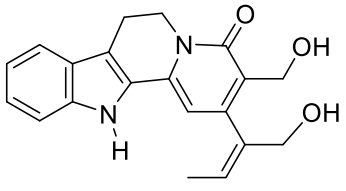
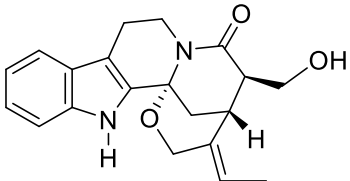
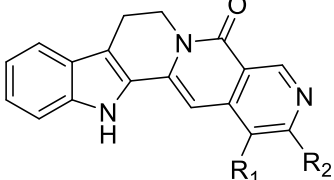
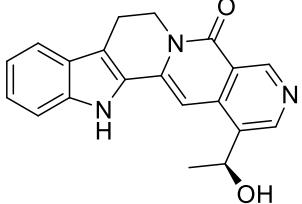
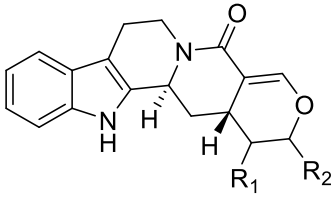
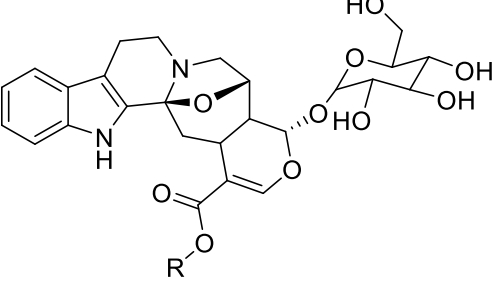
 <p>Latifolianine A (76)</p>	<p><i>N. latifolia</i> (heartwood)</p>	<p>Bankeu <i>et al.</i>, 2019</p>
 <p>R = β-OH (+)-Naucleofficine D (77) R = O Pobeginine (78)</p>	<p><i>N. pobeginii</i> (stem bark)</p>	<p>Bankeu <i>et al.</i>, 2018</p>
 <p>H-16α Naucleamide A (79) H-16β Naucleamide B (80)</p>	<p><i>N. latifolia</i> (trunk bark, wood)</p>	<p>Shigemori <i>et al.</i>, 2003</p>
 <p>Naucleamide C (81)</p>		
 <p>Naucleamide D (82)</p>		

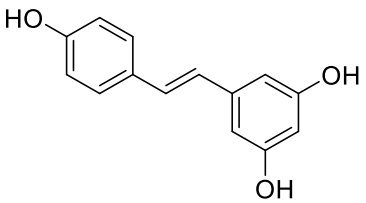
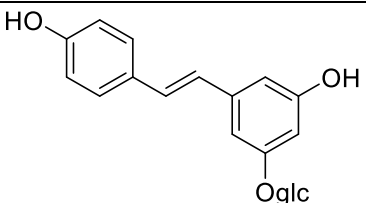
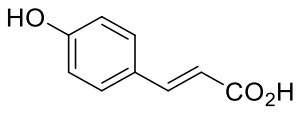
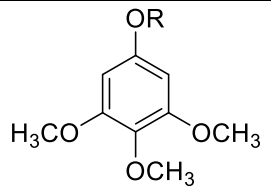
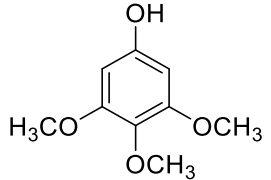
Table 17: Some alkaloids isolated from the genus *Nauclea* (continued)

 <p>Naucleamide E (83)</p>	<p><i>N. latifolia</i> (trunk bark, wood)</p>	<p>Shigemori <i>et al.</i>, 2003</p>
 <p>$R_1 = R_2 = H$ Nauclefine (84) $R_1 = CH=CH_2, R_2 = H$ Angustine (85)</p>	<p><i>N. latifolia</i> (root bark)</p>	<p>Hotellier and Delaveau, 1975</p>
 <p>Angustoline (86)</p>		
 <p>$R_1 = (R)\text{-CH=CH}_2, R_2 = (S)\text{-Oglc}$ Strictosamide (87) $R_1 = (S)\text{-CHO}, R_2 = (R)\text{-CH}_3$ Naucleidinal (88)</p>	<p><i>N. latifolia</i> (root bark, leaves and stems)</p>	<p>Bourchele <i>et al.</i>, 2016</p>
 <p>$R = CH_3$ Cadambine (89) $R = H$ Cadambine acid (90)</p>		

1.4.1.2.4. Phenolic compounds

Some phenolic compounds isolated from species of the *Nauclea* genus are presented in Table 18.

Table 18: Some phenolic compounds isolated from plants of the genus *Nauclea*

Structures	Species and sources	References
 <p>Resveratrol (91)</p>	<i>N. pobeguinii</i> (fruits)	Kuete <i>et al.</i> , 2015
 <p>Resveratrol glucoside (92)</p>		
 <p><i>p</i>-Hydroxycinnamic acid (93)</p>	<i>N. pobeguinii</i> (bark)	Xu <i>et al.</i> , 2012
 <p>R = Apiosyl-(1→4)-glc Kelampayoside (94)</p>		
 <p>Antiarol (95)</p>	<i>N. diderrichii</i>	Maclean and Murray, 1972

1.4.1.3. Previous chemical investigations on plants of the genus *Baphia*

Although this genus has not been extensively investigated chemically, previous chemical studies on species belonging to the genus *Baphia* have been reported, with isolation of several secondary metabolites such as: flavonoids, terpenoids, xanthenes, steroids and benzophenones (Kapingu *et al.*, 2008; Kapingu and Magagula, 2008).

I.4.1.3.1. Flavonoids

Table 19 below shows some flavonoids isolated from *Baphia* species.

Table 19: Some flavonoids isolated from *Baphia* species

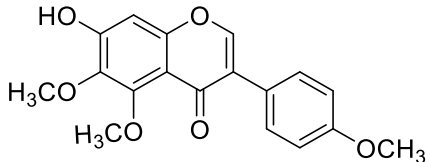
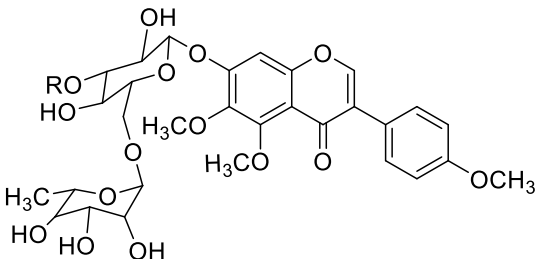
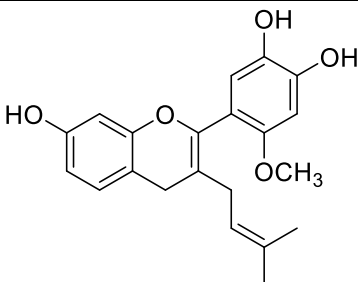
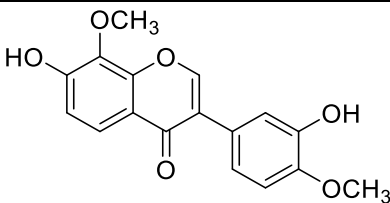
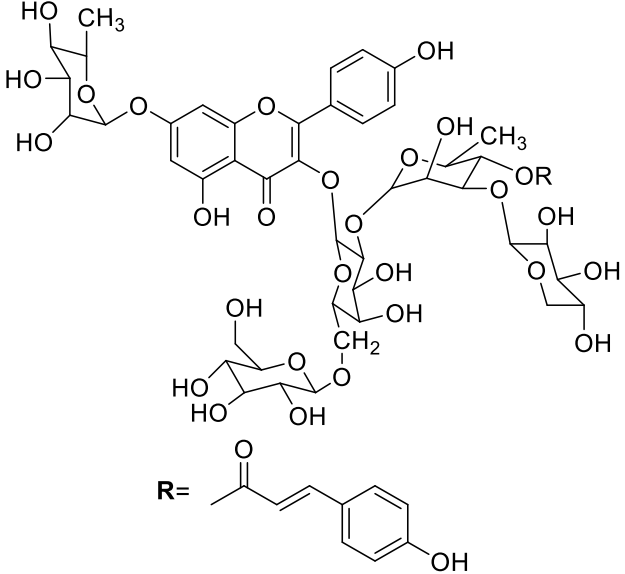
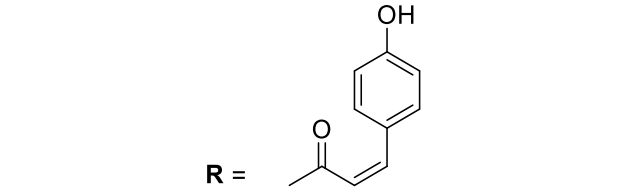
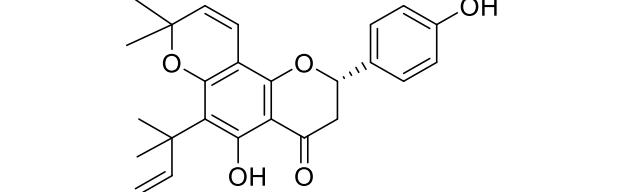
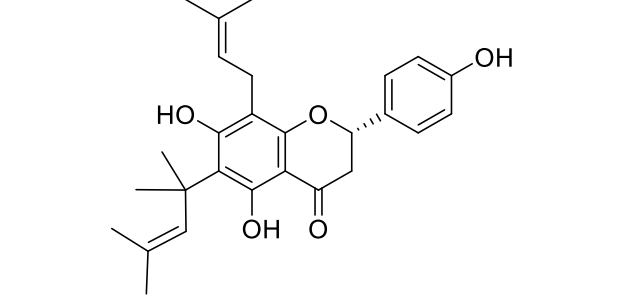
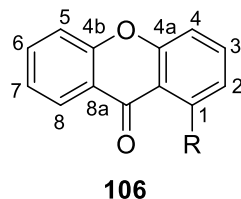
Structures	Species and sources	References
 <p>7-Hydroxy-4',5,6-trimethoxyisoflavone (96)</p>		
 <p>R = glc-(1→4)-rha-(1→6)-glc- 4',5,6-Trimethoxyisoflavone-7-O-β-D- glucopyranosyl(1→4)-α-L-rhamnopyranosyl(1→6)- β-D-glucopyranosyl(1→3)-[α-L- rhamnopyranosyl(1→6)]-β-D-glucopyranoside (97)</p> <p>R = rha-(1→6)-glc- 4',5,6-Trimethoxyisoflavone-7-O-α-L- rhamnopyranosyl(1→6)- β-D-glucopyranosyl(1→3)-[α-L- rhamnopyranosyl(1→6)]-β-D-glucopyranoside (98)</p> <p>R = H 4',5,6-Trimethoxyisoflavone-7-O-α-L- rhamnopyranosyl-(1→6)-β-D-glucopyranoside (99)</p>	<i>B. bancoensis</i> (root)	Yao-Kouassi <i>et al.</i> , 2008
 <p>Baphiflavene A (100)</p>	<i>B. massaiensis</i> (stem bark, twig)	Keroletswe <i>et al.</i> , 2018
 <p>3',7-Dihydroxy-4',8-dimethoxyisoflavone (101)</p>		

Table 19: Some flavonoids isolated from *Baphia* species (continued)

 <p>R=</p> <p>Kaempferol 3-<i>O</i>-β-D-xylopyranosyl(1\rightarrow3)-(4-<i>O</i>-<i>E</i>-<i>p</i>-coumaroyl-α-L-rhamnopyranosyl(1\rightarrow2))[β-D-glucopyranosyl(1\rightarrow6)]-β-D-galactopyranoside-7-<i>O</i>-α-L-rhamnopyranoside (102)</p>	<p><i>B. nitida</i> (leaves)</p>	<p>Chaabi <i>et al.</i>, 2009</p>
 <p>R =</p> <p>Kaempferol 3-<i>O</i>-β-D-xylopyranosyl(1\rightarrow3)-(4-<i>O</i>-<i>Z</i>-<i>p</i>-coumaroyl-α-L-rhamnopyranosyl(1\rightarrow2))[β-D-glucopyranosyl(1\rightarrow6)]-β-D-galactopyranoside-7-<i>O</i>-α-L-rhamnopyranoside (103)</p>		
 <p>Puguflavanone A (104)</p>	<p><i>B. puguensis</i> (root bark)</p>	<p>Kapingu <i>et al.</i>, 2008</p>
 <p>Puguflavanone B (105)</p>		

I.4.1.3.2. Prenylated xanthenes

Xanthenes are a class of secondary metabolites which exist in higher plant families, fungi, and lichen. They exist generally as yellow compounds and their structure are related to that of flavonoids.



Depending on the substituent R, the position 1 could interchange with positions 4, 5 and 8. Xanthenes are classified into six main groups: simple xanthenes, xanthone glycoside, prenylated xanthenes, xanthonolignoids, bisxanthenes, miscellaneous xanthenes (Negi *et al.*, 2013).

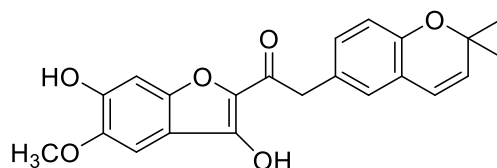
Some prenylated xanthenes isolated from plant species of the genus *Baphia* are given in Table 20.

Table 20: Some prenylated xanthenes from plants of the genus *Baphia*

Structures	Species and source	Reference
<p>1,3,5,7-Tetrahydroxy-2,4-bi(3-methylbut-2-enyl)xanthone (Baphikixanthone A) (107)</p>	<i>B. Kirkii</i> (stem)	Kapingu and Magadula, 2008
<p>1-Hydroxy-6-methoxy-2',2'-dimethyldihydropyrano-(5',6':3,4)-2'',2''-dimethyldihydropyrano-(5'',6'':7,8)xanthone (Baphikixanthone C) (108)</p>		

I.4.1.3.3. Benzofurane

Compound **109** below with a benzofurane backbone has been isolated from the stem of *B. kirkii* (Kapingu and Magagula, 2008).



Baphikinone (**109**)

I.4.1.3.4. Iminosugars

Some iminosugars isolated from the genus *Baphia* are presented in table 21 below.

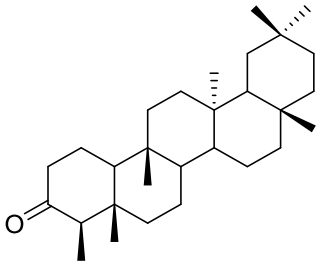
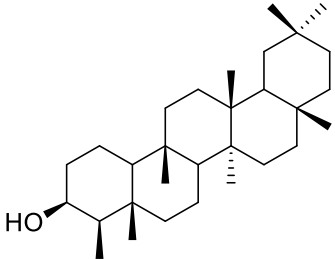
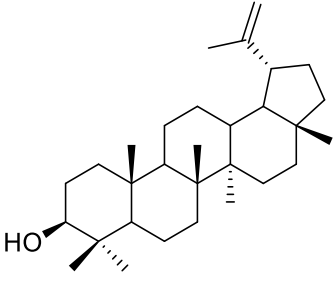
Table 21: Some iminosugars isolated from plants of the genus *Baphia*

Structures	Species and source	Reference
<p>1-Deoxynojirimycin (DNJ) (110) $R_1 = R_2 = H$</p>	<i>B. nitida</i> (leaves)	Kato <i>et al.</i> , 2008
<p>3-<i>O</i>-β-D-glucopyranosyl-DNJ (111) $R_1 = \beta\text{-D-glucopyranose}, R_2 = H$</p>		
<p>1-Deoxymannojirimycin (DMJ) (112)</p>		
<p>3-Epi-fagomine (113)</p>		
<p>DMDP (2<i>R</i>,5<i>R</i>-dihydroxymethyl-3<i>R</i>,4<i>R</i>-dihydropyrrolidine) (114) $R = H$</p>		
<p>3-β-<i>O</i>-D-glucopyranosyl-DMDP (115)</p>		

I.4.1.3.5. Triterpenoids

Some triterpenoids isolated from the genus *Baphia* are shown in Table 22 below.

Table 22: Some triterpenoids isolated from plants of the genus *Baphia*

Structures	Species and sources	References
 Friedelin (116)	<i>B. massaiensis</i> (stem bark)	Keroletswe <i>et al.</i> , 2018
 Friedelan-3 α -ol (117)		
 Lupeol (118)		

In order to confirm the therapeutic virtues of plants in folk medicine, biological screenings were carried out on crude extracts and isolated compounds.

I.4.2. Previous biological investigations on the studied plants

I.4.2.1. Previous biological investigations on plants of the Gardenieae tribe

Some of the biological activities from plant parts of the Gardenieae and isolated compounds are as follows:

➤ The methanol extract of *Rothmannia longiflora* leaves was reported to display analgesic, anti-inflammatory and antibacterial activities (Awosan *et al.*, 2014; Mallam *et al.*, 2016). The crude methanol extract of the stems of *Gardenia erubescens* showed sedative, analgesic, hypotensive and diuretic effects *in vivo* on rats, mice and cats (Hussain *et al.*, 1991).

➤ Gardenin B (**34**) isolated from the leaves of *Gardenia gummifera* displayed antiviral activity against the encephalo-myocardial virus *in vitro* (Parmar *et al.*, 1994).

➤ 6- β -Hydroxy-10-*O*-acetylgenipine (**24**) isolated from the leaves and bark of *R. witti*, was reported to exhibit strong antimycobacterial activity with a minimal inhibitory concentration (MIC) of 12.50 $\mu\text{g}/\text{mL}$ on *Mycobacterium tuberculosis*. In addition, the iridoid 10-*O*-acetylmacrophyllide exhibited cytotoxicity on the cancer cell line with an IC_{50} value of 6.82 $\mu\text{g}/\text{mL}$ (Chaipukdee *et al.*, 2016).

I.4.2.2. Previous biological investigations on plants of the genus *Nauclea*

Biological assays carried out on extracts and secondary metabolites isolated from the genus *Nauclea* revealed interesting biological activities. Some of them are listed below:

- The dichloromethane and methanol extracts of the trunk bark of *N. latifolia* were reported to have shown moderate activity (between 10 and 20% survival) against the amastigote and promastigote forms of *Leishmania major* and no significant toxicity appeared against macrophages (Ahua *et al.*, 2007).
- Naucleamide A (**79**) isolated from different parts of plants of the genus *Nauclea* showed an inhibitory activity on the glutathione-s-transferase enzyme of *Candida albicans* with IC_{50} value of 27.2 $\mu\text{g}/\text{mL}$ (Ata *et al.*, 2009).
- Strictosamide (**87**) isolated from extracts of different parts of *N. latifolia* and *N. pobeguinii* induces inhibitions on the chloroquine-resistant and chloroquino sensitive-strains of *P. falciparum* with IC_{50} values of 0.90 and 0.74 $\mu\text{g}/\text{mL}$, respectively (Mesia *et al.*, 2010; Abreu and Pereira, 2001). The same compound was reported to display a very weak cytotoxic activity ($\text{IC}_{50} > 100 \mu\text{g}/\text{mL}$) against the lung A549, the lung MRC5, the liver HepG2, the breast cancer cells MCF-7 and leukemic K562 (Mesia *et al.*, 2010; Li *et al.*, 2015).
- The 80% ethanol-water extract of the bark of *N. pobeguinii* displayed antiplasmodial activity by reducing by 86% the symptoms of malaria due to *P. bergeri* (Mesia *et al.*, 2010).
- The hydromethanolic extract of the bark of the stem of *N. latifolia* was reported to contain inhibitors against roundworms with an IC_{50} value of 15 mg/mL (Fakae *et al.*, 2000).
- The decoction of the root bark of *N. latifolia* administered antiperitoneally in mice at doses of 16, 40, 80 and 160 mg/kg was reported to display anticonvulsant, anxiolytic and sedative properties (Ngo *et al.*, 2009).

- Aqueous extract of the bark of *N. pobeguunii* showed good inhibition of α -amylase with an IC₅₀ of 248 $\mu\text{g/mL}$ (Agnaniet *et al.*, 2016).
- Angustine (**85**) isolated from *N. latifolia* and *N. pobeguunii* inhibited the enzymes monoamine oxidase A (MAO-A), butyrylcholinesterase (BChE) and acetylcholinesterase (AChE) with IC₅₀ values of 1.1 $\mu\text{g/mL}$, 3.47 $\mu\text{g/mL}$ and 3.47 $\mu\text{g/mL}$, respectively (Passos *et al.*, 2013).
- The aqueous decoction of the roots of *N. latifolia* on the maturation of the trophozoites of *P. falciparum* in schizonts after 24 h., gave an IC₅₀ of 22 $\mu\text{g/mL}$ (Badiaga, 2016).
- The aqueous decoction of the trunk bark and roots of *N. latifolia* showed antiplasmodial activities on two *P. falciparum* with IC₅₀ between 3-7 $\mu\text{g/mL}$ for the trunk bark and between 0.9-3.8 $\mu\text{g/mL}$ for the roots (Traoré, 1999).

I.4.2.3. Previous biological investigations on plants of the genus *Baphia*

The previous biological results revealed interesting biological activities of plants of the genus *Baphia*, including antiplasmodial, anti-inflammatory, antimicrobial, antiseptic and inhibitory activities (Ihekwereme *et al.*, 2016; Agyare *et al.*, 2016). Details on some of these biological activities are as follows:

- The hydroethanolic extract of *B. pubescens* was reported to have shown antiplasmodial activity at the dose 400 mg/kg, which is greater than that of the standard drug (artemether-lumefantrine). The extract is considered to be safe since the lethal dose was greater than 5000 mg/kg (Ihekwereme *et al.*, 2016).
- The ethanol extracts of the leaves and roots of *B. nitida* were assessed for their antibacterial potentials on two Gram-positive bacteria (*Staphylococcus aureus* and *Bacillus subtilis*), two Gram-negative bacteria (*Escherichia coli* and *Pseudomonas aeruginosa*) and a fungus (*Candida albicans*). It was found that the leaf extract was active against all tested microorganisms with a MIC of 50 mg/mL, while the root extract exhibited activity with MICs of 50 mg/mL on *B. subtilis*, *C. albicans* and *S. aureus*; 100 mg/mL on *P. aeruginosa* and 200 mg/mL on *E. coli* (Agyare *et al.*, 2016).
- The ethanol extracts from leaves and roots of *B. Nitida* were also reported to exhibit *in vitro* DPPH radical scavenging with IC₅₀ values of 1.21, 2.79 and 4.65 $\mu\text{g/mL}$, respectively (Agyare *et al.*, 2016).
- The ethanol extracts from the leaves and roots of *B. nitida* inhibited the edema of the foot pad induced by carrageenan at doses of 800 and 200 mg/kg, respectively (Agyare *et al.*, 2016).

➤ baphiflavene A (**100**) exhibited moderate antibacterial activity (zone of inhibition ≥ 10 mm) and good antifungal activity against *C. albicans* (zone of inhibition of 23 mm) as compared to chloramphenicol and miconazole, whose zone of inhibition is 19 mm (Keroletswe *et al.*, 2018).

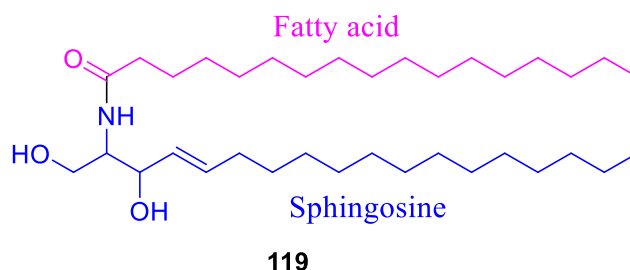
This work led to the isolation of forty-five compounds including a new ceramide. It will be therefore important to give a brief overview of this class of compounds.

I.5. OVERVIEW ON CERAMIDES

I.5.1. Definition and general classification of lipids

Lipids may be defined as substances that are soluble in non polar organic solvents (as chloroform, ether, *n*-hexane etc.), usually insoluble in water. Along with proteins and carbohydrates, lipids constitute the principal structural components of living cells. Lipids include fats, waxes, phosphatides, cerebrosides and related compounds (Vance and Vance, 2008). Scheme 1 shows the different classes of lipids containing fatty acid moiety.

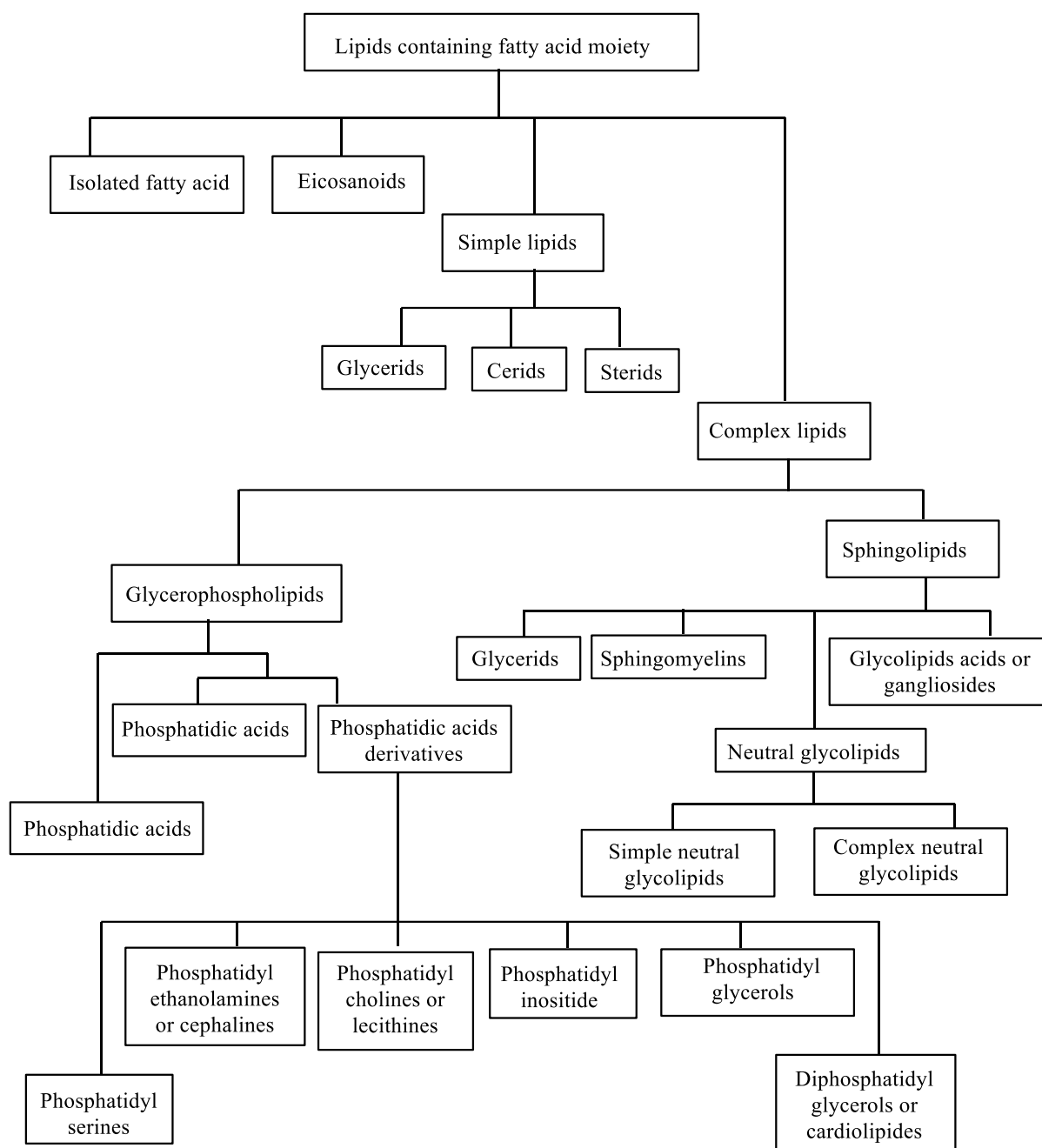
Sphingolipids are long chains or sphingoid bases linked to fatty acids via an amide bond. They are found in plants and animals, and are common in the nervous system (Kolter and Sandhoff, 1999). Ceramides (*N*-acyl-sphingoid bases) (**119**) are a major subclass of sphingolipids with an amide-linked fatty acid.



I.5.2. Definition and occurrence of ceramides

Ceramides are the hydrophobic part of sphingophospholipids and sphingoglycolipids (Minamino *et al.*, 2003). They are a family of lipid molecules that are made of long-chain bases (LCB) or sphingoid bases linked to fatty acids via an amide bond (Grassmé *et al.*, 2007). Ceramides are found in high concentrations within the membrane of cells (Kolter and Sandhoff, 2006).

Ceramides are formed as the key intermediates in the biosynthesis of all the complex sphingolipids, in which the terminal primary hydroxy group of ceramides is linked to carbohydrate, phosphate etc. (Wertz and Bergh, 1998). Unlike the sphingoid precursors, they are not soluble in water and are located in membranes where they participate in raft formation (Wertz and Bergh, 1998).



Scheme 1: Classification of lipids containing fatty acid moiety (Vance and Vance, 2008)

I.5.3. Biosynthesis and preparation of ceramides

The basic mechanism for the biosynthesis of sphinganine involves condensation of palmitoyl-coenzyme A (**120**) with serine (**121**), catalysed by a membrane-bound enzyme, serine palmitoyl transferase on the cytosolic side of the endoplasmic reticulum in animal cells as illustrated, to form 3-keto-sphinganine (**122**) (Merrill and Sandhoff, 2002). The specificity of this enzyme controls the chain-length of the base. The keto group is then reduced to a hydroxy by a specific reductase, on the cytosolic side of the endoplasmic reticulum, a step

that must occur rapidly as these intermediates are rarely encountered in tissues (Kolter and Sandhoff, 1999).

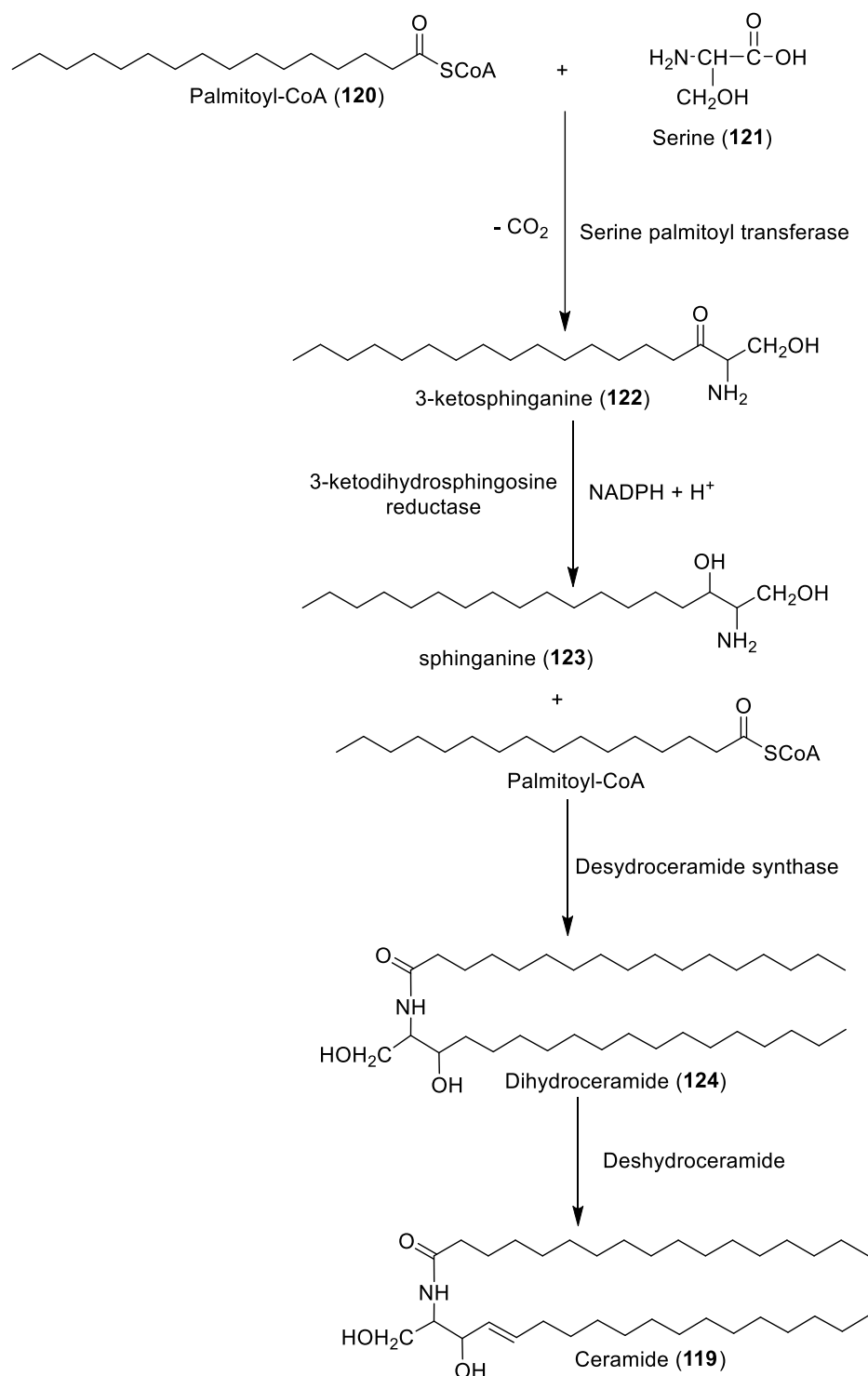
The enzymes are presumed to be in a similar location in plant cells. The free sphinganine (**123**) is rapidly *N*-acylated by acyl-CoA to form dihydroceramides (**124**) by dihydroceramide synthases, which in animals are located on the cytosolic face of the endoplasmic reticulum (Merrill and Sandhoff, 2002). Animals and plants have multiple isoforms of this enzyme, each with characteristic specificities for the chain-length of the base and fatty acyl-CoA moieties, suggesting that ceramides containing different fatty acids have distinct roles in cellular physiology. For example, animals have six ceramide synthases of which ceramide synthase 2 is the most abundant and is specific for CoA esters of very long-chain fatty acids (C₂₀ to C₂₆) (Kolter and Sandhoff, 1999). Scheme 2 shows biosynthesis of ceramides from palmitoyl-coenzyme.

Insertion of the *trans*-double bond at position 4 to produce sphingosine occurs only after the sphinganine has esterified to form a ceramide. The desaturases were first characterized in plants and this subsequently simplified the isolation of the appropriate enzymes in humans and other organisms (Kolter and Sandhoff, 1999).

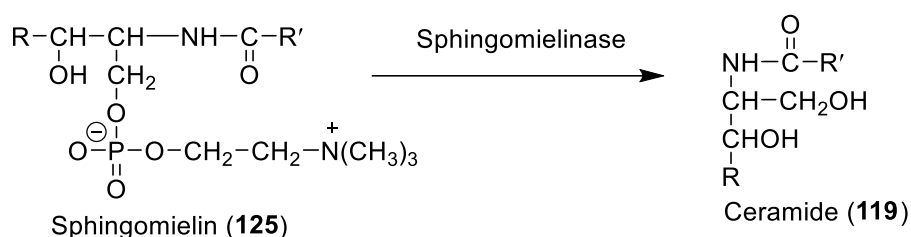
In addition, ceramides are also produced by other methods:

-The catabolism of the complex sphingolipids: it occurs by the action of sphingomyelinase or phospholipase C on sphingomyelin (**125**) (Scheme 3) (Merrill and Sandhoff, 2002; Kolter and Sandhoff, 2006).

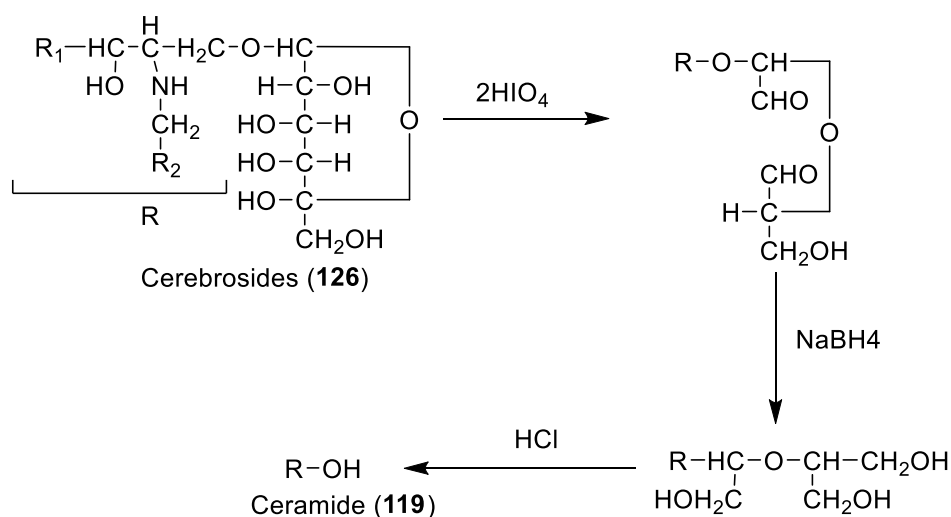
-The hydrolysis of glycosphingolipids by glycosidases: It is less important in quantitative term. Carter *et al.* (1961) proposed another chemical route to obtain ceramides from cerebroside (**126**) by oxidation using periodic acid (HIO₄) (Scheme 4) (Merrill and Sandhoff, 2002).



Scheme 2: Biosynthesis of ceramides from palmitoyl-coenzyme



Scheme 3: Biosynthesis of ceramides from sphingomyelin



Scheme 4: Conversion of cerebrosides to ceramides (Carter *et al.*, 1961)

I.5.4. Biological function of ceramides

Sphingolipids are widely present in the plasma membranes of eukaryotic cells of both terrestrial and marine organisms involved in many physiological processes (Muralidhar *et al.*, 2003). Usually, in animal tissues, ceramides and other sphingolipids are concentrated preferentially into different lateral membranes (rafts or caveolae).

Ceramides influence many biological functions. They have a role in the regulation of apoptosis. The deregulation of apoptosis can cause many diseases such as cancer, diabetes neuropathies, Alzheimer's disease, Parkinson's disease, and atherosclerosis (Zheng *et al.*, 2006). Ceramide has been implicated in the actions of tumor necrosis factor and in the cytotoxic responses to amyloid AB peptide, which are involved in Alzheimer's disease and neurodegeneration. Ceramides are also involved in many aspects of the biology of aging and male and female fertility. Furthermore, ceramides are involved in the induction of autophagy, the maintenance process by which cellular proteins and excess organelles are removed from cells (Vaena *et al.*, 2004).

Some biological functions of ceramides in animal tissues require the presence of the 4,5-double bond in the long-chain base, nevertheless the *trans* conformation may not be

essential, in that, ceramides containing a *cis*-4,5-double bond are an equally potent inducers of apoptosis at least (Zheng *et al.*, 2006). Also, it has been suggested that ceramides containing different fatty acids have distinct roles in cellular physiology. For example, C₁₆ ceramides appear to be especially important in apoptosis in non-neuronal tissues, while C₁₈ ceramides have growth arresting properties and may be involved in the apoptosis in some carcinomas treated with chemotherapeutic agents (Zheng *et al.*, 2006).

Ceramides are the predominant lipids of human epidermal stratum corneum, acting as a water barrier to prevent loss of body water (Masuda and Mori, 2005). Some of them also exhibit biological activities such as cytotoxic, antitumour, immunomodulatory, antiviral, antifungal and Ca²⁺ ATPase activities (Muralidhar *et al.*, 2005).

Comparatively, little information is available on the role of ceramides in cell signalling in plants, but there are suggestions that sphingolipid catabolic products may be linked to programmed cell death, signal transduction, membrane stability, host-pathogen interactions and stress responses (Kolter and Sandhoff, 1999).

I.5.5. General method for the structure elucidation of ceramides

Ceramides are made of one long-chain base and one fatty acid; their chemical structures are defined when the patterns of each of these constituents are determined. They can be analyzed by several techniques such as Infra-Red (IR), Mass Spectrometry (MS) and Nuclear Magnetic Resonance (NMR) spectroscopy. In addition to these techniques, chemical degradative methods are still an important tools in the determination of ceramide structures.

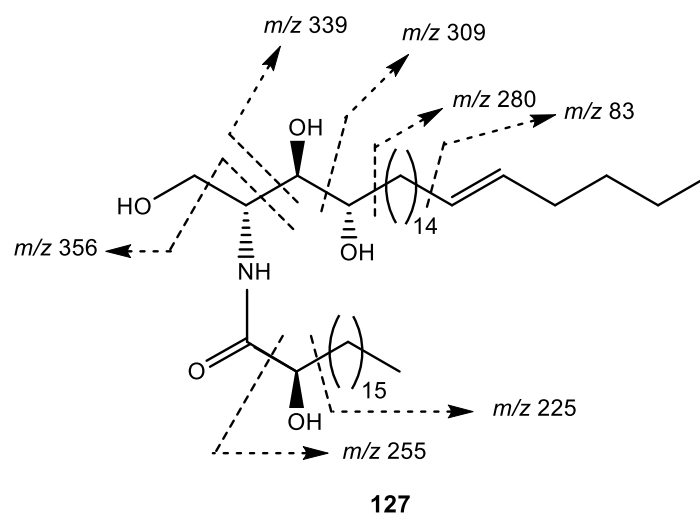
I.5.5.1. IR spectroscopy

IR analysis is usually used in order to determine the presence of secondary amides, hydroxy groups, fatty acid and olefinic functions. Therefore, the typical absorption bands around 3400, 1660 and 1530 cm⁻¹ suggest an amide linkage (Francisco *et al.*, 2006; Yaoita *et al.*, 2002). In addition, IR absorption bands closer to 3600 cm⁻¹ indicate the presence of hydroxy groups (Yaoita *et al.*, 2002). Furthermore, the absorption bands near to 2940, 2850 and 1455 cm⁻¹ (aliphatic) suggest the presence of fatty acid amides (Viqar *et al.*, 2004; Yaoita *et al.*, 2002). In addition, an absorption band around 1630 cm⁻¹ is due to the olefinic function (Muhammad *et al.*, 2007).

I.5.5.2. Mass spectroscopy

Mass spectrometry analysis has a salient role in the determination of the structures of ceramides. It permits to determine the molecular formula and the degree of unsaturation in the molecule. It helps to determine the length of both carbon chains and the position of olefinic

bond. This is possible with the help of the mass fragmentation pattern (Muhammad *et al.*, 2007; Muralidhar *et al.*, 2005). To obtain this information, different mass spectrometry methods are used. For example, High Resolution Fast Atomic Bombardment Mass Spectrometry (HRFABMS), Electrospray Ion Mass Spectrometry (ESIMS) and High-Resolution Electron Ionization Mass Spectrometry (HR-EI-MS). The Gas Chromatography (GC) coupled to EI is highly recommended in the analysis of ceramides after chemical degradative reactions. To illustrate this, let us take the case of tithoniamide B (**127**) isolated by Meffo *et al.* in 2006. Scheme 5 below shows the different fragments of tithoniamide B (Meffo *et al.*, 2006).



Scheme 5: Mass fragmentation pattern of tithoniamide (Meffo *et al.*, 2006)

1.5.5.3. Proton nuclear magnetic resonance spectroscopy

Proton Nuclear Magnetic Resonance (^1H NMR) spectroscopy has been widely employed as a method for ceramides structure determination. The ^1H NMR spectrum appears in the range of 0-10 ppm downfield from the reference signal of tetramethylsilane. This spectrum shows some characteristic signals: the resonance of the primary methyl groups ($-\text{CH}_3$) of both side chains appear as triplet of six protons around δ_{H} 0.86 ppm with the coupling constant between 7.0-7.8 Hz depending on the solvent (Muralidhar *et al.*, 2005; Eyong *et al.*, 2005). The resonance of methylene groups ($-\text{CH}_2-$) of the side chains appears as a broad singlet between δ_{H} 1.23-1.30 ppm (Muralidhar *et al.*, 2005; Naveen *et al.*, 2002). The Ha and Hb resonances of the hydroxymethylene at position C-1 appear as a pair of doublet of doublets (dd) around δ_{H} 4.50 and 4.40 ppm ($J = 10.5, 6.0$ Hz), respectively in pyridine (Eyong *et al.*, 2005). Also, they appear close to δ_{H} 3.95 and 3.70 ppm ($J = 11.0, 4.0$ Hz) in CDCl_3 (Eyong *et al.*, 2005; Naveen *et al.*, 2002). These values depend on the chemical environment

around carbon C-1. The resonance of olefinic proton appear as a pair of doublets of triplets or as multiplets near to δ_{H} 5.52 and 5.48 ppm (Cateni *et al.*, 2003). If one of the J -values of these protons is around 15.0 Hz, it reveals the E -orientation (Muhammad *et al.*, 2007). A proton attached to the amide nitrogen has resonance as a doublet around δ_{H} 8.55 ppm with the coupling constant in the range 8.8-9.1 Hz in pyridine (Takahiro *et al.*, 2006). A proton vicinal to amide group usually appears in the range of 5.00-5.23 ppm. However, all of these values can slightly change depending upon the type of solvent and the chemical environment.

I.5.5.4. Carbon nuclear magnetic resonance spectroscopy

The broad-band proton decoupled ^{13}C NMR spectrum of an unknown ceramide permits ready differentiation between ceramides containing double bonds and ceramides lacking the double bonds. Signals of olefinic carbons appear in the range of 127.0-135.0 ppm (Yaoita *et al.*, 2007; Viqar *et al.*, 2004). The ^{13}C NMR of ceramides also show some characteristic signals. The resonance of amide carbonyl appears between δ_{C} 175.0-177.0 ppm and methine carbon linked to amide nitrogen appear around δ_{C} 53.0 ppm (Meffo *et al.*, 2006; Muhammad *et al.*, 2007). The signal of the downfield hydroxymethylene group appears close to δ_{C} 62.2 (Yaoita *et al.*, 2007; Wouamba *et al.*, 2020). Methylenes of both side chains show their signals between δ_{C} 22.0-30.0 ppm (-CH₂-) (Yaoita *et al.*, 2007). Hydroxymethine carbons appear between δ_{C} 72.0-78.0 ppm (Meffo *et al.*, 2006; Muhammad *et al.*, 2007). Primary methyls of both side chains appeared around δ_{C} 14.3 ppm (-CH₃) (Muralidhar *et al.*, 2005; Wouamba *et al.*, 2020).

It is important to know that all these values depend on the nature of solvent and the chemical environment. Therefore, these shifts can slightly change.

I.5.5.5. Heteronuclear multiple bond connectivity (HMBC) and ^1H - ^1H correlation spectroscopy (COSY) techniques

These two techniques are of great importance in the structure determination of ceramides. They help specifically in the location of hydroxy groups and the double bonds in some ceramides. The connectivities between the olefinic protons of the double-bond and the carbons adjacent to this double-bond give the crucial information on its geometry. It is known that the geometry of the double-bond in the long-chain alkene can be determined on the basis of the ^{13}C NMR chemical shift of the allylic carbons, which is observed at $\delta_{\text{C}} \approx 27$ in (Z) isomers and at $\delta_{\text{C}} \approx 32$ in (E) isomers (Bankeu *et al.*, 2010; Wouamba *et al.*, 2020).

I.5.5.6. Chemical degradative methods in the structure determination of ceramides

The nature of each of the constituents of ceramides is determined through the methanolysis with methanolic hydrochloric acid. The fatty acid methyl ester (FAME) obtained together with a long chain base (LCB) from the methanolysis is extracted with *n*-hexane and this layer is evaporated and subjected to gas chromatography-mass spectrometry (GCMS) analysis to determine the nature of FAME (Kawatake *et al.*, 2002; Bankeu *et al.*, 2010). The layer can also be subjected to Liquid Chromatography-mass spectrometry (LCMS) analysis to determine the nature of the LCB.

Especially in the case of ceramides containing double-bond, an additional reaction is required to determine the position of the double-bond on one of the long-chains. This produces the dimethyl disulfide (DMDS) derivatives of ceramides. The positive mode FAB and the ESI mass spectrum of the DMDS derivatives of ceramides shows a remarkable fragment ion peak due to cleavage of the bond between the carbons bearing a methylthio group. These data indicate the position of the double-bond in the LCB or in the FAME of ceramides (Kawatake *et al.*, 2002; Cateni *et al.*, 2003; Bankeu *et al.*, 2010).

In view to rationalize and promote the uses of these plants in traditional medicine, the diversity of biological activities presented by their extracts, given the fact that *R. hispida* and *Nauclea latifolia* fruits are very little studied and also that *B. leptobotrys* has never been studied, we have undertaken as part of our research work, the chemical investigation of these three medicinal plants as well as the evaluation of their antileishmanial properties.

PART II: RESULTS AND DISCUSSION

II.1. Chemical study of *Rothmannia hispida*, *Nauclea latifolia* and *Baphia leptobotrys*

II.1.1. Extraction of plant material

The leaves of *R. hispida* were collected in June 2017 at Nkol-Afamba (GPS coordinates: Latitude 3°51'32"N, Longitude 11°39'53"E), a locality in the Centre Region of Cameroon and identified by Mr Nana Victor, a botanist at the National Herbarium of Cameroon, where a voucher specimen (N° 46515 HNC) is conserved. The air-dried and ground leaves of the plant (1.9 kg) were macerated three times at room temperature in 10 L of CH₂Cl₂/MeOH (1:1) for 48 h each and filtered. The crude extract was obtained as a green paste (251.8 g) after removing the solvent mixture by evaporation under vacuum at low temperature.

The ripe fruits of *Nauclea latifolia* were harvested in March 2017 at Makenene (GPS coordinates: Latitude 4°88'39"N, Longitude 10°79'44"E), a locality in the Centre Region of Cameroon and identified by Dr. Tacham Walter Ndam, Botanist at the Faculty of Science of The University of Bamenda, Cameroon, and compared with voucher specimens formerly kept at the Cameroon National Herbarium under the registration number 20144/SFR/Cam.

The air-dried and ground fruits of the plant (2.1 kg) were macerated three times at room temperature in 20 L of MeOH for 48 h each. The crude extract was obtained as a red paste (459.7 g) after removing the solvent mixture by evaporation under vacuum at low temperature.

The trunk bark and leaves of *B. leptobotrys* were harvested in April 2018 and September 2019, respectively in the Kompia forest (GPS coordinates: Latitude 3°33'38"N, Longitude 12°49'16"E), located in the East Region of Cameroon. The plant was identified by Mr Nana Victor, a botanist at the National Herbarium of Cameroon and compared with voucher specimen formerly kept at the Cameroon National Herbarium under the reference number 52328 HNC.

The air-dried and ground trunk bark (5.06 kg) and leaves (880.3 g) of the plant were separately macerated three times at room temperature, respectively with 25 L and 10 L of CH₂Cl₂/MeOH (1:1) for 48 h. The trunk bark crude extract was obtained as a chestnut oily paste (132.6 g) and the leaves crude extract as a green paste (102.2 g) after removing the solvent mixture by evaporation under vacuum at low temperature.

II.1.2. Antileishmanial screening and cytotoxicity assay

The CH₂Cl₂/MeOH (1:1) crude extract of *R. hispida* showed good antileishmanial activity *in vitro* during preliminary screening with IC₅₀ value of 15.50 µg/mL against *Leishmania donovani* 1S (MHOM/SD/62/1S) promastigotes and no cytotoxicity towards RAW 264.7 macrophage cells (CC₅₀ >100 µg/mL, SI > 6.45).

The MeOH crude extract of *N. latifolia* showed potent antileishmanial activity *in vitro* during preliminary screening with IC₅₀ value of 2.20 µg/mL against the same strain and no cytotoxicity towards RAW 264.7 macrophage cells (CC₅₀ > 100 µg/mL, SI > 43.35).

The CH₂Cl₂/MeOH (1:1) trunk bark crude extract showed moderate antileishmanial activity *in vitro* during preliminary screening with IC₅₀ value of 63.40 µg/mL while the leaves crude extract was non active (IC₅₀ > 100 µg/mL) against the same strain and no cytotoxicity towards RAW 264.7 macrophage cells (CC₅₀ > 100, SI > 1.57) was observed for the trunk bark extract.

II.1.3. Acute toxicity study

Knowing that fruits of *N. latifolia* are highly consumed by population and the fact that the MeOH crude extract displayed the best antileishmanial activity without cytotoxicity on macrophage cells, some tests were done to evaluate its safety. For this purpose, we evaluated the effects of the methanol crude extract on some clinical parameters, weight change and relative mass of certain organs.

➤ Effects of the extract on some clinical parameters

The Table 23 below shows the effects of administration in rats of the methanol crude extract (NLFFr) at a dose of 2000 mg/kg/BW (Body Weight) on selected clinical parameters. According to this table, it was noted that the plant extract was not harmful or showed no signs of toxicity with regard to the clinical parameters evaluated. Animals that received the methanol plant extract did not show aggression and chills. In addition, the animals that received plant extract in the same way as normal animals that received distilled water show normal stool appearance, sensitivity to sound and touch and mobility.

Table 23: Effects of the methanol extract on some clinical parameters

Parameters	Witness			NLFr 2000 mg/kg			NLFr 5000 mg/kg		
	30 min	4 h	14 days	30 min	4 h	14 days	30 Min	4 h	14 days
Number of deaths	0	0	0	0	0	0	0	0	0
Thrill	-	-	-	-	-	-	-	-	-
Aggressiveness	-	-	-	-	-	-	-	-	-
Mobility	+	+	+	+	+	+	+	+	+
Appearance of faeces	N	N	N	N	N	N	N	N	N
Horripilation	-	-	-	-	-	-	-	-	-
Touch sensitivity	+	+	+	+	+	+	+	+	+
Noise sensitivity	+	+	+	+	+	+	+	+	+

N= normal, + = Present, - = Absent

➤ **Effects on weight change**

The figure 8 below shows the effects of the administration of the methanol extract in rats on the weight gain. According to this figure, there is a non-significant variation in weight gain from day 0 to day 14 in normal animals that received the plant extract at different doses compared to those that received distilled water.

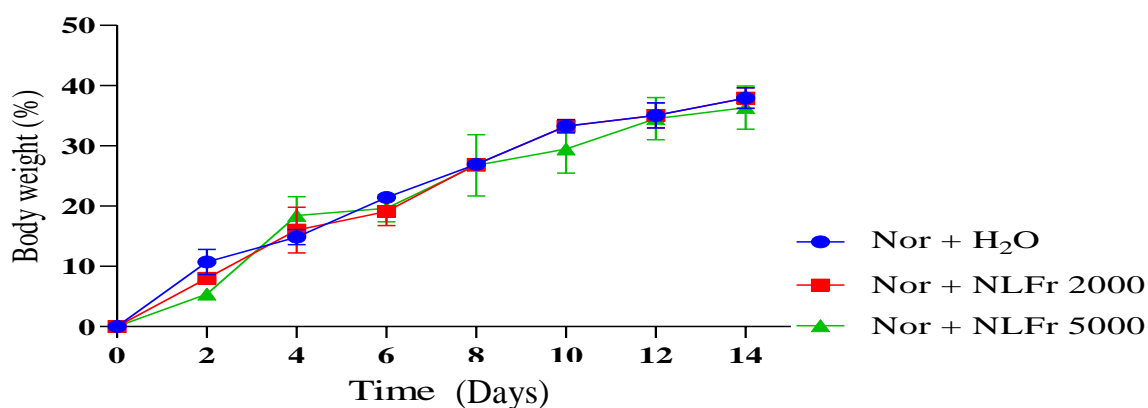


Figure 8: Effects of the methanol extract on the weight development of rats in acute toxicity

Each value represents the mean ± ESM; n = 3; Nor + H₂O: healthy rats treated with distilled water; Nor + NLFr 2000, Nor + NLFr 5000: rats treated with methanol extract of NLFr (*Nauclea latifolia* fruit extract) at doses of 2000 and 5000 mg/kg, respectively.

➤ Effects on the relative mass of certain organs

The figure 9 below is an illustration of the effects of administration of the extract on the relative mass of the liver, kidney, heart and lung. According to this figure, the administration for 14 days of the plant extract did not cause any significant variation in the relative mass of the various organs mentioned above as compared to normal animals which received distilled water.

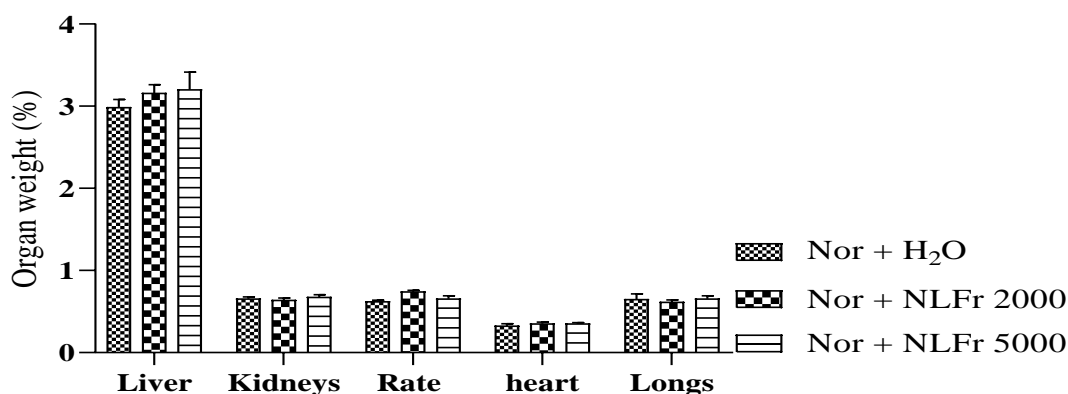


Figure 9: Effects of methanol extract of NLFr on the relative weight of organs in acute toxicity

Each value represents the mean \pm ESM; $n = 3$; Nor + H₂O: healthy rats treated with distilled water; Nor + NLFr 2000, Nor + NLFr 5000: rats treated with methanol extract of NLFr at doses of 2000 and 5000 mg/kg, respectively.

The present study was conducted to assess the toxicity effects of the methanol extract of *N. latifolia* for acute toxicity in female rats. This extract at the tested limit doses of 2000 and 5000 mg/kg did not cause any death during the 14 days of experimentation indicating that the Lethal Dose 50 (LD₅₀) is greater than 5000 mg/kg. In addition, no apparent signs of toxicity, neither on the behavior of the animals, nor on the clinical signs observed, nor on the body weight of the animals, nor on the relative weight of the organs involved in the toxicity were noted. In addition, slight differences in color observed on the macroscopic appearance of the organs after dissection are believed to be due to the specific physiology of each animal. Our results are in close agreement with the WHO data which suggests that the methanol extract of *N. latifolia* would be classified according to the Globally Harmonized Classification System (GHCS) in category 5 of substances of little or no toxicity (OECD, 2001).

II.1.4. Isolation of compounds

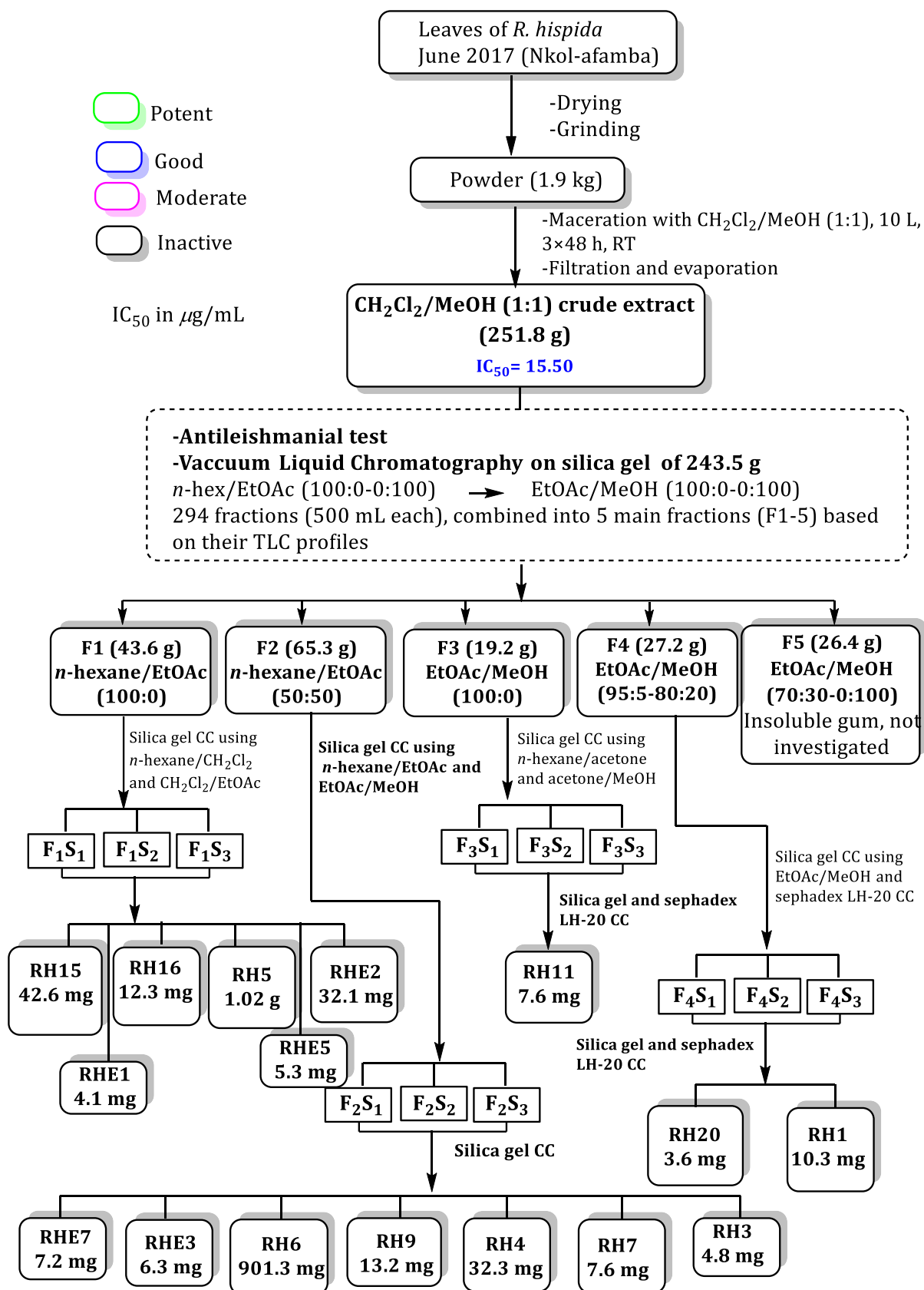
Part of *R. hispida* CH₂Cl₂/MeOH (1:1) crude extract (243.5 g) was subjected to vacuum liquid chromatography using the mixtures of *n*-hexane/EtOAc and EtOAc/MeOH in increasing polarities. Two hundred and ninety four (294) sub-fractions of 500 mL each, were

obtained and combined according to their TLC profiles to yield five main fractions labelled F1 (43.6 g, *n*-hexane/EtOAc, 100:0), F2 (65.3 g; *n*-hexane/EtOAc, 50:50), F3 (19.2 g; EtOAc/MeOH, 100:0), F4 (27.2 g; EtOAc/MeOH; 95:5–80:20) and F5 (26.4 g; EtOAc/MeOH, 70:30–0:100). The purification of these fractions over silica gel and Sephadex LH-20 led to the isolation of seventeen compounds (Scheme 6).

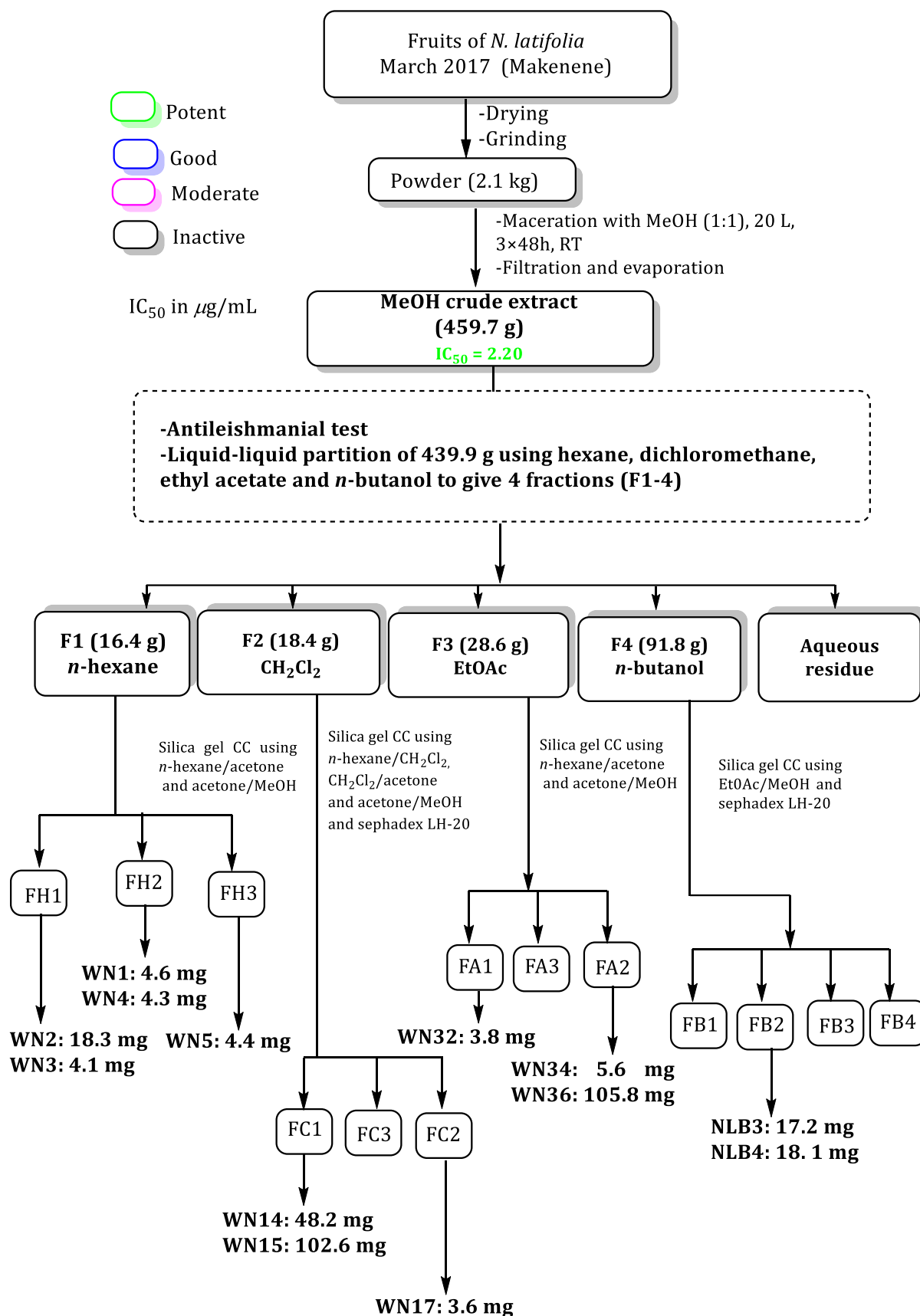
Part *N. latifolia* MeOH crude extract (439.0 g) was successively and exhaustively partitioned with *n*-hexane, CH₂Cl₂, EtOAc and *n*-butanol (1.5 L each) to give the *n*-hexane (16.4 g), CH₂Cl₂ (18.4 g), EtOAc (28.6 g) and *n*-butanol (91.8 g) soluble fractions along with a solid residue, respectively. The bioassay-guided purification through repeated silica gel and sephadex LH-20 columns of the active fractions using mixture of *n*-hexane/CH₂Cl₂, *n*-hexane/acetone, acetone/MeOH and EtOAc/MeOH at increasing polarities led to the isolation of thirteen compounds. In view to contribute to the chemophenetic study of this plant, the non active fraction was also studied (Scheme 7).

Part of *B. leptobotrys* CH₂Cl₂/MeOH (1:1) trunk bark crude extract (124.8 g) was separated on CC using silica gel and *n*-hexane, EtOAc and MeOH solvent systems of increasing polarities. Two hundred and ten (210) fractions of 500 mL each were obtained and combined based on their TLC profiles into five main fractions labelled FT1 (35.4 g; *n*-hexane/EtOAc, 100:0–80:20), FT2 (38.6 g; *n*-hexane/EtOAc, 80:20–60:40), FT3 (10.2 g; *n*-hexane/EtOAc, 50:50–30:70), FT4 (12.4 g; EtOAc/MeOH, 100:0–90:10) and FT5 (21.3 g; EtOAc/MeOH, 80:20–0:100).

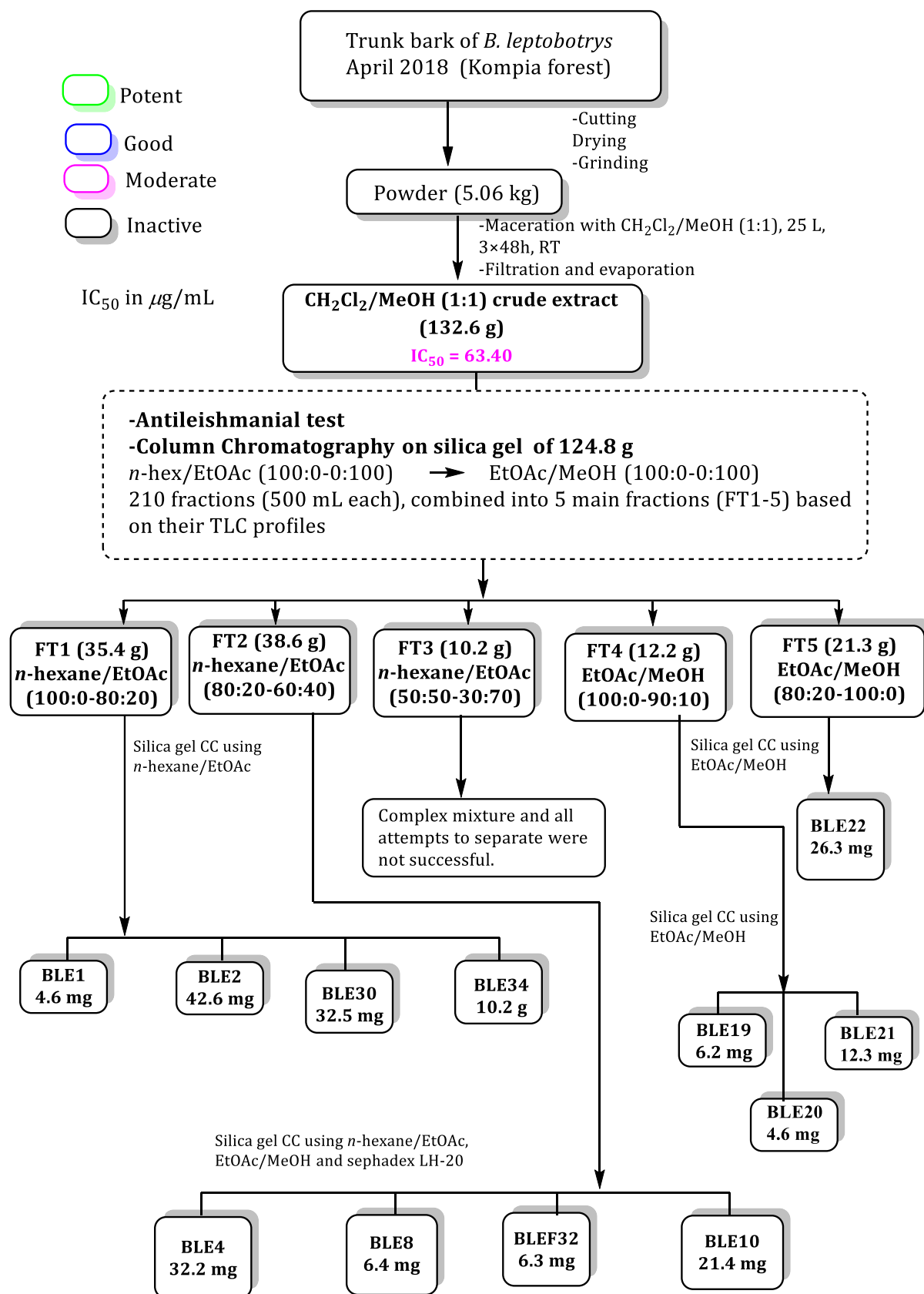
Part of *B. leptobotrys* CH₂Cl₂/MeOH (1:1) leaves crude extract (98.1 g) was separated over CC using silica gel and *n*-hexane, EtOAc and MeOH solvent systems of increasing polarities. Two hundred and eight (208) fractions of 250 mL each were obtained and combined based on their TLC profiles into five fractions labelled FL1 (15.3 g; *n*-hexane/EtOAc, 100:0–80:20, v/v), FL2 (24.7 g; *n*-hexane/EtOAc, 80:20–40:60), FL3 (15.9 g; EtOAc/MeOH, 100:0–80:20), FL4 (14.4 g; EtOAc/MeOH/H₂O, 95:5:2–80:20:10) and FL5 (13.3 g; MeOH/H₂O, 95:5–90:10). The purification through repeated silica gel and Sephadex LH-20 columns of all these fractions led to the isolation of twelve compounds from the trunk bark (Scheme 8) and seven compounds from the leaves (Scheme 9).



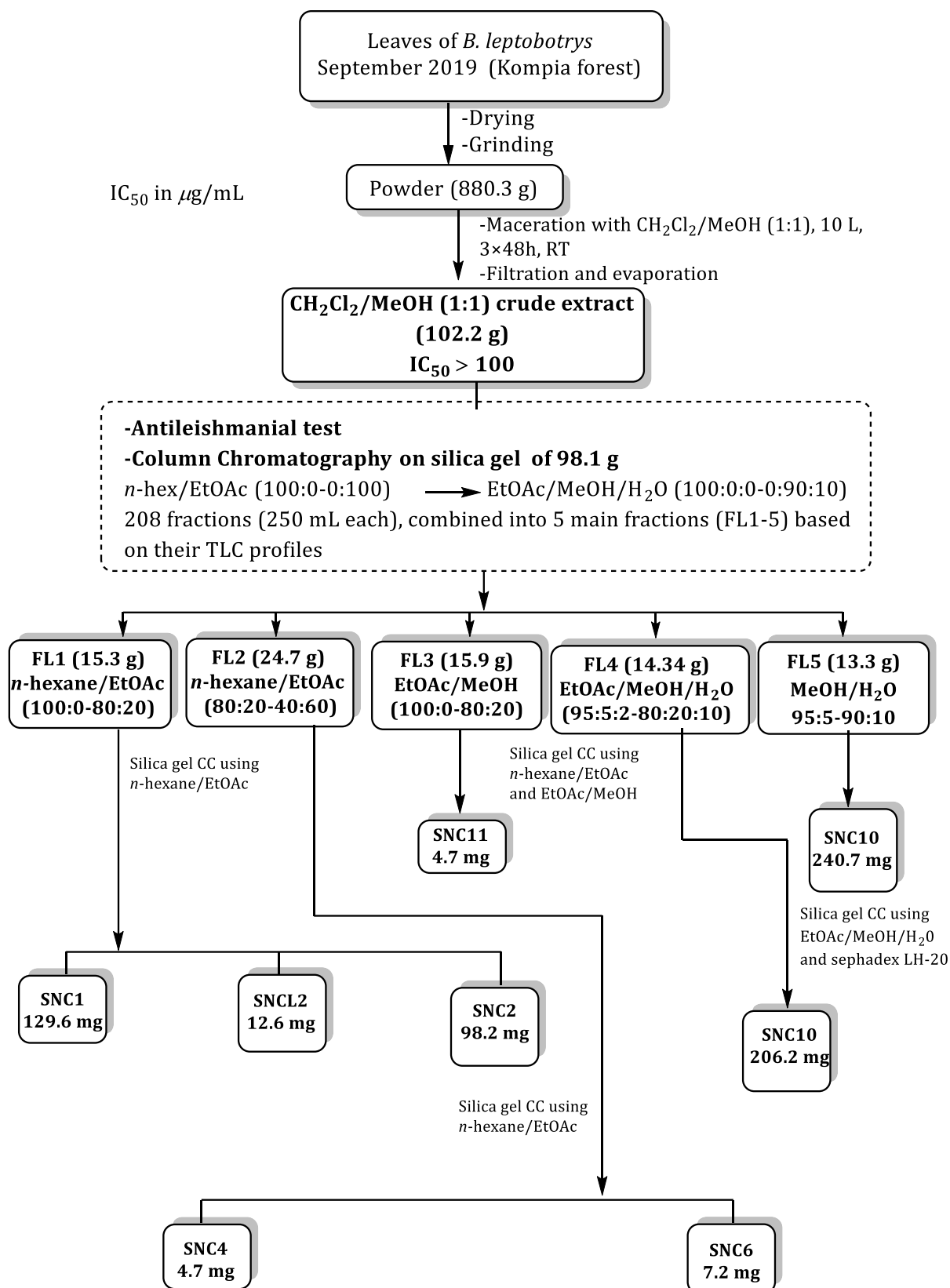
Scheme 6: Protocol of extraction and isolation of compounds from the leaves of *R. hispida*



Scheme 7: Protocol of extraction and isolation of compounds from the fruits of *N. latifolia*



Scheme 8: Protocol of extraction and isolation of compounds from the trunk bark of *B. leptobotrys*



Scheme 9: Protocol of extraction and isolation of compounds from the leaves of *B. leptobotrys*

II.1.5. Structural elucidation of the isolated compounds

A total of forty five different compounds have been totally characterized using physical and spectroscopic methods (MS, IR, NMR). They belong to eleven classes of secondary metabolites including:

- one new ceramide (**RHE7**);
- four phenolic derivatives (**RHE3**, **WN14**, **RHE1**, **RH20**);
- seventeen triterpenoids (**BLE4**, **BLE10**, **RH11 = WN4**, **WN1**, **RH5**, **RH6**, **RH9**, **WN5**, **RH16 = BLE1**, **BLE30**, **RH15**, **SNC11**, **SNC1**, **SNC2**, **SNCL2**, **SNC4**);
- three citric acid derivatives (**WN15**, **WN34**, **WN36**);
- two amino acid derivatives (**SNC6**, **SNC10**);
- one pyrrole derivative (**WN17**);
- one iridoid (**NLB3**);
- seven steroids (**BLE8**, **BLEF32**, **RHE2**, **RH4 = BLE2 = WN2**, **BLE19 = RH7**);
- four sugar derivatives (**BLE22 = RH1**, **BLE21**, **NLB4**);
- four fatty derivatives (**RHE5**, **RH3**, **BLE34**, **WN3**);
- one benzoic acid derivative (**WN32**).

II.1.5.1. Ceramide

II.1.5.1.1. Structural elucidation of compound RHE7

Compound RHE7 was isolated as a white powder in *n*-hexane/EtOAc (30:70). It is soluble in pyridine with an optical rotation $[\alpha]_D^{22} = -112.6^\circ$ (*c* 0.0563, pyridine).

Its molecular formula $C_{44}H_{89}NO_5$ was deduced from the HRESIMS (Figure 10a), which showed the sodium adduct peak $[M+Na]^+$ at m/z 734.6636 (calcd. for $C_{44}H_{89}NO_5Na$, 734.6633) implying one degree of unsaturation.

Its IR spectrum (Figure 11) displayed characteristic absorption bands for hydroxy groups (3333 cm^{-1}), aliphatic groups (2915 cm^{-1}) and amide group (1618 cm^{-1}) of ceramides (Yaoita *et al.*, 2000).

Its ^{13}C spectrum (Figure 12) displayed carbon resonances which were sorted by DEPT (Figure 13) and HMQC (Figure 14) techniques into:

- one quaternary carbon of an amide group at δ_C 174.9 (C-1');
- four methine carbon signals [including three oxymethine at δ_C 76.6 (C-3), 72.7 (C-4), and 72.2 (C-2') and an azomethine at δ_C 52.7 (C-2)], and an oxymethylene carbon at δ_C 61.7 (C-1);

- signals for long-chain aliphatic methylene carbons between δ_C 22.7-35.4 (C-7 to C-13 and C-5' to C-29');

- the resonances of two terminal methyl carbons at δ_C 14.0 (C-14 and C-30').

Its ^1H NMR spectrum (Figure 15) exhibited from downfield to upfield, resonances of:

- an amide proton at δ_H 8.59 (d, $J = 9.0$ Hz, NH);
- four hydroxyl groups at δ_H 7.64 (1H, d, $J = 4.4$ Hz, 2'-OH), 6.71 (2H, d, $J = 4.9$ Hz, 1-OH/3-OH) and 6.23 (1H, br s, 4-OH);
- a methine proton vicinal to the nitrogen atom of an amide group at δ_H 5.12 (1H, m, H-2) (Wouamba *et al.*, 2020; Simo *et al.*, 2008);
- non equivalent methylene proton signals at δ_H 4.52 (1H, dd, $J = 4.2, 10.6$ Hz, H-1a) and 4.43 (1H, dd, $J = 4.9, 10.6$ Hz, H-1b);
- three oxymethine protons at δ_H 4.63 (1H, br d, $J = 3.6$ Hz, H-2'), 4.36 (1H, m, H-3) and 4.29 (1H, m, H-4);
- two alkyl long chains appearing as broad singlets between δ_H 1.30-1.24;
- two primary methyl groups (CH₃-14 and CH₃-30) which appeared as a triplet of protons at δ_H 0.85 (6H) and supporting that compound RHE7 is a ceramide (Bankeu *et al.*, 2017).

Analysis of the ^1H - ^1H COSY (Figure 16), HMQC and HMBC (Figure 17) spectra led to the assignment of proton and carbon signals for RHE7. The ^1H - ^1H COSY spectrum exhibited the correlations between:

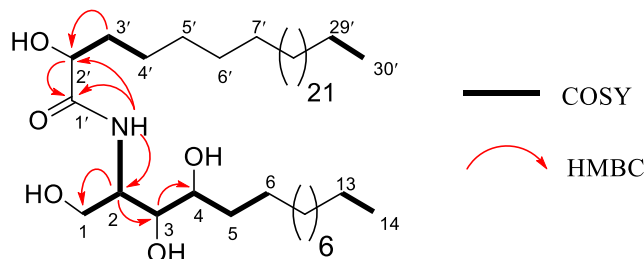
- the oxymethylene protons at δ_H 4.52 (H-1a) and 4.43 (H-1b) with the azomethine at δ_H 5.12 (H-2) which in turn was connected to the oxymethine proton H-3 (δ_H 4.36) and the amide proton N-H (δ_H 8.59);
- the proton H-3 (δ_H 4.36) also correlated with the oxymethine proton H-4 (δ_H 4.29) confirming the location at C-3 and C-4 for the two hydroxyl groups, respectively (Scheme 10).

This was further confirmed by the HMBC spectrum which showed correlations between:

- the azomethine H-2 (δ_H 5.12) and the oxymethine carbon C-3 (δ_C 76.6) and C-4 (δ_C 72.7);
- no cross peaks were observed between H-2' (δ_H 4.63) and downfield proton signals of the amide side chain.

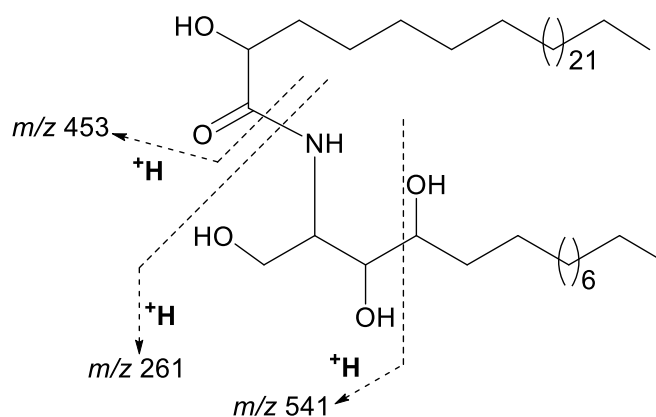
The location of the hydroxyl group at C-2' was deduced from the coupling observed on the ^1H - ^1H COSY spectrum between the H-2' (δ_H 4.63) and H-3' (δ_H 2.05) and also from the

correlation of the HMBC spectrum between H-2' (δ_H 4.63) and C-1' (δ_C 174.9) and the proton of the amide NH (δ_H 8.59) and carbon C-2' (δ_C 72.2) and C-1' (δ_C 174.9). This suggested that the fourth hydroxyl group is present at C-2' of the fatty acid chain, thus indicating the presence of a -COCH(OH)-CH₂-moiety in RHE7 (Radhika *et al.*, 2004).



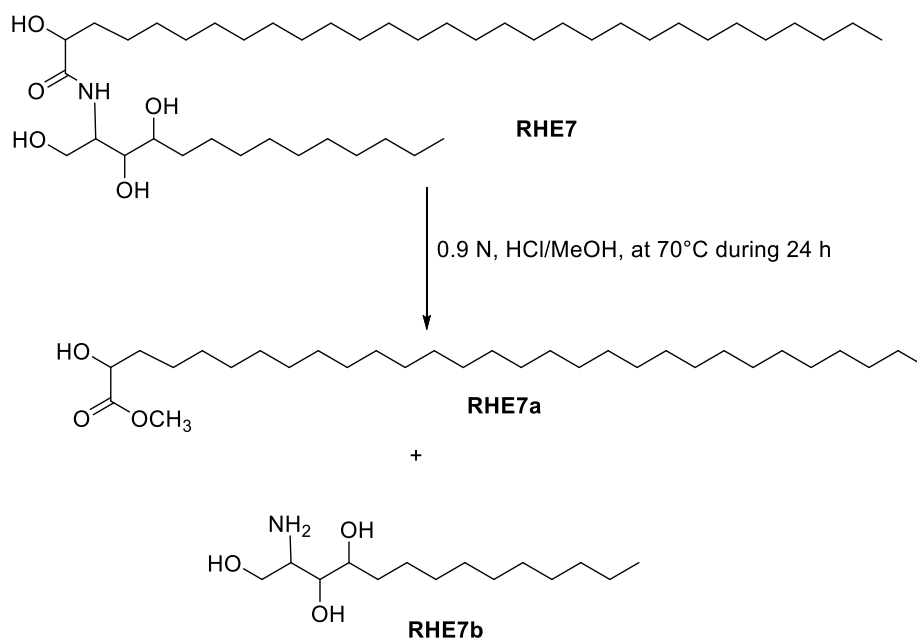
Scheme 10: Important HMBC and COSY correlations of RHE7

The length of the fatty acid moiety was confirmed by the ion peak at m/z 453 [CH₃(CH₂)₂₇CH(OH)CO+2H]⁺ and the length of the long chain base by the ion peak at m/z 261 [CH₃(CH₂)₉CH(OH)CH(OH)CH(NH)CH₂(OH)+H]⁺ in the ESIMS (Figure 10b).



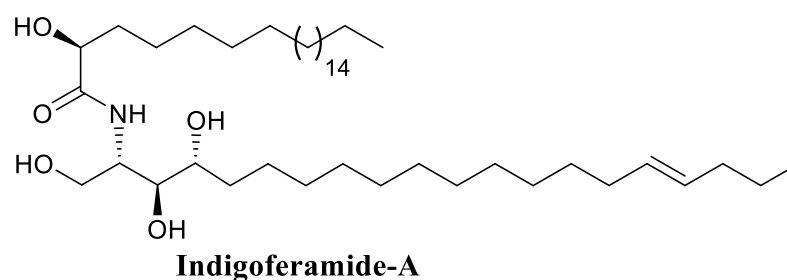
Scheme 11: Mass fragmentation pattern of RHE7

This was further confirmed by the methanolysis (0.9 N, HCl/MeOH, at 70°C during 24 h) of RHE7, which gave the fatty acid methyl ester (RHE7a) and the long chain base (RHE7b) after ESI-MS analysis. So, the peak at m/z 262.2 [M+H]⁺ corresponding to the molecular formula C₁₄H₃₂NO₃ was attributable to the long-chain base (RHE7b) (Figure 18, Scheme 12).



Scheme 12: Methanolysis of RHE7

Considering the HMBC and ^1H - ^1H COSY correlations, the biogenesis and steric hindrance of sphingolipids, the chemical shift of the H-2 signal and the chemical shifts of C-1 to C-4, C-1' and C-2' are generally known to determine the absolute configuration of the phytosphingosine (Simo *et al.*, 2008). The optical rotation $[\alpha]_D^{22}$: -112.6 and the chemical shifts of C-atoms C-1 (δ_C 61.7), C-4 (72.7), C-1' (δ_C 175.0) and 72.2 (δ_C C-2') in RHE7 were closely identical with those of indigoferamide-A $[\alpha]_D^{22}$: -16, C-1 (62.1), C-4 (72.9), C-1' (175.4) and C-2' (72.3) (Rahman *et al.*, 2017).



Based on the above data, RHE7 was concluded to be a new ceramide and trivially named rothmanniamide ((2*R*')-2-hydroxy-*N*-((2*S*,3*S*,4*R*)-1,3,4-trihydroxytetradecan-2-yl)triacontanamide).

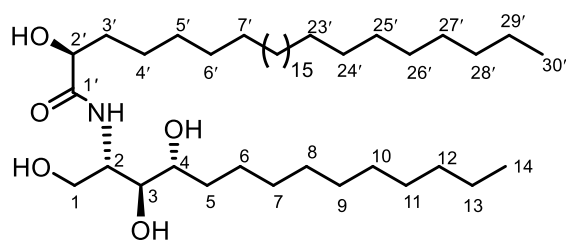


Table 24: ^1H (500 MHz) and ^{13}C (125 MHz) NMR data of rothmanniamide in pyridine- d_5

Position	$\delta^{13}\text{C}$	$\delta^1\text{H}$ (m, J in Hz)
Long chain base		
1a	61.7 (CH ₂)	4.52 (1H, dd, 4.2, 10.6)
1b		4.43 (1H, dd, 4.9, 10.6)
2	52.7 (CH)	5.12 (1H, m)
3	76.6 (CH)	4.36 (1H, m)
4	72.7 (CH)	4.29 (1H, m)
5	33.9 (CH ₂)	2.23 (1H, m), 1.94 (1H, m)
6	25.6 (CH ₂)	1.70 (1H, m), 1.77 (1H, m)
7-13 (CH ₂ groups)	22.7-31.8 (CH ₂)	1.30-1.24 (br s)
14	14.0 (CH ₃)	0.85 (3H, t, 6.8)
NH	-	8.59 (1H, d, 9.0)
1-OH	-	6.71 (1H, d, 4.9)
3-OH	-	6.71 (1H, d, 4.9)
4-OH	-	6.23 (1H, br s)
N-acyl moiety		
1'	174.9 (C)	-
2'	72.2 (CH)	4.63 (1H, brd, 3.6)
3'	35.4 (CH ₂)	2.23 (1H, m), 2.05 (1H, m)
4'	26.4 (CH ₂)	1.70 (1H, m), 1.94 (1H, m)
5'-29' (CH ₂ groups)	22.7-31.8 (CH ₂)	1.30-1.24 (br s)
14, 30'	14.0 (CH ₃)	0.85 (3H, t, 6.8)
2'-OH	-	7.64 (1H, d, 4.4)

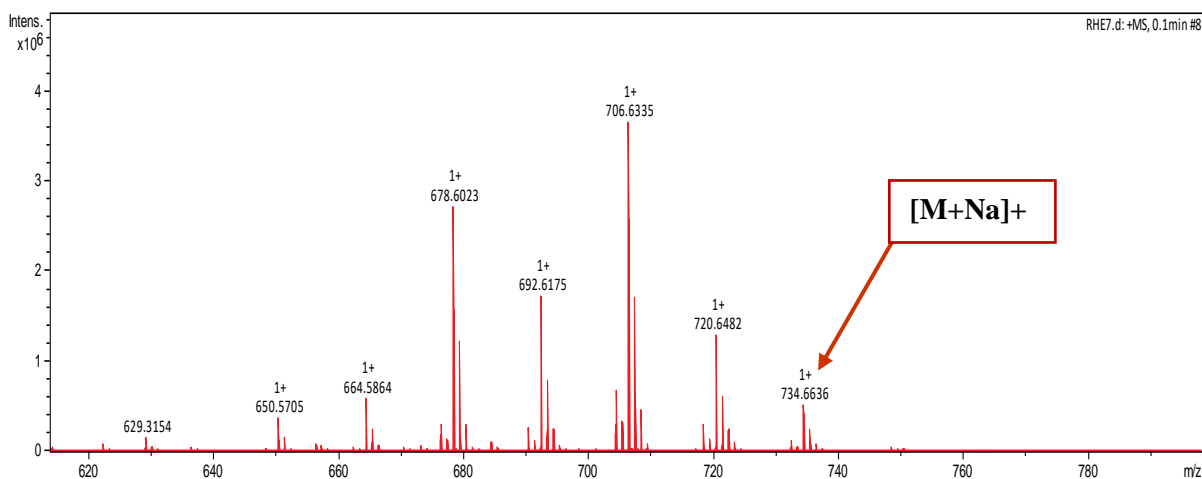


Figure 10a: HRESI mass spectrum of RHE7

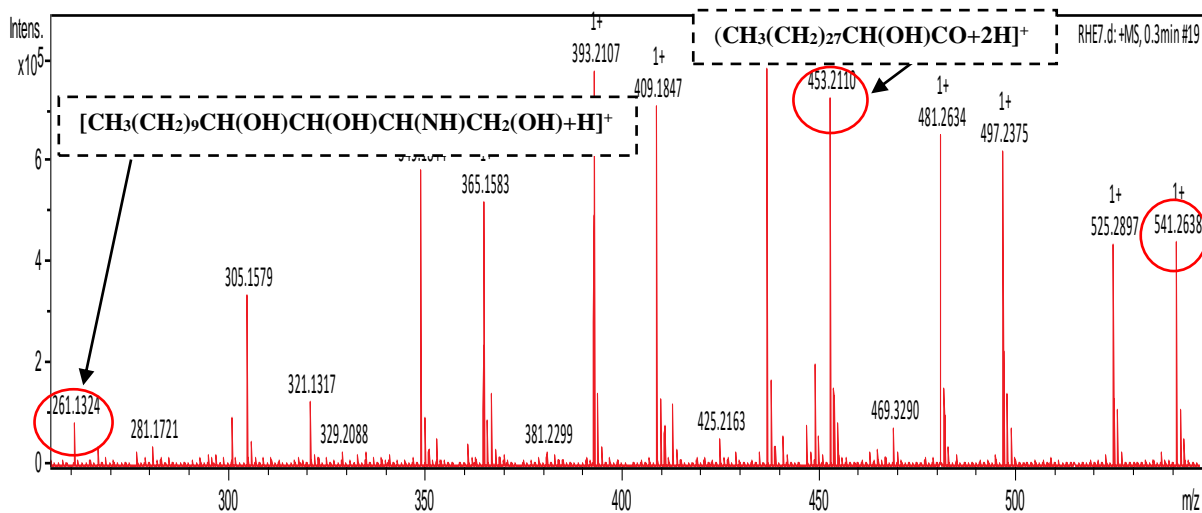


Figure 10b: ESI mass fragments of RHE7

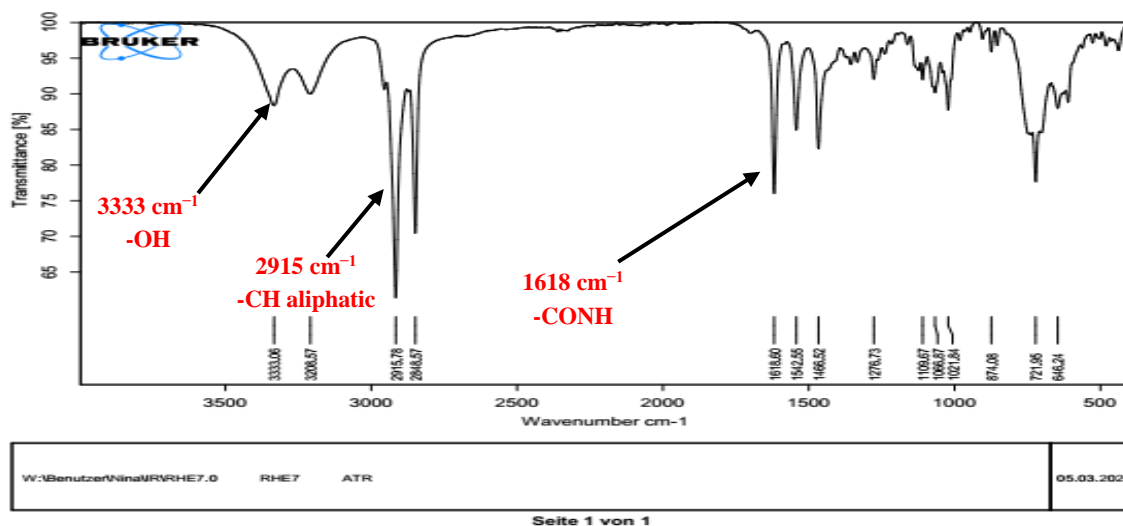


Figure 11: IR spectrum of RHE7

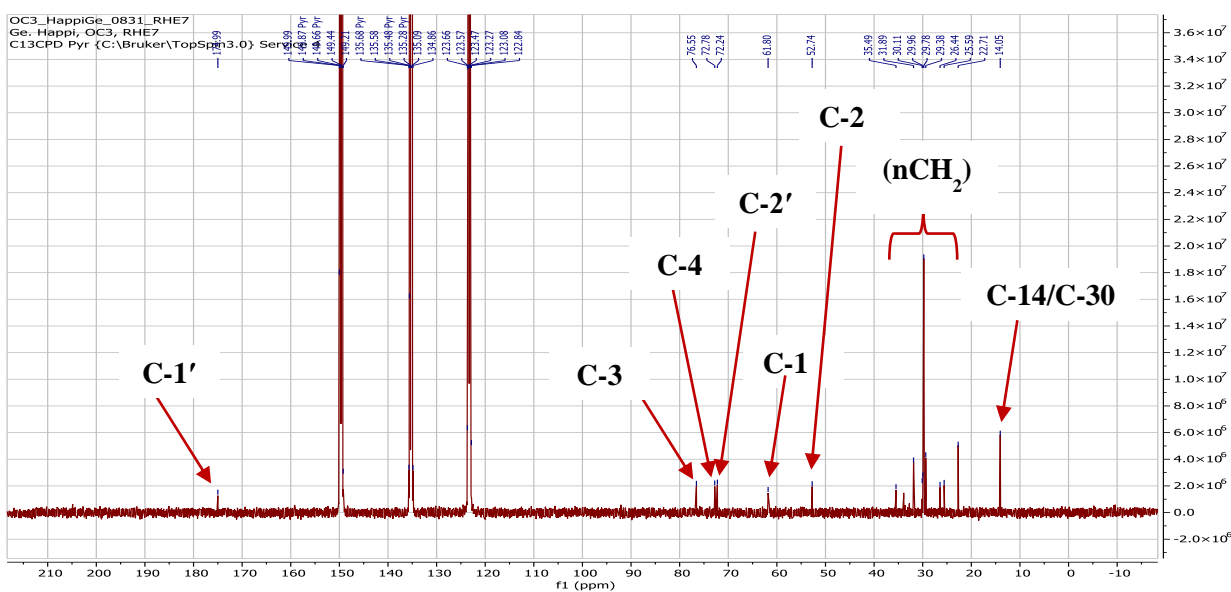


Figure 12: ^{13}C NMR spectrum of RHE7 (pyridine- d_5 , 125 MHz)

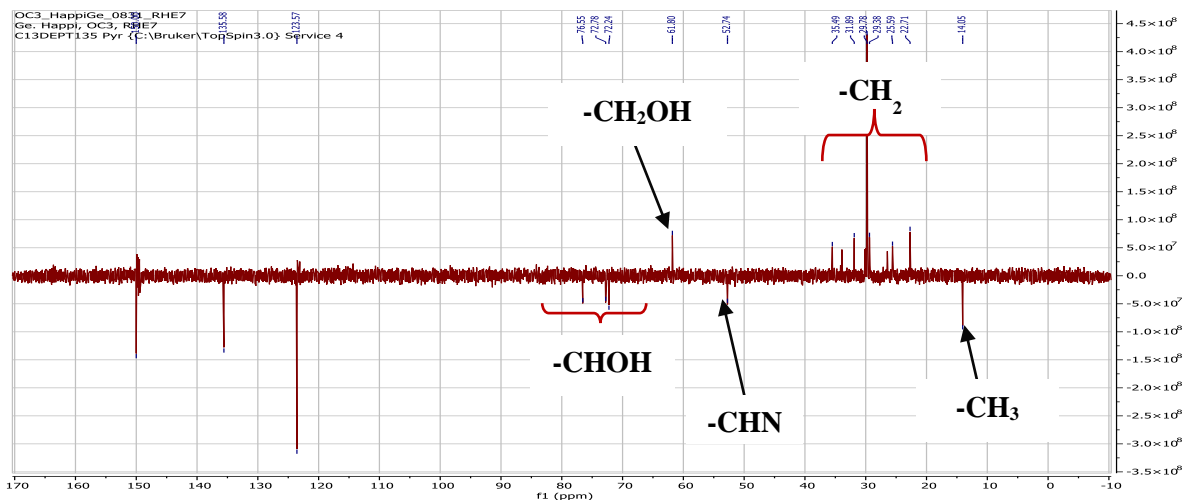


Figure 13: DEPT spectrum of RHE7

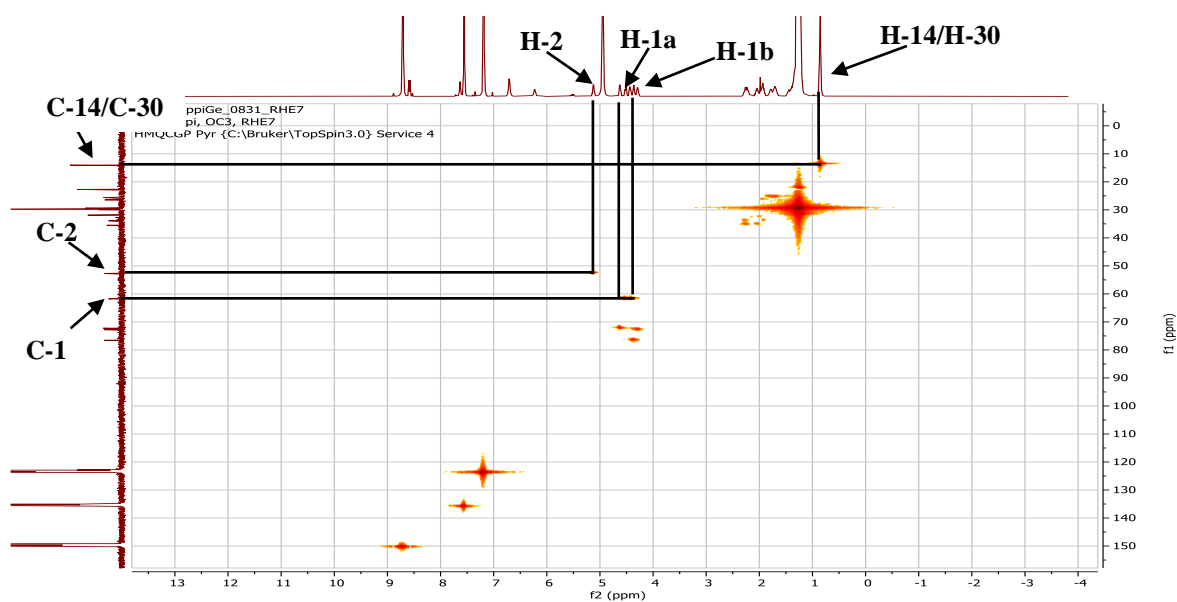


Figure 14: HMQC spectrum of RHE7

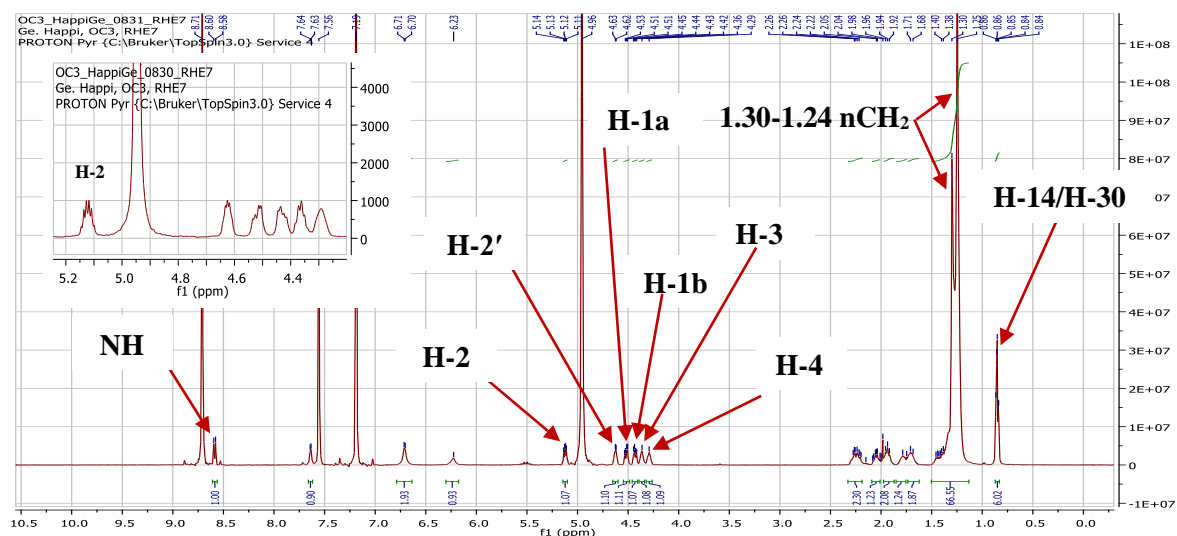


Figure 15: ^1H NMR of RHE7 (pyridine- d_5 , 500 MHz)

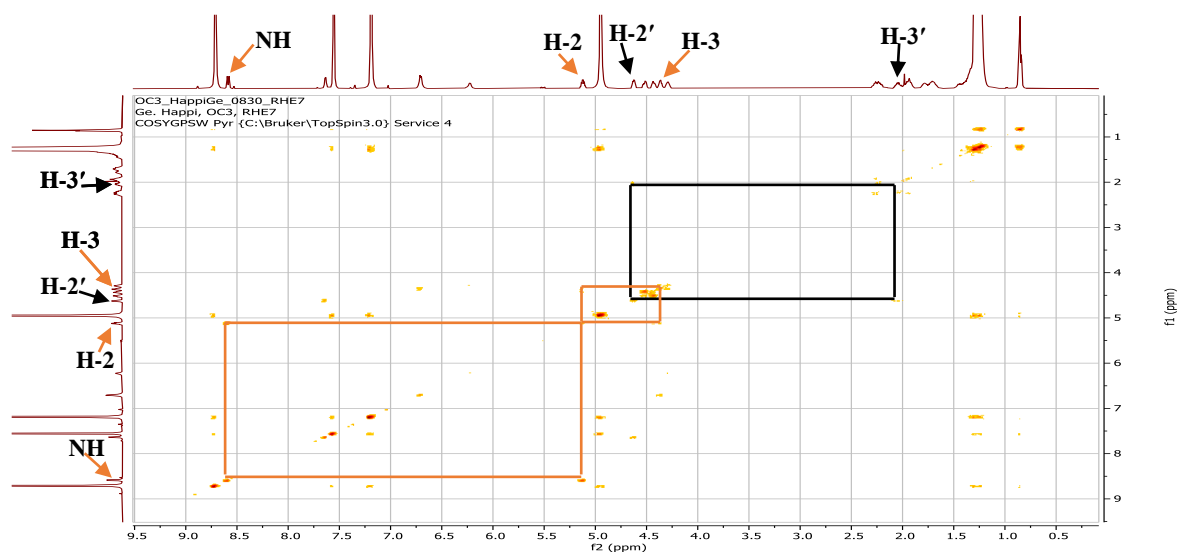


Figure 16: COSY spectrum of RHE7

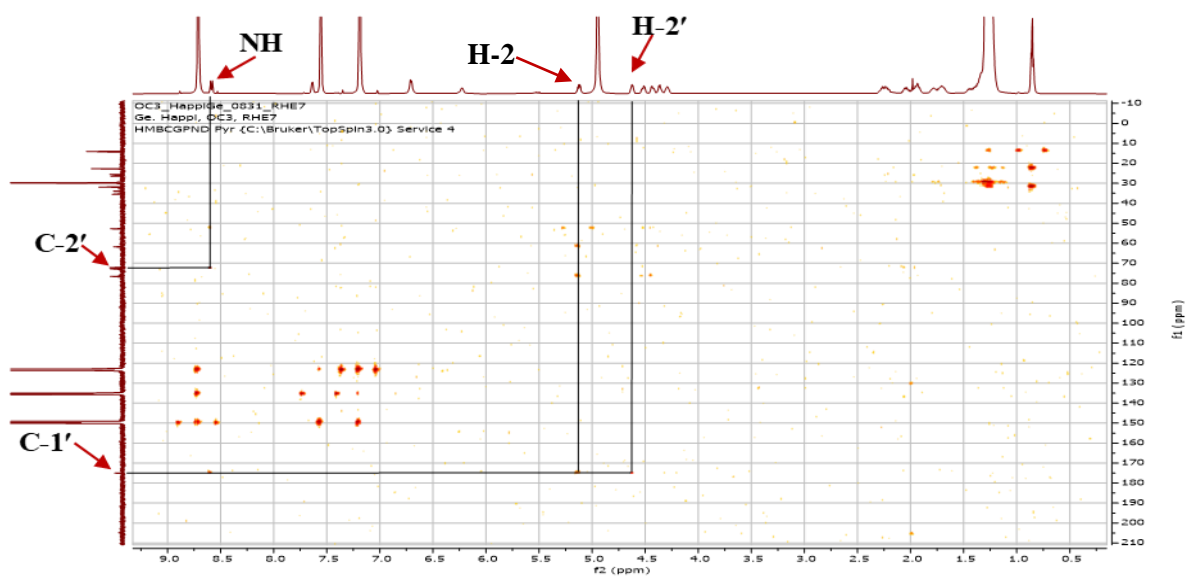


Figure 17: HMBC spectrum of RHE7

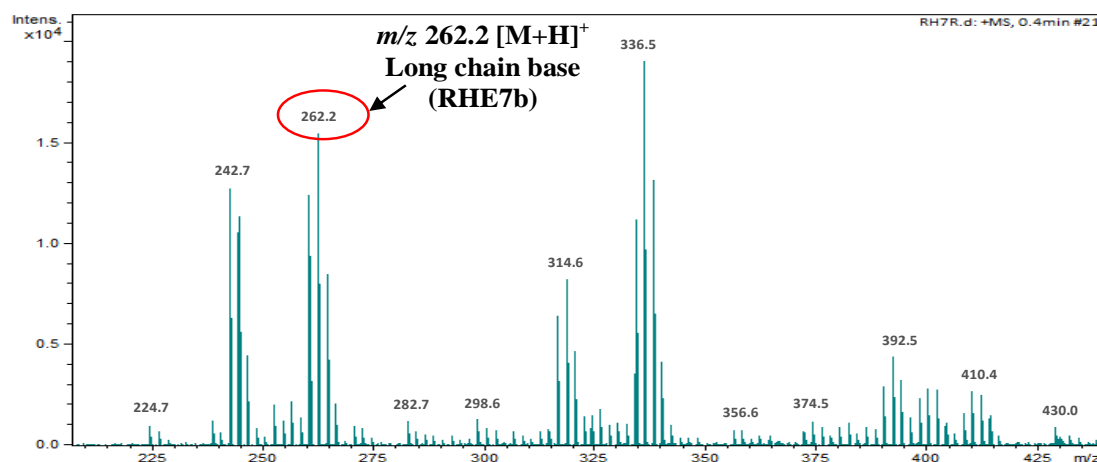


Figure 18: ESI mass spectrum of long-chain base of RHE7

II.1.5.2. Phenolic derivatives

II.1.5.2.1. Structural elucidation of compound RHE3

RHE3 was isolated as a white powder in *n*-hexane/EtOAc (80:20). It is soluble in pyridine and give a blue coloration to the ferric chloride test characteristic of phenolic compounds.

Its molecular formula $C_{26}H_{42}O_3$ was deduced from the HRESIMS spectrum (Figure 19), which showed the sodium adduct peak $[M+Na]^+$ at m/z 425.3028 (calcd. for $C_{26}H_{42}O_3Na$, 425.3032) implying six degrees of unsaturation.

Its 1H NMR spectrum (Figure 20) exhibited characteristic resonances of:

- a *trans* 4-hydroxy cinnamoyl moiety at δ_H 7.62 (2H, d, $J = 8.1$ Hz, H-2, H-6), 7.16 (2H, d, $J = 8.1$ Hz, H-3, H-5), 8.01 (1H, d, $J = 15.9$ Hz, H-1') and δ_H 6.67 (1H, d, $J = 15.9$ Hz, H-2') (Kuo *et al.*, 2002);
- signals of a heptadecyloxy moiety at δ_H 4.30 (2H, t, $J = 6.6$ Hz, H-1''), 1.68-1.28 (brs, H-2''-H-16'', $15CH_2$) and δ_H 0.85 (3H, t, $J = 6.1$ Hz, H-17'') (Chang *et al.*, 2001; Kuo *et al.*, 2002).

Its ^{13}C NMR spectrum (Figure 21) displayed signals for 26 carbons which were sorted by HMQC (Figure 22) technique into:

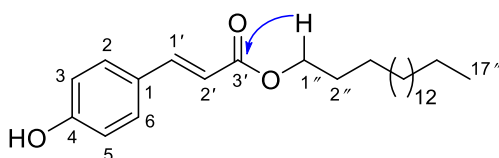
- three quaternary carbons among which the carbon of a carbonyl group of an ester at δ_C 167.2 (C-3'), an oxygenated aromatic ring carbon at δ_C 161.2 (C-4) and an other aromatic ring carbon at δ_C 125.9 (C-1);
- six methine group carbons among which two olefinic carbons at δ_C 144.8 (C-1') and δ_C 115.0 (C-2') and four aromatic ring carbons at δ_C 130.4 (C-2, C-6) and δ_C 116.2 (C-3, C-5);

- sixteen methylene groups among which one oxymethylene at δ_C 64.2 (C-1'') and others belonging to the alkyl long chain between δ_C 31.8-22.6 (C-2''-C-16'');
- one methyl group at δ_C 14.0 (C-17'').

The ^1H - ^1H COSY spectrum (Figure 23) showed correlations between protons:

- H-2/H-6 (δ_H 7.62) and H-3/H-5 (δ_H 7.16); H-1' (δ_H 8.01) and H-2' (δ_H 6.67) of the *trans* 4-hydroxy cinnamoyl moiety;
- H-1'' (δ_H 4.30) and H-2'' of the long chain.

All these data clearly indicate that RHE3 is an ester of *trans* cinnamic acid and heptadecyl-1-ol. This was confirmed by the correlation observed on its HMBC spectrum (Scheme 13, Figure 24) between the oxymethylene proton of the heptadecyloxy moiety at δ_H 4.30 (H-1'') and the carbonyl of the ester C-3' (δ_C 167.2).



Scheme 13: Key HMBC correlation of RHE3

From the above data, RHE3 was concluded to be *n*-heptadecyl-4-hydroxy-*trans*-cinnamate (**129**), previously identified by gas chromatography coupled to mass spectrometry in the leaves and roots of *Typha domingensis* Pers. and *T. latifolia* L. (Typhaceae) (He *et al.*, 2015). Herein, this secondary metabolite is isolated for the first time from natural source.

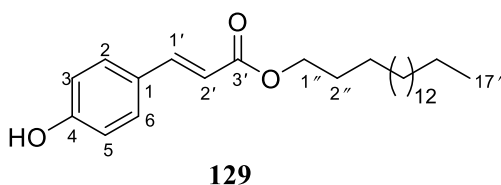


Table 25: ^1H (500 MHz) and ^{13}C (125 MHz) NMR data of *n*-heptadecyl-4-hydroxy-*trans*-cinnamate in pyridine-*d*₅

Position	$\delta^{13}\text{C}$	$\delta^1\text{H}$ (m, <i>J</i> in Hz)
1	125.9 (C)	-
2/6	130.4 (CH)	7.62 (2H, d, 8.1)
3/5	116.2 (CH)	7.16 (2H, d, 8.1)
4	161.2 (C)	-
1'	144.8 (CH)	8.01 (1H, d, 15.9)
2'	115.0 (CH)	6.67 (1H, d, 15.9)
3'	167.2 (C)	-
1''	64.2 (CH ₂)	4.30 (2H, t, 6.6)
2''-16''	31.8-22.6 (CH ₂)	1.68-1.28 (brs)
17''	14.0 (CH ₃)	0.85 (3H, t, 6.1)

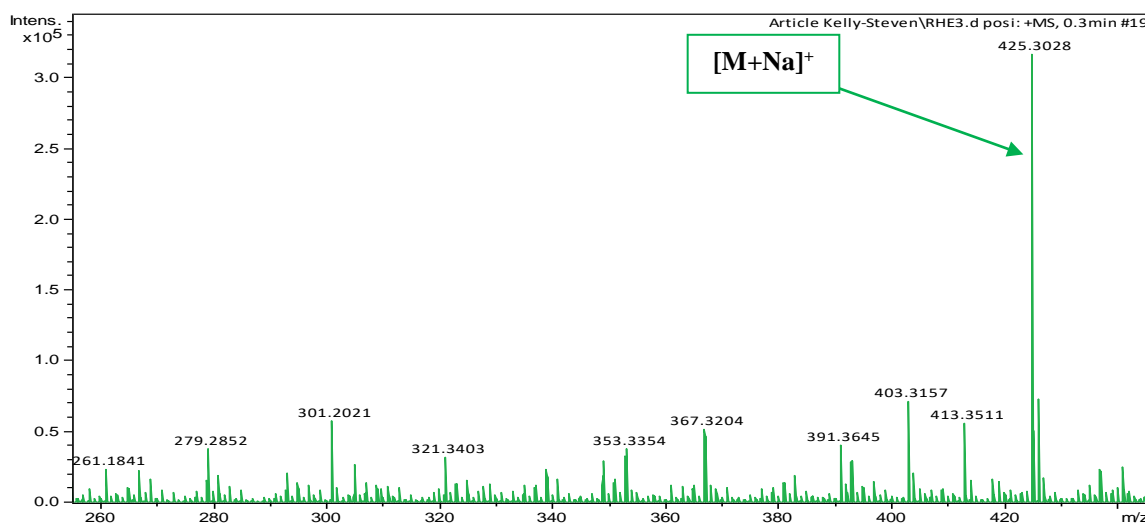


Figure 19: HRESI mass spectrum of RHE3

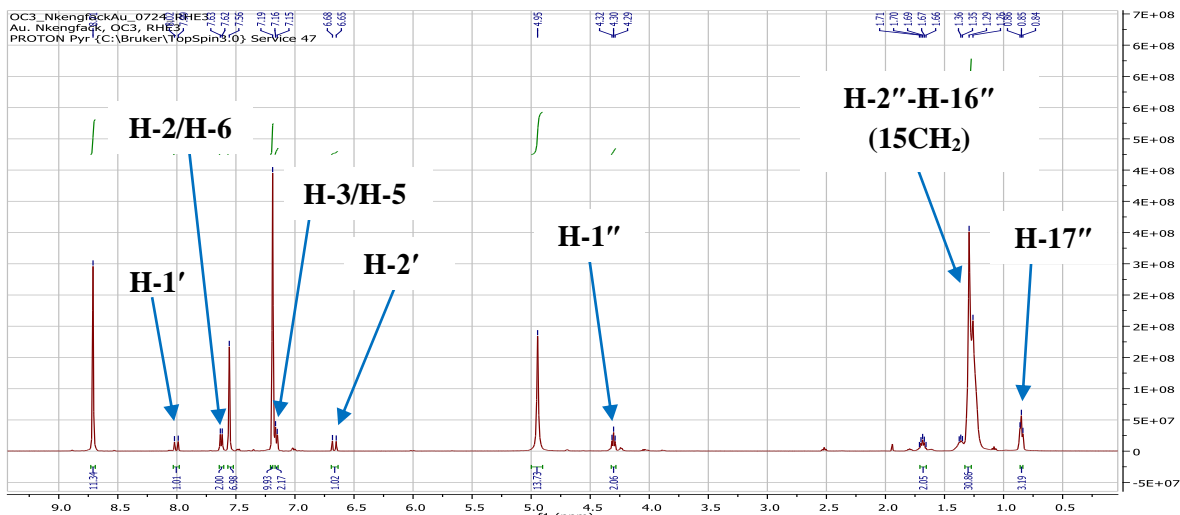


Figure 20: ^1H NMR spectrum (pyridine- d_5 , 500 MHz) of RHE3

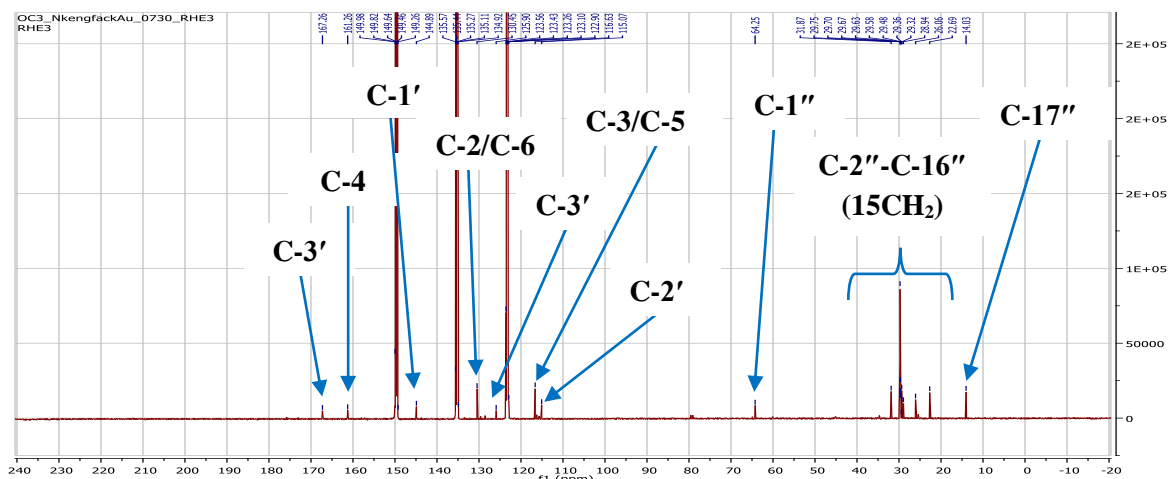


Figure 21: ^{13}C NMR spectrum (Pyridine- d_5 , 125 MHz) of RHE3

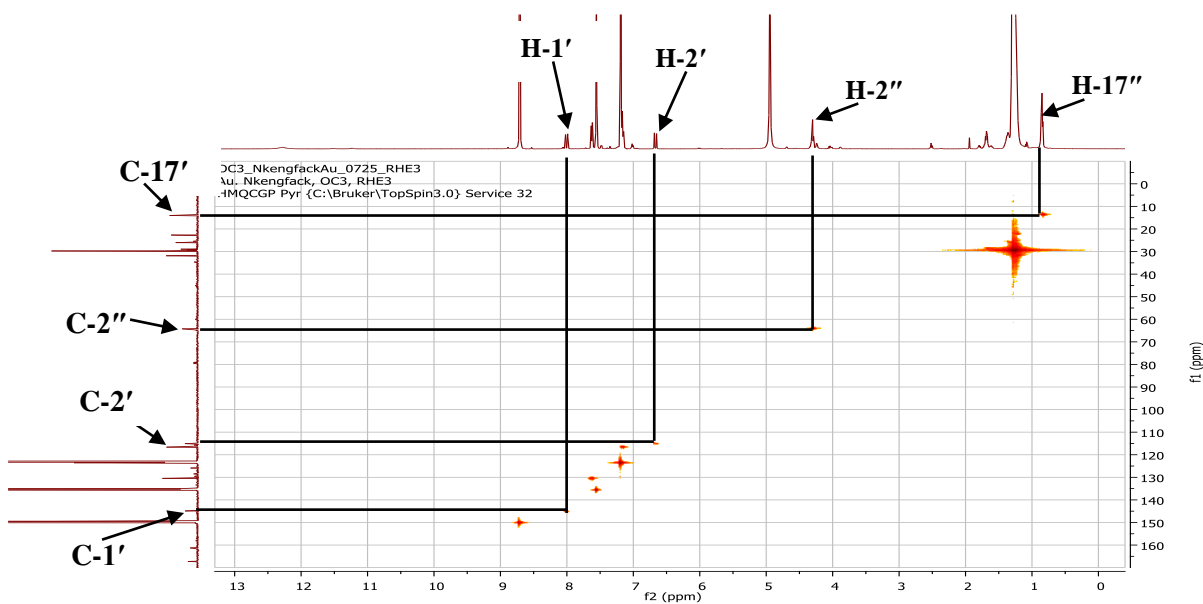


Figure 22: HMQC spectrum of RHE3

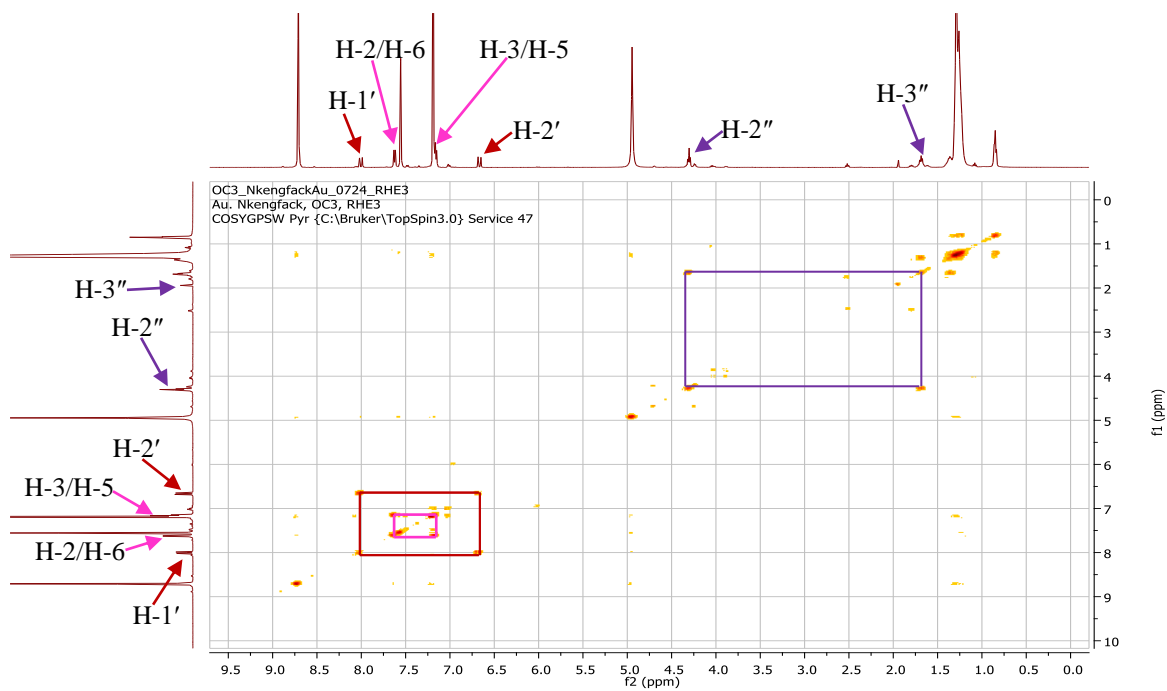


Figure 23: COSY spectrum of compound RHE3

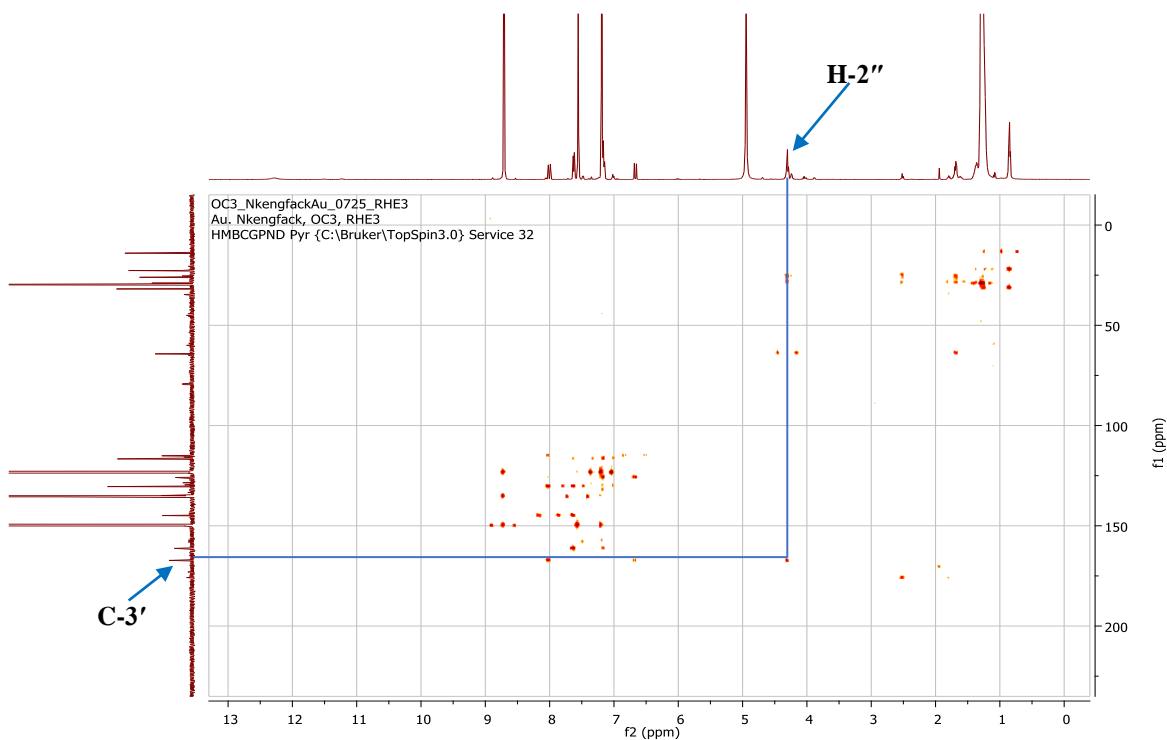


Figure 24: HMBC spectrum of RHE3

II.1.5.2.2. Structural identification of compound WN14

WN14 was obtained as yellow needles in *n*-hexane/CH₂Cl₂ (30:70). It is soluble in dichloromethane and reacted positively to Bornträger test, characteristic of anthraquinones and quinones.

Its molecular formula C₈H₈O₄ was deduced from the HRESIMS spectrum (Figure 25) which showed the sodium adduct peak [2M+Na]⁺ at *m/z* 359.0788 (calcd. for C₁₆H₁₆O₈Na, 359.0743), implying five degrees of unsaturation.

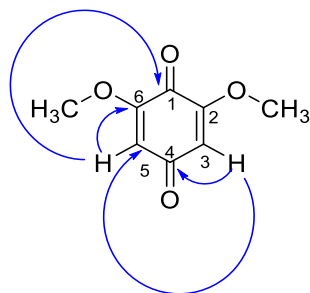
Its ¹H NMR spectrum (Figure 26) showed resonances of:

- methoxy groups at δ_H 3.80 (6H, s);
- olefinic protons at δ_H 5.83 (2H, s, H-3/H-5).

Its ¹³C NMR spectrum (Figure 27) exhibited five carbon signals, which were sorted by DEPT (Figure 28) and HMQC (Figure 29) techniques into:

- three quaternary carbons including two benzoquinone carbonyl groups at δ_C 186.8 (C-4) and δ_C 177.1 (C-1), and the other carbons at δ_C 157.3 (C-2/C-6);
- two olefinic carbons at δ_C 107.4 (C-3/C-5);
- two methoxy groups at δ_C 56.5 (OCH₃).

The position of the carbonyl groups was deduced from the correlations observed on the HMBC (Figure 39) spectrum between protons H-3/H-5 (δ_H 5.83) and carbons C-4 (δ_C 186.8), C-1 (δ_C 177.1), C-2/C-6 (δ_C 157.3) and C-3/C-5 (δ_C 107.4).



Scheme 14: HMBC correlations of WN14

All these data of WN14 were in agreement with those described in the literature for 2,6-dimethoxybenzoquinone (**130**), previously isolated from *Rauwolfia vomitoria* by Kupchan and Mang (1960).

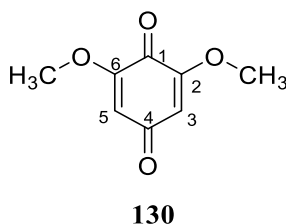


Table 26: ^1H (500 MHz) and ^{13}C (125 MHz) NMR data of WN14 in CDCl_3 compared to 2,6-dimethoxybenzoquinone [CDCl_3 , NMR ^{13}C (100 MHz), NMR ^1H (400 MHz)]

WN14			2,6-dimethoxybenzoquinone (Kupchan and Mang, 1960)	
Position	$\delta^{13}\text{C}$	$\delta^1\text{H}$ (m, J in Hz)	$\delta^{13}\text{C}$	$\delta^1\text{H}$ (m, J in Hz)
1	177.1	-	175.2	-
2, 6	157.3	-	154.5	-
3, 5	107.4	5.83 (2H, s)	106.9	5.63 (2H, s)
4	186.8	-	186.1	-
OCH_3	56.5	3.80 (6H, s)	56.3	3.92 (6H, s)

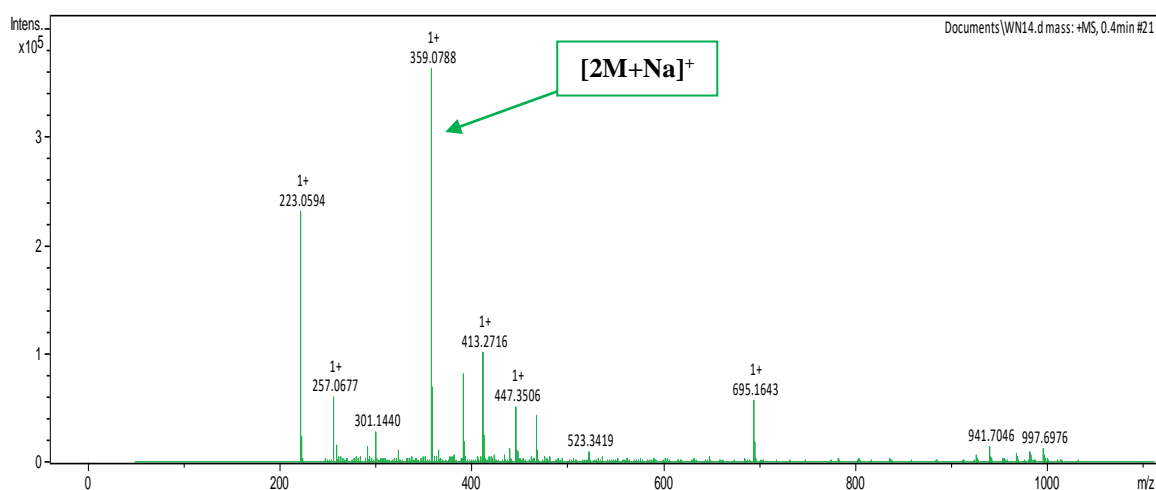


Figure 25: HRESI mass spectrum of WN14

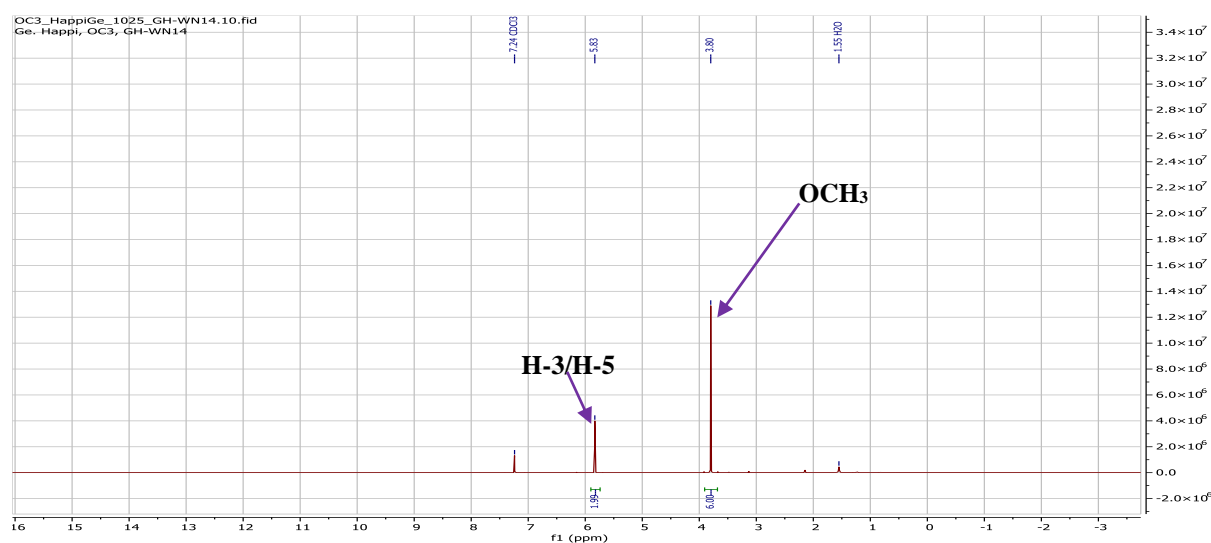


Figure 26: ^1H NMR spectrum (CDCl_3 , 500 MHz) of WN14

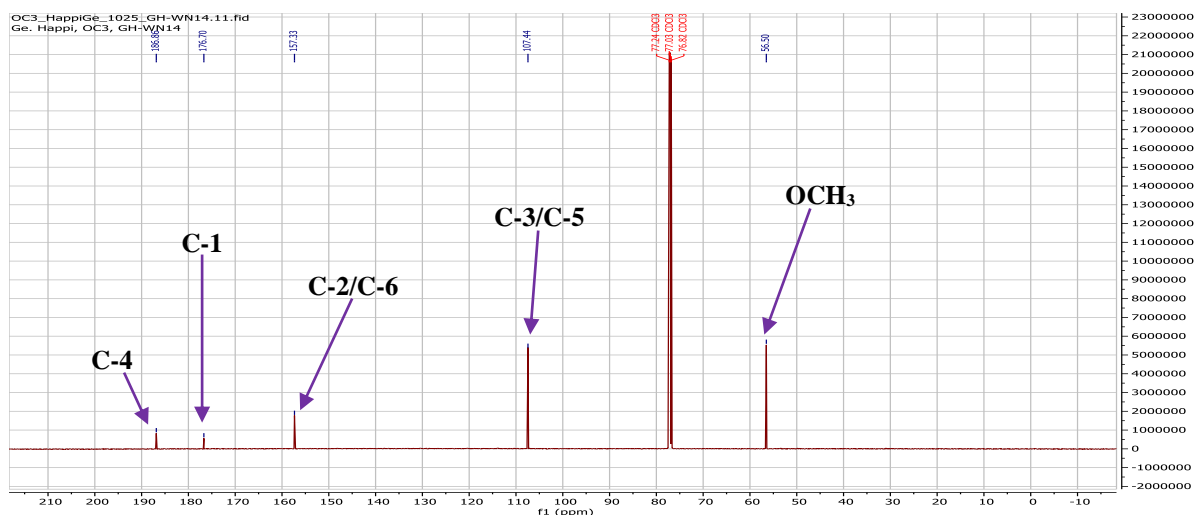


Figure 27: ^{13}C NMR spectrum (CDCl_3 , 125 MHz) of WN14

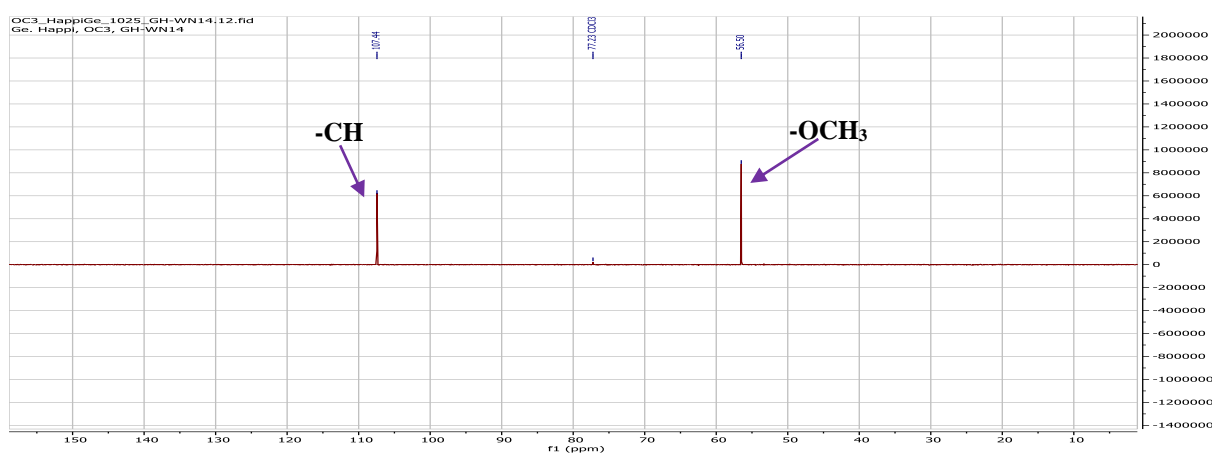


Figure 28: DEPT spectrum of WN14

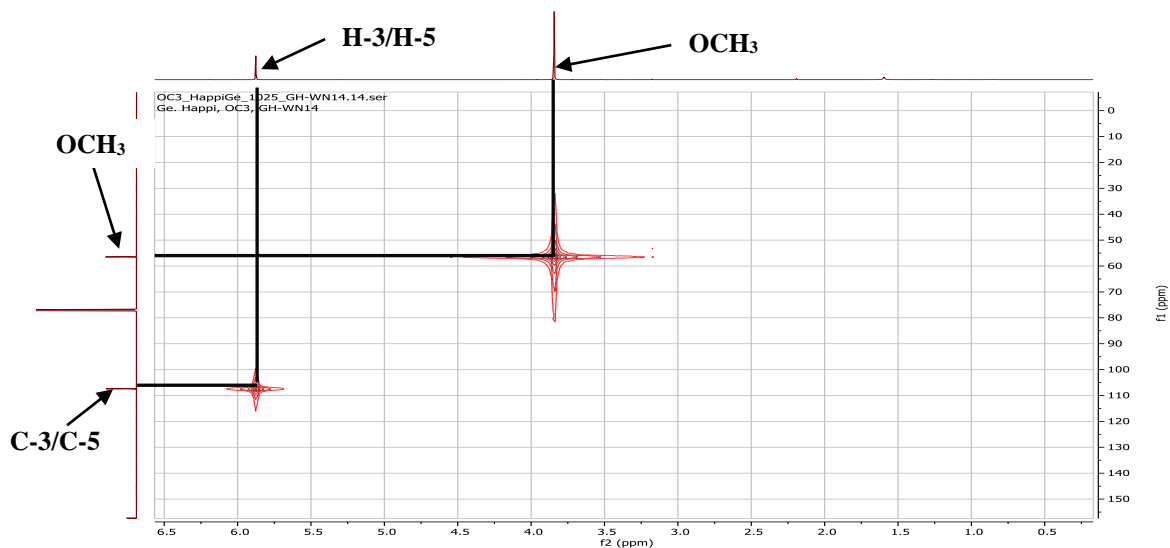


Figure 29: HMQC spectrum of WN14

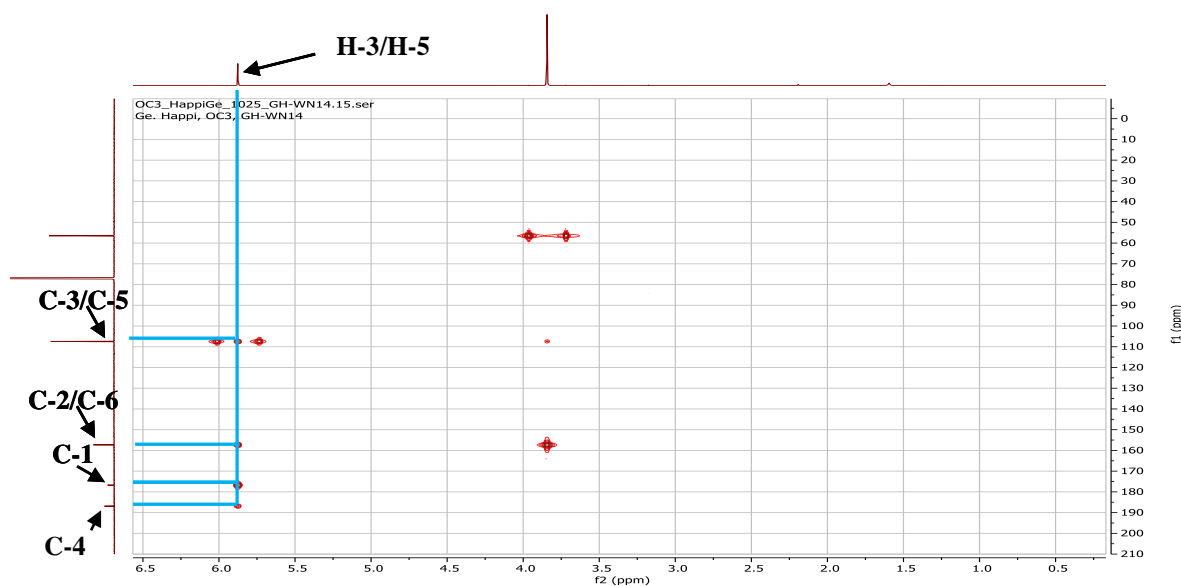


Figure 30: HMBC spectrum of WN14

II.1.5.2.3. Structural identification of compound RH20

RH20 was obtained as a yellow powder in EtOAc/MeOH (30:70). It is soluble in pyridine and reacts positively to ferric chloride test and Shinoda test, characteristic of phenolic compounds and flavonoids, respectively.

Its molecular formula $C_{21}H_{20}O_{11}$ was deduced from the HRESIMS spectrum (Figure 31) which showed the pseudomolecular ion peak $[M-H]^-$ at m/z 447.0961 (calcd. for $C_{21}H_{19}O_{11}$, 447.0927), implying twelve degrees of unsaturation.

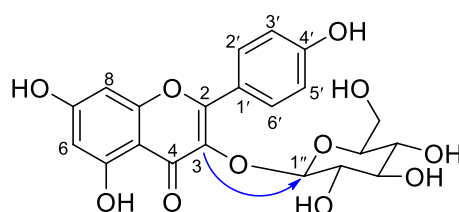
Its 1H NMR spectrum (Figure 32) displayed:

- a singlet of two aromatic protons at δ_H 6.68 (2H, d, $J = 2.2$ Hz, H-6/H-8);
- two doublets of two protons each at δ_H 8.48 (2H, d, $J = 8.8$ Hz, H-2'/H-6') and 7.15 (2H, d, $J = 8.8$ Hz, H-3'/H-5') attributable to protons of an AA'BB' system, characteristic of a para-substituted aromatic system (Wei *et al.*, 2011);
- resonance of a chelated hydroxyl group at δ_H 13.23 (1H, OH);
- signals of protons of a sugar moiety including the anomeric proton at δ_H 6.19 (1H, d, 7.8 Hz, H-1'') and the other protons at δ_H 4.78 (1H, dd, 7.8, 3.1 Hz, H-2''), 4.27 (1H, m, H-3''), 4.59 (1H, m, H-4''), 4.13 (1H, t, 5.8 Hz, H-5''), 4.24 (1H, m, H-6a'') and 4.39 (1H, dd, 10.8, 6.3 Hz, H-6b''). The β configuration of this sugar is due to the high value of the coupling constant of the anomeric proton ($J = 7.8$ Hz) (Agrawal, 1992).

Its ^{13}C NMR spectrum (Figure 33) exhibited carbon signals, which were sorted by HMQC (Figure 34) technique into:

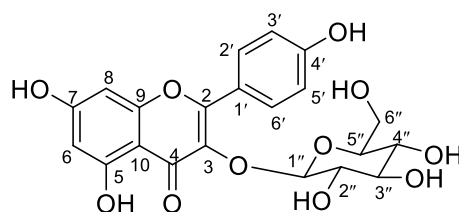
- nine quarternary carbons including the carbonyl at δ_C 181.2 (C-4) and carbon at δ_C 134.8 (C-3), characteristics of flavonol (Markham, 1982). The other carbons at δ_C 105.0 (C-10), 122.8 (C-1'), 157.2 (C-2/C-9), 161.0 (C-4'), 162.5 (C-5), 165.5 (C-7);
- six methine groups at δ_C 94.2 (C-8), 99.6 (C-8), 115.9 (C-3'/C-5') and 131.5 (C-2'/C-6');
- carbons of the sugar moiety at δ_C 104.5 (C-1''), 73.1 (C-2''), 75.2 (C-3''), 69.5 (C-4''), 77.2 (C-5'') and 61.8 (C-1''). A comparative analysis of chemical shifts and coupling constants with data from the literature (Agrawal, 1992) contributed to identify this sugar as β -D-glucopyranoside.

The fixation of this sugar on the aglycone was done using the correlation observed in the HMBC spectrum (Figure 35) between proton H-1'' (δ_H 6.19) and carbon C-3 (δ_C 134.8).



Scheme 15: Key HMBC correlation of RH20

All these data, compared with those described in the literature, were concluded to be that of kaempferol 3-*O*- β -D-glucopyranoside (astragalins) (**131**), previously isolated from *Flaveria bidentis* by Wei *et al.* (2011).



131

Table 27: ^1H (600 MHz) and ^{13}C (150 MHz) NMR data of RH20 in pyridine- d_5 compared to astragalins [DMSO- d_6 , NMR ^{13}C (150 MHz) and DMSO- d_6 +D $_2$ O, NMR ^1H (600 MHz)]

RH20			Astragalins (Wei <i>et al.</i> , 2011)	
Position	$\delta^{13}\text{C}$	$\delta^1\text{H}$ (m, J in Hz)	$\delta^{13}\text{C}$	$\delta^1\text{H}$
1	-	-	-	-
2	157.2	-	156.7	-
3	134.8	-	133.6	-
4	181.2	-	177.9	-
5	162.5	-	161.6	-
6	99.6	6.68 (1H, d, 2.2)	99.1	6.30 (1H, d, 2.4)
7	165.3	-	164.5	-
8	94.2	6.68 (1H, d, 2.2)	94.1	6.55 (1H, d, 2.4)
9	157.2	-	156.8	-
10	105.0	-	104.4	-
1'	122.8	-	121.3	-
2', 6'	131.5	8.48 (2H, d, 8.8)	131.3	8.16 (2H, d, 9.0)
3', 5'	115.9	7.15 (2H, d, 8.8)	115.5	6.84 (2H, d, 9.0)
4'	161.0	-	160.4	-
1''	104.5	6.19 (1H, d, 7.8)	101.3	5.29 (1H, d, 7.8)
2''	73.1	4.78 (1H, dd, 7.8, 3.1)	74.6	
3''	75.2	4.27 (1H, m)	76.8	
4''	69.5	4.59 (1H, m)	70.3	3.27-3.67 (m, 5H)
5''	77.2	4.13 (1H, t, 5.8)	77.9	
6''	61.6	4.24 (1H, m); 4.39 (1H, dd, 10.8, 6.3)	61.3	

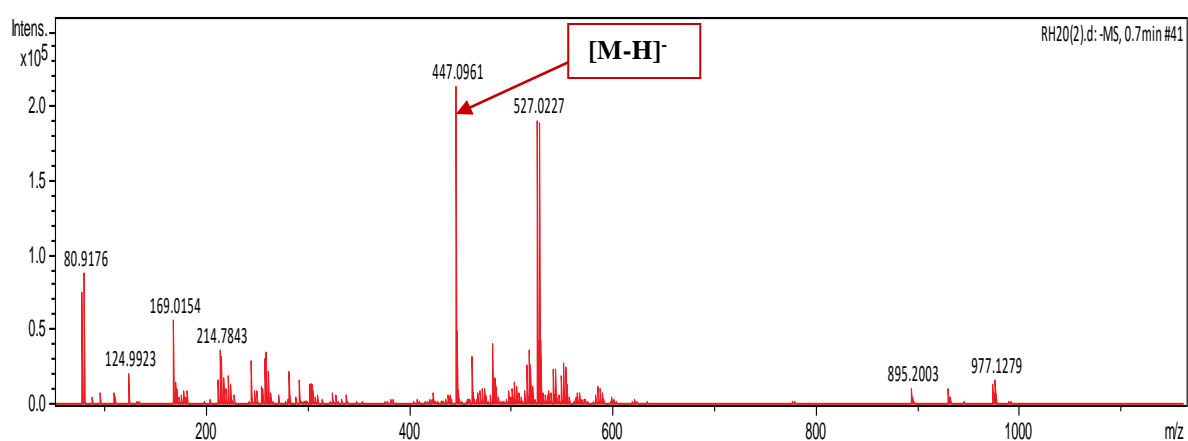


Figure 31: HRESI mass spectrum of RH20

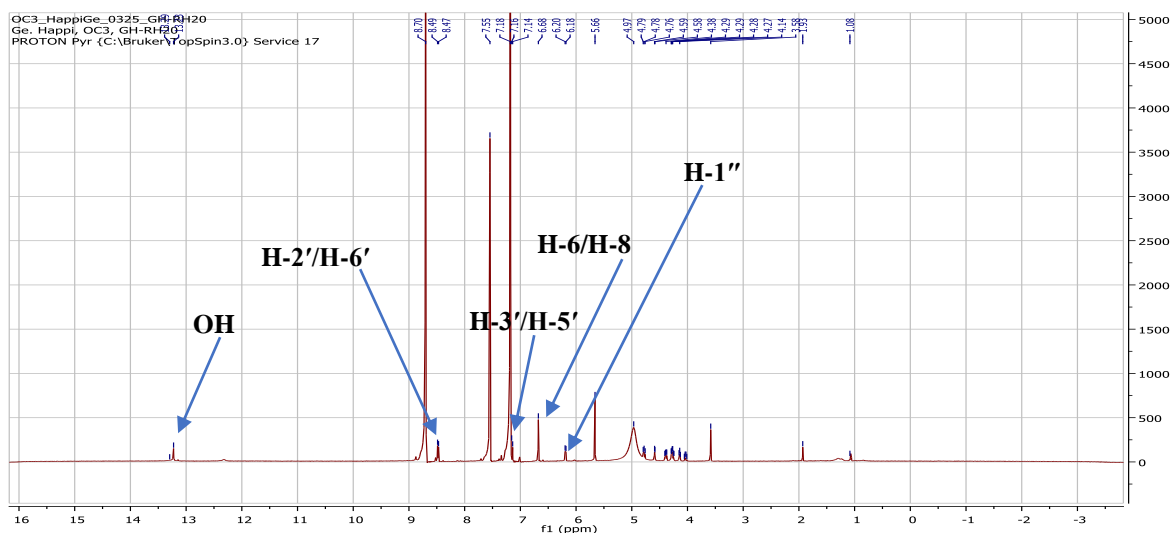


Figure 32: ^1H NMR spectrum (pyridine- d_5 , 600 MHz) of RH20

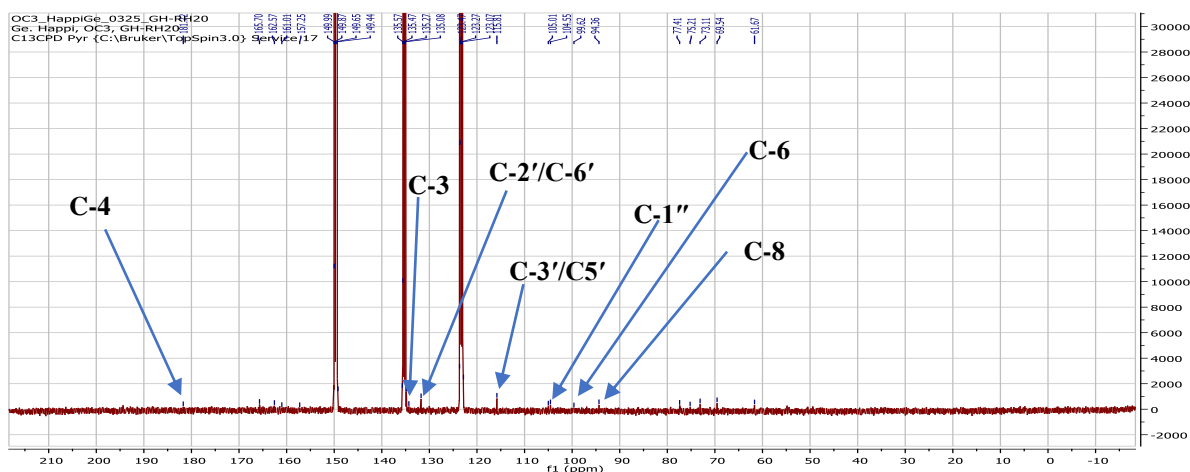


Figure 33: ^{13}C NMR spectrum (pyridine- d_5 , 150 MHz) of RH20

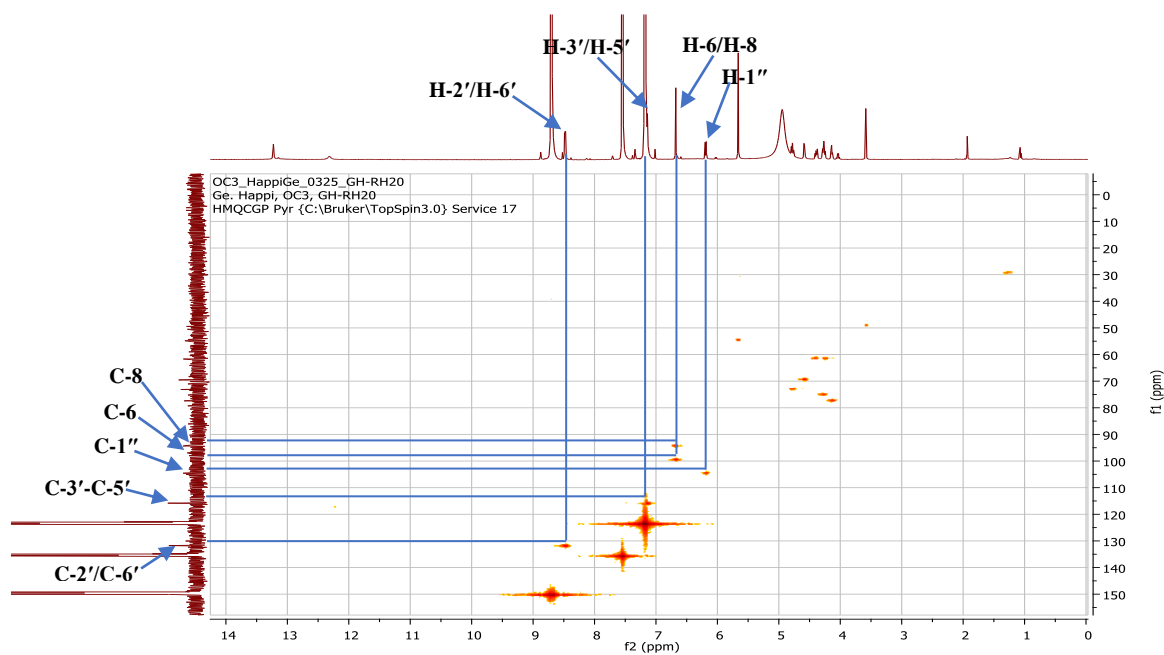


Figure 34: HMQC spectrum of RH20

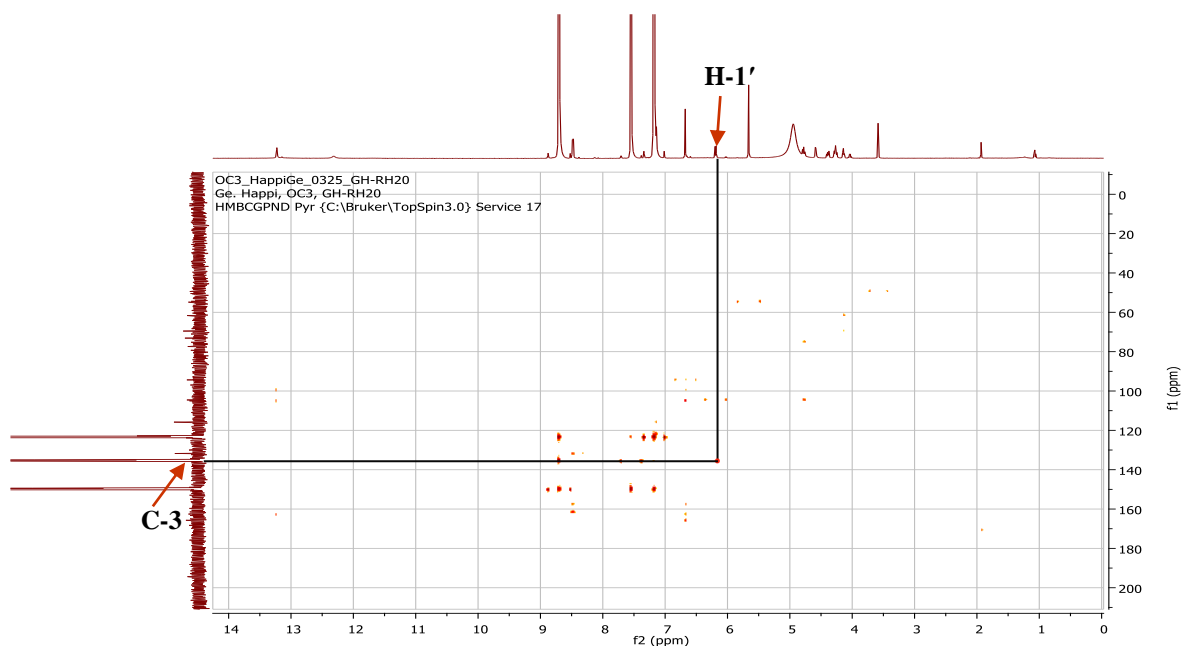


Figure 35: HMBC spectrum of RH20

II.1.5.2.4. Structural identification of compound RHE1

RHE1 was obtained as a yellow crystal in *n*-hexane/CH₂Cl₂ (80:20). It is soluble in dichloromethane and reacts positively to ferric chloride test, characteristic of phenolic compounds.

Its molecular formula C₁₆H₁₄O₅ was deduced from the HRESIMS spectrum (Figure 36) which showed the pseudomolecular ion peak [M+H]⁺ at *m/z* 287.0938 (calcd. for C₁₆H₁₅O₅, 287.0919), implying ten degrees of unsaturation.

Its ¹H NMR spectrum (Figure 37) displayed:

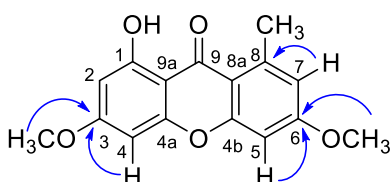
- one singlet at δ_H 2.78 (3H, s, 8-CH₃), attributable to a methyl attached to a Csp²-hybridized carbon;
- two singlets at δ_H 3.80 (3H, s, 3-OCH₃) and 3.83 (3H, s, 6-OCH₃), attributable to two methoxy groups;
- four doublets at δ_H 6.24 (1H, d, *J* = 2.3 Hz, H-2), 6.27 (1H, d, *J* = 2.3 Hz, H-4), 6.60 (1H, d, *J* = 2.2 Hz, H-7) and 6.63 (1H, d, *J* = 2.2 Hz, H-5), corresponding to two unsaturated rings (Silva and Pinto, 2005);
- a signal at δ_H 13.32 (1H, OH-1), attributable to a chelated proton.

Its ¹³C NMR spectrum (Figure 38) exhibited carbon resonances of xanthone type skeleton (Silva and Pinto, 2005), which were sorted by HMQC (Figure 39) technique into:

- nine quaternary carbons at δ_C 103.9 (C-9a), 113.1 (C-8a), 143.3 (C-8), 156.8 (C-4a), 159.5 (C-4b), 163.9 (C-1/C-6), 165.8 (C-3) including a carbonyl of 1 or 8 hydroxylated xanthone at δ_C 182.4 (C-9) (Silva and Pinto, 2005);
- four methine groups at δ_C 92.0 (C-4), 96.7 (C-2), 98.4 (C-5) and 115.4 (C-7);
- three methyl groups at δ_C 23.4 (8-CH₃), 55.6 (6-OCH₃) and 55.7 (3-OCH₃).

The position of the different substituents was determined by the correlations observed on the HMBC spectrum (Figure 40) between protons:

- H-5 (δ_H 6.63), H-7 (δ_H 6.60) and carbons C-6 (δ_C 163.9), 8-CH₃ (δ_C 23.4);
- H-2 (δ_H 6.24), H-4 (δ_H 6.27) and carbons C-3 (δ_C 165.8), C-1 (163.9);
- 3-OCH₃ (δ_H 3.80), 6-OCH₃ (δ_H 3.83) and carbons C-3 (δ_C 165.8) and C-6 (δ_C 163.9), respectively.



Scheme 16: Key HMBC correlations of RHE1

All these data, compared with those described in the literature, was in agreement with that of 1-hydroxy-3,6-dimethoxy-8-methylxanthone (lichexanthone) (**132**), previously isolated from *Cassipourea malosana* by Nishiyama *et al.* (2019).

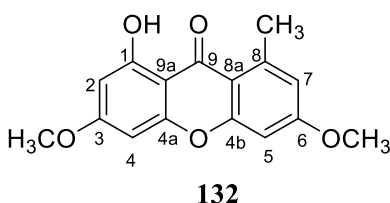


Table 28: ^1H (500 MHz) and ^{13}C (125 MHz) NMR data of RHE1 in CDCl_3 compared to lichexanthone [CDCl_3 , NMR ^{13}C (125 MHz), NMR ^1H (500 MHz)]

RHE1			Lichexanthone (Nishiyama <i>et al.</i> , 2019)	
Position	$\delta^{13}\text{C}$	$\delta^1\text{H}$ (m, J in Hz)	$\delta^{13}\text{C}$	$\delta^1\text{H}$ (m, J in Hz)
1	163.9	-	163.8	-
2	96.7	6.24 (1H, d, 2.3)	96.8	6.30 (1H, d, 2.0)
3	165.8	-	165.8	-
4	92.0	6.27 (1H, d, 2.3)	92.1	6.34 (1H, d, 2.0)
4a	156.8	-	157.0	-
4b	159.5	-	159.4	-
5	98.4	6.63 (1H, d, 2.2)	98.5	6.69 (1H, d, 2.0)
6	163.9	-	163.8	-
7	115.4	6.60 (1H, d, 2.2)	115.5	6.67 (1H, d, 2.0)
8	143.3	-	143.5	-
8a	113.1	-	113.0	-
9	182.4	-	182.4	-
9a	103.9	-	104.2	-
3-OCH ₃	55.7	3.80 (3H, s)	55.7	3.87 (3H, s)
6-OCH ₃	55.6	3.83 (3H, s)	55.7	3.89 (3H, s)
8-CH ₃	23.4	2.78 (3H, s)	23.5	2.85 (3H, s)
1-OH	-	13.32 (1H, s)	-	13.39 (1H, s)

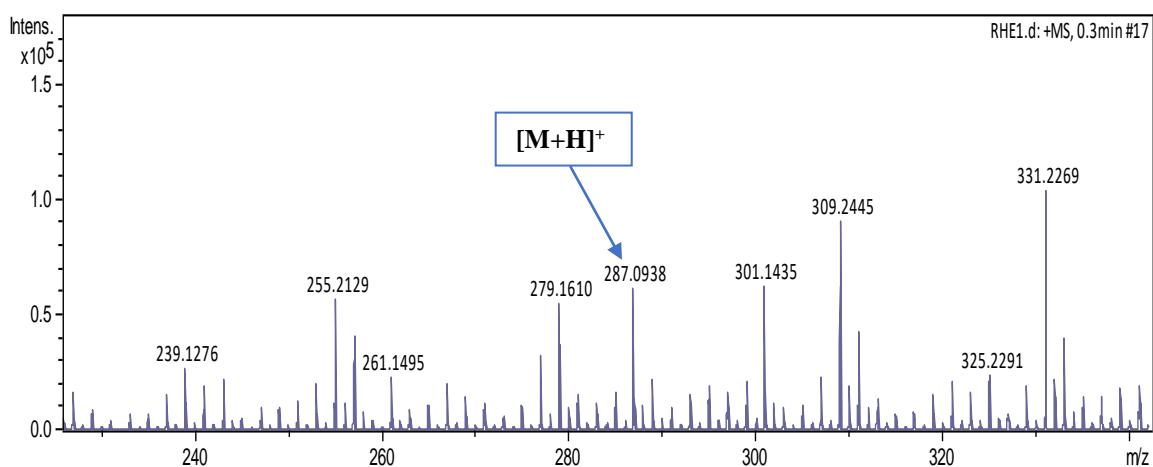


Figure 36: HRESI mass spectrum of RHE1

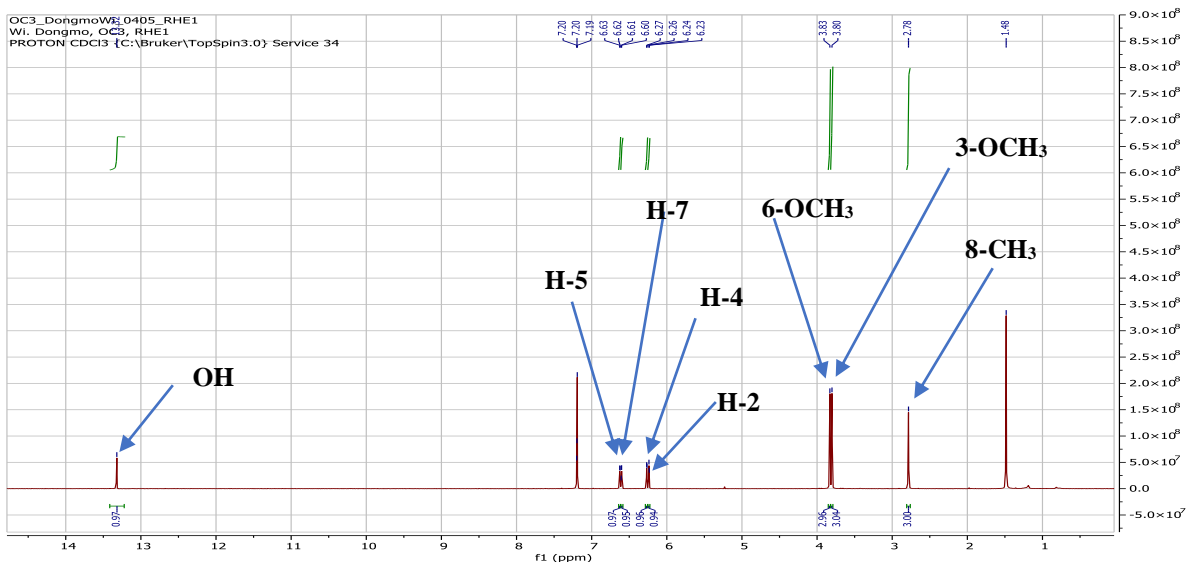


Figure 37: ^1H NMR spectrum (CDCl_3 , 500 MHz) of RHE1

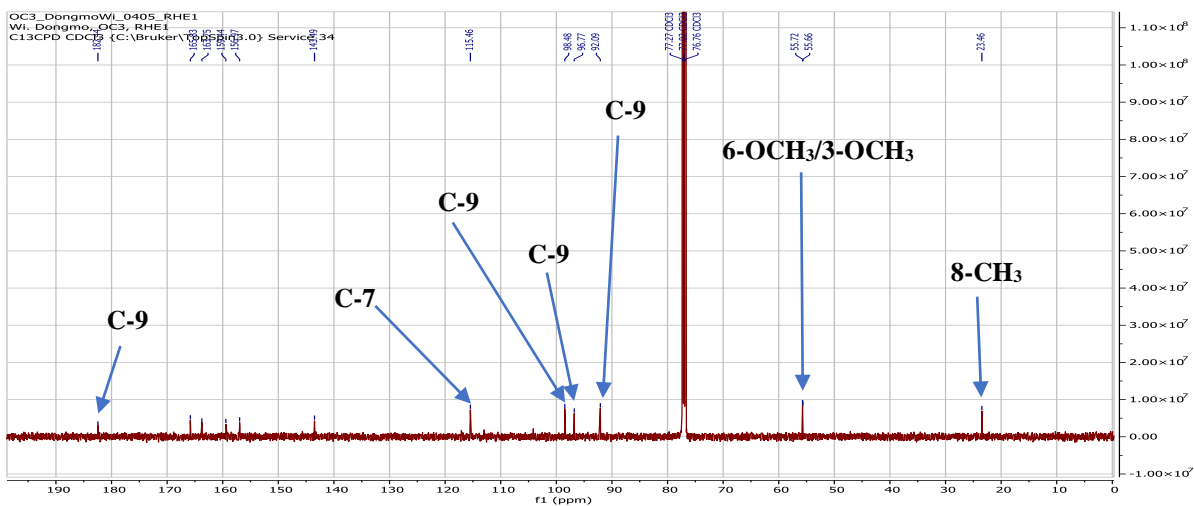


Figure 38: ^{13}C NMR spectrum (CDCl_3 , 125 MHz) of RHE1

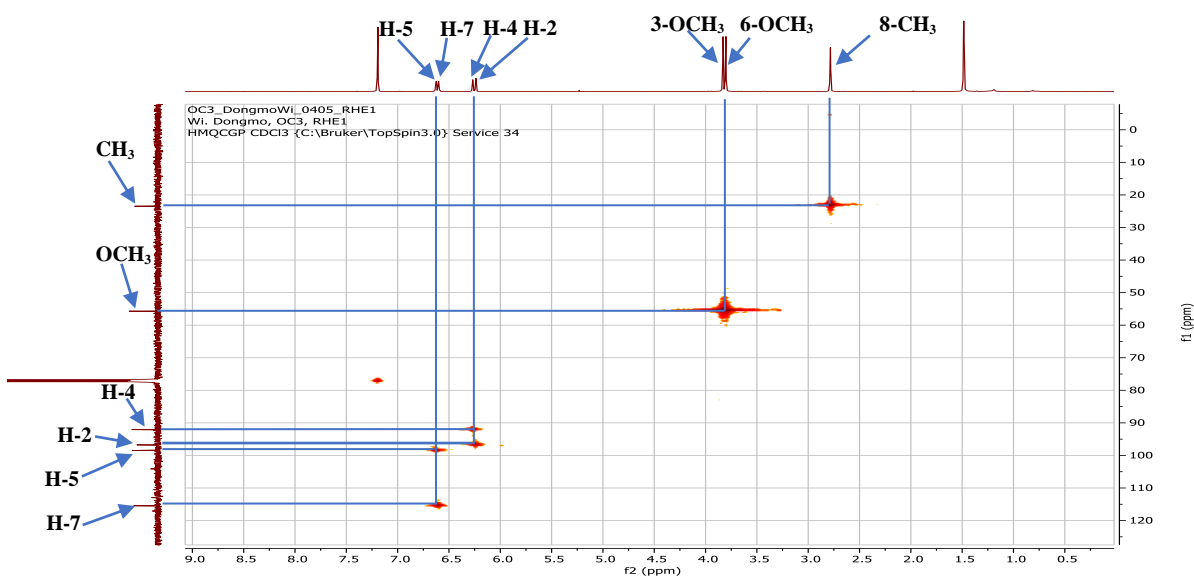


Figure 39: HMQC spectrum of RHE1

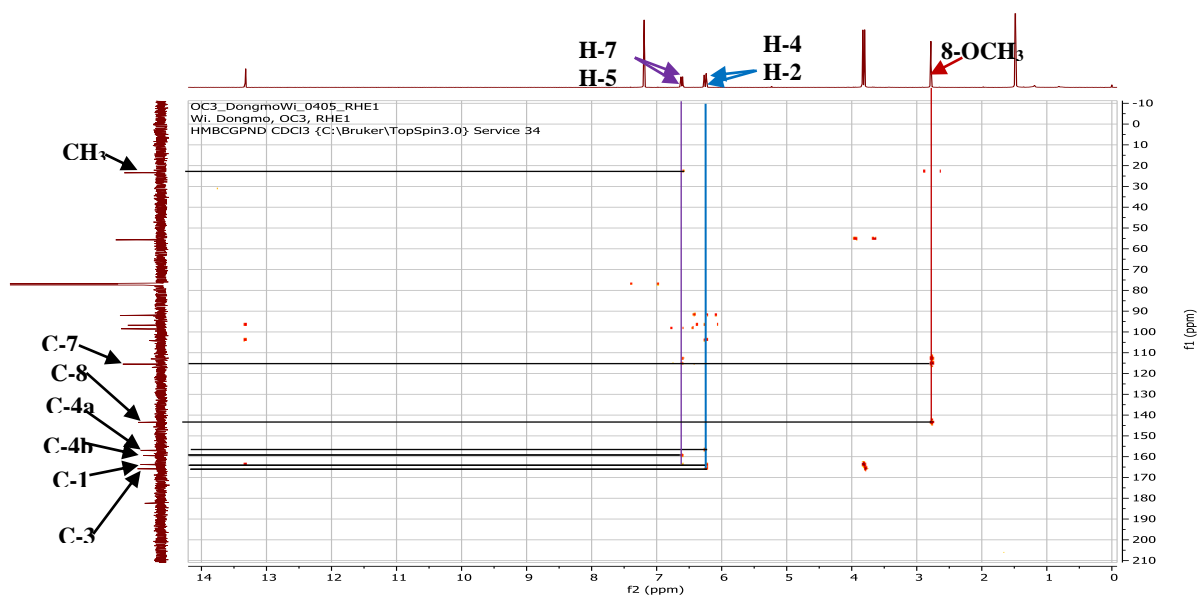


Figure 40: HMBC spectrum of RHE1

II.1.5.3. Triterpenoids

II.1.5.3.1. Structural identification of compound BLE4

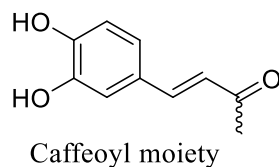
BLE4 was obtained as a white powder in *n*-hexane/EtOAc (80:20). It is soluble in dichloromethane and give a red color which turns purple to the Liebermann-Burchard test characteristic of triterpenoids.

Its molecular formula $C_{39}H_{56}O_4$ was deduced from the HRESIMS spectrum (Figure 41) which showed the sodium adduct peak $[M+Na]^+$ at m/z 611.4091 (calcd. for $C_{39}H_{56}O_4Na$, 611.4076), implying twelve degrees of unsaturation.

Its 1H NMR spectrum (Figure 42), displayed:

- eight singlets of three protons each at δ_H 0.77 (3H, s, H-27), 0.90 (3H, s, H-23), 0.94 (3H, s, H-24), 0.95 (3H, s, H-29), 0.96 (3H, s, H-30), 0.97 (3H, s, H-25), 1.04 (3H, s, H-28) and 1.11 (3H, s, H-26) which were attributed to the protons of the eight angular methyl groups of oleanane type pentacyclic triterpenoid skeleton (Mahato and Kundu 1994);
- signal of an oxymethine proton at δ_H 4.64 (1H, dd, $J = 7.1, 9.4$ Hz, H-3);
- signal of an olefinic proton singlet at δ_H 4.89 (1H, s, H-19);
- signals of aromatic protons at δ_H 7.14 (1H, d, $J = 2.0$ Hz, H-5'), 6.90 (1H, d, $J = 8.2$ Hz, H-8') and 7.04 (1H, dd, $J = 2.0, 8.2$ Hz, H-9'). The large coupling constant $J = 15.9$ Hz between H-2' (δ_H 6.30) and H-3' (δ_H 7.59) indicated *trans* coupling, while the coupling constants for the aromatic protons suggested meta ($J = 2.0$ Hz) and ortho ($J = 8.2$ Hz) coupling hence, a 1,3,4-trisubstituted benzene; resonances for conjugated

olefinic protons at δ_{H} 6.30 (1H, d, $J = 15.9$ Hz, H-2') and δ_{H} 7.59 (1H, d, $J = 15.9$ Hz, H-3'); two broad singlets at δ_{H} 6.06 (1H, OH-6') and δ_{H} 5.811 (1H, OH-7') represented hydroxyl group protons. These data suggested a caffeoyl moiety attached to the pentacyclic triterpenoid skeleton.

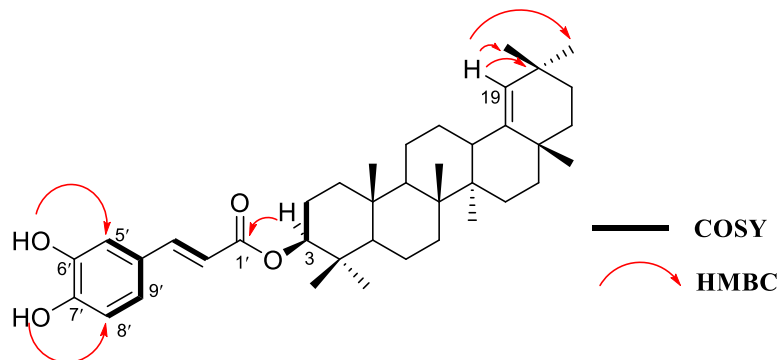


Its ^{13}C NMR spectrum (Figure 43) exhibited thirty nine carbon resonances, which were sorted by HMQC (Figure 44) technique into:

- eight methyl groups at δ_{C} 28.0 (C-23), 16.7 (C-24), 16.8 (C-25), 16.1 (C-26), 14.6 (C-27), 25.3 (C-28), 31.3 (C-29) and 29.2 (C-30);
- ten methylene groups at δ_{C} 38.9 (C-1), 23.8 (C-2), 18.1 (C-6), 34.4 (C-7), 21.1 (C-11), 26.1 (C-12), 27.5 (C-15), 37.7 (C-16), 33.3 (C-21) and 37.3 (C-22);
- seven quaternary carbons at δ_{C} 38.1 (C-4), 40.3 (C-8), 37.3 (C-10), 34.5 (C-17), 43.4 (C-14), and 32.3 (C-20), including a carbonyl of a conjugated ester at δ_{C} 167.6 (C-1');
- four methine groups at δ_{C} 55.6 (C-5), 51.3 (C-9) and 38.4 (C-13), including an oxymethine carbon at δ_{C} 81.3 (C-3);
- six aromatic ring carbons at δ_{C} 127.6 (C-4'), 114.6 (C-5'), 146.2 (C-6'), 143.7 (C-7'), 115.4 (C-8') and 122.3 (C-9');
- four olefinic carbons at δ_{C} 142.8 (C-18), 129.8 (C-19), 116.3 (C-2') and 144.5 (C-3');
- two olefinic carbons at δ_{C} 142.6 and 129.7 attributable respectively to C-18 and C-19 which are characteristic to olean-18-ene triterpenoids (Mahato and Kundu 1994).

The positions of these carbons on the pentacyclic triterpene skeleton were further confirmed by the correlations of proton H-19 (δ_{H} 4.89) with C-29 (δ_{C} 31.3), C-30 (δ_{C} 29.2), C-20 (δ_{C} 32.3) and C-21 (δ_{C} 33.3) observed on the HMBC spectrum (Figure 45). The position of the two oxyaromatic carbons was deduced from the correlations observed on the same spectrum between protons OH-6' (δ_{H} 6.06), OH-7' (δ_{H} 5.811) and carbons C-5' (114.4) and C-8' (115.4), respectively. These resonances indicated that BLE4 is a pentacyclic triterpenoid of the type olean-18-ene with a caffeoyl ester substituent at position 3 of the pentacyclic triterpenoid skeleton. The attachment of this group to the triterpenoid moiety was confirmed by the correlation observed on the HMBC spectrum between the proton H-3 (δ_{H} 4.64) and the carbonyl carbon of the ester C-1' (δ_{C} 167.6).

The ^1H - ^1H COSY spectrum (Figure 46) provided further conclusive structural evidence for BLE4. Some main correlations like that between H-9' (δ_{H} 7.04) with H-5' (δ_{H} 7.14) and H-8' (δ_{H} 6.90); H-2' (δ_{H} 6.30) and H-3' (δ_{H} 7.59); H-3 (δ_{H} 4.64) and H-2 (δ_{H} 1.75, δ_{H} 1.76) were displayed.



Scheme 17: Some Key HMBC and COSY correlations of BLE4

All these data compared to those described in the literature were in agreement to that of germanicol caffeoyl ester (**133**), previously isolated from *Barringtonia asiatica* (Lecythidaceae) by Ragasa *et al.* (2011).

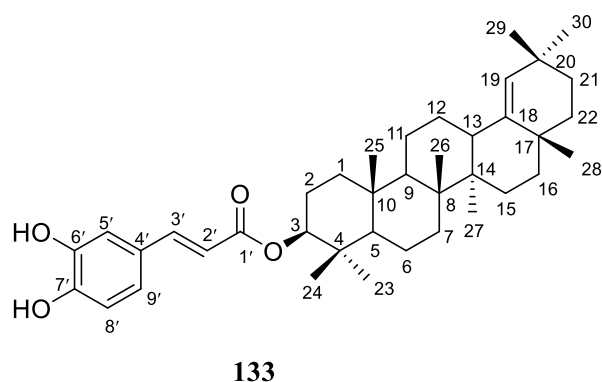


Table 29: ¹H (500 MHz) and ¹³C (125 MHz) NMR data of BLE4 in CDCl₃ compared to germanicol caffeoyl ester [CDCl₃, NMR ¹³C (150 MHz) and NMR ¹H (600 MHz)]

BLE4			Germanicol caffeoyl ester (Ragasa <i>et al.</i> , 2011)	
Position	$\delta^{13}\text{C}$	$\delta^1\text{H}$ (m, J in Hz)	$\delta^{13}\text{C}$	$\delta^1\text{H}$
1	38.6	1.07 (1H, m); 1.72 (1H, m)	38.4	1.05 (1H, m); 1.78 (1H, m)
2	23.8	1.75 (1H, m); 1.76 (1H, m)	23.8	1.68 (1H, m); 1.72 (1H, m)
3	81.3	4.64 (1H, dd, 7.1, 9.4)	81.2	4.59 (1H, dd, 7.2, 9.6)
4	38.1	-	38.1	-
5	55.6	0.86 (1H, d, 10.9)	55.6	0.82 (1H, d, 10.9)
6	18.1	1.39 (1H, m); 1.53 (1H, m)	18.2	1.40 (1H, m); 1.52 (1H, m)
7	34.4	1.39 (1H, m); 1.50 (1H, m)	34.5	1.36 (1H, m); 1.48 (1H, m)
8	40.3	-	40.8	-
9	51.3	1.30 (1H, m)	51.1	1.30 (1H, m)
10	37.3	-	37.4	-
11	21.1	1.30 (1H, m); 1.56 (1H, m)	21.1	1.30 (1H, m); 1.56 (1H, m)
12	26.1	1.22 (1H, m); 1.50 (1H, m)	26.2	1.20 (1H, m); 1.48 (1H, m)
13	38.4	2.29 (1H, d, 11.9)	38.6	2.26 (1H, d, 11.9)
14	43.4	-	-	-
15	27.5	1.14 (1H, m); 1.82 (1H, m)	27.5	1.08 (1H, m); 1.80 (1H, m)
16	37.7	1.33 (1H, m); 1.36 (1H, m)	37.7	1.32 (1H, m); 1.38 (1H, m)
17	34.5	-	34.3	-
18	142.8	-	142.7	-
19	129.8	4.89 (1H, s)	129.8	4.85 (1H, s)
20	32.3	-	32.3	-
21	33.3	1.33 (1H, m); 1.47 (1H, m)	33.3	1.32 (1H, m); 1.44 (1H, m)
22	37.3	1.41 (1H, m); 1.45 (1H, m)	37.2	1.40 (1H, m); 1.45 (1H, m)
23	28.0	0.90 (3H, s)	28.0	0.87 (3H, s)
24	16.7	0.94 (3H, s)	16.8	0.90 (3H, s)
25	16.8	0.97 (3H, s)	16.7	0.91 (3H, s)
26	16.1	1.11 (3H, s)	16.1	1.07 (3H, s)
27	14.6	0.77 (3H, s)	14.6	0.73 (3H, s)
28	25.3	1.04 (3H, s)	25.3	1.00 (s)
29	31.3	0.95 (3H, s)	31.3	0.93 (s)
30	29.20	0.96 (3H, s)	29.2	0.94 (s)
1'	167.6	-	167.5	-
2'	116.3	6.30 (1H, d, 15.8)	116.4	6.25 (1H, d, 15.6)
3'	144.5	7.59 (1H, d, 15.8)	144.3	7.54 (1H, d, 15.6)
4'	127.6	-	127.7	-
5'	114.4	7.14 (1H, d, 2.0)	114.3	7.09 (1H, d, 1.8)
6'	146.2	-	143.8	-
7'	143.7	-	146.2	-
8'	115.4	6.90 (1H, d, 8.2)	115.4	6.85 (1H, d, 7.8)
9'	122.3	7.04 (1H, dd, 2.0; 8.2)	122.4	6.99 (1H, dd, 1.8; 7.8)
OH-6', OH-7'	-	5.81 brs, 6.06 brs	-	5.80 brs, 6.00 brs

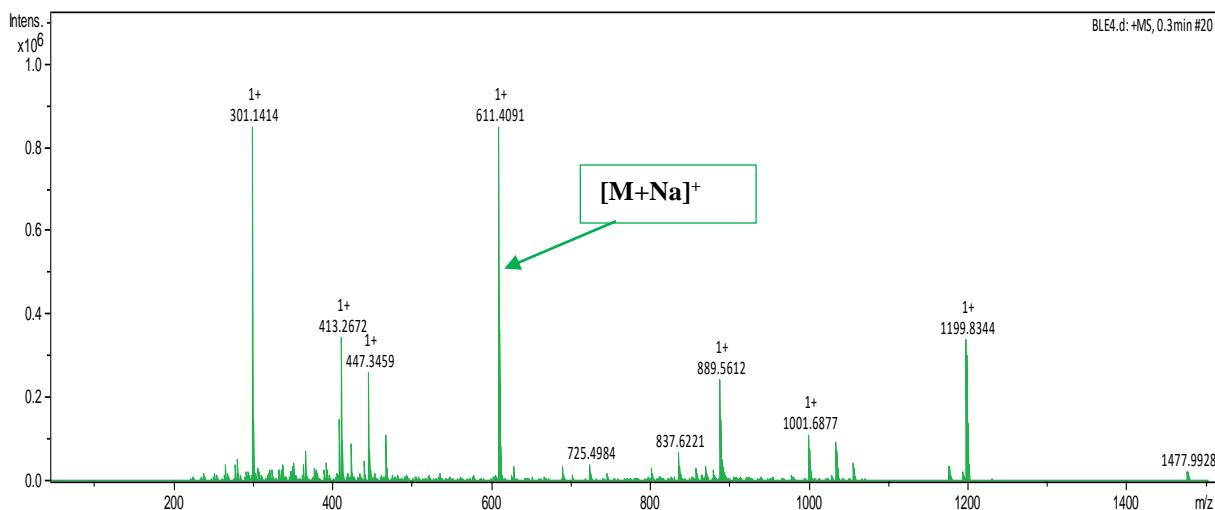


Figure 41: HRESI mass spectrum of BLE4

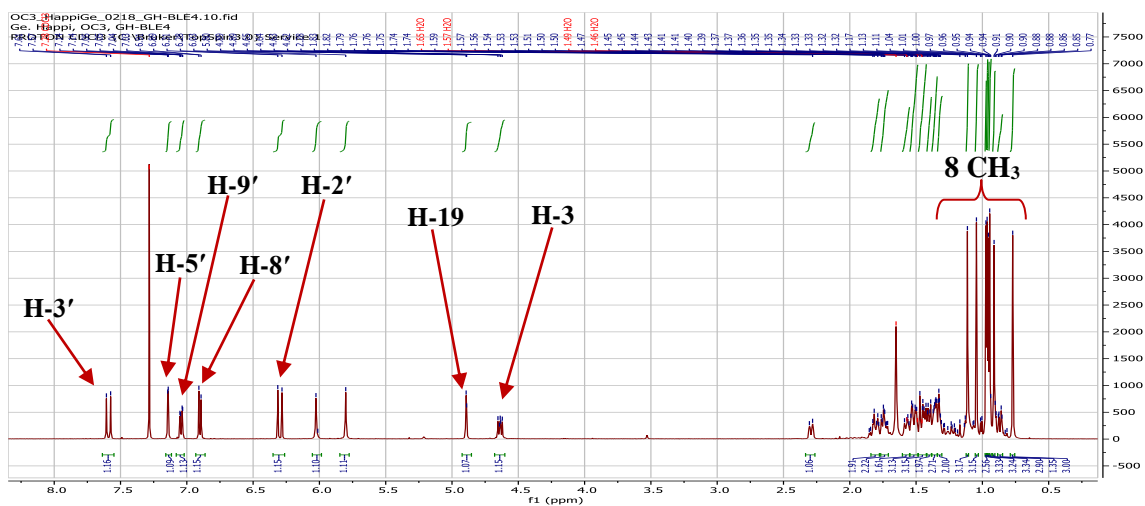


Figure 42: ¹H NMR spectrum (CDCl₃, 500 MHz) of BLE4

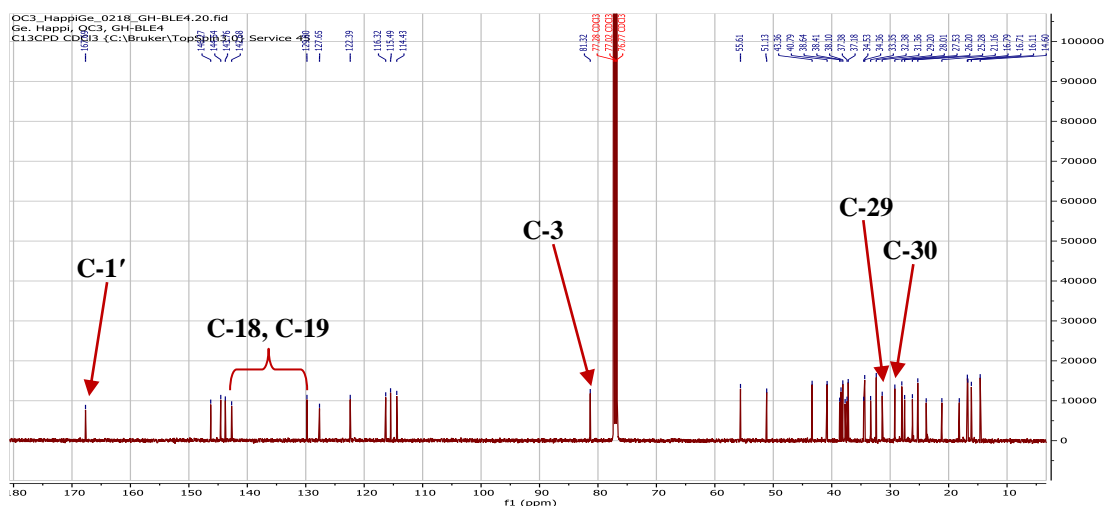


Figure 43: ¹³C NMR spectrum (CDCl₃, 125 MHz) of BLE4

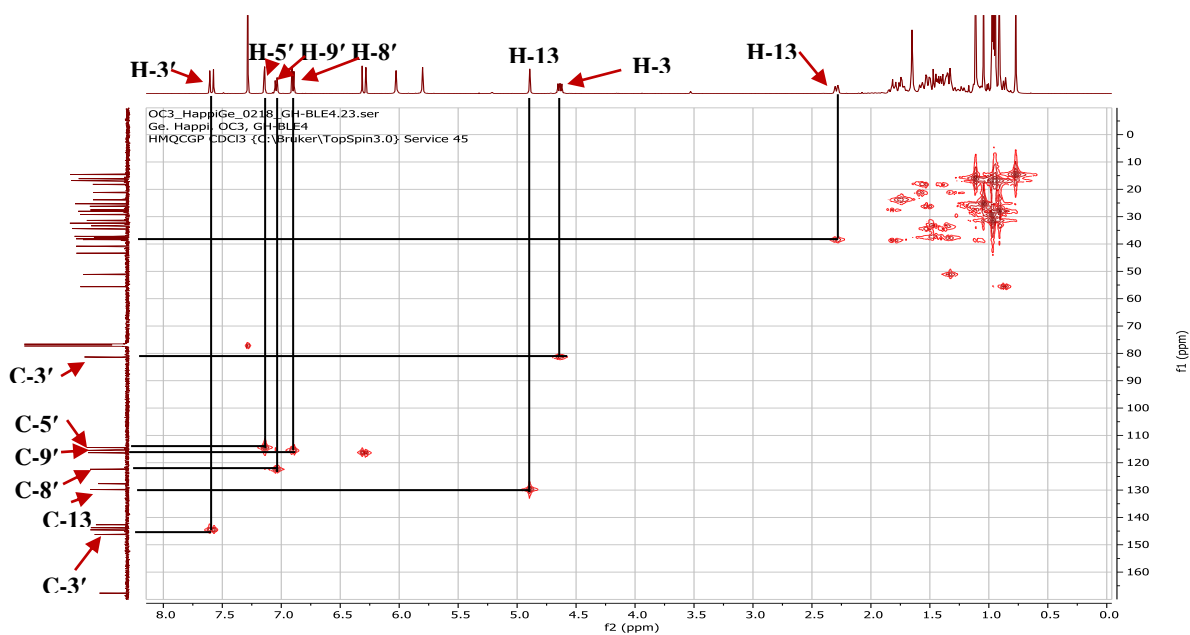


Figure 44: HMQC spectrum of BLE4

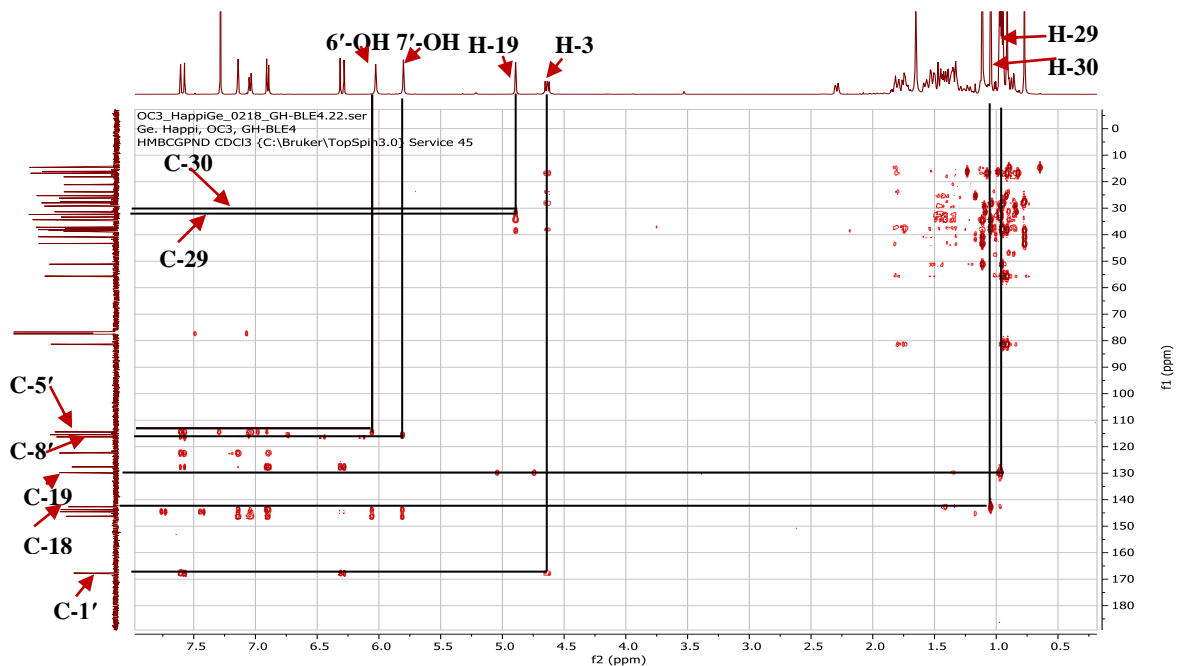


Figure 45: HMBC spectrum of BLE4

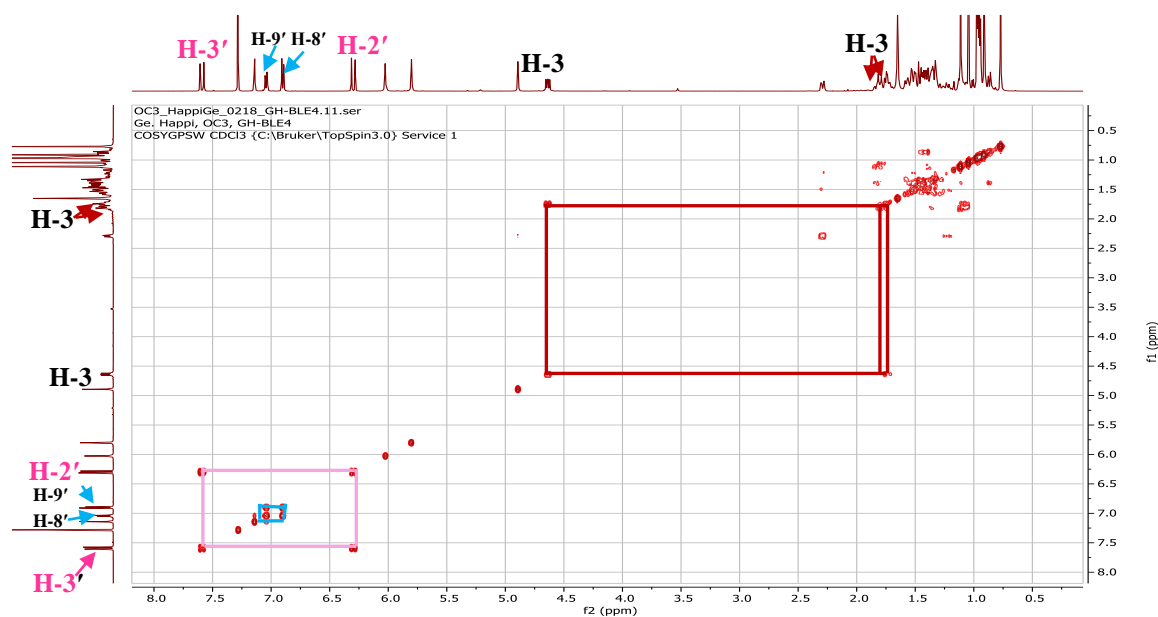


Figure 46: COSY spectrum of BLE4

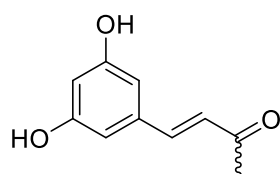
II.1.5.3.2. Structural identification of compound BLE10

BLE10 was obtained as a white powder in *n*-hexane/ethyl acetate (70:30). It is soluble in pyridine and give a red color which turns purple to the Liebermann-Burchard test characteristic of triterpenoids.

Its molecular formula $C_{39}H_{54}O_5$ was deduced from the HRESIMS spectrum (Figure 47) which showed the pseudomolecular ion peak $[M+H]^+$ at m/z 603.4060 (calcd. for $C_{39}H_{55}O_5Na$, 603.4049), with thirteen degrees of unsaturation.

Its 1H NMR spectrum (Figure 48), displayed signals of:

- eight singlets of three protons each at δ_H 0.82 (3H, s, H-28), 0.83 (3H, s, H-30), 0.88 (3H, s, H-29), 0.96 (3H, s, H-24), 1.00 (3H, s, H-23), 1.10 (3H, s, H-26), 1.29 (3H, s, H-25) and 1.34 (3H, s, H-27), attributable to the eight angular methyl of oleanane type pentacyclic triterpenoid skeleton (Mahato and Kundu 1994);
- an oxymethine proton at δ_H 4.91 (1H, dd, $J = 11.3, 5.2$ Hz, H-3);
- one singlet at δ_H 5.75 (1H, s, H-12) assigned to the proton of an enone group;
- two singlets of three aromatic protons at δ_H 7.24 (2H, s, H-5'/H-9') and 7.68 (1H, s, H-7'); suggesting a 1,3,5-substituted benzene ring;
- two olefinic protons at δ_H 6.71 (1H, d, $J = 15.8$ Hz, H-2') and 8.04 (1H, d, $J = 15.8$ Hz, H-3'), standing for *trans* methylene protons; thus suggesting a 3,5-dihydroxycinnamoyl moiety in BLE10.



3,5-dihydroxycinnamoyl moiety

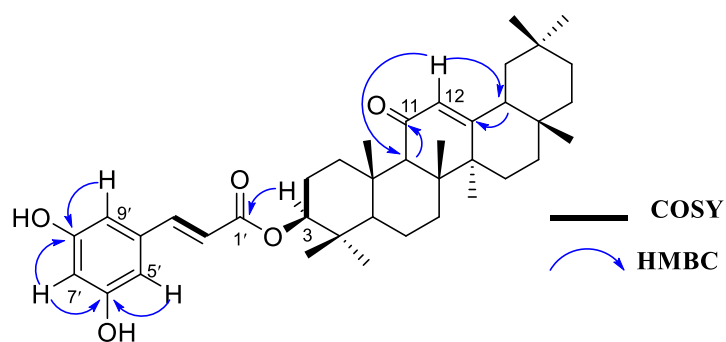
Its ^{13}C NMR spectrum (Figure 49), displayed 39 carbon signals; 30 belonging to pentacyclic triterpenoid skeleton and 9 signals for the conjugated ester substituent (cinnamoyl moiety) with the following functionalities:

- eight quaternary carbons at δ_{C} 38.2 (C-4), 44.9 (C-8), 37.1(C-10), 43.3 (C-14), 32.5 (C-17) and 30.8 (C-20), including a carbonyl carbon of a conjugated ester at δ_{C} 167.1 (C-1') and a conjugated carbonyl (enone) carbon at δ_{C} 199.1 (C-11);
- four methine carbons at δ_{C} 54.8 (C-5), 61.6 (C-9) and 47.4 (C-18), including an oxymethine carbon at δ_{C} 79.9 (C-3);
- six aromatic ring carbons at δ_{C} 126.8 (C-4'), 121.8 (C-5'), 147.5 (C-6'), 116.5 (C-7'), 150.2 (C-8'), 115.6 (C-9');
- four olefinic carbons at δ_{C} 145.4 (C-3'), 115.6 (C-2'), 170.0 (C-13), 128.1 (C-12);
- nine methylene carbons at δ_{C} 38.9 (C-1), 23.9 (C-2), 17.4 (C-6), 32.2 (C-7), 26.4 (C-15), 26.2 (C-16), 44.9 (C-19), 34.3 (C-21) and 36.4 (C-22);
- eight methyl carbons at δ_{C} 27.9 (C-23), 16.9 (C-24), 16.5 (C-25), 18.5 (C-26), 23.3 (C-27), 28.5 (C-28), 23.2 (C-29) and 32.8 (C-30).

The structure of the 3,5-dihydroxycinnamoyl moiety was confirmed by the correlations displayed on the HMBC (Figure 51) spectrum between the aromatic protons H-5'/H-7' (δ_{H} 7.24) and carbons C-3' (δ_{C} 145.3), C-4' (δ_{C} 126.8), C-2' (δ_{C} 115.6), C-6' (δ_{C} 147.5) and C-8' (δ_{C} 150.2), between H-9' (δ_{H} 7.68) and C-5' (δ_{C} 121.8), C-3' (δ_{C} 145.4), C-8' (δ_{C} 150.2) and between proton H-3' (δ_{H} 8.04) and carbons C-1' (δ_{C} 167.1), C-4' (δ_{C} 126.8) and C-9' (δ_{C} 115.6).

Also, the ^1H - ^1H COSY spectrum (Figure 52) displayed a correlation between H-3' (δ_{H} 8.04) and H-2' (δ_{H} 6.71), H-3 (δ_{H} 4.91) and H-2 (δ_{H} 1.84).

The conjugated ester group was placed at C-3 position due to the correlation between the proton H-3 (δ_{H} 4.91) and the carbon C-1' (δ_{C} 167.1) observed on the HMBC spectrum and the position of the conjugated ketone group was determined by the correlation between proton H-12 (δ_{H} 5.75) and carbons C-9 (δ_{C} 61.6), C-18 (δ_{C} 47.4); proton H-9 (δ_{H} 2.45) and carbon C-11 (δ_{C} 199.1); proton H-18 (δ_{H} 2.11) and carbon C-13 (δ_{C} 170.0) on the same spectrum.



Scheme 18: Some Key HMBC and COSY correlations of BLE10

All these data, compared to those described in the literature were concluded to be that of 3- β -*O*-*E*-3,5-dihydroxycinnamoyl-11-oxo-olean-12-ene (**134**), previously isolated from *Drypetes tessmanniana* by Dongfack *et al.* (2008).

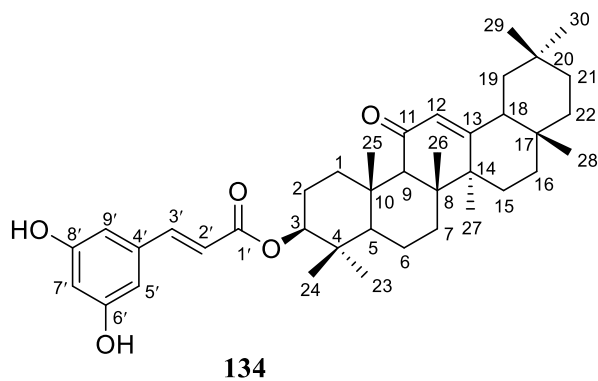


Table 30: ^1H (500 MHz) and ^{13}C (125 MHz) NMR data of BLE10 in pyridine-*d*₅ compared to 3- β -*O*-*E*-3,5-dihydroxycinnamoyl-11-oxo-olean-12-ene [Pyridine-*d*₅, NMR ^{13}C (100 MHz) and NMR ^1H (400 MHz)]

BLE10			3- β - <i>O</i> - <i>E</i> -3,5-dihydroxycinnamoyl-11-oxo-olean-12-ene (Dongfack <i>et al.</i> , 2008)	
Position	$\delta^{13}\text{C}$	$\delta^1\text{H}$ (m, <i>J</i> in Hz)	$\delta^{13}\text{C}$	$\delta^1\text{H}$ (m, <i>J</i> in Hz)
1	38.9	3.16 (1H, dt, 13.4, 3.6); 1.20 (1H, m)	39.1	1.18 (1H, m); 1.22 (1H, m)
2	23.9	1.84 (1H, m)	24.2	1.83 (1H, m); 1.91 (1H, m)
3	79.9	4.91 (1H, dd, 11.3, 5.2)	80.2	4.90 (1H, dd, 11.1, 4.8)
4	38.2	-	38.5	-
5	54.8	0.84 (1H, m)	55.1	0.85 (1H, m)
6	17.4	1.49 (1H, m); 1.32 (1H, m)	18.8	1.40 (1H, m); 1.53 (1H, m)
7	32.2	1.27 (1H, m); 1.57 (1H, m)	33.0	1.28 (1H, m); 1.60 (1H, m)
8	44.9	-	45.2	-
9	61.6	2.45 (1H, s)	61.9	2.45 (1H, s)
10	37.1	-	37.4	-
11	199.1	-	199.4	-
12	128.1	5.75 (1H, s)	128.3	5.75 (1H, s)
13	170.0	-	170.2	-
14	43.3	-	43.6	-
15	26.4	1.03 (1H, m); 1.68 (1H, m)	26.7	1.07 (1H, m); 1.72 (1H, m)
16	26.2	1.98 (1H, m); 1.67 (1H, m)	26.5	2.03 (1H, m); 1.69 (1H, m)
17	32.5	-	32.5	-
18	47.4	2.11 (1H, dd, 13.4, 4.5)	45.5	1.67 (1H, s)
19	45.3	1.64 (1H, d, 13.6); 0.94 (1H, m)	47.7	2.09 (1H, m); 2.12 (1H, m)
20	30.8	-	31.1	-
21	34.3	1.07 (1H, m); 1.38 (1H, m)	34.6	1.08 (1H, m); 1.35 (1H, m)
22	36.4	1.20 (1H, m); 1.39 (1H, m)	36.7	1.21 (1H, m); 1.43 (1H, m)
23	27.9	1.00 (3H, s)	28.7	1.00 (3H, s)
24	16.9	0.96 (3H, s)	16.7	0.96 (3H, s)
25	16.5	1.29 (3H, s)	17.1	1.29 (3H, s)
26	18.5	1.10 (3H, s)	17.6	1.10 (3H, s)
27	23.3	1.34 (3H, s)	23.5	1.37 (3H, s)
28	28.5	0.82 (3H, s)	28.2	0.82 (3H, s)
29	32.8	0.88 (3H, s)	32.7	0.88 (3H, s)
30	23.2	0.83 (3H, s)	23.6	0.83 (3H, s)
1'	167.1	-	167.3	-
2'	115.4	6.71 (1H, d, 15.8)	115.9	6.66 (1H, d, 15.8)
3'	145.4	8.04 d (1H, d, 15.8)	145.6	8.00 (1H, d, 15.8)
4'	126.8	-	128.4	-
5'	116.5	7.24 (1H, s)	116.7	7.23 (1H, s)
6'	147.5	-	147.7	-
7'	121.8	7.68 (1H, s)	122.0	7.69 (s)
8'	150.2	-	150.4	-
9'	115.6	7.24 (1H, s)	115.6	7.23 (1H, s)

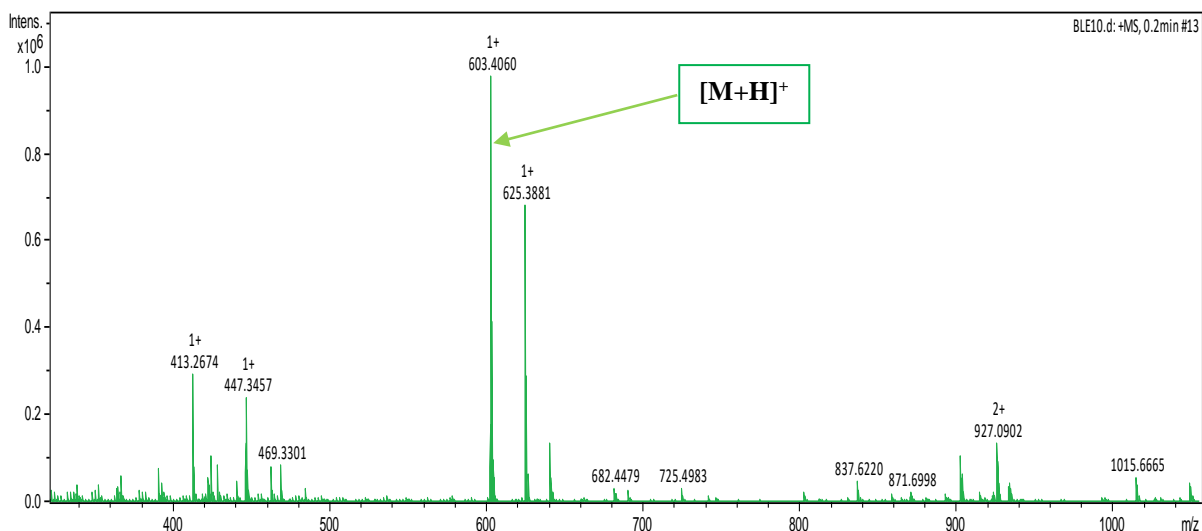


Figure 47: HRESI mass spectrum of BLE10

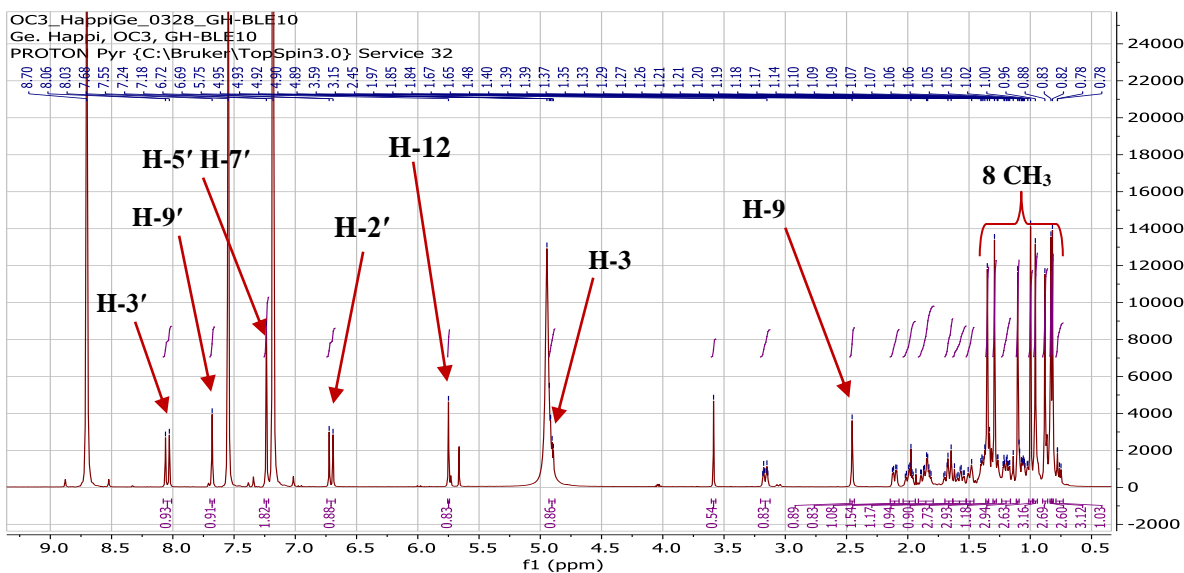


Figure 48: ^1H NMR spectrum (Pyridine- d_5 , 500 MHz) of BLE10

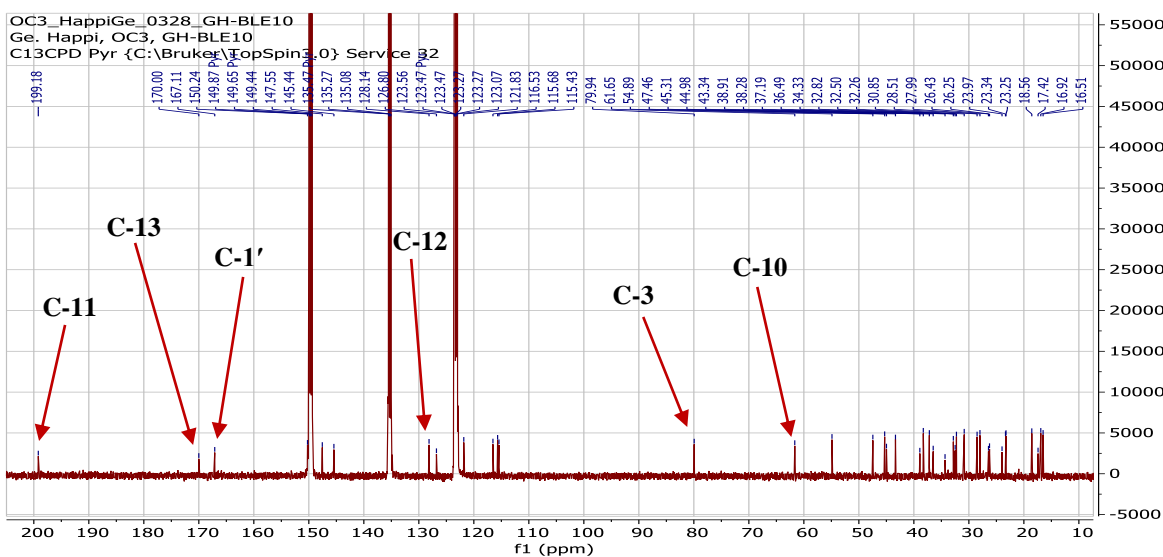


Figure 49: ^{13}C NMR spectrum (Pyridine- d_5 , 125 MHz) of BLE10

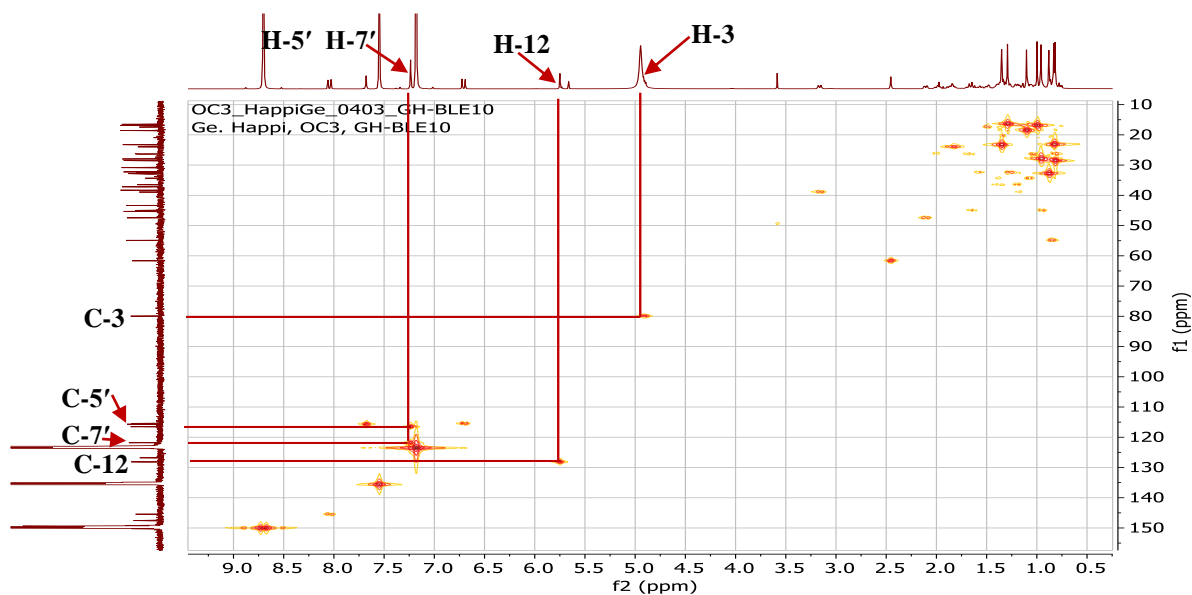


Figure 50: HMQC spectrum of BLE10

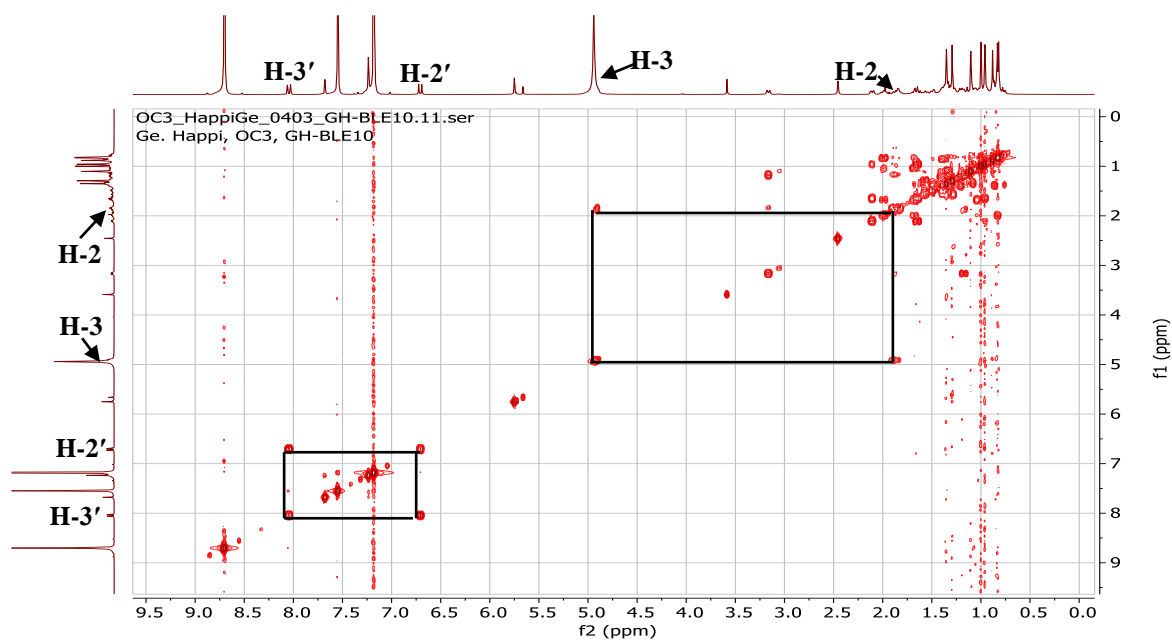


Figure 51: COSY spectrum of BLE10

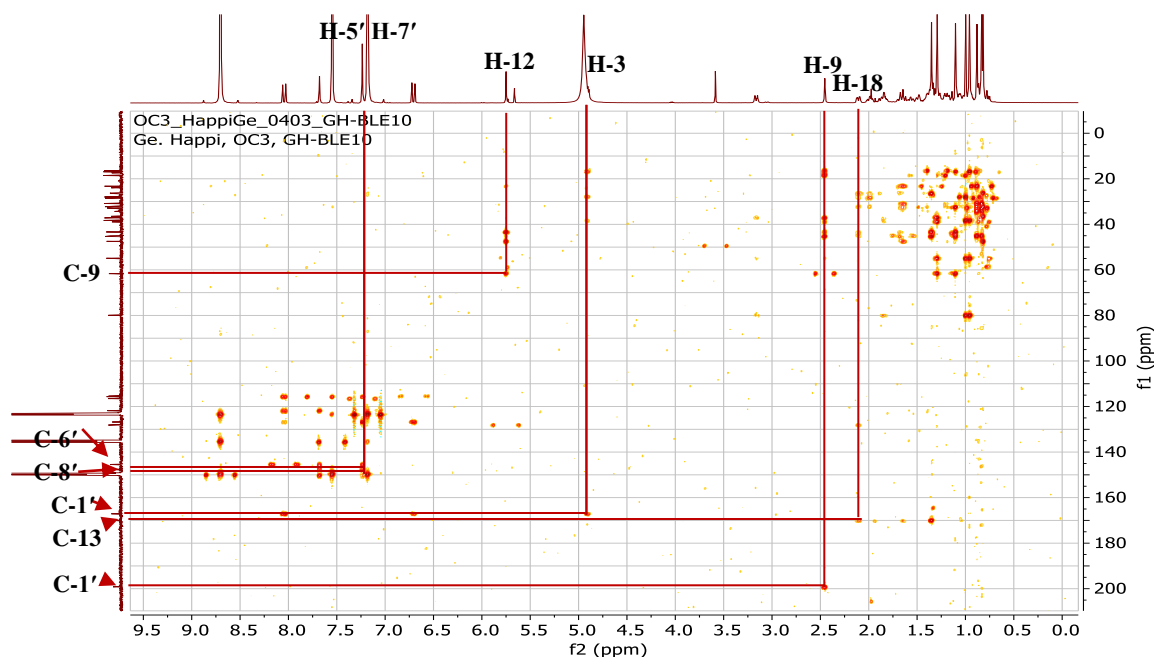


Figure 52: HMBC spectrum of BLE10

II.1.5.3.3. Structural identification of compound RH11

RH11 was obtained as a white powder in *n*-hexane/acetone (60:40). It is soluble in pyridine and give a red color which turns purple to the Liebermann-Burchard test characteristic of triterpenoids.

Its molecular formula $C_{30}H_{48}O_4$ was deduced from the HRESIMS spectrum (Figure 53) which showed the sodium adduct peak $[M+Na]^+$ at m/z 495.3487 (calcd. for $C_{30}H_{48}O_4Na$, 495.3450), implying seven degrees of unsaturation.

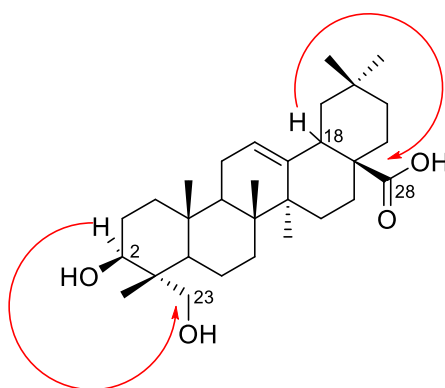
Its 1H -NMR spectrum (Figure 54) showed:

- six singlets of three protons each at δ_H 0.91 (3H, s, H-29), 0.95 (3H, s, H-25), 0.98 (3H, s, H-30), 1.03 (3H, s, H-26), 1.04 (3H, s, H-23), 1.22 (3H, s, H-27) attributable to six angular methyl groups of oleanane type pentacyclic triterpenoid skeleton (Mahato and Kundu, 1994);
- signal of three methine protons at δ_H 3.29 (1H, dd, $J = 13.8, 4.0$ Hz, H-18), including an oxymethine proton at δ_H 4.19 (1H, dd, $J = 18.0, 7.6$ Hz, H-3) and an olefinic methine proton at δ_H 5.48 (1H, t, $J = 3.0$ Hz, H-12),
- signals of two oxymethylene protons at δ_H 4.17 (1H, d, $J = 10.1$, H-23a) and δ_H 3.71 (1H, d, $J = 10.3$ Hz, H-23b);

Its ^{13}C spectrum (Figure 55) displayed 30 carbon resonances which were sorted by HMQC (Figure 56) technique into:

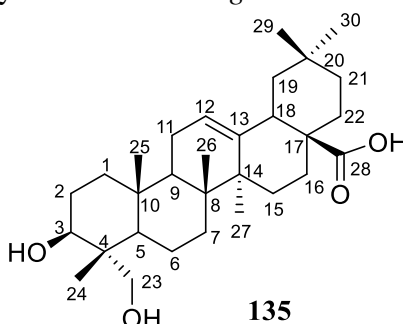
- six methyl groups at δ_C 12.9 (C-24), 15.7 (C-25), 17.2 (C-26), 23.5 (C-30), 25.9 (C-27) and 32.9 (C-29);
- eleven methylene groups at δ_C 18.3 (C-6), 23.4 (C-16), 23.6 (C-11), 28.1 (C-15), 27.4 (C-2), 32.9 (C-22), 32.7 (C-7), 33.9 (C-21), 38.5 (C-1), 46.3 (C-19), including an oxymethylene at δ_C 67.8 (C-23);
- four aliphatic methine groups at δ_C 41.7 (C-18), 36.9 (C-9), 48.3 (C-5), including an oxymethine carbon at δ_C 73.4 (C-3) which is attributable to carbon C-3 of pentacyclic triterpenoids;
- two olefinic carbons at δ_C 122.3 (C-12) and 144.6 (C-13), characteristic of the olean-12-ene pentacyclic triterpene skeleton (Mahato and Kundu, 1994);
- seven quarternary carbons amongst which: six sp^3 -hybride carbons at δ_C 30.7 (C-20), 36.9 (C-10), 39.5 (C-8), 41.9 (C-14), 46.4 (C-17), 42.6 (C-4) and one sp^2 -hybridized carbons at δ_C 179.9 (C-28) corresponding to the carbon of a carboxylic acid group.

On its HMBC spectrum (Figure 57), the correlation between the proton H-18 (δ_H 3.29) and the carbon C-28 (δ_C 179.9) allows us to attach the carboxyl group at position 28. Also, the correlations between proton H-3 (δ_H 4.19) and carbon C-23 (δ_C 67.8); proton H-23b (δ_H 3.71) and carbon C-3 (δ_C 73.4) allowed us to fix the oxymethylene group at position 23.



Scheme 19: Key HMBC correlations of RH11

All these data, compared with those of the literature, was in agreement with that of hederagenin (**135**), previously isolated from *Nigella sativa* by Joshi *et al.* (1999).



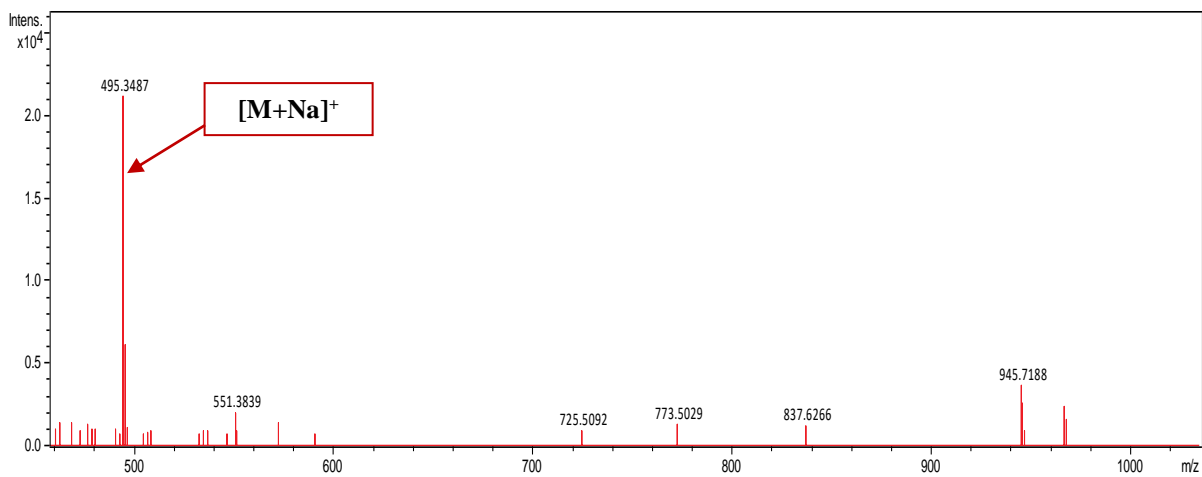


Figure 53: HRESI mass spectrum of RH11

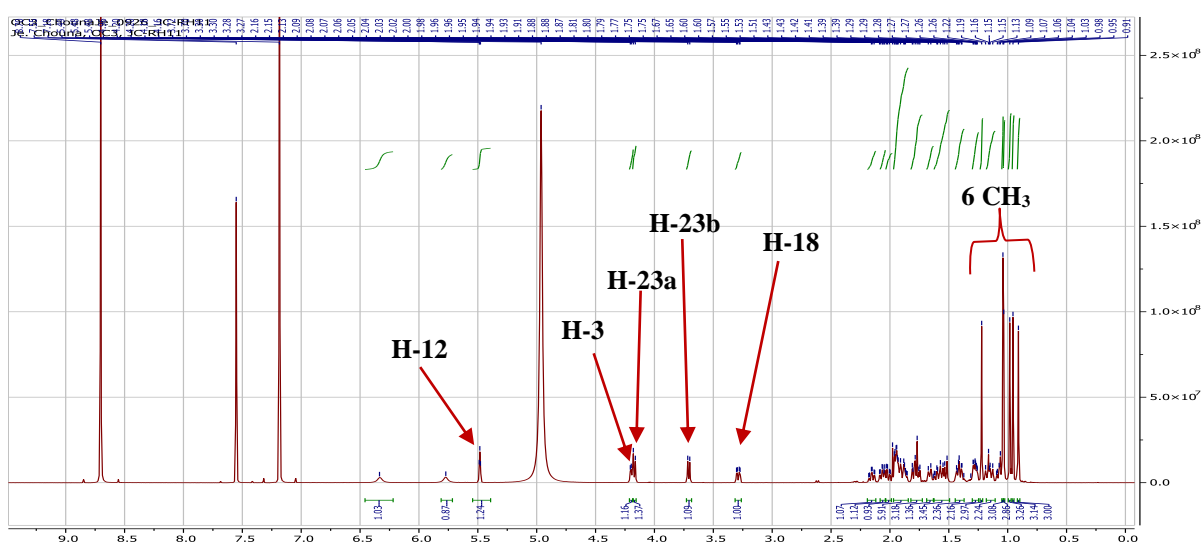


Figure 54: ^1H NMR spectrum (pyridine- d_5 , 500 MHz) of RH11

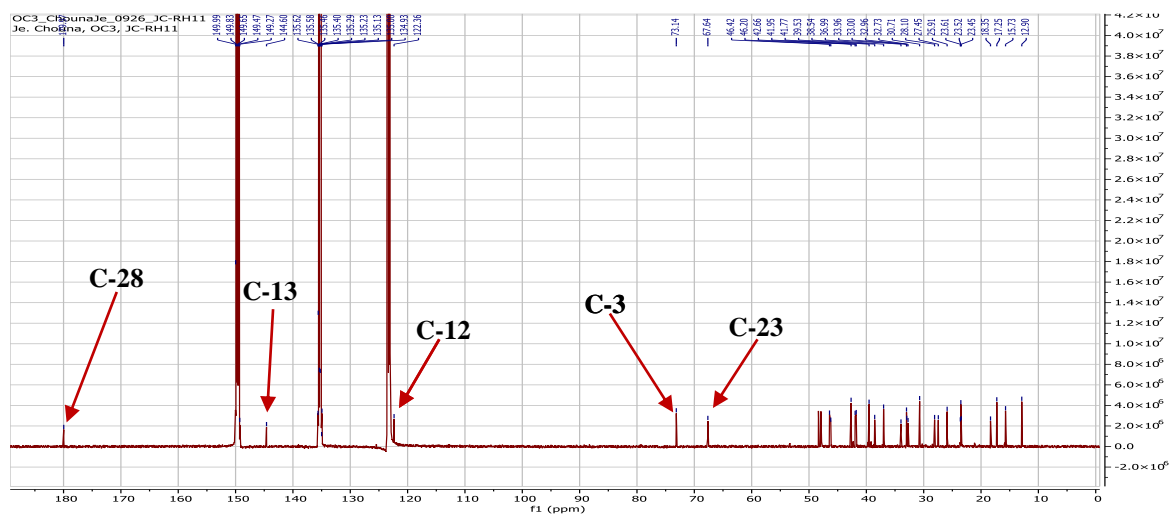


Figure 55: ^{13}C NMR spectrum (pyridine- d_5 , 125 MHz) of RH11

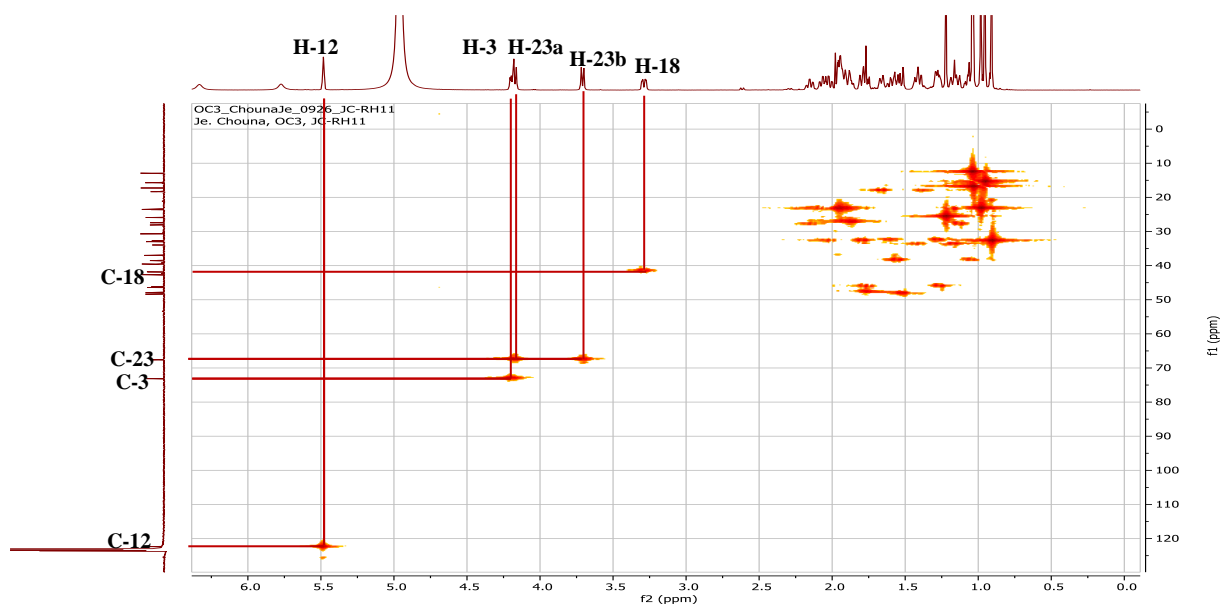


Figure 56: HMQC spectrum of RH11

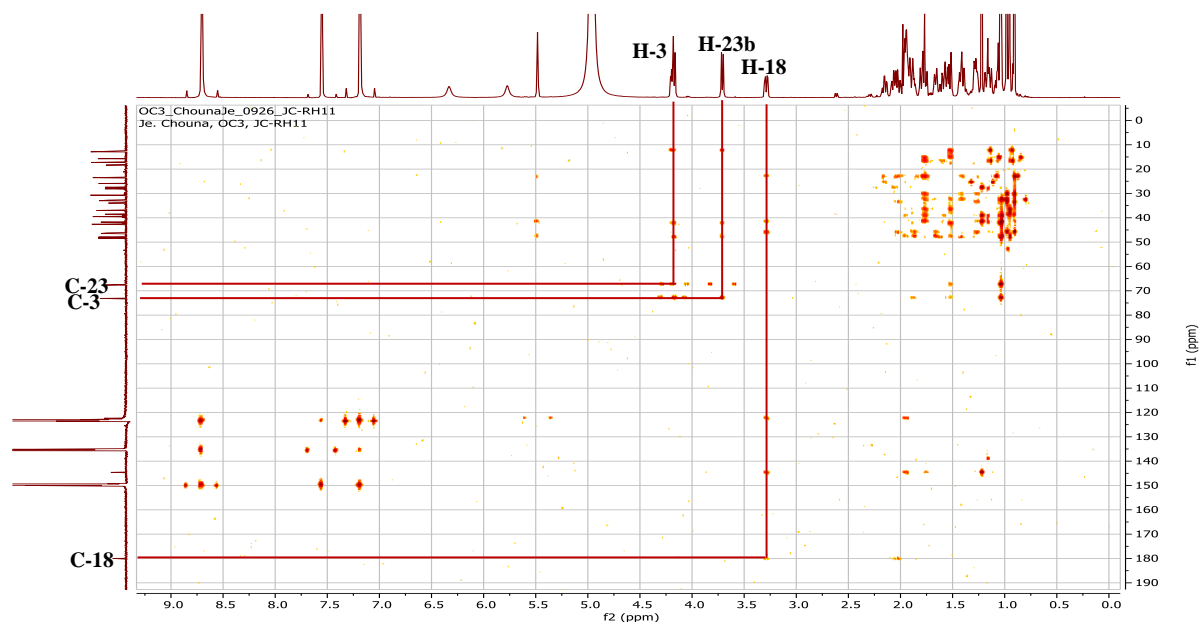


Figure 57: HMBC spectrum of RH11

II.1.5.3.4. Structural identification of compound WN1

WN1 was obtained as a white powder in *n*-hexane/EtOAc (80:20). It is soluble in the mixture of dichloromethane/methanol and give a red color which turns purple to the Liebermann-Burchard test characteristic of triterpenoids.

Its ¹H NMR spectrum (Figure 58) showed signals of:

- seven singlets of three protons each at δ_{H} 0.91 (3H, s, H-25), 0.76 (3H, s, H-24), 0.79 (3H, s, H-26), 0.92 (3H, s, H-30), 1.14 (3H, s, H-27), 0.96 (3H, s, H-23), 0.89 (3H, s,

H-29) attributable to seven angular methyl groups of a pentacyclic triterpenoid skeleton;

- three methine protons including an oxymethine proton at δ_{H} 3.17 (1H, dd, $J = 10.7, 5.4$ Hz, H-3), an olefinic methine proton at δ_{H} 5.24 (1H, t, $J = 3.7$ Hz, H-12) and a methine proton at δ_{H} 2.82 (1H, dd, $J = 14.1, 4.6$ Hz, H-18), which is characteristic of olean-12-ene triterpenoids (Mahato and Kundu, 1994);

Its ^{13}C spectrum (Figure 59) displayed carbon resonances which were sorted by HMQC and DEPT techniques into:

- seven methyl groups at δ_{C} 15.0 (C-25), 15.3 (C-24), 16.6 (C-26), 23.1 (C-30), 25.6 (C-27) 27.7 (C-23) and 32.7 (C-29);
- three aliphatic methine groups at δ_{C} 41.2 (C-18), 47.6 (C-9), 55.2 (C-5) and one oxymethine carbon at δ_{C} 78.5 (C-3) which is attributable to carbon C-3 of pentacyclic triterpenoids;
- two olefinic carbons at δ_{C} 122.2 (C-12) and 144.8 (C-13), characteristic of the olean-12-ene pentacyclic triterpene skeleton (Mahato and Kundu, 1994);
- ten methylene groups at δ_{C} 18.2 (C-6), 22.9 (C-16), 23.3 (C-11), 26.5 (C-15), 27.5 (C-2), 32.4 (C-22), 32.6 (C-7), 33.7 (C-21), 38.5 (C-1) and 45.9 (C-19);
- seven quaternary carbons amongst which: six sp^3 -hybridized carbons at δ_{C} 30.5 (C-20), 36.9 (C-10), 39.2 (C-8), 41.6 (C-14), 46.3 (C-17), 38.6 (C-4) and one sp^2 -hybridized carbon at δ_{C} 180.6 (C-28) corresponding to the carbon of a carboxylic acid group.

All these data, compared to those in the literature were in agreement with that of oleanolic acid (**70**) (Mahato and Kundu, 1994).

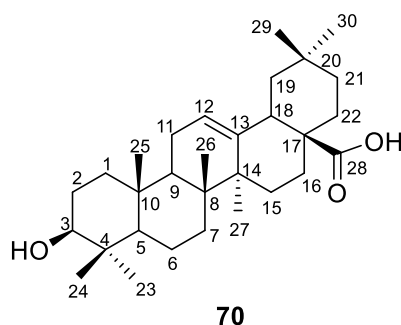


Table 31: ^{13}C (125 MHz) NMR data of WN1 ($\text{CDCl}_3/\text{methanol-}d_4$) and RH11 (pyridine- d_5) compared to oleanolic acid and hederagenin

	WN1	Oleanolic acid (Mahato and Kundu, 1994)	RH11	Hederagenin (Joshi <i>et al.</i> , 1999)
Position	$\delta^{13}\text{C}$	$\delta^{13}\text{C}$	$\delta^{13}\text{C}$	$\delta^{13}\text{C}$
1	38.5	38.5	38.5	38.9
2	27.5	27.4	27.4	27.6
3	78.5	78.7	73.4	73.5
4	38.6	38.7	42.6	43.0
5	55.2	55.2	48.3	48.7
6	18.2	18.3	18.3	18.7
7	32.6	32.6	32.7	33.1
8	39.2	39.3	39.5	39.9
9	47.6	47.6	47.9	48.3
10	36.9	37.0	36.9	37.4
11	23.3	23.1	23.6	24.0
12	122.2	122.1	122.3	122.7
13	144.8	143.4	144.6	145.0
14	41.6	41.6	41.9	42.3
15	26.5	27.7	28.1	28.5
16	22.9	23.4	23.3	23.8
17	46.3	46.6	46.4	46.9
18	41.2	41.3	41.7	42.1
19	45.9	45.8	46.2	46.6
20	30.5	30.6	30.7	31.1
21	33.7	33.8	34.3	33.9
22	32.4	32.3	32.9	33.4
23	27.7	28.1	67.6	67.8
24	15.3	15.6	12.9	13.3
25	15.0	15.3	15.7	16.1
26	16.6	16.8	17.2	17.7
27	25.6	26.0	25.9	26.3
28	180.6	181.0	179.9	180.6
29	32.7	33.1	32.9	32.9
30	23.1	23.6	23.5	23.5

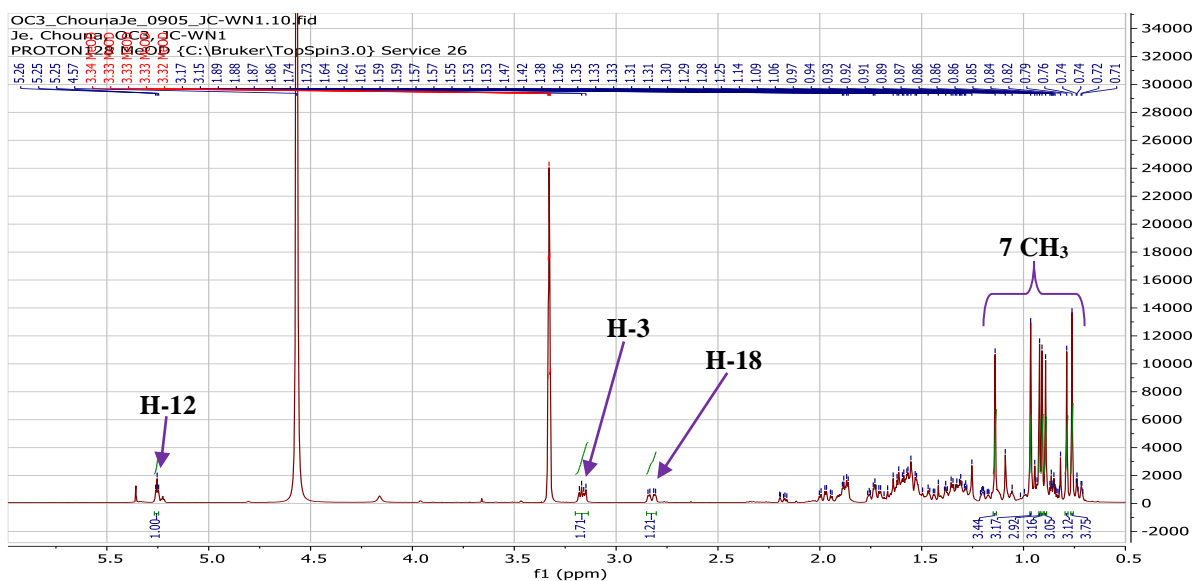


Figure 58: ^1H NMR spectrum ($\text{CDCl}_3/\text{methanol-}d_4$, 500 MHz) of WN1

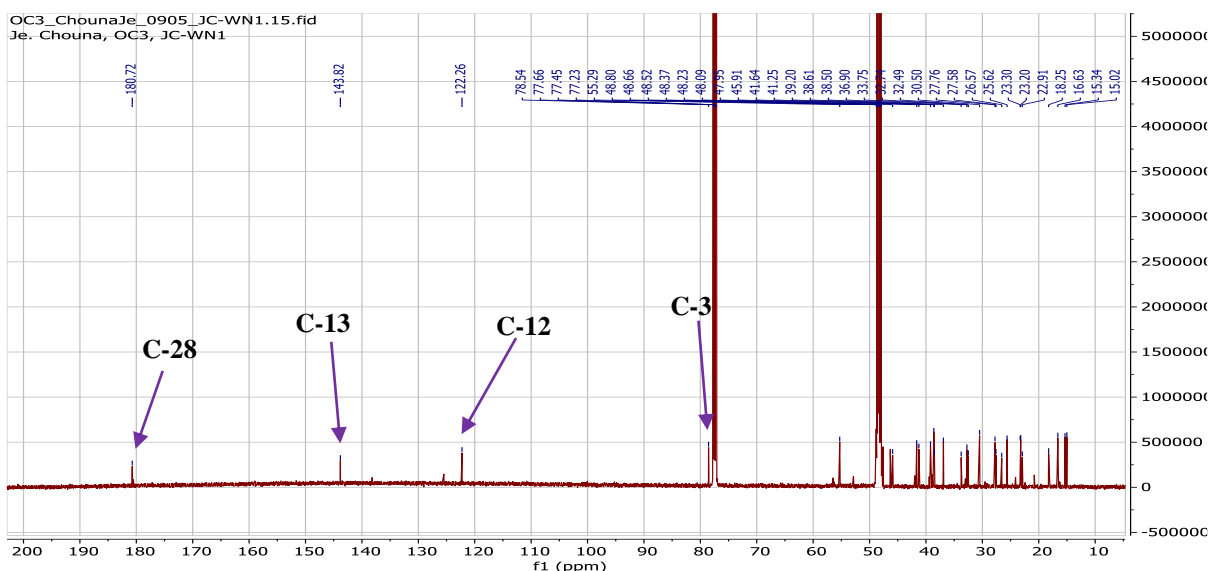


Figure 59: ^{13}C NMR spectrum ($\text{CDCl}_3/\text{methanol-}d_4$, 125 MHz) of WN1

II.1.5.3.5. Structural identification of compound RH5

RH5 was obtained as a white powder in $\text{CH}_2\text{Cl}_2/\text{EtOAc}$ (70:30). It is soluble in dichloromethane and give a red color which turns purple to the Liebermann-Burchard test characteristic of triterpenoids.

Its molecular formula $\text{C}_{30}\text{H}_{50}\text{O}_2$ was deduced from the HRESIMS spectrum (Figure 60) which showed the sodium adduct peak $[\text{M}+\text{Na}]^+$ at m/z 465.3694 (calcd. for $\text{C}_{30}\text{H}_{50}\text{O}_2\text{Na}$, 465.3709), implying six degrees of unsaturation.

Its ^1H NMR spectrum (Figure 61) showed:

- twelve singlets of three protons each attributable to the angular methyl of ursane type pentacyclic triterpenoid skeleton (Mahato and Kundu, 1994) at δ_{H} 0.72 (3H, s, H-23),

0.81 (3H, s, H-29), 0.82 (3H, s, H-30), 0.87 (3H, s, H-25), 0.88 (3H, s, H-26), 0.93 (3H, s, H-24), 1.10 (3H, s, H-27) and oleanane type pentacyclic triterpenoid skeleton (Mahato and Kundu, 1994) at δ_{H} 0.72 (3H, s, H-23), 0.86 (3H, s, H-25), 0.92 (3H, s, H-26), 0.93 (3H, s, H-24) and 1.03 (3H, s, H-27);

- two doublets of three protons each at δ_{H} 0.74 (3H, d, $J = 6.4$ Hz, H-30) and 0.87 (3H, d, $J = 6.4$ Hz, H-29), characteristic of the ursane type triterpenoid;
- two signals of methine protons at δ_{H} 1.31 (1H, m, H-18) and 1.91 (1H, dd, 13.7, 4.8 Hz, H-18) attributable to protons at position 18 and characteristic to urs-12-ene and oleanan-12-ene series, respectively (Mahato and Kundu, 1994);
- a signal at δ_{H} 3.14 (2H, m, H-3) and attributable to two oxymethine protons at position 3 of both series;
- two signals of oxymethylene protons at δ_{H} 3.14 (2H, m, H-28) and 3.47 (2H, d, 11.3 Hz, H-28);
- two signals at δ_{H} 5.07 (1H, t, $J = 3.6$ Hz, H-12) and 5.13 (1H, t, $J = 3.5$ Hz, H-12) attributable to olefinic protons at position 12 of pentacyclic triterpenoids of the urs-12-ene and oleanan-12-ene series, respectively (Mahato and Kundu, 1994).

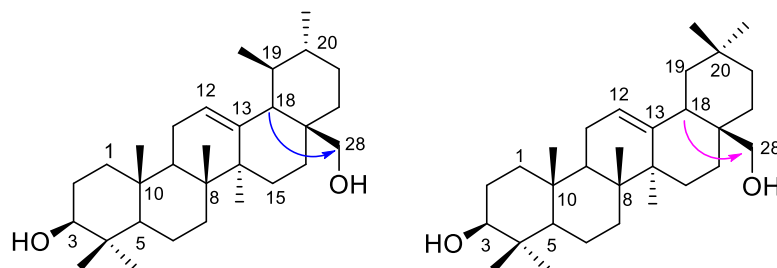
All these data shows that RH5 is a mixture of an oleanane and ursane type triterpenoids (Mahato and Kundu, 1994)

Its ^{13}C spectrum (Figure 62) displayed carbon resonances which were sorted by HMQC (Figure 63) technique into:

- fourteen methyl groups attributable to urs-12-ene serie at δ_{C} 15.5 (C-24), 15.7 (C-25), 16.7 (C-26), 17.3 (C-29), 21.3 (C-30), 23.3 (C-27) and 28.1 (C-23) and oleanan-12-ene serie at δ_{C} 15.5 (C-24), 15.6 (C-25), 16.7 (C-26), 23.5 (C-30), 25.9 (C-27), 28.1 (C-23) and 33.2 (C-29);
- twenty one methylene groups attributable to urs-12-ene and oleanan-12-ene series at δ_{C} 18.3 (C-6), 23.3 (C-11), 23.3 (C-16), 29.3 (C-15), 27.2 (C-2), 30.9 (C-21), 33.5 (C-7), 30.7 (C-22), 38.7 (C-1), 69.9 (C-28) and at δ_{C} 18.3 (C-6), 23.5 (C-11), 22.0 (C-16), 25.5 (C-15), 27.2 (C-2), 34.0 (C-21), 32.5 (C-7), 30.8 (C-22), 38.7 (C-1), 46.4 (C-19), 69.7 (C-28), respectively;
- ten methine groups attributable to the two series at δ_{C} 79.0 (C-3), 55.1 (C-5), 47.6 (C-9), 54.0 (C-18), 39.3 (C-19), 39.4 (C-20) and at δ_{C} 78.9 (C-3), 55.1 (C-5), 47.5 (C-9), 42.3 (C-18), respectively;

- eleven quaternary carbons belonging to the two series at δ_C 36.9 (C-10), 38.5 (C-4), 40.0 (C-8), 42.0 (C-14), 36.8 (C-17), 179.6 (C-20) and at δ_C 31.0 (C-20), 36.8 (C-10), 38.0 (C-4), 39.4 (C-8), 41.7 (C-14), 36.9 (C-17), respectively;
- four olefinic carbons attributable to urs-12-ene and oleanan-12-ene triterpenoids at δ_C 138.7 (C-13) and 125.0 (C-12) and at δ_C 144.2 (C-13) and 122.3 (C-12), respectively (Mahato and Kundu, 1994);

On its HMBC spectrum (Figure 64), the correlations between the proton H-18 (δ_H 1.31) and the carbon C-28 (δ_C 69.9) and between the proton H-18 (δ_H 1.91) and the carbon C-28 (δ_C 69.7) allowed us to fix the oxymethylene groups at position 28.



Scheme 20: Key HMBC correlations of RH5

All these data, compared to those in the literature, allowed us to identify RH5 as a mixture of uvaol (**136**) and erythrodiol (**137**), respectively (Mahato and Kundu, 1994).

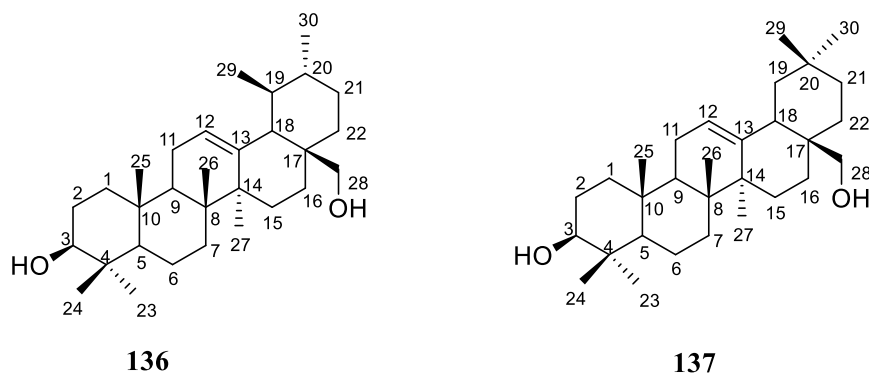


Table 32: ^{13}C (125 MHz) NMR data of RH5 in CDCl_3 compared to uvaol and erythrodiol

	RH5	Uvaol (Mahato and Kundu, 1994)	RH5	Erythrodiol (Mahato and Kundu, 1994)
Position	$\delta^{13}\text{C}$	$\delta^{13}\text{C}$	$\delta^{13}\text{C}$	$\delta^{13}\text{C}$
1	38.7	38.8	38.7	38.6
2	27.2	27.3	27.2	27.2
3	79.0	79.0	78.9	78.8
4	38.5	38.8	38.0	38.7
5	55.1	55.4	55.1	55.2
6	18.3	18.4	18.3	18.4
7	32.8	32.9	32.5	32.7
8	40.0	39.4	39.7	39.7
9	47.6	47.8	47.5	47.6
10	36.9	37.2	36.8	36.8
11	23.3	23.4	23.5	23.6
12	125.0	125.0	122.3	122.1
13	138.7	138.6	144.2	144.4
14	42.0	42.0	41.7	41.7
15	29.3	29.2	25.5	25.6
16	23.3	22.6	22.0	22.0
17	36.8-	36.8	36.9	36.9
18	54.0	54.1	42.3	42.3
19	39.3	38.9	46.4	46.5
20	39.4	39.4	31.0	31.0
21	30.8	30.7	34.0	34.1
22	30.8	30.7	30.6	31.0
23	28.1	28.1	28.0	28.1
24	15.5	15.4	15.5	15.5
25	15.7	15.6	15.6	15.5
26	16.7	16.9	16.7	16.8
27	23.3	23.4	25.9	25.9
28	69.9	69.7	69.7	69.7
29	17.3	17.2	33.2	33.2
30	21.3	21.3	23.5	23.6

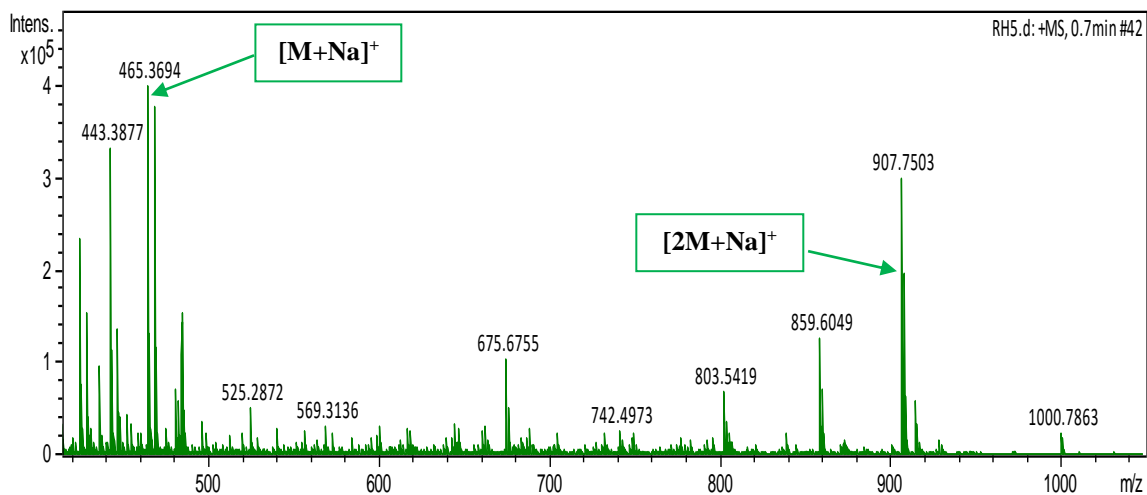


Figure 60: HRESI mass spectrum of RH5

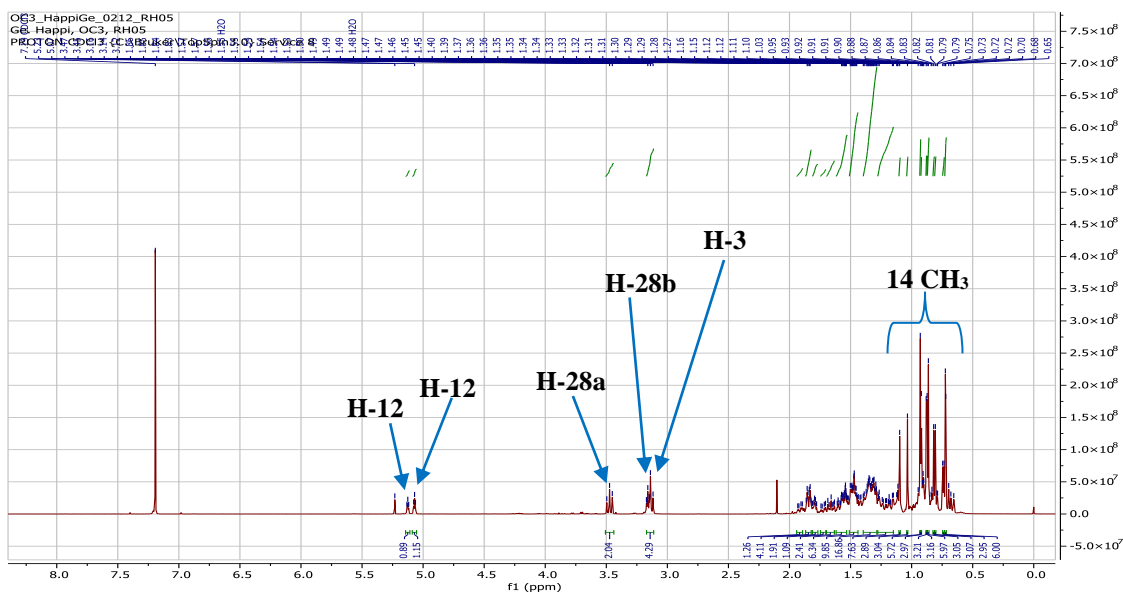


Figure 61: ^1H NMR spectrum (CDCl_3 , 500 MHz) of RH5

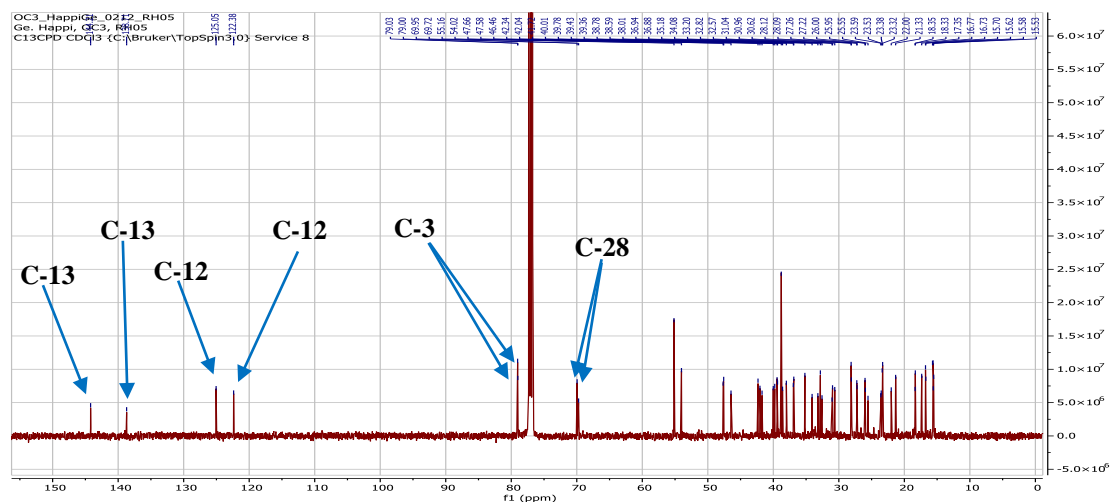


Figure 62: ^{13}C NMR spectrum (CDCl_3 , 125 MHz) of RH5

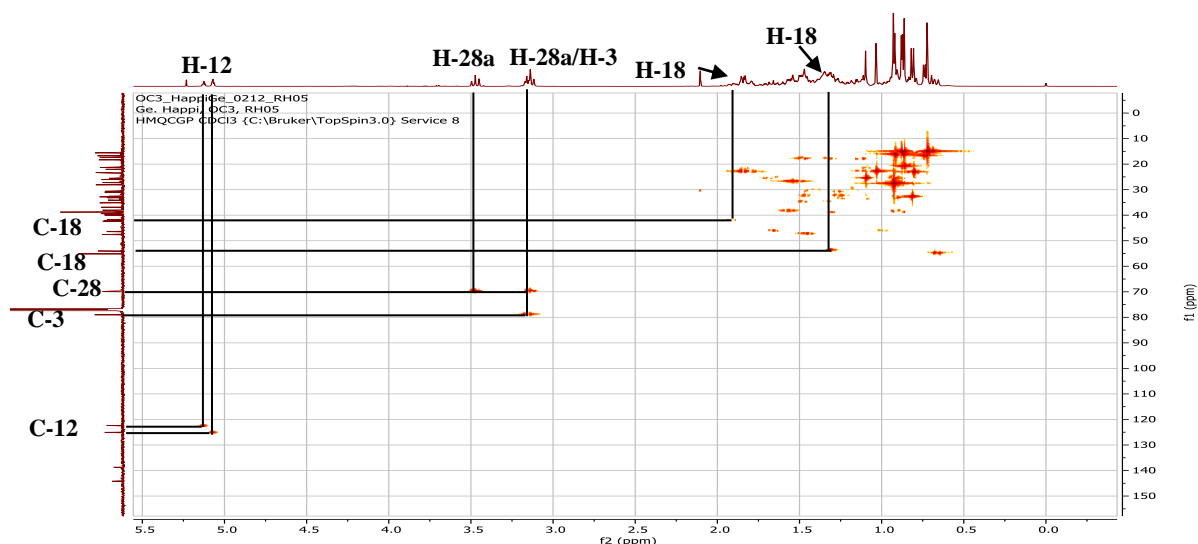


Figure 63: HMQC spectrum of RH5

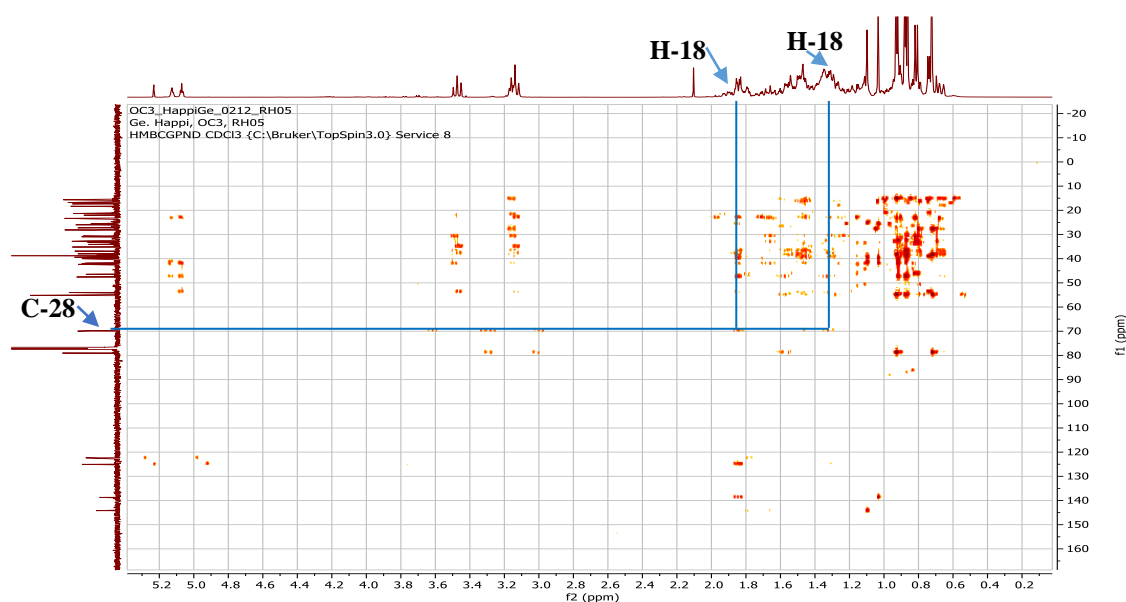


Figure 64: HMBC spectrum of RH5

II.1.5.3.6. Structural identification of compound RH6

RH6 was obtained as a white powder in *n*-hexane/EtOAc (70:30). It is soluble in pyridine and give a red color which turns purple to the Liebermann-Burchard test characteristic of triterpenoids.

Its molecular formula $C_{30}H_{48}O_3$ was deduced from the HRESIMS spectrum (Figure 65) which showed the sodium adduct peak $[M+Na]^+$ at m/z 479.3542 (calcd. for $C_{30}H_{48}O_3Na$, 479.3501), with seven degrees of unsaturation.

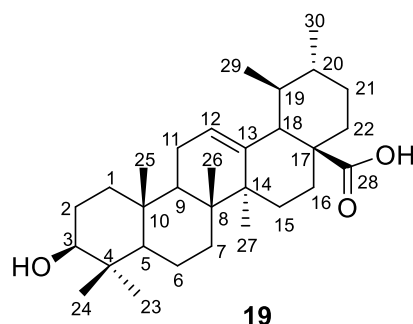
Its 1H NMR spectrum (Figure 66) exhibited:

- five singlets of three protons each at δ_H 0.89 (3H, s, H-25), 0.80 (3H, s, H-24), 0.85 (3H, s, H-26), 1.12 (3H, s, H-27) and 1.02 (3H, s, H-23) attributable to five angular methyl groups of pentacyclic triterpenoid skeleton (Mahato and Kundu, 1994);
- two doublets of 3 protons each at δ_H 0.95 (3H, d, $J = 6.4$ Hz, H-30) and 1.00 (3H, d, $J = 6.4$ Hz);
- another doublet of one proton at δ_H 2.63 (1H, d, $J = 11.3$ Hz, H-18) attributable to the proton H-18, which is characteristic to urs-12-ene series (Mahato and Kundu, 1994);
- a signal at δ_H 3.45 (1H, dd, $J = 10.2, 5.9$ Hz, H-3) attributable to the oxymethine proton at position 3;
- a signal at δ_H 5.49 (1H, t, $J = 3.3$ Hz, H-12) attributable to the olefinic proton at position 12 of the urs-12-ene series (Uddin *et al.*, 2011; Mahato and Kundu, 1994).

Its ^{13}C spectrum (Figure 67) displayed carbon resonances which were sorted by DEPT and HMQC techniques into:

- seven methyl groups at δ_C 15.4 (C-25), 16.3 (C-24), 17.2 (C-26), 17.3 (C-29), 21.1 (C-30), 23.6 (C-27) and 28.5 (C-23);
- nine methylene groups at δ_C 18.6 (C-6), 23.4 (C-11), 24.6 (C-16), 27.9 (C-15), 28.4 (C-2), 30.8 (C-21), 33.3 (C-7), 37.2 (C-22) and 38.8 (C-1);
- six methine groups at δ_C 77.8 (C-3), 55.5 (C-5), 47.8 (C-9), 53.3 (C-18), 39.2 (C-19) and 39.1 (C-20);
- six quaternary carbons at δ_C 37.0 (C-10), 39.1 (C-4), 39.7 (C-8), 42.2 (C-14), 47.8 (C-17) and δ_C 179.6 (C-28) attributable to the carbon of a carboxyl group;
- two olefinic carbons at δ_C 139.0 (C-13) and 125.4 (C-12) attributable respectively to C-13 and C-12 which are characteristic to urs-12-ene triterpenoids. (Mahato and Kundu 1994);

All these data, compared with those in the literature, allowed us to identify RH6 as ursolic acid (**19**), previously isolated from *Gentiana vietchiorun* (Gentianaceae) by Hong-Peng *et al.* (2014).



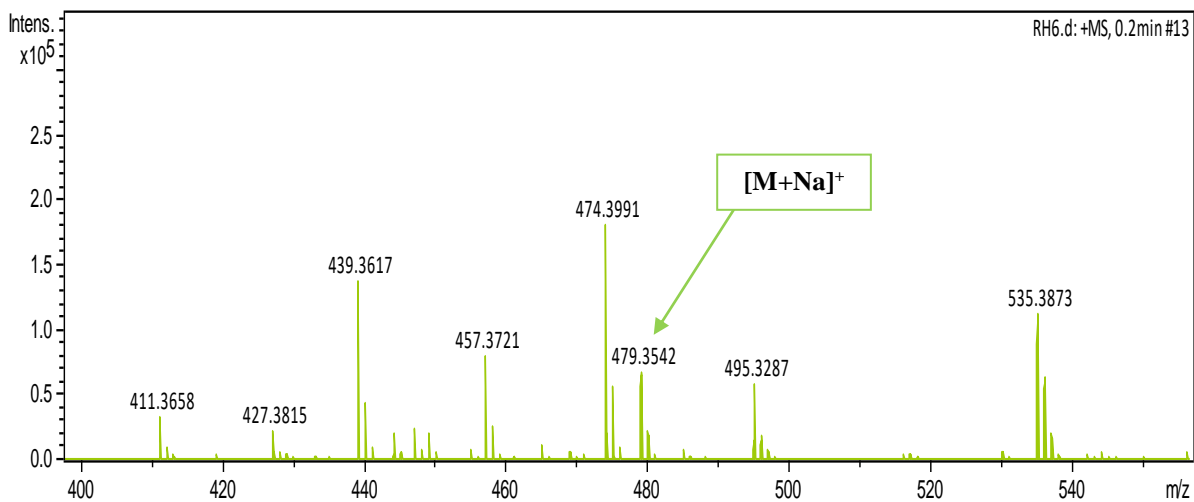


Figure 65: HRESI mass spectrum of RH6

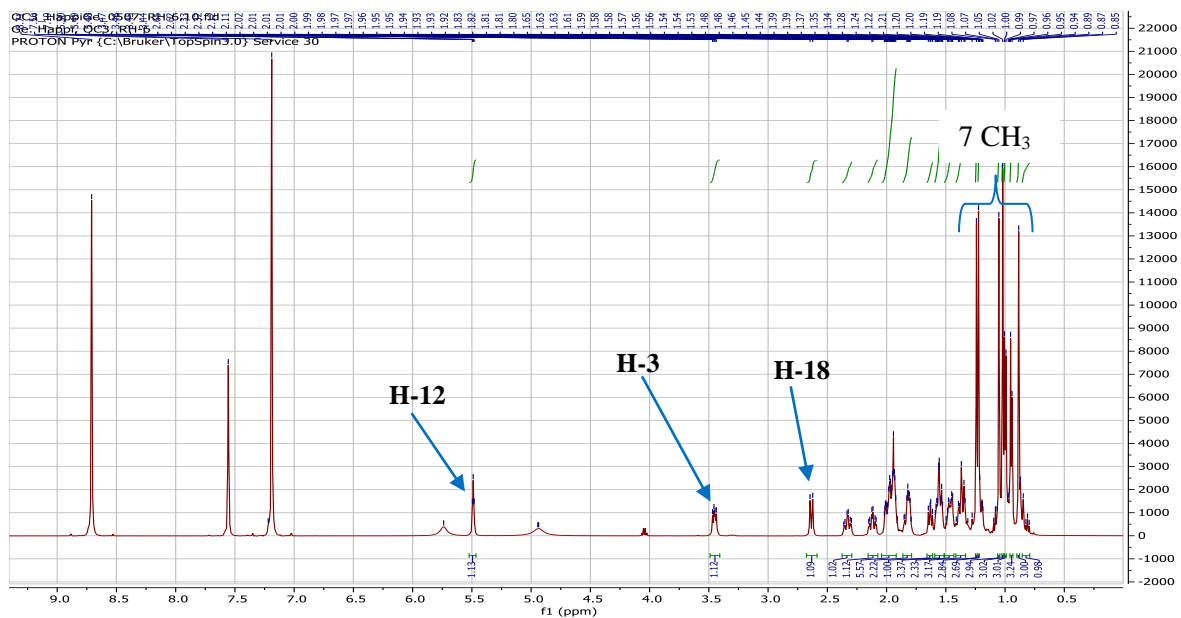


Figure 66: ¹H NMR spectrum (500 MHz, pyridine-*d*₅) of RH6

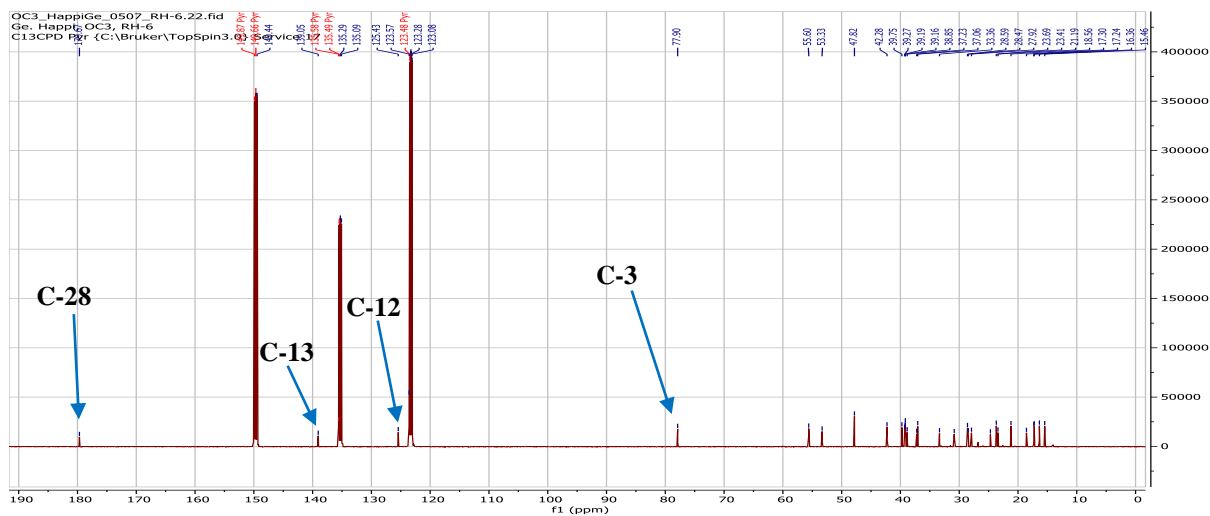


Figure 67: ¹³C NMR spectrum (pyridine-*d*₅, 125 MHz) of RH6

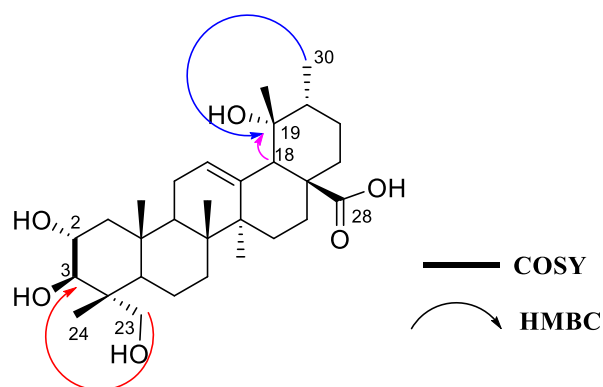
II.1.5.3.7. Structural identification of compound WN5

WN5 was obtained as a white powder in *n*-hexane/EtOAc (40:60). It is soluble in pyridine and give a red color which turns purple to the Liebermann-Burchard test characteristic of triterpenoids.

The ^1H (Figure 68) and ^{13}C (Figure 69) NMR spectra of WN5 were very similar to those of RH6. Except for the additional peaks on the proton spectrum of WN5 at δ_{H} 3.37 (1H, d, $J = 11.0$ Hz, H-23) and 3.50 (1H, d, $J = 11.0$ Hz, H-23) assignable to two oxymethylene protons and at δ_{H} 3.87 (1H, ddd, $J = 11.9, 4.6, 2.9$ Hz, H-2) assignable to an oxymethine proton. The carbon spectrum of WN5 sorted by HMQC (Figure 70) technique displayed additional peaks at δ_{H} 65.6 (C-2), 70.1 (C-23) and 72.0 (C-19).

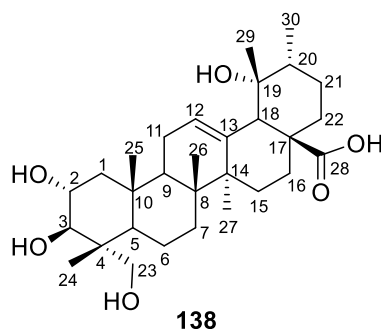
The ^1H - ^1H COSY spectrum (Figure 71) of WN5 showed correlations between protons H-2 (δ_{H} 3.87) and H-3 (δ_{H} 3.60) confirming the position of carbon C-2 (δ_{C} 65.6).

On the HMBC spectrum of WN5 (Figure 72), the correlations observed between the protons H-23 (δ_{H} 3.37, 3.50) and the carbon C-3 (δ_{C} 70.1), confirmed the position of carbon C-23. Also, the correlations observed between the protons H-18 (δ_{H} 2.50), H-30 (δ_{H} 0.91) and the carbon C-19 (72.0), allowed us to fix a hydroxyl group at position 19. The configuration of protons H-2 and H-3 was deduced from the value of the coupling constant $J = 11.9$ Hz between these protons.



Scheme 21: Some key COSY and HMBC correlations of WN5

All these data, compared to those in the literature were in agreement with that of myrianthic acid (**138**), previously isolated from *Gambeya boukokoensis* (Sapotaceae) by Wandji *et al.* (2003).



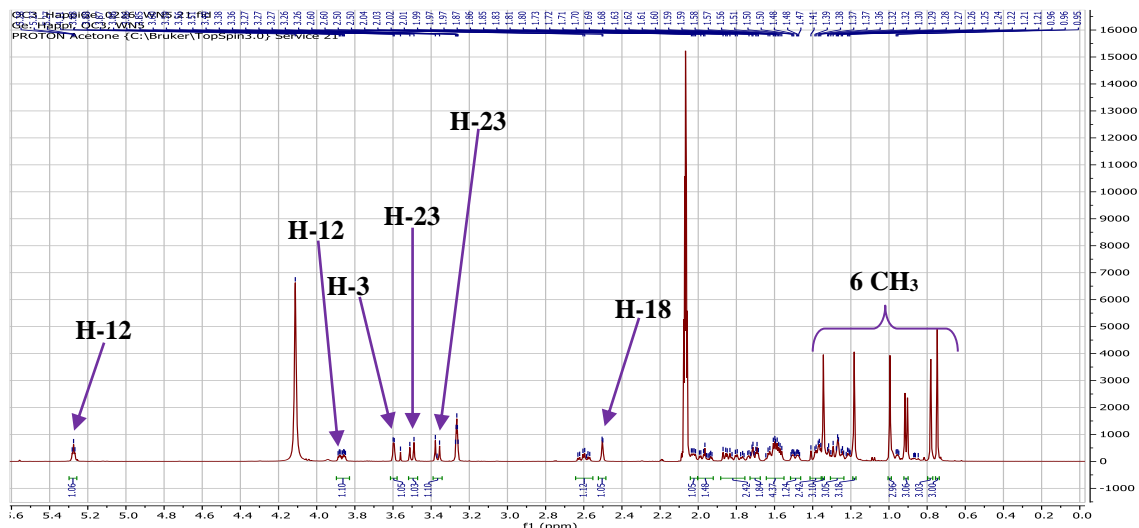


Figure 68: ^1H NMR spectrum (acetone- d_6 /methanol- d_4 , 500 MHz) of WN5

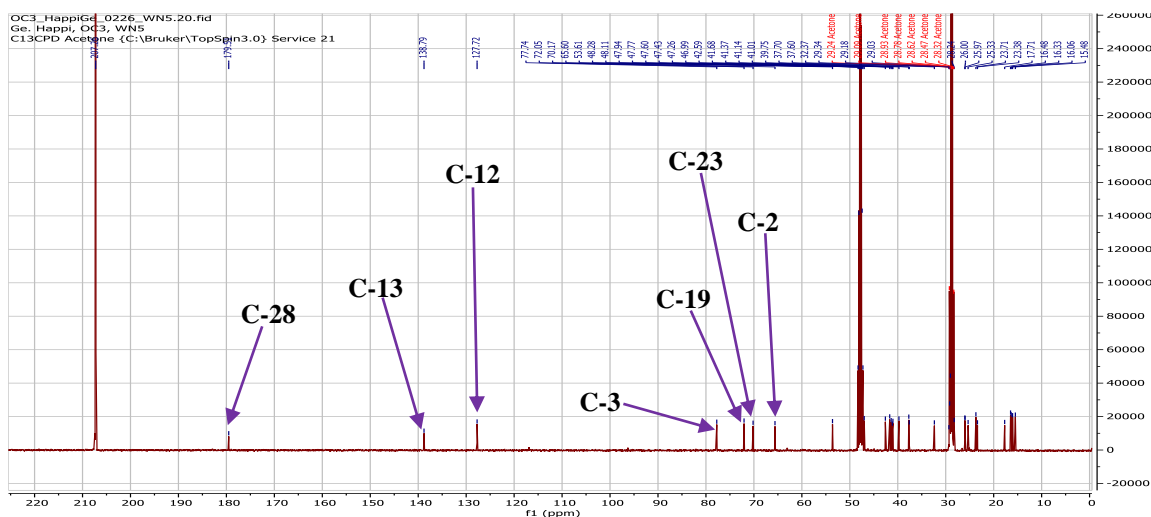


Figure 69: ^{13}C NMR spectrum (acetone- d_6 /methanol- d_4 , 125 MHz) of WN5

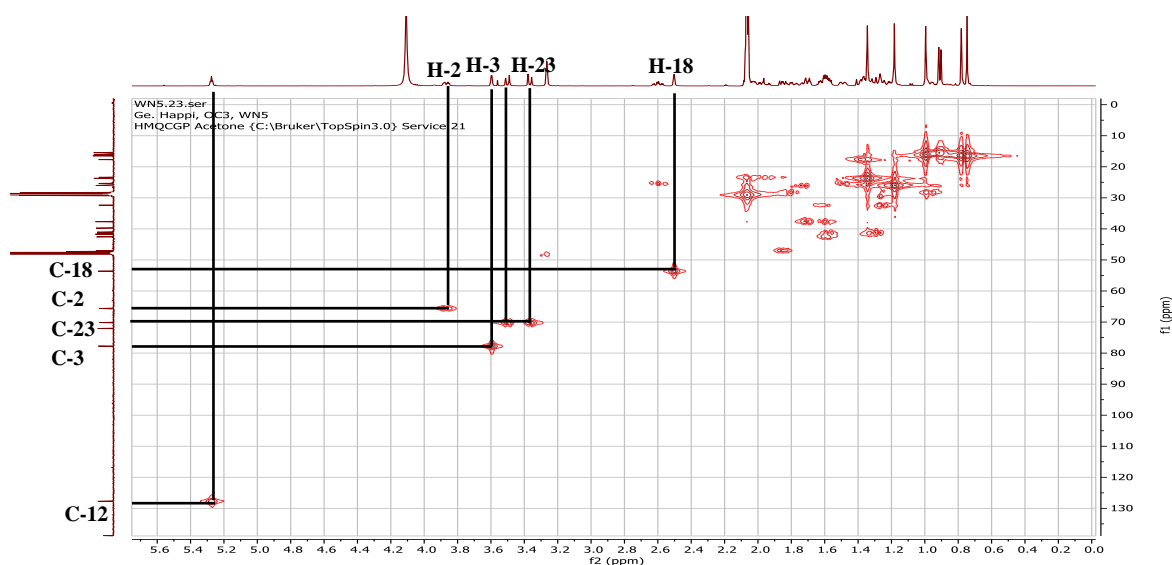


Figure 70: HMBC spectrum of WN5

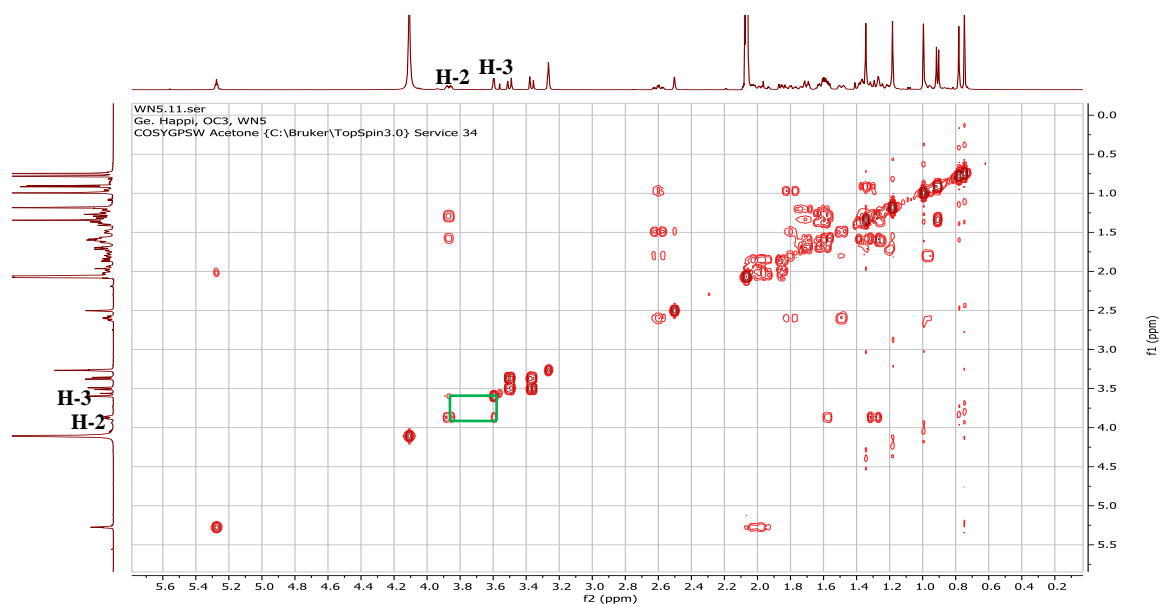


Figure 71: COSY spectrum of WN5

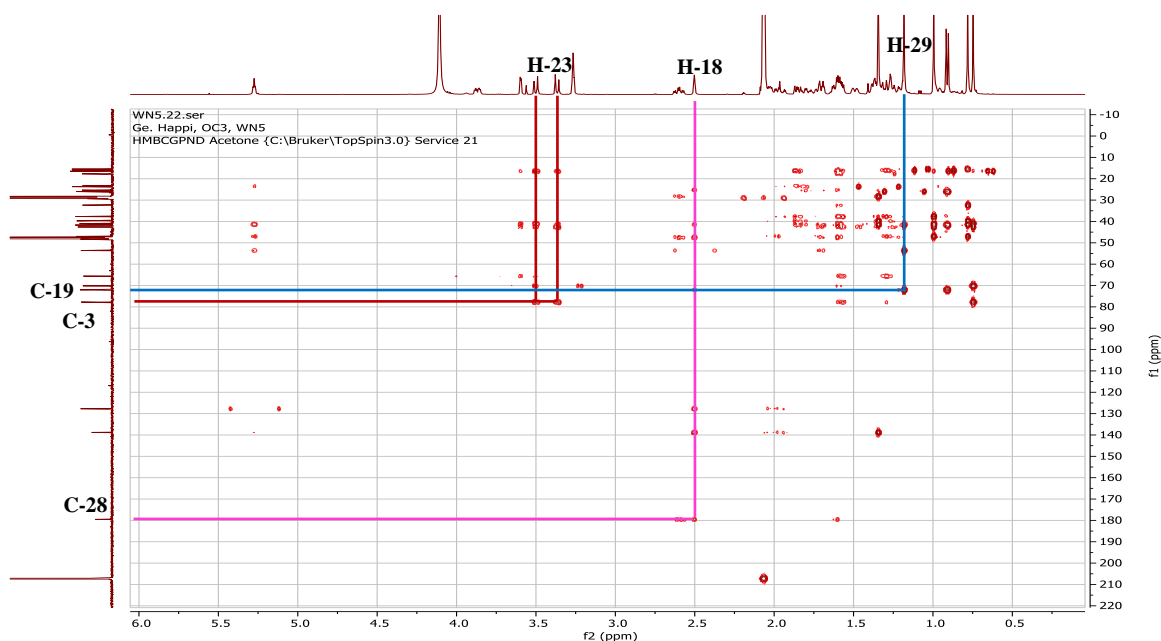


Figure 72: HMBC spectrum of WN5

II.1.5.3.8. Structural identification of compound RH9

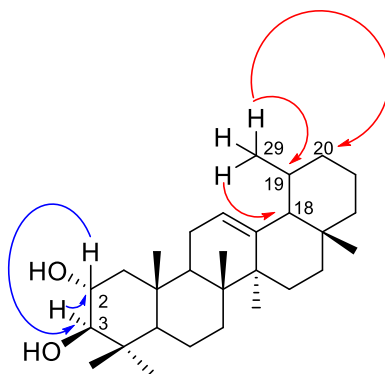
RH9 was obtained as a white powder in hexane/EtOAc (60:40). It is soluble in the mixture acetone/methanol and give a red color which turns purple to the Liebermann-Burchard test characteristic of triterpenoids.

Its molecular formula $C_{29}H_{48}O_2$ was deduced from the HRESIMS spectrum (Figure 73) which showed the pseudomolecular ion peak $[M-2H_2O+H]^+$ at m/z 393.3564 (calcd. for $C_{29}H_{45}$, 393.3521), implying six degrees of unsaturation.

The 1H (Figure 74) and ^{13}C (Figure 75) NMR spectra of RH9 were very similar to those of RH6. Except for the additional peaks on the proton spectrum of RH9 at 3.66 (1H,

ddd, $J = 11.3, 9.7, 4.5$ Hz, H-2), attributable to an oxymethine proton at position 2 and the absence of the peak of the methyl at position 30. The ^{13}C NMR spectrum (Figure 75) sorted by HMQC spectrum (Figure 76) displayed an additional peak at $\delta_{\text{C}} 69.2$ (C-2) and we noted the disappearance of the peak of the carboxylic acid group at position 28.

The correlation observed in the HMBC spectrum (Figure 77) between proton H-3 ($\delta_{\text{H}} 2.96$) and carbon C-2 ($\delta_{\text{C}} 69.2$) and between proton H-2 ($\delta_{\text{C}} 3.66$) and carbon C-3 ($\delta_{\text{C}} 84.1$), confirmed the position of the second oxymethine carbon at position 2. The absence of the methyl doublet at position 30 was supported on the HMBC spectrum by the correlations between proton H-29 and carbons C-20 ($\delta_{\text{C}} 30.5$), C-19 ($\delta_{\text{C}} 40.1$) and C-18 ($\delta_{\text{C}} 54.1$). The configuration of proton H-2 and proton H-3 was deduced from the value of the coupling constant $J = 9.7$ Hz between these protons.



Scheme 22: Some key COSY and HMBC correlation of RH9

All these data, compared to those in the literature were in agreement with that of 30-*nor-2 α ,3 β -dihydroxyurs-12-ene* (Carisursane A) (**139**), previously isolated from *Carissa opaca* (Apocynaceae) by Parveen *et al.* (2016).

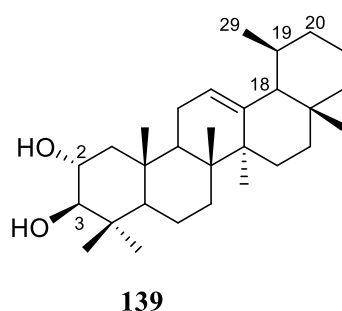


Table 33: ^{13}C (125 MHz) NMR data of WN5, RH6 (pyridine- d_5) and RH9 (acetone- d_6 /methanol- d_4) compared to myrianthic acid, ursolic acid [DMSO- d_6 , NMR ^{13}C (100 MHz)] and carisursane A [methanol- d_4 , NMR ^{13}C (100 MHz)]

	RH6	Ursolic acid (Hong-Peng <i>et al.</i> , 2014)	RH9	Carisursane A (Parveen <i>et al.</i> , 2016)	WN5	Myrianthic acid (Wandji <i>et al.</i> 2003)
Position	$\delta^{13}\text{C}$	$\delta^{13}\text{C}$	$\delta^{13}\text{C}$	$\delta^{13}\text{C}$	$\delta^{13}\text{C}$	$\delta^{13}\text{C}$
1	38.8	38.6	48.0	48.5	41.6	42.4
2	28.4	28.2	69.2	69.5	65.6	65.8
3	77.8	78.7	84.1	84.4	77.7	77.0
4	39.1	38.5	40.2	40.5	42.5	44.4
5	55.5	55.2	56.4	56.6	46.9	47.9
6	18.6	18.3	19.3	19.5	17.7	18.6
7	33.3	32.9	34.0	34.2	32.3	33.4
8	39.7	39.5	40.2	40.8	41.0	40.8
9	47.8	47.3	49.6	49.8	46.9	47.2
10	37.0	37.0	39.0	39.2	37.6	38.7
11	23.6	23.7	24.3	24.4	23.3	24.3
12	125.5	125.9	126.4	126.7	127.7	127.8
13	139.0	137.9	139.6	139.7	138.7	139.7
14	42.2	42.0	43.1	43.3	39.7	42.3
15	27.9	28.1	29.0	29.1	29.3	29.1
16	24.6	25.0	25.2	25.3	25.9	26.2
17	47.8	48.1	40.6	40.8	47.9	48.0
18	53.3	53.8	54.1	54.3	53.3	54.2
19	39.2	38.5	40.1	40.4	72.0	72.7
20	39.1	38.5	30.5	30.7	41.3	42.2
21	30.8	30.3	31.6	31.7	28.2	27.0
22	37.2	37.4	37.9	38.1	37.7	38.2
23	28.5	28.9	29.2	29.3	70.1	70.2
24	16.3	15.6	17.2	17.2	16.3	17.5
25	15.4	15.4	17.5	17.5	16.0	17.7
26	17.2	17.1	17.6	17.6	16.4	17.8
27	23.6	23.5	24.1	24.0	23.7	25.1
28	179.6	179.6	17.8	17.8	179.5	180.0
29	17.3	17.0	21.5	21.5	26.0	26.2
30	21.1	21.4			15.4	15.6

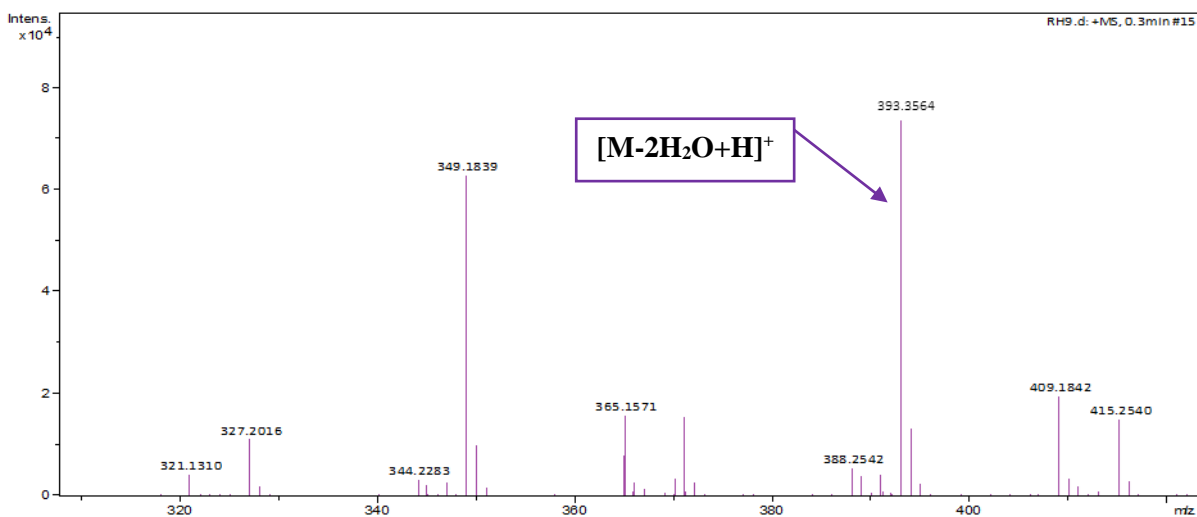


Figure 73: HRESI mass spectrum of RH9

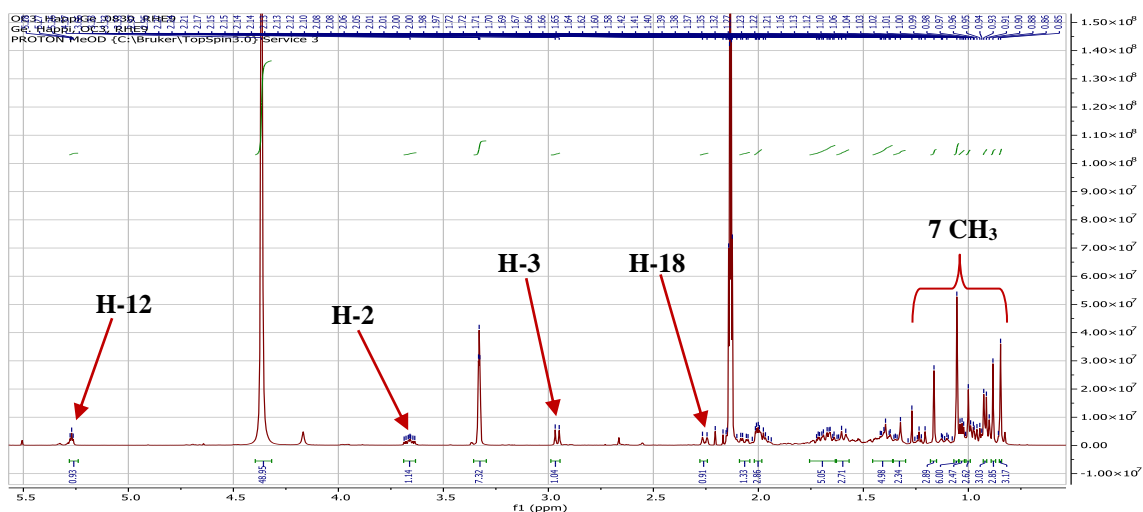


Figure 74: ¹H spectrum (acetone-*d*₆/methanol-*d*₄, 500 MHz) of RH9

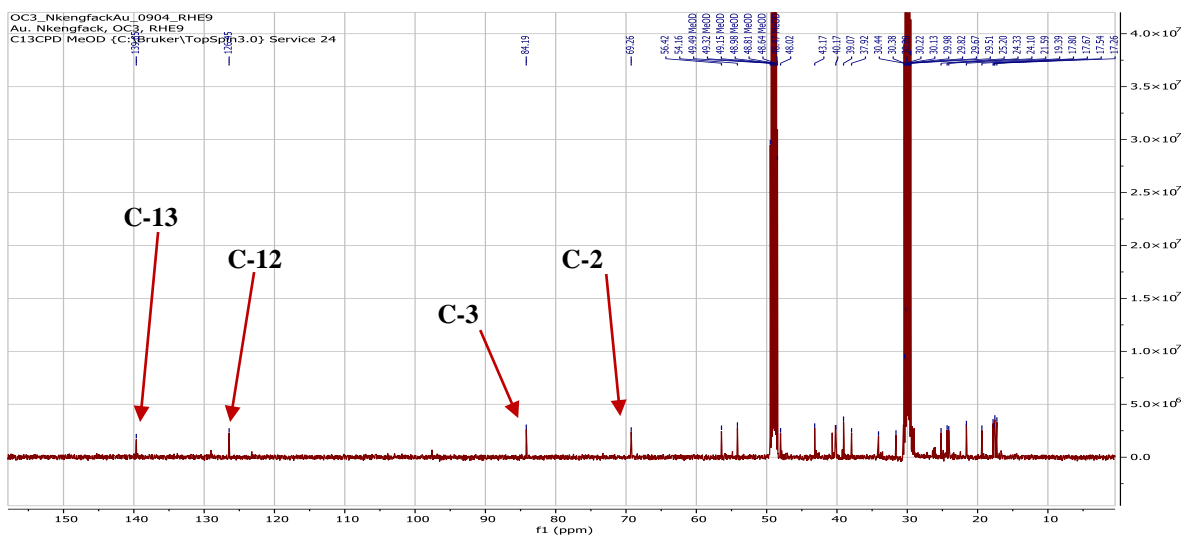


Figure 75: ¹³C spectrum (acetone-*d*₆/methanol-*d*₄, 125 MHz) of RH9

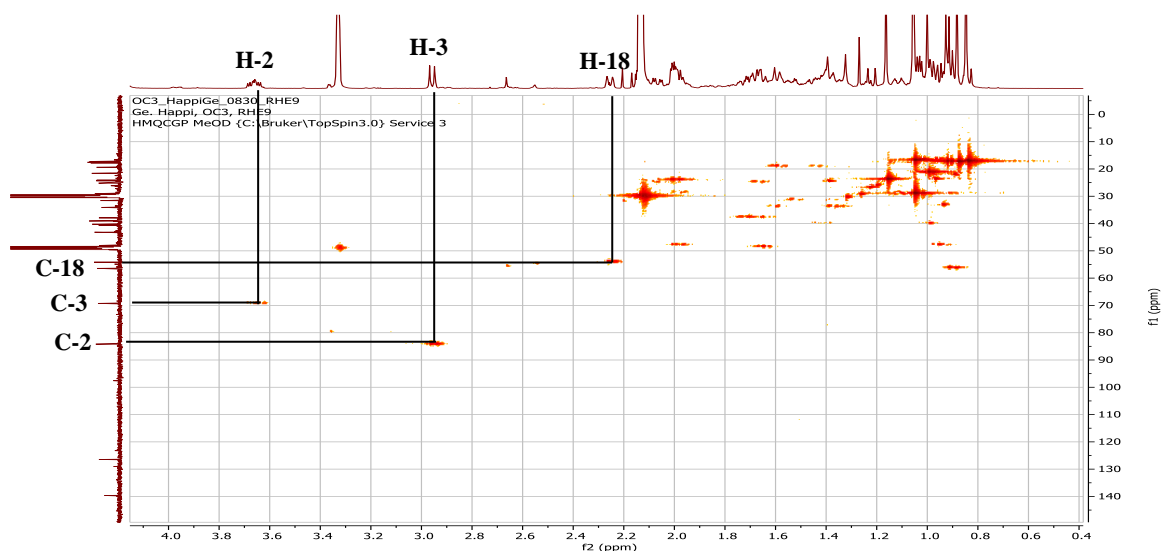


Figure 76: HMQC spectrum of RH9

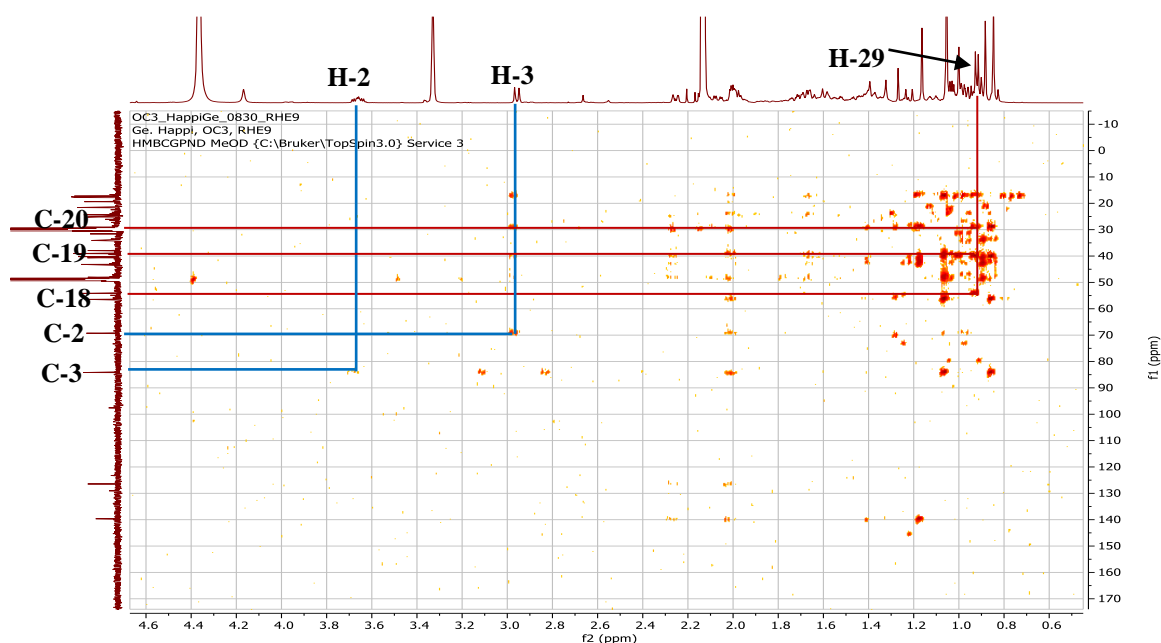


Figure 77: HMBC spectrum of RH9

II.1.5.3.9. Structural identification of compound RH15

RH15 was obtained as a white powder in *n*-hexane/CH₂Cl₂ (98:2). It is soluble in methylene chloride and give a red color which turns purple to the Liebermann-Burchard test characteristic of triterpenoids.

Its molecular formula C₄₆H₈₀O₂ was deduced from the HRESIMS spectrum (Figure 78) which showed the sodium adduct peak [M+Na]⁺ at *m/z* 687.6055 (calcd. for C₄₆H₈₀O₂Na, 687.6056), with seven degrees of unsaturation.

Its ¹H NMR spectrum (Figure 79) displayed resonance of:

- six singlets of three protons each at δ_{H} 0.71 (3H, s, H-28), 0.77 (3H, s, H-23), 0.78 (3H, s, H-25), 0.80 (3H, s, H-24), 0.87 (3H, s, H-27), and 0.96 (3H, s, H-26)

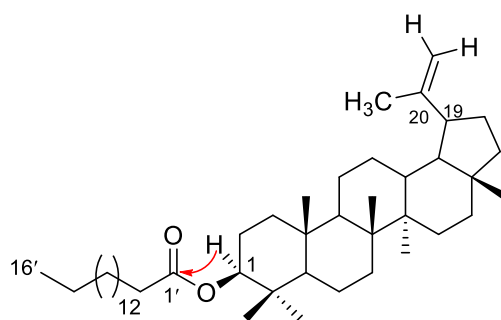
attributable to angular methyl groups of lupane type pentacyclic triterpenoid skeleton (Mahato and Kundu, 1994);

- singlet of three protons at δ_H 1.62 (3H, s, H-30) attributable to vinyl methyl;
- signal at δ_H 2.31 (1H, td, $J = 11.0, 5.7$ Hz, H-19) attributable to the proton at position 19 of the lup-20(29)-ene series (Mahato and Kundu, 1994);
- a signal at δ_H 4.40 (1H, dd, $J = 10.8, 5.5$ Hz, H-3) attributable to the oxymethine proton at position 3;
- two signals each at δ_H 4.50 (1H, brs, H-29a) and 4.62 (1H, brs, H-29b) attributable to the protons of the terminal methylene group at position C-29 of lup-20(29)-ene (Mahato and Kundu, 1994);
- a signal at δ_H 2.22 (2H, t, $J = 7.2$ Hz, H-1') characteristic of the protons of a methylene at position α of the carboxylate group;
- a broad peak at δ_H 1.21 (m, 14CH₂) integrating for several protons attributable to a long aliphatic chain;
- a terminal methyl at δ_H 0.81 (3H, t, $J = 6.2$ Hz, H-16').

Its ¹³C NMR spectrum (Figure 80) displayed carbon resonances which were sorted by HMQC technique in:

- seven methyl groups each at δ_C 14.5 (C-27), 15.9 (C-26), 16.1 (C-24), 16.5 (C-25), 18.0 (C-28), 19.2 (C-30) and 28.0 (C-23);
- two olefinic carbons at δ_C 150.9 (C-20) and 109.3 (C-29), characteristic of triterpenoids of the lup-20(29)-ene series (Mahato and Kundu, 1994);
- one oxymethine signal at δ_C 80.6 (C-3) attributable to the carbon C-3 and five methine signals at δ_C 37.8 (C-13), 48.1 (C-19), 48.2 (C-18), 50.3 (C-9) and 55.4 (C-5);
- ten methylene groups each at δ_C 18.2 (C-6), 20.9 (C-11), 25.1 (C-12), 27.4 (C-2), 27.9 (C-15), 29.8 (C-21), 34.2 (C-7), 35.5 (C-16), 38.3 (C-1) and 40.0 (C-22);
- five quaternary carbons at δ_C 37.4 (C-4), 40.8 (C-8), 37.0 (C-10), 42.8 (C-14) and 43.0 (C-17);
- a signal at δ_C 173.7 (C-1') attributable to the carbon of an ester carbonyl;
- a set of peaks between δ_C 29.8-29.1 attributable to the aliphatic long chain;
- a terminal methyl at δ_C 14.1 (C-16').

Its HMBC spectrum (Figure 81), displayed a correlation between the proton H-3 (δ_H 4.40) and the carbon at δ_C 173.7 (C-1'), allowing us to attach the fatty acid at position 3.



Scheme 23: Key HMBC correlation of RH15

The length of this fatty acid is confirmed on the APCI mass spectrum (Figure 82) by the peak at m/z 409.4167 corresponding to $[M-C_{16}H_{31}O_2]$.

Based on the above mentioned data, **RH15** was identified as lupeol palmitate (**140**), previously isolated from *Ficus vallis-choudae* Delile (Moraceae) by Bankeu *et al.* (2017).

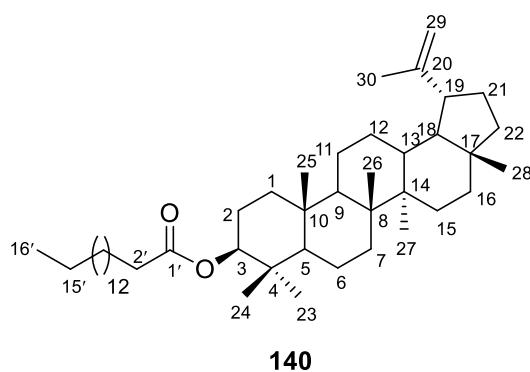


Table 34: ^1H (500 MHz) and ^{13}C (125 MHz) NMR data of RH15 in CDCl_3 compared to lupeol palmitate [CDCl_3 , NMR ^{13}C (100 MHz)]

RH15			Lupeol palmitate (Bankeu <i>et al.</i> , 2017)
Position	$\delta^{13}\text{C}$	$\delta^1\text{H}$ (m, J in Hz)	$\delta^{13}\text{C}$
1	38.3	1.61 (1H, m)	38.3
2	27.4	1.95 (1H, m), 1.53 (1H, m)	27.4
3	80.6	4.40 (1H, dd, 10.8; 5.6)	80.6
4	37.8	-	37.8
5	55.4	0.70 (1H, m)	55.4
6	18.2	1.34 (1H, m), 1.44 (1H, m)	18.3
7	34.2	1.33 (1H, m)	34.7
8	40.8	-	40.9
9	50.3	1.22 (1H, m)	50.4
10	37.0	-	37.1
11	20.9	1.35 (1H, m)	21.0
12	25.1	1.54 (1H, m)	25.1
13	37.8	1.60 (1H, m)	38.1
14	42.8	-	42.8
15	27.9	1.54 (1H, m)	27.4
16	35.5	1.31 (1H, m), 1.42 (1H, m)	35.6
17	43.0	-	43.0
18	48.2	1.30 (1H, m)	48.3
19	48.1	2.31 (1H, td, 11.0, 5.7)	48.0
20	150.9	-	151.0
21	29.8	1.85 (1H, m)	29.8
22	40.0	1.30 (1H, m), 1.12 (1H, m)	40.0
23	28.0	0.77 (3H, s)	28.0
24	16.1	0.80 (3H, s)	16.0
25	16.5	0.78 (3H, s)	16.6
26	15.9	0.96 (3H, s)	16.2
27	14.5	0.87 (3H, s)	14.5
28	18.0	0.71 (3H, s)	18.0
29	109.3	4.62 (1H, brs) 4.50 (1H, brs)	109.3
30	19.2	1.62 (3H, s)	19.3
1'	173.7	-	173.7
2'	34.8	2.22 (2H, t, 7.2)	31.9
3'	25.1	1.49 (1H, m)	25.2
(CH ₂) _{4'-14'}	29.1-29.8	1.25-1.17 (1H, m)	29.4-29.9
15'	22.7	1.50 (1H, m)	22.7
16'	14.1	0.81 (3H, t, 6.2)	14.1

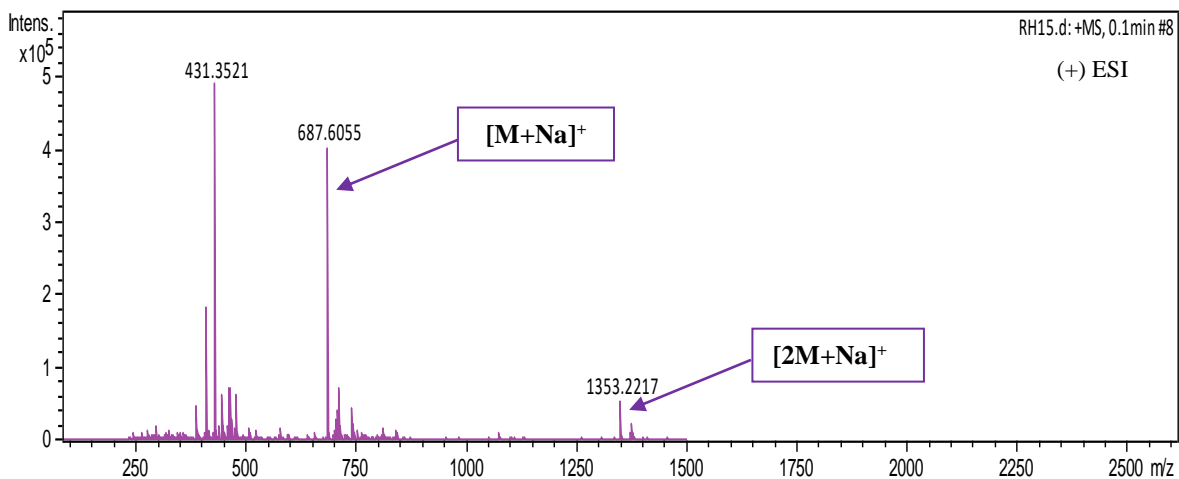


Figure 78: HRESI spectrum of RH15

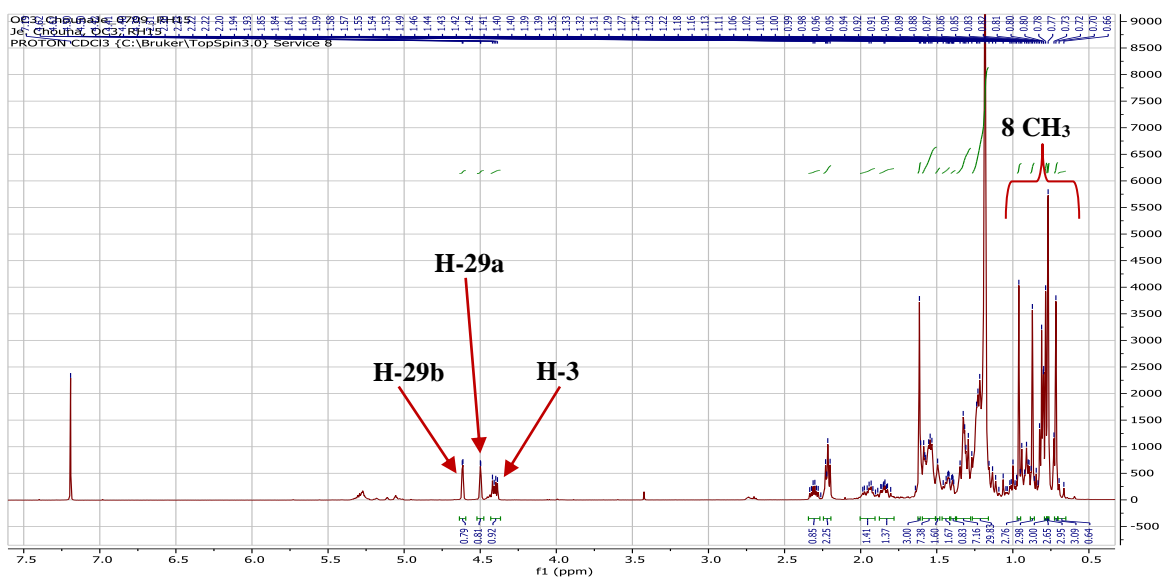


Figure 79: ¹H NMR spectrum (CDCl₃, 500 MHz) of RH15

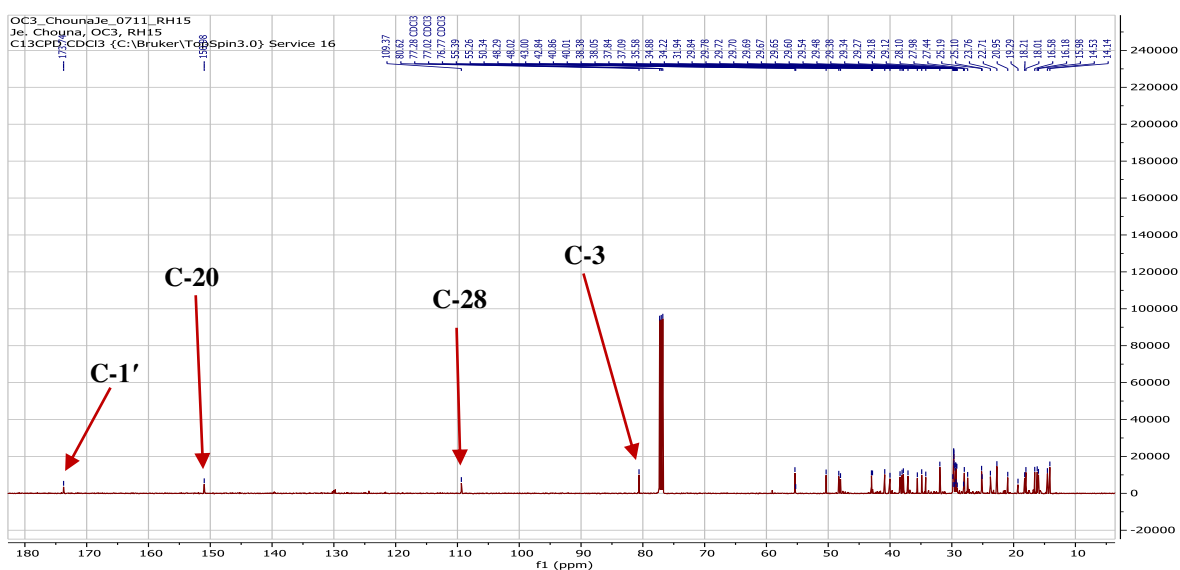


Figure 80: ¹³C NMR spectrum (CDCl₃, 125 MHz) of RH15

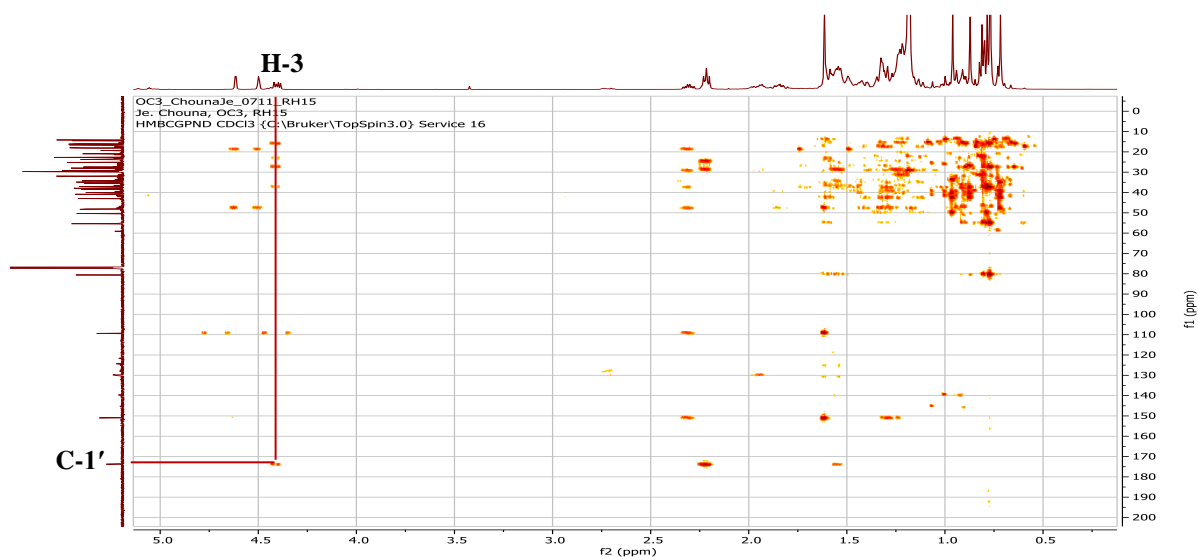


Figure 81: HMBC spectrum of RH15

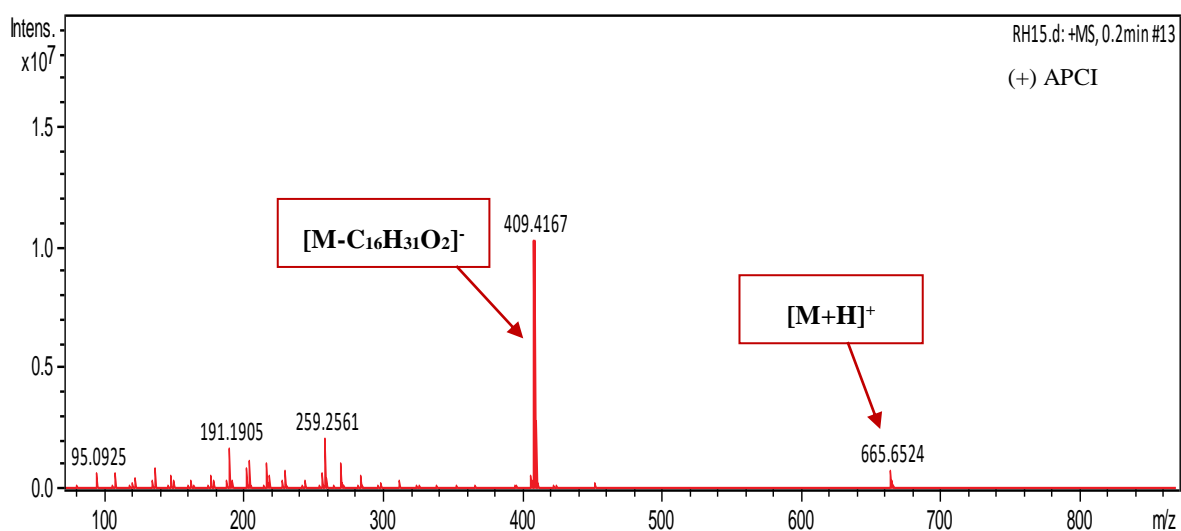


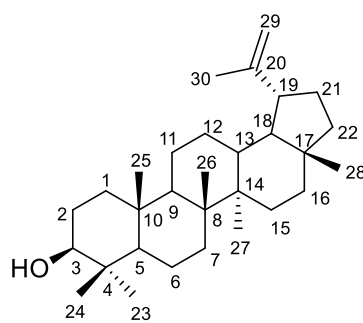
Figure 82: HRAPCI spectrum of RH15

II.1.5.3.10. Structural identification of compound RH16

RH16 was obtained as a white powder in *n*-hexane/CH₂Cl₂ (60:40). It is soluble in methylene chloride and give a red color which turns purple to the Liebermann-Burchard test characteristic of triterpenoids.

The ¹H (Figure 83) and ¹³C (Figure 84) NMR spectra of RH16 were very similar to those of RH15. However, we noted the disappearance of the peaks of the acid long chain at position 3 on the spectra of RH16.

The above data, were in agreement compared with those described in the literature for lupeol (**118**), previously isolated from *Diospyros rubra* (Rubiaceae) by Supaluk *et al.* (2010).



118

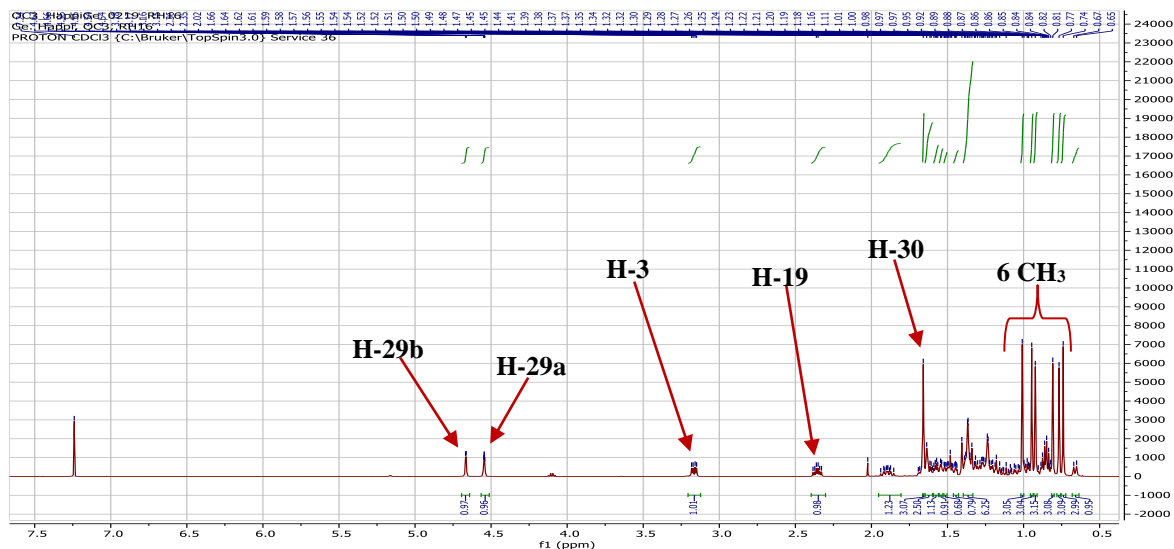


Figure 83: ¹H NMR spectrum (CDCl₃, 500 MHz) of RH16

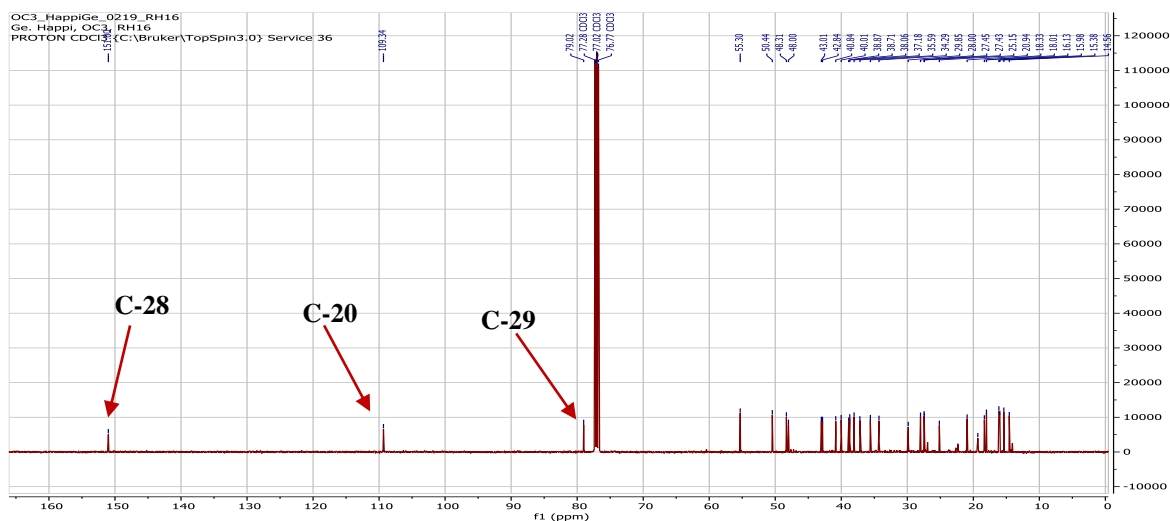


Figure 84: ¹³C NMR spectrum (CDCl₃, 125 MHz) of RH16

II.1.2.3.11. Structural identification of compound BLE30

BLE30 was obtained as a white powder in *n*-hexane/EtOAc (95:5). It is soluble in methylene chloride and gave a red color which turns purple to the Liebermann-Burchard test characteristic of triterpenoids.

Its molecular formula $C_{30}H_{48}O$ was deduced from the HRESIMS spectrum (Figure 85) which showed the sodium adduct peak $[M+Na]^+$ at m/z 447.3590 (calcd. for $C_{30}H_{48}ONa$, 447.3605), implying six degrees of unsaturation.

The 1H (Figure 86) and ^{13}C (Figure 87) NMR spectra of BLE30 are very similar to those of RH16. However, we noted the absence of a peak on the proton spectrum of BLE30 at δ_H 3.17 (1H, dd, $J = 11.4, 4.9$ Hz, H-3), attributable to the oxymethine proton at position 3 and the presence of a carbonyl group at δ_C 218.2 (C-3) on the ^{13}C NMR spectrum which replaced the oxymethine carbon group at δ_C 79.0 (C-3) (Figure 83).

All these data were similar to those described in the literature for lupenone (**140**), previously isolated from *Diospyros rubra* by Supaluk *et al.* (2010).

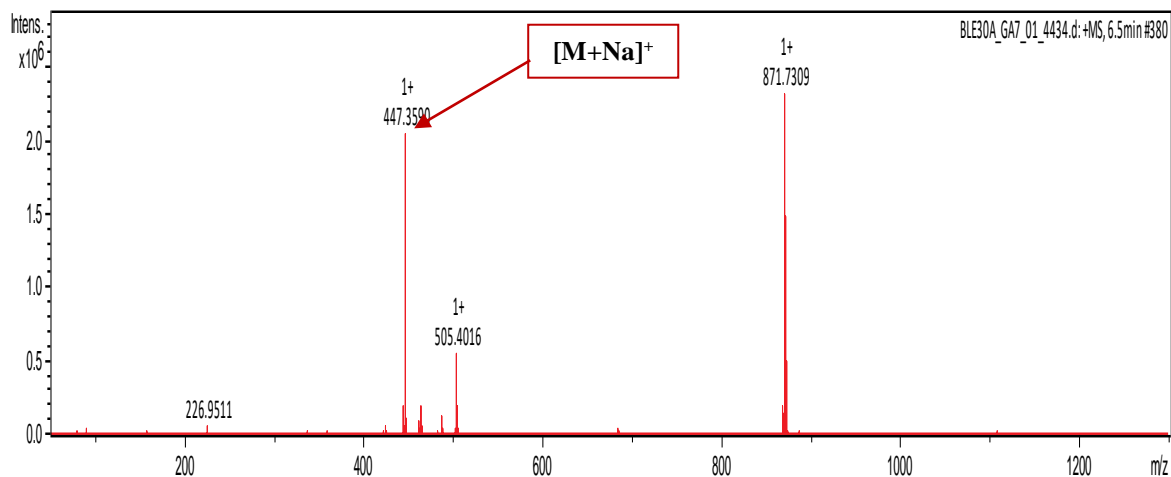
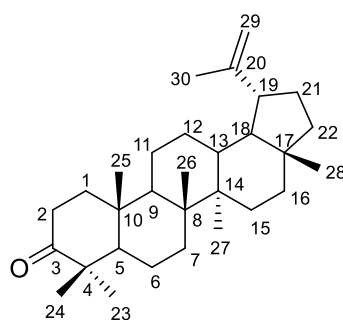


Figure 85: HRESIMS mass spectrum of BLE30

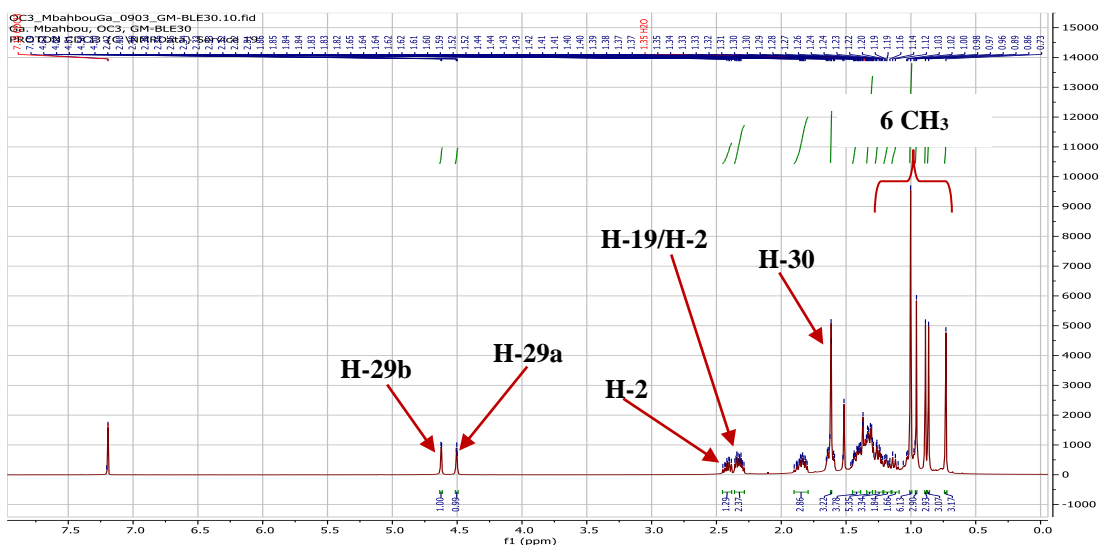


Figure 86: ^1H NMR spectrum (500 MHz, CDCl_3) of BLE30

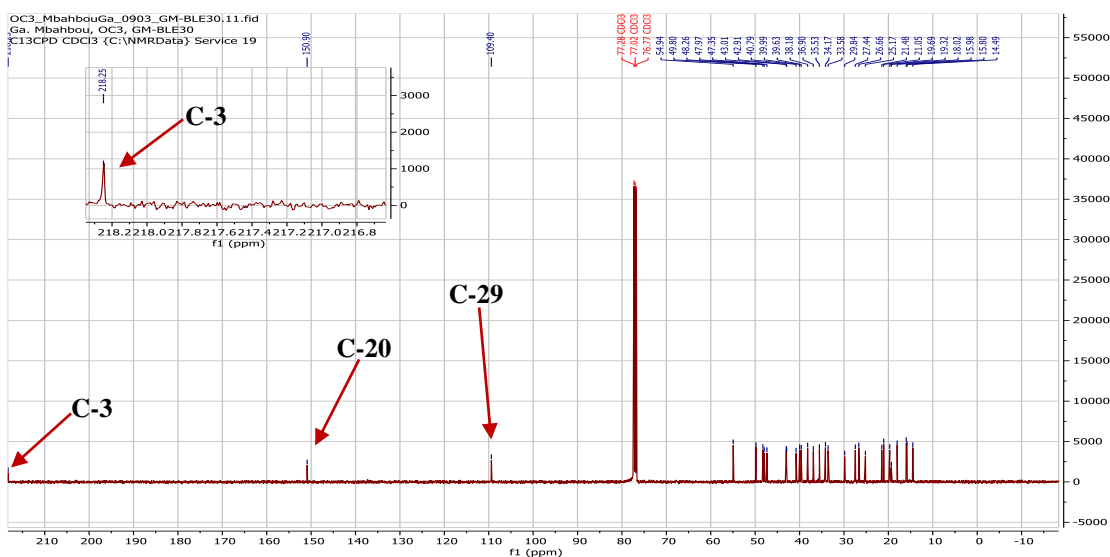


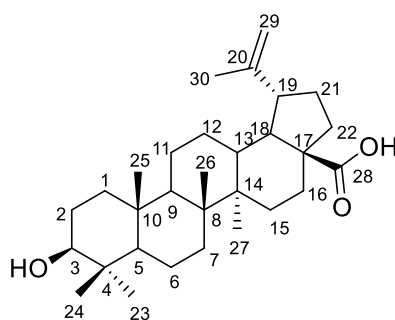
Figure 87: ^{13}C NMR spectrum (125 MHz, CDCl_3) of BLE30

II.1.5.3.12. Structural identification of compound SNC11

SNC11 was obtained as a white powder in *n*-hexane/EtOAc (70:30). It is soluble in pyridine and give a red color which turns purple to the Liebermann-Burchard test characteristic of triterpenoids.

The ^1H (Figure 88) and ^{13}C (Figure 89) NMR spectra of SNC11 are very similar to those of RH16. However, we noted the presence of an additional peak on the ^{13}C NMR spectrum of SNC11 at δ_{C} 178.6 (C-28), corresponding a carboxylic acid group.

The structure (**64**) was assigned to SNC11, which is that of betulinic acid, previously isolated from *Combretum laxum* by Eder *et al.* (2008).



64

Table 35: ^{13}C (125 MHz) NMR data of SNC11 (pyridine- d_5), BLE30 and RH16 in CDCl_3 compared to betulinic acid [CDCl_3 , NMR ^{13}C (100 MHz)], lupenone [CDCl_3 , NMR ^{13}C (75 MHz)] and lupeol

	SNC11	Betulinic acid (Eder et al., 2008)	BLE30	Lupenone (Supaluk et al., 2010)	RH16	Lupeol (Ragasa et al., 2015)
Position	$\delta^{13}\text{C}$	$\delta^{13}\text{C}$	$\delta^{13}\text{C}$	$\delta^{13}\text{C}$	$\delta^{13}\text{C}$	$\delta^{13}\text{C}$
1	39.0	39.3	39.6	39.6	38.7	38.7
2	28.0	28.3	34.1	34.1	27.4	27.4
3	77.3	78.2	218.2	218.2	79.0	79.0
4	39.2	39.6	47.4	47.3	38.8	38.8
5	54.7	56.0	54.9	54.9	55.3	55.3
6	18.5	18.8	19.6	19.3	18.2	18.3
7	34.6	34.9	33.5	33.5	34.2	34.3
8	40.8	41.2	40.7	40.7	40.8	40.8
9	50.7	51.0	49.8	49.7	50.4	50.4
10	37.2	37.6	36.9	36.8	37.1	37.1
11	20.9	21.3	21.4	21.4	20.9	20.9
12	25.8	26.2	25.1	25.1	25.1	25.1
13	38.3	38.7	38.1	38.1	38.0	38.0
14	42.6	42.9	42.9	42.8	42.8	42.8
15	30.9	31.3	27.4	27.4	27.9	27.4
16	32.6	32.9	35.5	35.5	35.6	35.6
17	56.4	56.7	43.0	42.9	43.0-	43.0-
18	49.5	47.8	48.2	42.7	48.3	48.3
19	47.5	49.8	47.9	47.9	48.0	48.0
20	151.1	152.5	150.9	150.8	151.0	150.9
21	30.0	30.3	29.8	29.6	29.8	29.7
22	37.3	37.6	39.9	39.9	40.0	40.0
23	28.5	28.7	26.6	26.6	28.0	28.0
24	16.1	16.4	21.0	21.0	15.9	15.9
25	16.2	16.5	15.9	15.9	16.1	16.1
26	16.2	16.5	15.8	15.7	15.3	15.3
27	14.6	15.0	14.4	14.4	14.5	14.1
28	178.6	178.9	18.0	17.9	18.0	18.0
29	109.7	110.0	109.4	109.3	109.3	109.3
30	19.2	19.5	19.3	19.6	19.3	19.3

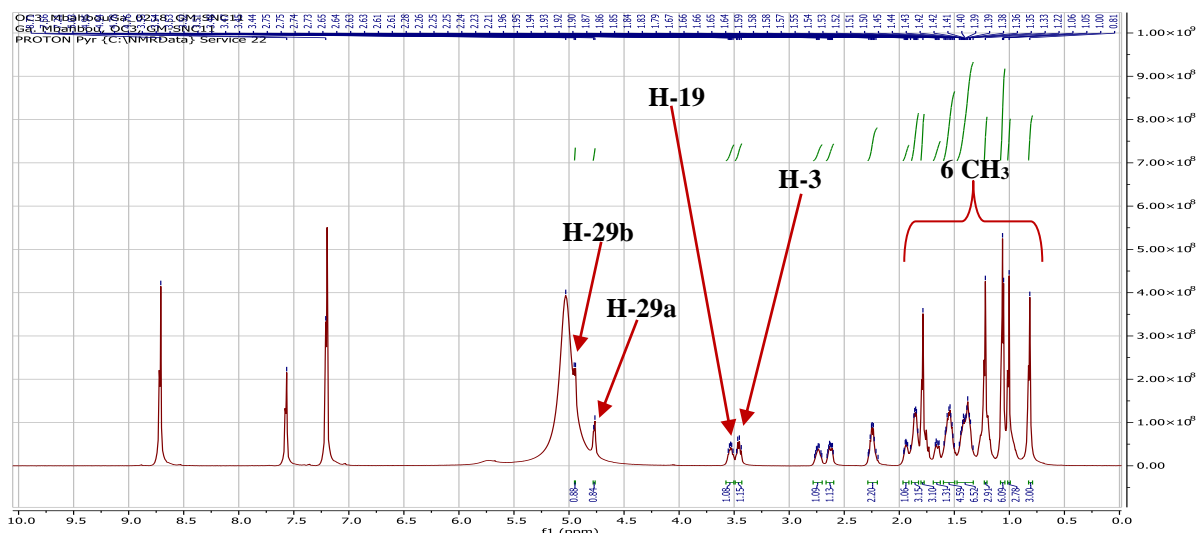


Figure 88: ^1H NMR spectrum (pyridine- d_5 , 500 MHz) of SNC11

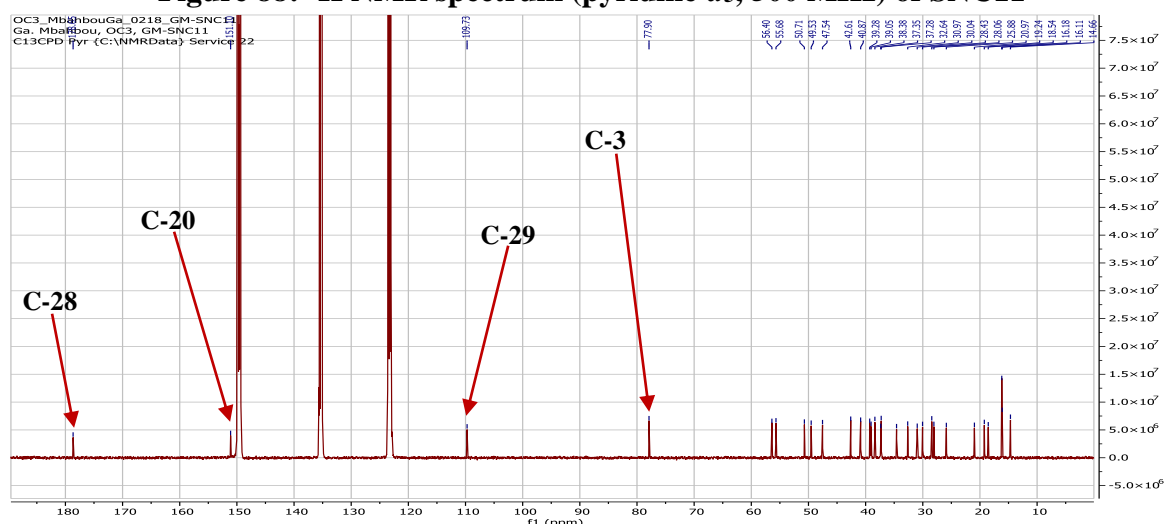


Figure 89: ^{13}C NMR spectrum (pyridine- d_5 , 125 MHz) of SNC11

II.1.5.3.13. Structural identification of compound SNC1

SNC1 was obtained as a white powder in *n*-hexane/EtOAc (95:5). It is soluble in dichloromethane and give a red color which turns purple to the Liebermann-Burchard test characteristic of triterpenoids.

Its molecular formula $\text{C}_{30}\text{H}_{50}\text{O}$ was deduced from the HRESIMS spectrum (Figure 90) which showed sodium adduct peak $[\text{M}+\text{Na}]^+$ at m/z 449.3767 (calcd. for $\text{C}_{30}\text{H}_{50}\text{ONa}$, 449.3759), implying six degrees of unsaturation.

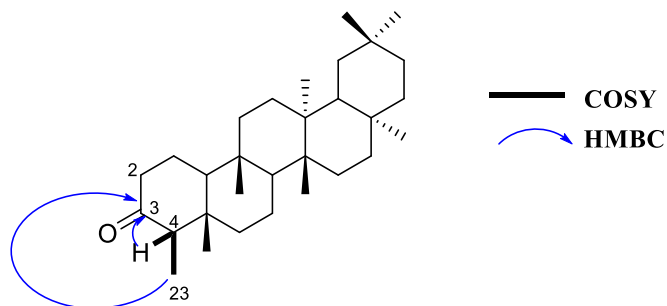
Its ^1H NMR spectrum (Figure 91) exhibited resonances of:

- seven singlets of three protons each at δ_{H} 0.71 (3H, s, H-24), 0.85 (3H, s, H-25), 0.93 (3H, s, H-26), 0.98 (3H, s, H-29), 0.99 (3H, s, H-30), 1.03 (3H, s, H-27) and 1.16 (3H, s, H-28);

- a doublet of 3 protons at δ_{H} 0.89 (3H, d, $J = 6.5$ Hz, H-23), characteristic of methyl at position 23 of pentacyclic triterpenoids of the friedelane series. This was conformed by the correlation observed in the ^1H - ^1H COSY spectrum (Figure 92) between the protons H-23 (δ_{H} 0.89) and the proton H-4 (δ_{H} 2.23, 1H, q, $J = 6.5$ Hz);
- signal of two methylene at the α position of a carbonyl at δ_{H} 2.40 (1H, dq, $J = 8.5, 3.5$ Hz, H-2) and 2.31 (1H, m, H-2);

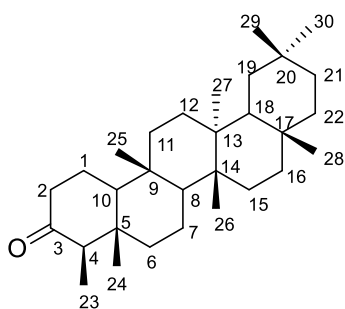
The analysis of its ^{13}C NMR (Figure 93) which was sorted by HMQC technique (Figure 94) displayed:

- eight methyl groups at δ_{C} 6.8 (C-23), characteristic of the methyl at position 23 of the friedelane series (Mahato and Kundu, 1994); 14.7 (C-24), 17.9 (C-25), 18.7 (C-27), 20.3 (C-26), 31.8 (C-30), 32.1 (C-29) and 35.3 (C-28);
 - seven quaternary carbons at δ_{C} 28.1 (C-20), 30.0 (C-17), 37.4 (C-9), 38.3 (C-14), 39.7 (C-13), 42.1 (C-5) and carbon of a ketone group at δ_{C} 213.3 (C-3);
 - four methine groups at δ_{C} 42.8 (C-18), 53.1 (C-8), 58.2 (C-4) and 59.4 (C-10);
 - eleven methylene groups at δ_{C} 18.2 (C-7), 22.3 (C-1), 30.5 (C-12), 32.4 (C-21), 32.7 (C-15), 35.3 (C-19), 35.6 (C-11), 36.0 (C-16), 39.2 (C-22), 41.3 (C-6) and 41.5 (C-2);
- On its HMBC (Figure 95), we observed correlations between protons H-4 (δ_{H} 2.23), H-23 (δ_{H} 0.89) and the carbonyl group C-3 (δ_{C} 213.3), which confirmed the presence of carbonyl at position 3.



Scheme 24: Some key COSY and HMBC correlations of SNC1

All these data were in agreement with those described in the literature for friedelin (**116**), previously isolated from *Maytenus robusta* (Rubiaceae) by Sousa *et al.* (2012).



116

Table 36: ^1H (500 MHz) and ^{13}C (125 MHz) NMR data of SNC1 in CDCl_3 compared to friedelin [CDCl_3 , NMR ^{13}C (100 MHz), NMR ^1H (400 MHz)]

SNC1			Friedelin (Sousa et al., 2012)	
Position	$\delta^{13}\text{C}$	$\delta^1\text{H}$ (m, J in Hz)	$\delta^{13}\text{C}$	$\delta^1\text{H}$ (m, J in Hz)
1	22.3	1.94 (1H, m), 1.66 (1H, m)	22.3	1.90 (1H, m), 1.65 (1H, m)
2	41.5	2.40 (1H, dq, 8.5, 3.5), 2.31 (1H, m)	41.5	2.38 (1H, d, 7.4), 2.22 (m)
3	213.3	-	212.9	-
4	58.2	2.23 (1H, q, 6.5)	58.3	2.18 (1H, q, 6.5)
5	42.1	-	42.8	-
6	41.3	1.75 (1H, m) 1.19 (1H, m)	41.3	1.66 (1H, m), 1.21 (1H, m)
7	18.2	1.46 (1H, m) 1.32 (1H, m)	18.3	1.45 (1H, m), 1.35 (1H, m)
8	53.1	1.32 (1H, m)	52.9	1.35 (1H, m)
9	37.4	-	37.5	-
10	59.4	1.50 (1H, m)	59.5	1.48 (1H, m)
11	35.6	1.37 (1H, m), 1.20 (1H, m)	35.7	1.38 (1H, m), 1.19 (1H, m)
12	30.5	1.27 (1H, m), 1.26 (1H, m)	30.5	1.31 (1H, m), 1.24 (1H, m)
13	39.7	-	39.7	-
14	38.3	-	38.3	-
15	32.7	1.24 (1H, m), 1.46 (1H, m)	32.4	1.49 (1H, m), 1.27 (1H, m)
16	36.0	1.50 (1H, m), 1.25 (1H, m)	36.0	1.50 (1H, m), 1.28 (1H, m)
17	30.0	-	30.0	-
18	42.8	1.56 (1H, m)	42.9	1.51 (1H, m)
19	35.3	1.33 (1H, m), 1.18 (1H, m)	35.3	1.31 (1H, m), 1.14 (1H, m)
20	28.1	-	28.2	-
21	32.4	1.46 (1H, m), 1.33 (1H, m)	32.7	1.42 (1H, m), 1.37 (1H, m)
22	39.2	1.44 (1H, m), 0.93 (1H, m)	39.2	1.41 (1H, m), 0.90 (1H, m)
23	6.8	0.89 (3H, d, 6.5)	6.8	0.88 (3H, d, 6.6)
24	14.7	0.71 (3H, s)	14.7	0.72 (3H, s)
25	17.9	0.85 (3H, s)	17.9	0.87 (3H, s)
26	20.3	0.93 (3H, s)	20.2	1.01 (3H, s)
27	18.7	1.03 (3H, s)	18.7	1.05 (3H, s)
28	35.3	1.16 (3H, s)	31.9	1.18 (3H, s)
29	32.1	0.98 (3H, s)	35.0	0.95 (3H, s)
30	31.8	0.99 (3H, s)	31.7	1.00 (3H, s)

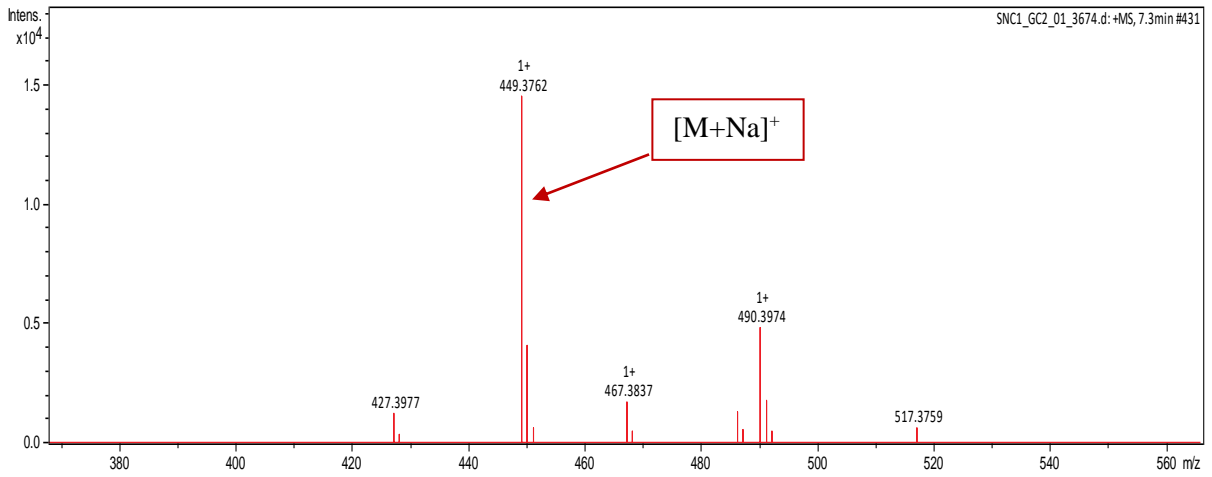


Figure 90: HRESI mass spectrum of SNC1

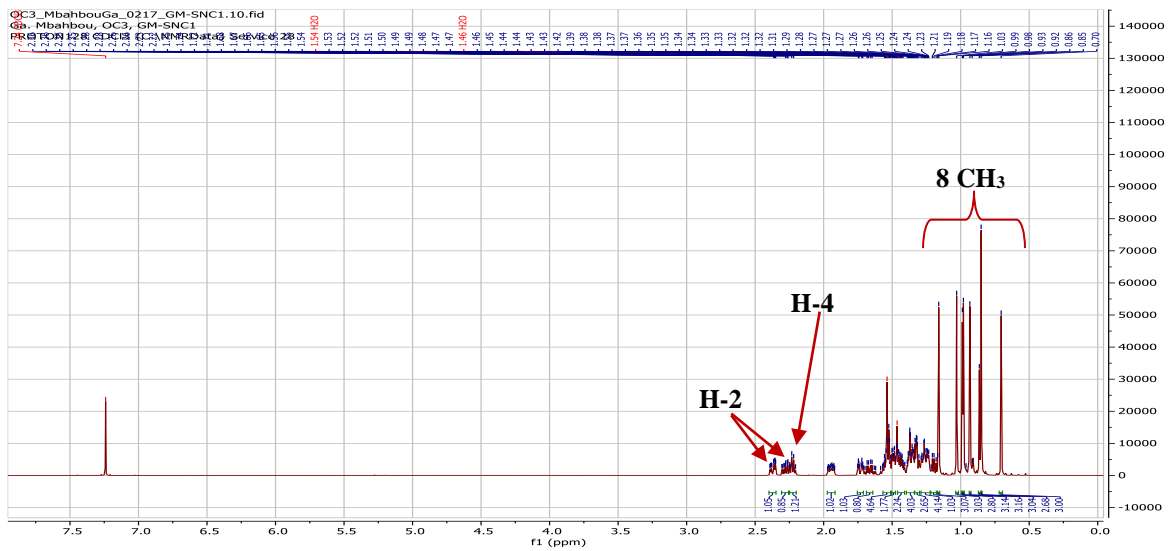


Figure 91: ¹H NMR spectrum (CDCl₃, 500 MHz) of SNC1

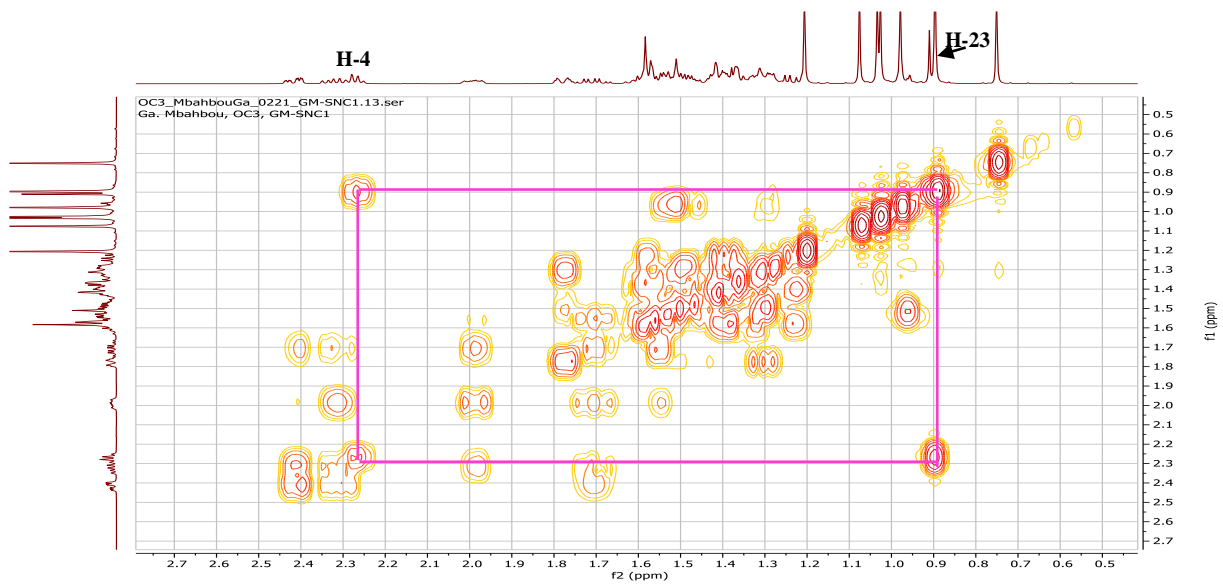


Figure 92: COSY spectrum of SNC1

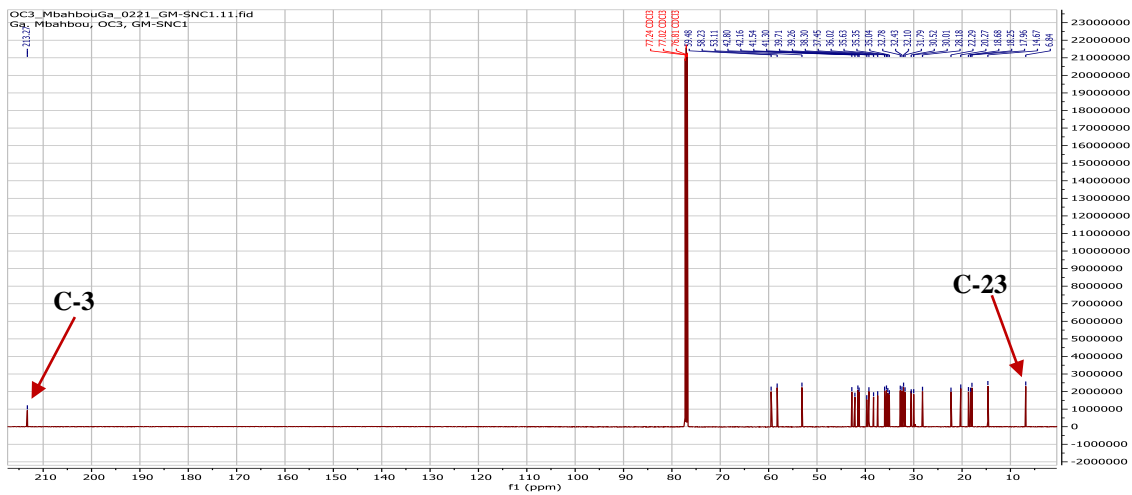


Figure 93: ^{13}C NMR spectrum (CDCl_3 , 125 MHz) of SNC1

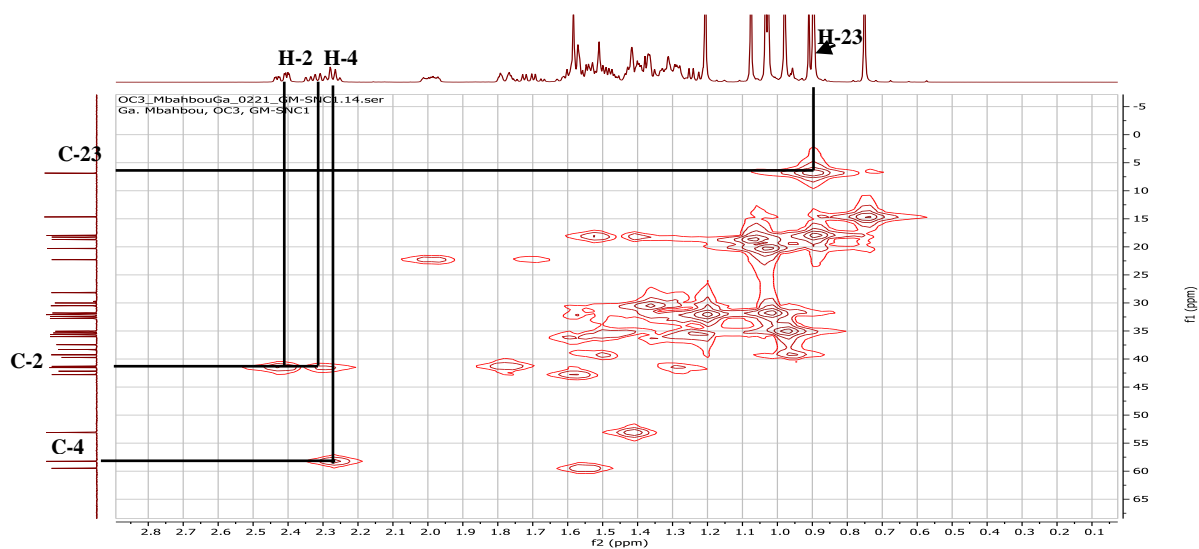


Figure 94: HMQC spectrum of SNC1

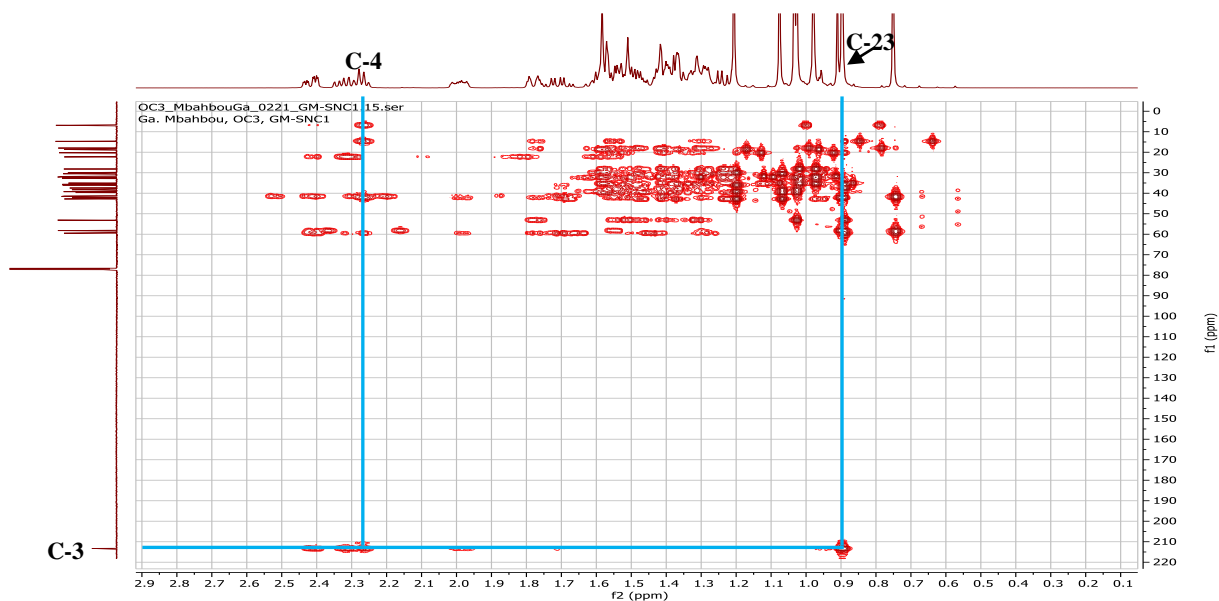


Figure 95: HMBC spectrum of SNC1

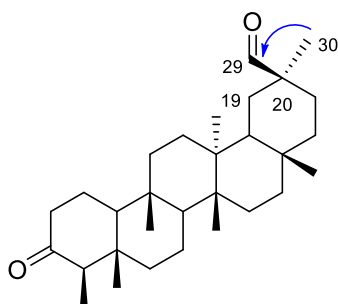
II.1.5.3.14. Structural identification of compound SNC2

SNC2 was obtained as a white powder in *n*-hexane/EtOAc (90:10). It is soluble in dichloromethane and give a red color which turns purple to the Liebermann-Burchard test characteristic of triterpenoids.

Its molecular formula $C_{30}H_{48}O_2$ was deduced from the HRESIMS spectrum (Figure 96) which showed the sodium adduct peak $[M+Na]^+$ at m/z 463.3504 (calcd. for $C_{30}H_{48}O_2Na$, 463.3552), implying seven degrees of unsaturation.

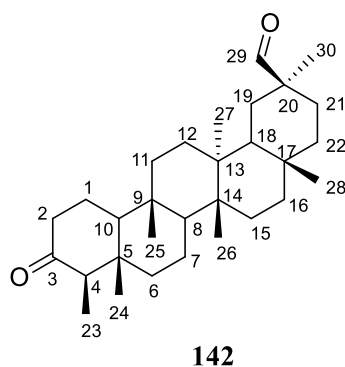
The 1H (Figure 97) and ^{13}C (Figure 98) spectra of SNC2 are very similar to those of SNC1 (friedelin). Except for the additional peak on the proton spectrum of SNC2 at δ_H 10.21 (1H, s, H-29) assignable to the proton of an aldehyde group and the presence of a carbon of aldehyde group at δ_C 204.9 (C-29) on the ^{13}C NMR spectrum which replace the methyl at δ_C 35.0 (C-29).

The position of the aldehyde group was confirmed by the correlation observed on the HMBC spectrum (Figure 99) of SNC2 between the proton H-30 (δ_H 1.07, s, 3H) and the carbon C-29 (δ_C 205.5).



Scheme 25: Key HMBC correlations of SNC2

All these data, compared with those in the literature, allowed us to identify SNC2 as 3-oxofriedelan-29-al (**142**), previously isolated from *Montonia diffusa* (Betancor *et al.*, 1980; Martínez *et al.*, 1988).



142

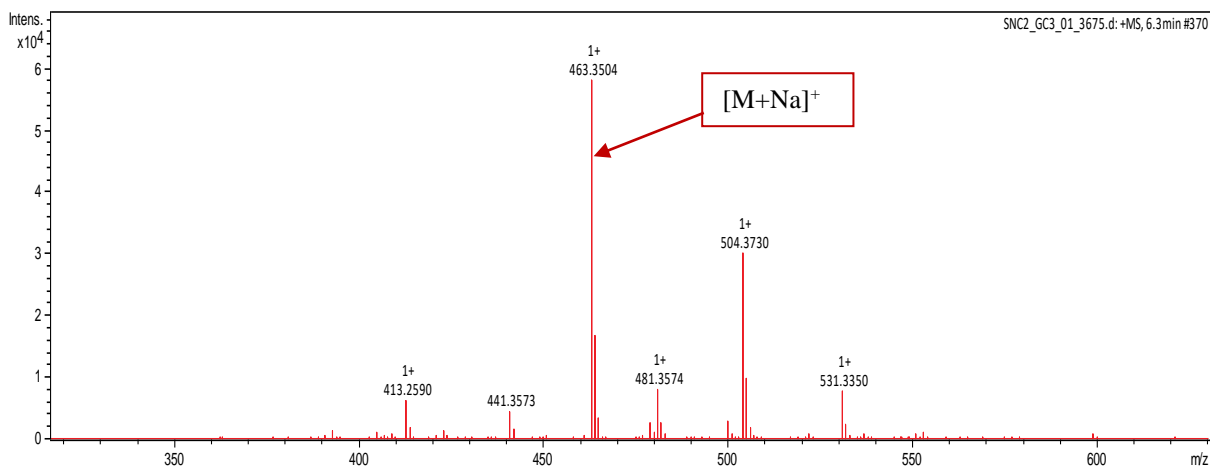


Figure 96: HRESI mass spectrum of SNC2

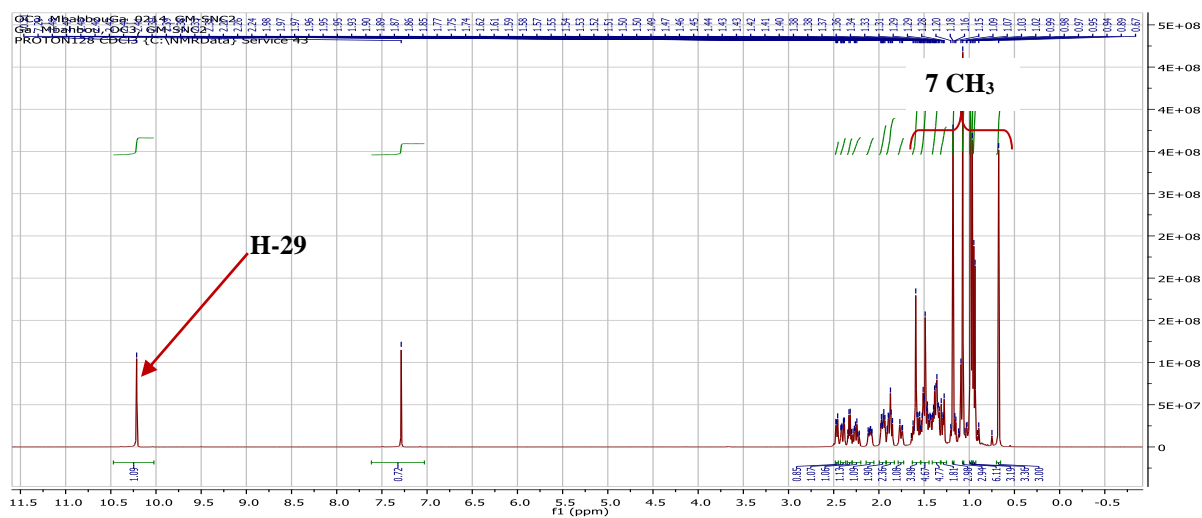


Figure 97: ¹H NMR spectrum (CDCl₃, 500 MHz) of SNC2

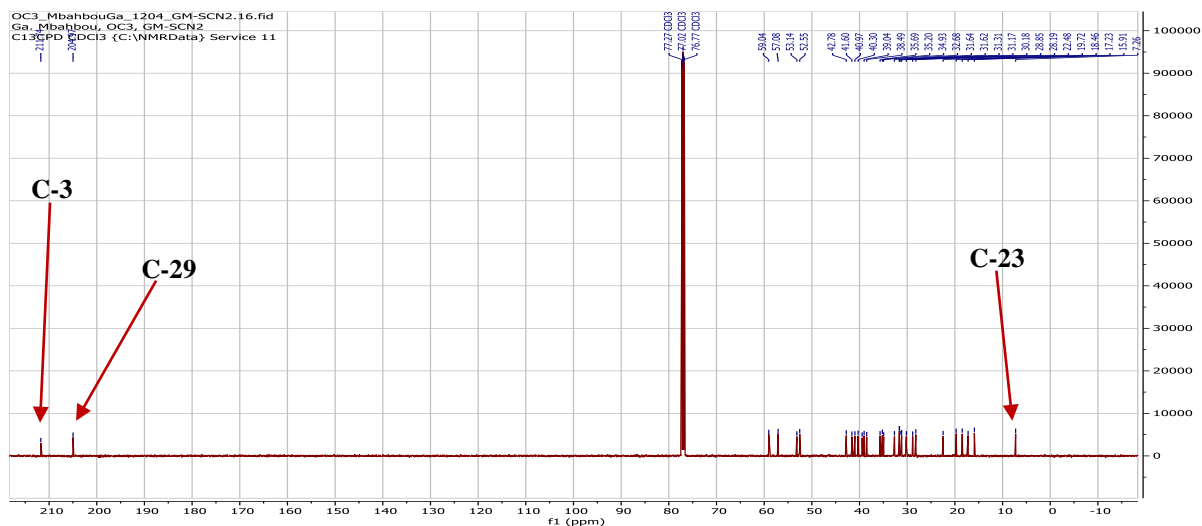


Figure 98: ¹³C NMR spectrum (CDCl₃, 125 MHz) of SNC2

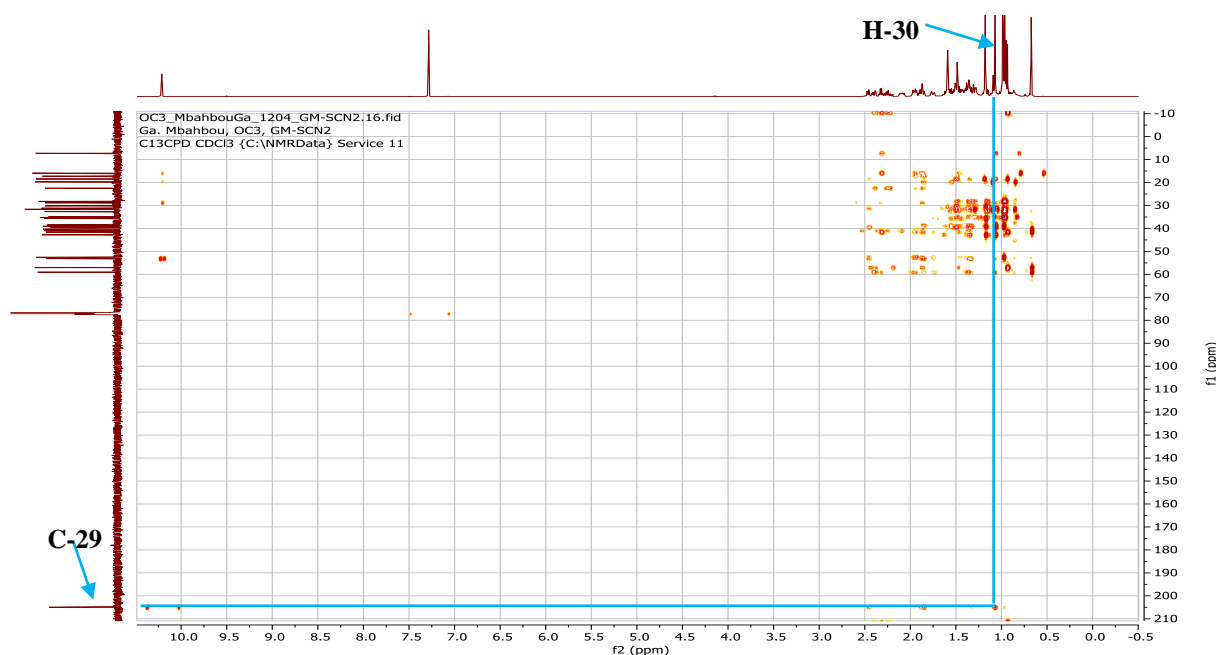


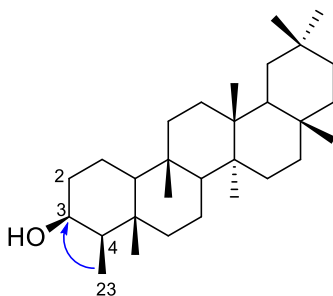
Figure 99: HMBC spectrum of SNC2

II.1.5.3.15. Structural identification of compound SNCL2

SNCL2 was obtained as a white powder in *n*-hexane/EtOAc (95:5). It is soluble in dichloromethane and gave a red color which turns purple to the Liebermann-Burchard test characteristic of triterpenoids.

The ^1H (Figure 100) and ^{13}C (Figure 101) NMR spectra of SNCL2 are very similar to those of SNC1 (friedelin). In fact, the proton spectrum of SNCL2 displayed an additional peak at δ_{H} 3.76 (1H, brs, H-3) corresponding to the proton of an oxymethine group and the presence of an oxymethine carbon group at δ_{C} 72.7 (C-3) on the ^{13}C spectrum which replaced the carbonyl group at δ_{C} 213.3 (C-3) on the ^{13}C spectrum of SNC1.

The position of the oxymethine group was confirmed by the correlation observed on the HMBC spectrum (Figure 102) of SNCL2 between proton H-23 (δ_{H} 0.96, s, 3H) and the carbon C-3 (δ_{C} 72.7).



Scheme 26: Key HMBC correlations of SNCL2

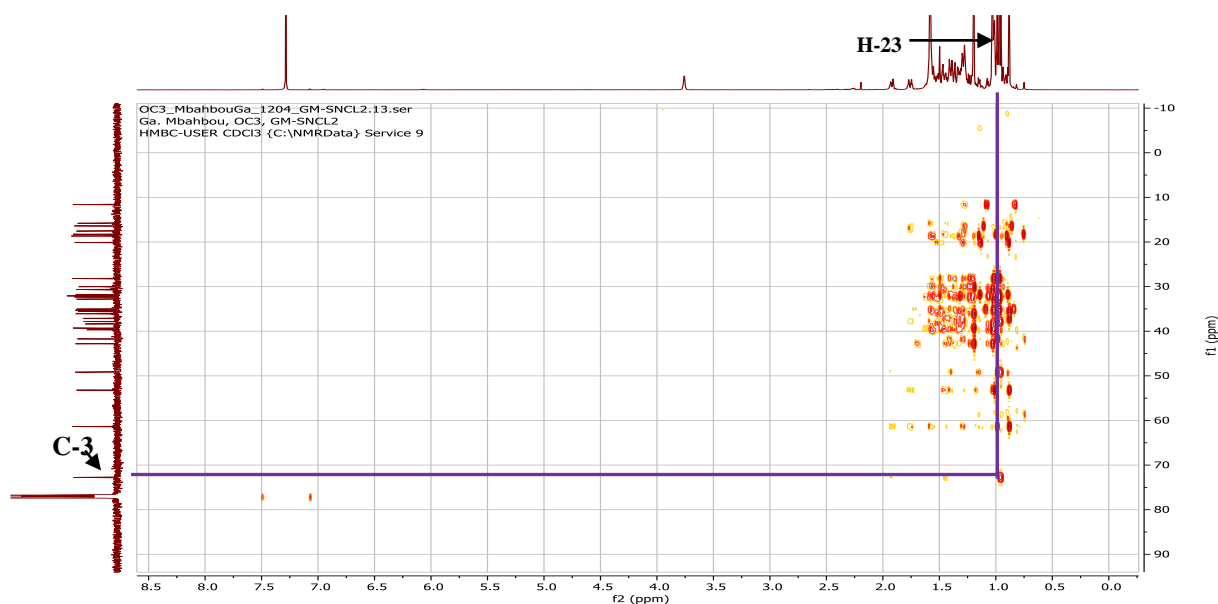


Figure 102: HMBC spectrum of SNC12

II.1.5.3.16. Structural identification of compound SNC4

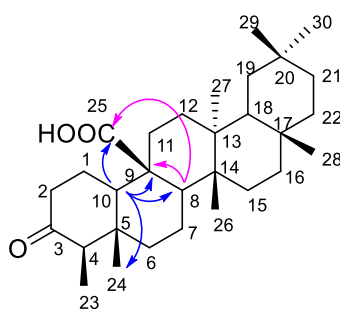
SNC4 was obtained as a white powder in *n*-hexane/EtOAc (85:15). It is soluble in pyridine and give a red color which turns purple to the Liebermann-Burchard test characteristic of triterpenoids.

Its molecular formula $C_{30}H_{48}O_3$ was deduced from the HRESIMS spectrum (Figure 103) which showed the sodium adduct peak $[2M+Na]^+$ at m/z 935.7002 (calcd. for $C_{60}H_{96}O_6Na$, 935.7105), implying seven degrees of unsaturation.

The 1H (Figure 104) and ^{13}C (Figure 105) NMR spectra of SNC4 were very similar to those of SNC1. However, there was an additional signal on the ^{13}C spectrum of SNC4 at δ_C 179.1 (C-25), corresponding to a carboxyl group.

On its HMBC (Figure 106), we observed correlations between protons:

- H-8 (δ_H 1.50, 1H, dd, $J = 12.1$ Hz, 2.4) and carbons C-25 (δ_C 179.1), C-10 (δ_C 58.9), C-9 (δ_C 49.6) and also between proton H-10 (δ_H 1.65, 1H, m) and carbons C-25 (δ_C 179.1), C-24 (δ_C 14.6), C-9 (δ_C 49.6), C-8 (δ_C 54.5), which confirm the presence of the carboxyl group at position 25.



Scheme 27: Some key HMBC correlations of SNC4

SNC4 was identified as 3-oxofriedelan-25-oic acid (**143**), trivially named roxburghonic acid and previously isolated from *Putranjiva roxburghii* by Garg and Mitra (1971).

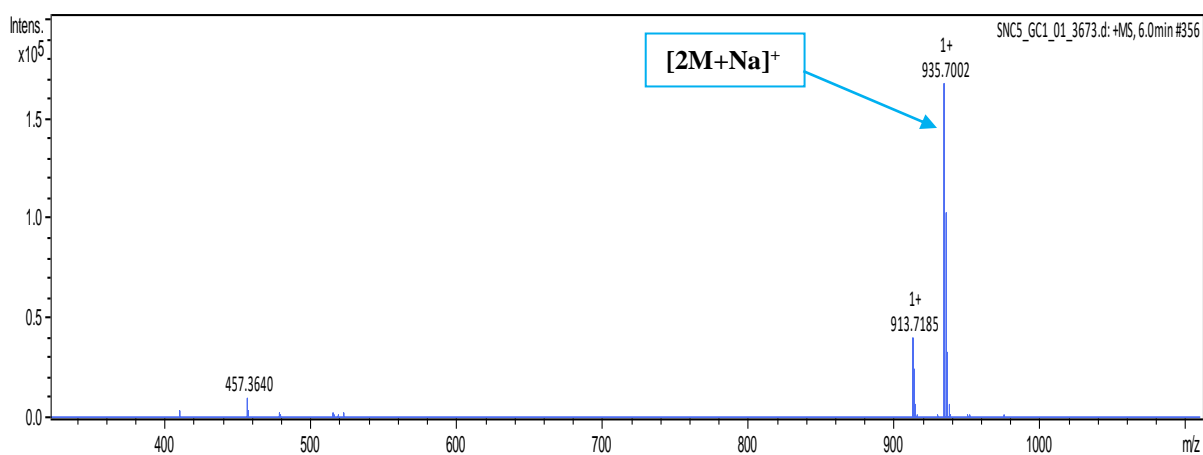
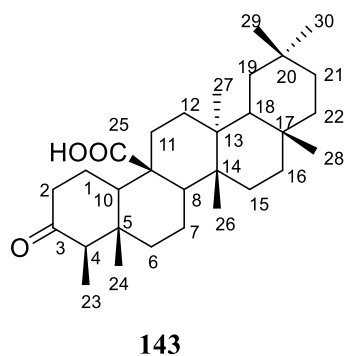


Figure 103: HRESI mass spectrum of SNC4

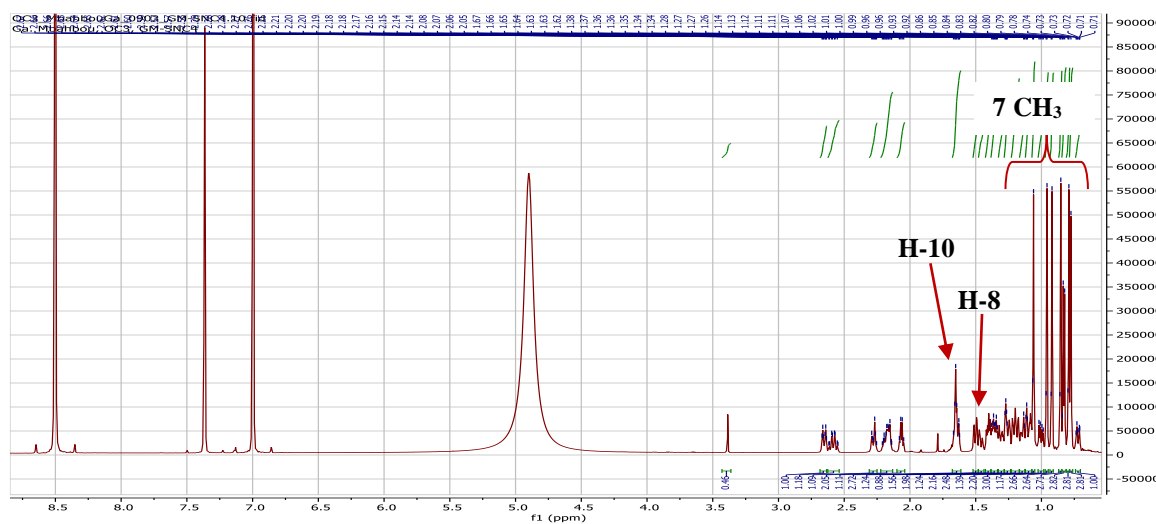


Figure 104: ¹H NMR spectrum (pyridine-*d*₅, 500 MHz) of SNC4

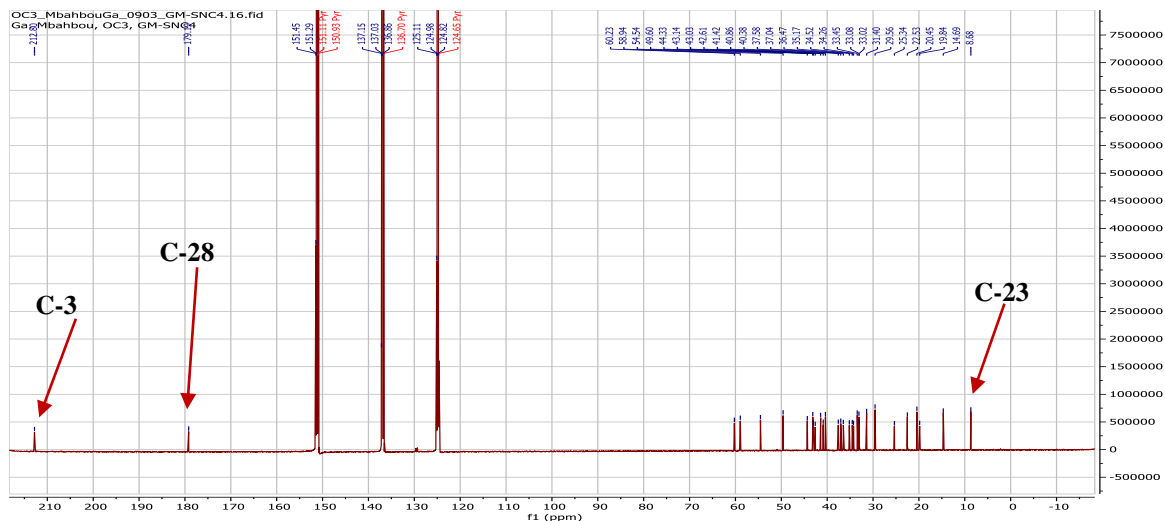


Figure 105: ^{13}C NMR spectrum (pyridine- d_5 , 125 MHz) of SNC4

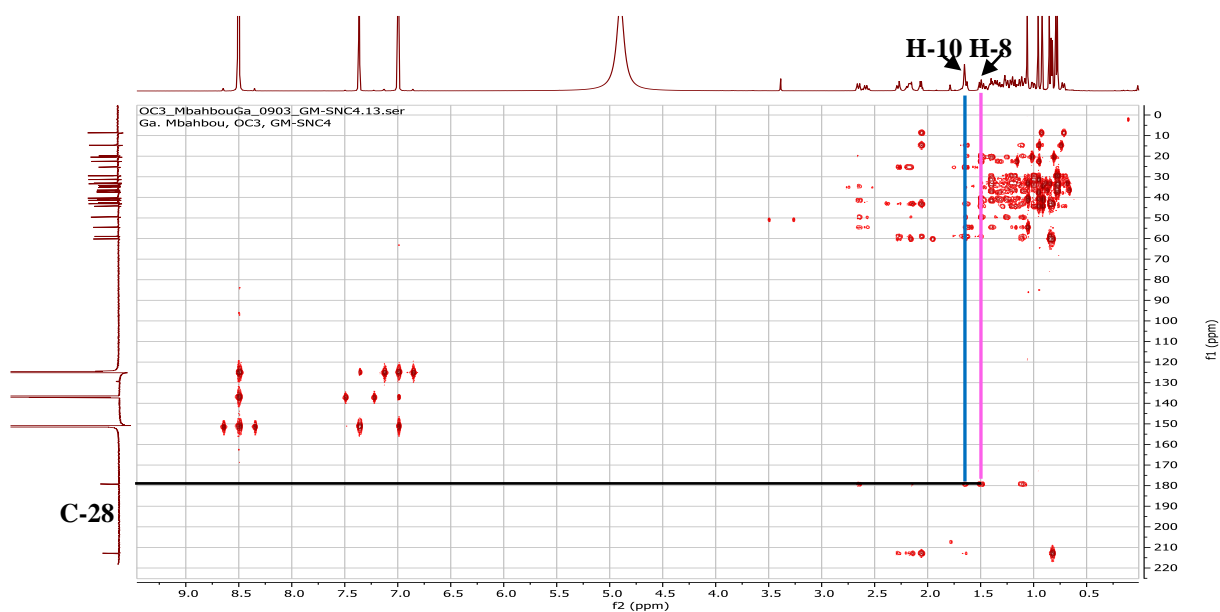


Figure 106: HMBC spectrum of SNC4

Table 37: ^1H (500 MHz) and ^{13}C (125 MHz) NMR data of SNCL2 (CDCl_3) and SNC4 (pyridine- d_5) compared to β -friedelinol [CDCl_3 , NMR ^{13}C (150 MHz)] and 3-oxofriedelan-25-oic acid [CDCl_3 , NMR ^{13}C (125 MHz), ^1H (500 MHz)]

SNC4			Roxburghonic acid (Garg and Mitra, 1971)	SNCL2	β -Friedelinol (Sousa et al., 2012)
Position	$\delta^{13}\text{C}$	$\delta^1\text{H}$ (m, J in Hz)	$\delta^1\text{H}$ (m, J in Hz)	$\delta^{13}\text{C}$	$\delta^{13}\text{C}$
1	25.3	2.18 (1H, m), 1.65 (1H, m)		15.8	15.8
2	43.0	2.27 (1H, m), 2.18 (1H, m)		36.0	36.1
3	212.8	-		72.7	72.8
4	60.2	2.06 (1H, q, 6.6)		49.1	49.1
5	43.1	-		37.8	37.8
6	42.6	1.65 (1H, m), 1.12 (1H, m)		41.7	41.7
7	19.8	2.58 (1H, qd, 13.0, 3.0), 1.36 (1H, m)		17.5	17.5
8	54.5	1.50 (1H, dd, 12.1, 2.4)		53.2	53.2
9	49.6	-		37.1	37.1
10	58.9	1.65 (1H, m)		61.3	61.3
11	35.1	2.65 (1H, dt, 13.4, 3.5), 1.20 (1H, m)		35.3	35.3
12	34.5	1.25 (1H, m), 1.10 (1H, m)		30.6	30.6
13	40.3	-		38.3	38.4
14	41.4	-		39.6	39.7
15	33.0	1.50 (1H, m), 1.40 (1H, m)		32.3	32.3
16	40.8	1.27 (1H, m), 0.72 (1H, m)		35.5	35.5
17	31.4	-		30.0	30.0
18	44.3	1.40 (1H, dd, 11.1, 5.7)		42.8	42.8
19	37.0	1.11 (1H, m), 1.01 (1H, m)		35.1	35.2
20	29.5	-		28.1	28.2
21	34.2	1.50 (1H, m), 1.25 (1H, m)		32.8	32.8
22	37.5	1.40 (1H, m), 1.11 (1H, m)		39.2	39.3
23	8.6	0.83 (3H, d, 6.7)	0.90 (3H, s)	11.6	11.6
24	14.6	0.85 (3H, s)	0.95 (3H, s)	16.4	16.4
25	179.1	-	-	18.2	18.2
26	20.4	0.92 (3H, s)	0.99 (3H, s)	20.1	20.1
27	22.5	1.06 (3H, s)	1.22 (3H, s)	18.6	18.6
28	33.4	0.96 (3H, s)	1.05 (3H, s)	32.0	32.1
29	36.4	0.78 (3H, s)	0.70 (3H, s)	35.0	35.0
30	33.0	0.79 (3H, s)	0.82 (3H, s)	31.8	31.8

II.1.5.4. Citric acid derivatives

II.1.5.4.1. Structural identification of compound WN15

WN15 was obtained as a colourless crystals in $\text{CH}_2\text{Cl}_2/\text{acetone}$ (95:5). It is soluble in dichloromethane and reacts positively to Lucas test characteristic of alcohol.

Its molecular formula $\text{C}_9\text{H}_{14}\text{O}_7$ was deduced from the HRESIMS spectrum (Figure 107) which showed the sodium adduct peak $[\text{M}+\text{Na}]^+$ at m/z 257.0649 (calcd. for $\text{C}_9\text{H}_{14}\text{O}_7\text{Na}$, 257.0637), implying three degrees of unsaturation.

The analysis of its ^1H NMR spectrum (Figure 108) showed:

- an AB system of two doublets integrating for two protons each at δ_{H} 2.74 (2H, d, $J = 15.6$ Hz, Ha) and δ_{H} 2.84 (2H, d, $J = 15.6$ Hz, Hb);
- two singlets of one and two methoxy groups at δ_{H} 3.77 (3H, s, Hd) and 3.63 (6H, s, Hc), respectively;
- a singlet of a proton at δ_{H} 4.05 (1H, s, OH) corresponding to the proton of a hydroxyl group.

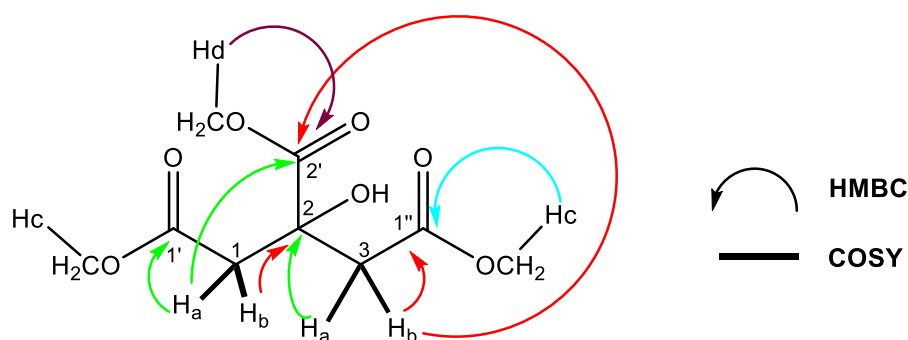
The analysis of its broad-band decoupled ^{13}C NMR spectrum (Figure 109) highlights the signals of nine carbon atoms that were sorted by the DEPT (Figure 110) and HMQC (Figure 111) techniques into:

- signals of two groups of quaternary carbons standing for three carbonyl groups at δ_{C} 170.2 (C-1'/C-1''), 173.8 (C-2') and 73.2 (C-2);
- a signal of two methylene groups at δ_{C} 43.0 (C-1/C-3);
- two signals of three methoxy groups at δ_{C} 53.2 (OCH₃) and δ_{C} 52.0 (2×OCH₃).

In fact, on the ^1H - ^1H COSY spectrum of WN15 (Figure 112), the coupling between the Ha protons (δ_{H} 2.74) and the Hb protons (δ_{H} 2.84) is observed.

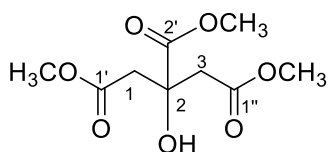
Taken together, these data indicate that WN15 is a citrate with three esterified acid groups. The positions of these substituents were deduced from the HMBC correlations (Figure 113) of protons:

- Hd (δ_{H} 3.63) and the carbons C-1'/1'' (δ_{C} 170.2);
- Ha (δ_{H} 2.74), Hb (δ_{H} 2.84) and carbons C-2' (δ_{C} 173.8), C-1'/C-1'' (δ_{C} 170.2) and C-2 (δ_{C} 73.2) revealing the symmetry in this molecule;
- Hc (δ_{H} 3.77) and carbon C-2' (δ_{C} 173.8).



Scheme 28: Some key COSY and HMBC correlations of WN15

Based on the above data and by comparison with those described in the literature, WN15 was identified as trimethyl citrate or methyl 2-hydroxypropane-1,2,3-tricarboxylate (**144**), previously isolated from *Nauclea pobeguinii* by Kuete *et al.* (2015).



144

Table 38: ^1H (500 MHz) and ^{13}C (125 MHz) NMR data of WN15 in CDCl_3 compared to trimethyl citrate

WN15			Trimethyl citrate (Sorensen, 2010)	
Position	$\delta^{13}\text{C}$	$\delta^1\text{H}$ (m, J in Hz)	$\delta^{13}\text{C}$	$\delta^1\text{H}$ (m, J in Hz)
1, 3	43.0	2.74 (2H, d, 15.6) 2.84 (2H, d, 15.6)	44.4	2.82 (2H, d, 15.3) 2.94 (2H, d, 15.3)
2	73.2	-	74.8	-
1', 1''	170.2	-	171.8	-
OCH_3	52.0	3.63 (6H, s)	52.4	3.65 (6H, s)
OCH_3	53.2	3.77 (3H, s)	53.3	3.76 (3H, s)

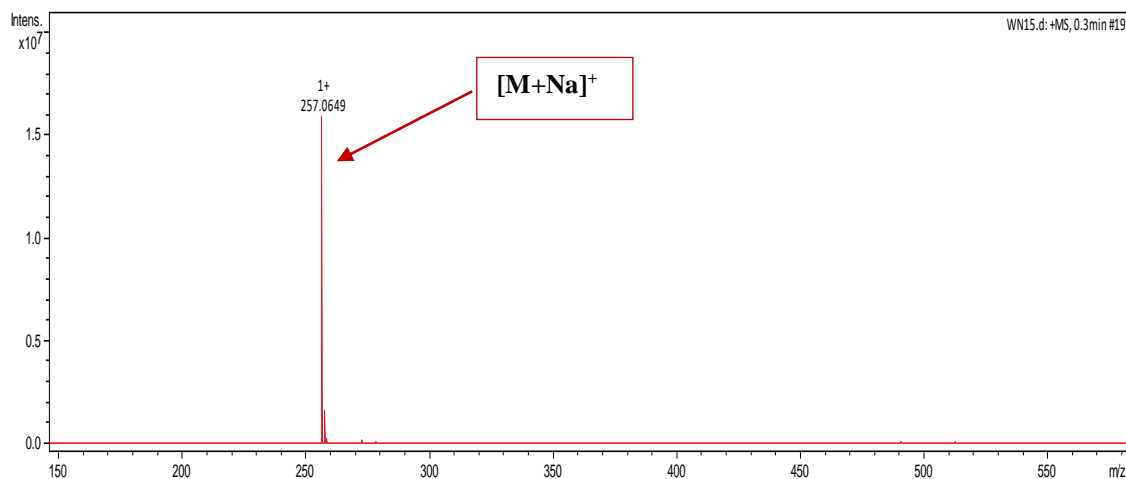


Figure 107: HRESI mass spectrum of WN15

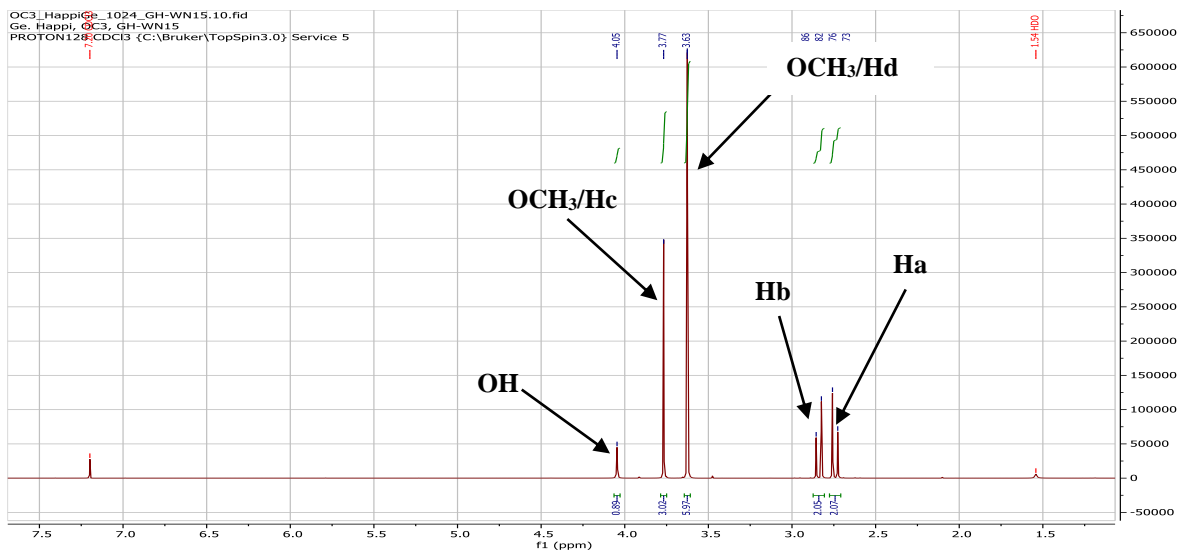


Figure 108: ^1H NMR spectrum (CDCl_3 , 500 MHz) of WN15

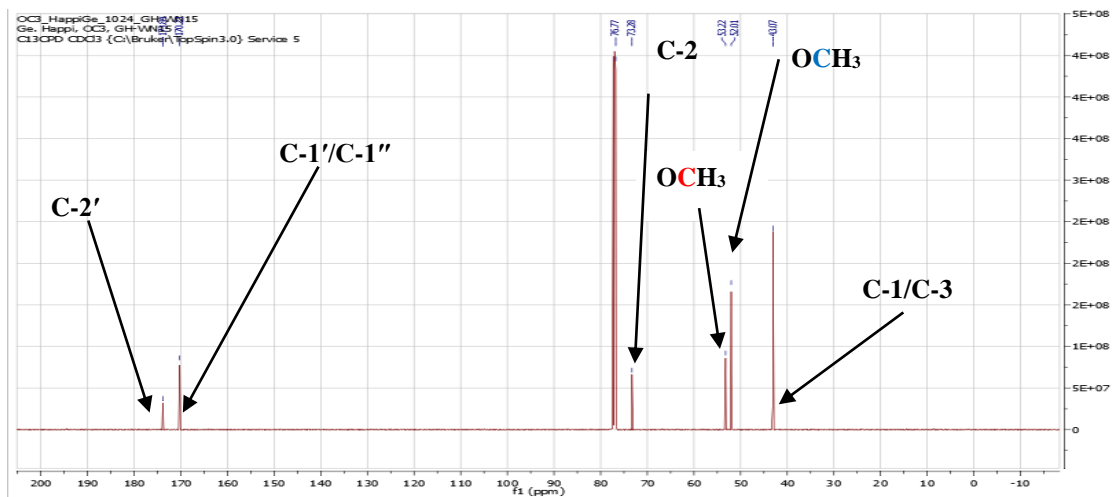


Figure 109: ^{13}C NMR spectrum (CDCl_3 , 125 MHz) of WN15

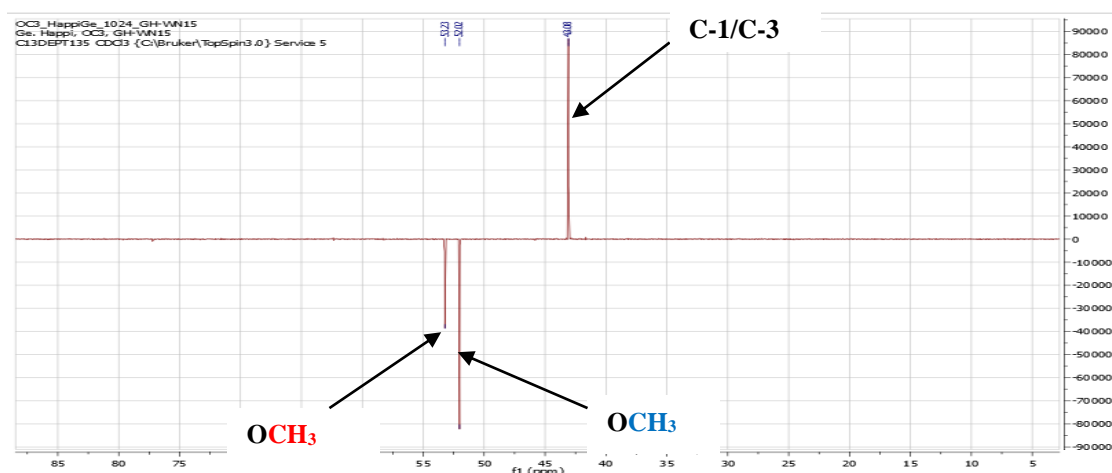


Figure 110: DEPT spectrum of WN15

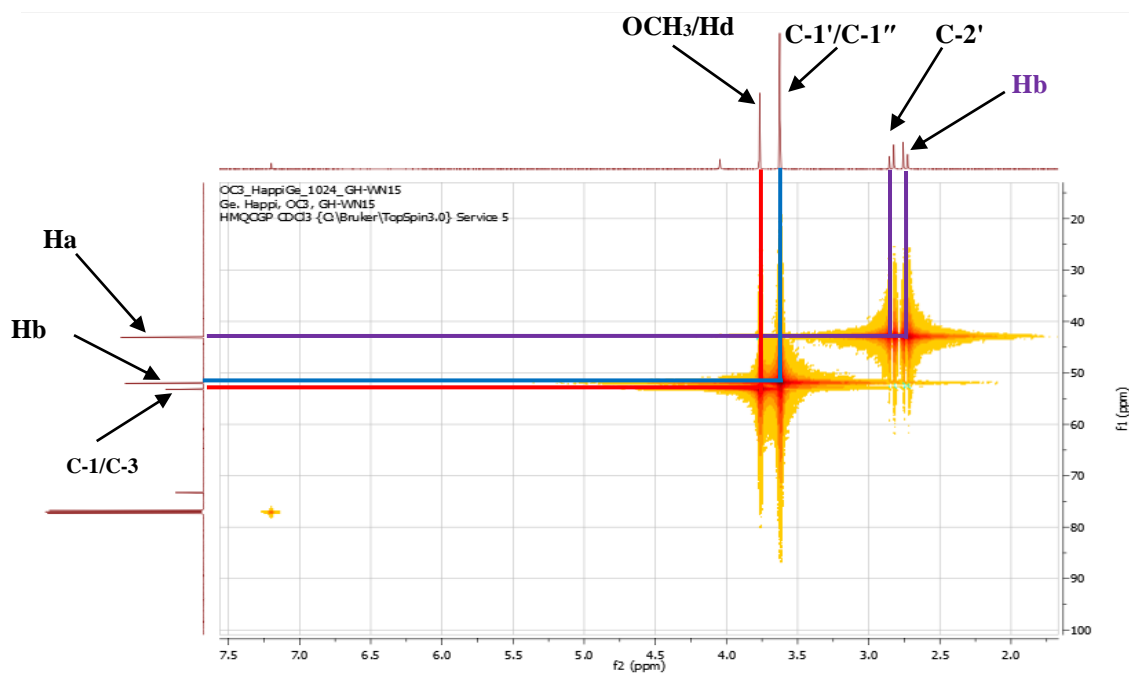


Figure 111: HMQC spectrum of WN15

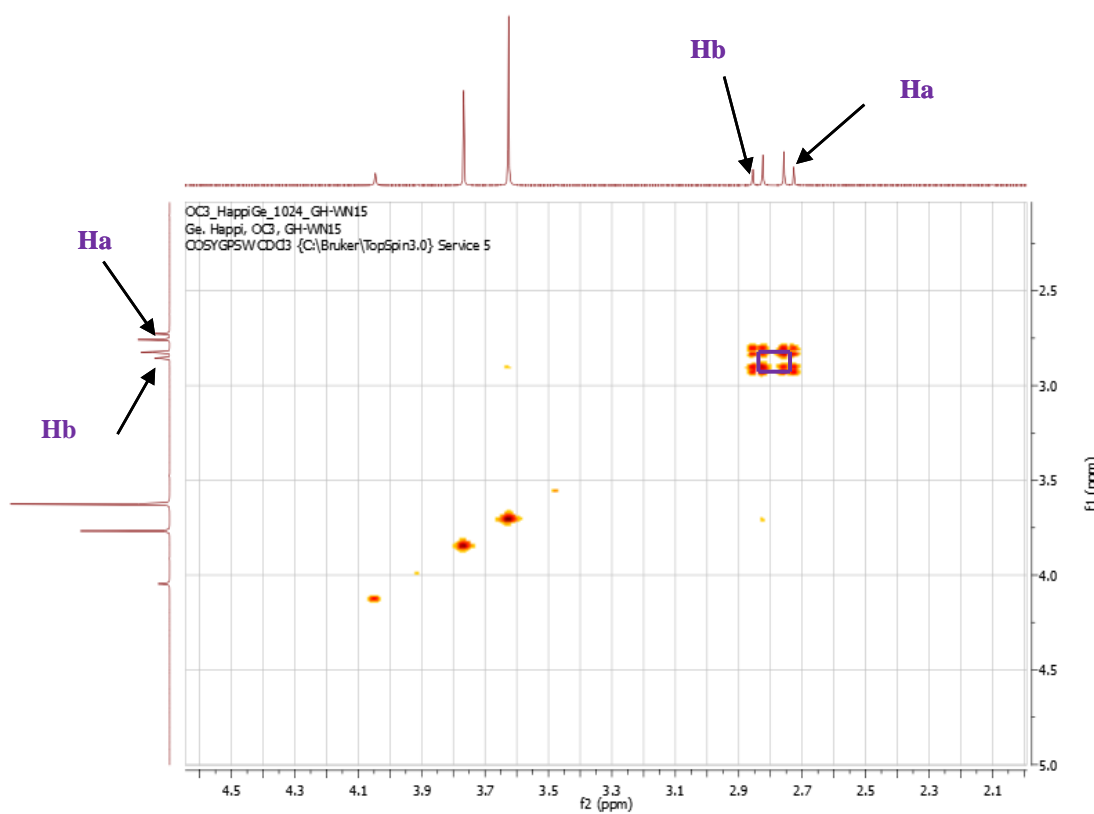


Figure 112: COSY spectrum of WN15

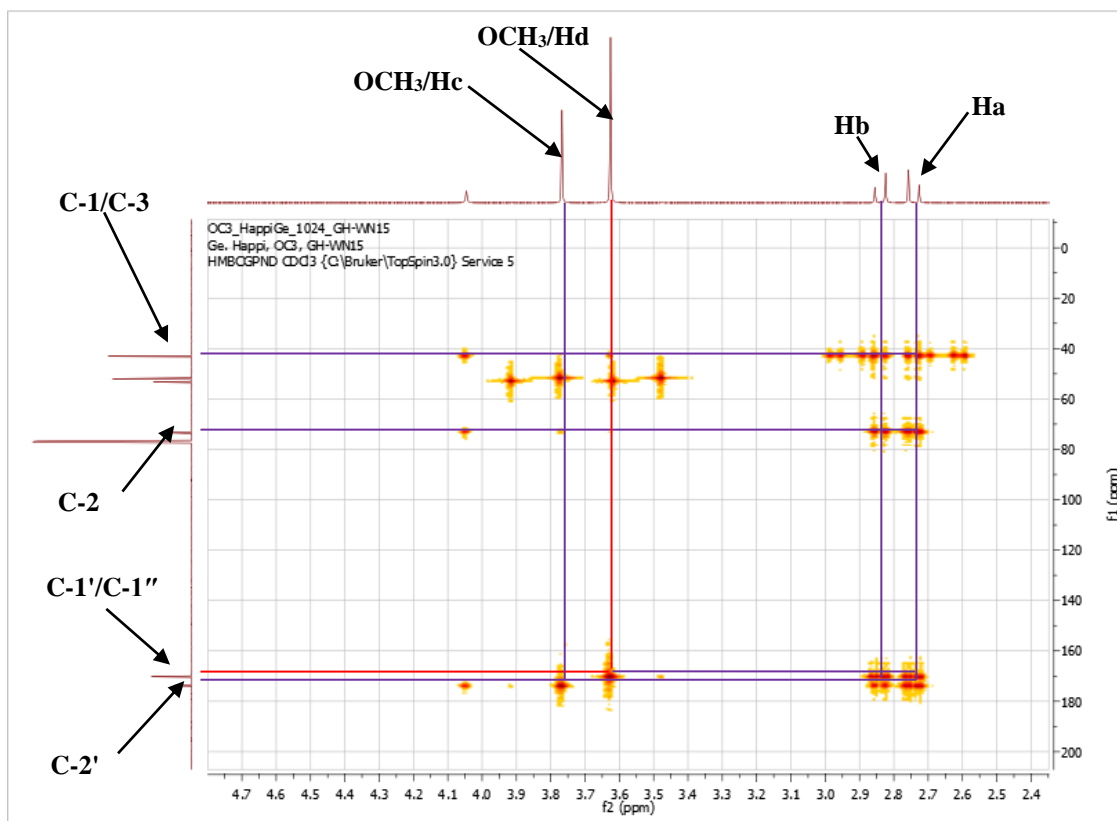


Figure 113: HMBC spectrum of WN15

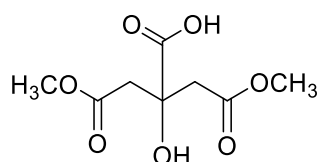
II.1.5.4.2. Structural identification of compound WN34

WN34 was obtained as a colourless crystals in $\text{CH}_2\text{Cl}_2/\text{acetone}$ (90:10). It is soluble in methanol and reacts positively to Lucas test and NaHCO_3 test characteristic of alcohol and carboxylic acid, respectively.

Its molecular formula $\text{C}_8\text{H}_{12}\text{O}_7$ was deduced from the HRESIMS spectrum (Figure 114) which showed the sodium adduct peak $[\text{M}+\text{Na}]^+$ at m/z 243.0484 (calcd. for $\text{C}_8\text{H}_{12}\text{O}_7\text{Na}$, 243.0481), implying three degrees of unsaturation. This mass is 14 u.m.a lower than that of the sodium adduct of WN15, suggesting the absence of CH_2 within WN34.

The ^1H NMR (Figure 115) and ^{13}C NMR (Figure 116) spectra of WN34 were close to that of the previously described WN5 with a little discrepancy. The only difference observed on the both spectra was the absence of the methoxy group at δ_{H} 3.77 (3H, s, Hd) on the proton spectrum and at δ_{C} 53.2 on the carbon spectrum of WN34.

These data were therefore in accordance with those of dimethyl citrate or 2-hydroxy-4-methoxy-2-(2-methoxy-2-oxoethyl)-4-oxobutanoic acid (**145**), previously isolated from *Aspergillus niger* by Sorensen (2010).



145

Table 39: ^1H (500 MHz) and ^{13}C (125 MHz) NMR data of WN34 in methanol- d_4 compared to dimethyl citrate

WN34			Dimethyl citrate (Sorensen, 2010)	
Position	$\delta^{13}\text{C}$	$\delta^1\text{H}$ (m, J in Hz)	$\delta^{13}\text{C}$	$\delta^1\text{H}$ (m, J in Hz)
1	175.0	-	176.5	-
2	72.8	-	74.4	-
3, 1'	42.6	2.96 (2H, d, 15.4)	44.2	2,79 (2H, d, 15.3)
		2.84 (2H, d, 15.4)		2,94 (2H, d, 15.3)
4, 2'	170.4	-	172.0	-
OCH ₃	50.7	3.63 (6H, s)	52.3	3.66 (6H, s)

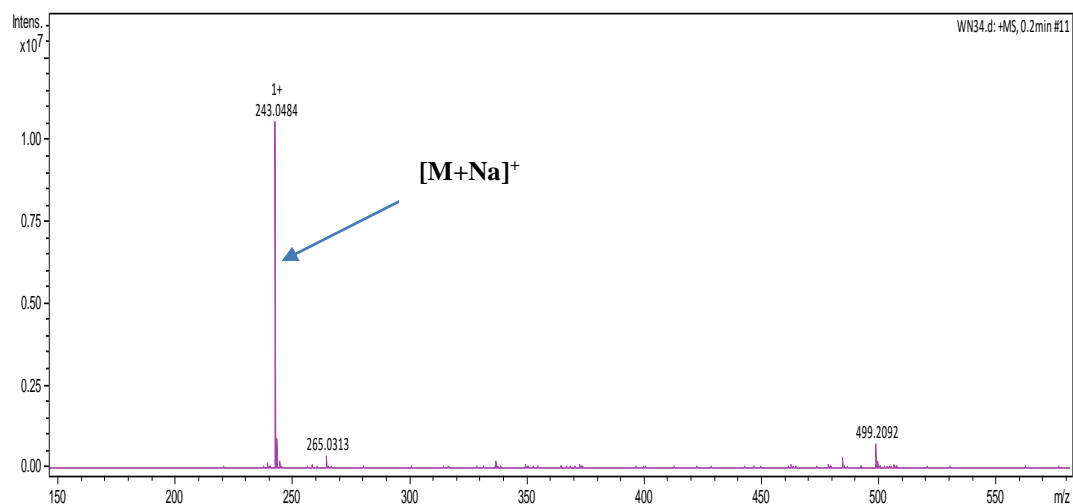


Figure 114: HRESI mass spectrum of WN34

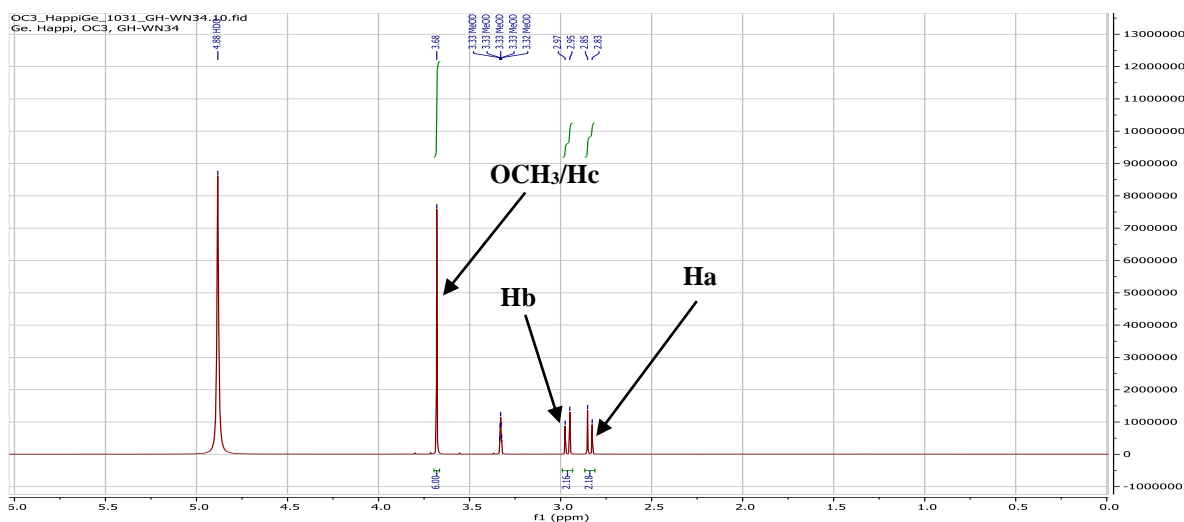


Figure 115: ^1H NMR spectrum (methanol- d_4 , 500 MHz) of WN34

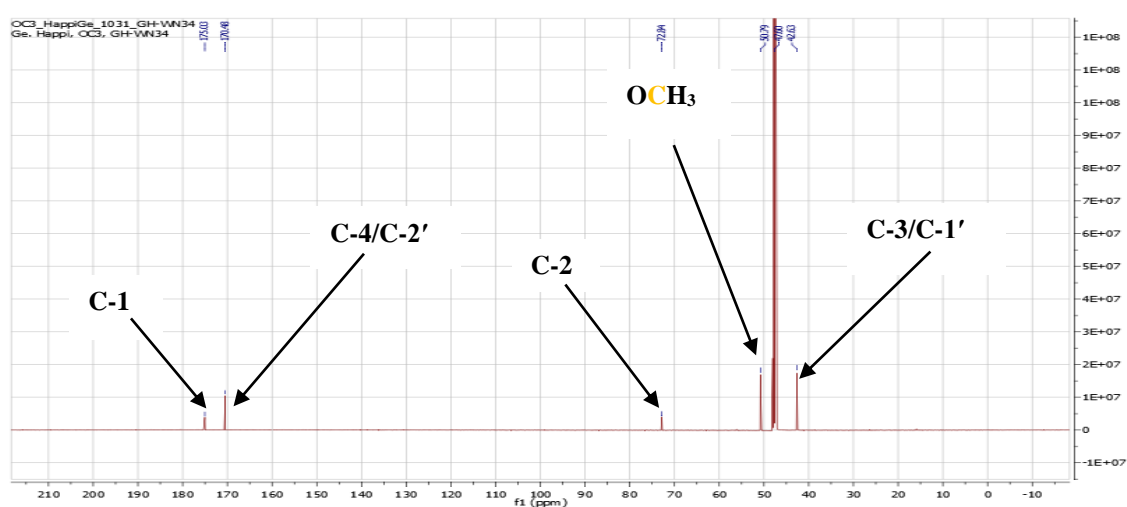


Figure 116: ^{13}C NMR spectrum (methanol- d_4 , 125 MHz) of WN34

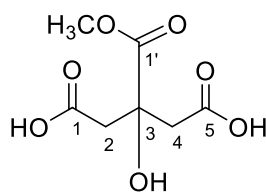
II.1.5.4.3. Structural identification of compound WN36

WN36 was obtained as a colourless crystals in $\text{CH}_2\text{Cl}_2/\text{acetone}$ (80:20). It is soluble in methanol and reacts positively to Lucas test and NaHCO_3 test characteristic of alcohol and carboxylic acid, respectively.

Its molecular formula $\text{C}_7\text{H}_{10}\text{O}_7$ was deduced from the HRESIMS spectrum (Figure 117) which showed the sodium adduct $[\text{M}+\text{Na}]^+$ peak at m/z 229.0302 (calcd. for $\text{C}_7\text{H}_{10}\text{O}_7\text{Na}$, 229.0427), implying three degrees of unsaturation. This mass is 28 u.m.a lower than that of the sodium adduct of WN15, suggesting the absence of two CH_2 within WN36.

Comparison of the ^1H NMR (Figure 118) and ^{13}C NMR spectra (Figure 119) of WN36 to that of WN15 revealed many similarities. The only difference observed was the absence of the singlet of two methoxy groups at δ_{H} 3.63 (6H, s, Hc) on the proton spectrum and at δ_{C} 52.0 (OCH₃) on the carbon spectrum of WN36.

Based on the above data and by comparison with those described in the literature, WN36 was identified as methyl citrate or 3-hydroxy-3-(methoxycarbonyl)pentanedioic acid (**146**), previously isolated from *Nauclea vanderghuchtii* by Nkouayeb *et al.* (2020).



146

Table 40: ^1H (500 MHz) and ^{13}C (125 MHz) NMR data of WN36 in methanol- d_4 compared to methyl citrate [DMSO- d_6 , NMR ^{13}C (125 MHz), NMR ^1H (500 MHz)]

WN36			Methyl citrate (Nkouayeb <i>et al.</i> 2020)	
Position	$\delta^{13}\text{C}$	$\delta^1\text{H}$ (m, J in Hz)	$\delta^{13}\text{C}$	$\delta^1\text{H}$ (m, J in Hz)
1	171.9	-	172.9	-
1'	174.1	-	175.1	-
1, 5	42.8	2.78 (2H, d, 15.6)	43.8	2,81 (2H, d, 15.3)
		2.93 (2H, d, 15.6)		2,95 (2H, d, 15.3)
2, 4	73.1	-	74.1	-
OCH ₃	51.6	3.77 (3H, s)	53.1	3.69 (3H, s)

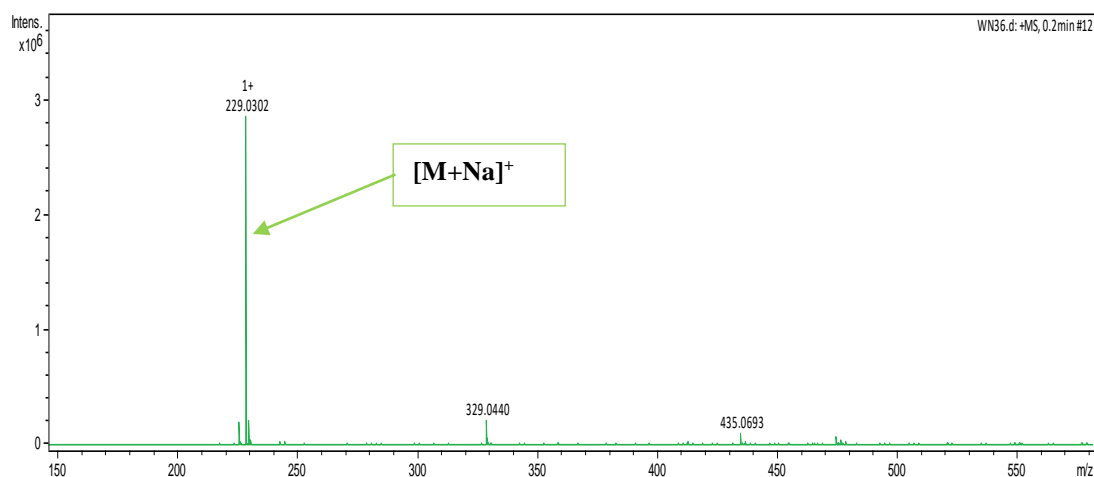


Figure 117: HRESI mass spectrum of WN36

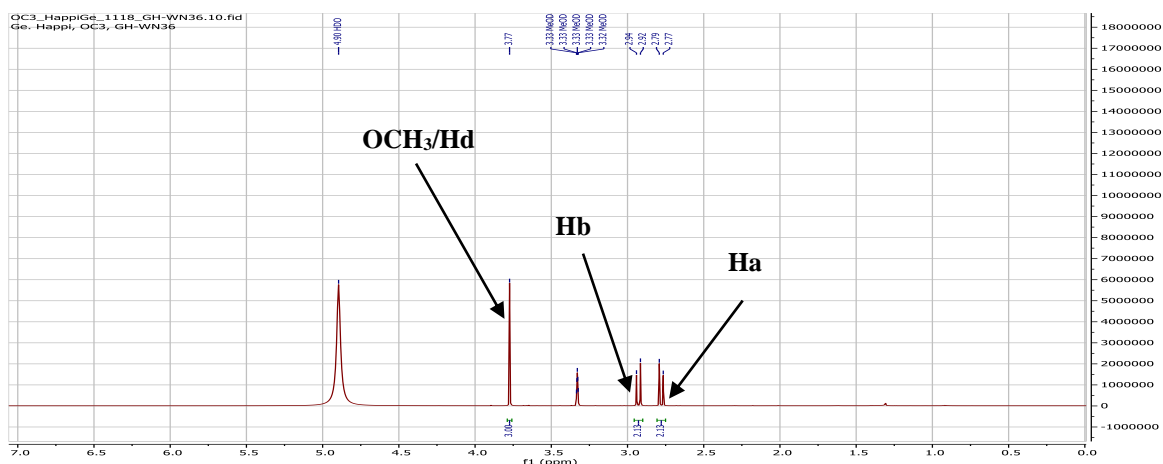


Figure 118: ^1H NMR spectrum (methanol- d_4 , 500 MHz) of WN36

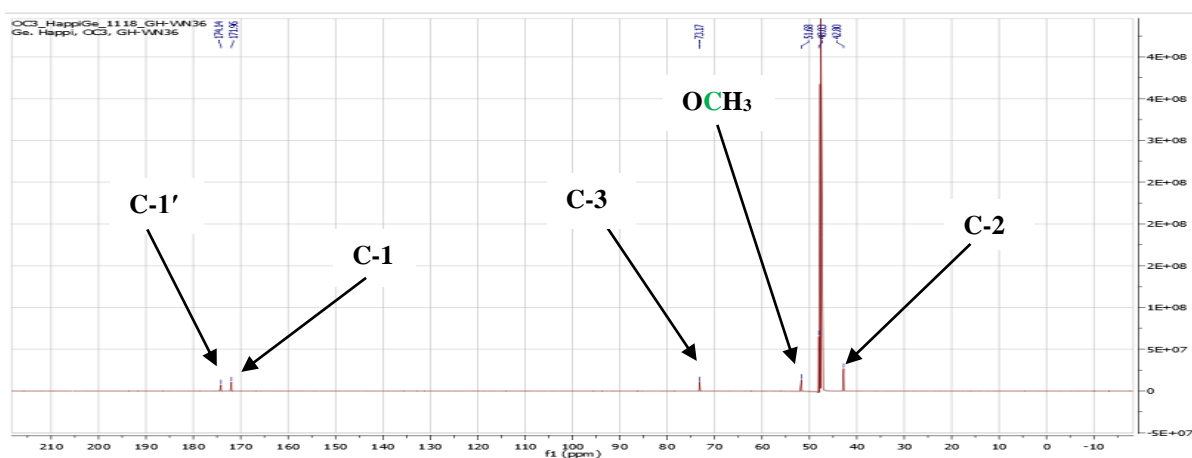


Figure 119: ^{13}C NMR spectrum (methanol- d_4 , 125 MHz) of WN36

II.1.5.5. Amino acid derivatives

II.1.5.5.1. Structural identification of compound SNC6

SNC6 was obtained as a white powder in *n*-hexan/EtOAc (80:20) and it is soluble in dichloromethane.

Its molecular formula $\text{C}_{32}\text{H}_{30}\text{N}_2\text{O}_4$ was deduced from the HRESIMS spectrum (Figure 120) which showed pseudomolecular ion peak $[\text{M}+\text{H}]^+$ at m/z 507.2278 (calcd. for $\text{C}_{32}\text{H}_{31}\text{N}_2\text{O}_4$, 507.2284), implying nineteen degrees of unsaturation.

Its ^1H NMR spectrum (Figure 121) showed signals of:

- three ABX coupling systems:
 - ✓ ABX1: at δ_{H} 4.64 (1H, m, H-2), 4.56 (1H, dd, $J = 11.4, 3.3$ Hz, H-1b) and 4.06 (1H, dd, $J = 11.4, 4.3$ Hz, H-1a);
 - ✓ ABX2: at δ_{H} 4.64 (1H, m, H-2), 3.02 (1H, dd, $J = 14.0, 6.5$ Hz, H-3b) and 2.91 (1H, dd, $J = 14.0, 8.5$ Hz, H-3a);

✓ ABX3: at δ_H 4.94 (1H, q, $J = 6.7$ Hz, H-2'), 3.32 (1H, dd, $J = 14.0, 6.5$ Hz, H-3b') and 3, 24 (1H, dd, $J = 14.0, 7.0$ Hz, H-3a');

- two secondary amine groups at δ_H 6.67 (1H, d, $J = 8.5$, NHb) and 6.57 (1H, d, $J = 6.5$ Hz, NHa);
- four monosubstituted phenyl groups between δ_H 7.72-7.19 (m).

The analysis of its broad-band decoupled ^{13}C NMR spectrum (Figure 122) showed the signals of thirty carbons which were sorted using the DEPT (Figure 123) and HMQC techniques (Figure 124) into:

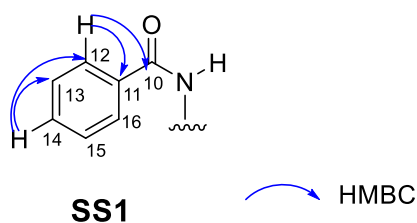
- seven quaternary carbons including three carbonyl groups at δ_C 171.9 (C-1') for ester and those at δ_C 167.5 (C-10') and 167.2 (C-10) for amides (Carvalho *et al.*, 2010);
- twenty two methine group carbons including two sp^3 carbons at δ_C 50.3 (C-2) and 54.5 (C-2');
- two carbons of benzyl methylene groups at δ_C 37.3 (C-3) and 37.4 (C-3');
- an oxymethylene group at δ_C 65.4 (C-1).

The 1H - 1H COSY and HMBC spectra of SNC6 brought sub-structures SS1, SS2, SS3 and SS4 together. In fact, the 1H - 1H COSY spectrum (Figure 125) displayed correlations between protons:

- of the amino group NHb (δ_H 6.67) and H-2 (δ_C 4.64), which in turn correlated with the H-1a (δ_C 4.56) and H-1b (4.06), H-3b (δ_C 3.02) and H-3a (2.91);
- of the amino group NHa (δ_C 6.57) and H-2' (δ_C 4.94), which in turn correlated with H-3a' (δ_C 3.32) and H-3b' (3.24).

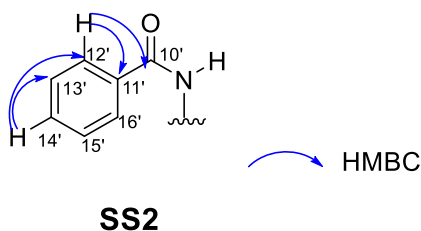
Its HMBC spectrum (Figure 126), showed correlations between protons:

- H-12/H-16 (δ_H 7.67) and carbons δ_C 167.2 (C-10), 134.2 (C-11), 131.4 (C-14) and 128.9 (C-13/C-15);
- H-14 (δ_H 7.68) and carbons C-13/C-15 (δ_C 128.9) and C-12/C-16 (127.1); given rise to following sub-structure SS1:

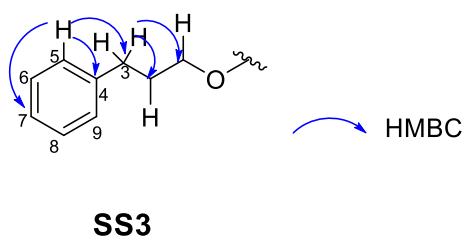


- H-12'/H-16' (δ_H 7.72) and carbons C-10' (δ_C 167.4), C-14' (132.0), C-11' (δ_C 133.3) and C-13'/C-15' (128.4);

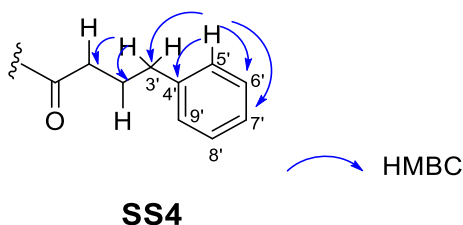
- H-14' (δ_H 7.69) and carbons C-13'/C-15' (δ_C 128.4) and C-12'/C-16' (δ_C 127.0); leading to the following sub-structure SS2:



- H-5/H-9 (δ_H 7.20) and carbons C-4 (δ_C 137.2), C-7 (δ_C 127.2) and C-3 (δ_C 37.3);
- H-3b (δ_H 3.02), H-3a (δ_H 2.91) and carbons C-2 (δ_C 50.3), C-1 (δ_C 65.4), C-4 (δ_C 137.2), C-5/C-9 (δ_C 129.2); which were in favor to the following sub-structure SS3:

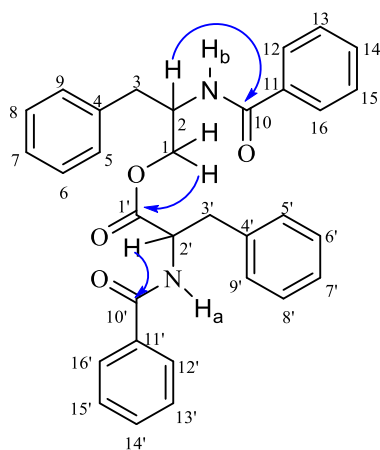


- H-5'/H-9' (δ_H 7.20) and carbons C-4' (δ_C 135.8), C-7' (δ_C 126.6) and C-3' (δ_C 37.4);
- H-3b' (δ_H 3.32) and H-3a' (δ_H 3.24) and carbons C-2' (δ_C 54.5), C-1' (δ_C 171.9), C-4' (δ_C 135.8) and C-5'/C-9' (δ_C 129.3);
- H-2' (δ_H 4.94) and carbon C-1' (δ_C 171.9); for the following SS4 substructure:



The connections between these sub-structures were made thanks to the correlations observed on the same HMBC spectrum between protons:

- H-1a (δ_H 4.56), H-1b (δ_H 4.06) and carbon δ_C 171.9 (C-1');
- H-2' (δ_H 4.94) and carbon C-10' (δ_C 167.4);
- H-2 (δ_C 4.64) and carbon C-10 (δ_C 167.2).



Scheme 29: Key HMBC correlations of SNC6

All these data of SNC6 were in agreement with those described by Carvalho *et al.* (2010) for *N*-benzoylphenylalaninyl-*N*-benzoylphenylalaninate (asperphenamate) (**147**), previously isolated from *Piptadenia gonoacantha*.

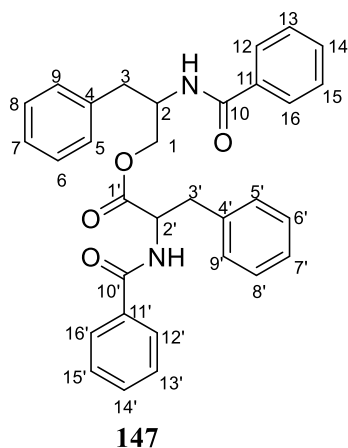


Table 41: ¹H (500 MHz) and ¹³C (125 MHz) NMR data of SNC6 in CDCl₃ compared to asperphenamate [CDCl₃, NMR ¹³C (175 MHz), NMR ¹H (700 MHz)]

SNC6			Asperphenamate (Carvalho <i>et al.</i> 2010)	
Position	$\delta^{13}\text{C}$	$\delta^1\text{H}$ (m, J in Hz)	$\delta^{13}\text{C}$	$\delta^1\text{H}$ (m, J in Hz)
1	65.4	4.56 (1H, dd, 11.4, 3.3) 4.06 (1H, dd, 11.4, 4.3)	66.4	4.52 (1H, dd, 11.0, 3.5) 4.02 (1H, dd, 11.0, 4.0)
2	50.3	4.64 (1H, m)	51.3	4.60 (1H, dddd, 8.0, 6.5, 4.0, 3.4)
3	37.3	3.02 (1H, dd, 14.0, 6.5) 2.91 (1H, dd, 14.0, 8.5)	38.3	2.98 (1H, dd, 14.0, 6.5) 2.87 (1H, dd, 14.0, 8.5)
4	137.2	-	138.2	-
5, 9	129.2	7.20 (2H, m)	130.3	7.20 (2H, dd, 8.0, 1.5)
6, 8	128.7	7.27 (2H, m)	129.7	7.27 (2H, td, 8.0, 1.5)
7	127.2	7.19 (1H, m)	127.8	7.20 (1H, tt, 8.0, 1.5)
10	167.2	-	168.2	-
11	134.2	-	135.2	-
12, 16	127.1	7.67 (2H, m)	128.1	7.69 (2H, m)
13, 15	128.7	7.52 (2H, m)	129.9	7.42 (2H, m)
14	131.4	7.68 (1H, m)	133.0	7.53 (1H, tt, 7.7, 1.4)
1'	171.9	-	172.9	-
2'	54.5	4.94 (1H, q, 6.7)	55.5	4.94 (1H, q, 7.0)
3'	37.4	3.32 (1H, dd, 14.0, 6.5) 3.24 (1H, dd, 14.0, 7.0)	38.5	3.32 (1H, dd, 14.0, 6.5) 3.24 (1H, dd, 14.0, 7.0)
4'	135.8	-	136.8	-
5', 9'	129.3	7.20 (2H, m)	130.2	7.23 (2H, dd, 7.7, 1.4)
6', 8'	128.7	7.27 (2H, m)	129.7	7.28 (2H, td, 7.7, 1.4)
7'	126.8	7.19 (1H, m)	128.4	7.23 (1H, tt, 7.7, 1.4)
10'	167.4	-	168.4	-
11'	133.3	-	134.3	-
12', 16'	127.0	7.72 (2H, m)	128.1	7.72 (2H, dd, 7.7, 1.4)
13', 15'	128.4	7.53 (2H, m)	129.4	7.34 (2H, td, 7.7, 1.4)
14'	132.0	7.69 (1H, m)	133.2	7.46 (1H, tt, 7.7, 1.4)
NHa	-	6.57 (1H, d, 6.5)	-	6.59 (1H, d, 6.3)
NHb	-	6.67 (1H, d, 8.5)	-	6.70 (1H, d, 8.4)

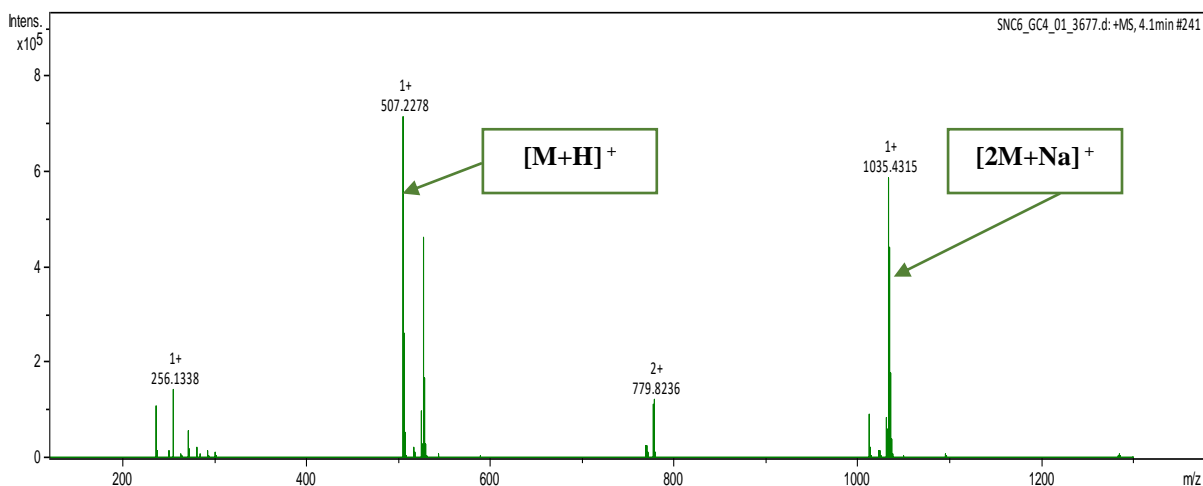


Figure 120: HRESI mass spectrum of SNC6

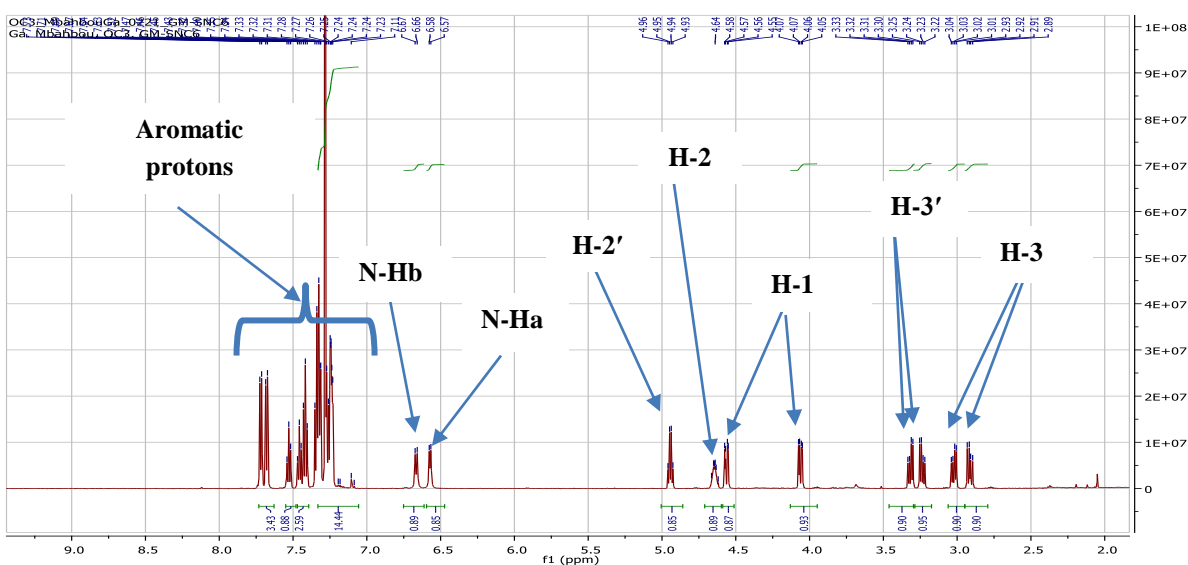


Figure 121: ¹H NMR spectrum (CDCl₃, 500 MHz) of SNC6

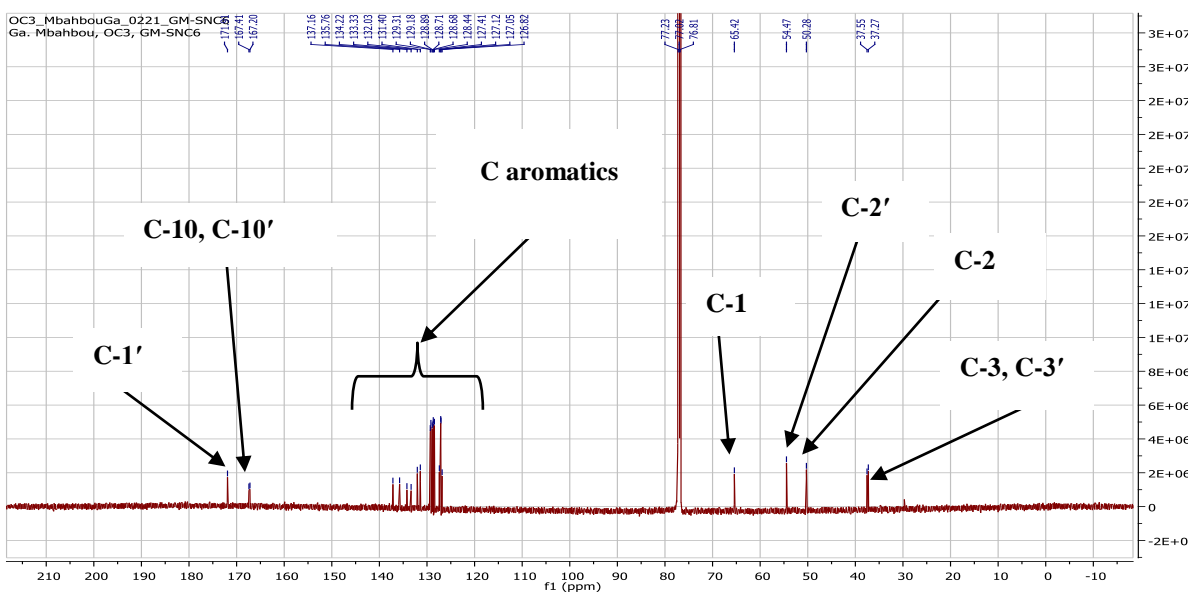


Figure 122: ¹³C NMR spectrum (CDCl₃, 125 MHz) of SNC6

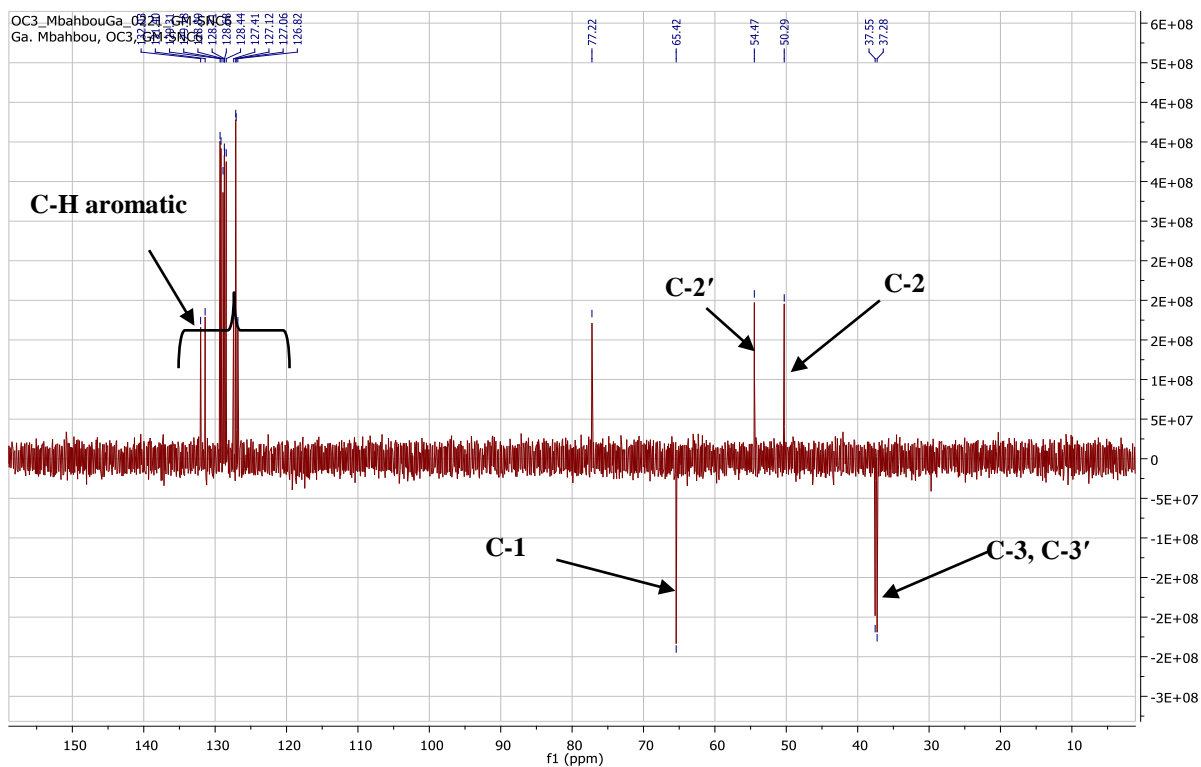


Figure 123: DEPT spectrum of SNC6

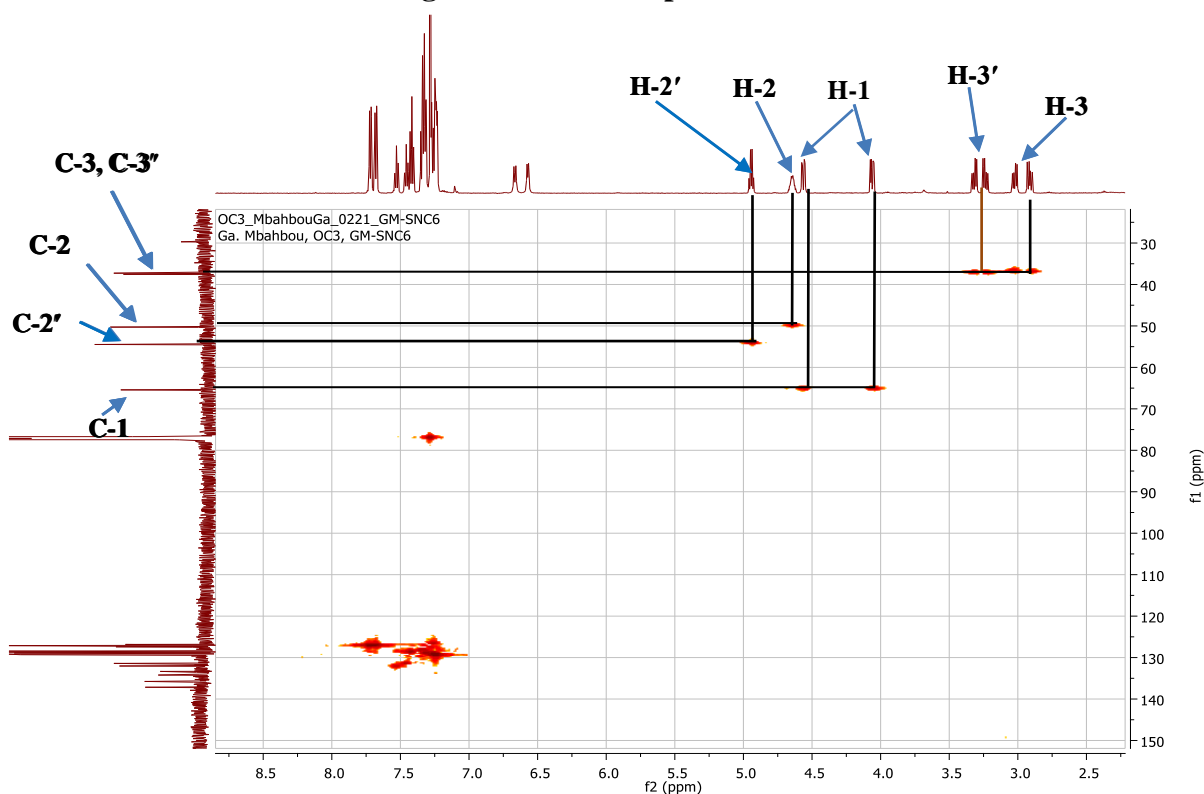


Figure 124: HMQC spectrum of SNC6

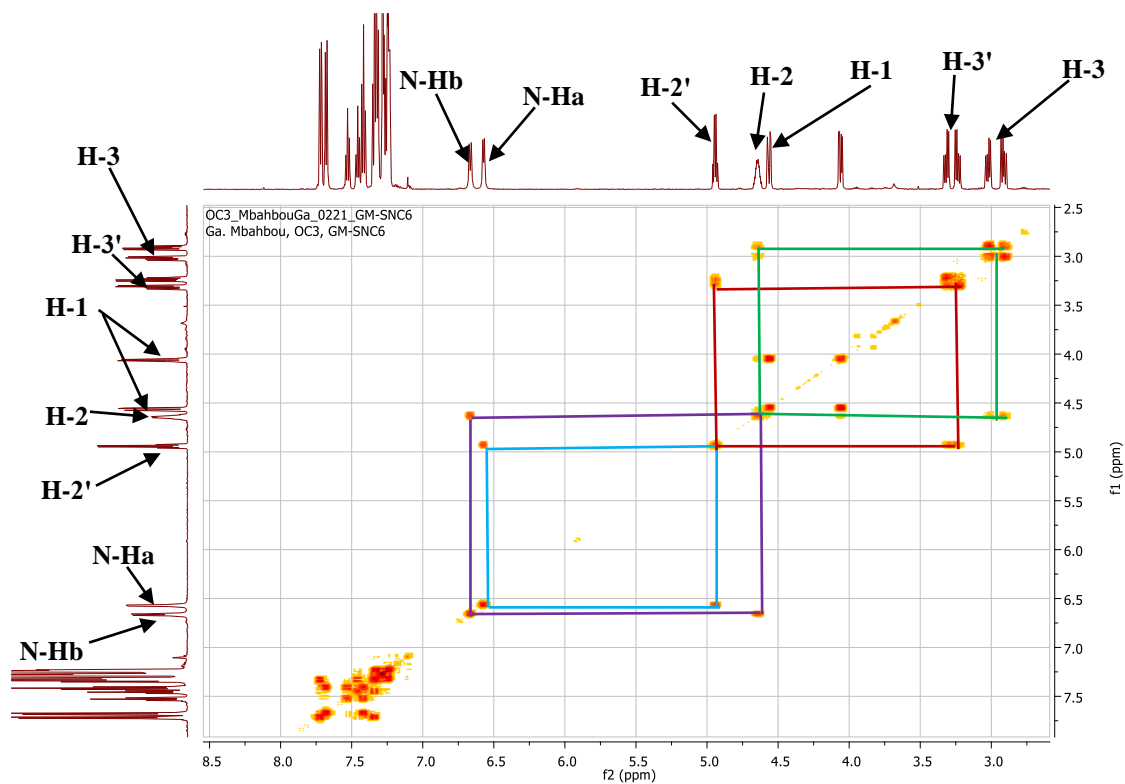


Figure 125: COSY spectrum of SNC6

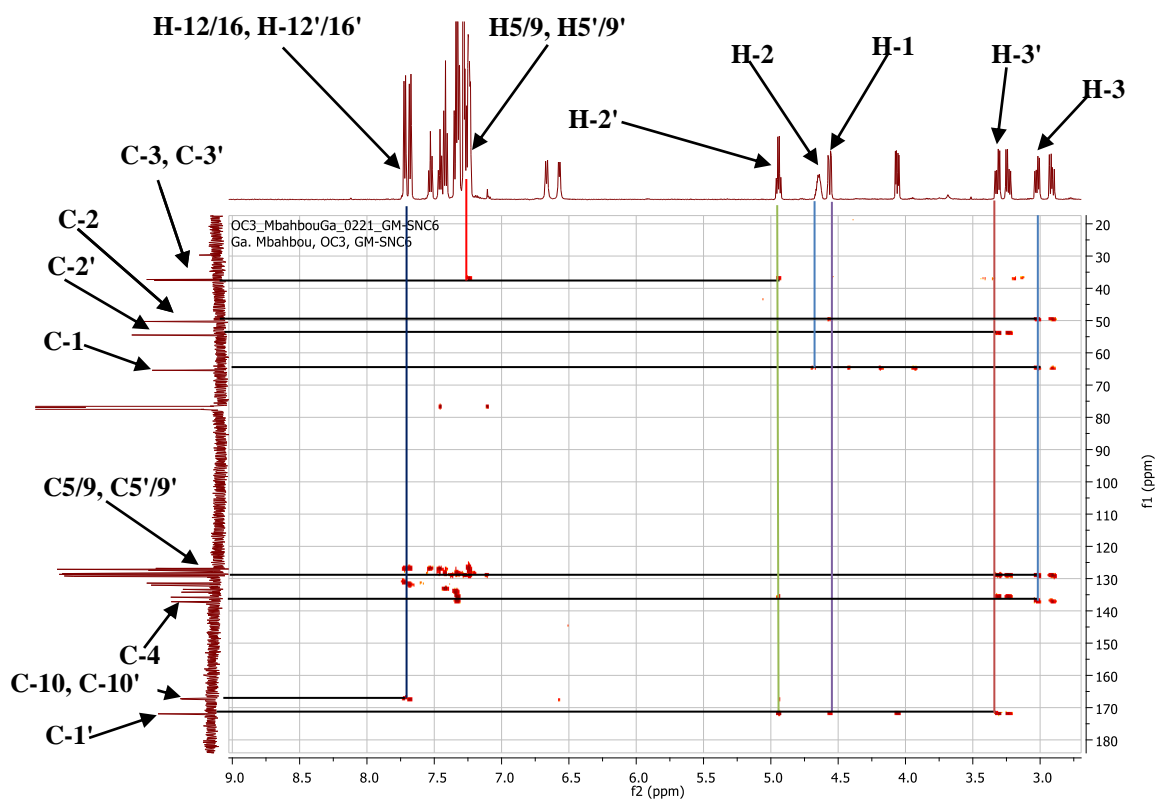


Figure 126: HMBC spectrum of SNC6

II.1.5.5.2. Structural identification of compound SNC10

SNC10 was obtained as a colourless crystals in EtOAc/MeOH/H₂O (80:20:10) and was soluble in water.

Its molecular formula C₆H₁₁NO₃ was deduced from the HRESIMS spectrum (Figure 127) which showed the sodium adduct [M+Na]⁺ peak at *m/z* 168.0683 (calcd. for C₆H₁₁NO₃Na, 168.0637), implying two degrees of unsaturation.

Its ¹H NMR spectrum (Figure 128) showed signals of:

- a singlet of three protons at δ_H 2.98 (3H, s, N-CH₃) attributable to an azomethyl group;
- two sets of methylene group protons at δ_H 2.42 (1H, m, H-3b), δ_H 2.18 (1H, dd, *J* = 14.2, 7.5 Hz, H-3a) and δ_H 3.91 (1H, dd, *J* = 13.0, 4.7 Hz, H-5b) and 3.13 (1H, m, H-5a);
- an azomethine proton at δ_H 4.13 (1H, d, *J* = 11.0, 7.5 Hz, H-2);
- an oxymethine proton at δ_H 4.57 (1H, m, H-4).

The analysis of its broad-band decoupled ¹³C NMR spectrum (Figure 129) exhibited the signals of six carbon atoms which were sorted by HMQC technique (Figure 130) into:

- a quaternary carbon at δ_C 172.9 (C-1) attributable to a carboxyl group;
- two methine groups at δ_C 69.5 (C-2) and 70.1 (C-4);
- two methylene groups at δ_C 38.2 (C-3) and 62.7 (C-5);
- an azomethyl group at δ_C 43.2 (N-CH₃).

All these spectral data suggest that SNC10 would have in its structure a cyclopentane ring substituted by a carboxyl group.

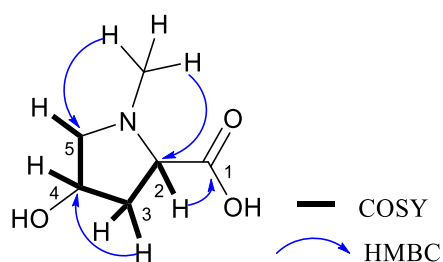
The positions of the hydroxyl and methyl group were established thanks to the correlations observed on the HMBC and ¹H-¹H COSY spectra.

In fact, its ¹H-¹H COSY spectrum (Figure 131) displayed correlations between protons:

- H-2 (δ_H 4.13) and H-3 (δ_H 2.42; 2.18);
- H-3 (δ_H 2.42; 2.18) and H-4 (δ_H 4.57);
- H-4 (δ_H 4.57) and H-5 (δ_H 3.91; 3.13).

Its HMBC spectrum (Figure 133) showed correlations between protons:

- H-5 (δ_H 3.91; 3.13) and carbons C-4 (δ_C 70.1), C-3 (δ_C 38.2),
- H-3 (δ_H 2.42; 2.18) and carbons C-2 (δ_C 69.5), C-1 (δ_C 172.9);
- H-2 (δ_H 4.13) and carbons C-1 (δ_C 172.9), C-3 (δ_C 38.2);
- of the azomethyl group N-CH₃ (δ_H 2.98) and carbons C-2 (δ_C 69.5), C-5 (δ_C 62.4).



Scheme 30: Some key COSY and HMBC of SNC10

These data were in agreement with those described in the literature for 4-hydroxy-*N*-methylproline (**148**), previously isolated from the red alga *Chondria coerulescens* by Scuito *et al.* (1983).

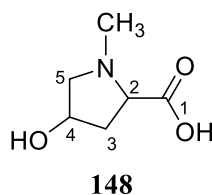


Table 42: ^1H (500 MHz) and ^{13}C (125 MHz) NMR data of SNC6 in D_2O compared to 4-hydroxy-*N*-methylproline [D_2O , NMR ^{13}C (20.1 MHz), NMR ^1H (270 MHz)]

SNC10			4-hydroxy- <i>N</i> -methylproline (Scuito <i>et al.</i> , 1983)	
Position	$\delta^{13}\text{C}$	$\delta^1\text{H}$ (m, <i>J</i> in Hz)	$\delta^{13}\text{C}$	$\delta^1\text{H}$ (m, <i>J</i> in Hz)
1	172.9	-	170.2	-
2	69.5	4.13 (1H, d, 11.0, 7.5)	69.1	4.02 (1H, d, 10.5, 7.5)
3a	38.2	2.18 (1H, dd, 14.2, 7.5)	38.7	2.20 (1H, dd, 13.5, 7.5)
3b		2.42 (1H, m)		2.43 (1H, dd, 10.5, 1.8)
4	70.1	4.57 (1H, m)	69.7	4.48 (1H, m)
5a	62.7	3.13 (1H, m)	62.4	3.10 (1H, dd, 12.6, 4.8)
5b		3.91 (1H, dd, 13.0, 4.7)		3.80 (1H, dd, 12.6, 2.1)
N-CH ₃	43.2	2.98 (3H, s)	43.4	2.96 (3H, s)

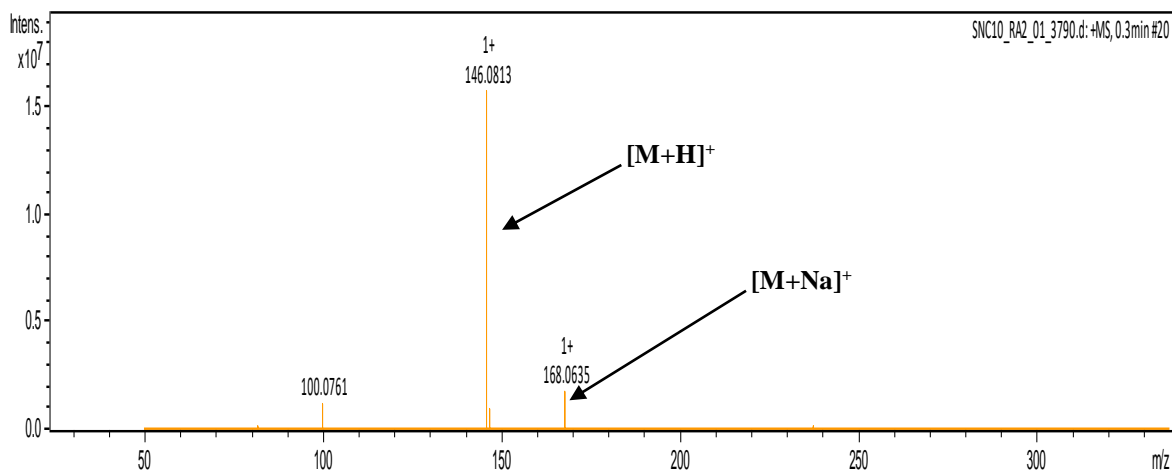


Figure 127: HRESI mass spectrum of SNC10

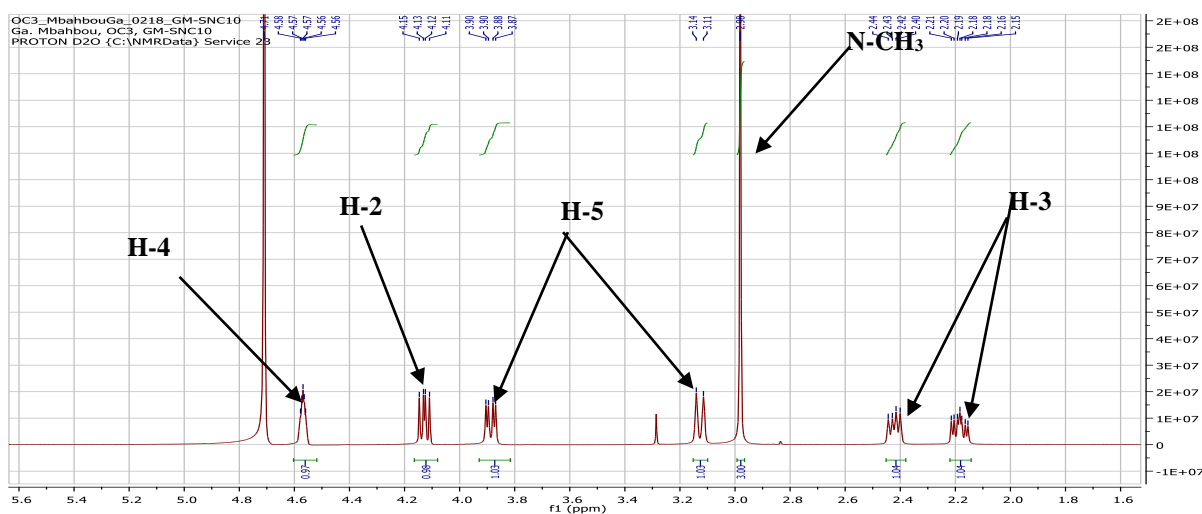


Figure 128: ¹H NMR spectrum (D₂O, 500 MHz) of SNC10

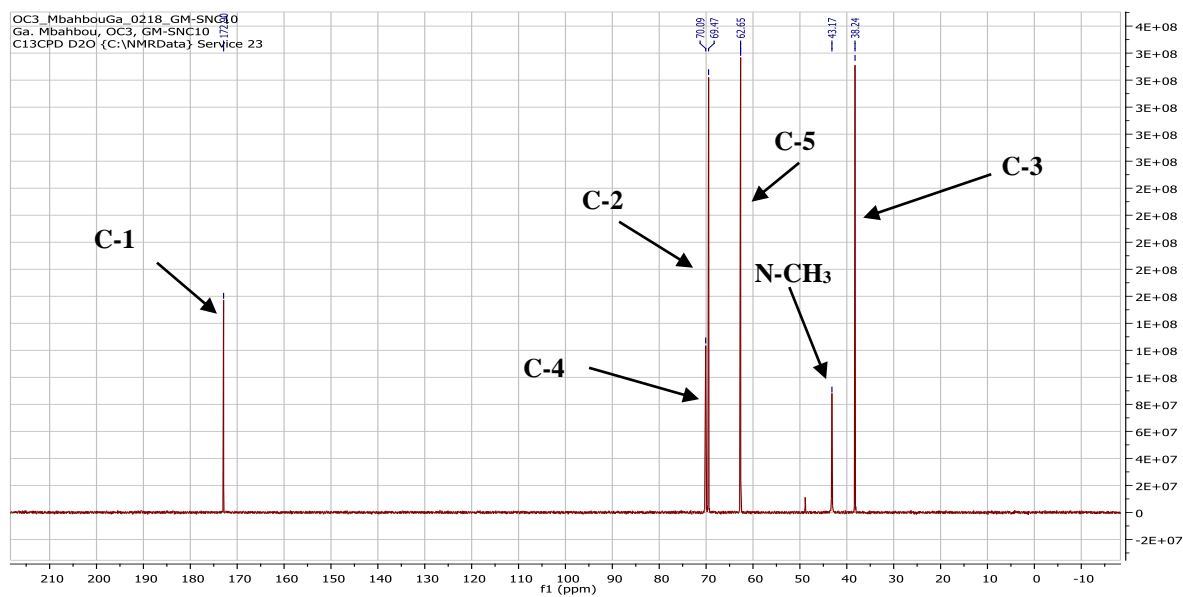


Figure 129: ¹³C NMR spectrum (D₂O, 125 MHz) of SNC10

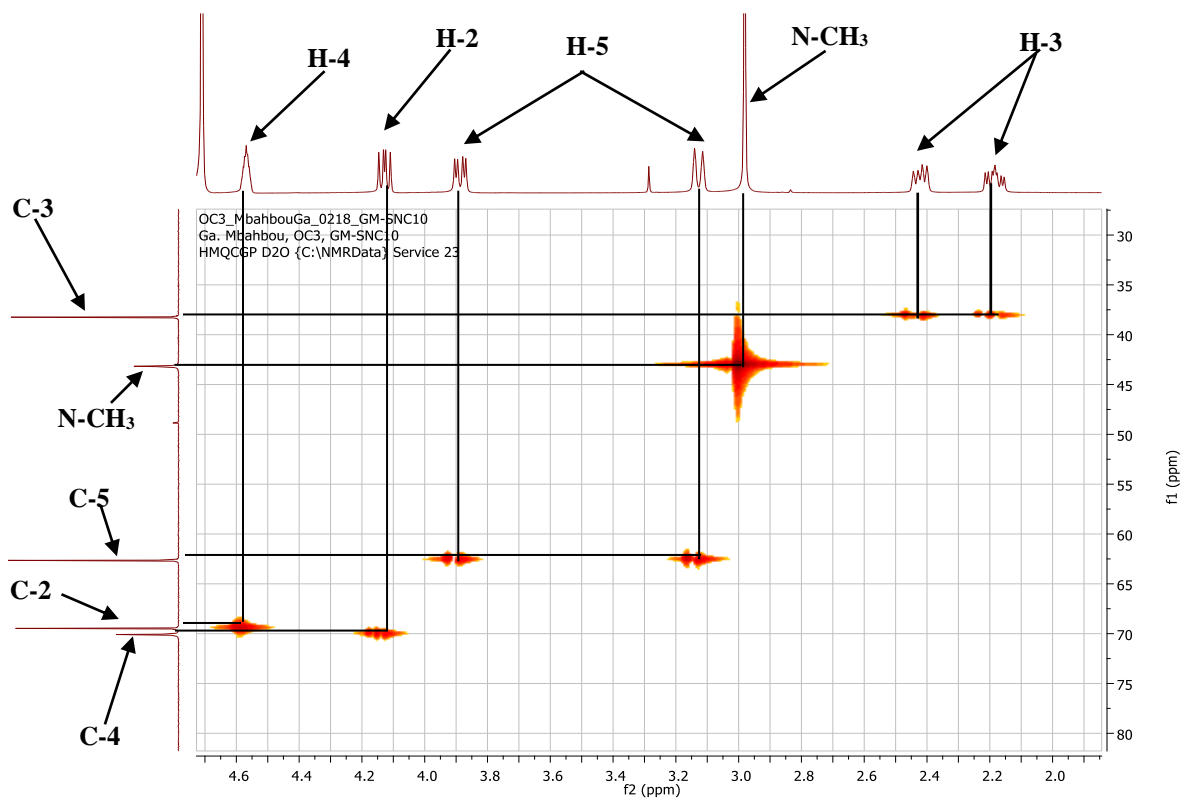


Figure 130: HMQC spectrum of SNC10

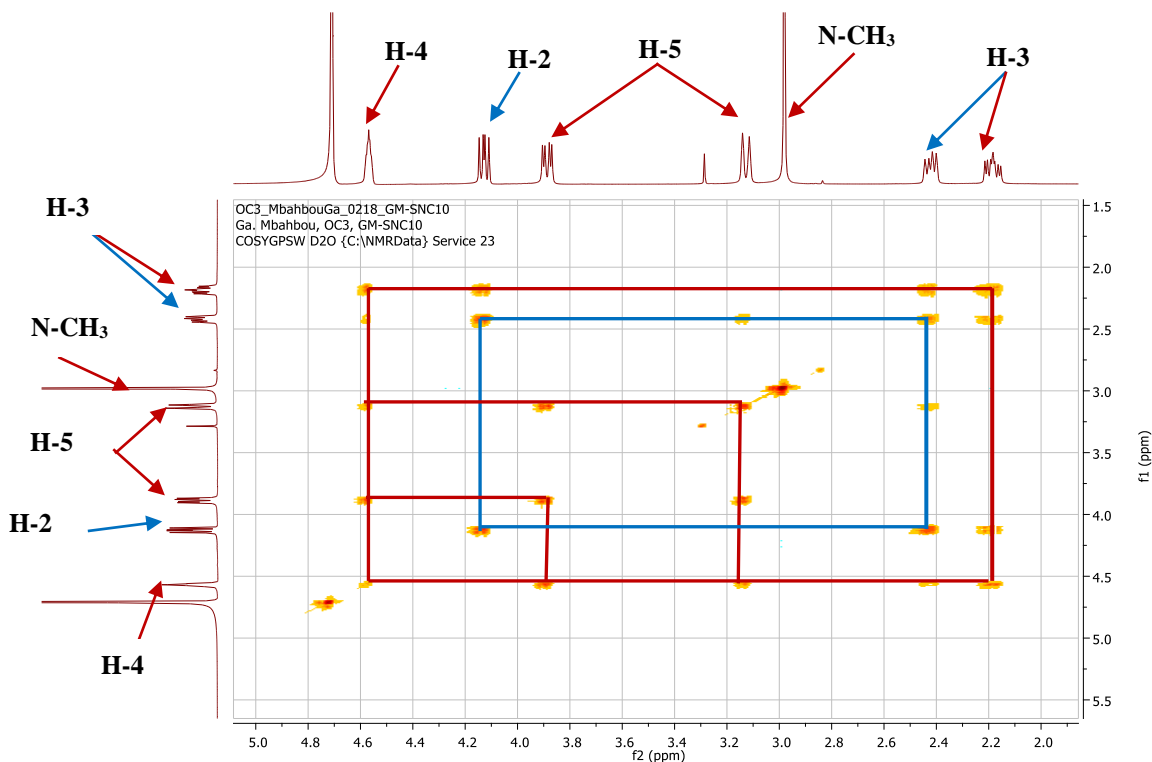


Figure 131: COSY spectrum of SNC10

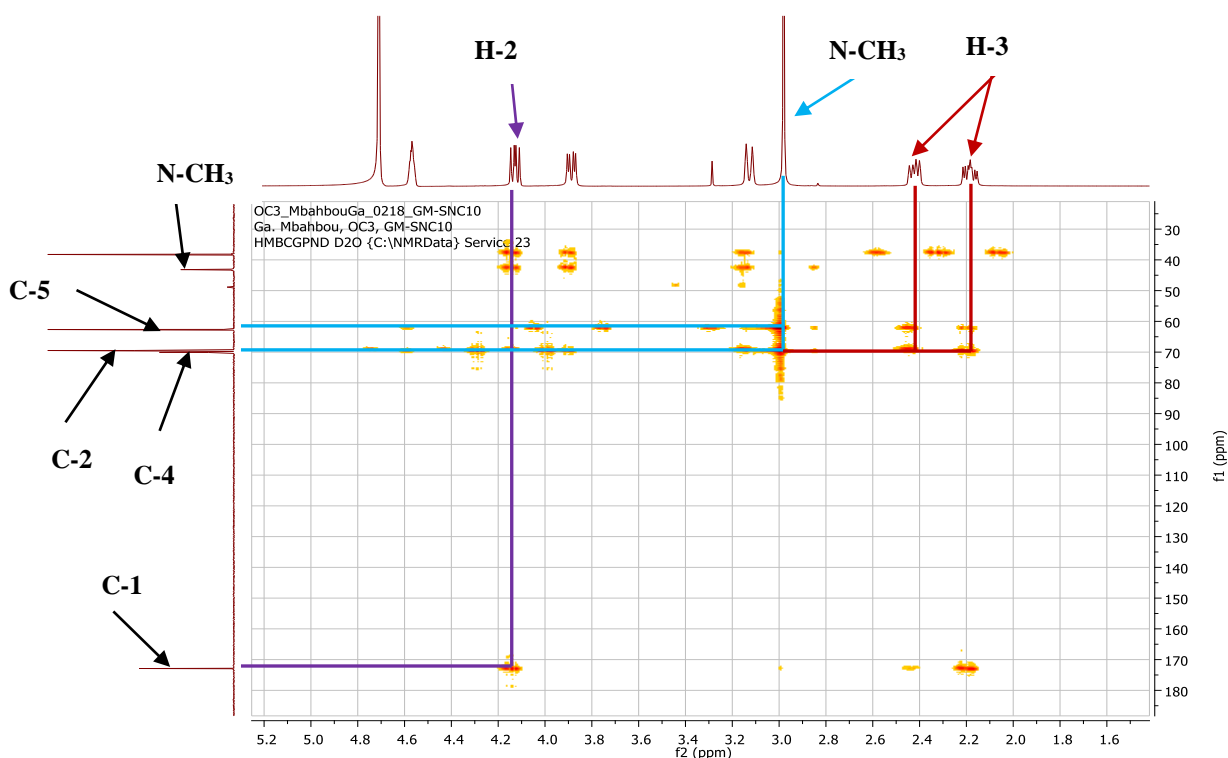


Figure 132: HMBC spectrum of SNC10

II.1.5.6. Pyrrole derivative

II.1.5.6.1. Structural identification of compound WN17

WN17 was obtained as orange crystals in $\text{CH}_2\text{Cl}_2/\text{acetone}$ (90:10) and it is soluble in methanol.

Its molecular formula $\text{C}_7\text{H}_7\text{NO}_4$ was deduced from the HRESIMS spectrum (Figure 133) which showed the sodium adduct peak $[3\text{M}+\text{Na}]^+$ at m/z 530.1056 (calcd. for $\text{C}_{21}\text{H}_{21}\text{N}_3\text{O}_{12}\text{Na}$, 530.1023), implying four degrees of unsaturation.

Its ^1H NMR spectrum (Figure 134) showed signals of:

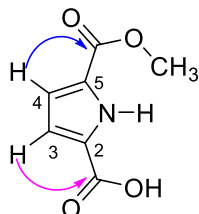
- two protons at δ_{H} 6.85 (1H, d, $J = 3.9$ Hz, H-4) and δ_{H} 6.86 (1H, d, $J = 3.9$ Hz, H-3);
- a methoxy group at δ_{H} 3.88 (1H, s, OCH_3).

Its ^{13}C NMR spectrum (Figure 135) exhibited carbon signals, which were sorted by DEPT (Figure 136) and HMQC (Figure 137) techniques into:

- four quaternary group carbons including a carboxyl group at δ_{C} 162.0 (2-COOH), a carboxylate group at δ_{H} 161.0 (5-COO) and the other carbons at δ_{C} 126.1 (C-5), δ_{C} 127.3 (C-2);
- two methine group carbons at δ_{C} 115.0 (C-3) and δ_{C} 115.1 (C-4);
- a methoxy group at δ_{C} 50.7 (OCH_3).

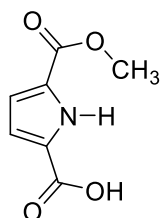
The position of the carboxylic and carboxylate groups was determined by the correlations observed on the HMBC spectrum (Figure 138) between protons:

- H-4 (δ_{H} 6.85) and carbon 2-COOH (δ_{C} 162.0);
- H-3 (δ_{H} 6.86) and carbon 5-COO (δ_{C} 161.0).



Scheme 31: Key HMBC correlations of WN17

All these data, compared with those described in the literature contributed to identify WN17 as monomethyl ester of 1H-pyrrole-2,5-dicarboxylic acid (**149**), previously isolated from *Berberis koreana* by Kostalova *et al.* (1992).



149

Table 43: ^1H (500 MHz) and ^{13}C (125 MHz) NMR data of WN17 in methanol- d_4 compared to monomethyl ester of 1H-pyrrole-2,5-dicarboxylic acid [DMSO- d_6 , NMR ^{13}C (125 MHz), NMR ^1H (500 MHz)]

WN17			Monomethyl ester of 1H-pyrrole-2,5-dicarboxylic acid (Kostalova <i>et al.</i> , 1992)	
Position	$\delta^{13}\text{C}$	$\delta^1\text{H}$ (m, J in Hz)	$\delta^{13}\text{C}$	$\delta^1\text{H}$ (m, J in Hz)
2	127.3	-	128.1	-
3	115.0	6.86 (1H, d, 3.9)	115.3	6.80 (1H, dd, 3.9, 2.4)
4	115.1	6.85 (1H, d, 3.9)	115.5	6.76 (1H, dd, 3.9, 2.4)
5	126.1	-	126.2	-
2-COOH	162.0	-	161.4	-
5-COO	161.0	-	160.5	-
O-CH ₃	50.7	3.88 (3H, s)	51.6	3.77 (3H, s)

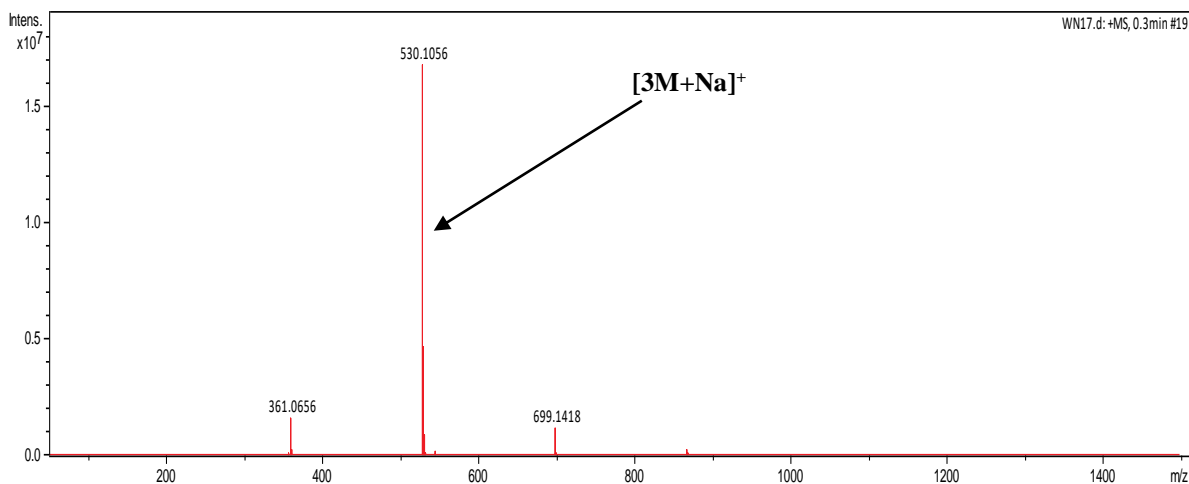


Figure 133: HRESI mass spectrum of WN17

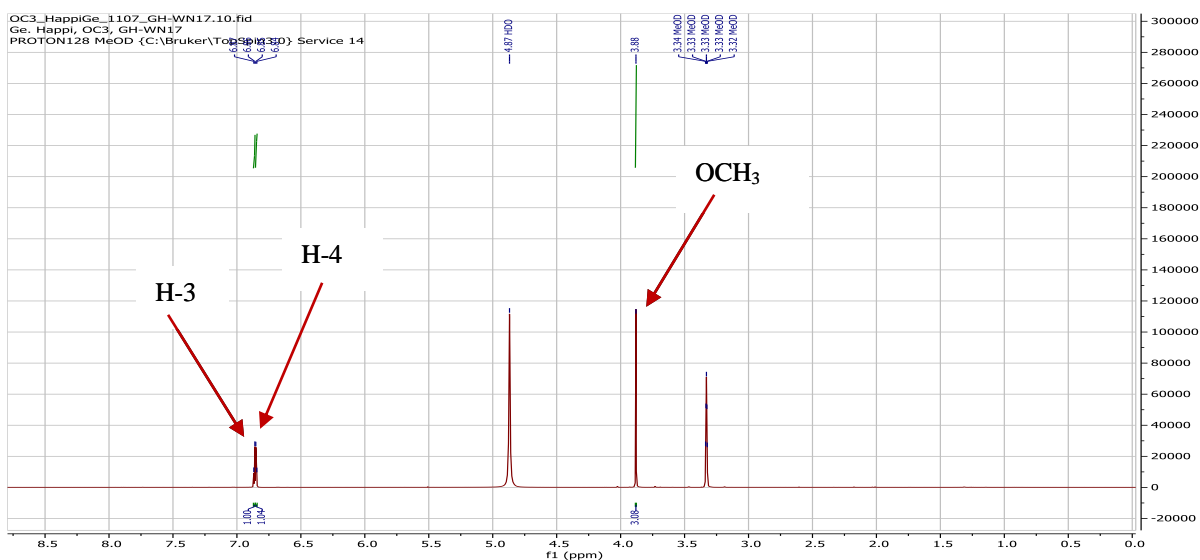


Figure 134: ^1H NMR spectrum (methanol- d_4 , 500 MHz) of WN17

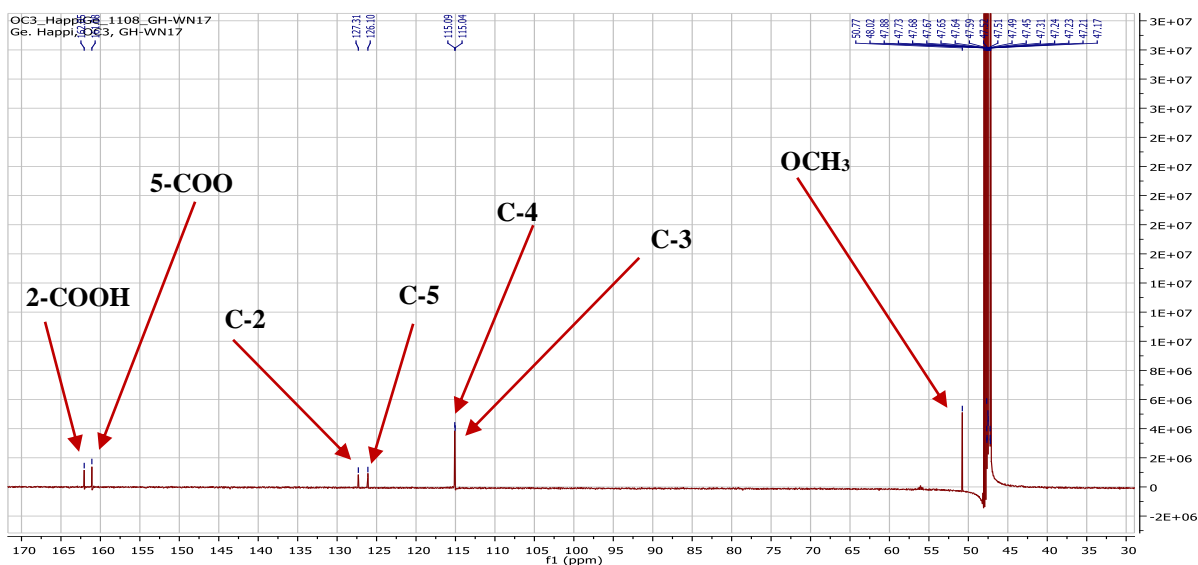


Figure 135: ^{13}C NMR spectrum (methanol- d_4 , 125 MHz) of WN17

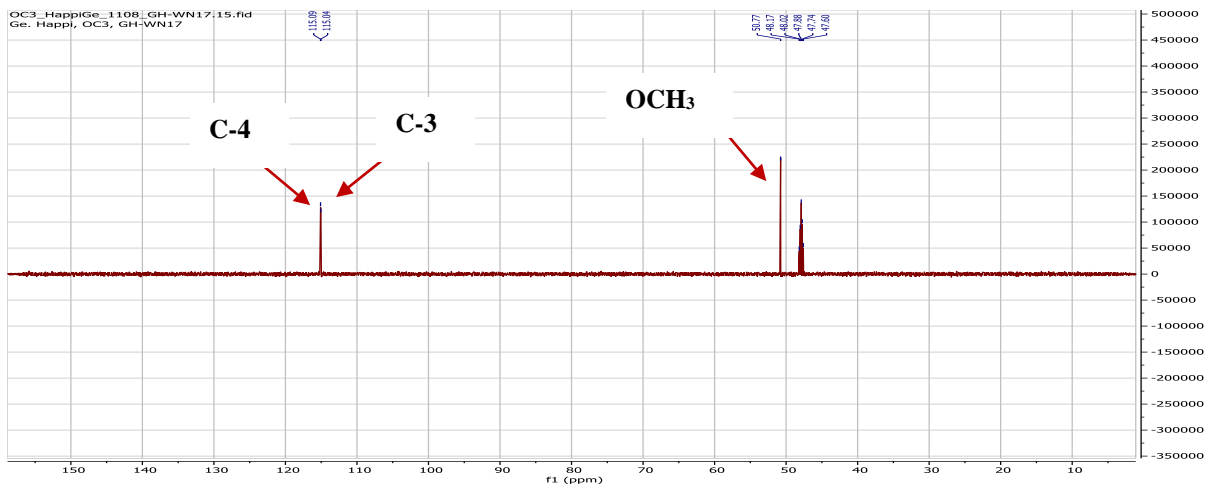


Figure 136: DEPT spectrum of WN17

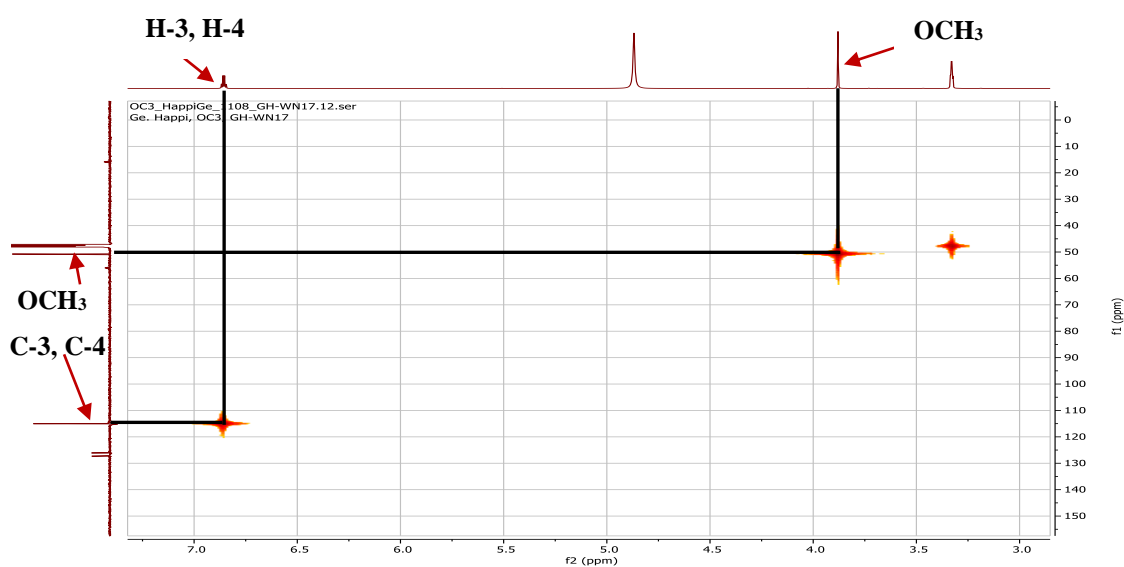


Figure 137: HMQC spectrum of WN17

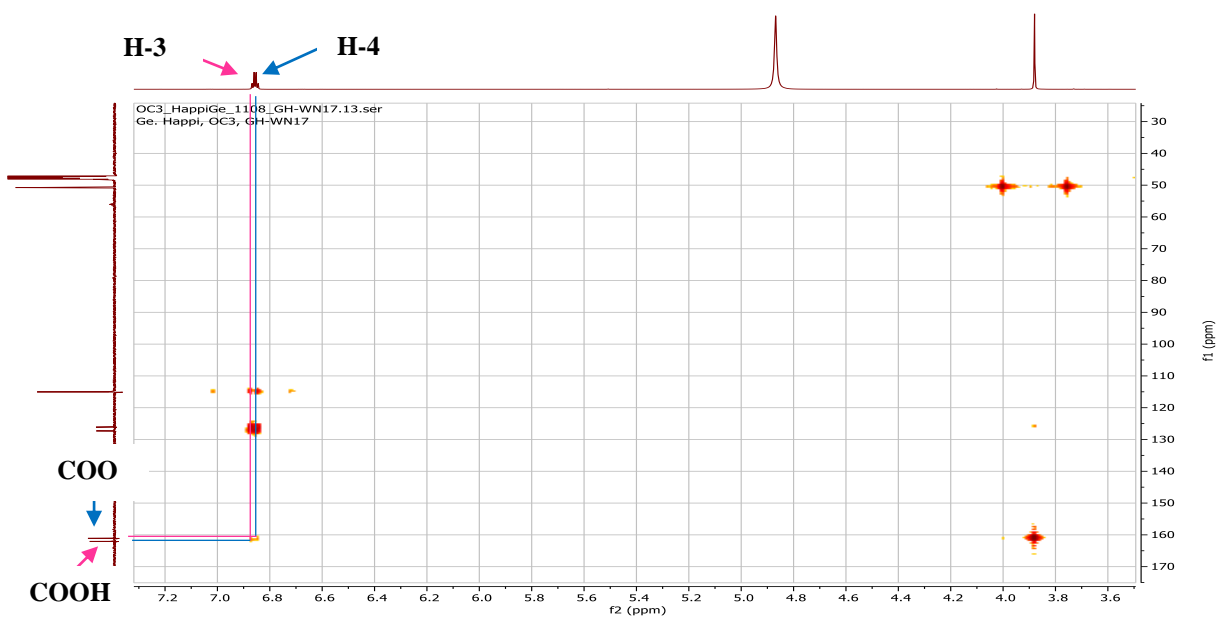


Figure 138: HMBC spectrum of WN17

II.1.5.7. Iridoid

II.1.5.7.1. Structural identification of compound NLB3

NLB3 was obtained as a chesnut paste in EtOAc/MeOH (80:20). It is soluble in methanol and reacts positively to Molisch test, characteristic of sugars.

Its molecular formula $C_{23}H_{36}O_{15}$ was deduced from the HRESIMS spectrum (Figure 139) which showed the sodium adduct peak $[M+Na]^+$ at m/z 575.1946 (calcd. for $C_{23}H_{36}O_{15}Na$, 575.1952), implying six degrees of unsaturation.

Its 1H NMR spectrum (Figure 140) showed resonances of:

- an olefinic proton at δ_H 7.42 (1H, s), characteristic of proton at position 3 of iridoids (Sang *et al.*, 2001);
- two oxymethine protons at δ_H 4.08 (1H, m, H-7) and 5.23 (1H, d, $J = 5.0$ Hz, H-1);
- three methine groups at δ_H 3.13 (1H, brq, $J = 8.2$ Hz, H-5), 2.02 (1H, td, $J = 8.8, 5.0$ Hz, H-9) and 1.91 (1H, m, H-8);
- two methylene protons at δ_H 1.65 (1H, m, H-6b) and 2.26 (1H, m, H-6a);
- a methyl group at δ_H 1.13 (3H, d, $J = 6.9$ Hz, H-10);
- methoxy protons at δ_H 3.69 (3H, s, OCH_3).
- protons of two sugar moieties including the two anomeric protons at δ_H 4.68 (1H, d, $J = 7.9$ Hz, H-1') and 4.39 (1H, d, $J = 7.8$ Hz, 1''). The β configuration of the two sugar moieties is due to the high value of the coupling constant of the anomeric protons ($J = 7.8$ Hz) (Agrawal, 1992).

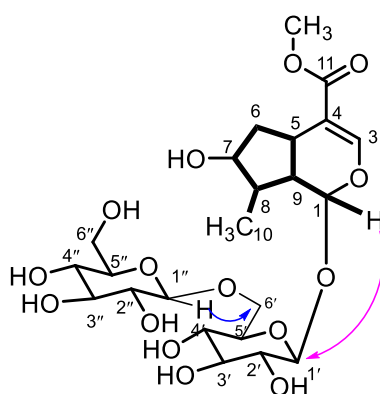
Its ^{13}C NMR spectrum (Figure 141) exhibited carbon signals, which were sorted by DEPT (Figure 142) and HMQC (Figure 143) techniques into:

- two quaternary carbons at δ_C 168.2 (C-11) and 112.4 (C-4), attributable to a carboxylate group and an olefinic carbon, respectively;
- six methine groups amongst which an olefinic at δ_C 150.9 (C-3), two oxymethines at δ_C 96.9 (C-1) and 73.6 (C-7) and the others at δ_C 45.0 (C-9), 40.9 (C-8) and 31.0 (C-5);
- one methylene group at δ_C 41.3 (C-6), one methyl group at δ_C 12.3 (C-10) and one methoxy group at δ_C 50.2 (OCH_3);
- carbons of the two sugar units amongst which carbons at δ_C 103.7 (C-1''), 98.9 (C-1'), 68.7 (C-6'). A comparative analysis of chemical shifts and coupling constants with data from the literature (Agrawal, 1992) contributed in identifying these sugar units as β -D-glucopyranoside.

The correlation observed on the HMBC spectrum (Figure 144) between proton H-1'' (δ_H 4.39) and carbon C-6' (δ_C 68.7) allowed us to link the two β -glucopyranosyl units at position 6'. The fixation of these two sugar units on the aglycon was made thanks to the correlation observed on the same spectrum between proton H-1 (δ_H 5.23) and C-1' (δ_C 98.9).

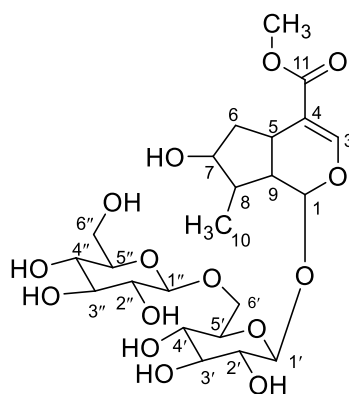
In addition, the 1H - 1H COSY spectrum of NLB3 (Figure 145) displayed correlations between protons:

- H-1 (δ_H 5.23) and H-9 (δ_H 2.02) which in turn was linked to H-5 (δ_H 3.13) and H-8 (δ_H 1.91);
- H-8 (δ_H 1.91) and H-10 (δ_H 1.13), H-7 (δ_H 4.08) which in turn was linked to H-6 (δ_H 1.65/2.26) which correlated also with H-5 (δ_H 3.13).



Scheme 32: Some key COSY and HMBC correlations of NLB3

All these data were in agreement with those described in the literature for loganin 6'-O- β -glucopyranoside (**150**), previously isolated from *Balanophora latisepala* by Kanchanapoom *et al.* (2001).



150

The NMR data of loganin 6'-O- β -glucopyranoside (**150**) is given here for the first time and were compared in table below to those of loganin

Table 44: ^1H (500 MHz) and ^{13}C (125 MHz) NMR data of NLB3 in methanol- d_4 compared to loganin [DMSO- d_6 , NMR ^{13}C (200 MHz) and DMSO- d_6 + D_2O , NMR ^1H (600 MHz)]

NLB3			Loganin (Calis <i>et al.</i> , 1984)	
Position	$\delta^{13}\text{C}$	$\delta^1\text{H}$ (m, J in Hz)	$\delta^{13}\text{C}$	$\delta^1\text{H}$
1	96.9	5.23 (1H, d, 5.0)	97.8	5.26 (1H, d, 4.5)
3	150.9	7.42 (1H, s)	152.8	7.38 (1H, d, 1.2)
4	112.4	-	113.1	-
5	31.0	3.13 (1H, brq, 8.2)	32.8	3.12 (1H, m)
6	41.3	1.65 (1H, m); 2.26 (1H, m)	40.5	1.62 (1H, m); 2.03 (1H, m)
7	73.6	4.08 (1H, m)	73.7	4.04 (1H, m)
8	40.9	1.91 (1H, m)	41.1	1.87 (1H, m)
9	45.0	2.02 (1H, td, 8.8, 5.0)	47.1	2.23 (1H, m)
10	12.3	1.13 (1H, d, 6.9)	14.0	1.09 (1H, d, 6.9)
11	168.2	-	169.4	-
OCH ₃	50.2	3.69 (3H, s)	52.0	3.69 (3H, s)
1'	98.9	4.68 (1H, d, 7.9)	100.3	4.64 (1H, d, 7.8)
2'	73.7	3.23 (1H, m)	74.8	3.40-3.19
3'	76.5	3.38 (1H, m)	78.0	3.40-3.19
4'	70.1	3.28 (1H, m)	71.6	3.40-3.19
5'	76.6	3.38 (1H, m)	78.3	3.40-3.19
6'	68.7	4.19 (1H, 11.7, 1.6); 3.78 (1H, 11.7, 6.5)	62.8	3.89 (1H, dd, 12.0, 1.8); 3.66 (1H, dd, 12.0, 5.7)
1''	103.7	4.39 (1H, d, 7.8)		
2''	73.2	3.23 (1H, m)		
3''	75.9	3.53 (1H, m)		
4''	70.1	3.28 (1H, m)		
5''	76.7	3.23 (1H, m)		
6''	61.3	3.69 (1H, m); 3.88 (1H, dd, 11.8, 1.8)		

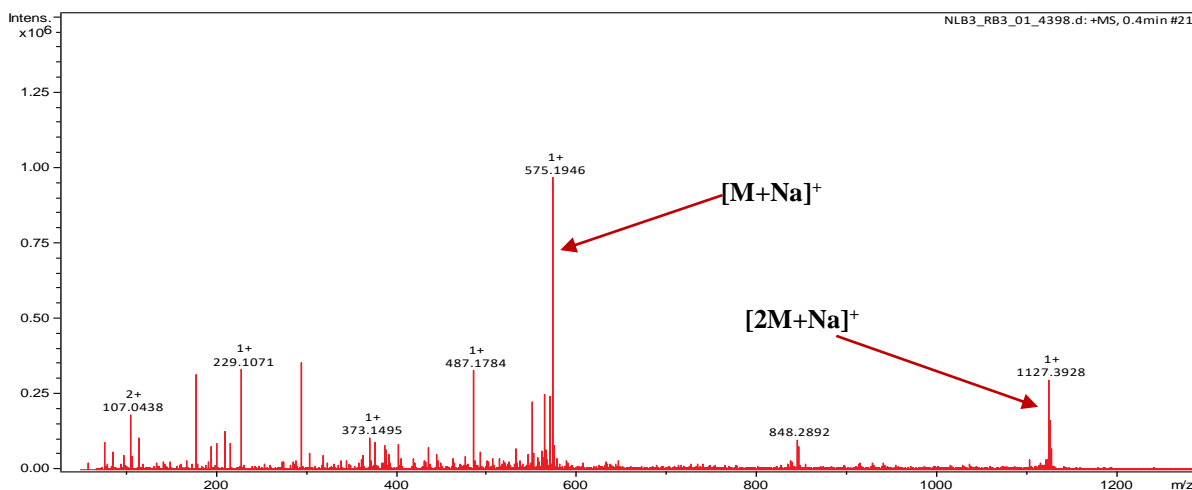


Figure 139: HRESI mass spectrum of NLB3

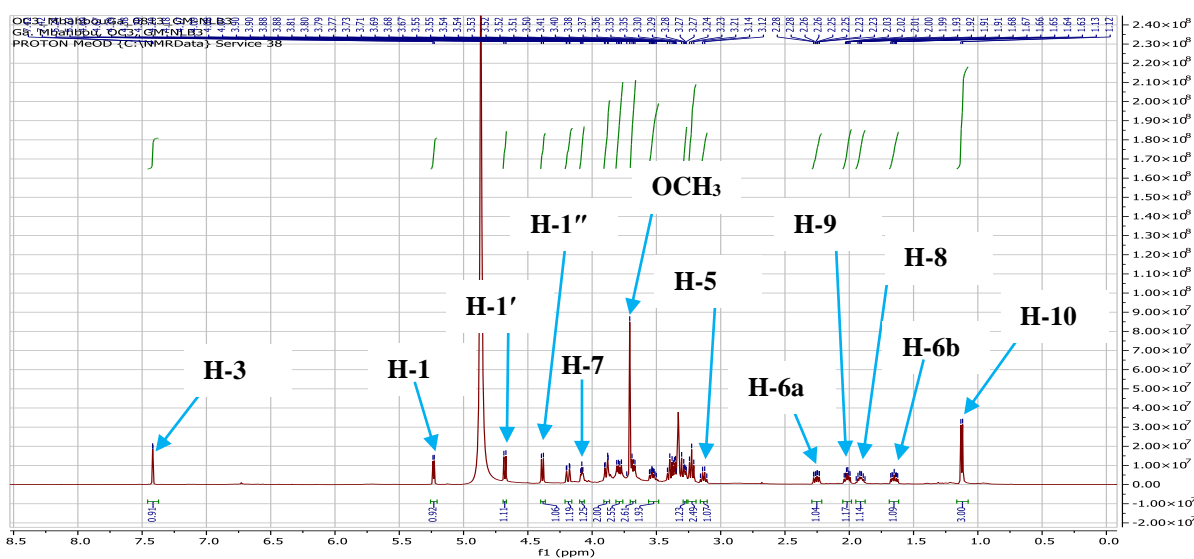


Figure 140: ^1H NMR spectrum (methanol- d_4 , 500 MHz) of NLB3

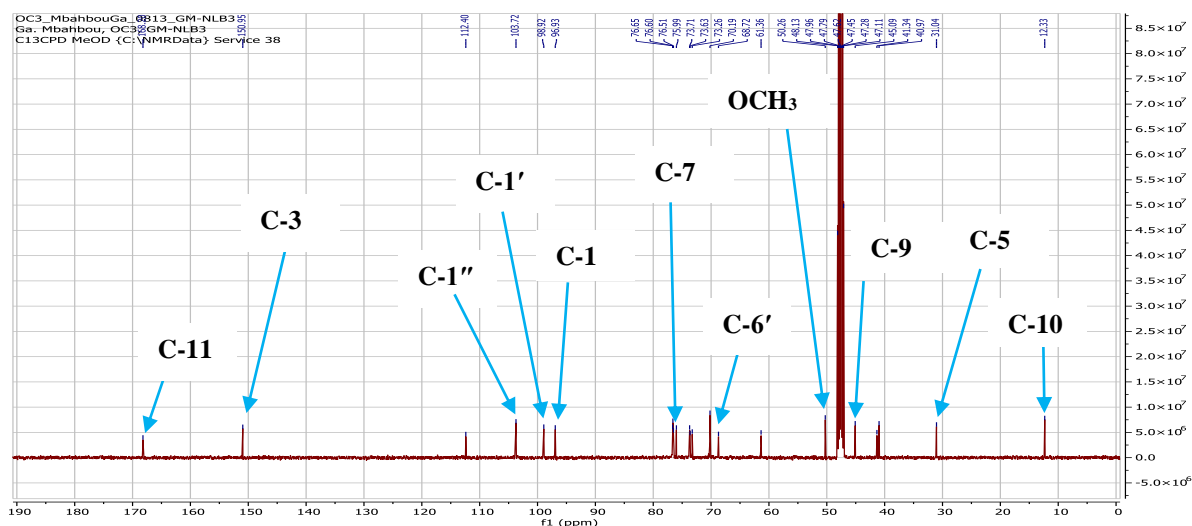


Figure 141: ^{13}C NMR spectrum (methanol- d_4 , 125 MHz) of NLB3

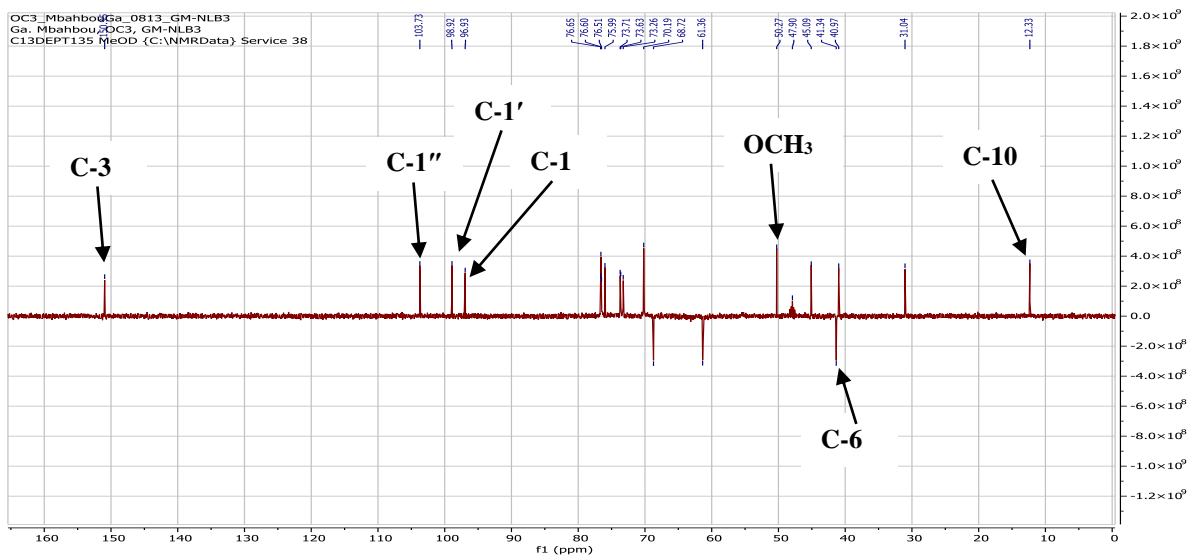


Figure 142: DEPT spectrum of NLB1

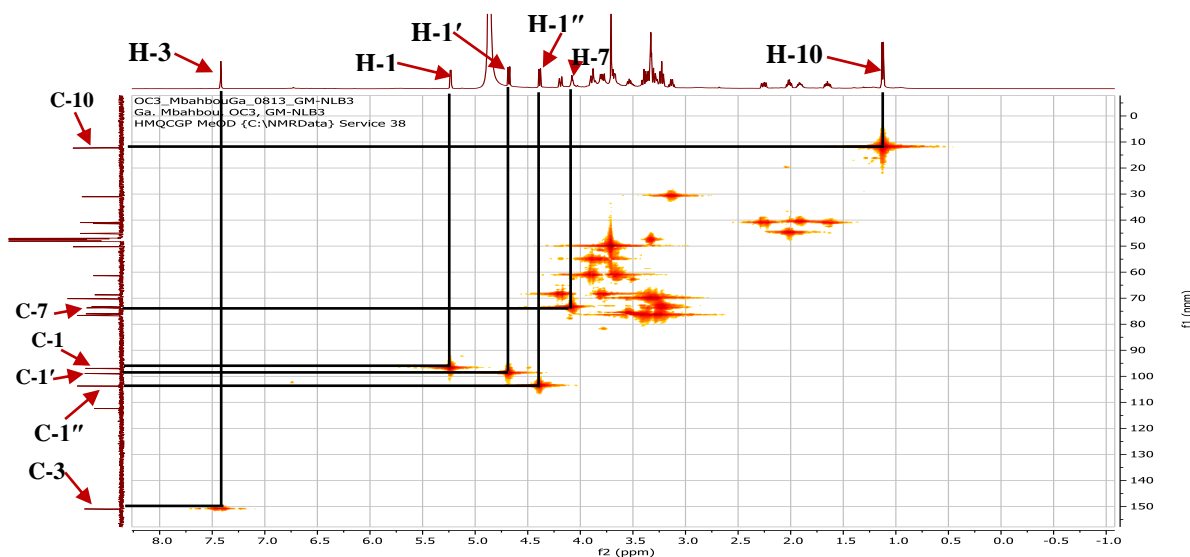


Figure 143: HMQC spectrum of NLB3

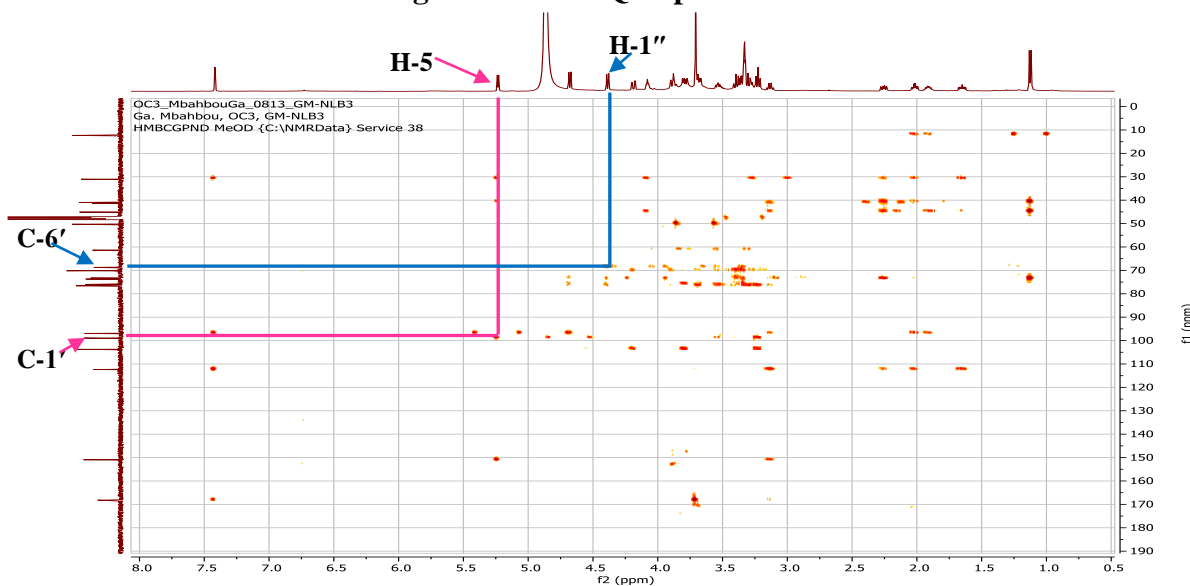


Figure 144: HMBC spectrum of NLB3

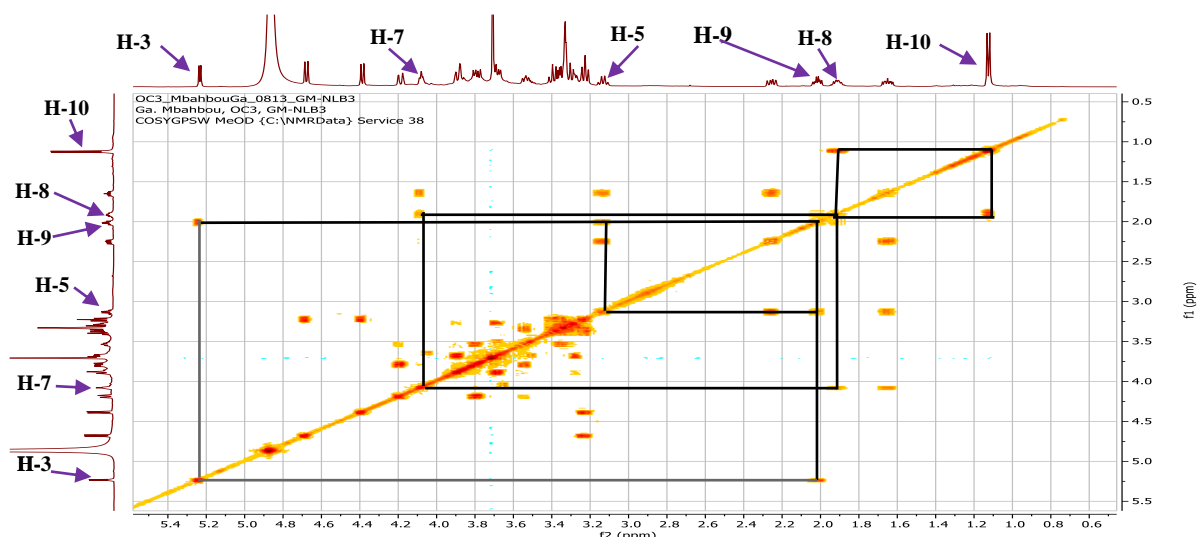


Figure 145: COSY spectrum of NLB3

II.1.5.8. Steroids

II.1.5.8.1. Structural identification of compound BLE8

BLE8 was obtained as a white powder in *n*-hexane/EtOAc (70:30). It is soluble in methanol and reacts positively to Lieberman Burchard test, characteristic of steroids by given a blue colour which turns quickly to dark green.

Its molecular formula $C_{28}H_{44}O_3$, with seven hydrogen deficiency was deduced from its NMR data and ESIMS spectrum (Figure 146) which showed the sodium adduct peak $[M+Na]^+$ at m/z 451.4.

Its 1H -NMR spectrum (Figure 147) displayed signals of:

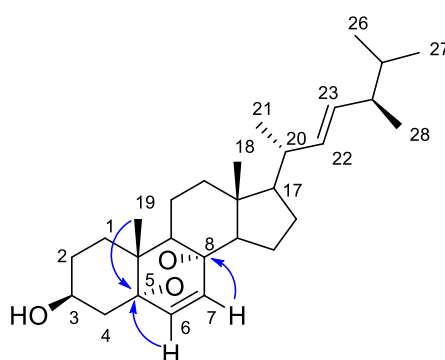
- six methyl groups including two singlets at δ_H 0.83 (3H, s, H-18), 0.89 (3H, s, H-19), and four doublets at δ_H 0.82 (3H, d, $J = 6.8$ Hz, H-26), 0.83 (1H, d, $J = 6.7$ Hz, H-27), 0.90 (1H, d, $J = 6.9$ Hz, H-28) and 1.00 (1H, d, $J = 6.6$ Hz, H-21);
- an oxymethine proton at δ_H 3.85 (1H, m, H-3);
- four olefinic protons at δ_H 5.14 (1H, dd, $J = 15.3$ Hz, 8.4, H-22), 5.22 (1H, dd, $J = 15.3, 7.6$ Hz, H-23), 6.25 (1H, d, $J = 8.5$ Hz, H-6) and 6.51 (1H, d, $J = 8.5$ Hz, H-7).

The analysis of its ^{13}C NMR spectrum (Figure 148) sorted by DEPT (Figure 149) and HMQC (Figure 150) techniques revealed C_{28} -sterol ergostane skeleton (Nowak *et al.* 2016), including signals of:

- six methyl groups at δ_C 12.5 (C-18), 17.2 (C-28), 17.7 (C-19), 19.1 (C-26), 19.5 (C-27) and 20.4 (C-21);
- two disubstituted olefins at δ_C 130.6 (C-7), 132.2 (C-23), 135.1 (C-22) and 135.5 (C-6);

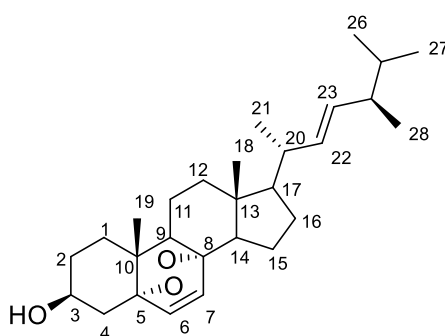
- two oxygenated quaternary carbons of δ_C 79.2 (C-8) and 82.2 (C-5) suggesting the presence of a peroxide structure (Nowak *et al.*, 2016);
- seven methine groups including an oxymethine at δ_C 65.6 (C-3), the others at δ_C 32.9 (C-25), 39.6 (C-20), 42.4 (C-24), 51.1 (C-9/C-13) and 56.6 (C-17).
- seven methylene groups at δ_C 20.3 (C-11), 23.2 (C-15), 28.4 (C-16), 29.4 (C-2), 34.6 (C-1), 36.4 (C-4) and 39.2 (C-12).

The position of the peroxide group was established using the HMBC spectrum (Figure 151) which showed the correlations between protons H-6 (δ_H 6.25), H-7 (δ_H 6.51) and carbons C-5 (δ_C 82.3) and C-8 (δ_C 79.2) and between H-19 (δ_H 0.89) and carbon C-5 (δ_C 82.2).



Scheme 33: key HMBC correlations of BLE8

All these data, compared with those described in the literature, were concluded to be that of ergosterol peroxide (**151**), previously isolated from *Hygrophoropsis aurantiaca* by Nowak *et al.* (2016).



151

Table 45: ^1H (500 MHz) and ^{13}C (125 MHz) NMR data of BLE8 in $\text{CDCl}_3/\text{methanol-}d_4$ compared to ergosterol peroxide [CDCl_3 , NMR ^{13}C (125 MHz) and NMR ^1H (500 MHz)]

BLE8			Ergosterol peroxide (Nowak <i>et al.</i> , 2016)	
Position	$\delta^{13}\text{C}$	$\delta^1\text{H}$ (m, J in Hz)	$\delta^{13}\text{C}$	$\delta^1\text{H}$
1	34.6	1.71 (1H, m); 1.67 (1H, m)	34.7	1.73 (1H, dd, 13.8, 3.4)
2	29.4	1.81 (1H, m); 1.79 (1H, m)	30.1	
3	65.6	3.85 (1H, m)	66.5	3.98 (1H, m)
4	36.4	2.05 (1H, m); 1.90 (1H, m)	37.0	
5	82.3	-	82.2	-
6	135.5	6.25 (1H, d, 8.5)	135.4	6.25 (1H, d, 8.5)
7	130.4	6.51 (1H, d, 8.5)	130.8	6.52 (1H, d, 8.6)
8	79.2	-	79.4	-
9	51.1	-	51.1	-
10	36.8	-	36.9	-
11	20.3	1.39 (1H, m); 1.54 (1H, m)	20.6	1.23 (1H, m); 1.55 (1H, m)
12	39.2	1.23 (1H, m); 1.96 (1H, m)	39.4	1.27 (1H, m); 1.98 (1H, m)
13	44.4	-	44.6	-
14	51.1	1.54 (1H, m)	51.7	1.59 (1H, m)
15	23.2	1.23 (1H, m); 1.55 (1H, m)	23.4	1.42 (1H, m); 1.66 (1H, m)
16	28.4	1.38 (1H, m); 1.76 (1H, m)	28.7	1.33 (1H, m); 1.81 (1H, m)
17	56.6	1.24 (1H, m)	56.2	1.25 (1H, m)
18	12.5	0.83 (3H, s)	12.9	0.83 (3H, s)
19	17.7	0.89 (3H, s)	18.2	0.89 (3H, s)
20	39.6	2.02 (1H, m)	39.7	2.05 (1H, m)
21	20.4	1.00 (3H, d, 6.6)	20.9	1.00 (3H, d, 6.7)
22	135.2	5.22 (1H, dd, 7.6, 15.3)	135.2	5.16 (1H, dd, 7.5, 15.3)
23	132.3	5.14 (1H, dd, 8.4, 15.3)	132.3	5.14 (1H, dd, 8.0, 15.3)
24	42.8	1.83 (1H, m)	42.8	1.86 (1H, m)
25	32.9	1.46 (1H, m)	33.1	1.60 (1H, m)
26	19.1	0.82 (3H, d, 6.8)	19.6	0.82 (3H, d, 6.8)
27	19.5	0.83 (3H, d, 6.7)	20.0	0.83 (3H, d, 6.6)
28	17.2	0.90 (3H, d, 6.9)	17.6	0.91 (3H, d, 6.8)

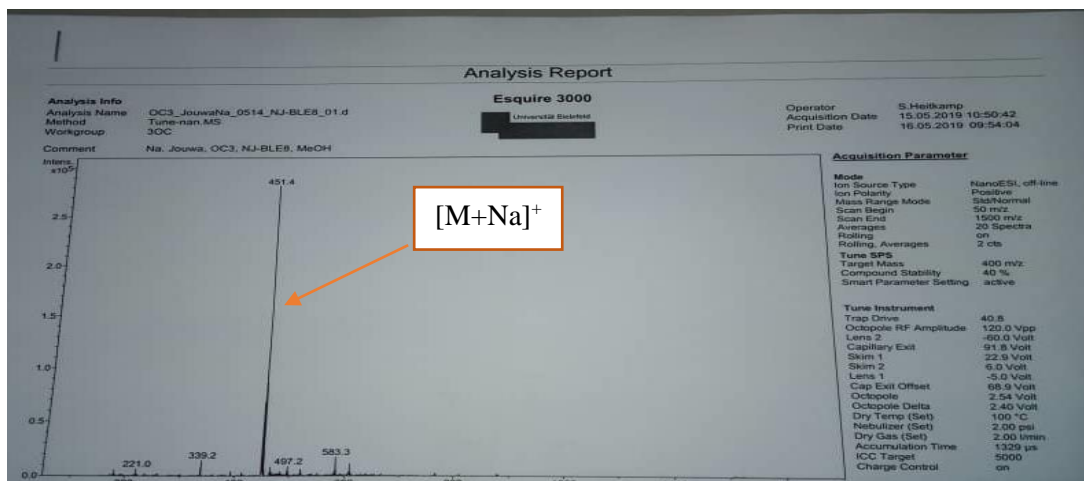


Figure 146: ESIMS spectrum of BLE8

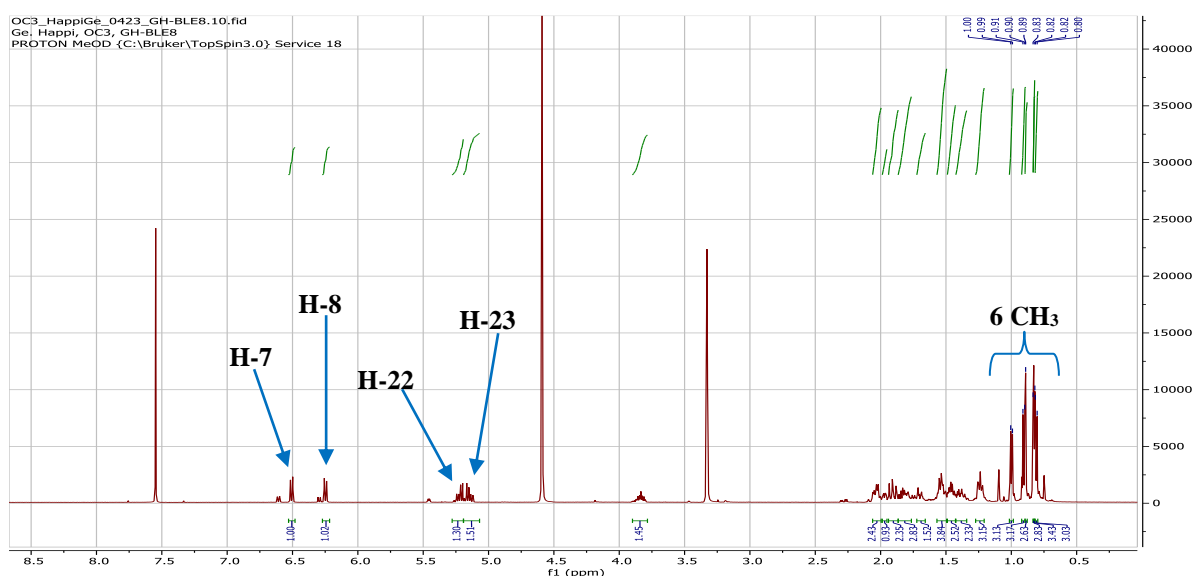


Figure 147: ¹H NMR spectrum (CDCl₃/methanol-*d*₄, 500 MHz) of BLE8

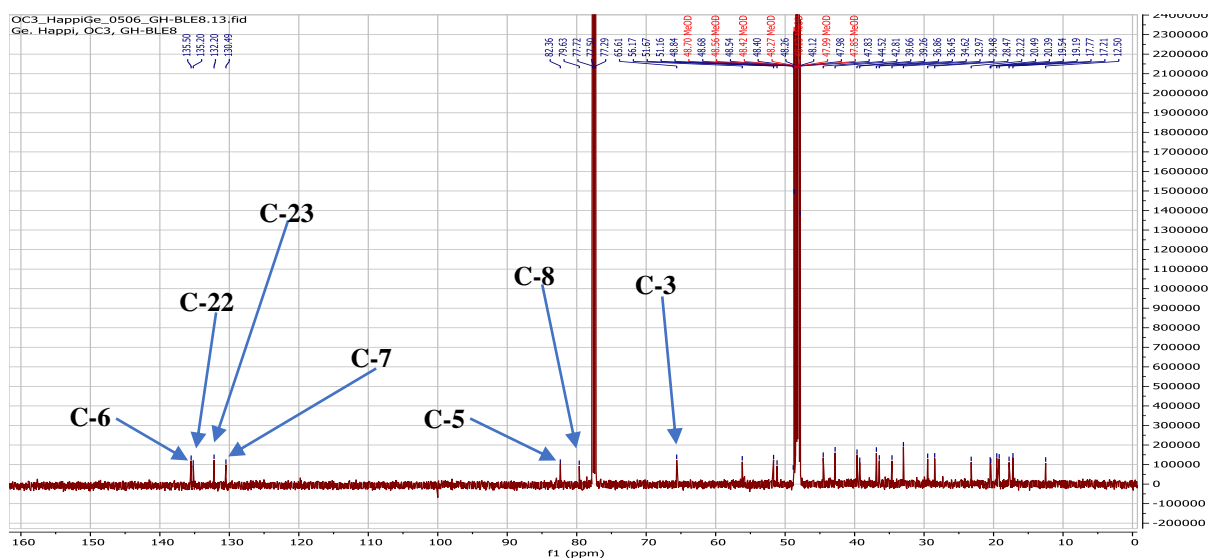


Figure 148: ¹³C NMR spectrum (CDCl₃/methanol-*d*₄, 125 MHz) of BLE8

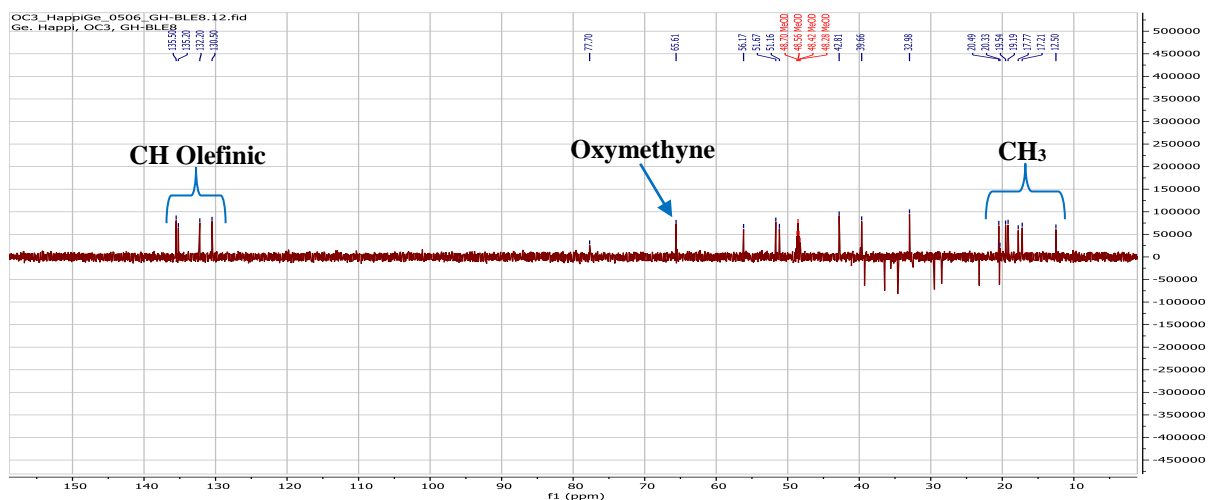


Figure 149: DEPT spectrum of BLE8

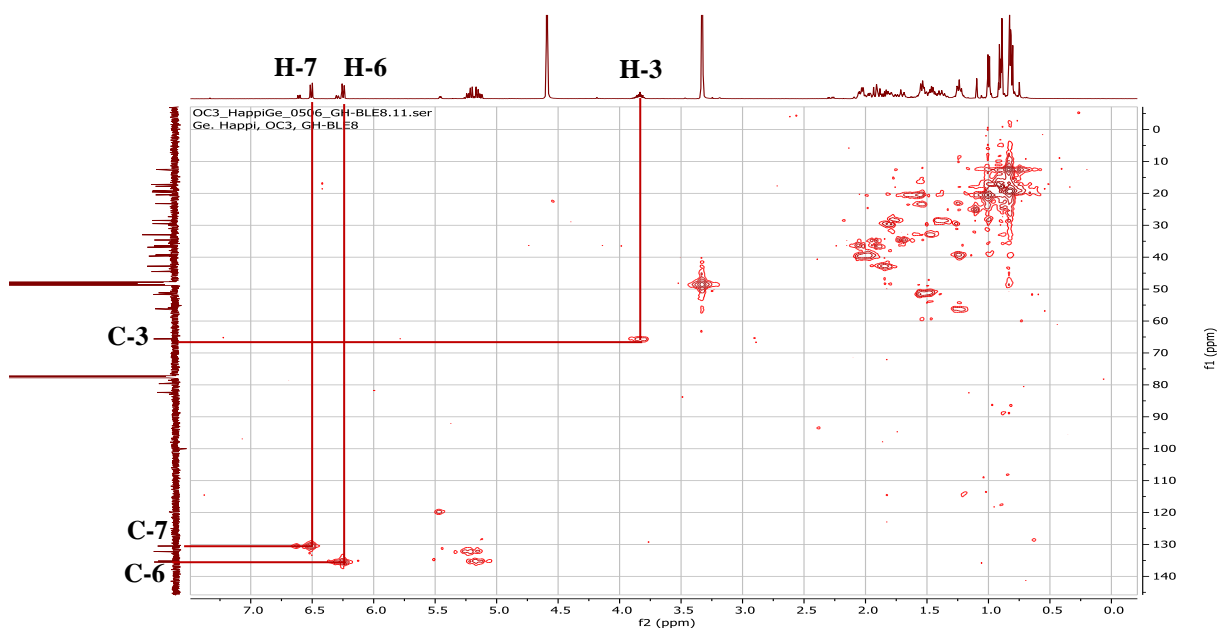


Figure 150: HMQC spectrum of BLE8

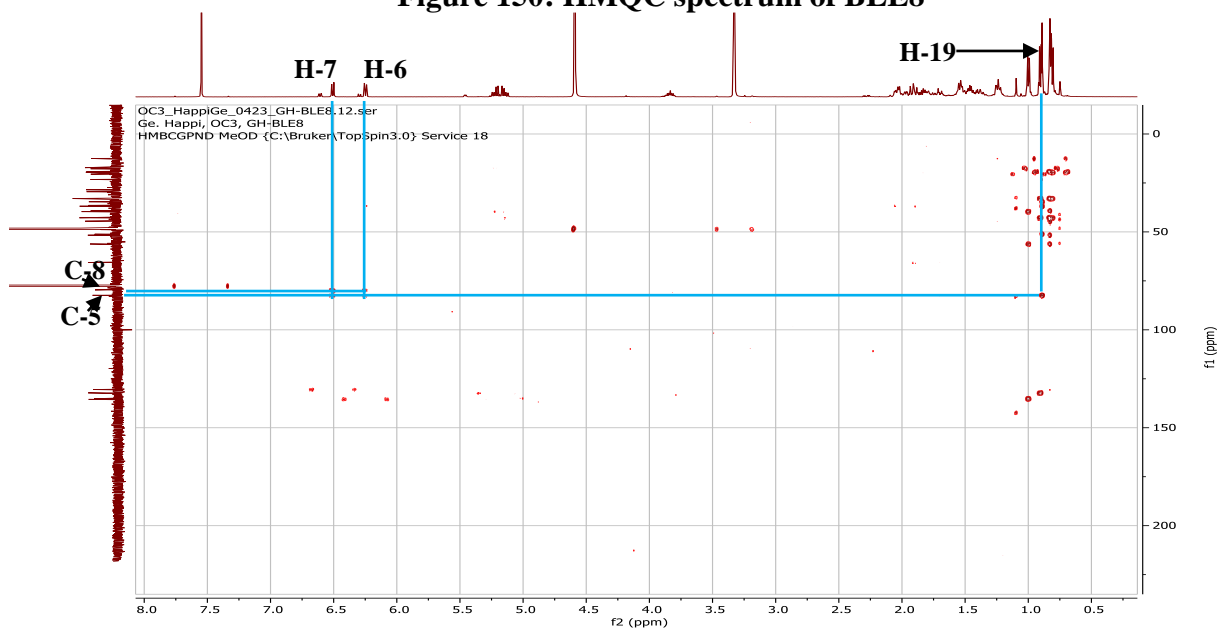


Figure 151: HMBC spectrum of BLE8

II.1.5.8.2. Structural identification of compound BLEF32

BLFE32 was obtained as a white powder in *n*-hexane/EtOAc (80:20). It is soluble in acetone and reacts positively to Lieberman Burchard test, characteristic of steroids by given a blue colour which turns quickly to dark green.

Its positive mode ESIMS spectrum (Figure 152) showed the sodium adduct peaks $[M+Na]^+$ at m/z 449.38 (calcd. for $C_{29}H_{46}O_2Na$, 449.3396) and m/z 451.38 (calcd. for $C_{29}H_{48}O_2Na$, 451.3352) which are different by the loss of two hydrogen atoms. These values, coupled with the NMR data, allowed them to be assigned the molecular formulas $C_{29}H_{46}O_2$ and $C_{29}H_{48}O_2$, implying seven and six degrees of unsaturation, respectively.

Its 1H NMR spectrum (Figure 153) showed signals of:

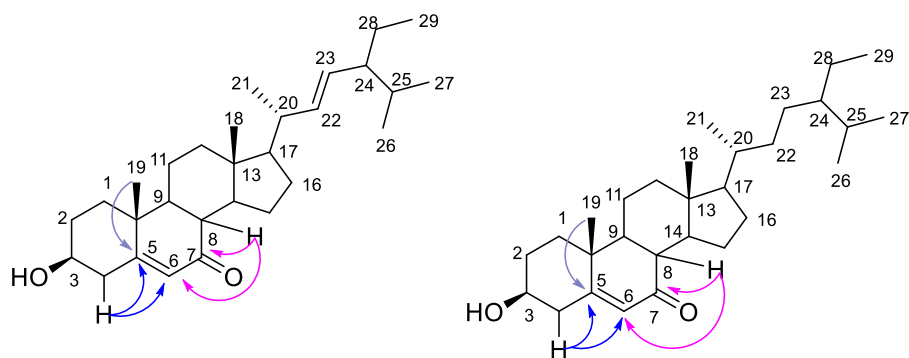
- four methyl groups singlets at δ_H 0.74 (3H, s, H-18), 0.75 (3H, s, H-18), 1.25 (1H, s, H-19) and 1.26 (1H, s, H-19);
- an oxymethine proton at δ_H 3.59 (2H, m, H-3);
- fourteen methine groups among which the proton at δ_H 2.28 (1H, ddd, 12.8, 10.7, 3.8, H-8);
- eighteen methylene groups among which the protons at δ_H 2.48 (1H, ddd, 13.9, 4.9 Hz, 2.3, H-4a) and 2.39 (1H, 13.6, 11.3, 2.0 Hz, H-4b);
- three olefinic protons at δ_H 5.25 (1H, dd, 15.2, 8.7 Hz, H-22), 5.11 (1H, dd, 15.2, 8.7 Hz, H-23), 5.61 (1H, s, H-6),

Its ^{13}C NMR spectrum (Figure 154) exhibited carbon signals, which were sorted by DEPT and HMQC techniques into:

- ten methyl groups at δ_C 11.3, 11.4 (C-29); 11.6, 11.7 (C-18); 16.7 (C-19); 18.4, 20.5 (C-27); 18.4, 20.9 (C-21), 19.1, 20.5 (C-26);
- four quaternary carbons including carbons of an enone group at δ_C 165.8 (C-5) and δ_C 200.5 (C-7);
- three olefinic carbons at δ_C 125.1 (C-6), 129.2 (C-23) and 138.4 (C-22).

The position of the enone group was confirmed by the correlations observed on the HMBC spectrum (Figure 155) between protons:

- H-4 (δ_H 2.48, 2.39) and carbons C-5 (δ_C 165.8), C-6 (δ_C 125.1);
- H-8 (δ_H 2.28) and carbons C-6 (δ_C 125.1) and C-7 (δ_C 200.5);
- H-19 (δ_H 1.25, 1.26) and carbon C-5 (δ_C 165.8).



Scheme 34: Some key HMBC correlations of BLEF32

All these data were in agreement with those described in the literature for 7-ketostigmasterol (**152**) and 7-keto- β -sitosterol (**153**), previously isolated from *Cassipourea malosana* by Nishiyama *et al.* (2019).

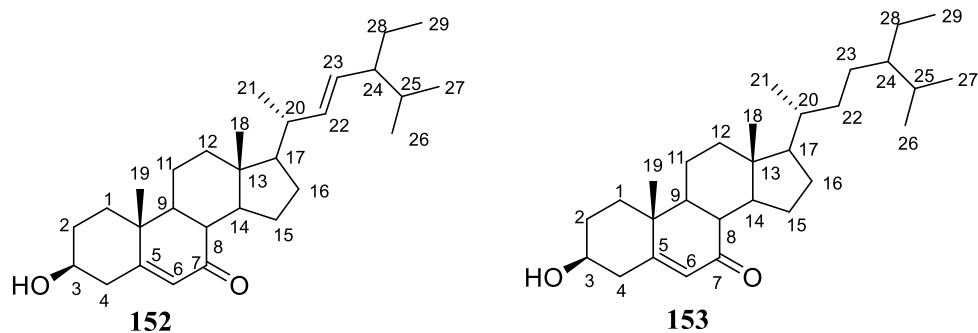


Table 46: ^{13}C (125 MHz) NMR data of BLEF32 in acetone- d_6 compared to 7-ketostigmasterol and 7-keto- β -sitosterol [CDCl_3 , NMR ^{13}C (150 MHz)]

Position	BLEF32	7-ketostigmasterol (Nishiyama <i>et al.</i> , 2019)	BLEF32	7-keto- β -sitosterol (Nishiyama <i>et al.</i> , 2019)
	$\delta^{13}\text{C}$	$\delta^{13}\text{C}$	$\delta^{13}\text{C}$	$\delta^{13}\text{C}$
1	36.4	36.2	36.4	36.4
2	31.2	31.8	31.2	31.2
3	69.8	70.4	69.8	70.5
4	41.9	41.7	41.9	41.8
5	165.8	164.9	165.8	165.0
6	125.1	126.0	125.1	126.1
7	200.5	202.7	200.4	202.3
8	45.1	45.2	45.8	45.8
9	50.3	49.9	51.2	50.0
10	38.2	38.1	38.2	38.3
11	21.0	21.2	21.0	21.2
12	38.6	38.4	38.7	38.7
13	42.9	42.8	42.9	43.1
14	50.0	49.8	50.0	49.9
15	26.1	26.3	26.2	26.3
16	29.3	29.0	28.3	28.5
17	54.7	54.6	54.7	54.7
18	11.7	12.0	11.4	11.6
19	16.7	17.2	16.7	17.3
20	150.9	40.3	36.0	36.0
21	20.9	21.3	18.4	18.4
22	138.4	137.9	33.8	34.0
23	129.2	129.3	25.9	26.1
24	45.1	45.1	26.2	45.4
25	29.1	29.1	31.8	29.1
26	20.5	20.9	19.1	19.0
27	18.4	18.4	20.5	19.8
28	25.1	25.2	22.8	23.1
29	11.4	11.7	11.3	11.0

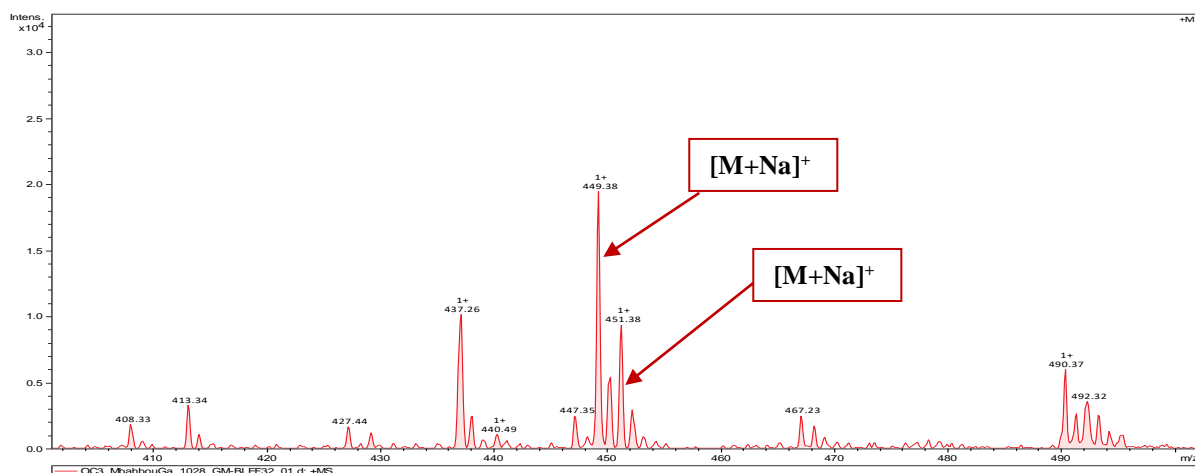


Figure 152: HRESI mass spectrum of BLEF32

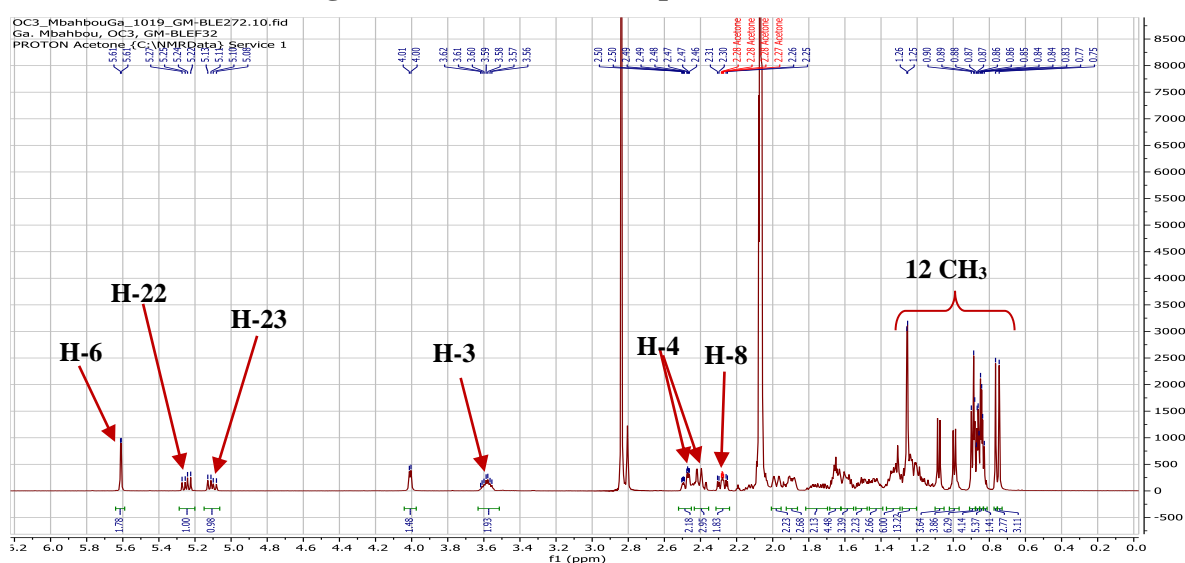


Figure 153: ¹H NMR spectrum (acetone-*d*₆, 500 MHz) of BLEF32

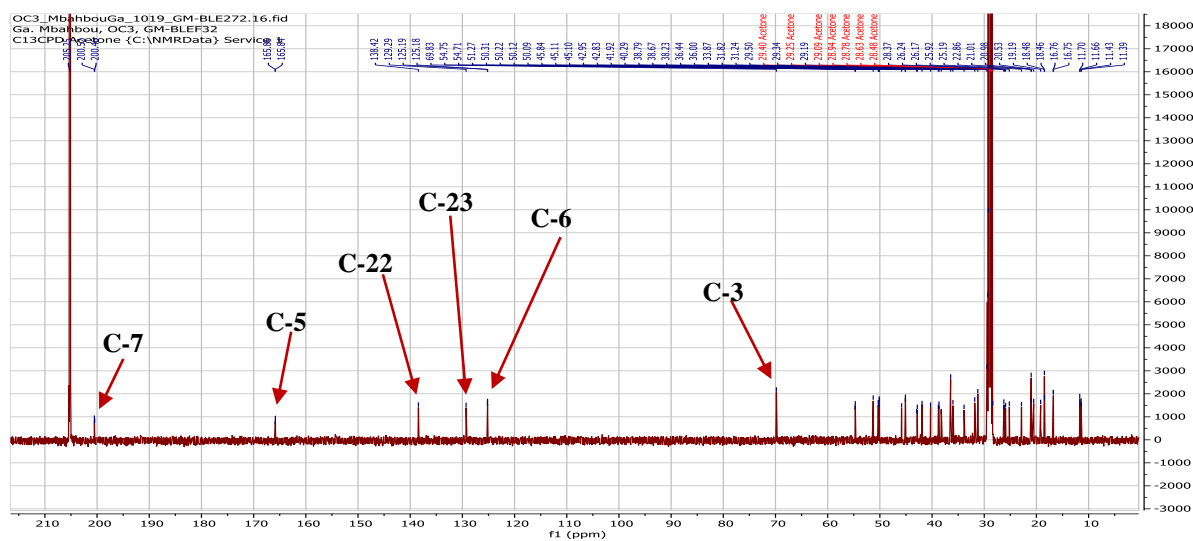


Figure 154: ¹³C NMR spectrum (acetone-*d*₆, 125 MHz) of BLEF32

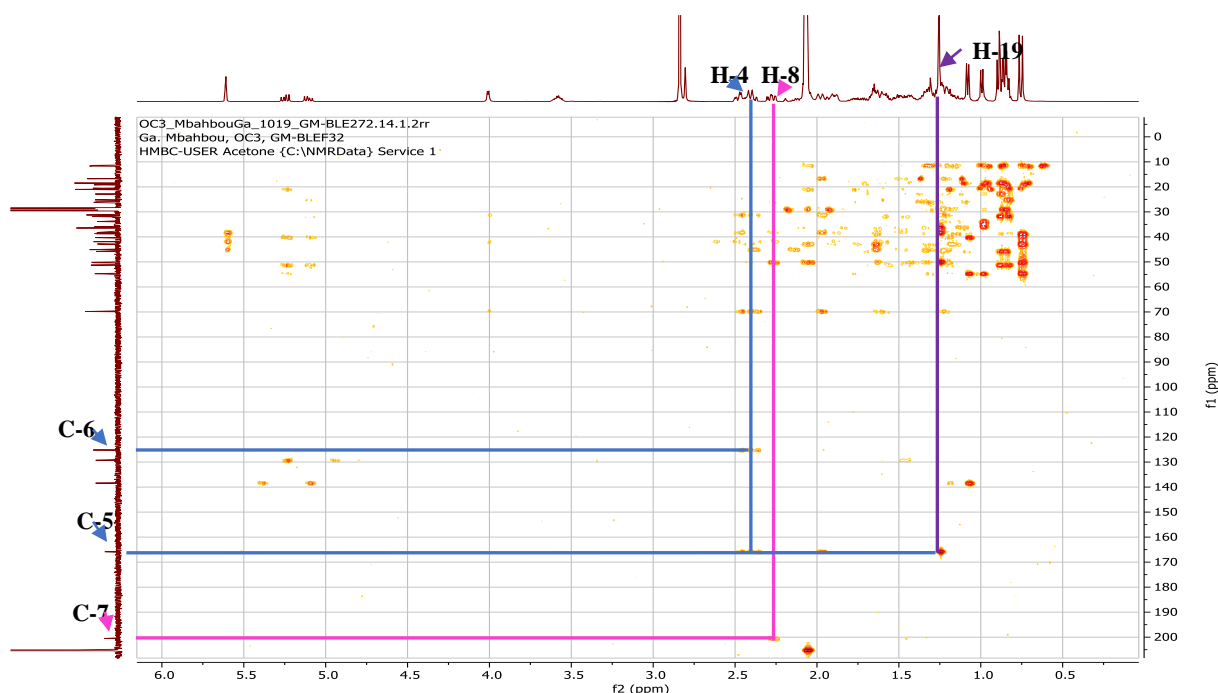


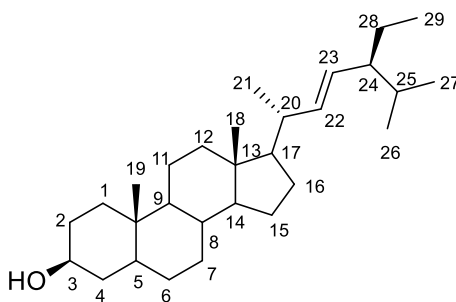
Figure 155: HMBC spectrum of BLEF32

II.1.5.8.3. Structural identification of compound RHE2

RHE2 was obtained as a white powder in *n*-hexane/ CH_2Cl_2 (40:60). It was soluble in dichloromethane and reacts positively to Liebermann Burchard test, characteristic of steroids by given a blue colour which turns quickly to dark green.

Its molecular formula $\text{C}_{29}\text{H}_{50}\text{O}$ was deduced from the HRESIMS spectrum (Figure 156) which showed the sodium adduct peak $[2\text{M}+\text{Na}]^+$ at m/z 851.7730 (calcd. for $\text{C}_{59}\text{H}_{100}\text{O}_2\text{Na}$, 851.7621), implying five degrees of unsaturation.

RHE2 was identified as stigmasta-22-en-3-ol (**154**) (Moreira *et al.*, 2017) thanks to its NMR data. In fact, its ^1H NMR spectrum (Figure 157) displayed characteristic proton resonances at δ_{H} 3.46 (1H, m, H-3), 5.08 (1H, dd, $J = 15.2, 8.6$ Hz, H-22) and 4.95 (1H, dd, $J = 15.1, 8.7$ Hz, H-23).



154

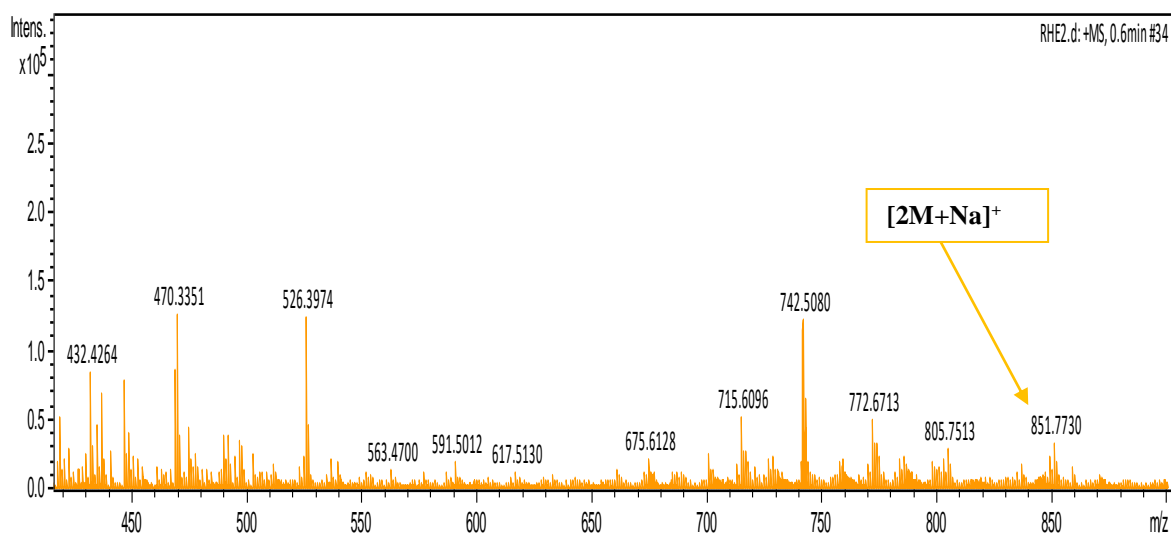


Figure 156: HRESI mass spectrum of RHE2

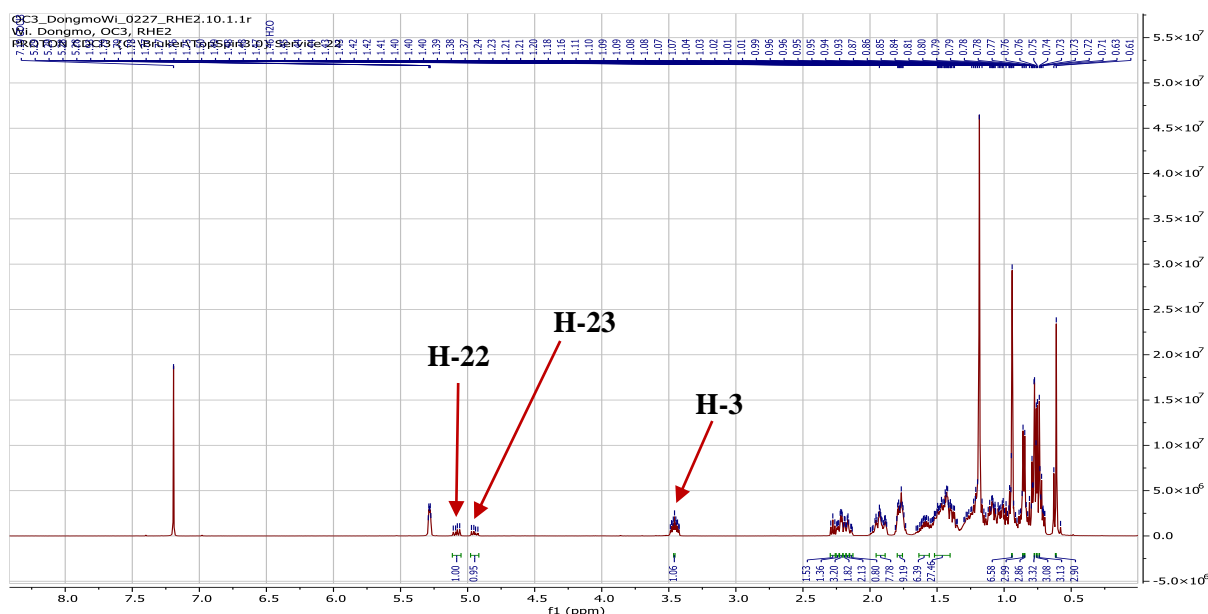


Figure 157: ^1H NMR spectrum (CDCl_3 , 500 MHz) of RHE2

II.1.5.8.4. Structural identification of compound RH4

RH4 was obtained as a white powder in *n*-hexane/EtOAc (90:10). It is soluble in dichloromethane and reacts positively to Liebermann Burchard test, characteristic of steroids by given a blue colour which turns quickly to dark green.

RH4 was identified as mixture of stigmasterol (**155**) and β -sitosterol (**56**) (Habib *et al.*, 2007) thanks to its NMR data and its TLC profile compared to a sample kept in the laboratory. Its proton spectrum (Figure 158), showed characteristic resonances of protons of steroids at δ_{H} 5.28 (2H, m, H-6), 3.46 (2H, m, H-3), 5.09 (1H, dd, $J = 15.2, 8.6$ Hz, H-22) and 4.94 (1H, dd, $J = 15.1, 8.7$ Hz, H-23).

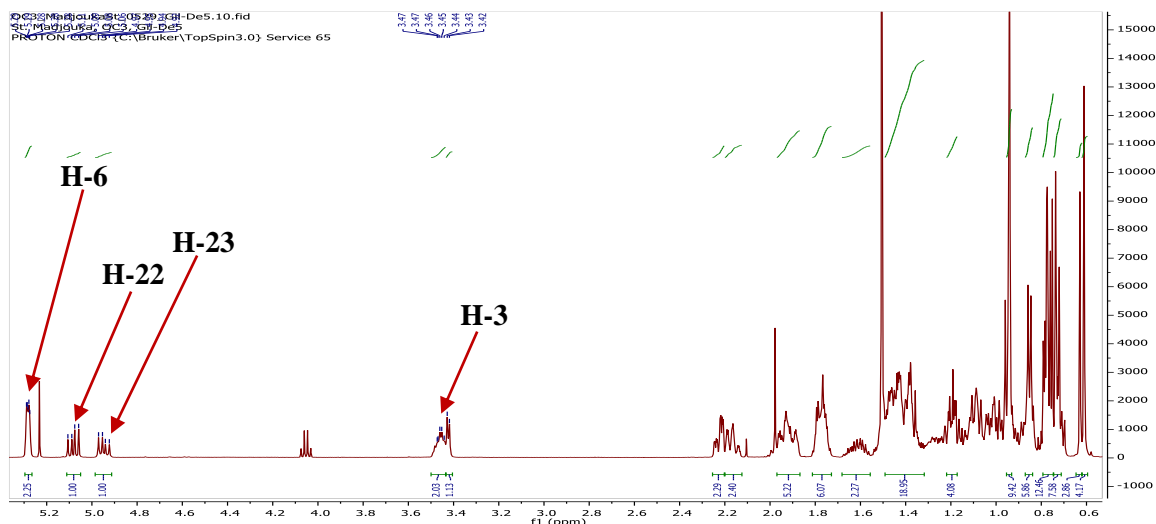
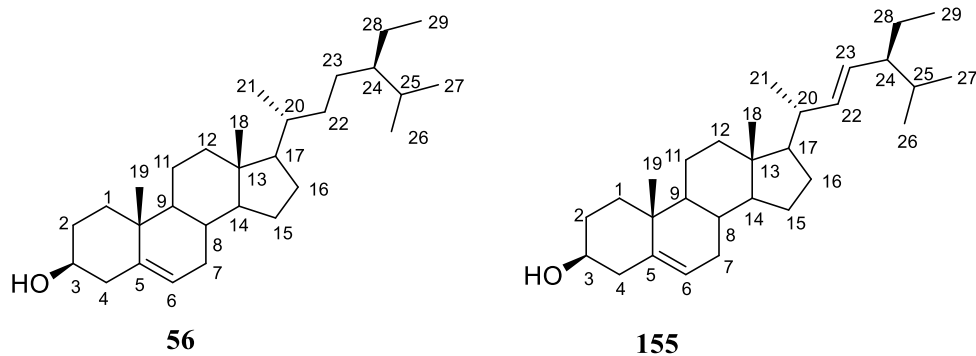


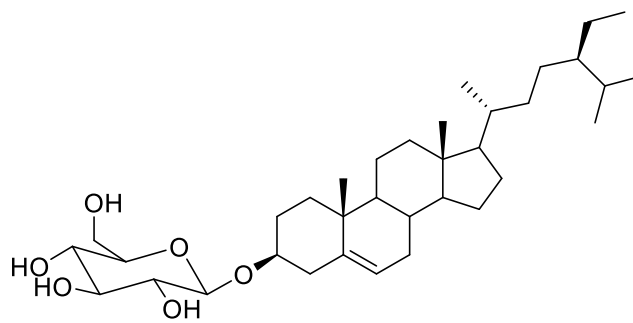
Figure 158: ¹H NMR spectrum (CDCl₃, 500 MHz) of RH4

II.1.5.8.5. Structural identification of compound BLE19

BLE19 was obtained as a white powder in EtOAc/MeOH (95:5). It is soluble in pyridine and reacts positively to Liebermann Burchard test, characteristic of steroids by given a blue colour which turns quickly to dark green.

Its molecular formula C₃₅H₆₀O₆ was deduced from the HRESIMS spectrum (Figure 159) which showed the sodium adduct peak [M+Na]⁺ at *m/z* 599.4279 (calcd. for C₃₅H₆₀O₆Na, 599.4288), implying six degrees of unsaturation.

These observations prompted us to compare ¹H (Figure 160) and ¹³C NMR (Figure 161) data of this compound with those of an authentic sample of β-sitosterol-3-*O*-β-D-glucopyranoside kept in the laboratory. Thus, BLE19 was identified as β-sitosterol-3-*O*-β-D-glucopyranoside (**58**) on TLC.



58

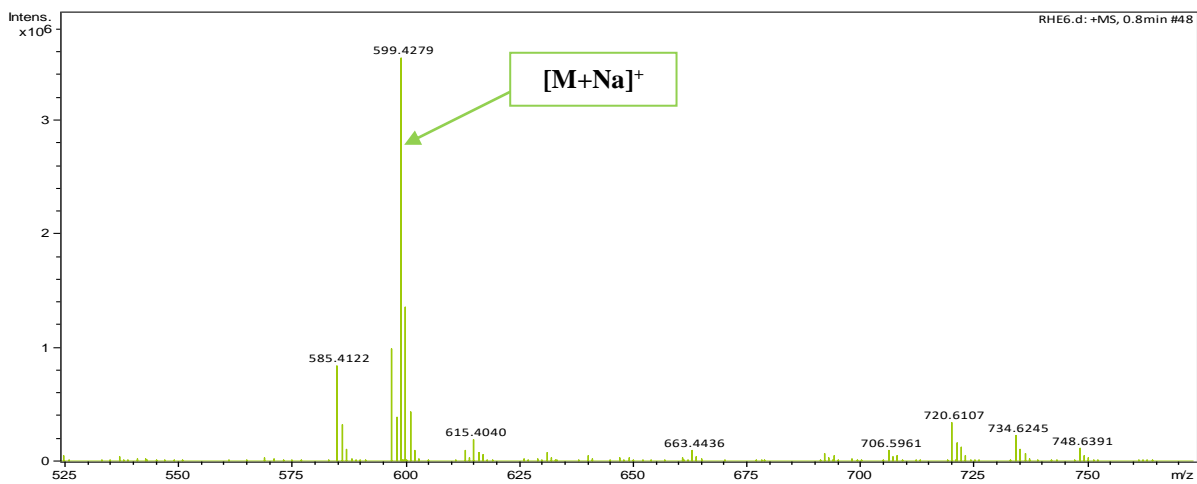


Figure 159: HRESI mass spectrum of BLE19

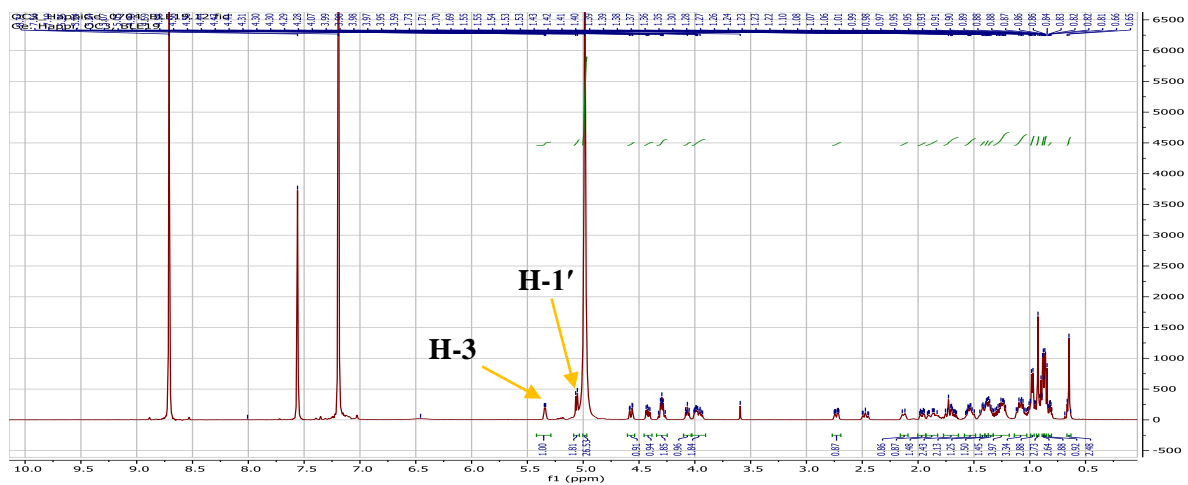


Figure 160: 1H NMR spectrum ($Pyridine-d_5$, 500 MHz) of BLE19

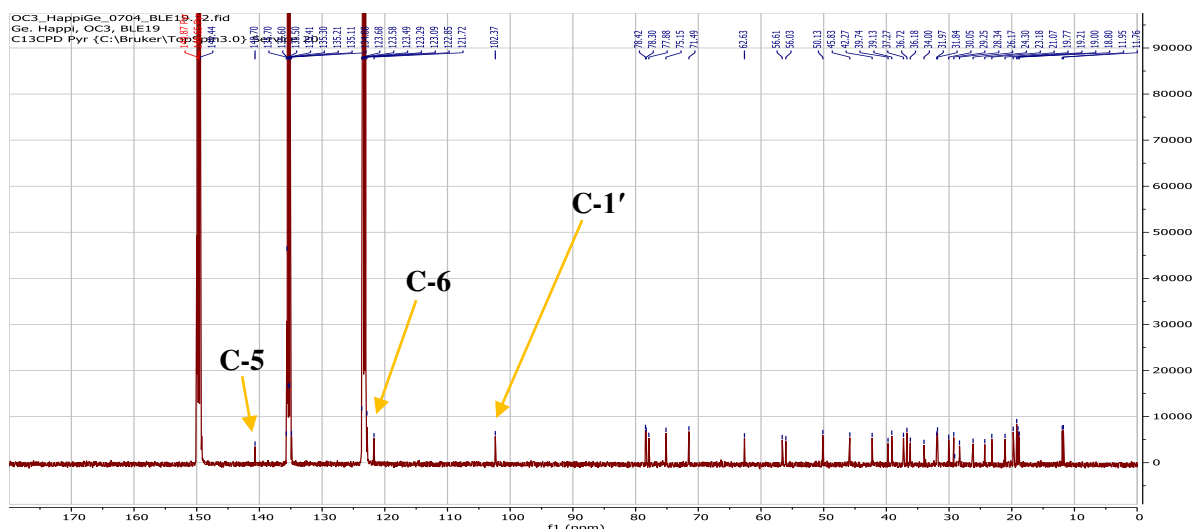


Figure 161: ^{13}C NMR spectrum (Pyridine- d_5 , 125 MHz) of BLE19

II.1.5.9. Sugar derivatives

II.1.5.9.1. Structural identification of compound BLE22

BLE22 was obtained as a white powder in EtOAc/MeOH (80:20). It is soluble in DMSO and reacts positively to Molish test, characteristic of sugars.

Its molecular formula $\text{C}_6\text{H}_{14}\text{O}_6$ was deduced from the HRESIMS spectrum (Figure 162) which showed the sodium adduct $[2\text{M}+\text{Na}]^+$ peak at m/z 387.1494 (calcd. for $\text{C}_{12}\text{H}_{28}\text{O}_{12}\text{Na}$, 387.1478), without unsaturation.

Its ^1H NMR (Figure 163) spectrum displayed signals of:

- two oxymethylene groups at δ_{H} 3.61 (2H, ddd, $J = 10.8, 5.8, 3.5$ Hz, H-1a/H-6a) and 3.39 (2H, dd, $J = 10.9, 5.8$ Hz, H-1b/H-6b);
- four oxymethine groups at δ_{H} 3.46 (2H, dtd, $J = 8.8, 5.8, 3.4$ Hz, H-2/H-5) and 3.55 (2H t, $J = 7.7$ Hz, H-3/H-4);
- six hydroxyl groups at δ_{H} 4.13 (2H, d, $J = 7.1$ Hz, OH-3/4), 4.32 (2H, t, $J = 5.7$ Hz, OH-1/6) and 4.40 (2H, d, $J = 5.5$ Hz, OH-2/5).

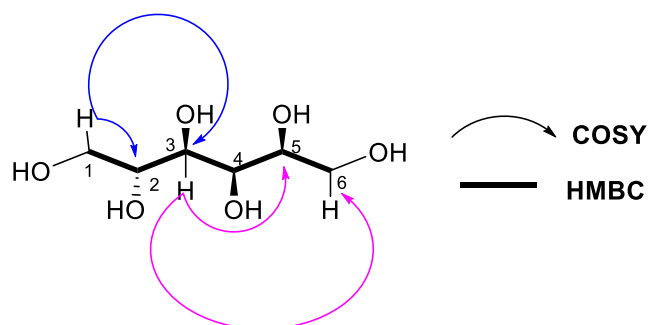
Its ^{13}C NMR spectrum (Figure 164) exhibited carbon signals, which were sorted by HMQC (Figure 165) technique into:

- two oxymethylene groups at δ_{C} 64.3 (C-1/C-6);
- four oxymethine groups at δ_{H} 71.7 (C-2/C-5) and 70.1 (C-3/C-4).

The ^1H - ^1H COSY (Figure 166) and HMBC spectra (Figure 167) of BLE22 allowed us to clearly establish its structure. In fact, its ^1H - ^1H COSY spectrum displayed correlations between protons H-1/H-6 (δ_{H} 3.61, 3.39) and H-2/H-5 (δ_{H} 3.46), which in turn was linked to protons H-3/H-4 (δ_{H} 3.55).

Its HMBC spectrum showed correlations between protons:

- H-1/H-6 (δ_H 3.61, 3.39) and carbons C-2/C-5 (71.7) and C-3/C-4 (70.1);
- H-3/H-4 (δ_H 3.55) and carbons C-1/C-6 (64.3) and C-2/C-5 (71.7).



Scheme 35: Some key COSY and HMBC correlations of BLE22

All these data, were in agreement with those of D-mannitol (**156**), previously isolated from *Gardenia aqualla* by Nyemb *et al.* (2018).

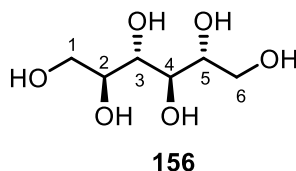


Table 47: ^1H (500 MHz) and ^{13}C (125 MHz) NMR data of BLE22 in DMSO- d_6 compared to D-mannitol (DMSO- d_6)

BLE22			D-mannitol (Nyemb <i>et al.</i> , 2018)	
Position	$\delta^{13}\text{C}$	$\delta^1\text{H}$ (m, J in Hz)	$\delta^{13}\text{C}$	$\delta^1\text{H}$ (m, J in Hz)
1, 6	64.3	3.61 (1H, ddd, 10.8, 5.8, 3.5)	63.8	3.62 (1H, ddd, 10.8, 5.7, 3.5)
		3.39 (1H, dd, 10.9, 5.8)		3.39 (1H, m)
2, 5	71.7	3.46 (2H, dtd, 8.8, 5.8, 3.4)	71.3	3.47 (2H, m)
3, 4	70.1	3.55 (2H t, 7.7)	69.7	3.56 (2H, t, 7.5) -
OH-1/6	-	4.32 (2H, t, 5.7)	-	4.33 (2H, t, 5.7)
OH-2/5	-	4.40 (2H, d, 5.5)	-	4.41 (2H, d, 5.5)
OH-3/4	-	4.13 (2H, d, 7.1)	-	4.13 (2H, d, 7.1)

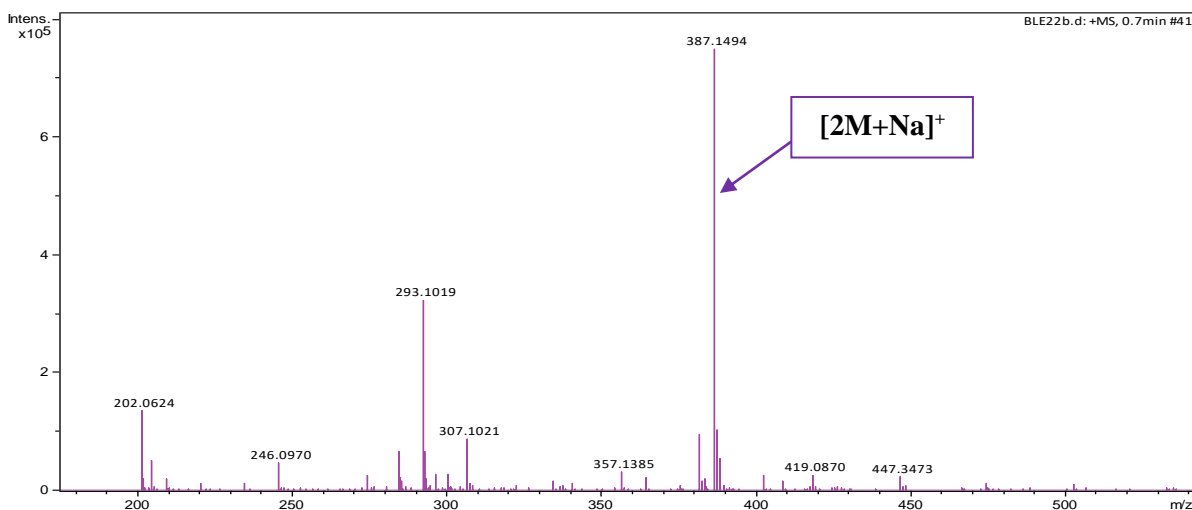


Figure 162: HRESI mass spectrum of BLE22

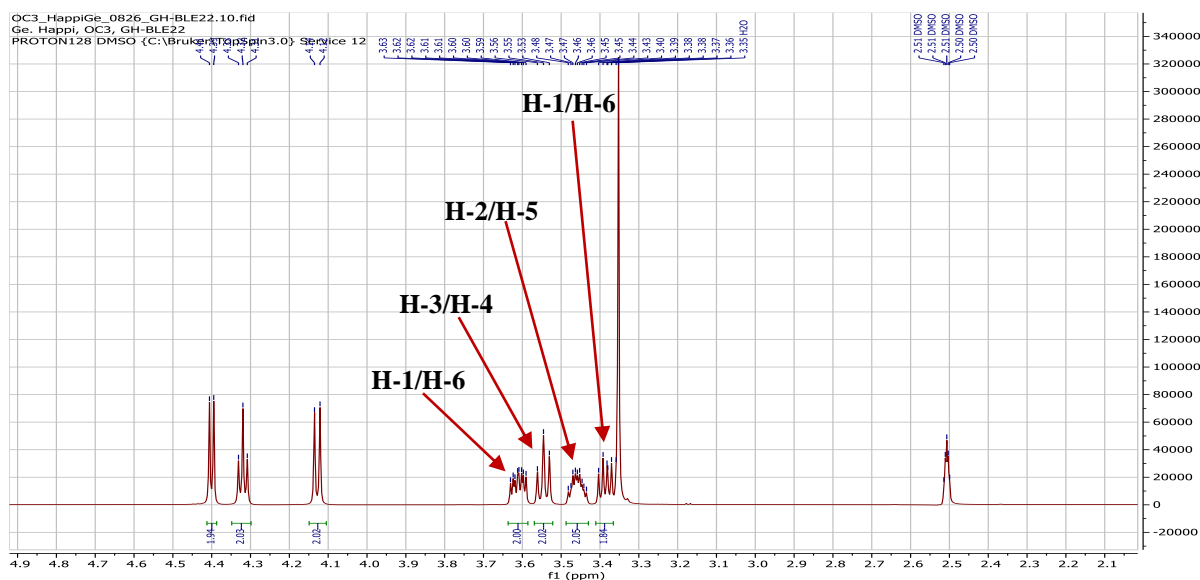


Figure 163: ¹H NMR spectrum (DMSO-*d*₆, 500 MHz) of BLE22

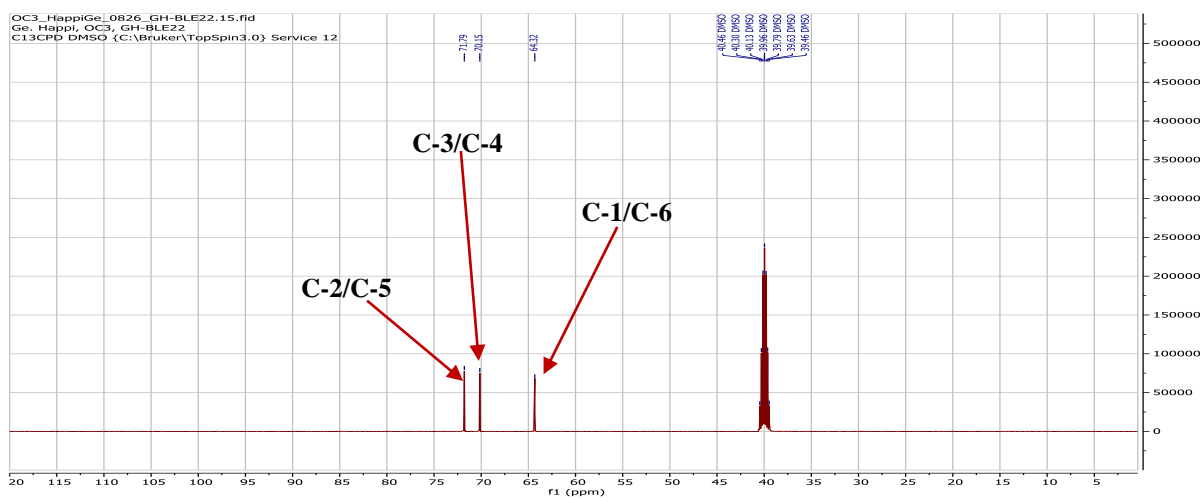


Figure 164: ¹³C NMR spectrum (DMSO-*d*₆, 125 MHz) of BLE22

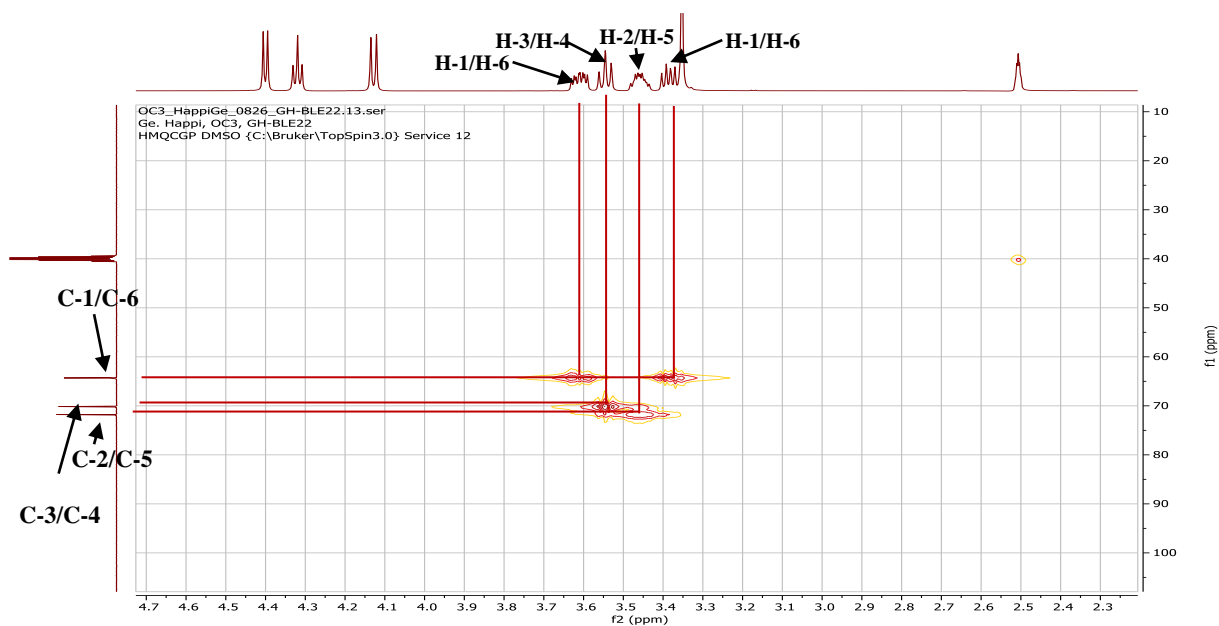


Figure 165: HMQC spectrum of BLE22

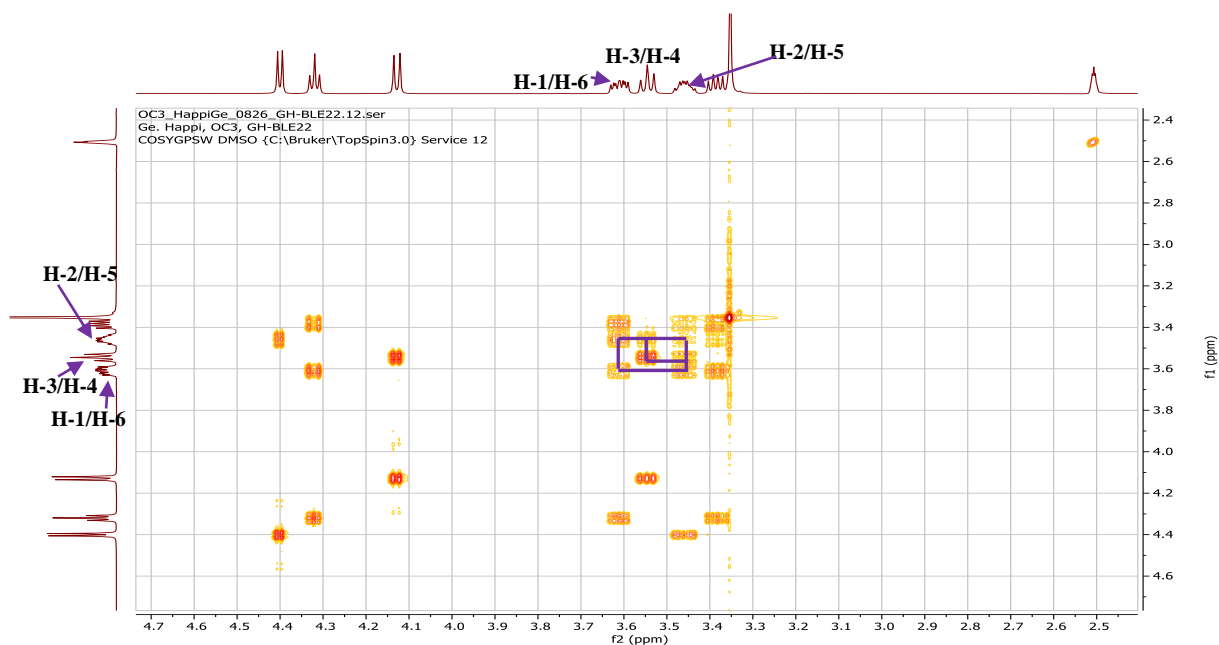


Figure 166: COSY spectrum of BLE22

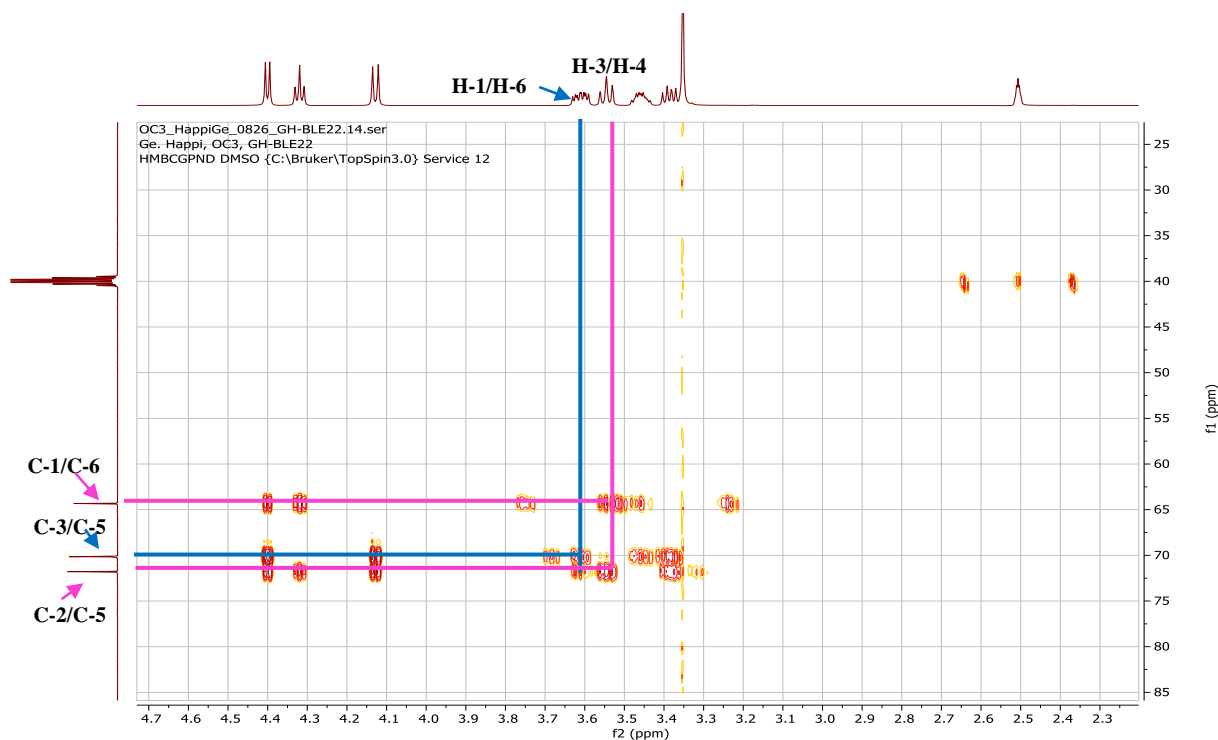


Figure 167: HMBC spectrum of BLE22

II.1.5.9.2. Structural identification of compound BLE21

BLE21 was obtained as a white powder in EtOAc/MeOH (90:10). It is soluble in methanol and reacts positively to Molish test, characteristic of sugars.

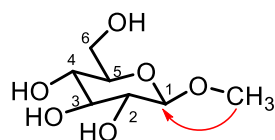
Its ^1H NMR (Figure 168) spectrum displayed signals of:

- a sugar moiety including four oxymethine groups among which an anomeric proton at δ_{H} 4.19 (1H, d, $J = 7.8$ Hz, H-1), the others at δ_{H} 3.18 (1H, dd, $J = 7.8, 9.1$ Hz, H-2), 3.37 (1H, t, $J = 9.0$ Hz, H-3), 3.29 (2H, m, H-4/H-5) and an oxymethylene group at δ_{H} 3.89 (1H, dd, $J = 11.9, 1.8$ Hz, H-6) and 3.69 (1H, dd, $J = 11.9, 5.3$ Hz, H-6). The β configuration of this sugar is due to the high value of the coupling constant of the anomeric proton ($J = 7.8$ Hz) (Agrawal, 1992).
- three protons at δ_{H} 3.55 (3H, s), attributable to a methoxy group.

Its ^{13}C NMR spectrum (Figure 169) exhibited carbon signals of:

- a sugar moiety at δ_{C} 61.3 (C-6), 70.2 (C-4), 73.6 (C-2), 76.5 (C-3), 76.6 (C-5) and 104.0 (C-1). A comparative analysis of chemical shifts and coupling constants with data from the literature (Agrawal, 1992) contributed in identifying this sugar as β -D-glucopyranoside.
- one methoxy group at δ_{C} 55.9 (OCH_3);

Its HMBC spectrum (Figure 170) showed correlation between the methoxy protons OCH_3 (δ_{H} 3.55) and carbon C-1 (δ_{C} 104.0).



Scheme 36: Key HMBC correlation of BLE21

All these data were in agreement with those described in the literature for methyl β -D-glucopyranoside (**157**) (Agrawal, 1992).

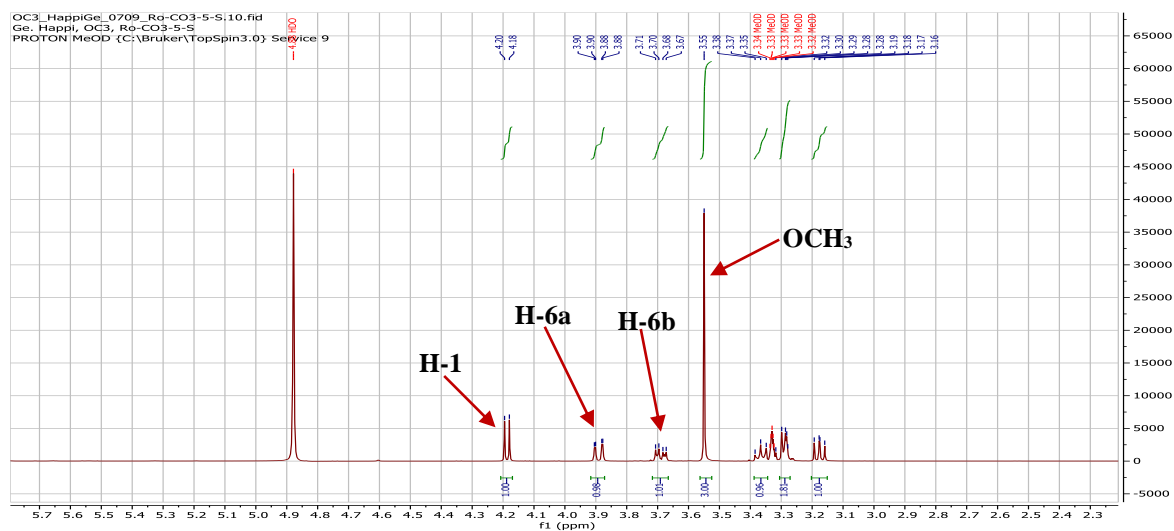
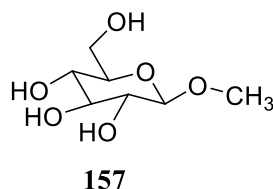


Figure 168: ^1H NMR spectrum (methanol- d_4 , 500 MHz) of BLE21

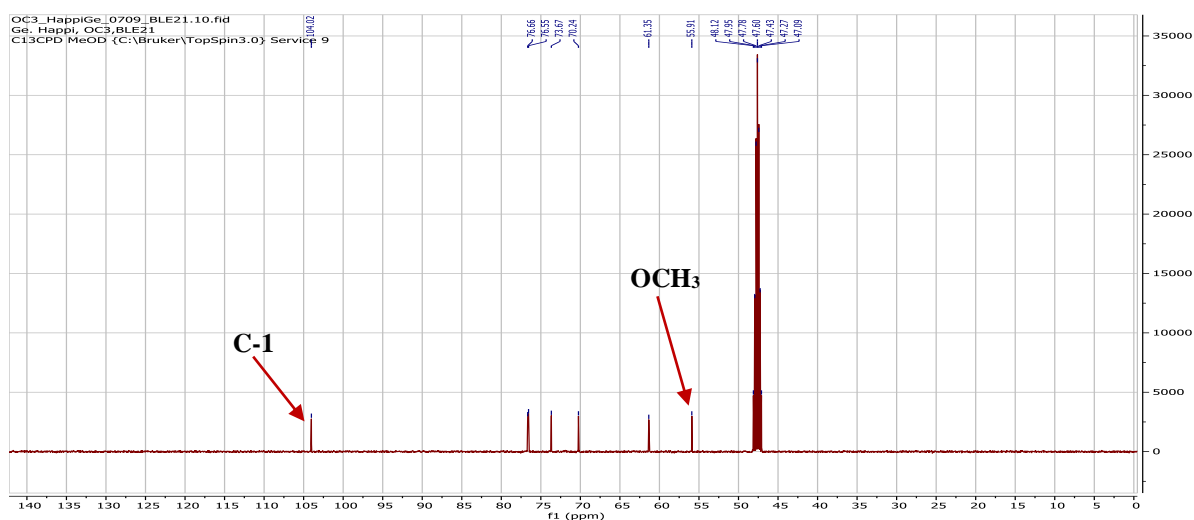


Figure 169: ^{13}C NMR spectrum (methanol- d_4 , 125 MHz) of BLE21

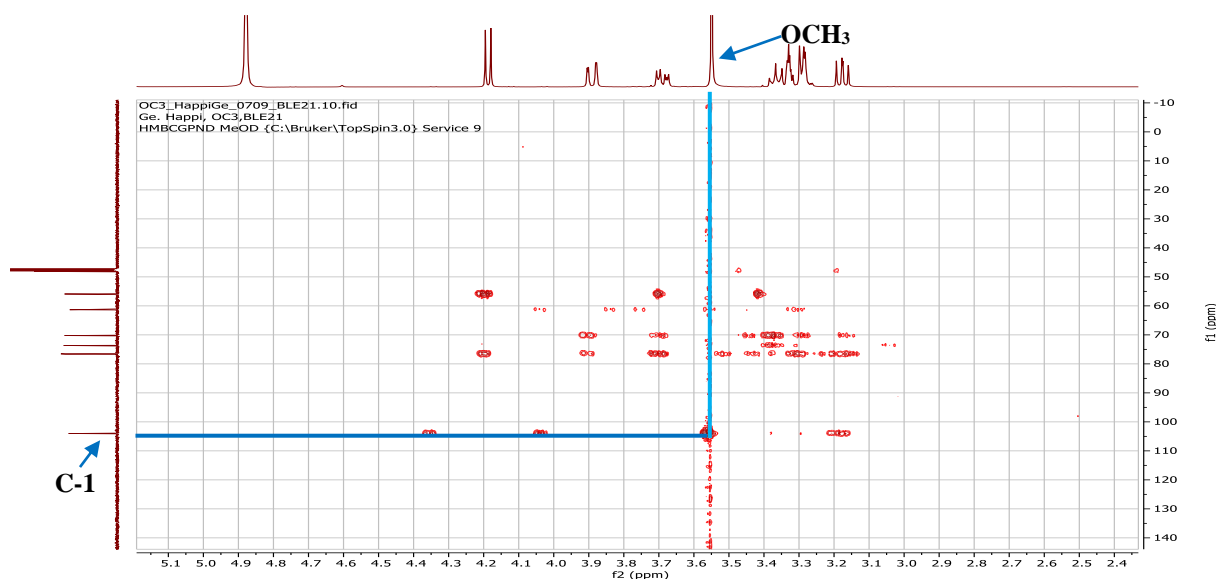


Figure 170: HMBC spectrum of BLE21

II.1.5.9.3. Structural identification of compound NLB4

NLB4 was obtained as a chesnut paste in EtOAc/MeOH (70:30). It is soluble in methanol and reacts positively to Molish test, characteristic of sugars.

Its molecular formula $C_6H_{12}O_6$ was deduced from the HRESIMS spectrum (Figure 171) which showed the sodium adduct peak $[M+Na]^+$ at m/z 203.0572 (calcd. for $C_6H_{12}O_6Na$, 203.0532), implying one degree of unsaturation.

The 1H (Figure 172) and ^{13}C (Figure 173) NMR spectra of NLB4 were very similar to those of BLE21 (methyl β -D-glucopyranoside). However, we noted the absence of the methoxyl signal (δ_H 3.55) on the 1H NMR spectrum of NLB4 and the presence of additional peaks including a second anomeric proton at δ_H 5.13 (1H, d, $J = 3.6$ Hz, H-1b). The α -configuration was assigned to the second sugar due to the low value of the coupling constant of the anomeric proton ($J = 3.6$ Hz) (Agrawal, 1992). On the ^{13}C NMR spectrum of NLB4, we observed the presence of additional carbon signals including the carbon at δ_C 92.7 (C-1b) and the absence of the methoxyl group signal at δ_C 55.9 ppm.

A comparative analysis of chemical shifts and coupling constants with data from the literature (Agrawal, 1992), supported the identification of the second sugar as α -D-glucopyranoside.

Based on the above data, NLB4 was concluded to be a mixture of α -D-glucopyranoside (**158**) and β -D-glucopyranoside (**159**) (Agrawal, 1992).

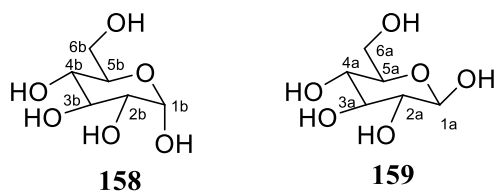


Table 48: ^{13}C (125 MHz) NMR data of BLE21 and NLB4 in methanol- d_4 compared to methyl β -D-glucopyranoside, β -D-glucopyranoside and α -D-glucopyranoside

	BLE21	Methyl β -D-glucopyranoside (Agrawal, 1992)	NLB4	α -D-glucopyranoside (Agrawal, 1992)	NLB4	β -D-glucopyranoside (Agrawal, 1992)
Position	$\delta^{13}\text{C}$	$\delta^{13}\text{C}$	$\delta^{13}\text{C}$	$\delta^{13}\text{C}$	$\delta^{13}\text{C}$	$\delta^{13}\text{C}$
1	104.0	104.0	92.7	93.0	96.7	96.8
2	73.6	74.1	71.5	72.4	74.8	75.2
3	76.5	76.8	73.4	73.7	76.6	76.7
4	70.2	70.6	70.3	70.7	70.4	70.7
5	76.6	76.8	72.4	72.3	76.7	76.7
6	61.3	61.8	61.3	61.8	61.4	61.8
OCH ₃	55.9	55.0	-	-	-	-

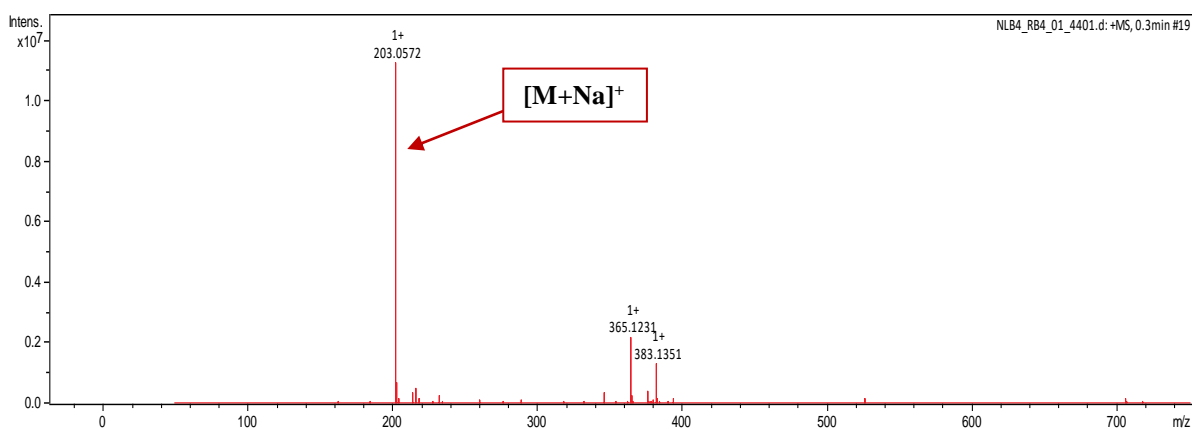


Figure 171: HRESI mass spectrum of NLB4

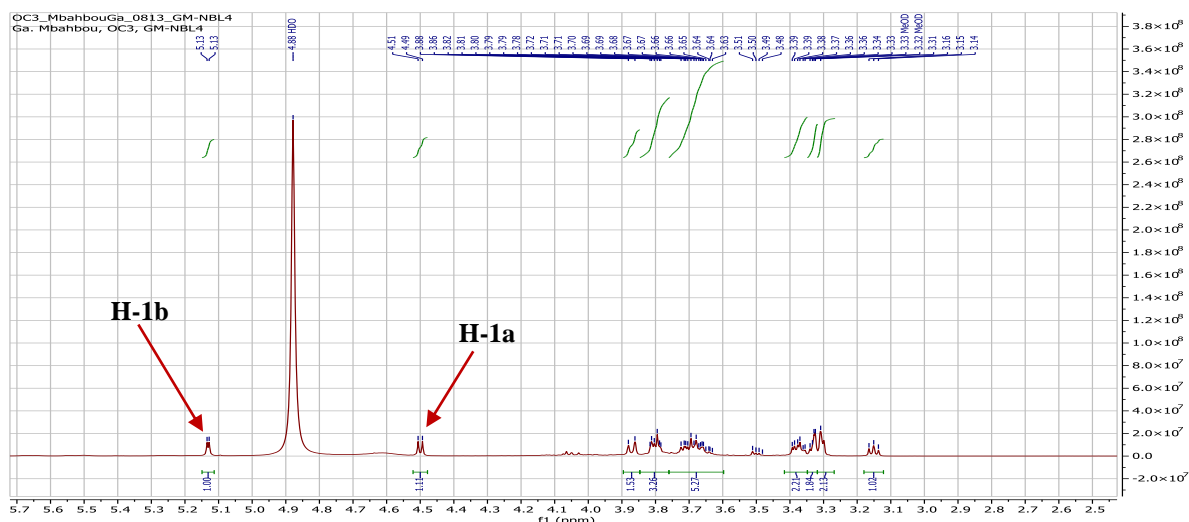


Figure 172: ^1H NMR spectrum (methanol- d_4 , 500 MHz) of NLB4

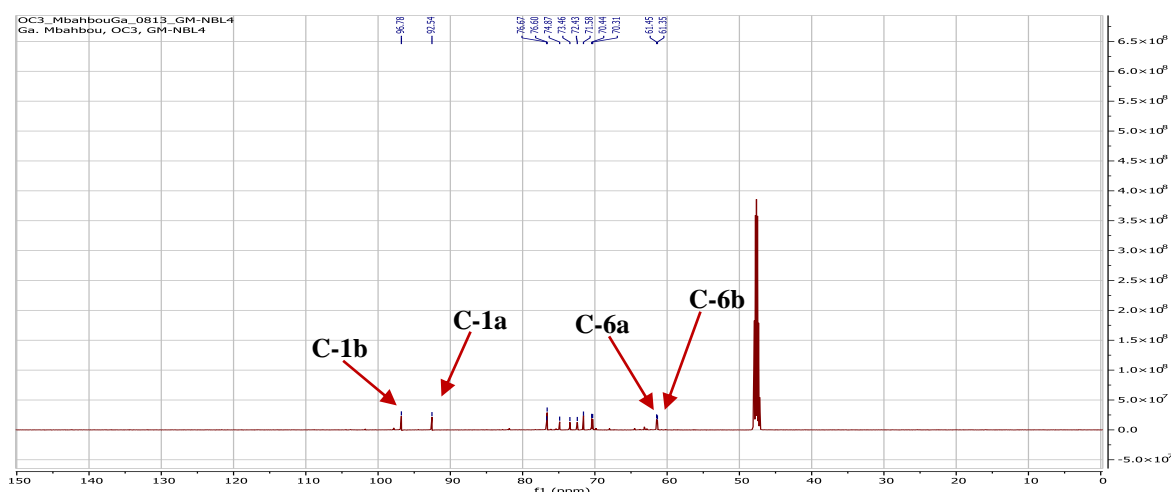


Figure 173: ^{13}C NMR spectrum (Methanol- d_4 , 125 MHz) of NLB4

II.1.5.10. Fatty derivatives

II.1.5.10.1. Structural identification of compound WN3

WN3 was obtained as a white powder in *n*-hexane/acetone (90:10) and it is soluble in dichloromethane.

Its molecular formula $\text{C}_{19}\text{H}_{38}\text{O}_4$ was deduced from the HRESIMS spectrum (Figure 174) which showed the sodium adduct peak $[\text{M}+\text{Na}]^+$ at m/z 353.2689 (calcd. for $\text{C}_{19}\text{H}_{38}\text{O}_4\text{Na}$, 353.2668), implying one degree of unsaturation.

Its ^1H NMR spectrum (Figure 175) showed signals of:

- an oxymethine proton at δ_{H} 3.95 (1H, tt, $J = 6.0, 4.3$ Hz, H-2);
- two oxymethylene groups at δ_{H} 4.23 (1H, dd, $J = 11.7, 4.6$ Hz, H-1a), 4.17 (1H, dd, $J = 11.7, 6.2$ Hz, H-1b) and δ_{H} 3.72 (1H, dd, $J = 11.5, 4.0$ Hz, H-3a), 3.62 (1H, dd, $J = 11.5, 5.8$ Hz, H-3b);

- a methylene at the α position of a carbonyl at δ_{H} 2.37 (2H, t, $J = 7.6$ Hz, H-2');
- methylene groups of an alkyl long chain at δ_{H} 1.56 (1H, m, H-3') and 1.28 (br s, 12CH₂);
- a terminal methyl group at δ_{H} 0.90 (3H, t, $J = 7.0$ Hz, H-16).

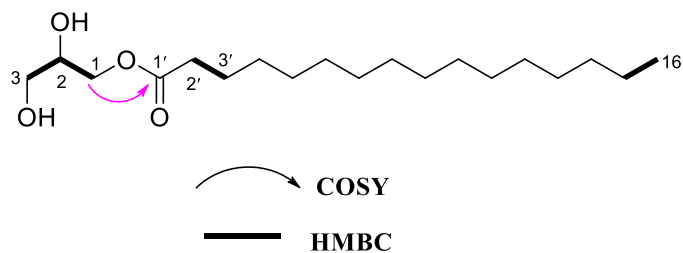
Its ¹³C NMR spectrum (Figure 176) displayed carbon resonances which were sorted by HMQC (Figure 177) technique into:

- an ester carbonyl at δ_{C} 174.4 (C-1');
- one oxymethine group at δ_{C} 70.3 (C-2), two oxymethylene groups at δ_{C} 65.2 (C-1) and 63.3 (C-3) characteristic of a glyceride derivative (Hernandez-Galicia *et al*, 2007);
- methylene groups at δ_{C} 34.1 (C-2'), 24.9 (C-3') and δ_{C} 31.9-22.7 (15CH₂);
- a terminal methyl at δ_{C} 14.1 (C-16).

The location of the alkyl long chain was confirmed by the correlation observed on the HMBC spectrum (Figure 179) between protons H-1 (δ_{H} 4.23, 4.17) and carbon C-1' (δ_{C} 174).

The ¹H-¹H COSY spectrum (Figure 180) of WN3 served to further confirm this structure by the correlations between protons:

- H-1 (δ_{H} 4.23, 4.17) and H-2 (δ_{H} 3.95), which in turn was linked to protons H-3 (δ_{H} 3.72, 3.62);
- H-2' and the alkyl long chain protons H-3 to H-15, which in turn were linked to the terminal methyl H-16 (δ_{H} 0.90).



Scheme 37: Some key COSY and HMBC correlations of WN3

All these data were in agreement with those described in the literature for glycerol palmitate (**160**), previously isolated from *Ibervillea sonora* by Hernandez-Galicia *et al.* (2007).

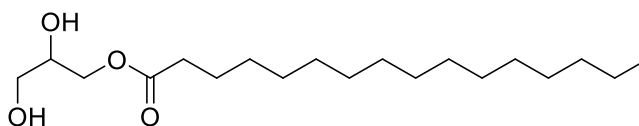


Table 49: ^1H (500 MHz) and ^{13}C (125 MHz) NMR data of WN3 in CDCl_3 compared to glycerol palmitate

WN3			Glycerol palmitate (Hernandez-Galicia <i>et al.</i> , 2007)	
Position	$\delta^{13}\text{C}$	$\delta^1\text{H}$ (m, J in Hz)	$\delta^{13}\text{C}$	$\delta^1\text{H}$ (m, J in Hz)
1	65.2	4.17 (1H, dd, 11.7, 6.2); 4.23 (1H, dd, 11.7, 4.6)	65.1	4.14 (1H, dd, 11.5, 6.0); 4.19 (1H, dd, 11.4, 4.9)
2	70.3	3.93 (1H, m)	70.2	3.93 (1H, m)
3	63.3	3.62 (1H, dd, 11.5, 5.8); 3.72 (1H, dd, 11.5, 4.0)	63.3	3.59 (1H, dd, 11.5, 6.0); 3.70 (1H, dd, 11.5, 4.0)
1'	174.4	-	174.3	-
2'	34.1	2.37 (2H, t, 7.6)	34.1	2.33 (2H, t, 7.5)
12CH ₂	31.9-22.7	1.28 (br s)	31.8-22.6	1.25 (br s)
16'	14.1	0.90 (3H, t, 7.0)	14.1	0.88 (3H, t, 7.2)

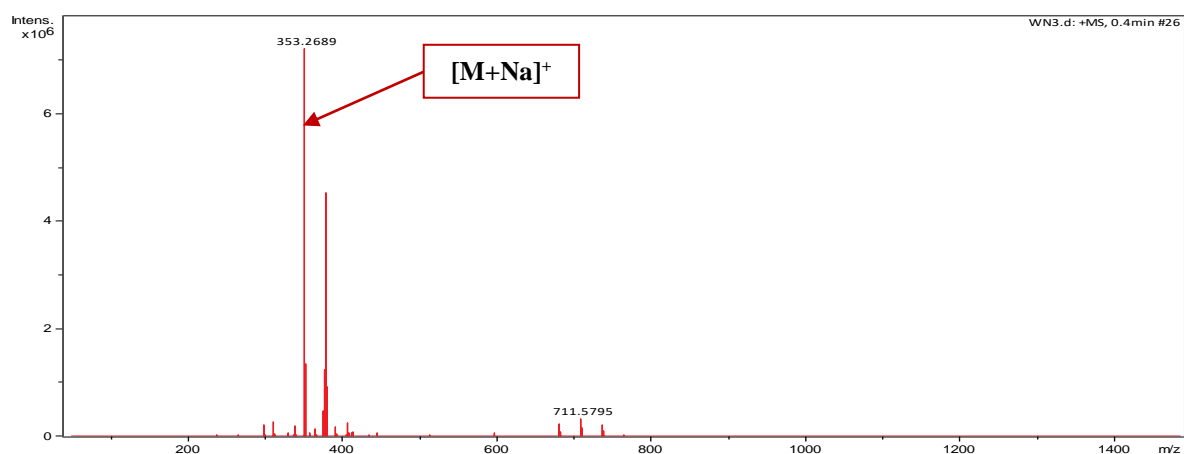


Figure 174: HRESI mass spectrum of WN3

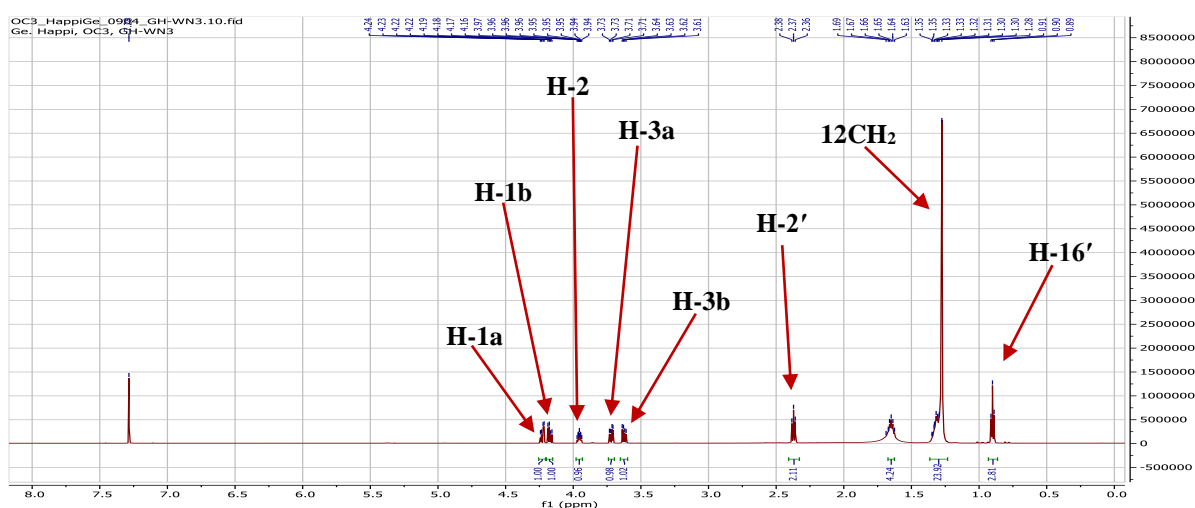


Figure 175: ^1H NMR spectrum (CDCl_3 , 500 MHz) of WN3

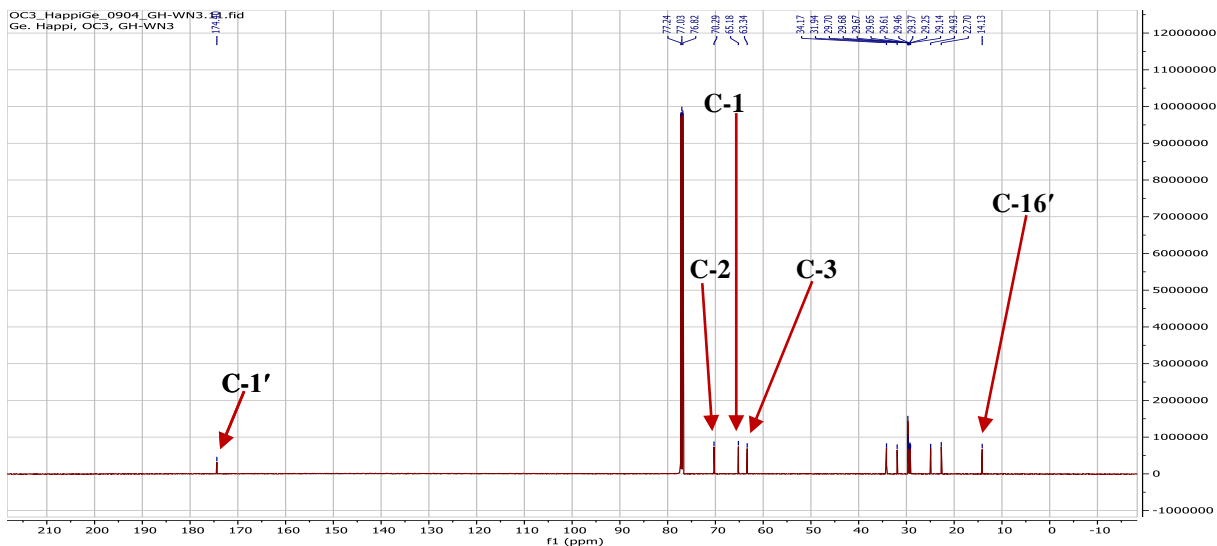


Figure 176: ^{13}C NMR spectrum (CDCl_3 , 125 MHz) of WN3

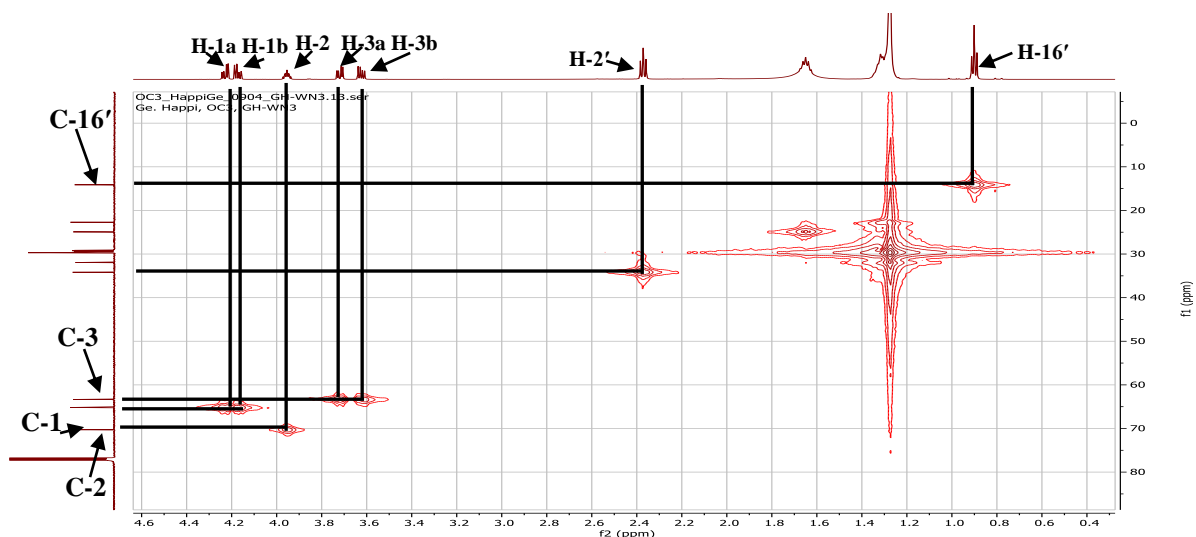


Figure 177: HMQC spectrum of WN3

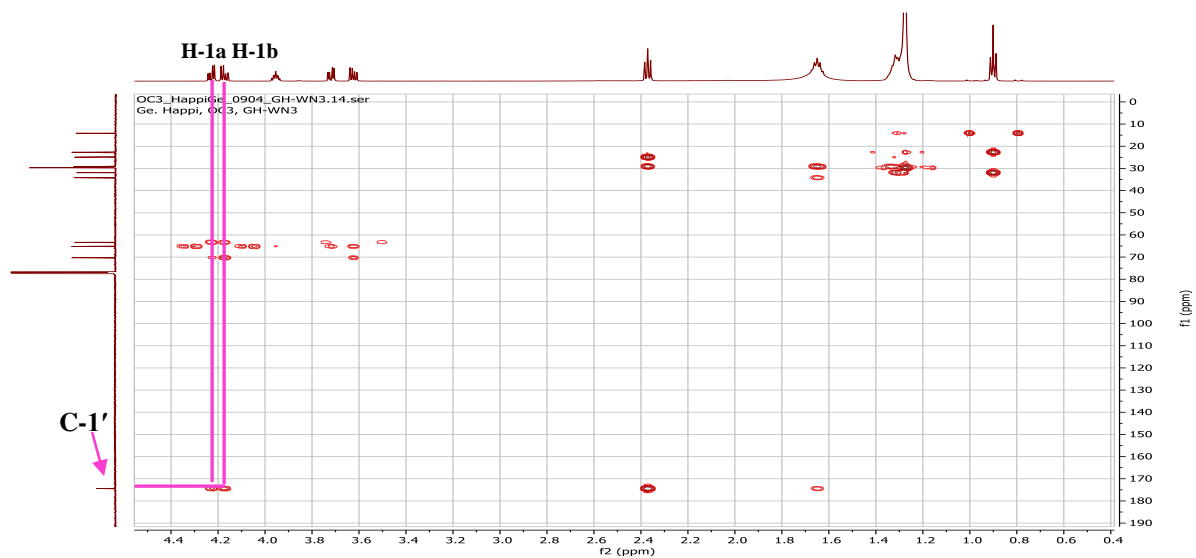


Figure 178: HMBC spectrum of WN3

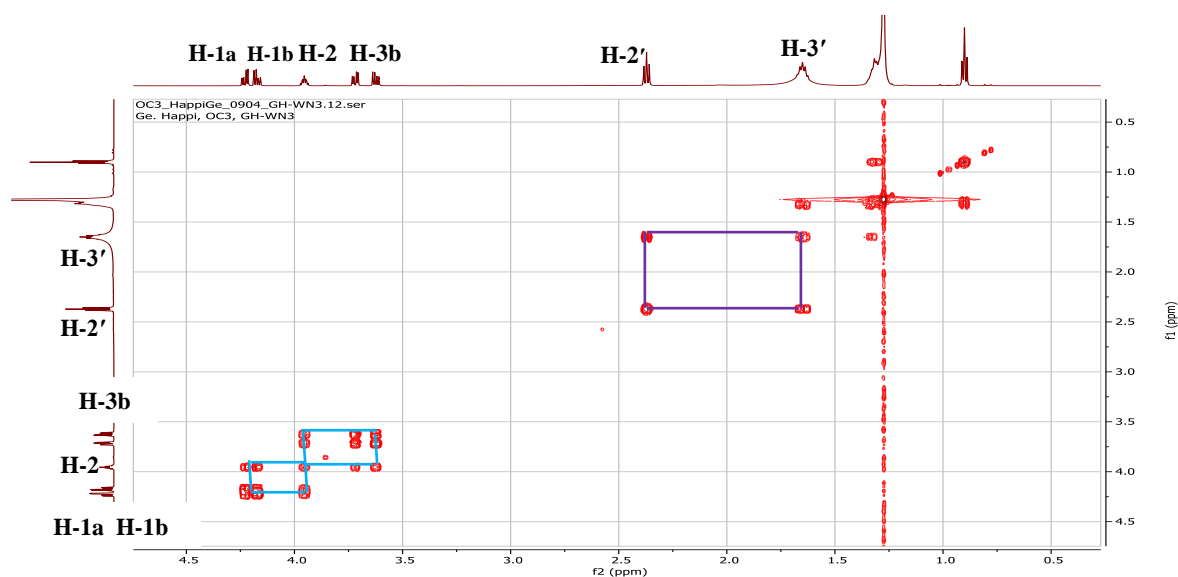


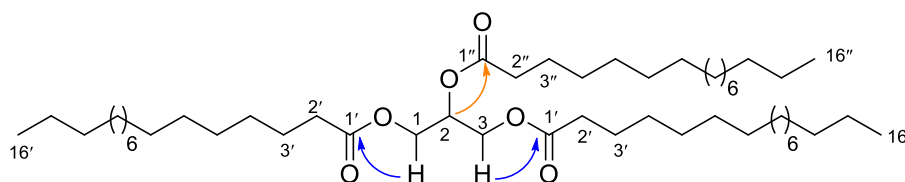
Figure 179: COSY spectrum of WN3

II.1.5.10.2. Structural identification of compound BLE34

BLE34 was obtained as a white powder in *n*-hexane and it is soluble in dichloromethane.

The ^1H (Figure 180) and ^{13}C NMR (Figure 181) spectra of BLE34 were very similar to those of WN3 (glycerol palmitate). However, we noted the presence of two additional palmitic acid moieties by the correlations observed on the HMBC spectrum (Figure 182) between protons of the glycerol moiety:

- H-1/H3 (δ_{H} 4.02, 4.22) and carbons C-1' (173.3);
- H-2 (δ_{H} 5.20) and carbon C-1'' (δ_{C} 172.9).



Scheme 38: Key HMBC correlations of BLE34

These data matched with those described in the literature for glycerol tripalmitate (**161**), previously synthesized (Lutton and Fehl, 1970). This stands as the first ever isolation of this compound from natural sources.

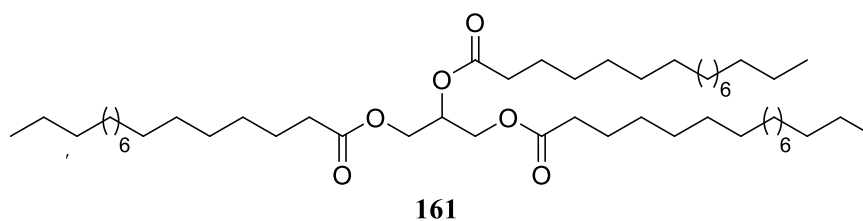


Table 50: ^1H (500 MHz) and ^{13}C (125 MHz) NMR data of BLE34 in CDCl_3

Glycerol tripalmitate		
Position	$\delta^{13}\text{C}$	$\delta^1\text{H}$ (m, J in Hz)
1, 3	62.1	4.08 (2H, dd, 11.9, 6.0); 4.22 (2H, dd, 11.9, 4.3)
2	68.8	5.20 (1H, tt, 5.9, 4.3)
1'	173.3	-
2'	34.0	2.24 (6H, t, 7.6)
3'	24.8	1.54 (6H, m)
1''	172.9	-
2''	34.2	2.24 (6H, t, 7.6)
3''	24.9	1.54 (6H, m)
36 CH_2	31.9-22.7	1.19 (br s, 36 CH_2)
Terminal CH_3	14.1	0.81 (9H, t, 7.0)

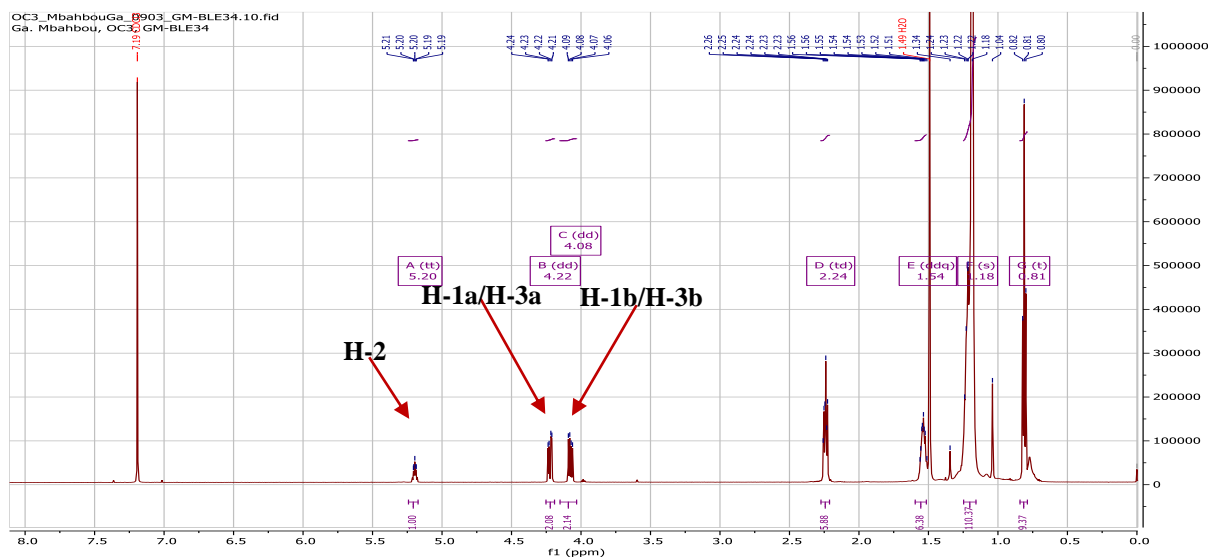


Figure 180: ^1H NMR spectrum (ppm) (CDCl_3 , 500 MHz) of BLE34

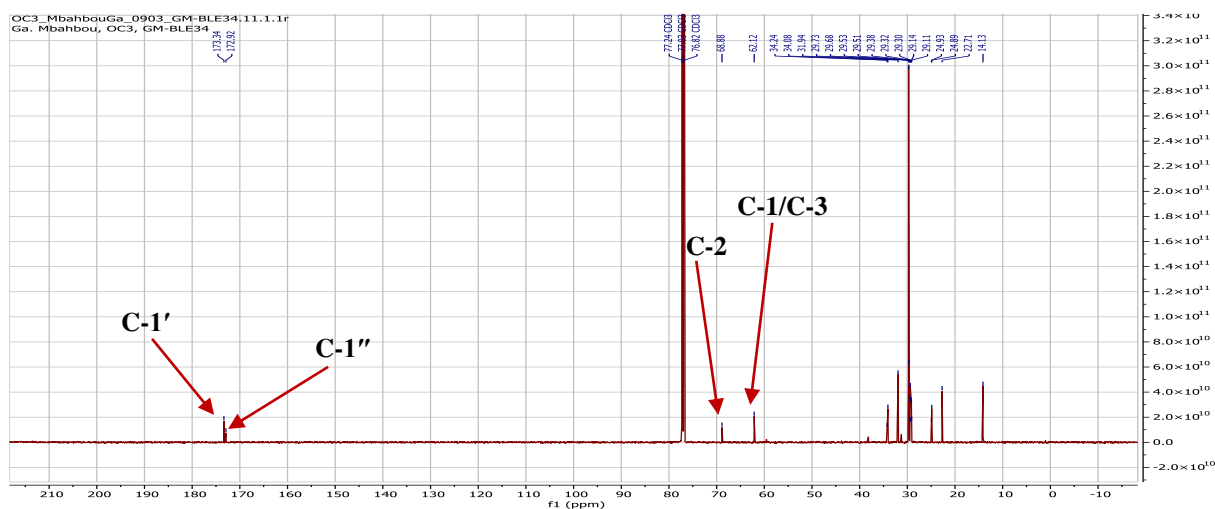


Figure 181: ^{13}C NMR spectrum (ppm) (CDCl_3 , 125 MHz) of BLE34

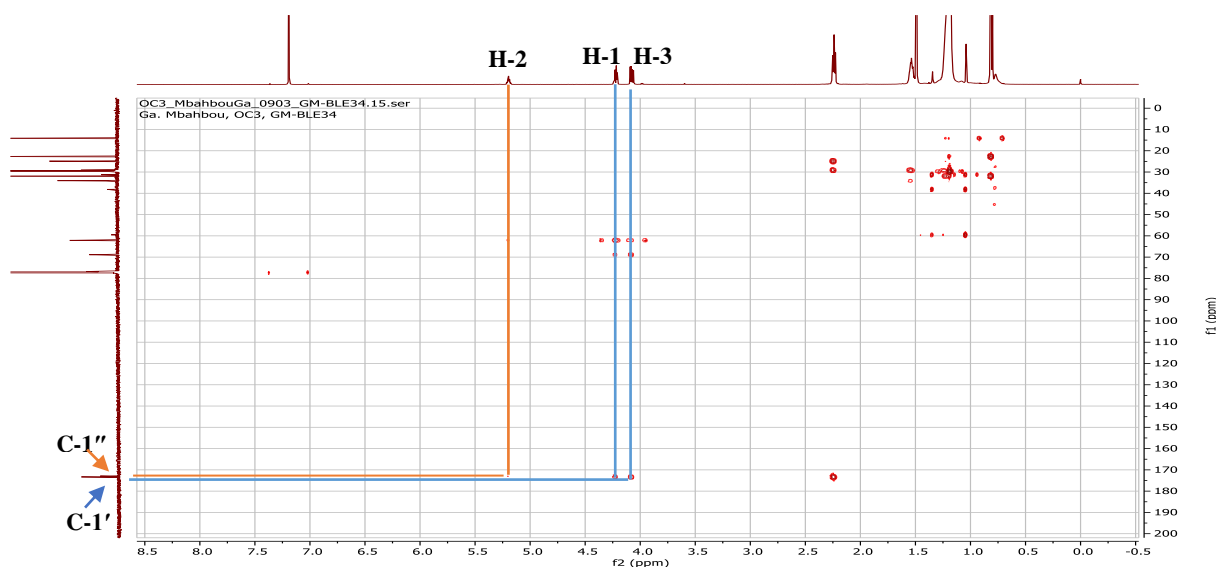


Figure 182: HMBC spectrum of BLE34

II.1.5.10.3. Structural identification of compound RHE5

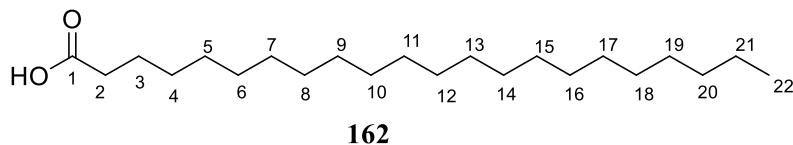
RHE5 was obtained as a white powder in *n*-hexane/CH₂Cl₂ (80:20) and it is soluble in pyridine.

Its molecular formula C₂₂H₄₄O₂ was deduced from the HRESIMS spectrum (Figure 183) which showed the sodium adduct [M+Na]⁺ peak at *m/z* 363.3317 (calcd. for C₂₂H₄₄O₂Na, 363.3339), implying one degree of unsaturation.

Its ¹H NMR spectrum (Figure 184) exhibited signals of:

- a methylene at the α position of a carbonyl at δ_{H} 2.52 (2H, t, $J = 7.4$ Hz, H-2);
- methylene groups of an alkyl long chain at δ_{H} 1.79 (1H, m, H-3), δ_{H} 1.39 (1H, m, H-4) and 1.27 (br d, 18CH₂);
- a terminal methyl at δ_{H} 0.85 (3H, t, $J = 6.8$ Hz, H-22).

These data contributed in identifying RHE5 as docosanoic acid (**162**) (Makhija *et al.*, 2010).



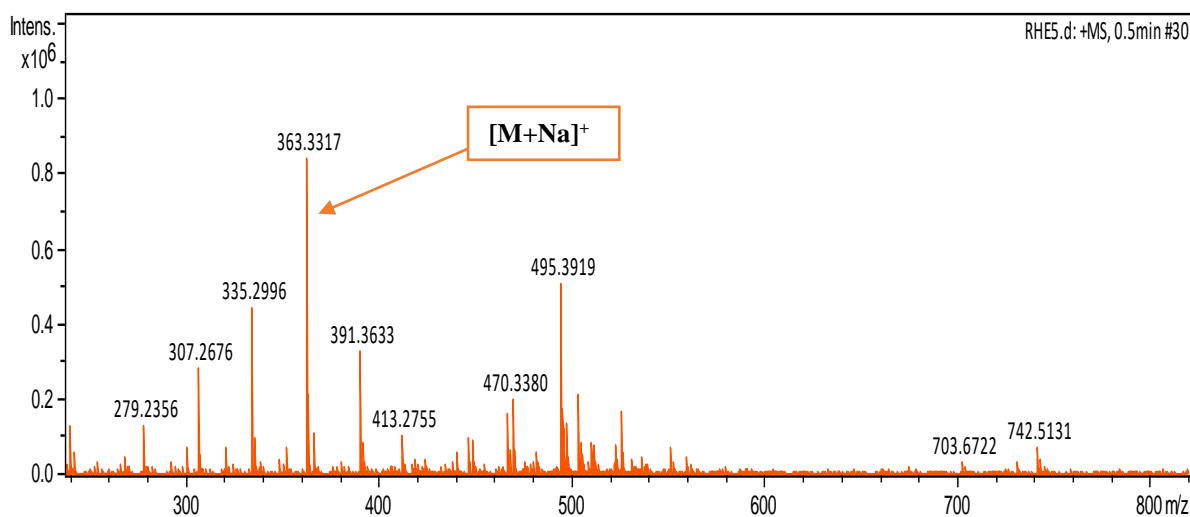


Figure 183: HRESI mass spectrum of RHE5

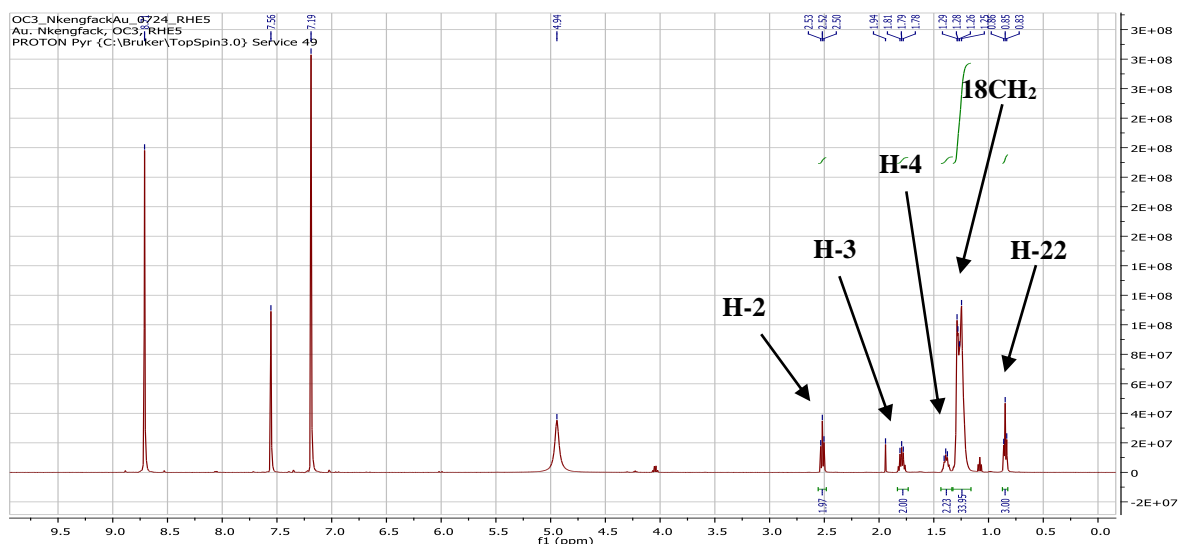


Figure 184: ^1H NMR spectrum (pyridine- d_5 , 500 MHz) of RHE5

II.1.5.10.4. Structural identification of compound RH3

RH3 was obtained as a white powder in *n*-hexane/EtOAc (90:10) and was soluble in dichloromethane.

Its molecular formula $\text{C}_{30}\text{H}_{62}\text{O}$ was deduced from the HRESIMS spectrum (Figure 185) which shows the peak of the sodium adduct $[\text{M}+\text{Na}]^+$ at m/z 461.4703 (calcd. for $\text{C}_{30}\text{H}_{62}\text{ONa}$, 461.4698), without unsaturation.

Its ^1H NMR spectrum (Figure 186) showed signals of:

- an oxymethylene group at δ_{H} 3.57 (2H, t, $J = 6.6$ Hz, H-1);
- a methylene group at δ_{H} 1.49 (2H, m, H-2);
- methylene groups of an alkyl long chain at δ_{H} 1.18 (br s, 27 CH_2);
- a terminal methyl at δ_{H} 0.81 (3H, t, $J = 6.9$ Hz, H-30).

These data helped in identifying RH3 as triacontanol (**163**) (Maruyama *et al.*, 1980).

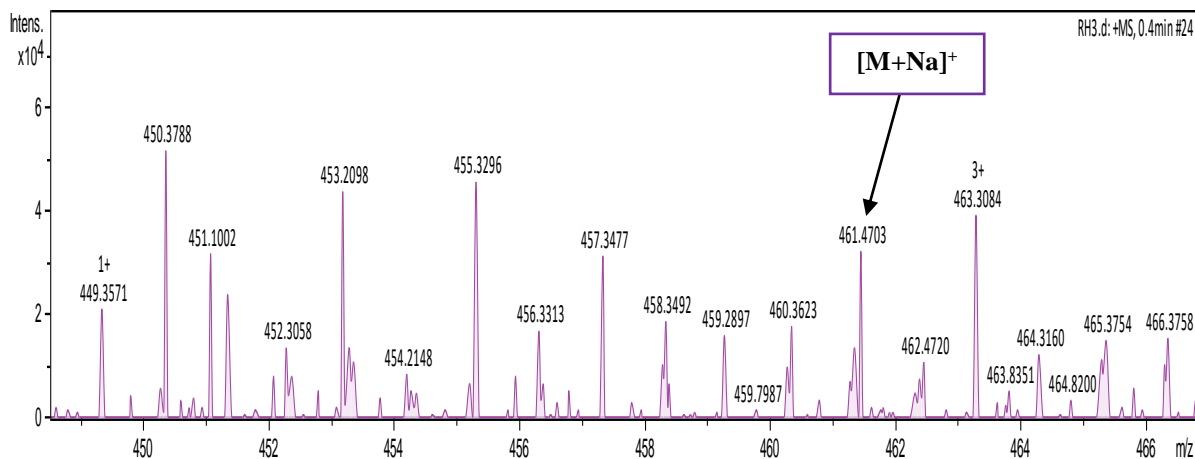
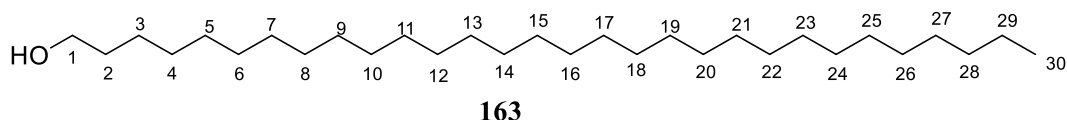


Figure 185: HRESI mass spectrum of RH3



Figure 186: ¹H NMR spectrum (CDCl₃, 500 MHz) of RH3

II.1.5.11. Benzoic acid derivative

II.1.2.11.1. Structural identification of compound WN32

WN32 was obtained as a white powder in *n*-hexane/EtOAc (90:10) and it is soluble in pyridine.

Its ¹³C NMR spectrum (Figure 187) exhibited signals of:

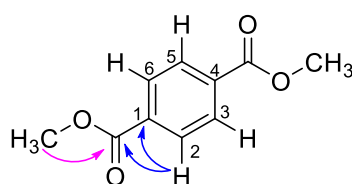
- methoxy groups at δ_H 4.71 (6H, s, OCH₃);
- aromatic group protons at δ_H 8.13 (4H, s, H-2/H-3/H-5/H-6).

Its ¹³C NMR spectrum (Figure 188) displayed four carbon resonances which were sorted by the HMQC spectrum (Figure 189) into:

- methoxy groups at δ_C 62.9 (OCH₃);
- aromatic methine groups at δ_C 129.6 (C-2/C-3/C-5/C-6), quaternary carbons at δ_C 134.0 (C-1/C-4), characteristic of a benzene ring disubstituted (Adeniran and Abimbade, 2014);
- carbonyl of ester at δ_C 165.5 (C-1').

The HMBC spectrum (Figure 190) of WN32 made it possible to determine the position of the two carbonyl groups by the correlations between:

- the aromatic proton H-2/H-3/H-5/H-6 (δ_H 8.13), protons of the methoxy groups (δ_H 4.71) and carbons C-1/C-4 (δ_C 134.0), C-1' (δ_C 165.5), revealing the presence of a symmetry in WN32.



Scheme 39: Key HMBC correlations of WN32

The above data of WN32 were in agreement with those of literature for 1,4-dimethylbenzene-1,4-dicarboxylate (**164**), previously isolated from *Cnidocolus aconitifolius* by Adeniran and Abimbade (2014).

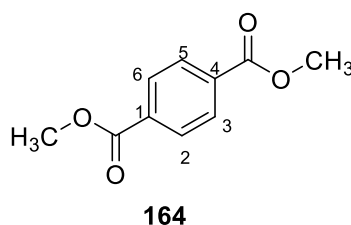


Table 51: ¹H (500 MHz) and ¹³C (125 MHz) NMR data of WN32 in CDCl₃ compared to 1,4-dimethylbenzene-1,4-dicarboxylate

WN32			1,4-dimethylbenzene-1,4-dicarboxylate (Adeniran et Abimbade, 2014)	
Position	$\delta^{13}\text{C}$	$\delta^1\text{H}$ (m, J in Hz)		
1,4	134.0	-	134.1	-
2, 3, 5, 6	129.6	8.13 (4H, s)	129.8	8.18 (4H, s)
1'	165.5	-	166.5	-
OCH ₃	62.9	4.71 (6H, s)	62.6	3.90 (6H, s)

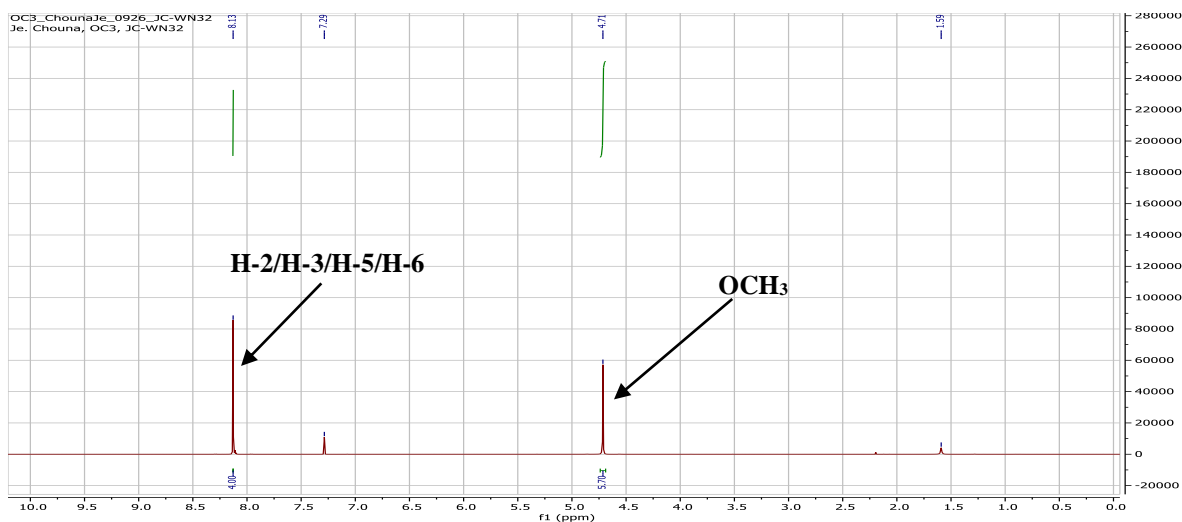


Figure 187: ^1H NMR spectrum (CDCl_3 , 500 MHz) of WN32

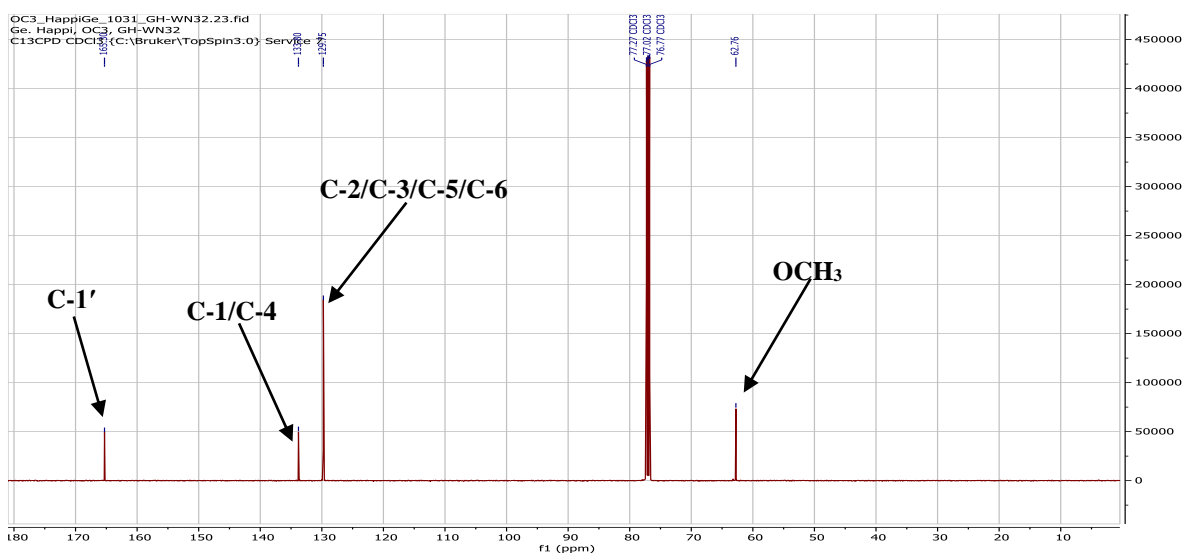


Figure 188: ^{13}C NMR spectrum (CDCl_3 , 125 MHz) of WN32

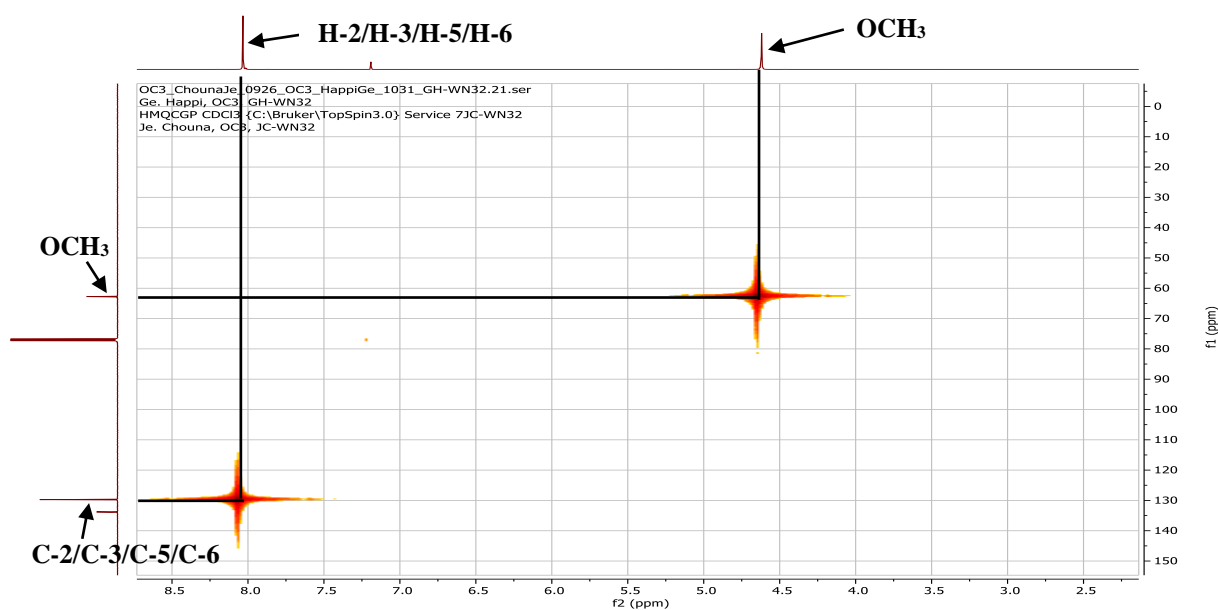


Figure 189: HMQC spectrum of WN32

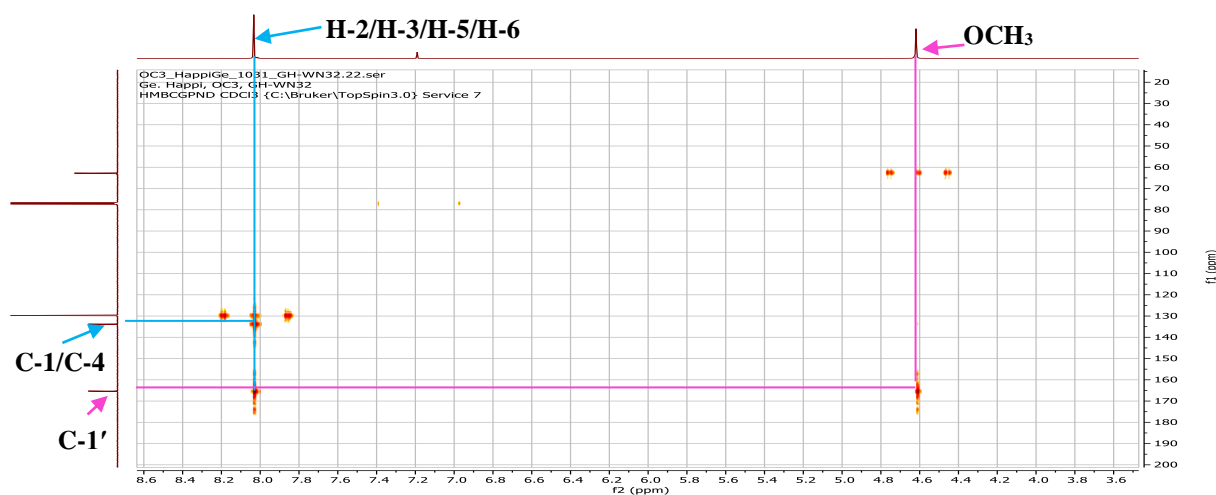


Figure 190: HMBC spectrum of WN32

II.2. CHEMOPHENETIC SIGNIFICANCE OF THE ISOLATED COMPOUNDS

➤ *R. hispida*

Seventeen compounds were isolated from the leaves of *R. hispida*, including a new ceramide (**128**), a naturally alkyl cinnamate derivative (**129**), seven triterpenoids (**19**, **118**, **135-137**, **139**, **140**), four steroids (**56**, **58**, **154**, **155**), one alcohol (**163**), two phenolic compounds including one flavonoid (**131**) and one xanthone (**132**) and one sugar derivative (**156**). Except for compounds **19** and **155**, all the remaining compounds are reported for the first time from *R. hispida*. *n*-Heptadecyl-4-hydroxy-trans-cinnamate (**129**), stigmast-22-en-3-ol (**154**), 30-nor-2 α ,3 β -dihydroxyurs-12-ene (**139**) and triacontan-1-ol (**163**) are newly isolated from the Rubiaceae family.

Although very little studies have been carried out on plants of the genus *Rothmannia*, it belongs to the subfamily Ixoroideae and the tribe of Gardenieae which have been the subject of numerous chemical works. Some of the isolated compounds have been reported from plants of this subfamily. It is the case of the triterpenoids lupeol palmitate (**140**), which has been previously isolated from *Mussaenda roxburghii* Hook. f. (Ghosh *et al.*, 2017). Lupeol (**118**) was reported from *R. hispida* (Dumaro *et al.*, 2016), *Fadogia homblei* De Wild (Mohammed *et al.*, 2013), *M. incana* Wall. (Dinda *et al.*, 2005), *Ixora coccinea* L. (Ikram *et al.*, 2013), *Gardenia saxatilis* Geddes (Suksamrarn *et al.*, 2003) and *Alibertia macrophylla* K. Schum. (da Silva *et al.*, 2007). Erythrodiol (**137**) was previously isolated from *G. gumnifera* L. f. (Reddy *et al.*, 1977). Ursolic acid (**19**) was reported from *R. hispida* (Dumaro *et al.*, 2017), *Wendlandia formosana* Cowan (Lakshmana *et al.*, 2004), *Augusta longifolia* (Spreng.) Rehder (Choze *et al.*, 2010), *F. homblei* (Mohammed *et al.*, 2013), *Sabicea brasiliensis* Wernham (Batista *et al.*, 2014), *I. coccinea* (Latha *et al.*, 2001), *Randia siamensis* Craib

(Jansakul *et al.*, 1999), *G. saxatilis* (Suksamrarn *et al.*, 2003), *G. jasminoides* J. Ellis (Yang *et al.*, 2013), *Duroia macrophylla* Huber (Martins *et al.*, 2013) and hederagenin (**135**) was isolated from *G. latifolia* Aiton (Reddy *et al.*, 1975).

The steroid β -sitosterol (**56**) has been isolated from *G. aqualla* Stapf & Hutch. (Nyemb *et al.*, 2018); stigmaterol (**155**) from *R. tabolti* (Wernham) Keay (Koagne *et al.*, 2017) and *R. witti* (Craib) Bremek. (Chaipukdee *et al.*, 2016).

Kaempferol 3-*O*- β -D-glucopyranoside (**131**) has been isolated from *Chimarrhis turbinata* DC (Cardoso *et al.*, 2005) and D-mannitol (**156**) from *R. tabolti* (Koagne *et al.*, 2017) and *G. aqualla* (Nyemb *et al.*, 2018).

Uvaol (**136**) has not been isolated from plants of the Ixoroideae subfamily, but it has been reported from plants of the other subfamilies of the Rubiaceae family namely Cinchonoideae and Rubioideae (Bremer and Eriksson, 2009). In fact, uvaol has been isolated from *Borreira articularis* (L. f.) F.N. Williams (Rubioideae) (Conserva *et al.*, 2012).

➤ *N. latifolia*

Fifteen compounds were isolated from the fruits of *N. latifolia*, including one quinone (**130**), four triterpenoids (**64**, **70**, **135**, **138**), three citric acid derivatives (**144-146**), one iridoid (**150**), one pyrrole derivative (**149**), one steroid (**155**), one benzoic acid derivative (**164**) two sugar derivatives (**158**, **159**) and one fatty derivative (**162**).

This work stands as the first report of the presence of 2,6-dimethoxybenzoquinone (**130**), myrianthic acid (**7**), monomethyl ester of 1H-pyrrole-2,5-dicarboxylic acid (**149**), dimethyl citrate (**145**), loganin 6-*O*- β -glucopyranoside (**150**) from plants of the genus *Nauclea*. Monomethyl ester of 1H-pyrrole-2,5-dicarboxylic acid and dimethyl citrate are isolated here for the first time from the Rubiaceae family.

The presence of the phthalate 1,4-dimethylbenzene-1,4-dicarboxylate (**164**) in the fruits of *N. latifolia* is not a surprise since many phthalates such as di-(1-hexen-5-yl) phthalate, monoethyl phthalate and 1,2-benzenedicarboxylic acid, dioctyl ester have been previously reported (Fadipe *et al.*, 2014a; Fadipe *et al.*, 2014b). Even though alkaloids are markers of plants of the genus *Nauclea*, no alkaloid was detected in the ripe fruits of the sample investigated. In fact, the Dragendorff and Mayer tests used to identify alkaloids were negative.

➤ *B. leptobotrys*

Nineteen compounds, including eight triterpenoids (**116-118**, **133**, **134**, **141-143**), six steroids (**56**, **58**, **151-153**, **155**), two amino acids (**147**, **148**), two sugar derivatives (**156**, **157**) and one glycerol derivative (**161**) were isolated from the leaves and trunk bark of *B.*

leptobotrys. To the best of our knowledge, all the compounds isolated from *B. leptobotrys* are reported for the first time. The compound glycerol tripalmitate (**161**) is isolated from the first time from natural source. It was previously synthesised. Amongst these compounds, lupeol (**118**) and friedelin (**116**) were isolated from *B. massaiensis* (Keroletswe *et al.*, 2018) while β -sitosterol (**56**) and stigmasterol (**155**) were isolated from *B. massaiensis* and *B. kirkii* (Kapingu *et al.*, 2008). Except for lupeol (**118**), friedelin (**116**), β -friedelinol (**117**), mixture of β -sitosterol (**56**) and stigmasterol (**155**), all the compounds were isolated for the first time from the genus *Baphia*. The compounds germanicol caffeoyl ester (**133**), 3- β -*O*-(*E*)-3,5-dihydroxycinnamoyl-11-oxo-olean-12-ene (**134**), 3-oxofriedelan-29-al (**142**), 3-oxofriedelan-25-oic acid (**143**) were isolated for the first time from the Fabaceae family. Eventhough compounds *N*-benzoylphenylalaninyl-*N*-benzoylphenylalaninate (**147**) and 4-hydroxy-*N*-methylproline (**148**) have not previously been isolated from plants of the genus *Baphia*, these compounds have previously been reported *Piptadenia gonoacantha* (Carvalho *et al.*, 2010) and *Inga umbellifera* (Coley *et al.*, 2005), respectively, two plants of the Fabaceae family (Caesalpinioideae) while compounds 7-ketostigmasterol (**152**) and 7-keto- β -sitosterol (**153**) were detected by GC/MS from the wood of *Chamaecytisus proliferus* spp. *palmensis* (Fabaceae) (Marques *et al.*, 2008). Ergosterol peroxide (**151**) was previously isolated from the fruits of *Enterolobium contortisiliquum* (Vell.) Morong (Fabaceae) (Miranda *et al.*, 2015) and from the fungus *Aspergillus* sp. EJC 04 (Trichocomaceae), an endophyte from *Bauhinia guianensis* Aubl. (Fabaceae) (Feitosa *et al.*, 2016). These findings enrich the chemical diversity of the *Baphia* genus and provide evidence for further chemotaxonomic studies.

II.3. BIOLOGICAL ACTIVITIES OF THE ISOLATED COMPOUNDS

II.3.1. Antileishmanial activity of extracts, fractions and isolated compounds

The isolated compounds were assessed for their antileishmanial activity against *Leishmania donovani* 1S (MHOM/SD/62/1S) promastigotes and their cytotoxicity towards RAW 264.7 macrophage cells.

The criteria of evaluation of the antileishmanial activity and cytotoxicity activity of natural products are represented in the tables 52 and 53 below:

Table 52: Criteria of evaluation of the antileishmanial activity of extracts, fractions and pure compounds

Antileishmanial activity of extracts/Fractions (Camacho, 2003)		Antileishmanial activity of pure compounds (Nwaka and Hudson, 2006; Sosa <i>et al.</i> , 2016)	
IC ₅₀ (μg/mL)	Qualification	IC ₅₀ (μg/mL)	Qualification
IC ₅₀ < 10	Potent activity	IC ₅₀ < 1	Hit/lead activity
10 < IC ₅₀ < 50	Good activity	IC ₅₀ < 10	Potent activity
50 < IC ₅₀ < 100	Moderate activity	10 < IC ₅₀ < 20	Moderate activity
IC ₅₀ > 100	Inactive	IC ₅₀ > 20	Inactive

Table 53: Criteria of evaluation of the cytotoxicity activity

Cytotoxicity activity criteria (Camacho, 2003; Nwaka and Hudson, 2006)	
Selectivity Index (SI)	Qualification
SI > 20	Hit selective
SI > 1	Selective
SI < 1	Non selective

II.3.1.1. *R. hispid*a

Concerning the leaves of *R. hispid*a, the results obtained are presented in Table 54 below.

Table 54: Antileishmanial activity and selectivity indices of crude extract and compounds from *R. hispid*a against promastigotes

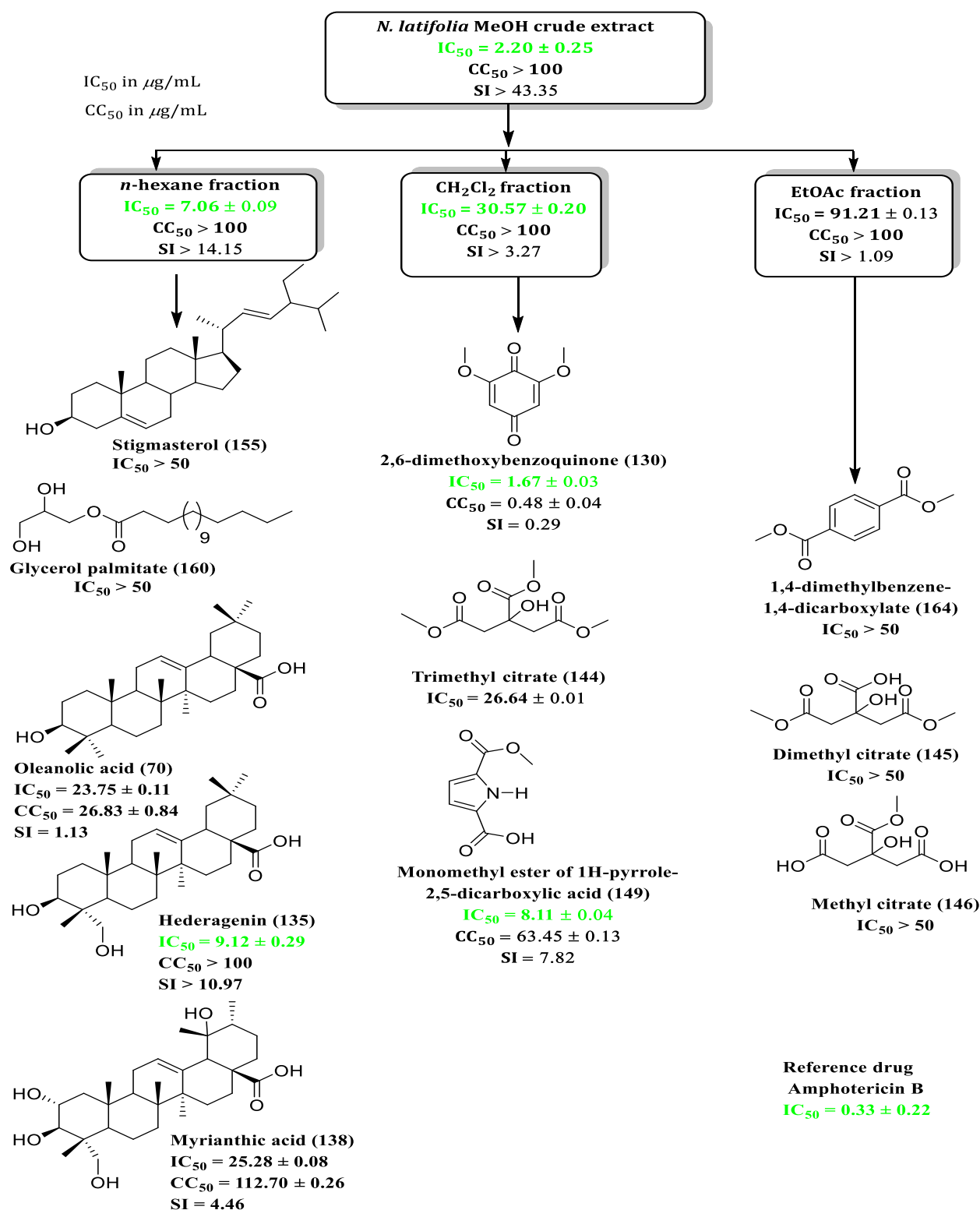
Extract/compounds	Promastigotes IC ₅₀ (μg/mL) ± SD	Macrophages CC ₅₀ (μg/mL) ± SD	Selectivity Index (SI) (CC ₅₀ /IC ₅₀)
CH ₂ Cl ₂ /MeOH (1:1) crude extract	15.50 ^h	> 100	> 6.45
Rothmannamide (128)	> 50	ND	ND
<i>n</i> -Heptadecyl-4-hydroxy- <i>trans</i> -cinnamate (129)	13.56 ± 0.31 ^f	> 100	> 7.37
Lupeol palmitate (140)	11.05 ± 0.31 ^e	> 100	> 9.05
Lupeol (118)	> 50	ND	ND
Uvaol (136) + erythrodiol (137)	14.30 ± 0.28 ^g	> 100	> 6.99
Ursolic acid (19)	0.88 ± 0.10 ^b	72.74 ± 0.46 ^a	82.94
30- <i>nor</i> -2 α ,3 β -dihydroxyurs-12-ene (139)	1.75 ± 0.09 ^c	> 100	> 57.21
Hederagenin (135)	9.12 ± 0.29 ^d	> 100	> 10.97
Stigmasta-22-en-3-ol (154)	> 50	ND	ND
Triacontan-1-ol (163)	> 50	ND	ND
Kaempferol 3- <i>O</i> - β -D-glucopyranoside (131)	44.34 ± 0.36 ^j	> 100	> 2.25
D-mannitol (157)	> 50	ND	ND
Amphotericin B	0.33 ± 0.22 ^a	-	-

ND: not determined; Data points are means from triplicate experiments. SD = Standard Deviation; Activity values were obtained from sigmoidal dose-response curves of concentration versus response. Along the columns, values with the different letter superscript are significantly different; Waller Duncan at $p \leq 0.05$.

From the active crude extract ($IC_{50} = 15.50 \mu\text{g/mL}$) of *R. hispida*, ursolic acid (**19**), 30-*nor-2 α ,3 β* -dihydroxyurs-12-ene (**138**) and hederagenin (**135**) exhibited highly potent antileishmanial activity against *L. donovani* promastigotes with IC_{50} values ranging from 0.88 to 9.12 $\mu\text{g/mL}$. In addition, lupeol palmitate (**140**), the mixture uvaol (**136**) and erythrodiol (**137**) and *n*-heptadecyl-4-hydroxy-trans-cinnamate (**129**) exhibited moderated activity with IC_{50} values between 11.05 and 14.30 $\mu\text{g/mL}$ (Table 54). Generally, all the tested active samples exhibited very low cytotoxicity ($CC_{50} > 70 \mu\text{g/mL}$) against RAW 264.7 cells. However, the most active compounds, ursolic acid (**19**) and 30-*nor-2 α ,3 β* -dihydroxyurs-12-ene (**139**) showed limited cytotoxicity towards RAW 264.7 cells with significant selectivity ($SI > 57$) (Table 54). Some authors suggested that the antileishmanial activity of triterpenoids could be related to the inhibition of leishmanial proteins and nucleic acids synthesis and/or to the inhibition of a membrane-associated calcium-dependent ATPase pump (Goijman *et al.*, 1984; Mishina *et al.*, 2007; Isah *et al.*, 2016). The difference in activity between the crude extract and some of the isolated compounds may be due to an antagonistic action of the isolated compounds. This antagonistic effect between extracts and constituents was previously discussed by Caesar and Cech (2019), who demonstrated that the complexity of crude extracts masks the biological activity of its chemical constituents on certain therapeutic targets.

II.3.1.2. *N. latifolia*

The methodology used here was the bioguided approach against the same strain and the results obtained are given in the scheme 40 below:



Scheme 40: Antileishmanial activity and selectivity indices of crude extracts, fractions and compounds from *N. latifolia*

From this scheme, the *n*-hexane was the most active fraction with IC₅₀ value of 7.06 µg/mL. But, it was less active than the crude extract with IC₅₀ value of 2.20 µg/mL. The CH₂Cl₂ and EtOAc fraction soluble fractions exhibited good and moderate activity with IC₅₀

of 30.57 and 91.21 $\mu\text{g/mL}$, respectively. The *n*-hexane and CH_2Cl_2 fractions of the fruits of *N. latifolia* were non cytotoxic with $\text{SI} > 3.27$.

From the most active *n*-hexane fraction, hegeragenin (**135**) was the most active compound with $\text{IC}_{50} = 9.12 \mu\text{g/mL}$ and with good selectivity ($\text{SI} > 10.97$). 2,6-dimethoxybenzoquinone (**130**) was the most active compound of the dichloromethane fraction with $\text{IC}_{50} = 1.67 \mu\text{g/mL}$, but showed lower selective ($\text{SI} = 0.29$) towards the macrophage cells. Monomethyl ester of 1H-pyrrole-2,5-dicarboxylic acid (**149**) showed also good activity with $\text{IC}_{50} = 8.11 \mu\text{g/mL}$. None of the compounds isolated from the ethyl acetate was active (Scheme 40).

From these results, one can conclude that the difference in activity between the crude extract fractions and the isolated compounds may be due to a synergistic action of the isolated compounds. This synergistic effect of chemical constituents in extracts was previously discussed by Caesar and Cech (2019), who demonstrated that the complexity of crude extracts enhance its biological activity on certain therapeutic targets.

The mechanisms involved in cytotoxicity of quinone derivatives are still largely unknown. So far, it is clear that quinones can alkylate essential proteins or inactivate enzymes either directly or following reduction. However, the most prominent characteristic of quinones is their ability to undergo reversible oxidation-reduction (Sun *et al.*, 1997; de Sena *et al.*, 2016).

II.3.1.3. *B. leptobotrys*

The table 55 below present the results obtained from the antileishmanial assay done on the trunk bark and leaves of *B. leptobotrys*.

Table 55: Antileishmanial activity and selectivity indices of crude extracts and compounds from *B. leptobotrys*

Extracts/compounds	Promastigotes IC ₅₀ (μg/mL) ± SD	Macrophages CC ₅₀ (μg/mL) ± SD	Selectivity Index (SI) (CC ₅₀ /IC ₅₀)
CH ₂ Cl ₂ /MeOH (1:1) trunk bark crude extract	63.40 ± 0.02 ^e	> 100	> 1.57
Glycerol tripalmitate (161)	> 50	ND	ND
Lupenone (141)	> 50	ND	ND
Germanicol caffeoyl ester (133)	6.03 ± 0.19 ^c	> 100	> 16.58
Ergosterol peroxide (151)	4.04 ± 0.09 ^b	15.56 ± 0.15 ^a	3.40
3-β-O-(E)-3,5-dihydroxycinnamoyl - 11-oxo-olean-12-ene (134)	45.33 ± 0.40 ^d	ND	ND
Methyl β-D-glucopyranoside (157)	> 50	ND	ND
CH ₂ Cl ₂ /MeOH (1:1) leaves crude extract	> 100	ND	ND
Friedelin (116)	> 50	ND	ND
3-oxofriedelan-29-al (142)	> 50	ND	ND
3-oxofriedelan-25-oic acid (143)	> 50	ND	ND
<i>N</i> -benzoylphenylalaninyl- <i>N</i> -benzoylphenylalaninate (147)	> 50	ND	ND
4-hydroxy- <i>N</i> -methylproline (148)	> 50	ND	ND
Amphotericin B	0.33 ± 0.22 ^a	-	-

ND: not determined; Data points are means from triplicate experiments. SD = Standard Deviation; Activity values were obtained from sigmoidal dose-response curves of concentration versus response. Along the columns, values with the different letter superscript are significantly different; Waller Duncan at $p \leq 0.05$.

The antileishmanial assay done on some of the isolated compound showed that germanicol caffeoyl ester (**133**) and ergosterol peroxide (**151**) exhibited potent antileishmanial activity with IC₅₀ of 4.04 and 6.03 μg/mL, respectively. These compounds were not cytotoxic towards RAW 264.7 macrophage cells with SI > 3.40 (Table 55). This is the first report of the antileishmanial activity of germanicol caffeoyl ester (**133**).

It is known that reactive oxygen species and nitrogen show high toxicity against intracellular protozoan parasites such as *Leishmania* and *Trypanosoma* within the mechanisms of innate host immune response and this process usually takes place within cells as an intracellular mechanism of the host's defence against infections caused by these parasites (Stafford *et al.*, 2002; Ramos-Ligonio *et al.*, 2012). The mechanism of action proposed for ergosterol peroxide involves the replacement of ergosterol, a structural component of the parasite cell membrane during the replication process. The subsequent breaking of the peroxide bond triggers a series of free radical reactions, which may cause the disruption of the parasite membrane (Leliebre-Lara *et al.*, 2016).

The difference in activity between the crude extracts, fractions and some of the isolated compounds may be due to an antagonistic action of the isolated compounds. This antagonistic effect between extracts and constituents was previously discussed by Caesar and Cech (2019), who demonstrated that the complexity of crude extracts masks the biological activity of its chemical constituents on certain therapeutic targets.

In order to search for other biological potentials of these three plants, the antibacterial screening of extracts and compounds was carried out. Considering the fact that complicated cases of visceral leishmaniasis are associated with bacterial infections and bleedings (Andrade *et al.*, 1990), the crude extracts and isolated compounds were evaluated for their antibacterial potential.

II.3.2. Attempt of preformulation of phytomedicine from *N. latifolia* fruits

The evaluation of the antileishmanial, cytotoxicity activities and subacute toxicity of the methanol fruits crude extract of *N. latifolia* led to interesting results; so, it seemed judicious to us to attempt a preformulation.

After carrying out the *in vitro* test on *L. donovani* 1S (MHOM/SD/62/1S) promastigotes and cytotoxicity towards Raw 264.7 macrophage cells, the results obtained showed that the ripe fruits of *N. latifolia* was a good candidate for the preformulation of a phytodrug. Thus, the acute toxicity test was performed and the extract showed no sign of toxicity. To optimize the use of the plant, we preformulated our phytomedicine using the smallest curative dose (1.283 mg/kg). The protocol used is that of Reagan-Shaw and collaborators, in 2007, entitled "Dose translation from animal to human studies revisited". The following formula was used:

Formula for Dose Translation Based on BSA (Body Surface Area)

$$\text{HED (mg/kg)} = \text{Animal dose (mg/kg)} \times \frac{\text{Animal Km}}{\text{Human Km}}$$

With HED: Human Effective Dose

In the present case, animal dose is 1.283 mg/kg. From the above formula, the Km factor are constant and known. The animal Km vary from one animal to another according to the species (Km of rat is 6 while the human Km is 37 for adult and 25 for child). The phytodrug has been preformulated as a syrup (Reagan-Shaw *et al.*, 2007), with the consumable doses evaluated as follows. This operation has several steps:

1st step: Human effective dose calculation

$$\text{HED} = 1.283 \times 6/25 = 0.308 \text{ mg/kg.}$$

2nd step: Calculation of the daily dose for children from 0 to 5 years

$$D = \text{HED} \times 20 = 0.308 \times 20 = 6.16 \text{ mg/day}$$

(The average body weight for child in 20 and for adult is 60)

3th step: Preparation of simple syrup

The standard formula for a saturated syrup is 6.7 g of sugar for 3.3 g of water for a total of 10 g of simple syrup. It is advisable to use demineralized or deionized water.

4th step: Determination of quantity of each ingredient

- Extract (active ingredient)

The daily dose is 6.16 mg for a child. The normal concentration of the active ingredient is 1.3 mg/mL. One teaspoon is 15 mL; i.e. a concentration of 19.5 g/15 mL. For the fruit extract, we will have $6.16/2 = 3.08$;

$(3.08/19500) \times 100 = 0.0158\%$ of active ingredient per spoon.

- for conservator or stabilizer (sodium benzoate)

It is advisable to vary the percentage of stabilizers in order to determine which stabilizes the product over a long period. This percentage varies between 0.05 and 0.5%.

- **for strawberry essence:** the percentage is standard for essences and it is 0.5%.

- **for aroma:** the percentage is also standard for aromas and it is 0.1%.

- simple syrup:

Its percentage is deducted from the percentages of the other ingredients:

$$\% \text{ syrup} = 100\% - (\% \text{ extract} + \% \text{ stabilizer} + \% \text{ strawberry essence} + \% \text{ flavour})$$

$$= 100\% - (0.0158\% + 0.3\% + 0.5\% + 0.1\%)$$

$$= 99.0842$$

So, in 100 mg of phytomedicine, we will have 99.0842 mg of saturated simple syrup (excipient), 0.0158 mg of crude extract (active principle), 0.3 mg of sodium benzoate (preservative), 0.5 mg of strawberry oil (ingredient) and 0.1 mg of flavour (ingredient).

The following syrup using the methanol soluble extract of *N. latifolia* was preformulated for the prevention of visceral leishmaniasis for children under 5 years (Figure 191). This syrup is administrated by oral voice as one teaspoon twice a day.

To ensure the efficacy of this syrup, antileishmanial assay and other toxicological assays must be performed to verify if the plant extract is still active and non toxic in that galenic form.

Therefore, many analysis are still necessary. These include pharmacokinetic study (absorption, distribution, metabolism, and excretion) and clinical trials.

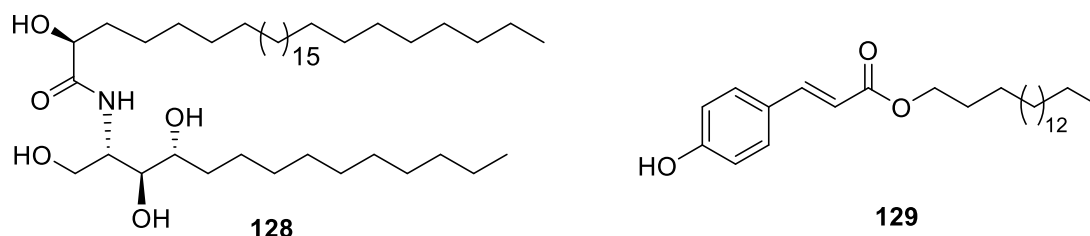


Figure 191: Preformulation from the fruits of *N. latifolia*

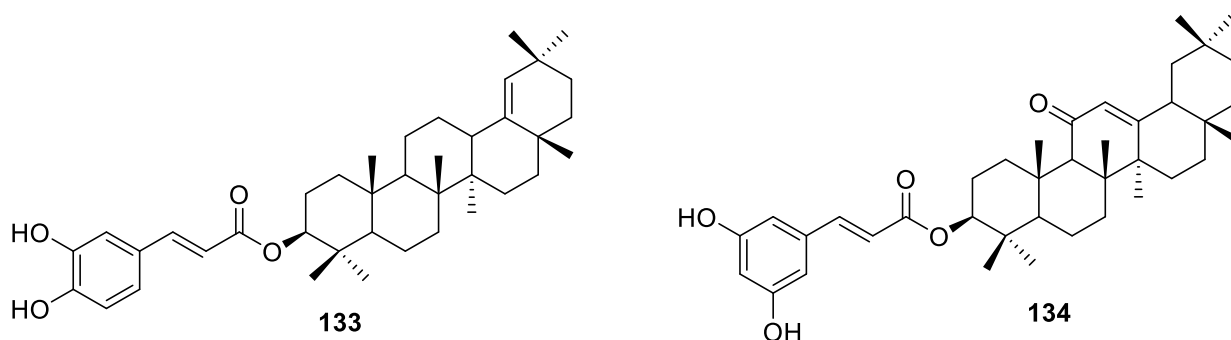
CONCLUSION AND PERSPECTIVES

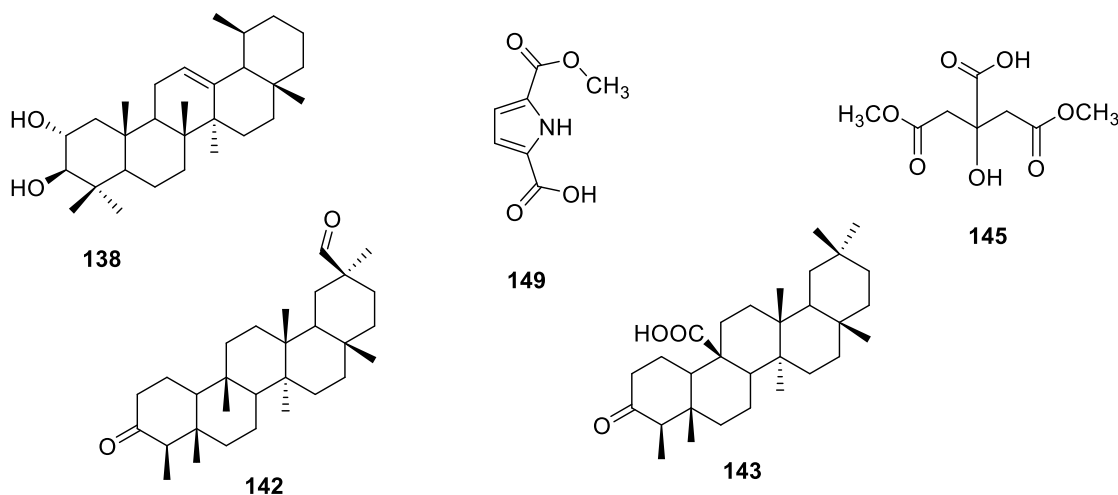
The objective of this work was to search for potential extracts, fractions from three Cameroonian medicinal plants namely *Rothmannia hispida*, *Nauclea latifolia* (Rubiaceae) and *Baphia leptobotrys* (Fabaceae) and compounds which can serve as lead for the development of new drugs against leishmaniasis.

The chemical investigation of the active extracts, fractions led to the isolation of forty five (45) compounds characterized using usual spectroscopic techniques (IR, HRESI mass spectrometry, 1D and 2D NMR) and divided into twelve classes among which one sphingolipid [rothmanniamide (**128**), a new derivative], seventeen pentacyclic triterpenoids, seven phytosteroids, three phenolic derivatives [*n*-heptadecyl-4-hydroxy-transcinnamate (**129**), isolated for the first time from natural source], three citric acid derivatives, one quinone, one pyrrole derivative, two amino acid derivatives, four carbohydrates, one iridoid, four fatty derivatives and one benzoic acid derivative.



All these compounds enrich the knowledge on the chemistry of these plants and provides further information in regard to the possible chemophenetic markers present in these species and showed the presence of uncommon metabolites encountered in Rubiaceae and Fabaceae families. Some compounds such as germanicol caffeoyl ester (**133**) and 3- β -O-(*E*)-3,5-dihydroxycinnamoyl-11-oxo-olean-12-ene (**134**), 3-oxofriedelan-29-al (**142**), 3-oxofriedelan-25-oic acid (**143**) are isolated for the first time from Fabaceae family and 30-*nor*-2 α ,3 β -dihydroxyurs-12-ene (**139**), monomethyl ester of 1H-pyrrole-2,5-dicarboxylic acid (**149**) and dimethyl citrate (**145**) are isolated for the first time from the Rubiaceae family.





The results obtained show also the antileishmanial and cytotoxicity potencies of some extracts, fractions and compounds.

The MeOH extract of the fruits of *N. latifolia* was the most potent extract ($IC_{50} = 2.20 \mu\text{g/mL}$) and the *n*-hexane fraction of the same plant was the most potent fraction ($IC_{50} = 7.06 \mu\text{g/mL}$) against *Leishmania donovani* 1S (MHOM/SD/62/1S) promastigotes and were selective with SI values of 43.35 and 14.15, respectively towards RAW 264.7 macrophage cells.

Ursolic acid (**19**) ($IC_{50} = 0.88 \mu\text{g/mL}$), 30-*nor*-2 α ,3 β -dihydroxyurs-12-ene (**139**) ($IC_{50} = 1.75 \mu\text{g/mL}$), ergosterol peroxide (**151**) ($IC_{50} = 4.04 \mu\text{g/mL}$), 2,6-dimethoxybenzoquinone (**130**) $IC_{50} = 1.67 \mu\text{g/mL}$, germanicol caffeoyl ester (**133**) ($IC_{50} = 6.03 \mu\text{g/mL}$), monomethyl ester of 1H-pyrrole-2,5-dicarboxylic acid (**149**) ($IC_{50} = 8.11 \mu\text{g/mL}$) and hederagenin (**135**) ($IC_{50} = 9.12 \mu\text{g/mL}$) were the most potent compounds compared to amphotericine B ($IC_{50} = 0.33 \mu\text{g/mL}$), the reference drug. Except for 2,6-dimethoxybenzoquinone (SI = 0.29), all the potent compounds were selective towards the macrophage cells (SI > 3.40).

The assessment of the toxic effects of the methanol extract of *N. latifolia* for acute toxicity in female rats showed that at the tested limit doses of 2000 and 5000 mg/kg, the extract did not cause any death during the 14 days of experimentation indicating that the Lethal Dose 50 (LD_{50}) is greater than 5000 mg/kg.

These results show that *R. hispida*, *N. latifolia* and *B. leptobotrys* could be sources of leishmaniacidal agents and contribute to the valorisation of the Cameroonian biodiversity.

In our future work, we intend to:

- Verify the safety and efficacy of the syrup by doing antileishmanial and toxicological assays;
- Do some chemical transformations of the most active compounds in view to increase their antileishmanial activity.

PART III: MATERIAL AND METHODS

III.1. APPARATUS AND PLANT MATERIALS

III.1.1. Apparatus

III.1.1.1. Evaporation, weighing and chromatographies

For this study, an ACCULAB SARTORIUS GROUP VICON type balance to weigh the plant material, crude extracts and fractions. An OHAUS Pioneer type balance (precision 0.001) was also used to weigh the isolated compounds. The crude extracts were evaporated using a HEIDOLPH brand rotary evaporator connected to a VACUUBRAND pump and a LAUDA chiller.

Test tubes of 500 mL, 100 mL, 10 mL of the respective brands Pobel, Dagra, Fortuna were used for the preparation of the different solvent systems.

Fractionation of the crude extracts were performed using vacuum liquid chromatography and column chromatography over silica gel, while the purification of compounds was carried out on column chromatography using silica gel 230–400 mesh (Merck, Darmstadt, Germany), 70–230 mesh (Merck) and sephadex LH-20 (Sigma-Aldrich, Munich, Germany) as stationary phase. The dimensions of the columns were chosen based on the amount of extract to be separated. The different eluents used were adapted to the stationary phases depending on the polarity of the compounds to be separated or analyzed. Analytical thin layer chromatography (TLC) was performed on Merck pre-coated silica gel (60 F254) aluminium foil (Merck, 20 × 20 cm) 0.2 mm thick. The identification of compound spots on TLC plates was carried out by visualizing under a UV lamp of type Spectroline, model VL-4-LC, with wavelength 254 and 366 nm, then pulverizing with sulphuric acid diluted at 20%, and heating the plate in an oven at about 100°C.

III.1.1.2. Mass spectra

High resolution mass spectra were obtained with a QTOF Compact Spectrometer (Bruker, Germany) equipped with a HRESI source. The spectrometer was operated in positive and negative modes (mass range: 50–1500, with a scan rate of 1.00 Hz) with automatic gain control to provide high-accuracy mass measurements within 0.4 ppm deviation using Na formate as calibrant. The following parameters were used for experiments: spray voltage of 4.5 kV, capillary temperature of 200°C. Nitrogen was used as sheath gas (4 L/min). The optical rotations were measured using a PerkinElmer polarimeter.

III.1.1.3. Nuclear Magnetic Resonance (NMR) spectra

The ^1H and ^{13}C NMR spectra were recorded on Bruker DRX 500 MHz and 600 MHz NMR spectrometers (Bruker Corporation, Brussels, Belgium) in deuterated solvents. Chemical shifts were reported in δ (ppm) using tetramethylsilane (TMS) (Sigma-Aldrich) as an internal standard, while coupling constants (J) were measured in Hz.

III.1.1.4. Optical rotation measurement and Infrared spectrum

The optical rotation were measured using a PerkinElmer polarimeter. The infrared spectra were recorded on a Bruker type spectrometer (Fourier Transform Infrared Spectrometer).

III.1.2. Plant materials

The leaves of *R. hispida* were collected in June 2017 at Nkol-Afamba (GPS coordinates: Latitude 3°51'32"N, Longitude 11°39'53"E), a locality in the Centre Region of Cameroon and identified by Mr Nana Victor, a botanist at the National Herbarium of Cameroon, where a voucher specimen (N° 46515 HNC) was deposited.

The ripe fruits of *N. latifolia* were harvested in March 2017 at Makenene, a locality in the Centre Region of Cameroon and identified by Dr. Tacham Walter Ndam, Botanist at the Faculty of Science of The University of Bamenda, Cameroon, and compared with voucher specimens formerly kept at the Cameroon National Herbarium under the registration number 20144/SFR/Cam.

The trunk bark and leaves of *B. leptobotrys* were harvested in April 2018 and September 2019, respectively in the Kompia forest, located in the East Region of Cameroon. The plant was identified by Mr Nana Victor, a botanist at the National Herbarium of Cameroon and compared with voucher specimen formerly kept at the Cameroon National Herbarium under the reference number 52328 HNC.

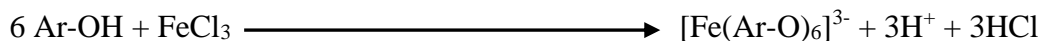
III.2. SOME CHARACTERISTIC TESTS USED IN THE IDENTIFICATION OF SECONDARY METABOLITES

III.2.1. Ferric chloride test

The purpose of this test is to identify phenolic compounds. The reagents used are ethanol and iron (III) chloride (FeCl_3).

Procedure: In 5 mL of ethanol contained in a test tube, a small amount of the compound was dissolved. Then a few drops of the ferric chloride (FeCl_3) solution were added to the solution obtained.

Results and interpretation: Gradually, the reaction medium turns to a greenish blue or purple color (transient or permanent) due to the formation of a complex of the type $[\text{Fe}(\text{OAr})_6]^{3-}$, which indicates the presence of the free phenolic hydroxyl groups. The formation of this complex is done according to the following equation:



III.2.2. Shinoda test

The purpose of this test is to identify flavonoids. The reagents used are methanol, hydrochloric acid (HCl), magnesium shaves (Mg).

Procedure: In 5 mL of methanol in a test tube, a small amount of the extract or compound was dissolved. To the resulting solution, a few drops of concentrated hydrochloric acid (HCl) and a few shaves of magnesium were added.

Results and Interpretation: The presence of flavonoids was confirmed by the appearance of a purple color.

III.2.3. Bornträger test

The purpose of this test is to identify quinones and anthraquinones. The reagents used are sodium hydroxide (NaOH), methylene chloride (CH_2Cl_2).

Procedure: In 5 mL of methylene chloride contained in a test tube, a small amount of the compound was dissolved. Then 10% of an aqueous sodium hydroxide solution was added to the resulting solution.

Results and interpretation: A red coloration develops in the aqueous phase is characteristic of anthraquinones, while a pink or purple coloration occurs in the aqueous phase for benzoquinones.

III.2.4. Libermann-Burchard test

The purpose of this test is to identify triterpenoids and steroids. The reagents used are chloroform (CHCl_3), acetic anhydride [$(\text{CH}_3\text{CO})_2\text{O}$], concentrated sulfuric acid (H_2SO_4).

Procedure: The dry residue was dissolved in 3 mL of chloroform. After having stirred it, the mixture is filtered and then distributed into 2 test tubes, the first of which serves as a control. Two drops of acetic anhydride were added to the second tube. The mixture was slightly stirred, then a few drops of 36 N H_2SO_4 was added to it.

Results and interpretation: The presence of terpenoids is indicated by a purplish red stain, while that of steroids are confirmed by a bluish green stain.

III.2.5. NaHCO₃ test

The purpose of this test is to identify carboxylic acids. The reagent used is NaHCO₃ (sodium bicarbonate).

Procedure: A small amount of the compound was dissolved in NaHCO₃.

Results and Interpretation: The presence of carboxylic acid was characterized by the complete dissolution of the product with release of CO₂. CO₂ is evidenced by cloudiness in lime water. The CO₂ discolors the filter paper soaked in an aqueous solution of purple KMnO₄.

III.2.6. Lucas test

The purpose of this test is to distinguish primary, secondary or tertiary alcohols. The Luca's reagents is a mixture of (ZnCl₂/HCl).

Procedure: A volume of 2 mL of Lucas's reagent was poured into a clean and dry test tube. Few drops of the compound was added; the tube was stoppered and vigorously shaken for one minute.

Results and interpretation: The almost immediate onset of cloudiness (cloudiness is due to chlorinated derivatives, insoluble in water) indicated the presence of tertiary alcohol.

III.2.7. Molish test

The purpose of this test is to identify sugars. The reagent used are ethanol, α -naphthol and concentrated H₂SO₄.

Procedure: In a test tube, a few milligrams of the extract or compounds was dissolved in ethanol and a 1% ethanolic solution of α -naphthol was added. After homogenization, a few drops of concentrated H₂SO₄ were slowly poured onto the wall of the test tube.

Results and interpretation: The presence of sugars was evidence by the appearance of a purplish red ring at the interface.

III.3. EXTRACTION, FRACTIONATION, ISOLATION AND PURIFICATION OF COMPOUNDS

III.3.1. Extraction

III.3.1.1. Preparation of *R. hispida* crude extract

The air-dried and ground leaves of the plant (1.9 kg) were macerated three times at room temperature with 10 L of dichloromethane/methanol (1:1) for 48 h each. The crude extract was obtained as a green paste (251.8 g) after removing the solvent mixture.

III.3.1.2. Preparation of *N. latifolia* crude extract

The air-dried and ground fruits of the plant (2.1 kg) were macerated three times at room temperature with 20 L of MeOH for 48 h each. The crude extract was obtained as a red paste (459.7 g) after removing the solvent under vacuum at low temperature.

III.3.1.3. Preparation of *B. leptobotrys* crude extracts

The air-dried and ground trunk bark (5.06 kg) and leaves (880.3 kg) of the plant were each macerated three times at room temperature, respectively with 25 L and 10 L of CH₂Cl₂/MeOH (1:1) for 48 h. The trunk bark crude extract was obtained as a chestnut oily paste (132.6 g) and the leaves crude extract as a green paste (102.2 g) after removing the solvent under vacuum at low temperature.

III.3.2. Fractionation of crude extracts and isolation of compounds

III.3.2.1. Fractionation of crude extract and isolation of compounds from *R. hispida*

A part of the extract (243.5 g) was subjected to vacuum liquid chromatography using the mixtures of *n*-hexane/EtOAc and EtOAc/MeOH of increasing polarities. Two hundred and ninety four (294) sub-fractions of 500 mL each, were obtained and combined according to their TLC profiles to yield five fractions labelled F1 (43.6 g, *n*-hexane/EtOAc, 100:0), F2 (65.3 g; *n*-hexane/EtOAc, 50:50), F3 (19.2 g; EtOAc/MeOH, 100:0), F4 (27.2 g; EtOAc/MeOH; 95:5–80:20) and F5 (26.4 g; EtOAc/MeOH, 70:30–0:100). The purification of these fractions over silica gel and sephadex LH-20 yielded eighteen compounds.

III.3.2.1.1. Study of the fraction F1

Fraction F1 (43.6 g) was subjected to CC over silica gel, eluted with mixtures of *n*-hexane/CH₂Cl₂ and CH₂Cl₂/EtOAc of increasing polarities. Two hundred and eighty two (282) sub-fractions of 250 mL each, were obtained and combined according to their TLC profiles to give three subfractions labelled F1S1, F1S2 and F1S3 (Table 56).

Table 56: Chromatogram of fraction F1

Fractions	Elution systems	Observation
1-151 (F1S1, 18.4 g)	<i>n</i> -hexane/CH ₂ Cl ₂ (100:0–60:40)	Mixture of at least seven compounds including RH15, RHE1, RHE5, RH16 and RHE2
152-229 (F1S2, 14.8 g)	<i>n</i> -hexane/CH ₂ Cl ₂ (30:70–0:100); CH ₂ Cl ₂ /EtOAc (100:0–80:20)	Oily mixture of at least nine compounds including and RHE5
230-282 (F1S3, 3.2 g)	CH ₂ Cl ₂ /EtOAc (70:30)	Mixture of at least four compounds including RH5

CC of F1S1 using mixture of *n*-hexane/CH₂Cl₂ and CH₂Cl₂/EtOAc at increasing polarities led to the isolation of compound RH15 (42.6 mg; *n*-hexane/CH₂Cl₂, 98:2) as a white powder, compound RH16 (12.3 mg; *n*-hexane/CH₂Cl₂, 60:40) as a white powder, compound RHE1 (4.1 mg; *n*-hexane/CH₂Cl₂, 80:20) as yellow crystals and compound RHE2 (32.1 mg; *n*-hexane/CH₂Cl₂, 40:60) as a white powder. Compound RH5 (1.02 g) precipitated in subfraction F1S3 as a white powder.

III.3.2.1.2. Study of the fraction F2

Fraction F2 (65.3 g) was also subjected to successive silica gel CC and eluted with a mixture of *n*-hexane/EtOAc and EtOAc/MeOH of increasing polarities. One hundred and seventy six (176) sub-fractions of 500 mL each, were obtained and combined according to their TLC profiles to give three subfractions labelled F2S1, F2S2 and F2S3 (Table 57).

Table 57: Chromatogram of fraction F2

Fractions	Elution systems	Observation
1-88 (F2S1, 16.7 g)	<i>n</i> -hexane/EtOAc (100:0–80:20)	Mixture of at least six compounds including RH3, RH4 and RHE3
89-132 (F2S2, 32.7 g)	<i>n</i> -hexane/EtOAc (70:30–40:60)	Mixture of at least seven compounds in chlorophyll including RH6 and RH9
133-176 (F2S3, 9.8 g)	<i>n</i> -hexane/EtOAc (30:70–0:100); EtOAc/MeOH (100:0–90:10)	Mixture of at least five compounds including RHE7 and RH7 with a trail

F2S1 was subjected to silica gel CC using mixture of *n*-hexane/EtOAc and EtOAc/MeOH at increasing polarities to yield compound RH3 (4.8 mg; *n*-hexane/EtOAc, 95:5), compound RH4 (32.3 mg; *n*-hexane/EtOAc, 90:10), compound RHE3 (6.3 mg; *n*-hexane/EtOAc, 80:20) as white powders.

Column chromatography of F2S2 over silica gel using mixture of *n*-hexane/EtOAc and EtOAc/MeOH at increasing polarities gave compound RH6 (1.04 g; *n*-hexane/EtOAc, 65:35) and compound RH9 (13.2 mg; *n*-hexane/EtOAc, 60:40) as white powders.

F2S3 was subjected to CC over silica gel using mixture of *n*-hexane/EtOAc and EtOAc/MeOH at increasing polarities to obtain compound RHE7 (7.2 mg; *n*-hexane/EtOAc, 30:70) and compound RH7 (7.6 mg; EtOAc/MeOH, 90:10) as white powders.

III.3.2.1.3. Study of the fraction F3

Fraction F3 (19.2 g) was subjected to successive silica gel CC and eluted with a mixture of *n*-hexane/acetone and acetone/MeOH of increasing polarities. One hundred and

sixteen (116) sub-fractions of 500 mL each, were obtained and combined according to their TLC profiles to give three subfractions labelled F3S1, F3S2 and F3S3 (Table 58).

Table 58: Chromatogram of fraction F3

Fractions	Elution systems	Observation
1-32 (F3S1, 47.2 mg)	<i>n</i> -hexane/acetone (80:20–70:30)	Mixture of at least six compounds including RH11
33-79 (F3S2, 7.3 g)	<i>n</i> -hexane/acetone (60:40–30:70)	Complex mixture of at least eight compounds
80-116 (F3S3, 8.1 g)	<i>n</i> -hexane/EtOAc (30:70–0:100); EtOAc/MeOH (95:5–85:15)	Trail

CC of F3S1 on sephadex LH-20 eluted with the mixture CH₂Cl₂/MeOH (30:70) afforded compound RH11 (7.6 mg) as white powder.

III.3.2.1.3. Study of the fraction F4 and F5

Finally, fraction F4 (27.2 g) was subjected to CC over silica gel and eluted with the mixtures EtOAc/MeOH (100:0–0:100) and sephadex LH-20, eluted with CH₂Cl₂/MeOH (30:70) to afford compound RH20 (3.6 mg; EtOAc/MeOH, 95:5) as yellow powder and RH1 (10.3 mg; EtOAc/MeOH, 80:20) as white powder.

Fraction F5 (26.4 g) was an insoluble gum that was not further investigated.

III.3.2.2. Fractionation of crude extract and isolation of compounds from *N. latifolia*

A part of the extract (439.0 g) was successively and exhaustively extracted with *n*-hexane, CH₂Cl₂, EtOAc and *n*-butanol (1.5 L each) to give the *n*-hexane (16.4 g), CH₂Cl₂ (18.4 g), EtOAc (28.6 g) and *n*-butanol (91.8 g) soluble fractions along with a solid residue.

III.3.2.2.1. Study of the *n*-hexane fraction

The active *n*-hexane fraction (15.2 g) was chromatographed over silica gel eluting with *n*-hexane/acetone and acetone/MeOH mixtures of increasing polarity to give one hundred and ninety three (193) fractions of 125 mL each. These fractions were combined based on their TLC profiles into three subfractions labelled FH1, FH2 and FH3 (Table 59).

Table 59: Chromatogram of the *n*-hexane fraction

Fractions	Elution systems	Observation
1-61 (FH1, 5.4 g)	<i>n</i> -hexane/acetone (100:0–90:10)	Mixture of at least six compounds including WN2 and WN3
62-114 (FH2, 4.2 g)	<i>n</i> -hexane/acetone (80:20–60:40)	Complex mixture of at least seven compounds including WN1 and WN4
115-193 (FH3, 5.6 g)	<i>n</i> -hexane/acetone (60:40–0:100); acetone/MeOH (100:0–95:5)	Mixture of at least five compounds including WN5

CC of subfraction FH1 using mixture of *n*-hexane/acetone at increasing polarities led to the isolation of compound WN2 (18.3 mg; *n*-hexane/acetone, 90:10) and compound WN3 (4.1 mg; *n*-hexane/acetone, 90:10) as white powders.

Subfraction FH2 was purified over silica gel using mixture of *n*-hexane/acetone at increasing polarities to give compound WN1 (4.6 mg; *n*-hexane/acetone, 80:20) and compound WN4 (4.3 mg; *n*-hexane/acetone, 70:30) as white powders.

Subfraction FH3 was subjected to CC over silica gel and isocratically eluted with *n*-hexane/acetone (60:40), followed by purification on sephadex LH-20, eluted with CH₂Cl₂/MeOH (30:70) to afford compound WN5 (4.4 mg, *n*-hexane/acetone, 40:60) as white powder.

III.3.2.2.2. Study of the dichloromethane fraction

The CH₂Cl₂ fraction (17.1 g) was subjected to CC over silica gel eluting with *n*-hexane/CH₂Cl₂ and CH₂Cl₂/acetone mixtures of increasing polarities to give one hundred and ninety two (192) fractions of 125 mL each. These fractions were combined on the basis of their TLC profiles into three subfractions labelled FC1, FC2 and FC3 (Table 60).

Table 60: Chromatogram of the dichloromethane fraction

Fractions	Elution systems	Observation
1-86 (FC1, 8.4 g)	<i>n</i> -hexane/CH ₂ Cl ₂ (70:30–0:100); CH ₂ Cl ₂ /acetone (100:0–90:10)	Complex mixture of at least twelve compounds including WN14 and WN15
87-140 (FC2, 3.4 g)	CH ₂ Cl ₂ /acetone (90:10–30:70)	Complex mixture of at least ten compounds including WN17 with a trail
142-192 (FC3, 5.6 g)	CH ₂ Cl ₂ /acetone (30:70–0:100); Acetone/MeOH (90:10–0:100)	Complex mixture of at least eight compounds with a trail

CC of subfraction FC1 over silica gel using mixtures of *n*-hexane/CH₂Cl₂, CH₂Cl₂/acetone at increasing polarities led to the isolation of compound WN14 (48.2 mg; *n*-hexane/CH₂Cl₂, 30:70) and compound WN15 (102.6 mg; CH₂Cl₂/acetone, 95:5) as colourless crystals. Subfraction FC2 (3.4 g; CH₂Cl₂/acetone, 90:10–30:70) was purified using silica gel followed by sephadex LH-20, eluting with CH₂Cl₂/MeOH (30:70) to give compound WN17 (3.8 mg; CH₂Cl₂/acetone, 90:10) as orange crystals.

III.3.2.2.3. Study of the ethyl acetate fraction

The EtOAc fraction (27.3 g) was subjected to CC over silica gel eluting with CH₂Cl₂/acetone and acetone/MeOH solvent systems of increasing polarities to give one

hundred and eighteen (118) fractions of 250 mL each. These fractions were combined based on their TLC profiles into three subfractions labelled FA1, FA2 and FA3 (Table 61).

Table 61: Chromatogram of the ethyl acetate fraction

Fractions	Elution systems	Observation
1-53 (FA1, 6.1 g)	CH ₂ Cl ₂ /acetone (100:0–70:30)	Complex mixture of at least fifteen compounds including WN32
54-82 (FA2, 14.7 g)	CH ₂ Cl ₂ /acetone (70:30–30:70); acetone/MeOH (100:0–95:5)	Complex mixture of at least eleven compounds including WN34 and WN36
83-118 (FA3, 4.3 g)	acetone/MeOH (95:5–80:20)	Trail

CC of subfraction FA1 over silica gel using mixtures of CH₂Cl₂/acetone at increasing polarities led to the isolation of compound WN32 (3.8 mg; CH₂Cl₂/acetone, 90:10) as white powder. Subfraction FC2 was subjected to CC over silica gel using mixture of CH₂Cl₂/acetone and acetone/MeOH at increasing polarities to give compound WN34 (5.6 mg; CH₂Cl₂/acetone, 90:10) and compound WN36 (1.02 g; CH₂Cl₂/acetone, 80:20) as colourless crystals.

III.3.2.2.4. Study of the *n*-butanol fraction

The *n*-butanol fraction (90.3 g) was subjected to CC over silica gel using EtOAc/MeOH (95:5–0:100) to yield sixty eight (68) fractions of 500 mL each. They were combined based on their TLC profiles into four subfractions labelled FB1 to FB4 (Table 62).

Table 62: Chromatogram of the *n*-butanol fraction

Fractions	Elution systems	Observation
1-19 (FB1, 7.4 g)	EtOAc/MeOH (95:5–90:10)	Mixture of at least four compounds with a trail
20-39 (FB2, 12.8 g)	EtOAc/MeOH (90:10–60:40)	Mixture of at least six compounds including NLB3 and NLB4 with a trail
40-50 (FB3, 15.6 g)	EtOAc/MeOH (50:50–40:60)	Complex mixture of at least eight compounds with a trail
51-68 (FB4, 40.6 g)	EtOAc/MeOH (30:70–0:100)	Trail

CC over silica gel of the subfraction FB2 using mixture of EtOAc/MeOH at different polarities followed by sephadex LH-20, eluting with MeOH, yielded compound NLB3 (17.2 mg; EtOAc/MeOH, 80:20) and compound NLB4 (18.1 mg; EtOAc/MeOH, 70:30) as chesnut pastes.

III.3.2.3. Fractionation of crude extract and isolation of compounds from *B. leptobotrys*

✚ Trunk bark of *B. leptobotrys*

Part of the extract (~124.8 g) was separated on CC over silica gel and *n*-hexane, EtOAc and MeOH solvent systems of increasing polarities. Two hundred and ten (210) fractions of 500 mL each were obtained and combined based on their TLC profiles into five fractions labelled FT1 (35.4 g; *n*-hexane/EtOAc, 100:0–80:20), FT2 (38.6 g; *n*-hexane/EtOAc, 80:20–60:40), FT3 (10.2 g; *n*-hexane/EtOAc, 50:50–30:70), FT4 (12.4 g; EtOAc/MeOH, 100:0–90:10) and FT5 (21.3 g; EtOAc/MeOH, 80:20–0:100) (Table 63).

Table 63: Chromatogram of the trunk bark crude extract of *B. leptobotrys*

Fractions	Elution systems	Observation
1-42 (FT1, 35.4 g)	<i>n</i> -hexane/EtOAc (100:0–80:20)	Mixture of at least ten compounds
43-129 (FT2, 38.6 g)	<i>n</i> -hexane/EtOAc (80:20–60:40)	Mixture of at least six compounds with a trail
130-157 (FT3, 10.2 g)	<i>n</i> -hexane/EtOAc (50:50–30:70)	Complex mixture of at least four compounds with a trail
158-163 (FT4, 12.4 g)	EtOAc/MeOH (100:0–90:10)	Complex mixture of at least six compounds with a trail
164-210 (FT5, 21.3 g)	EtOAc/MeOH (80:20–0:100)	Complex mixture of at least seven compounds with a trail

III.3.2.3.1. Study of the fraction FT1

The CC of fraction FT1 (35.4 g) over silica gel using mixtures of *n*-hexane/EtOAc (100:70–0:30) gave compound BLE34 (10.2 mg; *n*-hexane/EtOAc, 100:0), BLE30 (32.5 mg; *n*-hexane/EtOAc, 95:5), BLE1 (4.6 mg; *n*-hexane/EtOAc, 90:10) and BLE2 (42.6 mg; *n*-hexane/EtOAc, 90:10).

III.3.2.3.2. Study of the fraction FT2

The CC of fraction FT2 (38.6 g) over silica gel using mixtures of *n*-hexane/EtOAc (90:10–0:100) and EtOAc/MeOH (100:0–90:10) followed by sephadex LH-20 eluting with CH₂Cl₂/MeOH (30:70) yielded compounds BLEF32 (6.3 mg; *n*-hexane/EtOAc, 80:20), compound BLE4 (32.2 mg; *n*-hexane/EtOAc, 80:20), BLE8 (6.4 mg; *n*-hexane/EtOAc, 70:30) and BLE10 (21.4 mg; *n*-hexane/EtOAc, 70:30).

III.3.2.3.3. Study of the fraction FT3

The CC of fraction FT3 (10.2 g) over silica gel using mixtures of *n*-hexane/acetone (100:0–30:70) and acetone/MeOH (100:0–90:10) afforded compounds BLE11 (15.3 mg; *n*-

hexane/acetone, 50:50) and BLE40 (21.6 mg; *n*-hexane/acetone, 30:70) which were not completely characterized.

III.3.2.3.4. Study of the fraction FT4

Fraction FT4 (12.2 g) was purified over silica gel using EtOAc/MeOH (100:0–70:30) to give compounds BLE19 (6.2 mg; EtOAc/MeOH, 95:5), BLE20 (4.6 mg; EtOAc/MeOH, 95:5) and BLE21 (4.6 mg; EtOAc/MeOH, 90:10).

III.3.2.3.5. Study of the fraction FT4

The CC of fraction FT5 (21.3 g) over silica gel using EtOAc/MeOH (90:10–0:100, v/v) afforded compound BLE22 (26.3 mg; EtOAc/MeOH, 80:20).

✚ Leaves of *B. leptobotrys*

Part of the leaves crude extract (98.1 g) was separated on CC using silica gel and *n*-hexane, EtOAc and MeOH solvent systems of increasing polarities. Two hundred and eight (208) fractions of 250 mL each were obtained and combined based on their TLC profiles into five fractions labelled FL1 (15.3 g; *n*-hexane/EtOAc, 100:0–80:20, v/v), FL2 (24.7 g; *n*-hexane/EtOAc, 80:20–40:60), FL3 (15.9 g; EtOAc/MeOH, 100:0–80:20), FL4 (14.4 g; EtOAc/MeOH/H₂O, 95:5:2–80:20:10) and FL5 (13.3 g; MeOH/H₂O, 95:5–90:10) (Table 64).

Table 64: Chromatogram of the leaves crude extract of *B. leptobotrys*

Fractions	Elution systems	Observation
1-78 (FL1, 15.3 g)	<i>n</i> -hexane/EtOAc (100:0–80:20)	Mixture of at least eight compounds
79-146 (FL2, 24.7 g)	<i>n</i> -hexane/EtOAc (80:20–40:60)	Mixture of at least ten compounds with chlorophyll
147-161 (FL3, 15.9 g)	EtOAc/MeOH (100:0–80:20)	Complex mixture of at least four compound with a green trail
162-180 (FL4, 14.4 g)	EtOAc/MeOH/H ₂ O (95:5:2–80:20:10)	Complex mixture of at least three compounds with a green trail
181-208 (FL5, 13.3 g)	MeOH/H ₂ O (95:5–90:10)	Trail

III.3.2.3.6. Study of the fraction FL1

The CC of fraction FL1 (15.3 g) over silica gel with *n*-hexane/EtOAc (100:0–60:30) solvent systems led to the isolation of compounds SNC1 (129.6 mg; *n*-hexane/EtOAc, 95:5), SNCL2 (12.6 mg; *n*-hexane/EtOAc, 95:5) and SNC2 (98.2 mg; *n*-hexane/EtOAc, 90:10).

III.3.2.3.7. Study of the fraction FL2

Fraction FL2 was purified over silica gel CC using *n*-hexane/EtOAc (95:5–40:60) to yield compounds SNC4 (5.7 mg; *n*-hexane/EtOAc, 85:15) and SNC6 (7.2 mg; *n*-hexane/EtOAc, 70:30).

III.3.2.3.8. Study of the fraction FL3

The CC of fraction FL3 over silica gel CC using *n*-hexane/EtOAc (70:30–30:70) and EtOAc/MeOH (100:0–80:20) afforded compound SNC11 (4.7 mg; *n*-hexane/EtOAc, 70:30).

III.3.2.3.9. Study of the fraction FL4 and FL5

Compound SNC10 (446.9 mg; EtOAc/MeOH/H₂O, 80:20:10) precipitated as a colourless crystals in fraction FL4 and FL5.

III.4. METHANOLYSIS

Compound RHE7 (1 mg) was heated with 0.9 N, HCl/MeOH, at 70°C during 24 h in a sealed small-volume vial. The reaction was monitored by TLC analysis and the reaction middle was analyzed using ESI-MS, to yield the long chain base peak at $[M+H]^+$ *m/z* 262.

III.5. EVALUATION OF BIOLOGICAL ACTIVITIES

III.5.1. Antileishmanial assay

The cryopreserved promastigote form of *Leishmania donovani* 1S (MHOM/SD/62/1S) was obtained from Bei Resources and was routinely maintained at the Antimicrobial and Biocontrol Agents Unit, University of Yaoundé 1, in M199 medium supplemented with 10% Heat-Inactivated Fetal Bovine Serum (HIFBS) (Sigma) with 100 IU/mL penicillin and 100 µg/mL streptomycin. The culture was maintained in 75 cm² cell culture flask at 28°C (Khanjani *et al.*, 2015) and checked for growth daily and sub-cultured everyday 72 h.

The antileishmanial effect of *R. hispida*, *N. latifolia* and *B. leptobotrys* crude extracts, some fractions and some isolated compounds on cultured *L. donovani* 1S (MHOM/SD/62/1S) promastigotes was evaluated using the resazurin colorimetric method as described by Siqueira-Neto *et al.* (2010). For this purpose, 4×10^5 promastigotes/mL/well were seeded in a 96 well microtiter plate and treated with different concentrations of extracts, fractions and isolated compounds for 72 h at 28°C. The viability rate of promastigotes had a direct relationship with the amount of pink resorufin that was produced through the reduction of blue resazurin by the dehydrogenase enzyme in the inner mitochondrial membrane of the living parasites. Briefly, the promastigotes from a logarithmic phase culture (4×10^5 cells/mL; 90 µL) were seeded in 96-well microtiter plates and were treated with 10 µL of inhibitors at

different concentrations. They were all assessed in triplicate at final concentrations of 100 $\mu\text{g/mL}$ –0.16 $\mu\text{g/mL}$ for extracts/fractions and 50 $\mu\text{g/mL}$ –0.08 $\mu\text{g/mL}$ for compounds and test plates were incubated for 28 h at 28°C, followed by the addition of 1 mg/mL resazurin. The negative and positive controls were 0.1% DMSO and amphotericin B (10–0.016 $\mu\text{g/mL}$), respectively. After an additional incubation for 44 h, plates were then read on a Magellan Infinite M200 fluorescence multi-well plate reader (Tecan) at an excitation and emission wave lengths of 530 and 590 nm, respectively.

III.5.2. Cytotoxicity assay

The cytotoxicity profile of the crude extract, fractions and compounds was assessed using the Alamar blue assay (Mosman, 1983) against Raw 264.7 cells duly cultivated in complete Dulbecco's Modified Eagle's Medium (DMEM) containing 13.5 g/L DMEM (Sigma Aldrich), 10% Fetal Bovine Serum (Sigma Aldrich), 0.2% sodium bicarbonate (w/v) (Sigma Aldrich) and 50 $\mu\text{g/mL}$ gentamycin (Sigma Aldrich). Globally, macrophages were seeded into 96-wells cell-culture flat-bottomed plates at a density of 104 cells in 100 μL of complete medium/well and incubated for 24 h at 37°C, 5% CO₂ to allow cell adhesion. 10 μL of each serially diluted test sample solutions were added and assay plates were then incubated for 48 h in same experimental conditions. Growth control (0.1% DMSO-100% growth) and positive control wells (Podophyllotoxin at 20 μM) were included in the experiment plates. Cell proliferation was checked by adding 10 μL of a stock solution of resazurin (0.15 mg/mL in sterile PBS) to each well followed by plates incubation during 4 h. Fluorescence was then read on a Tecan Infinite M200 fluorescence multi-well plate reader (Tecan) at an excitation/emission of 530/590 nm. Results were expressed as 50% cytotoxic concentration (CC₅₀) and selectivity indices (SI) (CC₅₀ Mammalian cell/IC₅₀ *Leishmania donovani*) were calculated for each tested substance.

The data were subjected to one-way analysis of variance (ANOVA) and results were presented as means \pm SD of the replicated values. Significant differences for multiple comparisons were determined by Waller Duncan post-Hoc test at $p \leq 0.05$ using the Statistical Package for the Social Sciences (SPSS, version 16.0) program.

III.5.3. Acute toxicity assay

The study was performed according to the protocol of OECD (2001), guideline 423. For this toxicity study, 9 adults, non-pregnant female rats were used. These animals were randomly divided into 3 groups of 3 animals each of which, group 1 taken as a test control, was treated with distilled water at a single dose of 10 mL/kg; the other two groups (test lots)

received the extract at the single doses of 2000 and 5000 mg/kg, respectively. The animals were starved from water 12 h before the start of the experiment and 4 h after. The oral administration of the extract and distilled water was done through a gastric tube. After administration, animals were observed individually for the first 4 h and daily for 14 days after treatment. Special care was taken during the first 30 min after administration of the substance. Any signs of immediate toxicity such as aggressiveness, mobility, possible tremors, changes in coat, convulsions and other apparent signs of toxicity were noted during the experiment as well as changes in body weight. At the end of the experiment, the animals were sacrificed, their organs (liver, kidneys, spleen, lungs and heart) were removed and weighed in order to perform an autopsy on a macroscopic scale (Figure 192).

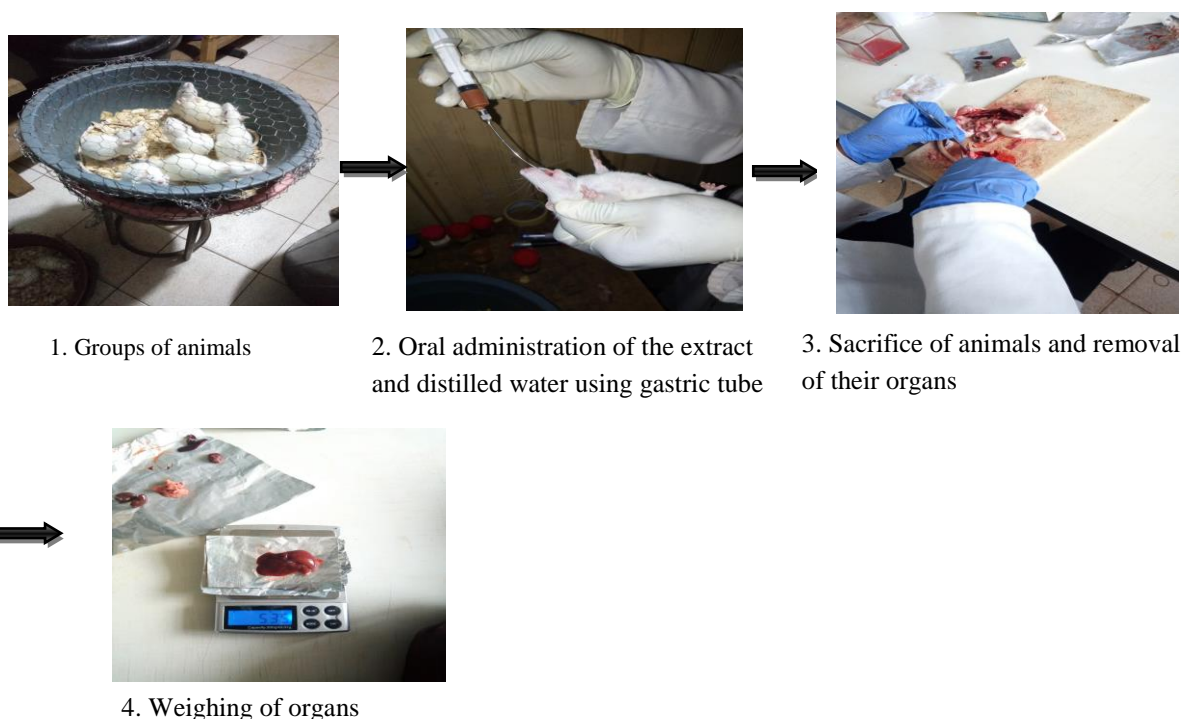


Figure 192: Steps involved in oral acute toxicity assay

III.5.4. Trial of preformulation

- Preparation of simple syrup

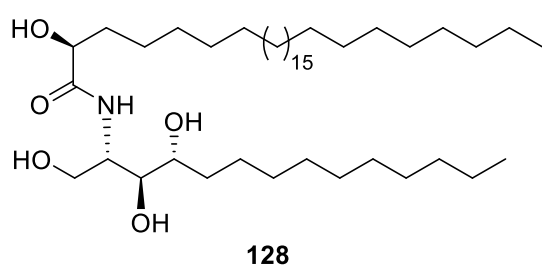
Introduce the previously weighed sugar powder into a conical flask with sufficient volume and then add a necessary and sufficient quantity of demineralized water. Heat the mixture to 50°C while stirring for about 1 hr, until a clear and homogeneous solution is obtained: this is simple syrup.

- Preparation of the phytodrug

Let the simple syrup cool then weigh it and deduce the mass of the active ingredient to be added to it, knowing that 0.0158% of extract corresponds to 99.0842% of simple syrup. Introduce a mass of active ingredient, previously weighed, into the simple syrup contained in a flask. Let the active ingredient dissolve until a limpid and homogeneous solution is obtained. Successively and gradually added the aroma, stabilizer and strawberry essence. The phytomedicine thus prepared is left to stand for 1 hr from time and finally bottled.

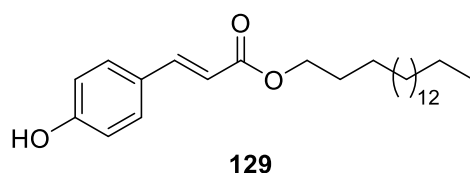
III.6. PHYSICAL AND CHEMICAL CHARACTERISTICS OF THE ISOLATED COMPOUNDS

Rothmanniamide



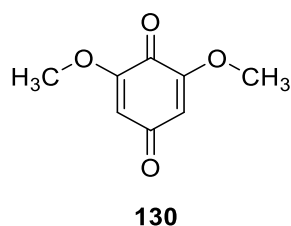
Molecular formula:	C ₄₄ H ₈₉ NO ₅
HRESI: [M+Na] ⁺	<i>m/z</i> 734.6636
Optical rotatory power	[α] _D ²² : -112.6
IR: OH	3333 cm ⁻¹
CH	2915 cm ⁻¹
NH	1618 cm ⁻¹
Physical aspect:	White powder
NMR ¹ H (methanol- <i>d</i> ₄ , 500 MHz):	Table 24
NMR ¹³ C (methanol- <i>d</i> ₄ , 125 MHz):	Table 24

n-Heptadecyl-4-hydroxy-trans-cinnamate



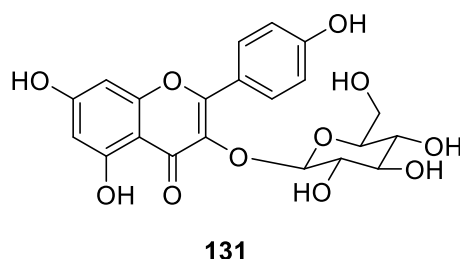
Molecular formula:	C ₂₆ H ₄₂ O ₃
HRESI: [M+Na] ⁺	<i>m/z</i> 425.3028
Physical aspect:	White powder
NMR ¹ H (pyridine- <i>d</i> ₅ , 500 MHz):	Table 25
NMR ¹³ C (pyridine- <i>d</i> ₅ , 125 MHz):	Table 25

2,6-dimethoxybenzoquinone



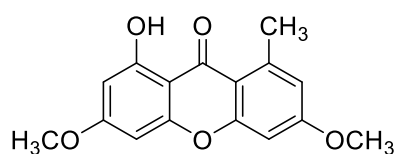
Molecular formula:	C ₈ H ₈ O ₄
HRESI: [2M+Na] ⁺	<i>m/z</i> 359.0788
Physical aspect:	Yellow crystals
mp	256°
NMR ¹ H (pyridine- <i>d</i> ₅ , 500 MHz):	Table 26
NMR ¹³ C (pyridine- <i>d</i> ₅ , 125 MHz):	Table 26

Kaempferol 3-O-β-D-glucopyranoside



Molecular formula:	C ₂₁ H ₂₀ O ₁₁
HRESI: [M+H] ⁺	<i>m/z</i> 287.0938
Physical aspect:	Yellow powder
mp	178°
NMR ¹ H (pyridine- <i>d</i> ₅ , 500 MHz):	Table 27
NMR ¹³ C (pyridine- <i>d</i> ₅ , 125 MHz):	Table 27

Lichexanthone



132

Molecular formula:

$C_{21}H_{20}O_{11}$

HRESI: $[M+H]^+$

m/z 287.0938

Physical aspect:

Yellow crystal

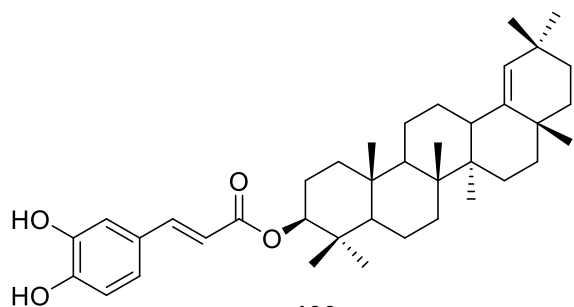
NMR 1H (pyridine- d_5 , 500 MHz):

Table 28

NMR ^{13}C (pyridine- d_5 , 125 MHz):

Table 28

Germanicol caffeoyl ester



133

Molecular formula:

$C_{39}H_{56}O_4$

HRESI: $[M+Na]^+$

m/z 611.4091

Physical aspect:

White powder

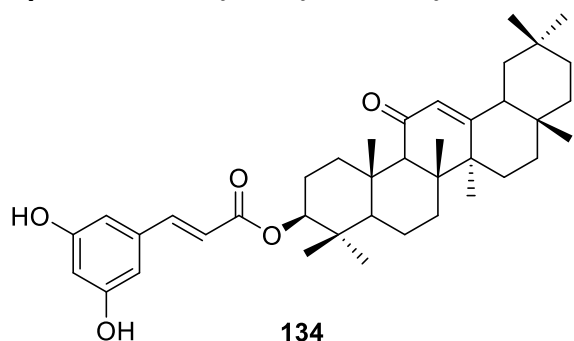
NMR 1H ($CDCl_3$, 500 MHz):

Table 29

NMR ^{13}C ($CDCl_3$, 125 MHz):

Table 29

3- β -O-E-3,5-dihydroxycinnamoyl-11-oxo-olean-12-ene



134

Molecular formula:

$C_{39}H_{54}O_5$

HRESI: $[M+H]^+$

m/z 603.4060

Physical aspect:

White powder

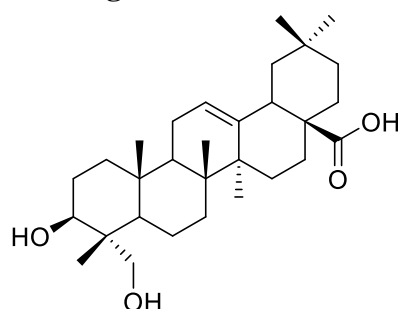
NMR 1H ($CDCl_3$, 500 MHz):

Table 30

NMR ^{13}C ($CDCl_3$, 125 MHz):

Table 30

Hederagenin



135

Molecular formula:

$C_{30}H_{48}O_4$

HRESI: $[M+Na]^+$

m/z 495.3487

Physical aspect:

White powder

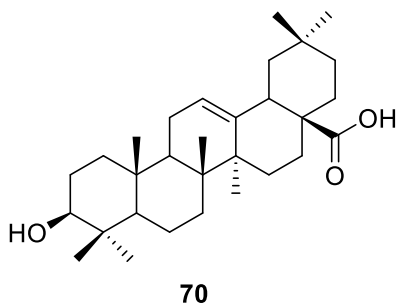
mp

332-334°

NMR ^{13}C (pyridine- d_5 , 125 MHz):

Table 31

Oleanolic acid



Molecular formula:

$C_{30}H_{50}O_2$

HRESI: $[M+Na]^+$

m/z 465.3694

Physical aspect:

White powder

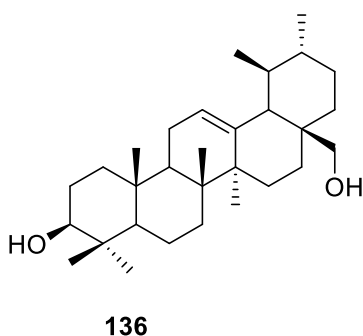
mp

306-308°

NMR ^{13}C ($CDCl_3$ /methanol- d_4 , 125 MHz):

Table 31

Uvaol



Molecular formula:

$C_{30}H_{50}O_2$

HRESI: $[M+Na]^+$

m/z 465.3694

Physical aspect:

White powder

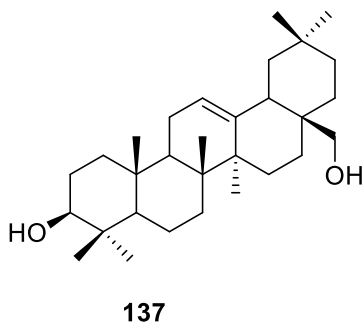
mp

232-233°

NMR ^{13}C ($CDCl_3$, 125 MHz):

Table 32

Erythrodiol



Molecular formula:

$C_{30}H_{50}O_2$

HRESI: $[M+Na]^+$

m/z 465.3694

Physical aspect:

White powder

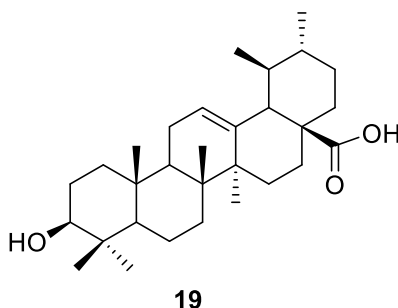
mp

230-231°

NMR ^{13}C ($CDCl_3$, 125 MHz):

Table 32

Ursolic acid



Molecular formula:

$C_{30}H_{48}O_3$

HRESI: $[M+Na]^+$

m/z 479.3542

Physical aspect:

White powder

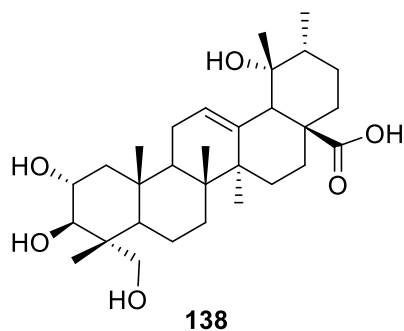
mp

285-288°

NMR ^{13}C (pyridine- d_5 , 125 MHz):

Table 33

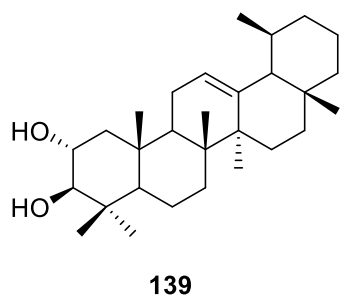
Myrianthic acid



Molecular formula:
Physical aspect:
NMR ^{13}C (pyridine- d_5 , 125 MHz):

$\text{C}_{30}\text{H}_{48}\text{O}_6$
White powder
Table 33

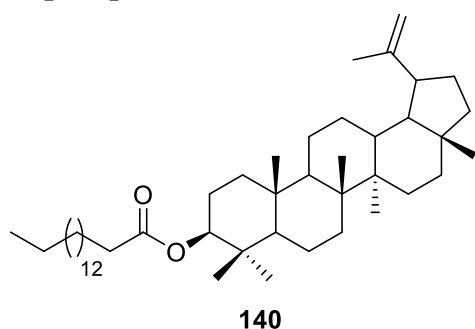
30-nor-2 α ,3 β -dihydroxyurs-12-ene (Carisursane A)



Molecular formula:
HRESI: $[\text{M}-\text{H}_2\text{O}+\text{H}]^+$
Physical aspect:
NMR ^{13}C (acetone- d_6 /methanol- d_4 ,
125 MHz):

$\text{C}_{29}\text{H}_{48}\text{O}_2$
 m/z 393.3564
White powder
Table 33

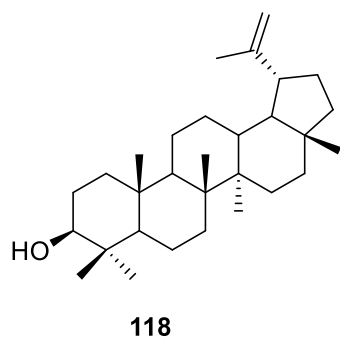
Lupeol palmitate



Molecular formula:
HRESI: $[\text{M}+\text{Na}]^+$
Physical aspect:
mp
NMR ^1H (CDCl_3 , 500 MHz):
NMR ^{13}C (CDCl_3 , 125 MHz):

$\text{C}_{46}\text{H}_{80}\text{O}_2$
 m/z 687.6055
White powder
52-56°
Table 35
Table 34

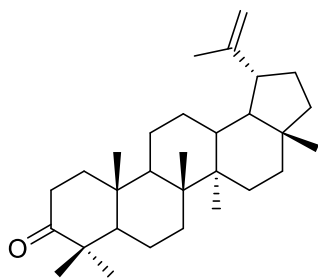
Lupeol



Molecular formula:
Physical aspect:
mp
NMR ^{13}C (CDCl_3 , 125 MHz):

$\text{C}_{30}\text{H}_{50}\text{O}$
White powder
215-216°
Table 35

Lupenone

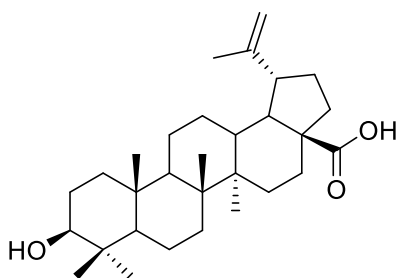


141

Molecular formula:
HRESI: $[M+Na]^+$
Physical aspect:
mp
NMR ^{13}C ($CDCl_3$, 125 MHz):

$C_{30}H_{48}O$
 m/z 447.3590
White powder
165-167°
Table 35

Betulinic acid

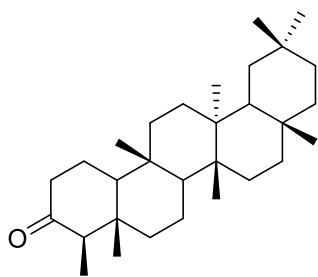


64

Molecular formula:
Physical aspect:
mp
NMR ^{13}C (pyridine- d_5 , 125 MHz):

$C_{30}H_{48}O_3$
White powder
316-318°
Table 35

Friedelin

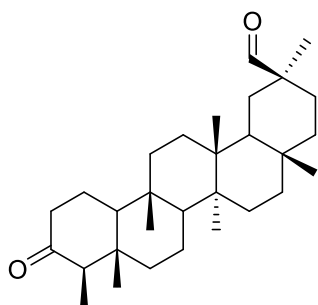


116

Molecular formula:
HRESI: $[M+Na]^+$
Physical aspect:
mp
NMR 1H ($CDCl_3$, 500 MHz):
NMR ^{13}C ($CDCl_3$, 125 MHz):

$C_{30}H_{50}O$
 m/z 449.3767
White powder
262-265°
Table 36
Table 36

3-Oxofriedelan-29-al

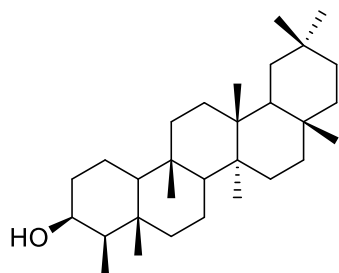


142

Molecular formula:
HRESI: $[M+Na]^+$
Physical aspect:

$C_{30}H_{52}O$
 m/z 463.3504
White powder

Friedelinol

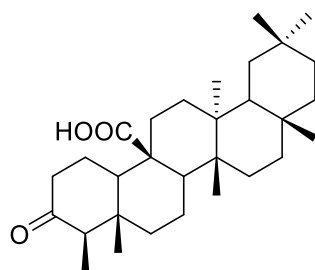


117

Molecular formula:
HRESI: $[M+Na]^+$
Physical aspect:
mp
NMR ^{13}C ($CDCl_3$, 125 MHz):

$C_{30}H_{48}O_2$
 m/z 463.3504
White powder
271-276°
Table 37

3-Oxofriedelan-25-oic

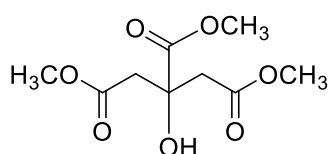


143

Molecular formula:
HRESI: $[2M+Na]^+$
Physical aspect:
NMR 1H (pyridine- d_5 , 500 MHz):
NMR ^{13}C (pyridine- d_5 , 125 MHz):

$C_{30}H_{48}O_3$
 m/z 935.7002
White powder
Table 37
Table 37

Trimethyl citrate

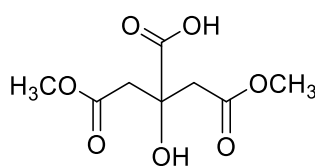


144

Molecular formula:
HRESI: $[M+Na]^+$
Physical aspect:
mp
NMR 1H ($CDCl_3$, 500 MHz):
NMR ^{13}C ($CDCl_3$, 125 MHz):

$C_9H_{14}O_7$
 m/z 257.0649
Colourless crystals
-55°
Table 38
Table 38

Dimethyl citrate

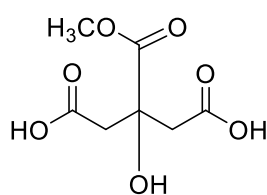


145

Molecular formula:
HRESI: $[M+Na]^+$
Physical aspect:
mp
NMR 1H (methanol- d_4 , 500 MHz):
NMR ^{13}C (methanol- d_4 , 125 MHz):

$C_8H_{12}O_7$
 m/z 243.0484
Colourless crystals
116°
Table 39
Table 39

Methyl citrate

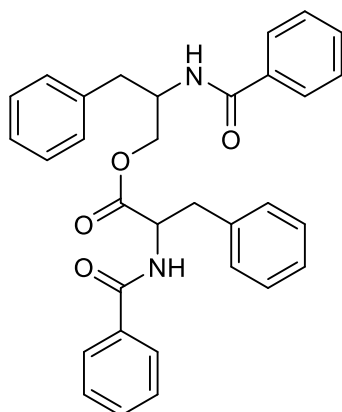


146

Molecular formula:
HRESI: $[M+Na]^+$
Physical aspect:
NMR 1H (methanol- d_4 , 500 MHz):
NMR ^{13}C (methanol- d_4 , 125 MHz):

$C_7H_{10}O_7$
 m/z 229.0302
Colourless crystals
Table 40
Table 40

***N*-benzoylphenylalaninyl *N*-benzoylphenylalaninate**



147

Molecular formula:

$C_{32}H_{30}N_2O_4$

HRESI: $[M+Na]^+$

m/z 507.2278

Physical aspect:

White powder

mp

209-210°

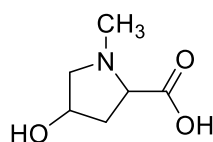
NMR 1H ($CDCl_3$, 500 MHz):

Table 41

NMR ^{13}C ($CDCl_3$, 125 MHz):

Table 41

4-Hydroxy-*N*-methylproline



148

Molecular formula:

$C_6H_{11}NO_3$

HRESI: $[M+Na]^+$

m/z 168.0683

Physical aspect:

Colourless crystals

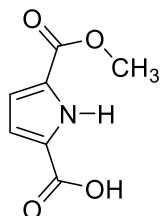
NMR 1H (D_2O , 500 MHz):

Table 42

NMR ^{13}C (D_2O , 125 MHz):

Table 42

Monomethyl ester of 1H-pyrrole-2,5-dicarboxylic acid



149

Molecular formula:

$C_7H_7NO_4$

HRESI: $[3M+Na]^+$

m/z 530.1056

Physical aspect:

Orange crystals

mp

241-242°

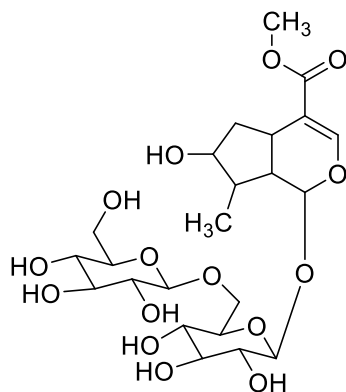
NMR 1H (methanol- d_4 , 500 MHz):

Table 43

NMR ^{13}C (methanol- d_4 , 125 MHz):

Table 43

Loganin 6'-O- β -glucopyranoside



150

Molecular formula:

$C_{23}H_{36}O_{15}$

HRESI: $[M+Na]^+$

m/z 575.1946

Physical aspect:

Chesnut paste

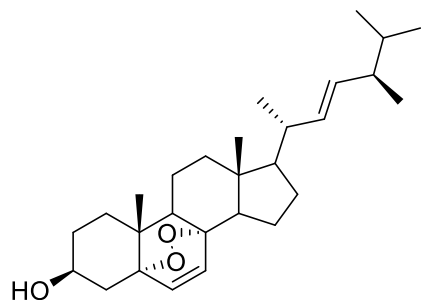
NMR 1H (methanol- d_4 , 500 MHz):

Table 44

NMR ^{13}C (methanol- d_4 , 125 MHz):

Table 44

Ergosterol peroxide



151

Molecular formula:

$C_{28}H_{44}O_3$

ESI: $[M+Na]^+$

m/z 451.4

Physical aspect:

White powder

mp

176°

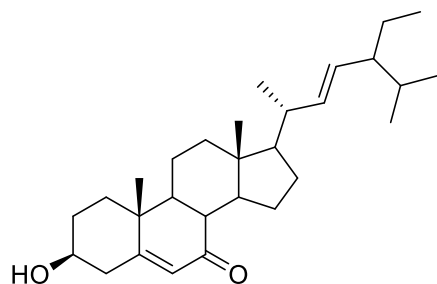
NMR 1H (methanol- d_4 , 500 MHz):

Table 45

NMR ^{13}C (methanol- d_4 , 125 MHz):

Table 45

7-Ketostigmasterol



152

Molecular formula:

$C_{29}H_{46}O_2$

ESI: $[M+Na]^+$

m/z 449.38

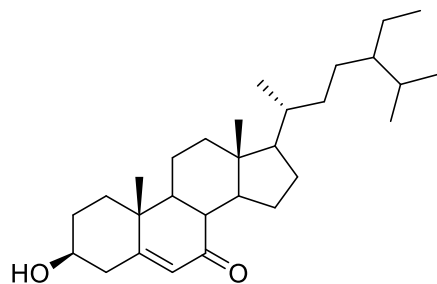
Physical aspect:

White powder

NMR ^{13}C (Acetone- d_6 , 125 MHz):

Table 46

7-Keto- β -sitosterol



153

Molecular formula:

$C_{29}H_{48}O_2$

ESI: $[M+Na]^+$

m/z 451.38

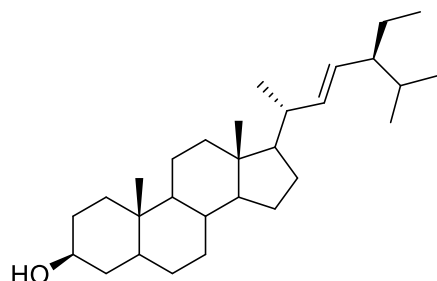
Physical aspect:

White powder

NMR ^{13}C (Acetone- d_6 , 125 MHz):

Table 46

Stigmasta-22-en-3-ol



154

Molecular formula:

$C_{29}H_{50}O$

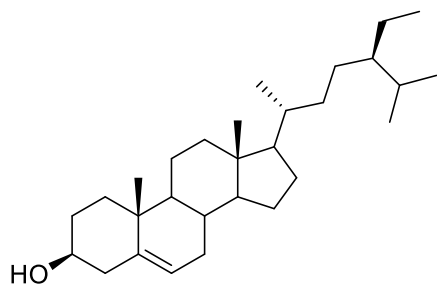
HRESI: $[2M+Na]^+$

m/z 851.7730

Physical aspect:

White powder

β -Sitosterol

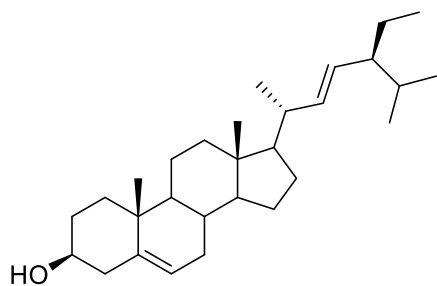


56

Molecular formula:
Physical aspect:

$C_{29}H_{50}O$
White powder

Stigmasterol

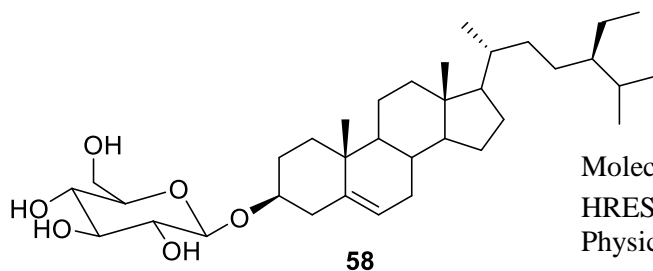


155

Molecular formula:
Physical aspect:

$C_{29}H_{48}O$
White powder

β -sitosterol-3-O- β -D-glucopyranoside

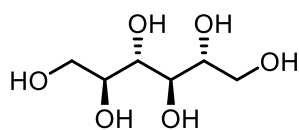


58

Molecular formula:
HRESI: $[M+Na]^+$
Physical aspect:

$C_{35}H_{60}O_6$
 m/z 599.4279
White powder

D-mannitol

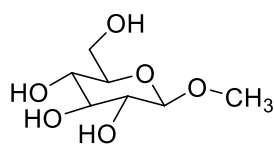


156

Molecular formula:
HRESI: $[2M+Na]^+$
Physical aspect:
mp
NMR 1H (DMSO- d_6 , 500 MHz):
NMR ^{13}C (DMSO- d_6 , 125 MHz):

$C_6H_{14}O_6$
 m/z 387.1494
White powder
164-169°
Table 47
Table 47

Methyl β -D-glucopyranoside

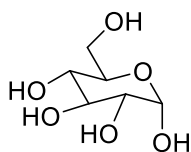


157

Molecular formula:
Physical aspect:
mp
NMR ^{13}C (methanol- d_4 , 125 MHz):

$C_6H_{14}O_6$
White powder
108-110°
Table 48

α -D-glucofuranoside

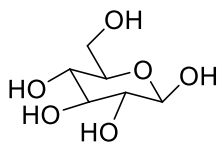


158

Molecular formula:
HRESI: $[M+Na]^+$
Physical aspect:
NMR ^{13}C (methanol- d_4 , 125 MHz):

$C_6H_{12}O_6$
 m/z 203.0572
Chesnut paste
Table 48

β -D-glucofuranoside

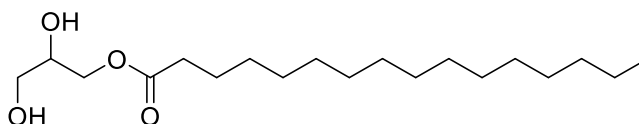


159

Molecular formula:
HRESI: $[M+Na]^+$
Physical aspect:
NMR ^{13}C (methanol- d_4 , 125 MHz):

$C_6H_{12}O_6$
 m/z 203.0572
Chesnut paste
Table 48

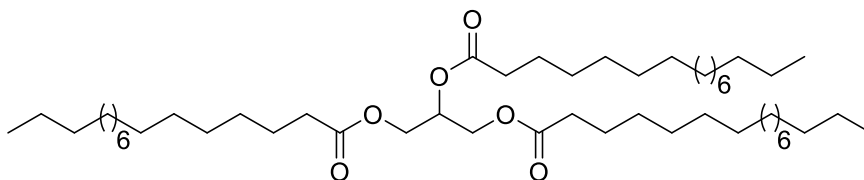
Glycerol palmitate



160

Molecular formula: $C_{19}H_{38}O_4$
HRESI: $[M+Na]^+$ m/z 353.2689
Physical aspect: White powder
mp $65-68^\circ$
NMR 1H ($CDCl_3$, 500 MHz): Table 49
NMR ^{13}C ($CDCl_3$, 125 MHz): Table 49

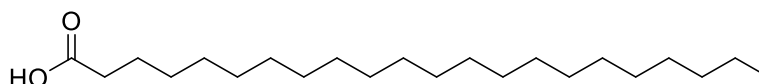
Glycerol tripalmitate



161

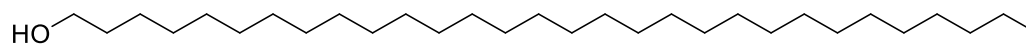
Molecular formula: $C_{51}H_{98}O_6$
Physical aspect: White powder
mp $44.7-67.4^\circ$
NMR 1H ($CDCl_3$, 500 MHz): Table 50
NMR ^{13}C ($CDCl_3$, 125 MHz): Table 50

Docosanoic acid



Molecular formula: **162** $C_{22}H_{44}O_2$
HRESI: $[M+Na]^+$ m/z 363.3317
Physical aspect: White powder
mp 80°

Triacontanol



163

Molecular formula:

$C_{30}H_{62}O$

HRESI: $[M+Na]^+$

m/z 461.4703

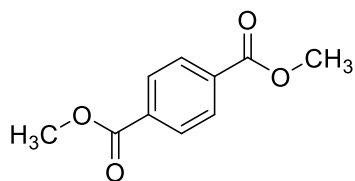
Physical aspect:

White powder

mp

87°

1,4-Dimethylbenzene-1,4-dicarboxylate



164

Molecular formula:

$C_{10}H_{10}O_4$

Physical aspect:

White powder

NMR 1H ($CDCl_3$, 500 MHz):

Table 51

NMR ^{13}C ($CDCl_3$, 125 MHz):

Table 51

REFERENCES

REFERENCES

- Abbasi I., Aramin S., Hailu A., Shiferaw W., Kassahun A., Belay S., Jaffe C., Warburg A., 2013. Evaluation of PCR procedures for detecting and quantifying *Leishmania donovani* DNA in large numbers of dried human blood samples from a visceral leishmaniasis focus in Northern Ethiopia. *BMC Infectious Diseases* **13**, 153.
- Abdel-Rahman N. A., Ismail I. A., Elshafe E. B. B., 2014. Characterization of some Sudanese edible forest fruits. *Journal of Agri-Food and Applied Sciences* **2**, 39-44.
- Abreu P., Pereira A., 2001. New indole alkaloids from *Sarcocephalus latifolius*. *Natural Product Letters* **15**, 43-48.
- Adelakun E., Okogun J. I., 1996. Flavonoid constituents of *Gardenia erubescens* stems. *Fitoterapia* **67**, 478.
- Adeniran O. I., Abimbade S. F., 2015. Characterization of compounds from leaf extracts of tree spinach-Cnidioscolus aconitifolius (Miller) I. M. Johnston. *International Journal of Scientific Research in Chemical Engineering* **1**, 82-86.
- Agnaniet H., Mbot E. J., Keita O., Fehrentz J.-A., Ankli A., Gallud A., Garcia M., Gary-Bobo M., Lebibi J., Cresteil T., 2016. Antidiabetic potential of two medicinal plants used in Gabonese folk medicine. *BMC Complementary and Alternative Medicine* **16**, 1-9.
- Agrawal P. K., 1992. NMR spectroscopy in the Structural identification of oligosaccharides and glycosides. *Phytochemistry* **31**, 3307-3330.
- Agyare C., Oguejiofor S., Bekoe E. O., Adu-Amoah L. and Boakye Y. D., 2016. Anti-inflammatory and anti-infective properties of ethanol leaf and root extracts of *Baphia nitida*. *British Microbiology Research Journal* **11**, 1-11.
- Ahua K M., Ioset J-R., Ioset N. K., Diallo D., Manuel J., Hostettman K., 2007. Antileishmanial activities associated with plants in the Malian traditional medicine. *Journal of Ethnopharmacology* **110**, 99-104.
- Akhoundi M., Kuhls K., Cannet A., Votýpka J., Marty P., Delaunay P., Sereno D., 2016. A historical overview of the classification, evolution and dispersion of *Leishmania* parasites and sandflies. *PLoS Neglected Tropical Diseases* **10**, 1-40.
- Alvar J., Yactayo S., Bern C., 2006. Leishmaniasis and poverty. *Trends in Parasitology* **22**, 552-557.
- Alvar J. I. D., Vélez C., Bern M., Herrero P., Desjeux J., Cano J., Jannin M., Den Boer M., 2012. Leishmaniasis worldwide and global estimates of its incidence. *PLoS One* **7**, e35671.

Andrade T. M., Carvalho E. M., Rocha H., 1990. Bacterial infections in patients with visceral leishmaniasis. *Journal of Infectious Diseases* **162**, 1354-1359.

Antai A. B., Ofem O. E., Nwosu O. J., Ukafia S. O., Iyadi K. C., Nia R., Osim E. E., 2010. Comparative effects of *Rothmannia hispida* leaves extract and protamine-Zinc insulin on alloxan-induced diabetic rats. *Journal of Biomedical Research* **13**, 47-54

Aquino R., de Tommasi N., Tapia M., Lauro M. R., Rastrelli L., 1999. New 3-methoxyflavones, an iridoid lactone and a flavonol from *Duroia hirsuta*. *Journal of Natural Products* **62**, 560-562.

Arnone A., Camarda L., Merlini L., Nasini G., Taylor D. A., 1981. Isoflavonoid constituents of the West African red wood *Baphia nitida*. *Phytochemistry* **20**, 799-801.

Ata A., Udenigwe C. C., Matochko W., Holloway P., Eze M. O., Uzoegwu P. N., 2009. Chemical constituents of *Nauclea latifolia* and their anti-GST and anti-fungal activities. *Natural Product Communications* **4**, 1185-1188.

Awosan E., Lawal I., Ajekigbe J., Borokini T., 2014. Antimicrobial potential of *Rothmannia longiflora* Salisb and *Canna indica* Linn extracts against selected strains of fungi and bacteria. *African Journal of Microbiology Research* **8**, 2376-2380.

Ayeleso A. O., Oguntibeju O. O., Brooks N. L., 2014. *In vitro* study on the antioxidant potentials of the leaves and fruits of *Nauclea latifolia*. *The Scientific World Journal* **2014**, 1-8.

Badiaga M., 2016. *Nauclea latifolia*: Ethnobotanique-phytochimie-activites biologiques. Éditions universitaires européennes, France, Pp 30-65.

Bankeu K. J. J., Kagho K. D. U., Fongang F. S. Y., Toghueo K. R. M., Mba'ning B. M., Feuya T. G. R., Fekam B. F., Tchouankeu J. C., Ngouela S. A., Sewald N., Lenta N. B., Ali S. M., 2019. Constituents from *Nauclea latifolia* with anti-*Haemophilus influenzae* Type b inhibitory activities. *Journal of Natural Products* **82**, 2580-2585.

Bankeu K. J. J., Madjouka S., Feuya R. T. G., Fongang S. F. Y., Siddiqui S., Iftikhar Ali, Mehreen L., Lenta N. B., Yousuf S., Nougoué T. D., Ngouela S. A., Ali. S M., 2018. Pobeguinine: a monoterpene indole alkaloid and other bioactive constituents from the stem bark of *Nauclea pobeguini*. *Zeitschrift für Naturforschung C* **73**, 335-344.

Bankeu J. J. K., Mustafa S. A. A., Gojayevev A. S., Lenta B. N., Nougoué D. T., Ngouela S. A., Assad K., Choudhary M. I., Prigge S., Guliyev A. A., Nkengfack A. E., Tsamo E., Ali M. S., 2010. Ceramide and cerebroside from the stem bark of *Ficus mucoso* (Moraceae). *Chemical and Pharmaceutical Bulletin* **58**, 1661-1665.

Bankeu K. J. J., Dawé A., Mbiantcha M., Feuya T. G. R., Ali I., Tchuenmogne T. M. A., Mehreen L., Lenta N. B., Ali S. M., Ngouela A. S., 2017. Characterization of bioactive compounds from *Ficus vallis-choudae* Delile (Moraceae). *Trends in Phytochemical Research* **1**, 235-242.

Bapela M. J., Kaiser M., Meyer J. J. M., 2017. Antileishmanial activity of selected South African plant species. *South African Journal of Botany* **108**, 342–345.

Batista J. C., Santin S. M. D. O., Schuquel I. T. A., Arruda L. L. M. D., Bersani-Amado C. A., Oliveira C. M. A. D., Kato L., Ferreira H. D., Silva C. C. D., 2014. Chemical constituents and evaluation of antioxidant and anti-inflammatory activities of roots of *Sabicea brasiliensis* wernh (Rubiaceae). *Quimica Nova* **37**, 638-642.

Beniddir A. M., 2012. Recherche de composés à activité antiplasmodiale à partir de la biodiversité malgache. Doctoral dissertation, Université Paris Sud, Paris XI, p 65.

Betancor C., Freire R., Gonzalez A. G., Salazar J. A., Pascard C., Prange T., 1980. Three triterpenes and other terpenoids from *Catha cassinoides*. *Phytochemistry* **19**, 1989-1993.

Betti J. L., Lejoly J., 2009. Contribution to the knowledge of medicinal plants of the Dja Biosphere Reserve, Cameroon: Plants used for treating jaundice. *Journal of Medicinal Plants Research* **3**, 1056-1065.

Borghi S. M., Fattori V., Conchon-Costa I., Pinge-Filho P., Pavanelli W. R., Verri W. A., 2017. Leishmania infection: painful or painless? *Parasitology Research* **116**, 465-475.

Borges F., Roleira F., Milhazes N., Santana L., Uriarte E., 2005. Simple coumarins and analogues in medicinal chemistry: occurrence, synthesis and biological activity. *Current Medicinal Chemistry* **12**, 887-916.

Boucherle B., Haudecoeur R., Ferreira Queiroz E., De Waard M., Wolfender J.-L., Robins R. J., Boumendjel A., 2016. *Nauclea latifolia*: biological activity and alkaloid phytochemistry of a West African tree. *Natural Product Reports* **33**, 1034-1043.

Boumendjel A., Sotoing Taiwe G., Ngo Bum E., Chabrol T., Beney C., Sinniger V., Haudecoeur R., Marcourt L., Challal S., Ferreira Queiroz E., Souard F., Le Borgne M., Lomberget T., Depaulis A., Lavaud C., Robins R. J., Wolfender J.-L., Bonaz B., De Waard M., 2013. Occurrence of the synthetic analgesic tramadol in an African medicinal plant. *Angewandte Chemie International Edition* **52**, 11780-11784

Bremer B., 2009. A review of molecular phylogenetic studies of Rubiaceae 1. *Annals of the Missouri Botanical Garden* **96**, 4-26.

Bremer B., Eriksson T., 2009. Time Tree of Rubiaceae: Phylogeny and dating the family, subfamilies and tribes. *International Journal of Plant Sciences* **170**, 766-793.

Brenzan M. A., Santos A. O., Nakamura C. V., Dias Filho B. P., Ueda-Nakamura T., Young M. C. M., Côrrea A. G., Júnior J. A., Morgado-Díaz J. A., Cortez D. A. G., 2012. Effects of (-) mammea A/BB isolated from *Calophyllum brasiliense* leaves and derivatives on mitochondrial membrane of *Leishmania amazonensis*. *Phytomedicine* **19**, 223-230.

Bringmann G., Hamm A., Kraus J., Ochse M., Noureldeen A., Jumbam D. N., 2001. Gardenamide A from *Rothmannia urcelliformis* (Rubiaceae). Isolation, absolute stereostructure, and biomimetic synthesis from genipine. *European Journal of Organic Chemistry* 2001, 1983-1987.

Bruneton J., 1999. Pharmacognosie, Phytochimie des plantes médicinales. 2^e Édition, Technique et Documentation Lavoisier, Paris, France, Pp 915-945.

Caesar L. K., Cech N. B., 2019. Synergy and antagonism in natural product extracts: when 1+1 does not equal 2. *Natural Product Reports* **36**, 869-888.

Calis I., Lahloub M. F., Sticher O., 1984. Loganin, loganic acid and periclymenoside, a new biosidic ester iridoid glucoside from *Lonicera periclymenum* L. (Caprifoliaceae). *Helvetica chimica acta* **67**, 160-165.

Camacho M. D. R., Phillipson J. D., Croft S. L., Solis P. N., Marshall, S. J., Ghazanfar S. A., 2003. Screening of plant extracts for antiprotozoal and cytotoxic activities. *Journal of ethnopharmacology* **89**, 185-191.

Cardoso L. C., Silva H. S. D., Castro-Gamboa I., Vanderlan da S. B., 2005. New biflavonoid and other flavonoids from the leaves of *Chimarrhis turbinata* and their antioxidant activities. *Journal of Brazilian Chemical Society* **16**, 1353-1359.

Carter H. E., Rothfus J. A., Gigg R., 1961. Biochemistry of the sphingolipids: XII. Conversion of cerebrosides to ceramides and sphingosine, structure of Gaucher cerebroside. *Journal of Lipids Research* **2**, 1-7.

Carvalho M. G., Cardozo M. R., Catundo F. E., Carvalho A. G., 2010. Chemicals constituents of *piptadenia gonoacantha* (Mart.). *Annals of the Brazilian Academy of Sciences*. **82**, 561-567.

Cateni F., Zilic J., Falsone G., Scialino G., Banfi E., 2003. New Cerebrosides from *Euphorbia peplis* L.: Antimicrobial activity evaluation. *Bioorganic and Medicinal Chemistry Letters* **13**, 4345-4350.

Chaabi M., Chabert P., Vonthron-Senecheau C., Weniger B., Ouattara M., Corstjens H., Sente I., Declercq L., Lobstein A., 2010. Acylated flavonol pentaglycosides from *Baphia nitida* leaves. *Phytochemistry Letters* **3**, 70-74.

Chaipukdee N., Kanokmedhakul K., Kanokmedhakul S., Lekphrom, Pyne S., 2016. Two new bioactive iridoids from *Rothmannia wittii*. *Fitoterapia* **113**, 97-101.

Chang S.-J., Lin T.-H., Chen C.-C., 2001. Constituents from the stems of *Dendrobium clavatum* var. *aurantiacum*. *Chinese Medicine* **12**, 211-218.

Cheek M., Kami E., Kami T., 2014. *Baphia vili* (Leguminosae: Papilionoideae), a new species from coastal thicket in the Republic of the Congo and Gabon. *Annals of the Botanic Garden and Botanical Museum Berlin* **44**, 39-44.

Chen L., Ma X., He J., Liu Y., Wang B., Yang Q., 2016. Anti-inflammatory activity of two new indole alkaloids from the stems of *Nauclea officinalis*. *Helvetica Chimica Acta* **99**, 742-746.

Choze R., Delprete P. G., Liao L. M., 2010. Chemotaxonomic significance of flavonoids, coumarins and triterpenes of *Augusta longifolia* (Spreng.) Rehder, Rubiaceae-Ixoroideae, with new insights about its systematic position within the family. *Revista Brasileira de Farmacognosia* **20**, 295-299.

Coley P. D., Lokvam J., Rudolph K., Bromberg K., Sackett T. E., Wright L., Brenes-Arguedas T., Dvoretz D., Ring S., Clark A., Baptiste C., Pennington R. T., Kursar T. A., 2005. Divergent defensive strategies of young leaves in two species of *Inga*. *Ecology* **86**, 2633-2643.

Conserva L. M., Jesu C. F. J., 2012. *Borreria* and *Spermacoce* species (Rubiaceae): a review of their ethnomedicinal properties, chemical constituents, and biological activities. *Pharmacognosy Reviews* **66**, 46-55

Croft S. L., Coombs G. H., 2003. Leishmaniasis-current chemotherapy and recent advances in the search for novel drugs. *Trends in Parasitology* **19**, 502-508.

Croft S. L., Seifert K., Yardley V., 2006. Current scenario of drug development for leishmaniasis. *Indian Journal of Medical Research* **123**, 399-410.

Croft S. L., Yardley V., 2002. Chemotherapy of leishmaniasis. *Current Pharmaceutical Design* **8**, 319-342.

Dacosta E., 2003. Les phytonutriments bioactifs. Yves Dacosta edition: Paris, p. 317.

da Silva E. R., Do Carmo M. C., Magalhães P. P., 2012. The leishmanicidal flavonols quercetin and quercitrin target *Leishmania (Leishmania) amazonensis* arginase. *Experimental Parasitology* **130**, 183-188.

da Silva V. C., De Oliveira F. A., da Silva B. V., Nasser L. M. A., 2007. New ent-Kaurane diterpene from stems of *Alibertia macrophylla* K. Schum. (Rubiaceae). *Helvetica Chimical acta* **90**, 1781-1785.

da Silva V. C., Giannini M. J. S. M., Carbone, V., Piacente S., Pizza C., Bolzani V. S., Lopes M. N., 2008. New antifungal terpenoid glycosides from *Alibertia edulis* (Rubiaceae). *Helvetica Chimica Acta* **91**, 1355-1362.

Daneshbod Y., Oryan A, Davarmanesh M., Shirian S., Negahban S., Aledavood A., Davarpanah M. A., Soleimanpoor H., Daneshbod K., 2011. Clinical, histopathologic, and cytologic diagnosis of mucosal leishmaniasis and literature review. *Archives of Pathology and Laboratory Medicine* **135**, 478-482.

de Sena P. V. S., De Oliveira C. B. S., Fumagalli F., da Silva E. F., da Silva N. B., De Andrade-Neto V. F., 2016. Cytotoxicity, hemolysis and *in vivo* acute toxicity of 2-hydroxy-3-anilino-1, 4-naphthoquinone derivatives. *Toxicology Reports* **3**, 756-762.

Desjeux P., 2004. Leishmaniasis: current situation and new perspectives. *Comparative Immunology, Microbiology and Infectious diseases* **27**, 305-318.

Dondji B., Dereure J., Pratlong F., Duhlińska D. D., Same-Ekobo A., Dedet J. P., 1998. Characterisation of *Leishmania major* causing cutaneous leishmaniasis in northern Cameroon. *Transactions of the Royal Society of Tropical Medicine and Hygiene* **92**, 677-678.

Dondji B., Dereure J., Poste B., Same-Ekobo A., Dedet J. P., 2001. Visceral leishmaniasis in Cameroon. Seroepidemiological survey in the Kousseri area, northern Cameroon. *Bulletin de la Société de Pathologie Exotique* **94**, 418-420.

Di Giorgio C., Lamidi M., Delmas F., Balansard G., Ollivier E., 2006. Antileishmanial activity of quinovic acid glycosides and cadambine acid isolated from *Nauclea diderrichii*. *Planta Medica* **72**, 1396-1402.

Dinda B., Debnath S., Majumder S., Arima S., Sato N., Harigaya Y., 2005. Chemical constituents of *Mussaenda incana*. *Indian Journal of Chemistry* **44B**, 2362-2366.

Do Socorro R. M. S., Mendonça-Filho R. R., Bizzo H. R., De Almeida R. I., Soares R. M., Souto-Pradrón T., Alviano C. S., Lopes A. H., 2003. Antileishmanial activity of a linalol-rich essential oil from *Croton cajucara*. *Antimicrobial Agents and Chemotherapy* **47**, 1895-1901.

Dongfack M. D. J., Van-dufat H. T., Lallemand M-C., Wansi J. D., Seguin E., Tillequin F., Wandji J., 2008. New Triterpenoids from the stem barks of *Drypetes tessmanniana*. *Chemical and Pharmaceutical Bulletin* **56**, 1321-1323.

Dumaro C. A., Etim E., Ahmadu A. A., 2016. Anti-inflammatory constituents of *Randia hispida* K. Schum (Rubiaceae). *Planta Medica* **82**.

Dumaro C. A., Etim E., Ahmadu A. A., 2017. Anti-inflammatory constituents of *Randia hispida* K. Schum (Rubiaceae). *Journal of Chemical Pharmaceutical Sciences* **9**, 160-164.

Eder B., Walmir S. G., Lidihone H., Caroline T., Fernanda R. G., 2008. Bioactive pentacyclic triterpenes from the stems of *Combretum laxum*. *Molecules* **13**, 2717-2728.

El-Amin M. H., 1990. Trees and shrubs of the Sudan, Ithaca Press, England 1st edition, Pp. 106, 400, 451.

Eloff J. N., 1998. A sensitive and quick microplate method to determine the minimal inhibitory concentration of plant extracts for bacteria. *Planta Medica* **64**, 16-21.

Eyong K. O., Krohn K., Hussain H., Folefoc G. N., Nkengfack A. E., Schulz B., Hu Q., 2005. Newbouldiaquinone and newbouldiamide: a new naphthoquinone-anthraquinone coupled pigment and a new ceramide from *Newbouldia laevis*. *Chemical and Pharmaceutical Bulletin* **53**, 616-619.

Fabri R. L., Garcia R. A., Florencio J. R., de Carvalho L. O., Pinto N. D. C. C., Coimbra E. S., de Souza-Fagundes E. M., Ribeiro A, Scio E., 2014. Pentacyclic triterpenoids from *Mitracarpus frigidus* (Willd. ex Roem. & Schult.) K. Shum: *in vitro* cytotoxic and leishmanicidal and *in vivo* anti-inflammatory and antioxidative activities. *Medicinal Chemistry Research* **23**, 5294-5304.

Fadipe A. L., Haruna K., Mohammed I., 2014a. Antibacterial activity of 1,2-benzenedicarboxylic acid, dioctyl ester isolated from the ethyl acetate soluble sub-portion of the unripe fruits of *Nauclea latifolia*. *International Journal of Pure and Applied Bioscience* **2**, 223-230.

Fadipe A. L., 2014b. Isolation and characterization of di-(1-hexen-5-yl) phthalate and monoethyl phthalate from the ethyl acetate extract of unripe fruits of *Nauclea latifolia*. *International Journal of Biology, Pharmacy and Allied Sciences* **3**, 776-784.

Fadipe A. L., 2014. Some fatty acid esters of the ripe fruits of *Nauclea latifolia* (Family Rubiaceae). *International Journal of Research in Pharmacy and Chemistry* **4**, 783-788.

Fakae B. B., Campbell A. M., Barrett J., Scott I. M., Teesdale-Spittle P. H., Liebau E., Brophy P. M., 2000. Inhibition of glutathione S-transferases (GSTs) from parasitic nematodes by extracts from traditional Nigerian medicinal plants. *Phytotherapy Research* **14**, 630-634.

Fang-min Q., Bai-Lian L., Ying Z., Grany-Xiang Z., 2015. A new triterpenoid from the fruits of *Gardenia jasminoides* Var. *Radicans* Makino. *Natural Product Research* **29**, 633-637.

Fatin R. J., Wahab, R., Daud J. M., Sudin M., Rasat M. S., Sulaiman O., 2012. Study on methanolic extracts of *Nauclea subdita* (Korth) Steud. Heartwood parts for the total phenolic contents and free radical scavenging activities. *Current Research Journal of Biological Sciences* **4**, 600-607.

Feitosa A. D. O., Dias A. C. S., Ramos G. D. C., Bitencourt H. R., Siqueira J. E. S., Marinho P. S. B., Barison A., Ocampos F. M. M., Marinho A. M. D. R., 2016. Lethality of cytochalasin B and other compounds isolated from fungus *Aspergillus* sp. (Trichocomaceae) endophyte of *Bauhinia guianensis* (Fabaceae). *Revista Argentina de Microbiología* **48**, 259-263.

Fournet A. B., Barrios A. A., Munoz V., Hocquemiller R., Cave A., 1992. Effect of natural naphthoquinones in BALB/c mice infected with *Leishmania amazonensis* and *L. venezuelensis*. *Journal of Ethnopharmacology* **37**, 159-64.

Francisco L., Ignacio B., Augusto R., Fernando T., Sara R., José Q., Francisco E., Jaime B., 2006. Isolation, structure elucidation, total synthesis, and evaluation of new natural and synthetic ceramides on human SK-MEL-1 melanoma cells. *Journal of Medicinal Chemistry* **49**, 5830-5839.

Garg H. S., Mitra C. R., 1971. Roxburghonic acid-a friedelane triterpenoid keto acid of the leaf of *Putranjiva roxburghii*. *Phytochemistry* **10**, 865-869.

Gbile Z. O., Adesina S. K., 1987. Nigerian flora and its pharmaceutical potential. *Journal of Ethnopharmacology* **19**, 1-16.

Ghosh R., Manash D. C., Sarkar A., Antu D., Sandhu P., Dinda B., Akhter Y., Bhattacharjee S., Utpal D. C., 2017. Exploration of phytoconstituents from *Mussaenda roxburghii* and studies of their antibiofilm effect. *Chemistry & Biodiversity* **14**, e1700165.

Gidado A., Ameh D. A., Atawodi S. E., 2005. Effect of *Nauclea latifolia* leaves aqueous extracts on bloods glucose levels of normal and alloxan-induced diabetic rats. *African Journal of Biotechnology* **4**, 91-93.

Gilbert G., Boutique R., 1952. Mimosaceae et Papilionaceae. Flore du Congo Belge, du Rwanda et du Burundi. I.N.E.A.C. (Institut National pour l'Etude Agronomique du Congo Belge). Jardin Botanique National de Belgique, Bruxelles **3**, Pp. 167-227.

Göhre A., Toto-Nienguesse A. B., Futuro M., Neinhuis C., Lautenschläger T., 2016. Plants from disturbed savannah vegetation and their usage by Bakongo tribes in Uige, Northern Angola. *Journal of Ethnobiology and Ethnomedicine* **12**, 1-28.

Goijman G., Turrens F., Marini-Bettolo B., Stoppani O., 1984. Inhibition of growth and macromolecular biosynthesis in *Trypanosoma cruzi* by natural products. Effects of miconidine and tingenone. *Journal of Herbmmed Pharmacology* **44**, 361-370.

Grassmé H., Riethmüller J., Gulbins E., 2007. Biological aspects of ceramide-enriched membrane domains. *Progress in Lipid Research* **46**, 161-170.

Gunatilaka L., Sirimanne S. R., Sotheeswaran S., Nakanishi T., 1979. Studies on medicinal and related Plants of Sri Lank Part 2. Three new flavones from *Gardenia fosbergii* Bud exudate. *Journal of Chemical Research* **21**, 216-217.

Habib M. R., Nikkon F., Rahman M., Haque M. E., Karim M. R., 2007. Isolation of stigmasterol and β -sitosterol from methanolic extract of root bark of *Calotropis gigantea* (Linn). *Pakistan Journal of Biological Sciences* **10**, 4174-4176.

Hamerski L., Carbonezi C. A., Cavalheiro A. J., Bolzani V. D. S., Young M. C. M., 2005. Triterpenoid saponins from *Tocoyena brasiliensis* Mart. (Rubiaceae). *Química Nova*, **28**, 601-604.

Haudecoeur R., Peuchmaur M., Peres B., Rome M., Taiwe G. S., Boumendjel A., Boucherle B., 2018. Traditional uses, phytochemistry and pharmacological properties of African *Nauclea latifolia* species: a review. *Journal of Ethnopharmacology* **212**, 106-136.

He Z. D., Ma C. Y., Zhanga H. J., Tana G. T., Tameza P., 2005. Antimalarial constituents from *Nauclea orientalis* (L.) L. *Chemistry and Biodiversity* **2**, 1578-1386.

He D., Bernd R. T., Simoneit J. B., Jaffe R., 2015. Gas chromatography mass spectrometry based profiling of alkyl coumarates and ferulates in two species of cattail (*Typha domingensis* P. and *Typha latifolia* L.). *Phytochemistry Letters* **13**, 91-98

Hernandez-Galicia E., Calzada F., Roman-Ramos R., Alarcon-Aguilar F. J., 2007. Monoglycerides and fatty acids from *Ibervillea sonora* root: isolation and hypoglycemic activity. *Planta medica* **73**, 236-240.

Hiemenz J. W., Walsh T. J., 1996. Lipid formulations of amphotericin B: recent progress and future directions. *Clinical infectious diseases* **22**, 133-144.

Hong-Peng Y., Shen Q., Yan-Ping S., Li-Tong B., 2014. Triterpenoids from *Gentiana vietchiorun*. *Journal of Chemical and Pharmaceutical Research* **7**, 1986-1990.

Hottellier F., Delaveau P., 1975. Nauclefine et Nauclefine deux nouveaux alcaloïdes de type indoloquinolizidine isolés de *Nauclea latifolia*. *Phytochemistry* **14**, 1407-1409.

Hotellier F.; Pousset J. L., Delaveau P., 1980. Naucleidinal et épinaucleidinal: nouveaux alcaloïdes de *Nauclea latifolia*. *Phytochemistry* **19**, 1884-1885.

Hussain M., Sokomba E., Shok M., 1991. Pharmacological effects of *Gardenia erubescens* in mice, rats and cats. *Natural Journal of Pharmacognosy* **29**, 94-100.

Igoli J. O., Tsenongo S. N., Tor-Anyiin T. A., 2011. A Survey of anti-venomous, toxic and other plants used in some parts of Tivland, Nigeria. *International Journal of Medicinal and Aromatic Plants* **1**, 240-244.

Ihekwereme C. P., Agbata C. A., Chukwueze D. K., Agu C. S., 2016. *In vivo* evaluation of antiplasmodial activity of hydroethanolic stem extract of *Baphia pubescens* in *Plasmodium berghei* infected albino mice. *Journal of Hebmed Pharmacology* **5**, 149-152.

Ikram A., Versian M. A., Shamshad S., Ahmed S. K., Ali S. T., Faizi S., 2013. Ixorene, a new dammarane triterpene from the leaves of *Ixora coccinea* Linn. *Record of Natural Products* **7**, 302-306.

Isah M. B., Ibrahim M. A., Mohammed A., Aliyu A. B., Masola B., Coetzer H. T. T., 2016. Systematic review of pentacyclic triterpenes and their derivatives as chemotherapeutic agents against tropical parasitic diseases. *Parasitology* **143**, 1219-1231.

James O., Ugbede H. H., 2011. Hypocholesterolemic effects of *Nauclea latifolia* (Smith) fruits studied in albino rats. *International Journal of Tropical Disease and Health* **1**, 11-21.

Jansakul C., Intarit K., Itharat A., Phadungcharoen T., Ruangrunsi N., Merica A., Lange G. L., 1999. Biological activity of crude extract and saponin pseudoginsenoside-RT1 derived from the fruit of *Randia siamensis*. *Pharmaceutical Biology* **37**, 42-45.

Jansen P. C. M., 2005. *Rothmannia longiflora* Salisb. Plant Resources of Tropical Africa. In: Jansen P. C. M. & Cardon D. (Editors). Wageningen, Netherlands.

Jiofack T., Fokunang C., Guedje N., Kemeuze V., Fongnzossie E., Nkongmeneck B. A., Mapongmetsem P. M., Tsabang N., 2010. Ethnobotanical uses of medicinal plants of two ethnoecological regions of Cameroon. *International Journal of Medical Sciences* **2**, 60-79.

Joshi B. S., Singh K. L., Roy R., 1999. Complete assignments of ¹H and ¹³C NMR spectra of the pentacyclic triterpene hederagenin from *Nigella sativa* Linn. *Magnetic Resonance Chemistry* **37**, 295-298.

Joshi K. C., Singh P., Pardasani R. T., 1979. Chemical examination of the roots of *Gardenia turgida* Roxb. *Journal of Indian Chemical Society* **56**, 327-328.

JSTOR Global Plants, 2020. *Baphia leptobotrys* Harms [family Leguminosae-Papilionoideae].

Kanchanapoom T., Picheansoonthon C., Kasai R. Yamasaki K., 2001. New Glucosides from Thai medicinal plant *Balanophora Iatisepala*. *Natural medicines* **55**, 213-216.

Kapingu M. C., Magadula J. J., Mbwambo Z. H., Mulholland D. A., 2008. Puguflavanones A and B; prenylated flavanones from *Baphia puguensis*. *Natural Product Communications* **3**, 749-753.

Kapingu M. C., Magadula J. J., 2008. Prenylated xanthenes and a benzophenone from *Baphia kirkii*. *Natural Product Communications* **3**, 1501-1504.

Kaptue L., Zekeng L., Fomekong E., Nsangou A., Tagu J. P., Tchuela J., 1992. Visceral leishmaniasis in Cameroon. Report of various cases and clinical study in the region of Kousseri, far-north of Cameroon. *Bulletin de la Société de Pathologie Exotique* **85**, 156-158.

Kato A., Kato N., Miyauchi S., Minoshima Y., Adachi I., Ikeda K., Asano N., Watson A. A., Nash R. J., 2008. Iminosugars from *Baphia nitida* Lodd. *Phytochemistry* **69**, 1261-1265.

Kawatake S., Nakamura K., Inagaki M., Higuchi R., 2002. Isolation and structure determination of six glucocerebrosides from the starfish *Luidia maculate*. *Chemical and Pharmaceutical Bulletin* **50**, 1091-1096.

Keroletswe N., Runner R. T. M., Masesanea I. B., 2018. A New 3-Prenyl-2-flavene and other extractives from *Baphia massaiensis* and their antimicrobial activities. *Natural Product Communications* **13**, 435-438.

Kevric I., Cappel M. A., Keeling J. H., 2015. New world and old world *Leishmania* Infections: A practical review. *Dermatology Clinical* **33**, 579-593.

Khan M. G., Bhaskar K. R., Kikuchi M., Salam M. A., Akther T., Haque R., Mondal D., Hamano S., 2014. Comparison of PCR-based diagnoses for visceral leishmaniasis in Bangladesh. *Parasitology International* **6**, 327-331.

Khan M. R., Rutaihua D. S. D., Mhehe G. L., 2003. 1-(3-hydroxy-4-methoxy-5-methylphenyl) ethanone, a new compound from the stem bark of *Lamprothamnus zanguebaricus*. *Fitoterapia* **74**, 741-742.

Khanjani J. S., Farazmand A., Amin M., Doroodgar A., Shirzadi M., Razavi M., 2015. Methanolic extract's activity of *Artemisia absinthium*, *Vitex agnus-castus* and *Phytolaca Americana* against *Leishmania major* in vitro and in vivo. *International Archives of Health Sciences* **2**, 69-74.

King F. E., Jurd L., 1953. The chemistry of extractives from hardwoods. Part XII. The cyclitols and steroids of opepe (*Sarcocephalus diderrichii*). *Journal of Chemical Society* **1953**, 1192-1195.

Koagne R. R., Bitchagno M. G. T., Fobofou T. S. A., Konga S. I., Tamokou J. D., Wessjohann L. A., Tane P., 2017. Rothtalazepane, a new azepane from the wood of *Rothmannia talbotii* (Rubiaceae). *Natural Product Communications* **12**, 1435-1436.

Kobets T., Grekov I., Lipoldova M., 2012. Leishmaniasis: Prevention, parasite detection and treatment. *Current Medicinal Chemistry* **19**, 1443-1474.

Kolter T., Sandhoff K., 1999. Sphingolipids-Their metabolic pathways and the pathobiochemistry of neurodegenerative diseases, *Angewandte Chemie International* **38**, 1532-1568.

Kolter T., Sandhoff K., 2006. Sphingolipid metabolism diseases. *Biochimica et Biophysica Acta (BBA)-Biomembranes* **1758**, 2057-2079.

Kostalova D., Hrochova V., Suchy V., Budesinsky M., Ubik K., 1992. Two pyrrole acids from *Berberis koreana*. *Phytochemistry* **31**, 3669-3670.

Krishnamurti M., Seshadri T. R., Sharma N. D., 1972. Chemical investigation of Dikamali gum: isolation of two new flavones, dimethoxyand trimethoxy wogonins, *Indian Journal of Chemistry* **10**, 23-25.

Kuete V., Sandjo L. P., Mbaveng A. T., Seukep J. A., Ngadjui B. T., Efferth T., 2015. Cytotoxicity of selected Cameroonian medicinal plants and *Nauclea pobeguinii* towards multi-factorial drug-resistant cancer cells. *BMC Complementary and Alternative Medicine* **15**, 1-6.

Kumara P. M., Soujanya K. N., Ravikanth G., Vasudeva R., Ganeshaiyah K. N., Shaanker R. U., 2014. Rohitukine, a chromone alkaloid and a precursor of flavopiridol, is produced by endophytic fungi isolated from *Dysoxylum binectariferum* Hook and *Amoora rohituka* (Roxb). Wight & Arn. *Phytomedicine* **21**, 541-546.

Kuo Y.-H., Lo J.-M., Chan Y.-F., 2002. Cytotoxic components from the leaves of *Schefflera taiwaniana*. *Journal of Chinese Chemical Society* **49**, 427-431.

Kupchan S. M., Mang E. O., 1960. A Note on the Occurrence of 2,6-dimethoxybenzoquinone in *Rauwolfia vomitoria*. *Journal of Pharmaceutical Sciences* **49**, 257-258.

Lakshmana R. B., Lin S. J., Hou W. C., Lai Z. Y., Liu P. C., Hsu F. L., 2004. Antioxidant iridoid glucosides from *Wendlandia formosana*. *Natural Product Research* **18**, 357-364.

Latha P. G., Nayar M. N. S., Sing O. V., George K. R., Panikkar K. R., Pushpangadan P., 2001. Isolation of antigenotoxic ursolic acid from *Ixora coccinea* flowers. *Actualidades Biologicas* **23**, 21-24.

Leliebre-Lara V., Monzote Fidalgo L., Pferschy-Wenzig E. M., Kunert O., Nogueiras Lima C., Bauer R., 2016. *In vitro* antileishmanial activity of sterols from *Trametes versicolor* (Bres. Rivarden). *Molecules* **21**, 1045.

Lewis W. H., Elvis-Lewis M. P. F., 1977. Medical Botany Plants Affecting Man's Health. John Willey & Sons, New York, Pp 402-521.

Li N., Cao, L., Ding G., Xiao W., 2012. Antibacterial and antiviral effects of strictosamide. *Chinese Journal of Experimental Traditional Medical Formulae* **18**, 170-174.

Liang H., Zheng H., Chen S., 1991. Pigment from the flower of *Gardenia sootepensis*, *Yunnan Zhiwu Yanjiu* **6**, 1395-96.

Lima T. C., Souza R. J., Santos A. D., Moraes M. H., Biondo N. E., Barison A, Steindel M., Biavatti M. W., 2015. Evaluation of leishmanicidal and trypanocidal activities of phenolic compounds from *Calea uniflora* Less. *Natural Product Research* **30**, 551-557.

Ling S. K., Tanaka T., Kouno I., 2001. Iridoids from *Rothmannia macrophylla*. *Journal of Natural Products* **64**, 796-798.

Löfstrand S. D., Krüger A, Razafimandimbison S. G., Bremer B., 2014. Phylogeny and generic delimitations in the sister tribes Hymenodictyeae and Naucleaeae (Rubiaceae). *Systematic Botany* **39**, 304-315.

LPWG (The Legume Phylogeny Working Group), 2017. A new subfamily classification of the Leguminosae based on a taxonomically comprehensive phylogeny. *Taxon* **66**, 44-77.

Luciano J. H. S., Lima M. A. S., Souza E. B., Silveira E. R., 2004. Chemical constituents of *Alibertia myrciifolia* Spruce ex K. Schum. *Biochemical Systematics and Ecology* **32**, 1227-1229.

Lutton E. S., Fehl A. J., 1970. The polymorphism of odd and even saturated single acid triglycerides, C8–C22. *Lipids* **5**, 90-99.

MacLean S., Murray D. G., 1972. The constituents of *Nauclea diderrichii*. Part IV. Miscellaneous substances; biogenetic considerations. *Canadian Journal of Chemistry* **50**, 1496-1501.

Mahato S. B., Kundu A. P., 1994. NMR ¹³C spectra of pentacyclic triterpenoids. A compilation and some salient features. *Phytochemistry* **37**, 1517-1575.

Maitera O. N., Khann M. E., James T. F., 2011. Phytochemical analysis and the chemotherapeutics of leaves and stem-bark of *Nauclea latifolia* grown in Hong, Adamawa State Nigeria. *Asian Journal of Plant Science and Research* **1**, 16-22.

Makhija I. K., Vignesh H., Chandrashekar K. S., Richard L., Prasanna K. S., 2010. Isolation of 3β -16 α -dihydroxy-5-cholesten-21-al, *n*-docosanoic acid and stigmasterol from petroleum ether extract of stem bark of *Michelia champaca*. *Archives of Applied Science Research* **2**, 344-348.

Mallam D., Anuka J., Abdulkadir U., Magaji G., Chindo A., Sani B., 2016. Analgesic and anti-inflammatory activities of *Rothmannia longiflora* Salisb in mice and rats. *Journal of Pharmacy* **6**, 1-7.

Markham K. R., 1982. Techniques of flavonoids identification. (ed). Academic Press: New-york, Pp 39-88.

Marques G., Gutiérrez A., José C., 2008. Chemical composition of lignin and lipids from tagasaste (*Chamaecytisus proliferus* spp. *palmensis*). *Industrial Crops and Products* **28**, 29-36.

Martínez V., M., Corona M. M., Vélez C. S., Rodríguez-Hahn L., Joseph-Nathan P., 1988. Terpenoids from *Montonia diffusa*. *Journal of Natural Products* **51**, 793-796.

Martins D., Carrion L. L., Ramos D. F., Salome K. S., da Silva P. E. A., Barison A., Nunez C. V., 2013. Triterpenes and the antimycobacterial activity of *Duroia macrophylla* hube (Rubiaceae). *BioMed Research International* **2013**, 1-7.

Maruyama K., Terada K., Yamamoto Y., 1980. Synthesis of triacontanol via metathesis-hydroboration-isomerization-oxidation. *Journal of Organic Chemistry* **45**, 737-738.

Masuda Y., Mori K., 2005. Synthesis and absolute configuration of 6-hydroxylated new ceramides in human skin, ceramides B, 4, 7, and 8. *European Journal of Organic Chemistry* **22**, 4789-4800.

Mativandlela S. P. N., Lall N., Meyer J., 2006. Antibacterial, antifungal and antitubercular activity of the roots of *Pelargonium reniforme* (CURT) and *Pelargonium sidoides* (DC) (Geraniaceae) root extracts. *South African Journal of Botany* **72**, 232-237.

Mauro, N. M., 2006. Synthèse d'alcaloïdes biologiquement actifs: la (+)-anatoxine et la camptothécine. Thèse de Doctorat, Université Joseph Fourier Grenoble, France, Pp 1-179.

Medić S. M., Jasprica, I., Smolcic, B. A., Mornar, A., 2004. Optimization of chromatographic conditions in thin layer chromatography of flavonoids and phenolic acids. *Croatica Chemica Acta* **77**, 361-366.

Meffo B. Y., Krohn K., Hussain H., Dongo E., Schulz B., Hu Q., 2006. Tithoniaquinone A and Tithoniamide B: a new anthraquinone and a new ceramide from leaves of *Tithonia diversifolia*. *Zeitschrift für Naturforschung* **61b**, 78-82.

Merrill A. H., Sandhoff K., 2002. Sphingolipids: metabolism and cell signalling. In: *Biochemistry of Lipids, Lipoproteins and Membranes*, 4th Edition, Elsevier, Amsterdam, Netherlands, 373-407.

Mesia K., Cimanga R. K., Dhooche L., Cos P., Apers S., Totté J., Tona G. L., Pieters L., Vlietinck A. J., Maes L., 2010. Antimalarial activity and toxicity evaluation of a quantified *Nauclea pobeguinii* extract. *Journal of Ethnopharmacology* **131**, 10-16.

Michel A., 2004. Trees, shrubs and lianas of West African dry zones. Margraf Publishers GMBH, Paris, Pp 135-515

Minamino M., Sakaguchi I., Naka T., Ikeda N., Kato Y., Tomiyasu I., Yano I., Kobayashi K., 2003. Bacterial ceramides and sphingophospholipids induce apoptosis of human leukaemic cells. *Microbiology* **149**, 2071-2081.

Miranda M. L. D., Garcez F. R., Garcez W. S., 2015. Triterpenos e outros constituintes dos frutos d'*Enterolobium contortisiliquum* (Vell.) Morong (Fabaceae). *Revista Virtual de Quimica* **7**, 2597-2605.

Mishina V., Krishna S., Haynes K., Meade C., 2007. Artemisinins inhibit *Trypanosoma cruzi* and *Trypanosoma brucei rhodesiense* *in vitro* growth. *Antimicrobial Agents and Chemotherapy* **51**, 1852-1854.

Mishra B. B., Gour J. K., Kishore N., Singh R. K., Tripathi V., Tiwari V. K., 2013. An antileishmanial prenyloxy-naphthoquinone from roots of *Plumbago zeylanica*. *Natural Product Research* **27**, 480-485.

Mohammed A. M. A., Coombes P. H., Crouch N. R., Mulholland D. A., 2013. Chemical constituents from *Fadogia homblei* De Wild (Rubiaceae). *International Letters of Chemistry, Physics and Astronomy* **14**, 116-124.

Moon H. I., Oh J. S., Kim J. S., Chen P. C., Zee O. P., 2002. Phytochemical compounds from the underground parts of *Gardenia jasminoides* var. *radicans* Makino. *Korean Journal of Pharmacognosy* **33**, 1-4.

Moreira V. F., Vieirab I. J. C., Braz-Filho R., 2017. Angelocunhol: new erythroxylyane diterpene and other compounds from *Simira sampaioana* (Rubiaceae). *Journal of Brazilian Chemical Society* **28**, 152-157.

Mosmann T., 1993. Rapid colorimetric assay for cellular growth and survival application to proliferation and cytotoxicity assays. *Journal of Immunological Methods* **65**, 55-63.

Moss G., 1989. Nomenclature of steroids (Recommandations 1989). *Pure and Apply Chemistry* **61**, 1783-1822.

Muanda F. N., 2010. Identification de polyphénols, évaluation de leur activité antioxydante et étude de leurs propriétés biologiques. Thèse de Doctorat. Université Paul Verlaine-Metz, France, Pp 55-86.

Muhammad S. A., Syed A. I., Shakeel A., Emil L., 2007. A new germacranolide and a new ceramide from *Salvia nubicola* (Lamiaceae). *Zeitschrift für Naturforschung* **62b**, 1333-1338.

Muralidhar N., Krishna N., Kumar M. M., Rao C. B., Rao D. V., 2003. New sphingolipids from marine sponge *Iotrochota baculifera*. *Chemical and Pharmaceutical Bulletin* **51**, 1193-1195.

Muralidhar P., Kumar M. M., Krishna N., Rao C. B., Rao D. V., 2005. New sphingolipids and a sterol from a *Lobophytum* species of the Indian Ocean. *Chemical and Pharmaceutical Bulletin* **53**, 168-171.

Murray H. W., Berman J. D., Davies C. R., Saravia N. G., 2005. Advances in leishmaniasis. *The Lancet* **366**, 1561-1577.

Nahrstedt A., Rockenbach J., Wray V., 1995. Phenylpropanoid glycosides, a furanone glucoside and geniposidic acid from members of the *Rubiaceae*. *Phytochemistry* **39**, 375-378.

Naveen M., Kiran I., Itrat A., Abdul M., 2002. Sphingolipids from *Conyza Canadensis*. *Phytochemistry* **61**, 1005-1008.

Negi J. S., Bisht V. K., Singh P., Rawat M. S. M., Joshi G. P., 2013. Naturally occurring xanthenes: Chemistry and biology. *Journal of Applied Chemistry* **2013**, 1-9.

Ngnokam D., Ayafor J. F., Connolly J. D., Nuzillard J. M., 2003. Nauclefolinine: a new alkaloid from the roots of *Nauclea latifolia*. *Bulletin of the Chemical Society of Ethiopia* **17**, 173-176.

Ngo B. E., Taiwe G. S., Moto F. C. O., Ngoupaye G. T., Nkantchoua G. C. N., Pelanken M. M., Rakotonirina S. V., Rakotonirina A., 2009. Anticonvulsant, anxiolytic, and sedative properties of the roots of *Nauclea latifolia* Smith in mice. *Epilepsy and Behavior* **15**, 434-440.

Ngouateu O. B., Kollo P., Ravel C., Dereure J., Kamtchouing P., Same-Ekobo A., von Stebut E., Maurer M., Dondji B., 2012. Clinical features and epidemiology of cutaneous

leishmaniasis and *Leishmania major*/HIV co-infection in Cameroon: results of a large cross-sectional study. *Transactions of the Royal Society of Tropical Medicine and Hygiene* **106**, 137-142.

Nishiyama Y., Noda Y., Nakatani N., Shitan N., Sudo T., Kato A., Mutiso P. B. C., 2019. Structure of constituents isolated from the bark of *Cassipourea malosana* and their cytotoxicity against a human ovarian cell line. *Journal of Natural Medicines* **73**, 289-296.

Nkouayeb B. M. N., Azebaze A. G. B., Tabekoueng G. B., Tsopgni W. D. T., Lenta B. N., Frese M., Sewald N., Vardamides J. C., 2020. Chemical Constituents of *Nauclea vanderghuchtii*. *Natural Product Sciences* **26**, 144-150.

Nowak R., Drozd M., Mendyk E., Lemieszek M., Krakowiak O., Kisiel W., Rzeski W., Szewczyk K., 2016. A new method for the isolation of ergosterol and peroxyergosterol as active compounds of *Hygrophoropsis aurantiaca* and *in vitro* antiproliferative activity of isolated ergosterol peroxide. *Molecules* **21**, 946.

Nwaka S., Hudson A., 2006. Innovative lead discovery strategies for tropical diseases. *Nature Reviews Drug Discovery* **5**, 941-955.

Nworgu Z. A. M., Onwukaeme D. N., Afolayan A. J., Amaechina F. C., Ayinde B. A., 2008. Preliminary studies of blood pressure lowering effect of *N. latifolia* in rats. *African Journal of Pharmacy and Pharmacology* **2**, 37-41.

Nyemb J. N., Magnibou M. L., Talla E., Tchinda T. A., Tchuenguem T. R., Henoumont C., Laurent S., Mbafor T. J., 2018. Lipids constituents from *Gardenia aqualla* Stapf and Hutch. *Open Chemistry* **16**, 371-376.

OECD, 2001. Toxicité orale aiguë-méthode par classe de toxicité aiguë. Ligne directrice de l'OCDE pour les essais de produits chimiques, Ligne directrice 423, p 14.

Ogunwa T. H., Adeyelu T. T., Fasimoye R. Y., Oyewale M. B., Ademoye T. A., Ilesanmi O. C., Sholanke D. R., Awe O. B., Ajiboye S. A., Oloye B. O., Ayenitaju F. C., 2017. Phytochemical profile and *in vitro* antioxidant properties of *Baphia pubescens* leaves. *Journal of Complementary and Alternative Medical Research* **4**, 1-10.

Omobuwajo O. R., Adesanya S. A. Babalola G. O., 1992. Isoflavonoids from *Pycnanthus angolensis* and *Baphia nitida*. *Phytochemistry* **31**, 1013-1014.

OMS (Organisation mondiale de la Santé), 2017. Leishmaniose, Aide-mémoire N°375.

Ono M., Ueno M., Masuoka C., Ikeda T., Nohara T., 2005. Iridoid glucosides from the fruit of *Genipa americana*. *Chemical and pharmaceutical bulletin* **53**, 1342-1344.

Onwukaeme N., 1995. Anti-inflammatory activities of flavonoids of *Baphia nitida* Lodd. (Leguminosae) on mice and rats. *Journal of ethnopharmacology* **46**, 121-124.

Onyekwere B. C., Onyekachi E. J-B., Izunwanne U. R., 2014. Isolation and Characterization of Baphianoside from the leaves of *Baphia nitida*. *Journal of Natural Sciences Research* **4**, 138-143.

Oryan A., 2015. Plant-derived compounds in treatment of leishmaniasis. *Iranian Journal of Veterinary Research* **16**, 1-19.

Pan L., Lezama-Davila C. M., Isaac-Marquez A. P., Calomeni E. P., Fuchs J. R., Satoskar A. R., Kinghorn A. D., 2012. Sterols with antileishmanial activity isolated from the roots of *Pentalinon andrieuxii*. *Phytochemistry* **82**, 128-135.

Parmar V. S., Bisht K. S., Sharma S. K., Jain R., Taneja P., Singh S., Simonsen O., Boll P. M., 1994. Highly oxygenated bioactive flavones from tamarix. *Phytochemistry* **36**, 507-511.

Parveen S., Saleem M., Rianza N., Ashrafab M., Qurat-ul-Ainb N. M. F., Jabbara A., 2016. New norterpenoids and a sphingolipid from *Carissa opaca*. *Journal of Asian Natural Products Research* **18**, 222-231

Passos C. S., Simões-Pires C., Nurisso A., Soldi T. C., Kato L., de Oliveira, C. M. A., de Faria E. O., Marcourt L., Gottfried C., Carrupt P.-A., Henriques A. T., 2013. Indole alkaloids of *Psychotria* as multifunctional cholinesterases and monoamine oxidases inhibitors. *Phytochemistry* **86**, 8-20.

Plassart L., 2015. *Sarcocephalus latifolius*: Etude botanique, chimique et pharmacologique; Thèse de Doctorat. Université de Rouen, France, Pp 11-69.

Radhika P., Rao V. L., Laatsch H., 2004. Chemical constituents of a marine soft coral of the genus *Lobophytum*. *Chemical and Pharmaceutical Bulletin* **52**, 1345-1348.

Ragasa C. Y., Espineli D. L., Shen C., 2011. New triterpenes from *Barringtonia asiatica*. *Chemical and Pharmaceutical Bulletin* **59**, 778-782.

Ragasa C.Y., Tan M. C. S., Fortin D. R., Shen C.-C., 2015. Chemical constituents of *Ixora philippinensis* merr. *Journal of Applied Pharmaceutical Science* **5**, 62-67.

Rahman T. U., Arfan M., Liaqat W., Uddin G., Choudhary M. I., 2014. Isolation of a novel indigoferamide-A from seeds of *Indigofera heterantha* Wall and its antibacterial activity. *Record of Natural Products* **8**, 412-416.

Ramos-Ligonio A., López-Monteon A., Trigos Á., 2012. Trypanocidal activity of ergosterol peroxide from *Pleurotus ostreatus*. *Phytotherapia Research* **26**, 938-943.

Reagan-Shaw S., Nihal M., Ahmad N., 2007. Dose translation from animal to human studies revisited. *The FASEB Journal* **22**, 659-661.

Reddy G. C. S., Ayengar K. N. N., Rangaswami S., 1973. Triterpenoids of *Gardenia turgida*. *Phytochemistry* **12**, 1831.

Reddy G. C. S., Ayengar K. N. N., Rangaswami S., 1975. Triterpenoids of *Gardenia latifolia*. *Phytochemistry* **14**, 307.

Reddy G. C. S., Rangaswami S., Sunder R., 1977. Triterpenoids of the stem bark of *Gardenia gummifera*. *Planta Medica* **32**, 206-211.

Reithinger R., Dujardin J. C., Louzir H., Pirmez C., Alexander B., Brooker S., 2007. Cutaneous leishmaniasis. *The Lancet Infectious Diseases* **7**, 581-596.

Sang S., Cheng X., Zhu N., Wang M., Jhoo J. W., Stark R. E., Badmaev V., Ghai G., Rosen R. T., Ho C. T., 2001. Iridoid glycosides from the leaves of *Morinda citrifolia*. *Journal of Natural products* **64**, 799-800.

Sangshetti J. N., Khan F. A. K., Kulkarni A. A., Arote, R., Patil R. H., 2015. Antileishmanial drug discovery: comprehensive review of the last 10 years. *Rsc Advances* **5**, 32376-32415.

Santana D. B., Da Costa R. C., Araújo R. M., De Paula J. E., Silveira E. R., Braz-Filho R., Espindola L. S., 2015. Activity of Fabaceae species extracts against fungi and *Leishmania*: vatacarpan as a novel potent anti-Candida agent. *Revista Brasileira de Farmacognosia* **25**, 401-406.

Sattar A. F., Ahmed F., Ahmed N., Sattar A. S., Malghani A. K. M., Choudarhy I. M., 2012. A doubled blind, randomized, clinical trial on the antileishmanial activity of a *Morinda citrifolia* (Noni) stem extract and its major constituents. *Natural Product Communications* **7**, 195-196.

Scuito S., Chillemi R., Piatelli M., Impellizzeri G., 1983. The identification of 4-hydroxy-N-methylproline in the red alga *chondria coerulescens*. *Phytochemistry* **22**, 2311-2312.

Shigemori H., Kagata T., Ishiyama H., Morah F., Ohsaki A., Kobayashi J., 2003. Naucleamides A-E, new monoterpene indole alkaloids from *Nauclea latifolia*. *Chemical and Pharmaceutical Bulletin* **51**, 58-61.

Silva S. M. A., Pinto A. G. C. D., 2005. Structure elucidation of xanthone derivatives: studies of nuclear magnetic resonance spectroscopy. *Current Medicinal Chemistry* **12**, 2481-2497.

Simo C. C., Kouam S. F., Poumale H. M., Simo I. K., Ngadjui B. T., Green I. R., Krohn K., 2008. Benjaminamide: a new ceramide and other compounds from the twigs of *Ficus benjamina* (Moraceae). *Biochemical Systematics and Ecology* **36**, 238-243.

Singh N., Mishra B. B., Bajpai S., Singh R. K., Tiwari V. K., 2014. Natural product based leads to fight against leishmaniasis. *Bioorganic and Medicinal Chemistry* **22**, 18-45.

Singh R. K., Pandey H. P., Sundar S., 2006. Visceral leishmaniasis (*kala-azar*): challenges ahead. *Indian Journal of Medical Research* **123**, 331-344.

Siqueira-Neto J. L., Song O. -R., Oh H., Sohn J. -H., Yang G., Nam J., Jang J., Cechetto J., Lee C. B., Moon S., Genovesio A., Chatelain E., Christophe T., Freitas J. L. H., 2010. Antileishmanial high-throughput drug screening reveals drug candidates with new scaffolds. *PLOS Neglected Tropical Disease* **4**, e675.

Soladoye M. O., 1985. A revision of *Baphia* (Leguminosae-Papilionoideae). *Kew Bulletin* **40**, 291-386.

Sonke B., Simo A. K., 1996. Systematic revision of the genus *Rothmannia* (Rubiaceae-Gardenieae) in Cameroon. *National Botanical Garden Belgium Bulletin* **65**, 219-247.

Sorensen J. L., 2010. The isolation of citric acid derivatives from *Aspergillus niger*. *FEMS Microbiology Letters* **306**, 123-124.

Sosa A. M., Amaya S., Salamanca C. E., Gilabert M., Bardón A., Giménez A., Vera N. R., Borkosky S. A., 2016. Active sesquiterpene lactones against *Leishmania amazonensis* and *Leishmania braziliensis*. *Natural Product Research* **30**, 2611-2615.

Sousa G., Duarte L., Alcântara A., Silva G., Vieira-Filho S., Silva R., Oliveira D., Takahashi J., 2012. New triterpenes from *Maytenus robusta*: Structural identification based on NMR experimental data and theoretical calculations. *Molecules* **17**, 13439-13456.

Staerk D., Lemmich E., Christensen J., Kharazmi A., Olsen C. E., Jaroszewski J. W., 2000. Leishmanicidal, antiplasmodial and cytotoxic activity of indole alkaloids from *Corynanthe pachyceras*. *Planta Medica* **66**, 31-536.

Stafford J. L., Neumann N. F., Belosevic M., 2002. Macrophage mediated innate host defense against protozoan parasites. *Critical Reviews in Microbiology* **28**, 187-248.

Sui-kiong L., Takashi T., Isao K., 2001. Iridoids from *Rothmannia macrophylla*. *Natural products* **64**, 796-798.

Suksamrarn A., Tanachatchairatana T., Kanokmedhakul S., 2003. Antiplasmodial triterpenes from twigs of *Gardenia saxatilis*. *Journal of Ethnopharmacology* **88**, 275-277.

Sun J. S., Tsuang Y. H., Huang W. C., Chen L. T., Hang Y. S., Lu F. J., 1997. Menadione-induced cytotoxicity to rat osteoblasts. *Cellular and Molecular Life Sciences* **53**, 967-976.

Sun J. Y., Lou H. X., Dai S. J., Xu H., Zhao F., Liu K., 2008. Indole alkaloids from *Nauclea officinalis* with weak antimalarial activity. *Phytochemistry* **69**, 1405-1410.

Sunderland T. C. H., Comiskey J. A., Besong S., Mboh H., Fonwebon J., Dione M. A., 2003. Vegetation assessment of Takamanda forest reserve, Cameroon. Smithsonian Institution.

Supaluk P., Puttirat S., Rungrot C., Somsak R., Virapong P., 2010. New bioactive triterpenoids and antimalarial activity of *Diospyros rubra* Lec. *EXCLI Journal* **9**, 1-10.

Taiwe G. S., Ngo Bum E., Talla E., Dimo T., Dawe A., Sinniger V., 2014. *Nauclea latifolia smith* (Rubiaceae) exerts antinociceptive effects in neuropathic pain induced by chronic constriction injury of the sciatic nerve. *Journal of Ethnopharmacology* **151**, 445-451.

Takahiro I., Tatsufumi O., Yosuke M., 2006. A ceramide and cerebroside from the starfish *Asterias amurensis* L. and their plant-growth promotion activities. *Journal of Natural Products* **69**, 1080-1082.

Takhtajan A., 2009. Class Magnoliopsida (Dicotyledons). Flowering Plants (Second edition). Springer, Pp. 518-519.

Tan A. M., Nicolo L. C., Alejandro J. D., Hiromitsu T., 2014. Chemotaxonomic relevance of the constituents from the leaves of *Rothmannia merrillii*. *Journal of Chemical and Pharmaceutical Research* **6**, 779-781.

Tateng A. N., Payne V. K., Ngouateu O. B., Kirstein O. D., Warburg A., von Stebut E., Maurer M., Dondji B., Krüger A., 2019. Inventory and taxonomy of phlebotomine sand flies of the Mokolo leishmaniasis focus, northern Cameroon, with description of new *Sergentomyia* taxa (Diptera: Psychodidae). *Acta tropica* **194**, 172-180.

Tchacondo T., Karou S. D., Batawila K., Agban A., Ouro-Bang'na K., Anani K. T., Gbeassor M., de Souza C., 2011. Herbal remedies and their adverse effects in Tem tribe traditional medicine in Togo. *African Journal of Traditional, Complementary and Alternative Medicines* **8**, 45-60.

Torres-Guerrero E., Quintanilla-Cedillo M. R., Ruiz-Esmenjaud J., Arenas R., 2017. Leishmaniasis: a review. *F1000Research* **6**, 1-38.

Towns A. M., 2014. Fertility and fontanel: women's knowledge of medicinal plants for reproductive health and childcare in Western Africa. Doctorat/PhD Thesis. Leiden University, Germany, p. 23.

Traore F. 1999. Evaluation de l'activité antimalarique de *Glinus oppositifolius* (L.), *Nauclea latifolia* (SM.), *Mitragyna inermis* (Willd), O. Kuntze, trois plantes-utilisées en médecine traditionnelle au Mali. Thèse de Doctorat, Marseille II, France, p.199.

Udenigwe C. C., Matochko W., Holloway P., Eze M. O., Uzoegwu P. N., 2009. Chemical constituents of *Nauclea latifolia* and their anti-GST and anti-fungal activities. *Natural Product Communications* **4**, 1185-1188.

Udia M., Antai B., Lapahand T., Ekeuwei B., 2013. Phytochemistry, proximate and elemental compositions of extracts from the leaves of *Rothmannia longiflora* and *Rothmannia hispida*. *Journal of Natural Products* **3**, 41-47.

Uddin G., Siddiqui B. S. H., Alam M., Sadat A., Ahmad A., Uddin A., 2011. Chemical constituents and phytotoxicity of solvent extracted fractions of stem bark of *Grewia optiva* Drummond ex burret. *Middle-East Journal of Scientific Research* **8**, 85-91.

Ullah N., Nadhman A., Siddiq S., Mehwish S., Islam A., Jafri L., Hamayun M., 2016. Plants as antileishmanial agents: current scenario. *Phytotherapy Research*, **30** 1905-1925.

Vaena de A. S., Jones J. A., Hannun Y. A., 2004. Ceramides in bioactive lipids, edited by Nicolaou A. and Kotkotos G., The oily press, Bridgwater, Pp 135-167.

Vance D. E., Vance J. E., 2008. Biochemistry of lipids, lipoproteins and membranes, 5th edition, Elsevier, Oxford, Paris, p. 624.

Viquar U. A., Javid H., Hidayat H., Umar F., Erum A., Sarfraz A. N., Muhammad I. C., 2004. Two ceramides from *Tanacetum artemesioides*. *Zeitschrift für Naturforschung* **59b**, 329-333.

Vivien J., Faure J. J., 2011. Arbres des forêts d'Afrique centrale. Ediprint, Saint Berthevin, France, p 945.

Wandji J., Tillequin F., Mulholland D. A., Shirri J. C., Tsabang N., Seguin E., Verite P., Libot F., Fomum Z. T., 2003. Pentacyclic triterpenoid and saponins from *Gambeya boukokoensis*. *Phytochemistry* **64**, 845-849.

Wang H.-Y., Liub K., Wang R.-X., Qina S.-H., Wang F.-L., Jing-Yong S., 2014. Two new triterpenoids from *Nauclea officinalis*. *Natural Product Research* **29**, 644-649.

Wei Y., Xie Q., Fisher D., Sutherland I. A., 2011. Separation of patuletin-3-O-glucoside, astragalin, quercetin, kaempferol and isorhamnetin from *Flaveria bidentis* (L.) Kuntze by elution-pump-out high-performance counter-current chromatography. *Journal of chromatography A* **1218**, 6206-6211.

Wertz P. W., Bergh V. D., 1998. The physical, chemical, and functional properties of lipids in the skin and other biological barriers. *Chemistry and Physics of lipids* **91**, 85-96.

WHO, 2000. Principes méthodiques généraux pour la recherche et l'évaluation relative à la médecine traditionnelle 2000: Résumé. WHO/EDT/TRMP. Organisation mondiale de la Santé, Genève, Suisse, p 87.

WHO, 2017. Global leishmaniasis update, 2006–2015: a turning point in leishmaniasis surveillance. *Weekly Epidemiological Record* **92**, 557-565.

WHO, 2020. Global leishmaniasis surveillance, 2017–2018, and first report on 5 additional indicators. *Weekly Epidemiological Record* **95**, 265-279.

Wouamba N. S. C., Happi M. G., Lenta N. B., Sewald N., Kouam F. S., 2020. Vernoguinaamide: a new ceramide and other compounds from the root of *Vernonia guineensis* Benth. and their chemophenetic significance. *Biochemical Systematics and Ecology* **88**, 103988.

Xu Y.-J., Foubert K., Dhooghe L., Lemièrre F., Cimanga K., Mesia K., Apers S., Pieters L., 2012. Chromatographic profiling and identification of two new iridoid-indole alkaloids by UPLC-MS and HPLC-SPE NMR analysis of an antimalarial extract from *Nauclea pobeguinii*. *Phytochemistry Letters* **5**, 316-319.

Yang L., Peng K., Zhao S., Zhao F., Chen L., Qiu F., 2013. 2-methyl-1-erythritol glycosides from *Gardenia jasminoides*. *Fitoterapia* **89**, 126-130.

Yaoita, Y., Ishizuka, T., Kakuda, R., Machida, K., Kikuchi, M., 2000. Structures of new ceramides from the fruits bodies of *Grifola frondosa*. *Chemical and Pharmaceutical Bulletin* **48**, 1356-1358.

Yaoita Y., Kohata R., Kakuda R., Machida K., Kikuchi M., 2002. Ceramide constituents from five mushrooms. *Chemical and Pharmaceutical Bulletin* **50**, 681-684.

Yaoita Y., Satoh Y., Kikuchi M., 2007. A new ceramide from *Ramaria botrytis* (Pers.) Ricken. *Journal of Natural Medicines* **61**, 205-207.

Yao-Kouassi P. A., Magid A. A., Richard B., Martinez A., Jacquier M.-J., Caron C., LeMagrex D. E., Gangloff S. C., Coffy A. A., Ze` C. M., 2008. Isoflavonoid glycosides from the roots of *Baphia bancoensis*. *Journal of Natural Products* **71**, 2073-2076.

Zahra A., Souroush S., 2010. An investigation into the antifungal property of Fabaceae using bioinformatics tools. *Avicenna Journal of Medical Biotechnology* **2**, 93-100.

Zheng W., Kollmeyer J., Symolon H., Momin A., Munter E., Wang E., Kelly S., Allegood J.C., Liu Y., Peng Q., Ramaraju H., Sullards M.C., Cabot M., Merrill A. H., 2006. Ceramides and other bioactive sphingolipid backbones in health and disease: lipidomic analysis, metabolism and roles in membrane structure, dynamics, signaling and autophagy. *Biochimica and Biophysica Acta* **1758**, 1864-1884.

ANNEXE

PUBLICATIONS RESULTING FROM THIS WORK:

1. **Wonkam A. K. N.**, Ngansop C. A. N., Wouamba S. C. N., Jouda J. B., Happi G. M., Boyom F. F., Sewald N., Lenta B. N., 2020. Rothmanniamide and other constituents from the leaves of *Rothmannia hispida* (K. Schum.) Fagerl. (Rubiaceae) and their chemophenetic significance. *Biochemical Systematics and Ecology* **93**, 104137. <https://doi.org/10.1016/j.bse.2020.104137>.
2. **Wonkam A. K. N.**, Ngansop C. A. N., Tchuenmogne M. A. T., Tcheegnitegni B. T., Bitchagno G. T. M., Awantu A. F., Bankeu J. J. K., Boyom F. F., Sewald N., Lenta B. N., 2021. Chemical constituents from *Baphia leptobotrys* Harms (Fabaceae) and their chemophenetic significance. *Biochemical Systematics and Ecology* **96**, 104260. <https://doi.org/10.1016/j.bse.2021.104260>.